Ingenieurfakultät Bau Geo Umwelt
Lehrstuhl für Hydrologie und Flussgebiets-management

Impacts of Changes in Climate, Land Cover and Water Management on Water Availability of the Upper Blue Nile River Basin, Ethiopia

Dagnenet Fenta Mekonnen

Vollständiger Abdruck der von der Ingenieurfakultät für Bau Geo Umwelt der Technischen Universität München zur Erlangung des akademischen Grades eines

Doktor-Ingenieurs (Dr.-Ing.)

genehmigten Dissertation.

Vorsitzender: Prof. Dr.sc.techn. Peter Rutschmann

Prüfer der Dissertation:

1. Prof. Dr.-Ing. Markus Disse
2. Prof. Dr.rer.nat. Ralf Ludwig (Ludwig-Maximilians-Universität München)
3. Prof. Dr. agr. Karl Auerswald

Die Dissertation wurde am 06.05.2019 bei der Technischen Universität München eingereicht und durch die Ingenieurfakultät Bau Geo Umwelt am 01.07.2019 angenommen.

Declarations of Authorship

I certify that this dissertation is the result of my own work, except where otherwise acknowledged. This doctoral dissertation was not previously presented to another examination board.

Doctoral candidate's signature **Munich, April 2019**

Parts of this dissertation have been published in the following journal articles:

Mekonnen, D.F., Disse, M.: Analyzing the future climate change of Upper Blue Nile River basin using statistical downscaling techniques. Hydrology and Earth System Sciences, 22(4), 2391, 2018a. DOI:10.5194/hess-22-2391-2018

Mekonnen, D.F., Duan, Z., Rientjes, T., Disse, M.: Analysis of combined and isolated effects of land-use and land-cover changes and climate change on the upper Blue Nile River basin's streamflow. Hydrology and Earth System Sciences, 22(12), 6187-6207, 2018b. DOI: https://doi.org/10.5194/hess-22-6187-2018

Abstract

The Nile basin is home to over 257 million people, which are about 54% of the total population of the 11 countries that share the Nile River. The water resources in the upper Blue Nile River basin (UBNRB) are the major source of life for the people living in the Nile basin. It provides more than 60% of the total Nile water. However, land degradation, deforestation, increasing water demand due to population and economic growth, urbanization, and climate change are becoming the major challenges and threatening issues by altering the dynamics of the hydrology and water availability of the basin. Hence, sustainable water resources management in the basin is necessary that requires in-depth understanding of the historical trends of hydro-climatic variables, hydrological processes and sources influencing water quantity, such as land use land cover (LULC) and climate changes. This dissertation is therefore aiming for the following objectives i) to assess the long-term trends of rainfall, maximum temperature (Tmax), minimum temperature (Tmin) and streamflow. ii) analyses responses by changes in LULC and climate over the past decades on streamflow in the UBNRB. iii) understand the future water development perspective in the UBNRB by considering the future climate change and proposed reservoirs in the basin. Different methods including long-term trend analysis, satellite remote sensing technique, climate and hydrological modeling were applied.

The long-term trends (1971-2010) of rainfall, temperature and streamflow were analyzed for 15 rainfall stations, 10 temperature stations and four streamflow gauging stations in the basin. Mann-Kendall (MK) and Pettitt tests were used for the trend and change point detection analysis, respectively. The results showed statistically significant increasing trend and related upward shifts in almost all temperature stations except Assosa station, which showed no change. However, precipitation time series did not reveal any statistically significant trends at 5% significance level in daily, mean annual and seasonal scales across the majority of examined stations. The MK test results for daily, monthly, annual and seasonal streamflow time series showed a positive trend, the magnitude of which is statistically significant at El Diem station. The Pettitt test also detected upward shift for daily, annual, and long rainy season streamflow at El Diem gauging station.

Landsat satellite images for 1973, 1985, 1995, and 2010 were used for LULC change-detection analysis. The LULC change-detection findings indicate that cultivated land increased while the forest coverage decreased prior to 1995, but forest area increased after 1995 with the area of cultivated land that decreased. Statistically, forest coverage changed from 17.4% to 14.4%, by 12.2 %, and by 15.6 %, while cultivated land changed from 62.9% to 65.6 %, by 67.5 %, and by 63.9% from 1973 to 1985, in 1995, and in 2010, respectively. The Soil and Water Assessment Tool (SWAT) is applied to study the hydrological impact of climate and LULC changes. Results of SWAT hydrological modeling indicate that mean annual streamflow increased by 16.9 % between the 1970s and 2000s due to the combined effects of LULC and climate change. The evapotranspiration change caused by the LULC change is minimal. As a result, the change for surface runoff and base flow due to LULC change is not significant. However, climate change significantly affected the surface runoff and base flow. This indicates that hydrological impacts by climate change are more significant as compared to the impacts of LULC change for streamflow of the upper Blue Nile River basin. Between the period 1970s and 2000s, the combined effects of LULC changes and climate change increased surface runoff by 20.9 mm.

The isolated effect of climate change contributed about 95.7 % (20 mm) while LULC change alone increased surface runoff by 0.3 mm, this accounted for 1.4 % of the total surface runoff change. Between this simulation period, combined changes of LULC and climate decreased baseflow by -11.5 mm, and the percent contributions were 94.8 % (-10.9 mm) for the climate change and 5.2 % (-0.6 mm) for the LULC changes.

Two widely used statistical downscaling techniques, namely the Long Ashton Research Station Weather Generator (LARS-WG) and the Statistical Downscaling Model (SDSM) were applied to downscale future climate scenarios of precipitation, maximum temperature (Tmax) and minimum temperature (Tmin) of the UBNRB. The calibration and validation result illustrates that both downscaling techniques (LARS-WG and SDSM) have shown comparable and good ability to simulate the current local climate variables. Further quantitative and qualitative comparative performance evaluation was done by equally weighted and varying weights of statistical indexes for precipitation only. The performance evaluation result showed that SDSM was more accurate to reproduce long-term mean monthly precipitation but LARS-WG performed best in capturing the extreme events and distribution of daily precipitation in the whole data range.

To overcome the uncertainties came from different general circulation models (GCMs), a multi-model approach was employed. In total, 27 systematically selected future climate scenarios were produced for the period 2030s, 2050s and 2080s. The result from the ensemble mean of the six coupled model inter-comparison project phase 3 (CMIP3) GCMs showed an increasing trend for precipitation, Tmax and Tmin. In contrary to CMIP3 GCMs, the downscaled precipitation from three coupled model inter-comparison project phase 5 (CMIP5) GCMs using representative concentration pathways (RCP 4.5 and RCP 8.5) scenarios showed a greater tendency towards a decrease in the future in the UBNRB. Furthermore, HadCM3 from CMIP3 using A2a and B2a scenarios and canESM2 from CMIP5 GCMs under RCP2.6, RCP4.5 and RCP8.5 scenarios were downscaled by SDSM method. The result from the two GCMs under five different scenarios showed that the three climate variables (precipitation, Tmax and Tmin) might increase in the future, which has an agreement with CMIP3 multi-model average result. The maximum increase of precipitation was obtained from canESM2 GCM downscaled using SDSM and maximum decrease from GFDL CMIP5 GCM downscaling using LARS-WG method. The wide-range of downscaled future precipitation results from multi-model GCMs over UBNRB showed the uncertainties' of GCMs outputs.

Finally, HEC-HMS semi-distributed hydrological model was used for quantifying the impacts of combined future climate change and water managements with 12 different scenarios on the hydrology and water availability of UBNRB. The statistical performance evaluation results obtained during the calibration and validation periods were satisfactory and acceptable. The downscaled outputs of canESM2 and GFDL GCMs under midrange scenarios of RCP4.5 are used for further impact analysis as they represented the wet and dry climate conditions respectively in the future. The hydrological response result indicates that under RCP4.5 scenario from canESM2 climate model, streamflow might increase by 22.6 %, 43 % and 55 % in the period 2030s, 2050s and 2080s respectively over the UBNRB. However, the streamflow might decrease by -21 %, -25 % and -21 % using climate variables downscaled from GFDL CMIP5 GCM under RCP4.5 scenario as input. The impact assessment result under wet climate condition

(canESM2 RCP4.5) and full development scenario indicates that the Lake Tana reservoir level and area might increase by maximum of 0.1m and 4.2 km^2 respectively from the area during the natural flow condition. In contrary, under the climate change projection of GFDL GCM RCP 4.5 scenario (dry climate condition) combined with full water resource developments in the UBNRB, the lake water levels lower up to by 1.03 m and the mean lake area reduced by a maximum of 47.4 km^2 from 3,053.2 km^2 to 3,005.8 km^2.

This dissertation also provide quantitative analysis of water resources management by considering the current and future climate change combined with the proposed cascades reservoirs for power generation. The model simulation results revealed that the total energy generation of Grand Ethiopian Renaissance Dam (GERD) might increase by 2,829 $GWhyr^{-1}$ from the target energy of 16,153 $GWhyr^{-1}$ to 18,982 $GWhyr^{-1}$ under wet climatic condition (i.e. canESM2 GCM RCP4.5 climate scenario). However, under dry climatic condition (i.e. GFDL GCM RCP4.5), it might decrease by 9,072 $GWhyr^{-1}$ to 7,081 $GWhyr^{-1}$. The proposed four large cascaded hydropower projects along the main stem of Abay River can generate a maximum total annual energy of 50,047 $GWhyr^{-1}$ and a minimum of 24,213 $GWhyr^{-1}$ at the end of 21^{st} century using canESM2 and GFDL GCMs respectively.

The model simulation results show that drastic impacts on the annual cycle of discharges can be expected, shifting from a strong seasonal to a completely balanced regime with almost constant discharges each month. The value of the coefficient of variance at El Diem gauging station under natural condition is 1.14 but for other scenarios, which are influenced by climate and water resource developments, it is reduced to less than 0.5. Lake Tana sub-basin is more susceptible to water scarcity because of the upstream large size future planned water resource developments and climate change effects. Hence, effective planning, management and regulation of water resource developments are highly recommended to prevent conflict between competing water users and sectors. In conclusion, this study has shown that climate change effect is more significant than the anthropogenic effects for altering the performance of water infrastructure developments and hydrology of the basin.

Zusammenfassung

Im Nilbecken leben über 257 Millionen Menschen, das sind etwa 54% der Gesamtbevölkerung der elf Länder, die sich das Nileinzugsgebiet teilen. Die Wasserressourcen im oberen Blue Nile River Basin (UBNRB) sind die wichtigste Lebensgrundlage für die Menschen im Nilbecken. Es liefert mehr als 60% des gesamten Nilwassers. Landdegradation, Entwaldung, steigender Wasserbedarf aufgrund von Bevölkerungs- und Wirtschaftswachstum, Urbanisierung und Klimawandel werden jedoch zu großen Herausforderungen und Bedrohungen, indem sie die Dynamik der Hydrologie und der Wasserverfügbarkeit des Beckens verändern. Daher ist eine nachhaltige Bewirtschaftung der Wasserressourcen im Einzugsgebiet erforderlich, die ein grundlegendes Verständnis der historischen Trends hydroklimatischer Variablen, hydrologischer Prozesse und wassermengenbeeinflussender Ursachen wie Landnutzungsänderungen (LULC) und Klimaänderungen erfordert. Diese Dissertation zielt daher auf die folgenden Ziele: i) Bewertung der langfristigen Trends von Niederschlag, maximaler Temperatur (Tmax), minimaler Temperatur (Tmin) und Durchfluss. ii) Analyse von LULC und Klimaänderungen in den letzten Jahrzehnten und Auswirkungen auf den Durchfluss im UBNRB. iii) zukünftige Wasserverfügbarkeit im UBNRB durch Berücksichtigung der zukünftigen Klimaänderung und der vorgeschlagenen Reservoirs im Becken. Verschiedene Methoden wie Langzeittrendanalyse, Satellitenfernerkundung, Klima- und hydrologische Modellierung wurden eingesetzt.

Die langfristige Entwicklung von Niederschlag wurde an 15 Stationen, Temperatur an zehn Stationen und Abfluss an vier Pegeln für den Zeitraum 1971-2010 analysiert. Für die Trend- und Sprungerkennung wurde der Mann-Kendall Test (MK) bzw. der Pettitt Test verwendet. Die Ergebnisse zeigten statistisch signifikant steigende Trends und einen damit verbundenen Temperaturanstieg an allen Messstellen außer in Assosa, die keine Veränderung zeigte. Die Niederschlagszeitreihen zeigten jedoch keine statistisch signifikanten Trends für Tages-, Monats- und Jahreswerte am Großteil der untersuchten Stationen bei 5% Signifikanzniveau. Die MK-Testergebnisse für tägliche, monatliche, jährliche und saisonale Abflusszeitreihen zeigten einen positiven Trend, dessen Ausmaß an der Station El Diem statistisch signifikant ist. Der Pettitt Test erkannte ebenfalls einen Abflussanstieg auf täglicher und jährlicher Ebene sowie während der langen Regenzeit an der Messstation El Diem.

Für die Erkennung und Analyse von LULC Veränderungen wurden Landsat Satellitenbilder der Jahre 1973, 1985, 1995 und 2010 verwendet. Die Ergebnisse der LULC-Änderungserkennung ergab für die Waldfläche in den Jahren 1973, 1985, 1995 und 2010 Flächenanteile von 17,4%, 14,4%, 12,2% und 15,6%, und für die Ackerfläche im selben Zeitraum Flächenanteile von 62,9%, 65,6%, 67,5% und 63,9%. Die Ergebnisse belegen, dass die landwirtschaftlich genutzte Fläche bis 1995 zunahm, während die Waldfläche gleichzeitig abnahm, allerdings hat sich diese Entwicklung nach 1995 umgekehrt. Zur Untersuchung der hydrologischen Auswirkungen von Klimaänderungen und LULC wird das Soil and Water Assessment Tool (SWAT) eingesetzt. Die Ergebnisse der hydrologischen SWAT-Modellierung deuten darauf hin, dass der mittlere jährliche Abfluss zwischen den 1970er und 2000er Jahren aufgrund der kombinierten Auswirkungen von LULC und Klimawandel um 16,9% gestiegen ist. Die durch LULC verursachte Evapotranspirationsänderung ist minimal. Infolgedessen ist die Änderung des Oberflächenabflusses und des Basisabflusses durch LULC nicht signifikant. Der Klimawandel hat jedoch den Oberflächen- und Basisabfluss erheblich beeinflusst. Dies deutet darauf hin, dass

die hydrologischen Auswirkungen des Klimawandels bedeutender sind als die Auswirkungen der LULC auf den Abfluss des oberen Blue Nile River Basins. Zwischen den 1970er und 2000er Jahren erhöhten die kombinierten Auswirkungen von LULC und Klimawandel den Oberflächenabfluss um 20,9 mm. Der isolierte Effekt des Klimawandels trug etwa 95,7 % (20 mm) bei, während LULC allein den Oberflächenabfluss nur um 0,3 mm erhöhte, was 1,4 % der gesamten Oberflächenabflussänderung ausmachte. In diesem Simulationszeitraum verringerten die kombinierten Veränderungen von LULC und Klima den Basisabfluss um -11,5 mm, und die prozentualen Beiträge betrugen 94,8 % (-10,9 mm) für den Klimawandel und 5,2 % (-0,6 mm) für die Landnutzungsveränderungen (LULC).

Zwei weit verbreitete statistische Downscalingverfahren, nämlich der Long Ashton Research Station Weather Generator (LARS-WG) und das Statistical Downscaling Model (SDSM), wurden zum Downscalen zukünftiger Klimaszenarien von Niederschlag, Maximaltemperatur (Tmax) und Minimaltemperatur (Tmin) des UBNRB eingesetzt. Die Kalibrier- und Validierungsergebnisse zeigen, dass beide Downscaling-Techniken (LARS-WG und SDSM) vergleichbare und gute Fähigkeiten zur Simulation der aktuellen lokalen Klimavariablen besitzen. Weitere quantitative und qualitative vergleichende Bewertungen wurden durch gleich gewichtete und variierende Gewichte von statistischen Indizes nur für Niederschläge durchgeführt. Das Auswertungsergebnis zeigte, dass SDSM in der Lage war, genauere langfristige mittlere monatliche Niederschläge zu reproduzieren, während LARS-WG bei der Erfassung der Extremereignisse und der Verteilung der täglichen Niederschläge im gesamten Datenbereich bessere Ergebnisse erzielte.

Um die Unsicherheiten zu überwinden, wurden verschiedene allgemeine Zirkulationsmodelle verwendet (GCMs) herrühren, wurde ein multimodell-Ansatz verwendet. Insgesamt wurden 27 systematisch ausgewählte Zukunftsszenarien für den Zeitraum 2030er, 2050er und 2080er Jahre erstellt. Das Ergebnis aus dem Ensemble-Mittelwert von sechs gekoppelten GCM Modellen (Projekt CMIP3) zeigte einen zunehmenden Trend für Niederschläge, Tmax und Tmin. Im Gegensatz zu CMIP3-GCMs zeigte der reduzierte Niederschlag aus drei gekoppelten modellübergreifenden Projektphasen-5 (CMIP5)-GCMs mit repräsentativen Konzentrationspfaden (RCP 4.5 und RCP 8.5) eine stärkere Tendenz zu einem zukünftigen Rückgang in der UBNRB. Darüber hinaus wurde HadCM3 aus CMIP3 unter Verwendung von A2a- und B2a-Szenarien und canESM2 aus CMIP5-GCMs unter RCP2.6, RCP4.5 und RCP8.5-Szenarien mittels SDSM-Methode herunterskaliert. Das Ergebnis der beiden GCMs unter fünf verschiedenen Szenarien zeigte, dass die drei Klimavariablen (Niederschlag, Tmax und Tmin) in Zukunft zunehmen könnten, was eine Übereinstimmung mit dem CMIP3-Multimodell-Durchschnittsergebnis darstellt. Die maximale Zunahme des Niederschlags wurde aus canESM2 GCM erhalten, das mit SDSM verkleinert wurde, und die maximale Abnahme aus GFDL CMIP5 GCM, das mit der LARS-WG-Methode verkleinert wurde. Die große Bandbreite der herunterskalierten zukünftigen Niederschlagsergebnisse von Multi-Modell-GCMs über UBNRB zeigte die Unsicherheiten der GCM-Outputs.

Schließlich wurde das teilverteilte hydrologische Modell HEC-HMS zur Quantifizierung der kombinierten Auswirkungen des zukünftigen Klimawandels und der Wasserbewirtschaftung mit zwölf verschiedenen Szenarien auf die Hydrologie und Wasserverfügbarkeit im UBNRB verwendet. Die Ergebnisse der statistischen Bewertung, die während der Kalibrierungs- und

Validierungszeiträume erzielt wurden, waren zufriedenstellend und akzeptabel. Die herunterskalierten Werte der GCMs „canESM2“ und „GFDL“ mit mittleren Szenarien RCP4.5 werden für die weitere Analyse der Auswirkungen auf den Klimawandel verwendet, da sie die nassen bzw. trockenen Klimabedingungen in der Zukunft darstellen. Das Ergebnis der hydrologischen Analyse deutet darauf hin, dass unter RCP4.5-Szenarien aus dem canESM2-Klimamodell der Abfluss im Zeitraum 2030er, 2050er und 2080er Jahre um 22,6 %, 43 % bzw. 55 % im UBNRB zunehmen könnte. Der Abfluss könnte jedoch um -21%, -25% bzw. -21% abnehmen, wenn die Klimavariablen aus GCM GFDL CMIP5 unter RCP4.5-Szenarien als Input verwendet werden. Die Ergebnisse der Folgenabschätzung unter feuchten Klimabedingungen (canESM2 RCP4.5) und des vollständigen Entwicklungsszenarios deuten darauf hin, dass der Wasserstand und die Fläche des Lake Tana um maximal 0,1 m bzw. 4,2 km^2 gegenüber dem Gebiet während der natürlichen Abflussbedingungen ansteigen könnten. Im Gegensatz dazu sinkt, im Rahmen der Klimaprognose des GCM GFDL RCP 4.5-Szenarios (trockene Klimabedingungen) in Kombination mit der vollständigen Erschließung der Wasserressourcen im UBNRB, der Wasserspiegel um bis zu 1,03 m und die mittlere Seefläche um maximal 47,4 km^2 von 3053,2 km^2 auf 3005,8 km^2.

Diese Dissertation bietet auch eine quantitative Analyse des Wasserressourcen-Managements durch die Berücksichtigung der aktuellen und zukünftigen Klimaänderungen in Kombination mit den vorgeschlagenen Kaskaden-Reservoirs für die Stromerzeugung. Die Modellsimulationsergebnisse zeigten, dass die gesamte Energieerzeugung des Grand Ethiopian Renaissance Dam um 2.829 $GWhyr^{-1}$ von der Soll-Energie von 16.153 $GWhyr^{-1}$ auf 18.982 $GWhyr^{-1}$ unter feuchten klimatischen Bedingungen (z.B. GCM CanESM2 RCP4.5 Klimaszenario) steigen könnte, aber unter trockenen klimatischen Bedingungen (z.B. GCM GFDL RCP4.5) könnte sie um 9.072 $GWhyr^{-1}$ auf 7.081 $GWhyr^{-1}$ sinken. Die vorgeschlagenen vier großen Kaskaden-Wasserkraftprojekte entlang des Hauptflusses des Abay River können am Ende des 21. Jahrhunderts mit CanESM2- und GFDL-GCMs eine maximale jährliche Gesamtenergie von 50.047 $GWhyr^{-1}$ und mindestens 24.213 $GWhyr^{-1}$ erzeugen.

Weitere Ergebnisse der Simulation des Kaskadenspeicher-Betriebsmodells zeigten, dass drastische Auswirkungen auf die monatlichen Abflüsse zu erwarten sind, die sich von einem starken saisonalen zu einem vollständig ausgeglichenen System mit nahezu konstanten Abflüssen pro Monat verschieben. Der Wert des Varianzkoeffizienten an der Messstation El Diem unter natürlichen Bedingungen beträgt 1,14, für andere Szenarien, die von der Entwicklung der Klima- und Wasserressourcen beeinflusst werden, wird sie jedoch auf weniger als 0,5 reduziert. Das Teileinzugsgebiet des Lake Tana ist aufgrund der großen, zukünftig geplanten Entwicklung der Wasserressourcen stromaufwärts und der Auswirkungen des Klimawandels stärker der Wasserknappheit ausgesetzt. Daher wird eine effektive Planung, Verwaltung und Regulierung der Entwicklung der Wasserressourcen dringend empfohlen, um Konflikte zwischen konkurrierenden Wassernutzern und -sektoren zu vermeiden. Zusammenfassend lässt sich sagen, dass diese Studie gezeigt hat, dass der Effekt des Klimawandels signifikanter ist als die anthropogenen Effekte für die Veränderung der Leistung von Wasserinfrastrukturen und der Hydrologie des Einzugsgebietes.

Acknowledgements

First and foremost, praises and thanks to the God, the Almighty, for His showers of blessings throughout my research work to complete the research successfully.

I would like to express my deepest gratitude to my supervisor Prof. Dr.-Ing Markus Disse, who has given me the opportunity to pursue my Ph.D. under his guidance at Technical University of Munich (TUM), Chair of Hydrology and River basin management, Germany. Moreover, I appreciate his constant guidance and encouragement throughout this Ph.D. work. I appreciate his timely response to all academic and non-academic matters related to my research. It was a great privilege and honor to study under his guidance. I am extremely grateful for what he has offered me. I am extending my heartfelt thanks to his wife and family for their kindness. I would also like to extend my sincere gratitude to Dr.-Ing Bernd Wiebusch, who helped me in many ways for creating a contact with Prof. Markus Disse.

I am also indebted to Prof. Dr. sc. techn. Peter Rutschmann, chairperson of my examination committee, who offered me to visit TUM for a strategic meeting with Prof. Markus Disse. I am grateful to the members of the examining board Prof. Dr. rer. nat. Ralf Ludwig and Prof. Dr. agr. Karl Auerswald for their commitment. My sincere thanks go to Dr.-Ing Annette Spengler for supporting my Ph.D. in many ways.

I would like to acknowledge my employer the Amhara regional state water, irrigation and energy development bureau and the Amhara regional government for granting me a study leaves to pursue this research work. This research has been possible thanks to the financial support of DAAD water–food–energy NeXus project and the TUM Graduate School (TUM-GS). I acknowledge Oskar von Miller Forum (OvMF) for granting me a scholarship for accommodation in Munich. I am also indebted to OvMF staffs (Prof. Dr.-Ing.Werner Lang (Director), Daniela Schäfer, Rosemarie Nöhbauer and sabelle Krier-Michaeli) for their assistance and kindness during my stay at OvMF.

I extend my acknowledgement to the Ministry of water, Irrigation and Energy, Ethiopian National Meteorological Agency, Abay basin authority and Tana-Beles project office for providing me all necessary hydro-meteorological data and other supporting documents for the research. I would also like to thank the Eastern Nile Technical Regional Office (ENTRO) for hosting me as visiting Ph.D student for three-week productive stay. I am thankful to Eng. Azeb Merisha and Mr. Fekahmed Negash (ENTRO Executive Director) for the opportunity they gave me to visit ENTRO.

There are people who should deserve a great acknowledgment for their contribution to me during the entire research period without whom this study would have only been a dream. All staffs of chair of hydrology and river basin management at Technical university of Munich, especial acknowledgement to our secretary Mrs. Christiane Zach-Cretaine, I really appreciate your support for every helpful assistance you have made for me, when it is needed throughout the research period. Mr. Georg Loy, Constantin Heffner, Prof. Dr.-Ing. Haimerl Gerhard, Helena Huber, Dr. Erwin, Katherina, Dr.Tatiana Stamou, Kordula Schwarzwälder, Daniela Schaufuß,

Sabine Thomma, and Führes Jakob are few of them, for their wholehearted assistance and kindness.

Special acknowledgement goes to my mentors Dr. Thomas Schneider and Dr. Duan Zheng, no words can truly express the level of gratitude and appreciation I have for you. I would like to offer special thanks to Eng. Simegnew Bekele (late project manager of GERD), who, although no longer with us, for his kindness and generosity during our GERD visits. Special acknowledgement goes to Aba Hitsane Dingil, no words can truly express the level of gratitude and appreciation I have for you. Thank you for being the father and for your prayers I needed when times were hard.

I am extremely grateful to my parents for their love, prayers, constant encouragement, moral support and the faith that made me who I am. I am very much thankful to my beloved wife, W/ro Yenezewud Belay, for her love, understanding, devotion and all she has done for me. She has always been a great source of inspiration and has made a great difference in my life. My daughters and sons Bethelihem, Hana, Mikiyas and Beniyas, thank you for your patience and understanding during the difficult time of my study. You are my real sources of inspiration.

Finally, my thanks go to all the people who have supported me in one way or the other during this amazing journey.

Acronyms and abbreviations

ACB	Absolute Cumulative Bias
AOGCM	Atmospheric Ocean General Circulation Model
ArcGIS	GIS software interface
ARS-USDA	Agricultural Research Service of the United States Department of Agriculture
Bm^3	Billion cubic meters
CDF	Cumulative probability Distribution Function
CGIAR-CSI	Consultative Group on International Agricultural Research-Consortium for Spatial Information
CMIP3	Coupled Model Intercomparison Project phase 3
CMIP5	Coupled Model Intercomparison Project phase 5
CN	Curve Number
CSA	Central Statistics Agency of Ethiopia
DEM	Digital Elevation Model
DSMW	Digital Soil Map of the World
ECCDI	Expert on Climate Change Detection and Indices
ENTRO	Eastern Nile Technical Regional Office
EPM	Semi-empirical Distribution
EROS	Earth Resources Observation and Science
FAO-UNESCO	Food and Agriculture Organization of the United Nations
FFW	Food For Work
FSL	Reservoir Full Supply Level
GCM	General Circulation Models
GCPs	Ground Control Points
GERD	Grand Ethiopian Renaissance Dam
GIS	Geographic Information System
GPS	Global Positioning System
GWh	Gigawatt hours
ha	Hectar
HBV	Hydrologiska Byrans Vattenbalansavdelning model
HEC-HMS	Hydrologic Engineering Center- Hydrological Model System
HFAM	Hydrocomp Forecast and Analysis Modeling
HPP	Hydropower Project
HRU	Hydrologic Response Unit
IPCC	Intergovernmental Panel on Climate Change
IRF	Interquartile Relative Fraction
ISODATA	Iterative Self-Organizing Data Analysis
ITCZ	Inter-Tropical Convergence Zone
KS	Kolmogorov–Smirnov
LARS-WG	Long Ashton Research Station Weather Generator
LULC	Land Use Land Cover
m^3s^{-1}	Cubic meter per second
MAE	Mean Absolute Error

m.a.s.l	Meters above sea level
MERET	Managing Environmental Resources to Enable Transition
MOL	Minimum Operating Level
mm	Millimeter
Mm^3	Million Cubic Meter
MoWR	Ministry of Water Resources of Ethiopia
MSS	Multi-spectral Scanner
MW	Mega watt
MWIE	Ministry of Water, Irrigation and Electricity of Ethiopia
NCEP	National Centers for Environmental Prediction
NDVI	Normalized Difference Vegetation Index
NMA	National Meteorology Agency of Ethiopia
NSE	Nash-Sutcliffe efficiency
PBIAS	Percent Bias
PDF	Probability Distribution Function
PSNP	Productive Safety Net Programs
RCP	Representative Concentration Pathway
RCM	Regional Climate Models
R^2	Correlation Coefficient
RMSE	Root Mean Square Error
SDSM	Statistical Downscaling Model
SLMP	Sustainable Land Management Project
SMA	Soil Moisture Accounting Algorithm
SRES	Special Report on Emission Scenario
SRTM	Shuttle Radar Topography Mission
SUFI-2	Sequential Uncertainty Fitting, Version2
SWAT	Soil and Water Assessment Tool
SWAT-CUP	SWAT-Calibration and Uncertainty Program
SWC	Soil and Water Conservation
SWM	Stanford Watershed Model
TM	Thematic Mapper
TUM	Technical University of Munich
UBNRB	Upper Blue Nile River Basin
USGS	United States Geological Survey
Yr^{-1}	per year

List of Tables

List of Figures

List of Appendices

Chapter 1 Introduction

1.1 Background

Nile is the world's longest river and has a drainage area of about 3.2 million km^2, which is nearly 10% of the landmass of the African continent. The Nile River has two important water supply sources: the Blue Nile (Ethiopia) which contributes almost 85% of the flow and White Nile (Nile Equatorial countries) that contributes the remaining 15% of the flow. The Nile basin is home to over 257 million people which is about 54% of the total population of the 11 countries that share the Nile (Abdulkarim H *et al.*, 2016). Hence, it is becoming a crucial resource for the socio-political and economic development of the Nile basin countries. Although, the Blue Nile River, originating from Ethiopian highland, contributes the major share of the Nile water with more than 60% of the total discharge (Conway, 2000), it is becoming one of the least developed sub-basin. To date, Ethiopia has utilized very little of the Blue Nile water. Until recently, the usable installed capacity of hydropower is 639.4MW: Amerti-Neshi-Fincha (95 MW), Tana Beles (460 MW) and Tis Abay I &II (84.4 MW), which account 16% of the country's current 3,814.6 MW with almost no large-scale irrigation development except Fincha (8,145 ha) and Koga (7,200 ha). Recently due to its large water resource potential, and suitability of land and topography for irrigation and power generation, the Ethiopian government has given due emphasis to significantly increase large reservoir water storage in the Blue Nile basin to support national development and alleviate poverty. Possible irrigation and hydropower projects have been investigated over a number of years, as a result, 815,581 ha of land suitable for potential irrigation and more than 10,000 MW hydropower schemes being anticipated in the Blue Nile Basin (BCEOM, 1998a).

Due to the high population growth and low productivity, cultivated land has been expanded with the objective of getting better economic benefits without looking at the environmental suitability. Several reasons are behind Ethiopia's ambitious plan to develop large-scale irrigation and hydropower projects. First, to combat the negative effects of the extreme spatial and temporal variability of both climate and hydrology, which cause recurring floods and droughts. Majority of the population rely on rain fed agriculture in which its productivity has a strong correlation with the climate variability linked to vulnerability. The cost of hydrological variability currently has been estimated to be more than one third of the annual GDP, which indicated that increased investment in multipurpose water infrastructure could contribute to the long term economic development and mitigate the adverse impacts of floods and droughts (Chen and Swain, 2014). Second, Ethiopia's hydropower capacity could contribute to economic growth particularly for generating foreign hard currency and a reliable source of electricity, which ultimately contribute for the sustainable economic development.

However, land degradation, deforestation, increasing water demand due to population and economic growth, urbanization, and climate change are becoming the major challenges and threatening issues for future water developments by altering the dynamics of the hydrology and water availability of the basin. To optimize food security and to establish better water management policies and strategies in the basin, land and water resource development and environmental sustainability of the basin, a good knowledge of the impacts of all these social and

environmental changes on the hydrology of the basin is becoming crucial. Understanding the hydrological processes and sources impacting water quantity, such as LULC change and climate change can achieve this as they are the key driving forces that can modify the watersheds hydrology and water availability (Oki and Kanae, 2006; Woldesenbet *et al.*, 2017b; Yin *et al.*, 2017). LULC change can modify the rainfall path to generate basin runoff by altering critical water balance components, such as, groundwater recharge, infiltration, interception, and evaporation. Climate variations affect water cycle process in terms of temperature, precipitation and evaporation, which leads to the temporal and spatial change of water and sediment resources. Meanwhile, LULC alter the hydrologic cycle and soil erosion by way of such processes as canopy interception and transpiration, and the redistribution of rainfall erosivity. UBNRB experiences significant spatial and temporal climate variability (Alemseged and Tom, 2015; McCartney *et al.*, 2012). Less than 500 mm of precipitation falls annually near the Sudanese border whereas more than 2000 mm falls annually in some areas of the southern basin (Awulachew *et al.*, 2008). Potential evapotranspiration (ET) also varies considerably and it is strongly correlated with altitude. At annual bases, it varies from more than 2200 mm near the Sudanese border to between about 1300 mm and 1700 mm in the Ethiopian highlands (McCartney *et al.*, 2012). The precipitation and ET cycles are characterized by seasonal and inter-annual variability, which affect the characteristic of the UBNRB streamflow. Hence, it is critical to quantify the change of river runoff through time, and to understand the drivers and mechanisms behind them. This would provide basic knowledge on the variation of change of streamflow in the upper Blue Nile River basin.

1.2 Problem statement

The UBNRB is characterized by large temporal variability in climate and hydrology both at seasonal and annual scale, which can be influenced by human activities such as modification in LULC, abstraction or change in water use. Identification of trends in hydro-climatic variables has enormous advantage for planning and management of limited water resources and for setting alternative strategies for future developments particularly to the shared water resource in the case of Blue Nile River. Changes in climate in conjunction with the changes in anthropogenic effects of the catchment could also influence the streamflow.

Climate change affects human kind in several ways. Drought and flooding are among the main effects of climate change, which significantly affect the livelihood of the people. Climate change affects the hydrological cycle, through changes in precipitation, maximum and minimum temperature and evapotranspiration. As it is clearly known that evapotranspiration is one of the main components of hydrological cycle, as the evaporation rate changes it has a direct impact on the hydrological regimes of a specific watershed. The higher the temperature the higher the rate of evaporation (Mohammed, 2013). This indicates that in addition to the changing pattern of the rainfall due to climate change there will be a direct influence on evaporation and ultimately on water resources potential. Hence, it is very important to understand how future climate change affects the availability and variability of basin water resource. So far, investigation of climate change on basin scale is not studied in detail especially in Ethiopia.

As upper Blue Nile basin covers about 14% of the total land area of Ethiopia and it is a basin, where 40% of the national agricultural product is generated, climate impact on the water

resources of the upper Blue Nile basin will have significant impact on the national food security. About two-thirds of the population who are entirely depending on farming is expected to reside on the highland parts of the basin, where there is relatively high amount of rainfall. However, the livelihood of the population is still below the poverty line, because of the erratic distribution of the rainfall both spatial and temporal, with the increase of dry spells that significantly reduce crop yields and sometimes lead to total crop failure (Gebrehiwot *et al.*, 2010).

Furthermore, the implication of climate change could be enormous on the performance of the planned large-scale irrigation and hydropower project as they are heavily relies on the availability of rainfall. During drought years, the hydropower generation is significantly affected due to shortage of water in the dams for power generation; meanwhile, the performance of the irrigation projects may reduce as the base flow of the rivers available for irrigation decreases. Climate variability, the way climate fluctuates yearly and seasonally above or below a long-term average value, caused by changes in forcing factors such as variation in seasonal extent of the Inter-tropical Convergence Zone (ITCZ) like El Niño and La Niña events, is already imposing a significant challenge to Ethiopia. It affects food security, water and energy supply, poverty reduction and sustainable socio-economic development efforts. For instance, recurrent droughts and floods in Ethiopia have resulted in loss of life and property as well as in the displacement of people. Changes in temperature and precipitation will have direct impact on the processes of runoff production. Consequently, any change in the spatial and temporal availability of water resources affects agriculture, industry and urban development. IPCC (2014a) findings indicate that developing countries such as Ethiopia will be more vulnerable to climate change because of its economic, climatic settings and limited water storage facilities.

One of the most important causes for vulnerability of Ethiopia to climate variability and change is very high dependence on rainfall amount and distribution, which has a direct effect on rain, fed agriculture. Climate variability also severely influences the water resources spatial and temporal availability and indirectly on the hydropower production capacity. These in turn affects the country‘s economy and its developmental goals and poverty reduction capacity. Over all, the impact may potentially embrace back economic progress or reverse the efforts made in development, and thus exacerbates social and economic challenges (Simane *et al.*, 2016). The country’s vulnerability to climate change is further increased by high levels of poverty, rapid population growth, and reliance on rain-fed agriculture.

Changes in land use and land cover (LULC) have also significant impacts on the regional hydrology by partitioning the rainfall into evapotranspiration and other water balance components such as surface runoff, lateral flow from the soil storage, ground water recharge. In the upper Blue Nile basin, due to high population growth and low productivity of the upland areas, changes in LULC are expected through expansion of cultivated land in low land areas of the basin. Furthermore, changes in LULC are expected through expansion of large scale irrigation and sugar cane plantation due to ambitious water resource development plan of the Ethiopian Government (Girma, 2013).

To mitigate these challenges, the Ethiopian government is therefore carried out a series of studies on upper Blue Nile river basin (UBNRB), which have been identified as an economic “growth corridor”, focused on identifying irrigation and hydropower potential of the basin (BCEOM,

1998a; USBR, 1964; WAPCOS, 1990). As the result, large scale irrigation and hydropower projects including the Grand Ethiopian Renaissance Dam (GERD), which will be the largest hydroelectric power plant in Africa after completion, have been identified and being constructed as mitigation measure for the impacts of climate change and reducing the conversion of forestland into cultivated land. The Ethiopian government argues that the GERD will supply electricity for the country as well as generate surplus cheap energy for export to neighboring countries. It has been suggested that a strong link exists between energy and development, and that access to electricity, including access in rural areas, is one of the keys to reducing poverty. It is also expected that the huge reservoir would generate positive externalities downstream by reducing flooding and sediment loads and by providing more constant and predictable flows. However, the implication of climate change effect on the availability of water resource should be a great concern for the sustainability of these large scale projects otherwise the consequences becomes catastrophic. In this regard, quantifying the effects of climate change on streamflow should be the first priority and crucial step for developing better water resource management policies and strategies in the basin and to provide concrete and concise information for water managers, policy and decision makers.

Therefore, understanding the relationships between the hydrologic regime, climate factors, and anthropogenic effects, patterns or trends of hydrological and meteorological variables of the basin will benefit efforts to manage water and ecological resources of the basin. It is a clear fact that in any water related engineering activities proper estimation of runoff magnitude is required for efficient design, planning, and management of the planned large-scale water resource developments that deals with preservation and utilization of water for various purposes.

The research was carried out in collaboration with a larger project on water resources management of the Nile River Basin also referred to as NIMA-NEX (NIle MAnagement Nexus EXpert tool).

1.3 Research objectives, questions and hypothesis

The main objective of this study is to quantify the combined and isolated impacts of climate change and LULC changes on the streamflow of UBNRB. Moreover, to analyze the combined impacts of future climate change, land and water management on the hydrology of UBNRB under different scenarios. Therefore, the specific objectives are

- To properly investigate and analyze the different methods available for filling gaps for the rainfall, temperature and streamflow data records and propose a method suitable for a basin
- To assess the long-term trend of rainfall and streamflow
- To evaluate the comparative performance of two widely used statistical downscaling techniques, namely the Long Ashton Research Station Weather Generator (LARS-WG) and the Statistical Downscaling Model (SDSM) over the UBNRB
- To downscale future climate scenarios of precipitation, maximum temperature (Tmax) and minimum temperature (Tmin) at acceptable spatial and temporal resolution, which can be used directly for further hydrological impact studies

- To analyze the changes in LULC for the past 4 decades (1973-2010)
- To quantify the combined and isolated effects of the changes in LULC and climate change on the streamflow and water balance components of UBNRB
- To quantify the potential impacts of climate change and water demands on the hydrology of the UBNRB.

Specific questions to be addressed during the completion of this research are:

- What is the general pattern of ground based measured precipitation, maximum temperature, minimum temperature and streamflow in the past 40 years (1971-2010)?
- Which driving factor is more significant for altering the hydrology of UBNRB? Is it LULC or climate change?
- Did LULC exhibits change in the past 37 years (1973-2010) in the UBNRB? Which land cover type has shown positive change and which one showed negative change?
- Can SWAT hydrological model be applied in the UBNRB in areas where the climate is monsoon tropical i.e. the soil moisture completely drying in dry season and saturate in rainy season unlike the temperate region where SWAT is originally developed?
- Which statistical downscaling methods better performs in representing the current climate of the basin?
- What will be the pattern of precipitation, maximum temperature, minimum temperature in the future for the UBNRB due to climate change effect? How do these patterns affect the streamflow and water balance components of the basin?
- How do the combined climate change and water resource developments that have planned to be developed by the Government of Ethiopia (GoE) in the future affects the Lake Tana reservoir?
- Could water scarcity be a big challenge for the region in the future?

Following the above research objectives and research questions the following hypotheses can be formulated

- Climate change effect is more significant than LULC changes for altering the streamflow of the basin.
- SWAT can be applied in monsoon tropical area if additional site-specific data containing soil and land use information is properly integrated into the model.
- SDSM statistical down scaling model based on regression of predictands and predictors might perform better than LARS-WG stochastically weather generator model in simulating the present climate condition of the UBNRB.
- In the future due to green house effect, precipitation and temperature may experience an increasing trend and as a result, streamflow may increase.
- Lake Tana sub-basin is more susceptible to water scarcity because of the large size future planned water resource developments and climate change effects.

- Climate change in portions of the UBNRB of Ethiopia may have the potential to increase the precipitation and flow regimes significantly. The increasing of precipitation in the basin could also result in increased water availability for rain-fed agricultural, domestic consumption and habitat.

This is doable by combining the analysis of statistical trend test, LULC classification and change detection derived from satellite remote sensing, and by employing semi-distributed hydrological models for simulating the past, present and future time periods streamflow under different forcing conditions.

1.4 Dissertation structure

The thesis is organized in eight chapters. In the first chapter, introduction of the research issues on the UBNRB, the problem statement, the objectives and hypothesis of the thesis were presented. **Chapter 2** summarizes the state of the art about the statistical trend analysis, hydrological and climate change modeling and remote sensing techniques for the LULC map classification and change detection analysis. In **Chapter 3** the description of the study area, topography, climate, hydrology, land use and soil characteristics are presented. **Chapter 4** briefly describes the hydro-meteorological data, in filling techniques for the missing data and evaluates their comparative performances. Furthermore, statistical trend analysis for precipitation, minimum temperature and maximum temperature for the 15 stations that have long time records and better data quality, and for streamflow of the four main streamflow stations (El Diem, Kessi, Gilgel Abay and Gumara) is carried out. Statistical Mann Kendall trend test and Pettittt homogeneity tests have been applied to assess the significance of trends and change point detection over different periods respectively. **Chapter 5** assesses the hydrological responses of the UBNRB to the changes in LULC and climate. It further identifies the major driving forces for the alteration of hydrology in the basin. In this chapter detail LULC classification and change detection analysis was carried out using remote sensing technique from Landsat images for the period 1973, 1985, 1995 and 2019 for the UBNRB. SWAT semi distributed hydrological model is applied for analyzing the combined and single effects of LULC and climate changes on the streamflow. **Chapter 6** analyzes the comparative performance of two widely used statistical downscaling methods (LARS-WG and SDSM) and projects the future precipitation, maximum temperature and minimum temperature. **Chapter 7** deals with the **c**ombined impacts of climate change and water managements on the hydrology of the basin and on the irrigation and hydropower sectors under different scenarios. HEC-HMS semi-distributed hydrological model is used for this task. Finally, **Chapter 8** summarizes the findings of the thesis, concluding remarks, recommendation, and outlooks for further studies in the basin.

Chapter 2 State of the Art

2.1 Statistical trend test for hydro-climatic variables of upper Blue Nile River basin

Detection of trends in hydro-climatic variables could be the priority task for planning and managing limited water resources and devise alternative strategies for future developments. It has significant importance in particular to the shared water resources in the case of the Blue Nile river basin (Gebrekristos, 2015). It is also one of the most important factors in explaining various socio-economic problems such as food security in a country whose economy is heavily dependent on low-productivity rain fed agriculture such as Ethiopia (Cheung *et al.,* 2008). Furthermore, the various developments made by human activity and hydro climatic changes can alter the time series of a streamflow. Determining of trends in long term streamflow is an important tool to detect any modification in hydrological systems (Salarijazi *et al.*, 2012).

Several individual studies have been done to investigate the historical trends in precipitation and streamflow in the UBNR basin, with most studies focusing on annual and seasonal total precipitation and streamflow. Taye *et al.* (2011) reviewed some of the research outputs and concluded that most studies reported no significant trend in annual and seasonal precipitation totals. For instance, (Conway, 2000) reported no change for a basin-wide time series of annual rainfall constructed from 11 gauges for the period 1900 to 1998 in the UBNRB. Whereas, over the period 1961 -1 990 the basin-wide series showed a strong negative correlation with time, r = -0.65). Seleshi and Zanke (2004) analyzed the changes in annual, rainy season and dry season rainfall and rainy days based on 11 key stations located in different climatic zones of Ethiopia over the common period 1965–2002 using Mann-Kendall (MK) trend test. They demonstrated that there is no trend in the annual rainfall total, the seasonal rainfall total or rainy days over central, northern and northwestern Ethiopia in the period 1965–2002. Changes in rainfall were examined using data from 134 stations in 13 watersheds across Ethiopia between 1960 and 2002 by Cheung *et al.* (2008). They analyzed the variability and trends in seasonal and annual rainfall at the watershed scale at the gauge, regional, and national levels. By regressing annual watershed rainfall on time, results from the one-sample *t* -test show no significant changes in rainfall for any of the watersheds examined. However, the seasonal rainfall averages against time, showed a significant decline in June to September rainfall (i.e. Kiremet) for the Baro-Akobo, Omo-Ghibe, Rift Valley, and Southern Blue Nile watersheds located in the southwestern and central parts of Ethiopia. Gebremicael *et al.* (2013) also analyzed the annual rainfall pattern at nine stations in the Upper Blue Nile and reported no change of annual rainfall in all nine stations except Assosa for the period (1970–2005). Gebrekristos (2015) investigated the monthly and seasonal rainfall trends at 13 rainfall stations in the UBNRB using MK test. He reported that the changes are not significant both at monthly and seasonal scale for the majority of investigated climate stations. Tesemma *et al.* (2010) applied both the Mann-Kendall and Sen's t tests to investigate the statistical trend tests for precipitation and streamflow in the UBNRB. Their report showed that there was no significant trend in the basin wide annual, dry season, short and long rainy season rainfall at 5% significant level for the Blue Nile basin for the period from 1963-2004.

Furthermore, (Meze-Hausken, 2004) analyzed long-term rainfall data up to 2002 for 4 stations in northern Ethiopia (Mekelle from 1960, Gondar from 1953, Bahr Dar from 1962, and Combolicha

from 1953). No trends were detected in these data during this extended period. (Hurni *et al.*, 2005) analyzed the trend change of rainfall from seven soil conservation and research programmes (SCRP) research sites. Their result confirmed the above conclusion of no significant trends in annual rainfall, during the period from1981 and 2002. Nevertheless, two of the stations, Maybar and Andit Tid along the Eastern escarpment, where a small rainy season (Belg) is common in the first half of the year, followed by the Kiremet season in the second half, showed slight to pronounced trends. In Maybar, both the Belg and Kiremet seasons showed a tendency towards increased total rainfall and in Andit Tid Kiremet showed a distinct increase, while Belg totals decreased over the same period.

At the UBNRB basin scale, no significant long-term trends were observed for mean streamflow at the annual and seasonal scales (Awulachew *et al.*, 2008; Conway, 2000; Melesse *et al.*, 2009). Tesemma *et al.* (2010) reported significant increases in discharge during the long wet season at three stations, Bahirdar, Kessie and El Diem, all situated on the main stem of UBNR. As a percentage of the 40-year seasonal mean, these increments were 26% at Bahir Dar, 27% at Kessie and 10% at El Diem. Discharge during the short rainy season streamflow increased significantly at Bahir Dar (33%) and at Kessie (51%), while the trend was not significant at El Diem in the period from 1963 to 2003. Dry season streamflow show no significant trend at Bahirdar and Kessie but a significant decreasing trend at El Diem (10%). Similarly, (Gebremicael *et al.*, 2013) find statistically significant increasing trends of annual and long wet season streamflow, while dry season streamflow show a significant decreasing trend at El Diem. This indicates trends towards more severe hydrological extremes, in both high and low streamflow directions. At the sub-basin scale, Rientjes *et al.* (2011a) reported that low streamflow in the Gilgel Abay sub-basin decreased during the past 30 years (1973–2001), specifically an 18.1% and 66.6% decrease for the periods 1982–2000 and 2001–2005, respectively. However, for the same periods, the high streamflow show an increase of 7.6% and 46.6%. For the Chemoga sub-basin, (Bewket and Sterk, 2005) observed a statistically significant decline of dry season streamflow (October–May) during 1960–1999, while high streamflow do not indicate any discernible trend. According to Bewket *et al.* (2005), these decreasing trends are explained by significant land cover changes in the basins observed during 1957–1998, specifically destruction of natural vegetative cover, expansion of cropland, overgrazing, and increased area under eucalypt plantations, spurring increased transpiration and declines in base flow.

According to Taye *et al.* (2015), although there are some contradictory findings across these studies, it appears there are no statistically significant precipitation trends in the Ethiopian highlands, while statistically significant streamflow trends are evident in some of the tributary catchments. They summarized the findings for high and low streamflow trends in the ten sub-basins over UBNRB. Low streamflow are shown to have significant decreasing or increasing trends in 11 out of 18 cases, or 61%. Comparatively, no significant change is evident for high streamflow in 13 out of 18 cases (72%). This illustrates that low streamflow in the basin are historically more sensitive to the natural and artificial changes than high streamflow. For the historical context, the discrepancies could be due to the period and length of data analyzed and the failure to consider stations, which can represent the spatial variability of the basin and errors induced from observed data.

2.2 Climate change modeling on upper Blue Nile River basin

General Circulation Models (GCMs) from Intergovernmental Panel on Climate Change (IPCC) Third and Fifth Coupled Model Inter-comparison Projects (CMIP3 and CMIP5) are tools used to simulate the current and future climate change of different climate variables under different climate change scenarios (Chisanga *et al.*, 2017) due to increasing greenhouse gases (GHGs). The GHG emissions scenarios reflect the uncertainty of the future climate and GCMs' striving to represent complex natural systems (Nkomozepi and Chung, 2013). The range of possible emission scenarios (forcing), internal variability, and intermodel differences are the major source of uncertainties in climate projections (Deser *et al.*, 2012; Meher *et al.*, 2017). Forcing uncertainty arises from incomplete knowledge of external factors influencing the climate system, including future trajectories of anthropogenic greenhouse gases (GHGs), aerosol, stratospheric ozone concentrations; land-use change, etc. were included in the emission scenario as external factors that influence the climate system significantly. Model uncertainty, also termed response uncertainty, occurs because different models may yield different responses to the same external forcing as a result of differences in, for example, in physical and numerical formulations. Internal variability is the natural variability of the climate system that occurs in the absence of external forcing, and includes processes intrinsic to the atmosphere, the ocean, and the coupled ocean-atmosphere system (Deser *et al.*, 2012). The combined effect of this variability's makes difficult in estimating precipitation accurately through GCMs.

GCMs perform reasonably well at larger spatial scales but poorly at finer spatial and temporal scales, especially precipitation, which is of interest to hydrological impact analysis (Goly et al., 2014). GCMs are the most important tools, which provide past and future climate change information at various grid locations over the globe (Meher *et al.*, 2017). To this day, output from the GCMs are not adequate to represent the regional, sub regional, or local-scale climate features properly because of their coarser resolution and inadequate representation of forcing and feedbacks like cloud, convections, evaporation, topography, etc. (Pervez and Henebry, 2014; Wilby *et al.*, 1999). Because of these inherent limitations, downscaling of the GCM simulations is essential for impact applications at local scale.

The impacts of climate change on the hydrological cycle in general and on water resources in particular are of high significance due to the fact that all natural and socio/economic system critically depends on water. The direct impact of climate change can be variation and changing pattern of water resources availability and hydrological extreme events such as floods and droughts, with many indirect effects on agriculture, food and energy production and overall water infrastructure (Ebrahim et al., 2013). The impact may be worse on trans-boundary Rivers like Upper Blue Nile River where competition for water is becoming high from different economic, political and social interests of the riparian countries and when runoff variability of upstream countries can greatly affect the downstream countries (Kim, 2008; Semenov and Barrow, 1997).

To this end, several individual researches have been done to study the impacts of climate change on the water resources of UBNRB from one or more GCMs, emission scenario(s), and

downscaled GCM output for driving a hydrological model. Regardless of its magnitude, better agreement among authors with regard to the prediction of the future increasing temperature was observed over the UBNRB. However, the accurate estimation of future prediction of precipitation over this region remains difficult because of its complex topography, sparse data availability, and poor data quality. As the result, inconsistent and conflicting research outputs are observed for predicting precipitation.

For example, Beyene et al. (2010) used 11 GCMs and observed data from CRU and their outputs for precipitation prediction ranges from -16 to 40% in 2020s (2010-2039) and -24% to 26% for 2080s (2070-2099). Conway (2005) considered the outputs of nine GCMs using A2 SRES scenario for the projection of rainfall and temperature. The result suggested that the changes in average seasonal climate for the period around the 2080s, relative to 1961-1990 climate ranges from -40 % to 100 % for the winter season (Dec-Feb), and from -40 % to 120 % for the summer season (June to Aug) precipitation. Kim (2008) used the outputs of six GCMs for the projection of future precipitations and temperature, the result suggested that the changes in mean annual precipitation from the six GCMs range from -11 % to 44 % while the weighted average projected with a change of 11% at 2050s. On the other hand, the changes in mean annual temperature range from 1.4°C to 2.6^{o}C with a weighted average change of 2.3^{o}C from the baseline. Likewise, Yates and Strzepek (1998a) used 3 GCMs and the result revealed that the changes in precipitation range from -5 % to 30 % and the change in temperature range from 2.2^{o}c to 3.5^{o}c. Yates and Strzepek (1998b) also used six GCMs and the result showed in the range from -9 % to 55 % for precipitation while temperature increased from 2.2^{o}c to 3.7^{o}c. Another study done by Elshamy et al. (2009b), used 17 GCMs and the result showed that changes in total annual precipitation range between −15 % to +14 % but the ensemble mean of all models showed almost no change in the annual total rainfall. While, all models predict the temperature to increase between 2^{o}C and 5^{o}C. Gebre and Ludwig (2014), used five biased corrected 50km x 50km spatial resolution GCMs for RCP4.5 and RCP8.5 scenarios to down scale the future climate change of 4 watershed (Gilgel Abay, Gumara, Rib and Megech) located in Tana sub basin for the time period of 2030s and 2050s. The result suggested that the selected five GCMs disagree on the direction of future prediction of precipitation but multimodal average monthly and seasonal precipitation may generally increases over the watersheds.

For the future context, discrepancies could be due to the difference of type and number of GCMs and scenarios used for downscaling, the downscaling techniques applied (can be dynamical and statistical), selection of representative predictors, the period of analysis, the type of observed data (gridded or station based), and spatial and temporal resolution of observed and predictor dataset (Cherie, 2013). So based on such differences, it is not clear which combination of inputs give a good insight for future plausible climate conditions of the UBNRB.

To address uncertainty in projected climate changes, the (IPCC, 2014b) thus recommends using a large ensemble of climate change scenarios produced from various combinations of Atmospheric Ocean General Circulation Model (AOGCMs) and forcing scenarios. However, it can become prohibitively time consuming to assess the climate change, using simultaneously many climate change scenarios and many statistical down scaling models. As a result, researchers typically assess the climate change and its impacts under only one or a few climate change scenarios selected arbitrarily with no justification for instance used only A1B and A2

scenarios. Yet, there is no any hard rule to select an appropriate subset of climate change scenarios among the wide range of possibilities (Casajus et al., 2016). Hence, the performance of downscaling that ensures to narrow down the scale discrepancy between the coarse scale GCMs and the required local scale climate variables for hydrological models should be investigated for their contribution, which is missed in previous studies of climate change analysis in the UBNRB.

Many researchers have been tried to compare the comparative skill of down scaling methods in different study areas such as (Dibike and Coulibaly, 2005; Ebrahim *et al.*, 2013; Fiseha *et al.*, 2012; Goodarzi *et al.*, 2015; Hashmi *et al.*, 2011; Khan *et al.*, 2006; Qian *et al.*, 2004; Wilby *et al.*, 2004b; Wilby and Wigley, 1997; Xu, 1999). However, no single model has been found to perform well over all the regions and time scales. Thus, evaluations of different models are critical to understand the applicability of the existing models.

Apart from the GCMs and downscaling techniques, most of the previous studies e.g. (Beyene et al., 2010; Elshamy et al., 2009b; Kim, 2008), used CRU, NFS and other gridded data sets constructed based on the interpolation of a few stations in Ethiopia, which has relatively less accurate as compared with the station based data (Worqlul et al., 2014). Therefore, a multi-model approach, to minimize the uncertainty of GCMs and incorporating acceptable number of weather stations which has long time series and reliable observed climate data to minimize the errors coming from the less accurate gridded data is recommended.

2.3 Hydrological modeling

Hydrological models and definitions

Water is one of the essential components of the environment, which requires proper planning and management to achieve its sustainable utilization. However, it is well known that the number and diversity of water-related challenges are large and are expected to increase in the future. In addition to climate change, land use change is one of the important human interventions altering the quality and quantity of both surface and ground water (Dwarakish and Ganasri, 2015). Both climate and land use change have adverse implications on the natural hydrologic system in terms of variation in the runoff regime, evapotranspiration (ET), subsurface flow, infiltration, etc., (Lørup *et al.*, 1998; McColl and Aggett, 2007; Xu and Singh, 1998). Due to complicated inter-relationship between various hydrological components such as precipitation, evaporation, transpiration, infiltration, and runoff, hydrological cycle and hydrological response of a catchment have become very complex. In response to these challenges, hydrological models have been developed to analyze and understand the natural hydrologic system, to investigate the relationship between climate, land use and hydrologic process (Bormann et al., 2009; Nandakumar and Mein, 1997; Tang et al., 2011), and to explore solutions for sustainable water management, in order to support decision makers and operational water managers. Therefore, hydrologic models have become increasingly important tools for the management of the water resources (Sarkar and Kumar, 2012; Shirke *et al.*, 2012; Suliman *et al.*, 2015) which can be used for flow forecasting to support reservoir operation, flood mitigation, spillway design studies, and many other purposes.

Hence, models are constructed to serve as proof of an idealized logical structure and they are an important element of methodical theories (Adem and Batelaan, 2006). A model is an expression to show a part of the natural or human created world which can be in the form of a physical, analog or mathematical model (Dingman, 2002). Generally, hydrological models are tools that integrate our knowledge of hydrologic systems to a set of interrelated equations that try to convert the physical laws, which govern extremely complex natural phenomena, to simulate the real world hydrologic processes.

Classification of hydrological modeling

Hydrologic models have become an indispensable tool for the study of hydrological processes and the impact of modern anthropogenic factors on the hydrologic system. Many researchers classified hydrological models based on; the basis of their function and objectives, their structure, and their level of spatial disaggregation. Proper classification can be helpful for engineers, experts and researchers to understand the characteristics of models before deciding to employ them for their works. Hence, models can be categorized into three main classes, namely, physical model, analogous and mathematical models. Physical model is a reduced-dimension representation of real world system. As a simple definition for models, a physical model is defined as a scaled-down form of a real system (Brooks et al., 2003; Salarpour et al., 2011). The analog model is the result of a simulated process that is used to represent a natural process. Mathematical models, on the other hand, include clear chronological set of relation, numerical and logical steps that change numerical inputs into numerical outputs(Jajarmizadeh et al., 2012).

In terms of hydrological model, mathematical models was given more consideration due to the rapid development of computer technology. These models are faster, high accuracy and more economical. On the contrary, deficiencies of a hydrologic model can be due to its user-unfriendliness, large data requirement, lack of reliable measuring and other unclear limitations (Singh and Frevert, 2005).

There are many hydrological models with unique and common characteristics that have been developed so far (Wang et al., 1996). Hydrologic models can be classified based on the representation of physical processes, space, time, or randomness. The classification of hydrologic models centered on physical process is based on the input and parameters needed for the model and the extent of physical principles represented within the model. Another method for classifying models includes the spatial representation of the basin either modeling the basin as whole where spatial variability is disregarded or by dividing the basin into spatially explicit sub-regions. Further classifications focus on whether randomness is incorporated into the model and if time is represented within the model. Figure 2-1 represents the classifications of the different hydrologic models.

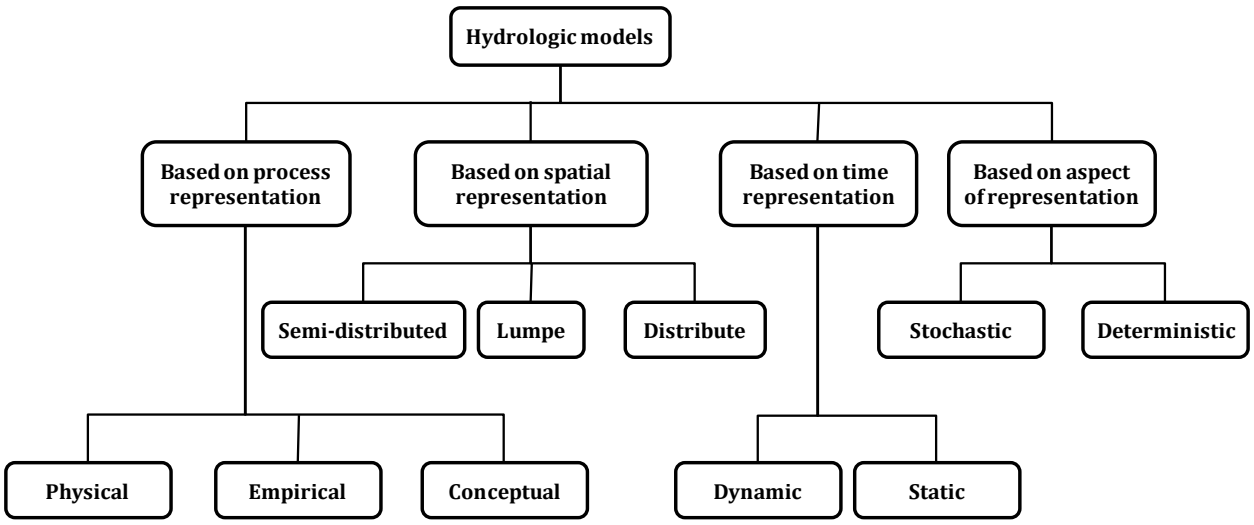

Figure 2-1: Classification of hydrological models after MARKERT et al. (2016)

Moreover, each category is subdivided into subcategories that are more detailed. Based on process representation includes physically based, conceptual and empirical. In addition, spatial representation category consists of lumped, distributed and semi-distributed, meanwhile temporal representation category comprises of dynamic and static. Finally, aspect of randomness category comprises stochastic and deterministic.

However, different authors classified the hydrological models into different classifications. For instance, Chow et al. (1988) classified the hydrological models into two major categories, namely physical models and mathematical models. Furthermore, he divided physical models into two classes again, namely scale models and analog models. Mathematical model c further divided into two subcategories, namely stochastic and deterministic. Figure 2-2 presents the classification of hydrological models according to Chow et al. (1988).

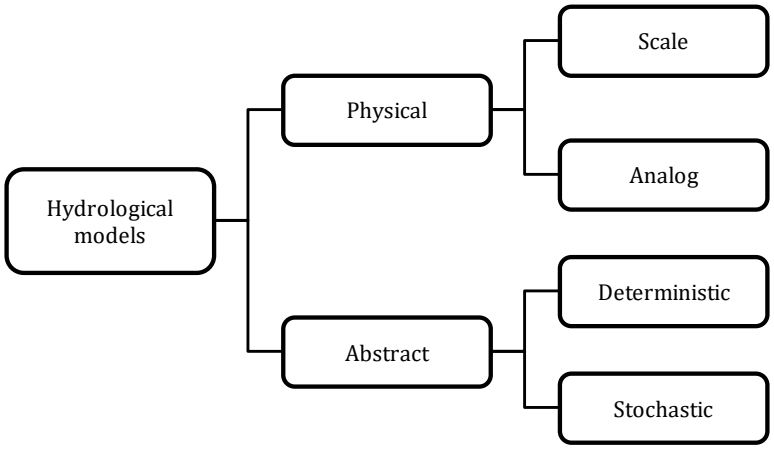

Figure 2-2: Hydrological models classification by Chow *et al.* (1988)

Cunderlik (2003) further classified deterministic hydrologic models into three major categories (lumped, semi-distributed and distributed). Oogathoo (2006) classified the mathematical hydrological model into five major different categories based on criteria such as law and assumptions, equations, parameters, time and procedure of computations, which further classified into ten different types. Figure 2-3 presents the classification of hydrological models according to the criteria mentioned above. Lewarne (2009) stated that hydrological models could be classified into five groups in accordance to the definition of mathematical models under polar condition. Category1 divides the models into two-linear and non-linear. Category2 divides the models into deterministic and probabilistic (stochastic) models. Category3 divides the models into static and dynamic, where the time element plays a significant role. Category4 is based on the role of parameters into lumped and distributed. Category5 divides the models into physical and conceptual models.

Gosain et al. (2009) noted that a broad classification for hydrological models can emerge from the development of hydrological models from the old days but generally the models can be simply defined as a black-box, conceptual or deterministic model. Undoubtedly, there are also subdivisions for these categories. Figure 2-4 presents the classification of hydrological models according to Gosain et al. (2009). Detail descriptions can be found in (Jajarmizadeh et al., 2012).

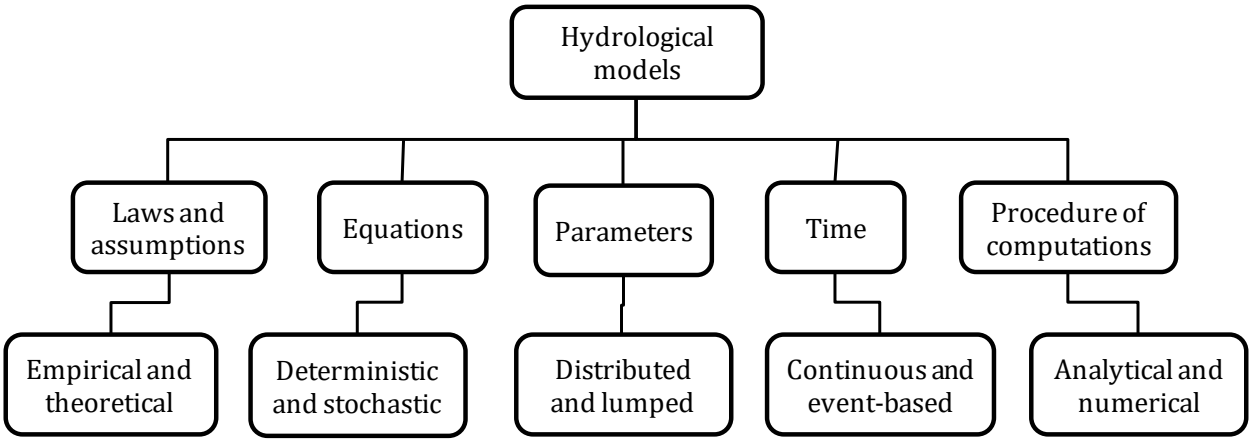

Figure 2-3: Hydrological models classification by criteria

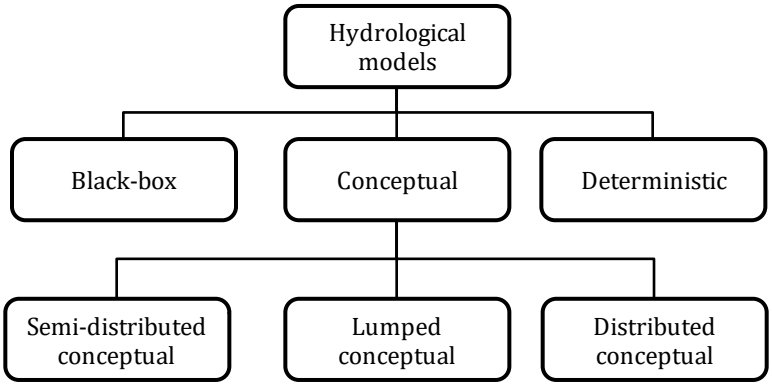

Figure 2-4: Hydrological models classification by Gosain *et al.* (2009)

Previous works of hydrological modeling in the upper Blue Nile River basin

A review by Awulachew *et al.* (2008) shows that the number of models simulating the streamflow from watersheds in the Blue Nile and other river basins in Ethiopia and Africa has increased exponentially in recent years. These models are from relatively simple engineering approaches, such as the rational method (Desta, 2003), to more complex models, such as SWAT (Cherie, 2013; Gashaw *et al.*, 2018; Gebremicael *et al.*, 2013; Girma, 2013; Setegn *et al.*, 2008; Teferi *et al.*, 2013). Others are the precipitation runoff modeling system (PRMS) (Legesse *et al.*, 2003), water erosion prediction project (WEPP) (Zeleke, 2000), the agricultural non-point source model (AGNPS) (Haregeweyn and Yohannes, 2003; Mohamed *et al.*, 2004) and water balance approaches (Ayenew and Gebreegziabher, 2006; Kim and Kaluarachchi, 2008a). Implementation of these models yielded mixed results. For example, AGNPS was tested in the highlands of Ethiopia on the Augucho Catchment but the observed runoff patterns could not be reproduced. PRMS was similarly tested by Legesse *et al*. (2003) for South Central Ethiopia, and needed extensive calibration to predict the monthly runoff.

The main conclusion of this overview of hydrological models used in the highlands of Ethiopia is that the daily simulation results of the more complex models is disappointing when compared with the relatively better predictions of the simple water balance models. The main reason is that most of the complex hydrological models are developed based on the SCS curve number approach, of which the parameter values are obtained statistically from plot data in the United States with a temperate climate. The watershed behavior in a temperate climate is different than in a monsoonal climate where during the dry period the soil dries out completely, something that does not happen in the United States (Steenhuis *et al.*, 2009).

The lack of available data for both input and calibration further hinders the use of complex models in Ethiopia. For these reasons, simple water balance models, that most efficiently utilize the available data, are the most appropriate choice for simulation of the hydrology of the Blue Nile. Hence, many simple water balance type approaches have been attempted for the Nile Basin. Kebede et al. (2006) developed a water balance model on Lake Tan sub-basin of UBNRB utilizing relatively long durations (>30 years) of data for precipitation, evaporation, inflows of major tributaries and outflows to the Blue Nile. A similar water balance type rainfall-runoff model was developed and tested by Collick *et al*. (2009) to predict the stream flow for four relatively small watersheds (<500 ha) in the Blue Nile Basin. The authors reported reasonable predictions on a daily or weekly time step using nearly identical parameters for watersheds, which are hundreds of kilometers apart. Steenhuis *et al.* (2009), were made minor modifications for the model developed by Collick *et al.* (2009) with respect to interflow generation for predicting the discharge and sediment of the entire Blue Nile. They reported satisfactory result both for simulating the discharge and sediment of the UBNRB.

Hence, it is to be noticed that simple water balance models often perform better, especially over monthly time steps than the complex counterparts that have many more calibration parameters in the UBNRB. However, simple water balance models have limitations such as different parameter sets are required for different basin sizes in the Blue Nile Basin as shown by Kim *et al.* (2008a)

and also hills and valleys were not differentiated in their simplified model (Kebede *et al.*, 2006). In addition, simple water balance could not be able to evaluate the likely implications of climate change and LULC changes on streamflow and water balance components. Therefore, several authors preferred to apply the complex hydrological models like SWAT for investigating the impacts of climate and LULC changes on the hydrology of the UBNRB.

Van Griensven *et al.* (2012) reviewed 22 peer-reviewed papers on the application of SWAT to the tropical high lands of the Nile basin countries for a variety of thematic areas including climate change impact modeling. They carried out a critical evaluation of model performance, physical representation of model parameters and correctness of the hydrological balance. Based on performance evaluation, they reported that majority of the SWAT models were classified as giving satisfactory to very good results.

Recently, several attempts have been made to evaluate the likely implications of climate change and LULC changes on streamflow to UBNRB and some other sub-watersheds using SWAT (e.g., (Chakilu and Moges, 2017; Cherie, 2013; Gashaw *et al.*, 2018; Gebremicael *et al.*, 2013; Girma, 2013; Kidane *et al.*, 2018; Setegn *et al.*, 2008; Teferi *et al.*, 2013; Teklay *et al.*, 2019; White *et al.*, 2011; Woldesenbet *et al.*, 2017b; Woldesenbet *et al.*, 2018), whereby the results obtained provide further evidence of the performance of SWAT model in these kinds of hydrological basin studies.

At basin scale, Cherie (2013) applied SWAT model to evaluate the climate change impacts on the streamflow of UBNRB at El Diem station. He reported that the future simulations of streamflow in the basin, using both SDSM and LARS-WG downscaled output in SWAT reveal a decline of -10% to -61% of the future Blue Nile streamflow. Girma (2013) also used SWAT model to study the hydrological impact of climate and land use changes on the UBNRB. Although the downscaling rainfall data may decrease by 6 – 12 % during the short rainy season in the basin, average annual projected runoff changes for the basin were 9.2% and -10.0% relative to the historical flow for 2041-2070 and 2071-2100 respectively. (Gebremicael *et al.*, 2013) applied SWAT model to simulate the runoff and sediment fluxes in the early 1970s and at the end of the time series in 2000s in order to interpret the physical causes of the trends and corroborate the statistical results. A comparison of model parameter values between the 1970s and 2000s showed significant change, which could explain catchment response changes during the period (1973-2005).

At sub-basin scale, Kidane *et al.* (2018) evaluated the impacts of climate and LULC dynamics on the hydrological responses of Guder sub-watershed located in the south of UBNRB (see Figure 3-2) using SWAT for the period 1973 - 2015. They reported the decreases of forest and shrub land by 38% and 48% while, settlement and cultivated land increased by 572% and 7% respectively. After LULC change detection analysis, individual and combined impacts of climate and LULC on hydrological dynamics of Guder watershed were evaluated by comparing the simulated flow generated by climate data of 1973–1982 and 2006–2015 and LULC data of 1973 and 2015. As the result, the SWAT simulation indicted that LULC change increased the wet season flow by 14.5% while decreasing by 9.65% in dry season. In wet season, the flow increased by 4.5% while decreased by 3.3% in dry season because of change in climate and seasonal variability. The combined effects of climate change and LULC changes results the

decline of dry season stream flow by 11.34% and the increment of wet season stream flow by 17.76%.

Gashaw *et al.* (2018) also applied remote sensing techniques for the LULC map classification and SWAT model to analyze the hydrological impacts of LULC changes in the Andasa watershed, which is located in the North Gojjam sub-basin of the UBNRB (Figure 3-2), for a baseline period of 1985–2015 and to the future changes of 2030 and 2045 periods. The results showed that there was a continuous expansion of cultivated land and built-up area, and withdrawing of forest, shrubland and grassland during the 1985–2015 periods, which are expected to continue in the 2030 and 2045 periods. The LULC changes, which had occurred during the period of 1985 to 2015, had increased the annual flow (2.2%); wet seasonal flow (4.6%), surface runoff (9.3%) and water yield (2.4%). Conversely, the observed changes had reduced dry season flow (2.8%), lateral flow (5.7%), groundwater flow (7.8%) and ET (0.3%). The 2030 and 2045 LULC states are expected to further increase the annual and wet season flow, surface runoff and water yield, and reduce dry season flow, groundwater flow, lateral flow and ET.

Teklay *et al.* (2019) also applied SWAT model to assess the impacts of land use change and climate change on hydrological responses such as surface runoff, evapotranspiration, and peak flow in Gumara watershed. The Gumara watershed is located in the eastern part of the Lake Tana Basin (Figure 3-2), which has an area of 1269 km^2. The elevation ranges between 1794 and 3704masl, with a mean elevation of 2272 masl. They reported the expansion of agricultural land use by 11.1% and the reduction of forest cover by 2.3% during the period from 1985 to 2015. As the result, the surface runoff simulation increased by 45.1 mm (12.4%) between 1985-199 and 2010-2015 due to the combined effects of LULC change and climate variation. The isolated LULC change increased surface runoff by 11.6mm (3.2%), which accounts for 25.7% of the total surface runoff change (45.1mm). The isolated effects of climate variation between 1985-1989 and 2010-2015 increased surface runoff by 33.5mm (9.2%), which accounted for about 74.3% of the total surface runoff increment. The above results showed that land use change and climate variation during 1985–1989 and 2010–2015 increased surface runoffs, but the contribution of land use change was smaller than that of climate variation. Between this simulation period, combined LULC change and climate variation increased peak flow by 3.7m^3s^{-1} (1.7%), and 2.4 m^3s^{-1} (1.1%) increase due to isolated LULC change and 1.3m^3s^{-1}(0.6%) increase for the isolated climate variability. The percent contributions were 64.9% for LULC change and 35.1% for climate variability.

The impacts of LULC dynamics and its impact on the low flow of Gumara sub-watershed of the UBNRB were evaluated through application of the SWAT model by Chakilu *et al.* (2017). They prepared three LULC data; 1973, 1986, and 2013 from Landsat satellite and these data were used for base map, model calibration and change study respectively. Based on the result, the extreme low flow of Gumara watershed has been decreasing from 0.53 m^3s^{-1} to 0.43 m^3s^{-1}, which showed decreasing by 0.1 m^{3-1} that is 18.87%. In general, the above studies illustrated that agricultural land has increased while the forest coverage has decreased in the UBNRB, which results the increase of surface runoff and peak flow and decreasing of dry season flow.

2.4 Remote sensing for land use/land cover

Land use and land cover change (LULC) has been a key research priority with multi-directional impacts on both human and natural systems (Turner et al., 2007) yet also a challenging research theme in the field of land change science. It can affect biodiversity (Hansen et al., 2004), hydrology (DeFries and Eshleman, 2004; Uhlenbrook, 2007), and ecosystem services (DeFries et al., 2004). Hence, it has increasingly become a topic of paramount importance for regional and international research programs examining LULC change. As is the case in many other developing countries, most of the population of Ethiopia lives in rural areas and depends directly on agriculture for its livelihood (Bewket *et al.*, 2005). This rural population is currently growing rapidly, and consequently inducing a very dynamic land use and land cover. Hence, several studies highlighted that LULC Change is a prevalent phenomenon in the highlands of Ethiopia (Bewket *et al.*, 2005; Gebremicael *et al.*, 2013; Kidane *et al.*, 2018; Teferi *et al.*, 2013; Zeleke, 2000). These studies found different types and rates of LULC in different parts of the country over the different periods. In most cases, however, expansion of forestland into cultivated land, deforestation and afforestation have been the common forms of transitions. In addition to the few published researches, as mentioned above, the Abay River Basin Master Plan Project prepared the LULC map of UBNRB at scales of 1:2,000,000 and 1:250,000 based on Landsat Thematic Mapper (TM) images from 1986 to 1990 (BCEOM, 1998a).

The impact of LULC change on stream flow pattern in a typical watershed called Chemoga in the Blue Nile basin of Ethiopia was investigated by Bewket et al. (2005). Their results show that, between 1960 and 1999, total annual stream flow decreased at a rate of 1.7 mm $year^{-1}$, whereas the annual rainfall decreased only at a rate of 0.29 mm $year^{-1}$. The decrease in the stream flow was more pronounced during the dry season (October to May), while the corresponding rainfall showed no discernible trend. The wet season (June to September) rainfall and stream flow did not show any trends. The observed adverse changes in the stream flow could be attributed due to changes in LULC that involved destruction of natural vegetative covers, expansion of croplands, overgrazing and increased area under eucalypt plantations.

Zeleke (2000) analyzed the LULC changes that occurred from 1957 to 1995 in the Dembecha area, Gojam, in the Northwestern highlands of Ethiopia. Their analysis showed that 99% of the forest cover that existed in 1957 was cleared in 1995. On the other hand, cultivated land increased from 39% in 1957 to 70% in 1982 and 77% in 1995. The greatest expansion occurred between 1957 and 1982 (about 78%) and slowed down between 1982 and 1995 (only 10%) because almost no land was left for further expansion.

Teferi et al. (2013) quantified long-term land use and land cover (LULC) changes and to identify the spatial determinants of locations of most systematic transitions for the period 1957–2009 in the Jedeb watershed, Upper Blue Nile Basin. It covers an area of 296.6 km^2 and thus is meso-scale in size. It is situated in the southwestern part of Mount Choke, which is a headwater of the Upper Blue Nile in Ethiopia with its elevation ranging from 2172 masl to nearly 4001 masl. They

reported that cultivated land and grassland were the major proportions as compared to the other LULC classes during the whole period 1957–2009. The percentage coverage of cultivated land increased from 53.4% to 69.5% while grassland decreased from 20.6% to 14.9% from the baseline period 1957 to 2009. About 46% of the study area experienced a transition over the past 52 years, out of which 20% was due to a net change while 26% was attributable to swap change (i.e. simultaneous gain and loss of a given category during a certain period).

Gebremicael et al. (2013) analyzed the impacts of LULC change on the runoff and sediment fluxes of the UBNRB during the period 1973 to 2000. Their findings indicate that the surface runoff (Qsurf) contribution to the total river discharge has increased by 75%, while the subsurface flow (Qlat) and the ground water (GWQ) flow has decreased by 25% and 50%, respectively and the total water yield at the outlet has increased by 25% with negligible change of rainfall between the two periods . This clearly depicts a modification of catchment response and thus a possible change of the physical characteristics of the basin between 1970s and 2000s. In the UBNRB, the areal coverage of rainfed cropland, grassland, water body and barren land showed a growth of 81%, 56%, 14% and 241%, respectively from 1973 to 2000. On the other hand, wooded grassland, woodland, shrubs and bushes, natural forest, afro-alpine vegetation showed a decline by 61%, 31%, 8%, 51%, and 5%, respectively.

Kidane et al. (2018) analyzed the impacts of climate and LULC dynamics on the Hydrological Responses of the Upper Blue Nile in the Guder sub-watershed. The watershed area is 46,654 ha with an elevation range between 1820 and 3271 masl. They used the Landsat satellite imageries to identify the LULC of the watershed during 3 periods: 1973, 1995 and 2015. According to their classification and change detection result, the area coverage of cultivated land raised from 62.7 to 67.1 % from 1973 to 2015. They also reported that during these periods the forest coverage decreases from 14% in 1973 to 9% in 2015, which indicates that about 37.5% of the forest ecosystems were converted to other LULC during the period 1973 to 2015.

Chapter 3 Description of study area

3.1 Location

The Nile River is regarded as the longest river in the world flowing to the north originated from northeastern Africa, which covers a drainage area of 3,400,000 km^2 (Onyutha and Willems, 2015). It is 6,853 km long, and it is a trans-boundary river as its drainage basin covers eleven African countries, namely, Tanzania, Uganda, Rwanda, Burundi, Democratic Republic of the Congo, Kenya, Ethiopia, Eritrea, South Sudan, Republic of the Sudan and Egypt (Figure 3-1). It has two major water supply sources, the White Nile and the Blue Nile. The White Nile originates in the Great Equatorial Lakes region, is considered the headwaters the Nile. The Blue Nile, however, is the major water resource contributor (85%) of the Nile water resource.

The Upper Blue Nile River basin (UBNRB) is the part of the Blue Nile basin which is under the Ethiopian territory (Cherie, 2013).The UBNRB (known as the Abay River in Ethiopia) is originated at the Lake Tana (largest fresh water Lake in Ethiopia) at an elevation of 1,800 m (Figure 3-1). It leaves the southeastern corner of the Lake, flowing first to the southeast, before looping back and flowing west and then turning north-west crossing the Sudan border and joining the White Nile at Khartum. In this analysis, the total area of UBNRB at El Diem station, excluding the Rahad and Dinder tributaries, which do not flow along the main stem of the Abay River, is 172,760 km^2. It is located between 7^{o}45' and 13^{o}N, and 34^{o}30' and 39^{o}45' E (see Figure 3-1). It shares common boundaries with the Tekeze basin to the north, the Awash basin to the east and southeast, the Omo-Gibe basin to the south, and the Baro-Akobo basin to the south-west.

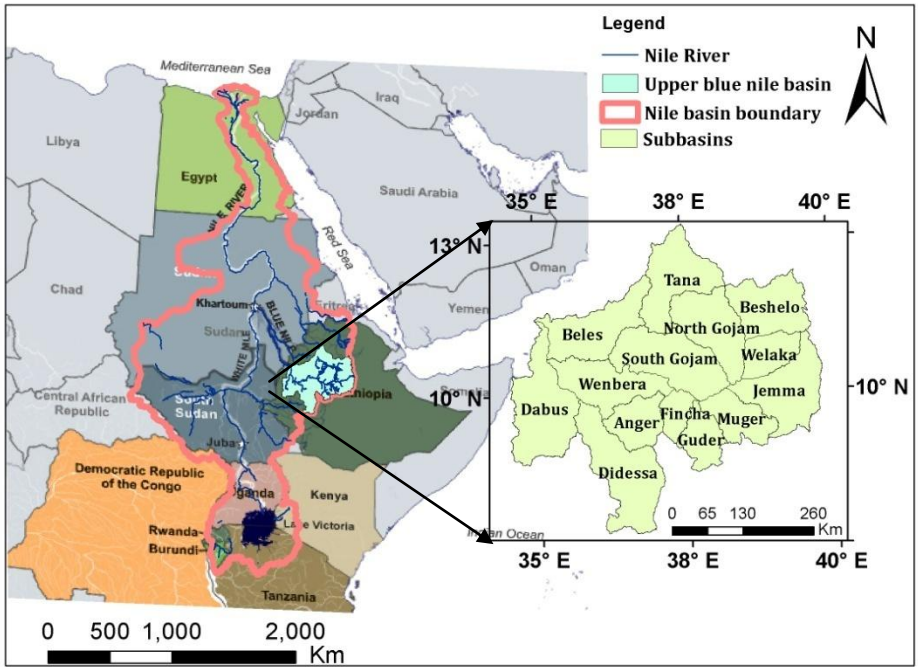

Figure 3-1: Location map of the study area

The UBNRB has 14 major sub-basins: Anger, Beles, Beshelo, Dabus, Didessa, Fincha, Guder, Jemma, Tana, Muger, North Gojam, South Gojam, Weleka and Wembera (Figure 3-1 and Table 3-5).

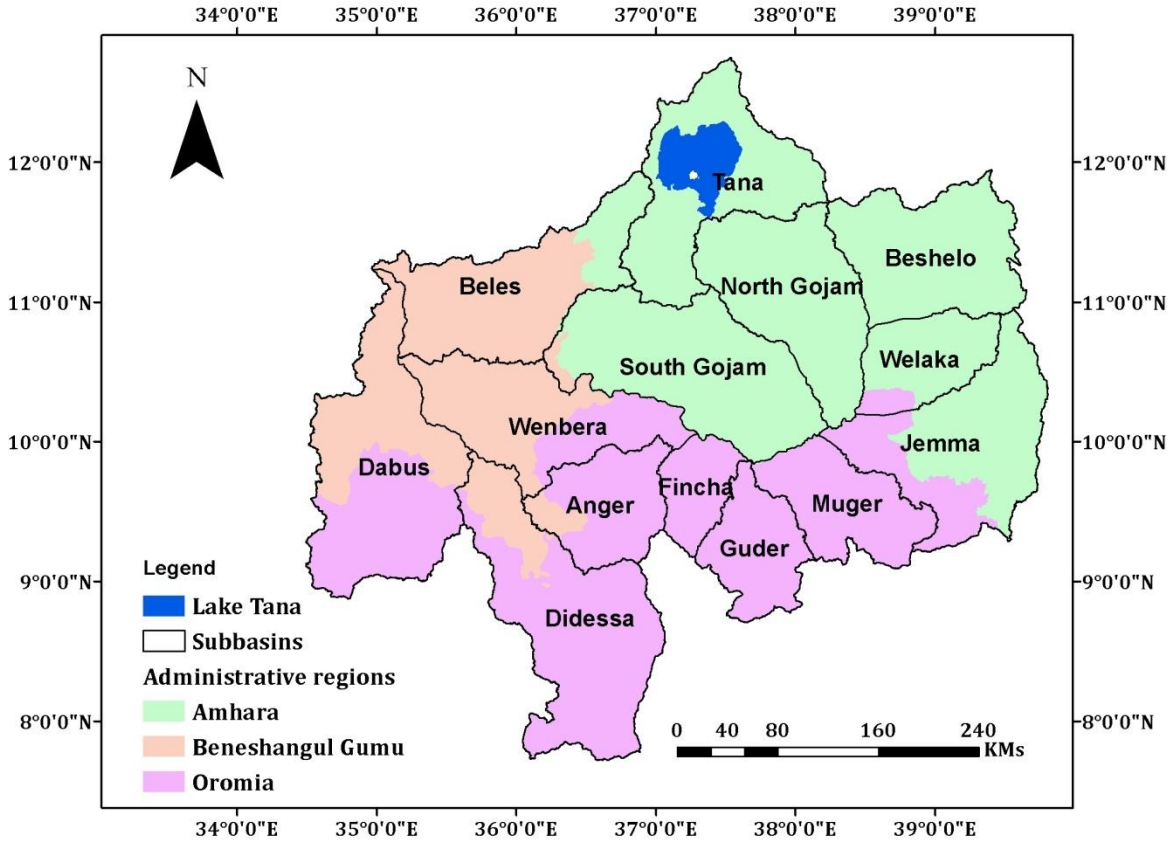

Figure 3-2: Administrative regions of the UBNRB

The administrative structure of Ethiopia is hierarchical, from regional states, to Zones, Weredas and Kebeles. According to the current regional structure, the study area covers some parts of three regional states; namely, Amhara regional state, Oromia regional state and Benshangul-Gumuz regional state Figure 3-2. The basin also contains 22 Zones (9 from Amhara, 8 from Oromia and 5 from Benshangul-Gumuz) and 237 Weredas from the three regions (Authority, 2015). About 46% of the basin area falls within the Amhara region, 31% corresponding for Oromiya and for Benshangul-Gumuz 22% (BCEOM, 1998a).

The Abay basin accounts for a major share of the country's irrigation and hydropower potential, however, to date, Ethiopia has utilized very little of the Blue Nile water. Until recently, only three relatively minor hydraulic structures have been constructed. The Chara-Chara weir and Finchaa dam were built primarily to provide hydropower. They regulate flow from Lake Tana and the Finchaa River respectively. In 2010, a new power station on the Beles River, which utilizes water diverted from Lake Tana started operation. According to the data collected from the Tana-Beles project office, an average 99 m^3s^{-1} of water is diverted to Tana Beles hydropower project (HPP) from Lake Tana reservoir to generate mean annual electricity of 2,230 GWh

during the period 2011-2016. Within the Blue Nile basin, the usable installed capacity is currently 639.4 MW, 16% of the country's current 3,814.6 MW. The Tis Abay I and Tis Abay II hydropower projects are standing as back up after the operation of Tana Beles hydropower, since water is subtracted from Lake Tana to operate the Tana-Beles hydropower project. Agriculture, the main occupation of the inhabitants in the basin, is primarily rain-fed with almost no irrigation. Currently, the only formal large and medium scale irrigation schemes are the Finchaa sugar cane plantation (8,145 ha), which utilizes water after it has passed through the Finchaa hydropower plant and the Koga scheme (7,020 ha), which uses water flowing into Lake Tana and was constructed in 2010. Apart from the irrigation schemes, modern irrigation is entirely in small-scale irrigation.

3.2 Topography

The topography of the UBNRB has high disproportion and variations which include high mountains, rolling ridges, deep gorges and flat areas (Girma, 2013). The elevations in UBNRB range between 483 masl at the El Diem near to the Sudan border, to 4,248 masl in the northeastern highlands (Figure 3-3**)**. UBNRB is characterized by the plateau highlands, in the central Ethiopian highlands with elevations ranging between 2,000–2,500 masl; the plateau valleys, in the eastern part of the basin which contain the main tributaries of the Abay; and the lower plains and hill lands in the western part of the basin close to the Sudanese border (Girma, 2013).

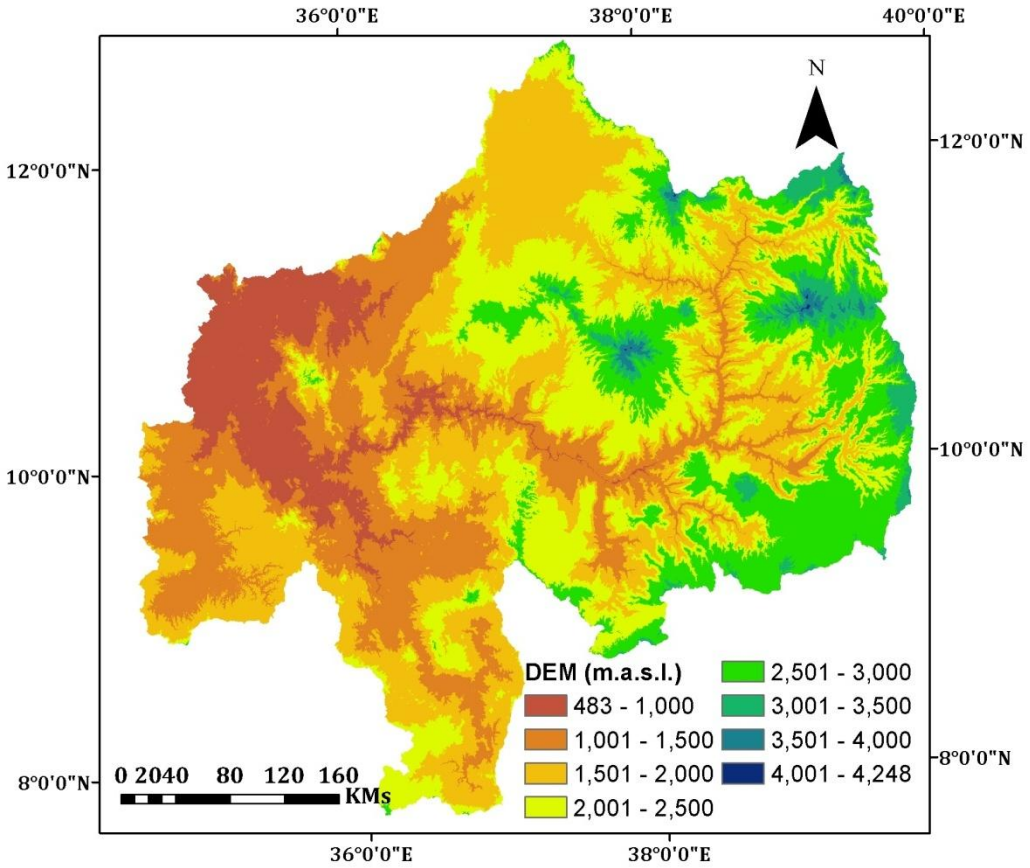

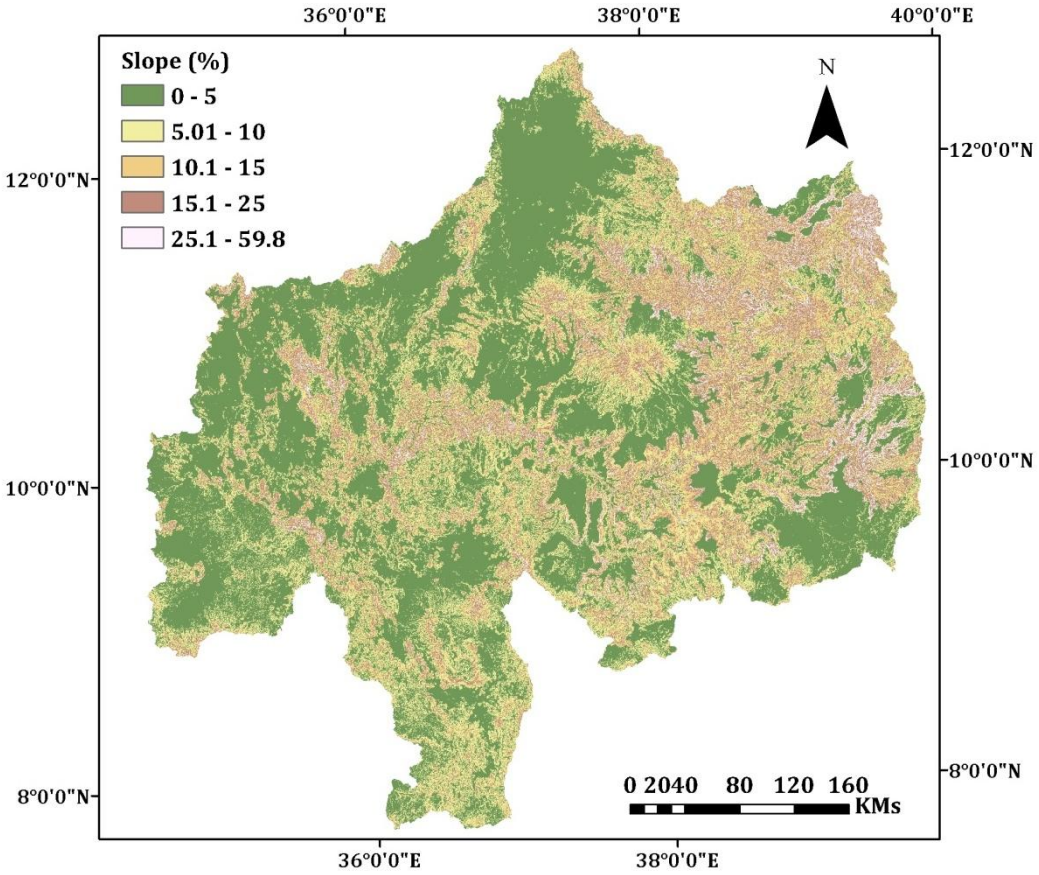

Figure 3-3: Topography of UBNRB, DEM (top) and slope (bottom)

The highlands extend from 1500 masl up to as high as 4248 masl, with a slope of greater than 30% in the eastern part (Figure 3-3), causes the rain-bearing air masses to uplift, leading to the dominantly plentiful rainfall which provides for both agriculture and hydro-power (BCEOM, 1998a). The high altitudes (above 1500 masl), of the dominant highland part of the basin (62%) have favored human settlement and agriculture by minimizing disease problem such as malaria. The deep dissection provides for rapid drops in altitude, providing the head benefiting for hydropower development. Conversely, extensive soil erosion due to steep slopes is becoming the big challenge and threatening for the country, which bases its economy on agriculture. The frequent and deep dissection also creates major barriers to communication, restricts the extension of groundwater reservoirs and their storage capacity. The lowlands flatten to 1000 masl to less than 500 masl with a slope of less than 5% is located in the western part of the basin, which is characterized by high temperature is almost untouched for developments.

3.3 Land cover

Land cover classification is used for many applications like: conservation measures, biodiversity assessment, water quality assessment, and for land cover change detection. It has also a great role for analyzing the impacts of soil moisture at a certain catchment because it directly affects the

infiltration capacity of the soil and the amount of evapotranspiration takes place (Mekonnen, 2009). BCEOM (1998a) classified the land use/land cover (LULC) based on the food and agriculture organization (FAO) classification system for the purpose of basin master plan studies. The land cover of the basin essentially follows the divide between highland and lowland. The highland area is dominantly covered with cultivation (Figure 3-4), which is a strong indicator of the upland soil erosion and problems faced by smallholders in extending cultivation into the lowlands. Forest leftovers remain in the south-west, where they are either under active conversion to cultivation or as shade for coffee trees, and along the divide line between the highlands and lowlands on steep slopes. The other major highland land cover is grassland, which occurs primarily in poorly drained depressions, within farmlands and on exposed high altitude locations. Similarly, bush and shrub occur as inclusions throughout the landscape, but rarely form significant areas.

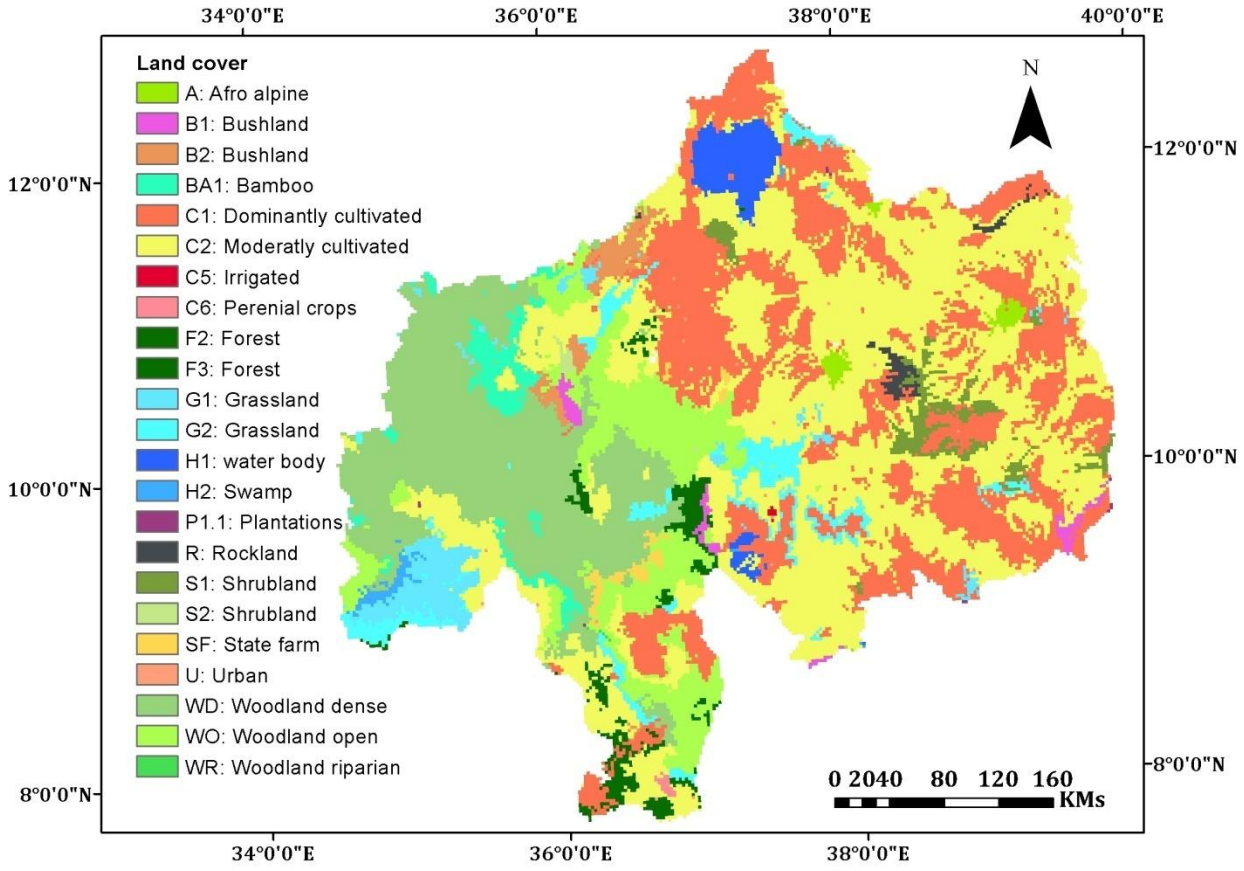

Figure 3-4: Land use/Land cover map of the UBNRB (BCEOM, 1998a)

On the map, areas with high conversion to farmland have been classed as ‘dominantly cultivated’ whereas those with lower land use for farmland are defined as ‘moderately cultivated’. According to the LULC classification by BCEOM (1998a), the three dominant land covers of the basin are cultivation, woodland and grassland (Table 3-1). Cultivation is the major land cover of the upper Blue Nile basin occupying about 57.8% of the basin. Most of the cultivation occurs in the highlands where the elevation is higher than 1500 masl. Woodland, which can be defined as

continuous stand of a single storey trees with a crown density of between 20–80% (Teferi *et al.*, 2013), bush land and shrub land cover 28.4% of the basin, which are dominantly found mainly in the western lowlands of the basin. Grassland covers 5.4 % of the basin, it occurs in both the lowlands and highlands and inter mixed to farmlands. The low land grasses occupy the lower humid valleys of the Beles, Anger, Dabus and Didessa sub-basins. Forestland covers only about 3.2% of the basin area and it is found mostly in the uplands. Plantations mainly include Eucalyptus tree species. These plantations are located around villages or in specialized areas set aside for reforestation and income generation used for fuel and construction material. Bamboo occupies about 1.8% of the upper Blue Nile basin. It is found in the lower areas of the western part of the basin. Afro-alpine vegetation, which is found in areas above 3,200 masl such as mount Guna and Choke area, covers only 0.5%. Rock cover accounts about 0.4% of the UBNRB. This is mostly consisting of exposed rock on ridges, escarpment sides and the Abay gorge as a result of geologic erosion.

Table 3-1: Summary of land cover in the Abbay River Basin (BCEOM, 1998a)

Land cover	Area (Km^2)	Area (%)
Afro alpine	852.3	0.5
Bamboo	3,120.0	1.8
Bushland	3,032.2	1.7
Dominated cultivated	38,948.8	22.3
Forest	5,527.3	3.2
Grassland	9,401.4	5.4
Irrigation land	41.3	0.0
Moderatly cultivated	61,088.6	34.9
Perenial crops	139.5	0.1
Plantations	62.0	0.0
Rockland	764.5	0.4
Shrubland	3,187.2	1.8
State farm	914.3	0.5
Swamp	604.4	0.3
Urban	170.5	0.1
Water body	3,507.5	2.0
Woodland	43,520.3	24.9
Total	174,882.1	

3.4 Soil

A soil can be defined as a continues natural body which has three spatial and one temporal dimension. The soils of the basin reflect the combined effects of the five factors including climate; biota; topography; time and geology, where numerous physical, chemical and biological processes takes place. These processes are driven by the changes in different kinds of energy. A portion of solar energy is converted into heat energy which results in an increase of soil

temperature in the soil surface (Mekonnen, 2009). The increase of soil temperature results in high evaporation of water inside the soil particle. The seasonal soil moisture pattern in the study area follows the pattern of rainfall. In the dry season, the soil moisture content is quite low, while the rainy season the soil moisture content increases. Soil classification is the categorization of soils into groups at varying levels of generalization according to their physical, mineralogical and chemical properties. The soils that covered the basin are classified based on technical classifications following the classifications of FAO (WRB, 2015).

Nitosols (30.8%), Cambisols (28.2%), Fluvisols (15.9%) and Arenosols (13.5%) dominate the soil type in the basin (see Table 3-2). The Nitosols are the most common and dominant soil types in the UBNRB, which is found in the central highlands, north-west and south- east part of the basin. It is deep, well-drained, red tropical soils with at least 30 percent clay, considerably more fertile (WRB, 2015). The deep and the stable soil structure of Nitosols permit deep rooting and make these soils quite resistant to erosion. The favorable physical properties (good workability, good internal drainage and fair water holding properties) complemented by chemical (fertility) properties makes the most productive soils of the humid tropics. Nitosols are formed by fine-textured material weathered from intermediate to basic parent rock (WRB, 2015). Leaching has left the soils nutrient poor and acid to very acid. The soil acidity further decreases nutrient availability and, in the extreme, can mobilize aluminum and lead to aluminum toxicity (BCEOM, 1998a).

Cambisols are the second largest dominant soil type in the basin, which are found in the north, north-west and northeast highlands of the basin (Table 3-2 and Figure 3-5). Erosion and deposition cycles explain the occurrence of Cambisols in mountain regions, and this is evident from weak, brownish discoloration and structure formation in its soil profile. It is characterized by slight or moderate weathering of parent material. Cambisols are mostly occurred in temperate and boreal regions where the parent material of the soil is young and the soil formation is slow. Cambisols also occur in dry regions but are less common in the humid tropics and subtropics where weathering and soil formation proceed at much faster rates than in temperate regions. The reason for the occurrence of the Cambisols in the UBNRB, where the climate is characterized by humid sub-tropical region is because of active geologic erosion, where they may occur in association with mature tropical soils (Polanco, 2017). Cambisols are considered the most productive and suitable for agriculture and are used intensively.

Fluvisols are the third largest soil types that covered the majority of western lowland of the UBNRB. Fluvisols occur on all continents and in all climates on level topography along rivers and lakes, in deltaic areas, that are flooded by surface water. Arenosols which comprise deep sandy soils are covered the deep gorges of the UBNRB following the river flows. Arenosols occupy large parts of arid and semi-arid regions in the world, and they characterized by coarse texture, accounting for high permeability and low water and nutrient storage capacity and high sensitivity to erosion. High percolation losses may make surface irrigation impracticable in areas where covered by Arenosols.

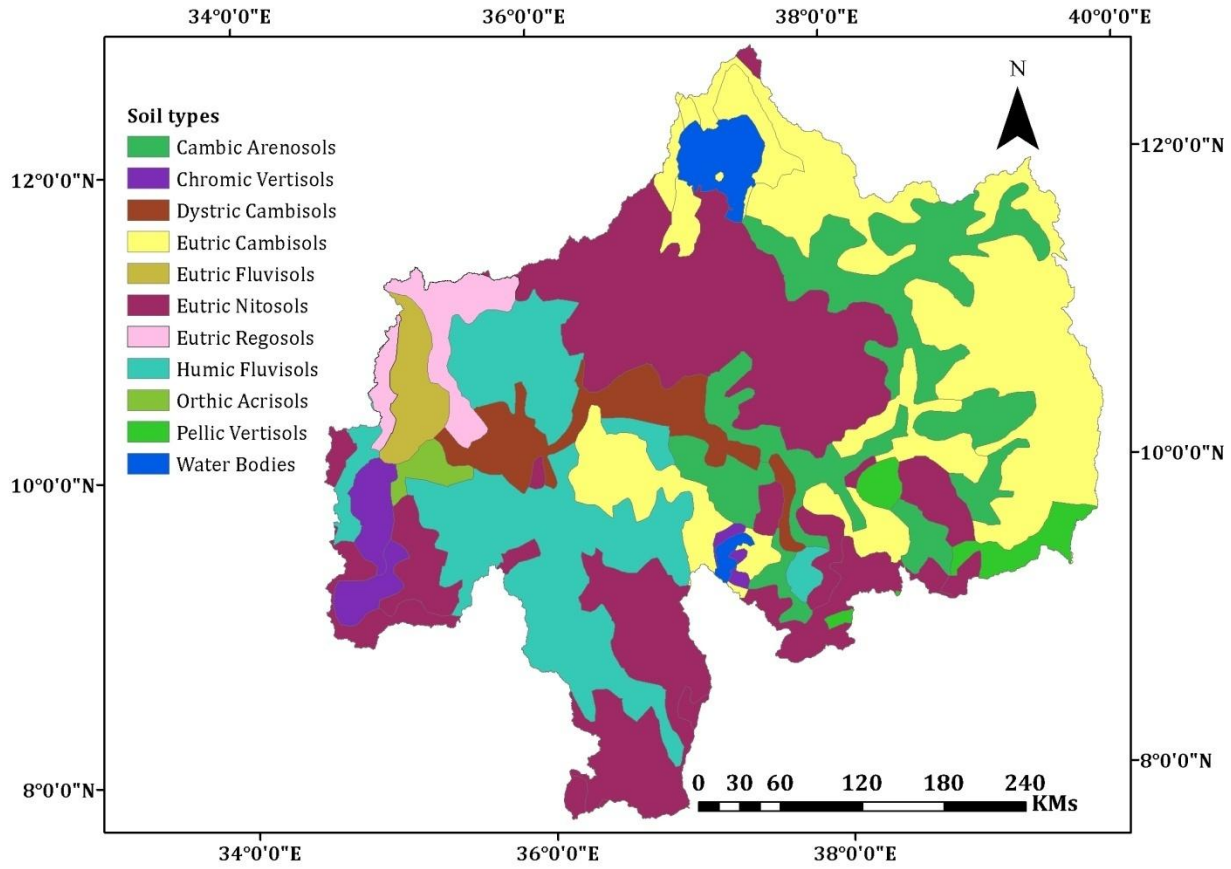

Figure 3-5: Spatial distributions of UBNRB soil type (BCEOM, 1998a)

Table 3-2: Soil types and distribution in the upper Blue Nile Basin (BCEOM, 1998a)

Soil type	Area	Area (%)
Cambic Arenosols	23,449.64	13.5
Chromic Vertisols	3,897.92	2.2
Dystric Cambisols	8,077.01	4.6
Eutric Cambisols	41,088.48	23.6
Eutric Fluvisols	3,473.49	2.0
Eutric Nitosols	53,530.89	30.8
Eutric Regosols	4,871.98	2.8
Humic Fluvisols	27,663.93	15.9
Orthic Acrisols	1,230.40	0.7
Pellic Vertisols	3,187.59	1.8
Water Bodies	3,571.18	2.1
Total	174,042.52	100.0

3.5 Climate

The climate of the UBNRB is characterized by high seasonal and inter- annual variations which is predominantly influenced by strongly varying altitudes and latitudes. The influence of these factors determine a rich variety of local climates, ranging from hot and arid along the Ethiopia-Sudan border to temperate at the highlands and even humid-cold at the mountain peaks in Ethiopia (Tekleab et al., 2014). The basin has three main seasons: a main rainy season, the wet summer season, which occurs between June and September (Kiremet), during which southwestern winds bring rains from the Atlantic Ocean. Some 70 %–90 % of the total rainfall occurs during this season. A dry winter season lasts from October to January (Bega) and the short rains of spring which may occur between February and May (BCEOM, 1998a; NMA, 2013). The short rains, originating from the Indian Ocean, are brought by south-east winds, while the heavy rains in the wet season originate mainly from the Atlantic Ocean and are related to south-west winds (BCEOM, 1998a). The spatial and temporal distribution of rainfall in Ethiopia is governed by the movement of air masses associated with the inter-tropical convergence zone (ITCZ),which moves seasonally from the South to the North and back (Conway, 2000).

According to Conway (2000), during the dry season (traditionally known as Bega) the ITCZ lies south of Ethiopia and rainfall may not occurs over the Blue Nile region, as it is affected by north-east continental air, which produces the dry season. From March, the ITCZ returns bringing small rains to the southern, and southwestern of the basin. This short period of rainfall is known as the Belg. In May, the northward movement of the ITCZ producing a short dry season before the main wet season, the *Kiremet.* Around June, the ITCZ moves further north and the south-west air stream extends over all highlands of Ethiopia to produce the main rainy season.

3.5.1 Rainfall

The UBNRB is relatively wet and its rainfall has a mono-modal pattern. Conway (2000) reported the mean annual rainfall values range between 1148-1757 mm during the period 1900-1998 and has a mean annual value of 1421 mm estimated from eleven rainfall gauges. 70 % of the rainfall falls between June and September. Awulachew *et al.* (2008) reported the average annual rainfall between 1400 and 1800 mm, ranging from an average of about 1000 mm near the Ethiopia–Sudan border to 1400 mm in the upper part of the basin, and in excess of 2000 mm in the Didessa and Beles sub basins. Abtew *et al.* (2009) studied the spatial and temporal distribution of meteorological parameters in the basin. According to their study, the mean annual rainfall is 1423 mm for the period of 1960-1990 based on the rainfall statistics of 32 stations. According to (Mekonnen and Disse, 2018a), the long term mean annual rainfall values calculated from 15 rainfall stations located in and around the study area using Thiessen polygon method in the period 1984-2011 range from 826.5 mm in the north (Wegel Tena) to 2366 mm in central highlands (Enjibara) with mean annual value of 1452 mm (Figure 4-1). The mean seasonal rainfall based on the above data showed that about 238, 1065 and 148mm occurred in Belg (October–January), Kiremet (June–September) and Bega (February–May) respectively, in which about 74% of rainfall is concentrated between June and September (Kiremet season), which has strong connection to the influence from the Indian Ocean (Onyutha *et al.*, 2015). The differences could be due to the period and length of data analyzed and the failure to consider the influence of multi-decadal oscillations.

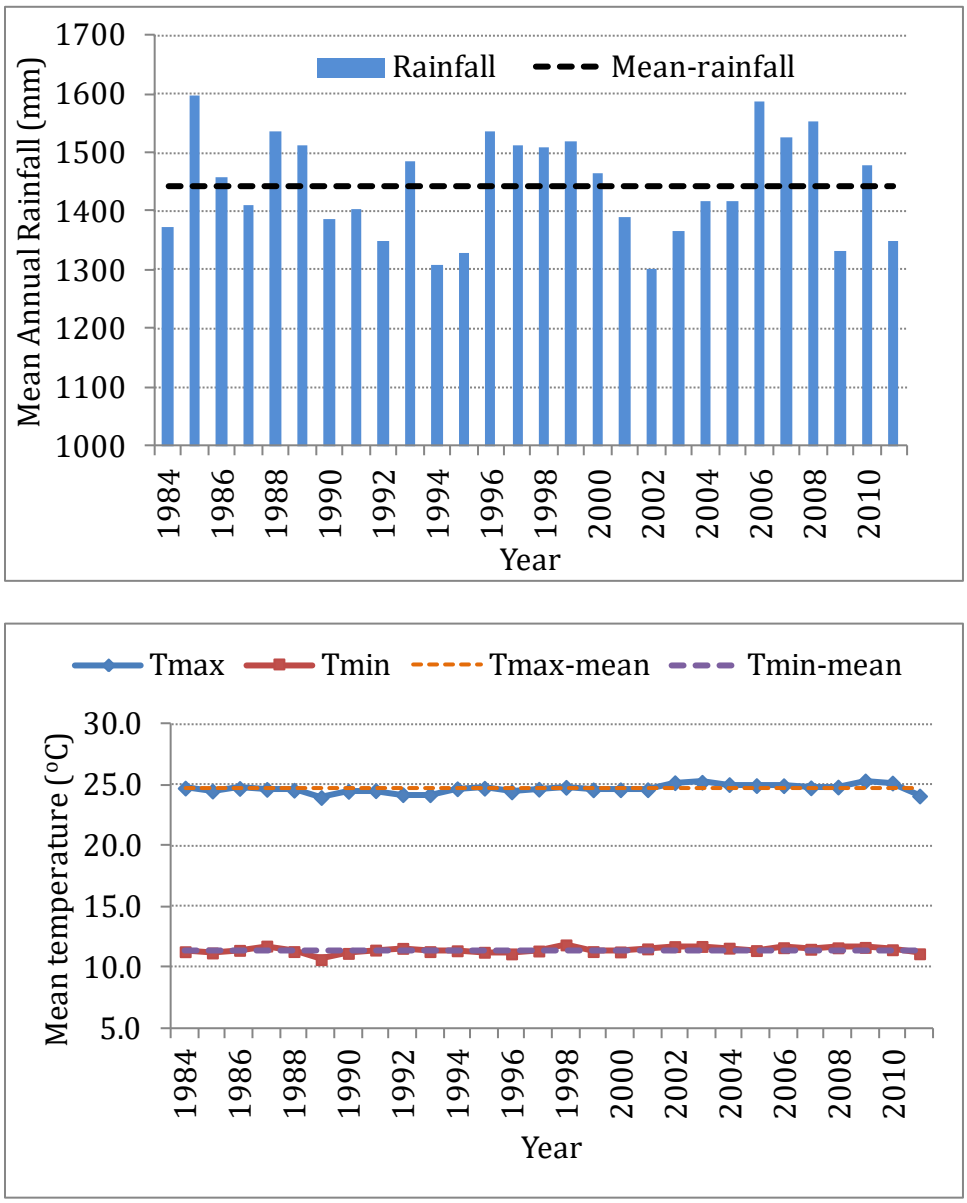

Figure 3-6: Annual rainfall and mean annual Tmax and Tmin for the UBNRB

Rainfall tends to increase with altitude while also being greatly affected by local rain-shadow and related effects as a result of the combination of these various a very substantial spatial variations in rainfall existed in the basin (BCEOM, 1998a). They identified four areas with distinct rainfalls, two with relatively high rainfall and two with relatively low rainfall:

i) A southeastern area is characterized by relatively high rainfall (1400-2200 mm) and a long wet season, which provides good conditions for agriculture.

ii) A central area also has relatively high rainfall (1400-2200 mm) but there is a more pronounced seasonal pattern, typified by a shorter wet season and longer dry season. The area provides the main grain surpluses in the basin.

iii) An area covering most of the eastern part of the basin, is characterized by relatively low annual rainfall (less than 1200 mm) distributed in both rainy seasons according to a bimodal pattern. It represents the main drought-prone area in the basin.
iv) A west and north-west area has relatively low rainfall (less than 1200 mm) falling predominantly in the main rainy season, and high average rates of evapotranspiration.

3.5.2 Temperature

Air temperature is a crucial parameter influencing numerous natural processes, for instance the plant growth, evaporation rates, wind movement, precipitation patterns and evapotranspiration variations (Polanco, 2017). The temperature in the basin is highly influenced with altitude and latitude. The climate is generally temperate at higher elevations and tropical at lower elevations (Conway, 2000). According to Conway (2000), on average temperatures fall by 5.3 -5.8^{o}C for every 1000 meters increase in elevation. The maximum average air temperatures in the UBNRB occur between March and June, while the lowest average air temperatures occur in December. During the summer, between July and September, high temperatures are reduced because of the rainfall, and cloudy conditions. Thus, the hottest period is experienced between March and May, before the major rainy season (Conway, 2000)**.** Furthermore, Tekleab *et al.* (2014) reported the mean annual temperature ranges from 13^{o}C in south eastern parts to 26°C in the lower areas of the south western part near to the Ethiopia-Sudan border for the period 1995-2004. The traditional Ethiopian classification of climate is based on elevation and recognizes at least three zones: the Kolla zone below 1800 meters with mean annual temperatures of 20-28°C; the Woina Dega zone between 1800 and 2400 meters with mean annual temperatures of 16-20°C; the Dega zone above 2400 meters with mean annual temperatures of 6-16°C.

According to the data analyzed in this dissertation, the long term mean annual maximum temperature ranges from 18.1º C at Mehal Meda to 30.9ºC at Dedesa from years (1984–2011). Meanwhile, the mean annual minimum temperature ranges from 6.33ºC at Debre Birhan to 16.19ºC at Anger Appendix 1. The mean annual minimum and maximum areal temperature of the UBNRB calculated from 26 temperature stations using Thiessen polygon method are 11.37^{o}C and 24.67 ^{o}C respectively Figure 3-6.

3.5.3 Hydrology

The Abay River (UBNR) in Ethiopia starts its journey from Lake Tana as an outflow and develops its course in a clockwise spiral. Shortly after leaving the lake, the river reaches the Tis Abay falls, which has a drop of 50 m, thereafter flowing in a deep gorge to the Sudan border. Deep ravines or canyons in which the Blue Nile and other rivers flow cut the basin. The valley of the Blue Nile is 1300 m deep in places, and the course of the river is often difficult to cross (Sutcliffe and Parks, 1999). Majority of the tributaries are found on the left bank, which include the Beshilo, Welaka, Jemma, Muger, Guder, Finchaa and Didessa. Right bank tributaries from the central highlands tend to be smaller, and include the Abeya, Suha, Chemoga, Birr, Fettam and Dura. Two major tributaries join in the lowlands, the Dabus on the left bank and the Beles the only major right bank tributary see Figure 4-2.

Table 3-3: Mean monthly flows (Mm^3) at Lake Tana outlet and El Diem (Sutcliffe *et al.*, 1999)

Jan	Feb	Mar	Apr	May	Jun	Jul	Aug	Sep	Oct	Nov	Dec	Total
Flow at outlet of Lake Tana (1920-1933)												
208	124	83	43	28	26	97	503	995	841	519	344	3810
Flow at El Diem (1912-1960)												
796	468	376	331	621	1648	6651	15647	12859	6889	2684	1385	50355
Flow at El Diem (1961-1997)												
716	417	348	315	600	1672	6911	14672	11119	5946	2394	1299	46411
Flow at El Diem (1912-1997)												
762	446	364	324	612	1659	6763	15963	14931	8245	2889	1497	52791

Table 3-4: Observed seasonal streamflow of the gauging stations (1971-2010), see their locations on the Figure 4-2

		Mean flow (m^3s^{-1})				Mean volume (Bm^3)				Contribution (%)		
Stations	Area (km^2)	Daily	LRS	DS	SRS	Annual	LRS	DS	SRS	LRS	DS	SRS
Eldiem	172,254	1645.1	3627.0	999.7	323.6	51.9	37.9	10.5	3.4	73.1	20.1	6.5
Kessi	65,784	613.3	1396.0	301.0	147.0	19.3	14.6	3.1	1.5	75.5	16.3	7.9
Tana	15,154	125.0	147.4	164.6	62.0	3.9	1.5	1.7	0.6	39.1	43.7	16.4
Gumara	1,394	36.2	86.3	14.9	8.0	1.1	0.9	0.2	0.1	79.0	13.7	7.3
Gilgel abay	1,664	52.1	128.2	23.4	5.3	1.6	1.3	0.2	0.1	81.6	14.9	3.4
Rib	1,664	15.5	40.8	4.2	1.8	0.5	0.4	0.0	0.0	87.2	9.0	3.8
Megech	462	7.8	18.8	3.0	1.8	0.2	0.2	0.0	0.0	79.6	12.9	7.6
Main beles	3,431	57.0	143.3	27.1	2.5	1.8	1.5	0.3	0.0	83.4	15.8	1.5
Gilgel beles	675	5.1	10.9	3.1	1.3	0.2	0.1	0.0	0.0	70.6	20.0	8.4
Koga	244	17.7	41.2	11.0	1.4	0.6	0.4	0.1	0.0	77.2	20.6	2.6
Andasa	573	5.3	11.5	3.4	1.0	0.2	0.1	0.0	0.0	71.8	21.1	6.2

Note:LRS; long rainy season, DS; dry season, SRS; short rainy season

The estimated mean annual discharge of UBNRB at El Diem (Ethio-Sudan boarder) varies considerably with the data period considered. Moreover, the flow in the basin is highly seasonal following the seasonality of rainfall in the basin. Sutcliffe *et al.* (1999) has summarized the flow records at the main sites Table 3-3. The runoff from Lake Tana is 3.8 km^3 in the period 1920-1933, with a range between 5.6 km^3 in 1929 and 1.9 km^3 in 1925 and 1930. The peak outflow occurs in September and October, with a long low flow recession from January to June, which indicated that its seasonal distribution is not greatly damped by the lake storage. The lake outflow contributes only some 7.7 % of the flow at El Diem. The long-term mean annual flow at El Diem from 1912 -1997 was 48.6 km^3 with a variation from low annual totals of 20.69 km^3 in 1913 and 29.6 km^3 in 1984, to high 69.7 km^3 in 1917 and 69.8 km^3 in 1929. The seasonal distribution of flows is very noticeable, with maximum mean monthly flows 15.23 km^3 in August contrasting with 0.32 km^3 in April Table 3-3. About 84% of the runoff occurs during the main rainy season (June - October). The mean annual flow of UBNRB for periods 1912-1960,

1961-1997 and 1912-1997 is 50.3, 46.4 and 48.6 km^3 respectively. Table 3-4 shows the observed mean daily and seasonal flows at different flow measuring stations, which are located in the UBNRB (see Figure 4-2 for their locations)

Conway (2000) reported that the occurrence of high fluctuation in the flow of UBNRB ranging from a 79.1km^3 in 1909 to a lowest 20.7km^3 in 1913. Moreover, the recent study by Tekleab *et al.* (2014) indicated that the mean annual flow at El Diem gauging station was 47.48 km^3 in the period 1965-2010, excluding the data gap and the whole 2005 data series.

According to BCEOM (1998a), at El Diem, average annual discharge is 49.4 km^3, with the low flow month (April) equivalent to less than 2.5 % of that for the high flow month (August). Four months (July-October) account for 82% of the annual total and the four low flow months (February-May) for only 4 %. The largest tributaries, Dabus, Didessa and Tana account for about 10%, 8.5% and 7% of the total flow at the border respectively. In general, the runoff generated from the UBNRB accounts approximately 40% of Ethiopia's total surface water resources of 122km^3.

Table 3-5: Main drainage sub-basins of UBN Basin and their mean annual runoff

S.No	Sub-basin Name	Area (km^2)	Gross Runoff (mm)	S.No	Sub-basin Name	Area (km^2)	Gross Runoff (mm)
1	Tana	15,054	514	8	Guder	7,011	537
2	North Gojam	14,389	486	9	Fincha	4,089	450
3	Beshlo	13,242	455	10	Didessa	19,630	651
4	Welaka	6,415	410	11	Anger	7,901	527
5	Jimma	15,782	422	12	Wonbera	12,957	410
6	South Gojam	16,762	543	13	Dabus	21,030	466
7	Muger	8,188	423	14	Beless	14,200	378
Total	Basin Area	176,652					

Chapter 4 Hydro-Meteorological data analysis

4.1 General

Understanding hydrological and climate variability both in space and time is essential for managing the available water resources for humans and ecosystem needs. The availability of reliable time series of rainfall and river flow data are therefore the key assets for the success of any climate and LULC changes impact assessment. The completeness of records is a crucial component for their utilization. Hydrological and meteorological understanding in the UBNRB is poor due to the sparseness of field data (limited operational data collection) poorly distributed across the basin and the poor quality measurement (Woldesenbet *et al.*, 2017a). Ground-based measurements are either missing or of poor quality for predicting and investigating changes in the hydrological system. In UBNRB, the spatial distribution of meteorological stations is poor, with the least coverage over remote and non-accessible areas, many stations are non-functioning, with significant missing data, and in some cases inefficient quality control systems. Encountering missing data in meteorological time series is inevitable because of instrument malfunctions, network reinstallation, communication-line breakdown, observation recording errors, absence and limited knowledge of observers, and civil war incidents. If data gaps are large, incomplete time series may hide the pattern of the data, and they may considerably distort the results of any statistical analysis and raise uncertainty in modeling results (Campozano *et al.*, 2014).

The availability of reliable, serially complete sets, and homogenous meteorological data on different spatial and temporal scales are vital for climate impact assessment, hydrological modeling and analysis, and design of water resource systems in this basin (Woldesenbet *et al.*, 2017a). The low quality and incompleteness of time series data strongly hinders and effects the planning, operation and management of water resources systems, hindering the calibration and validation of modeling tools and their use for predicting the hydrological responses under changed climate conditions (Adeloye, 1996). Estimations of missing data are therefore vital where meteorological stations are scarce and the observed data are influenced by topography. Regarding the issue of missing climatological data, it is essential to handle in a careful manner using one of the many available optimal infilling the missing data techniques. Woldesenbet *et al.* (2017a) reviewed the previous studies related to water balance for the UBNRB, and conclude that all studies overlooked gap filling and/or in homogeneities in climate time series. To minimize this data-limitation, huge efforts and different techniques are tried in this study to improve the quality and extend the length of available meteorological data.

4.2 Meteorological and hydrological data description

The meteorological data analyzed in this study include rainfall (RF), maximum (Tmax), minimum temperatures (Tmin), relative humidity (RH), wind speed (WS), and sunshine hours (SH). Although there are many meteorological gauging stations in the study area, most of the gauges either have short record periods, or have abundance of missing and erroneous data. Among the stations in the UBNRB, 40 rainfall and 35 temperature stations are considered for further analysis (see Figure 4-1). The basic characteristics of the meteorological gauging stations used are listed in Appendix 1. The data from these stations are collected from the Ethiopian National Meteorological Service Agency (ENMSA) in the period 1952-2015. In spite of this 73-

years long record length, most of the stations suffer from a variety of errors which include significant missing records and recording errors, such as, for example, that the minimum temperature is greater than the maximum temperature within a particular period. The occurrences of civil war, defective and outdated devices were the main causes for the missing data records. After screening and rigorous analyses of the weather data, stations were selected for daily maximum and minimum temperatures and rainfall time series, depending on the length of record, percent of the missing record and purpose of the studies. As a result, only the 15 stations, in which rainfall data is relatively more complete, proved to be suitable for trend analysis. Some 10 stations having complete climate variables, such as Tmax, Tmin, RH, WS, and SH were used as input for the SWAT model for analyzing the impacts of combined and isolated effects to the changes of climate and LULC (Figure 4-1). All errors, except those due to missing records, such as misplaced decimal digits and zero value for missing records are corrected by a careful investigation using UBNRB master plan study and by communicating professionals and experts from the ENMSA. As indicated in Appendix 1, the percentage of missing daily rainfall ranges from 0.4 % to 60.8% while for temperature it ranges from 1.2% to 48.1%.

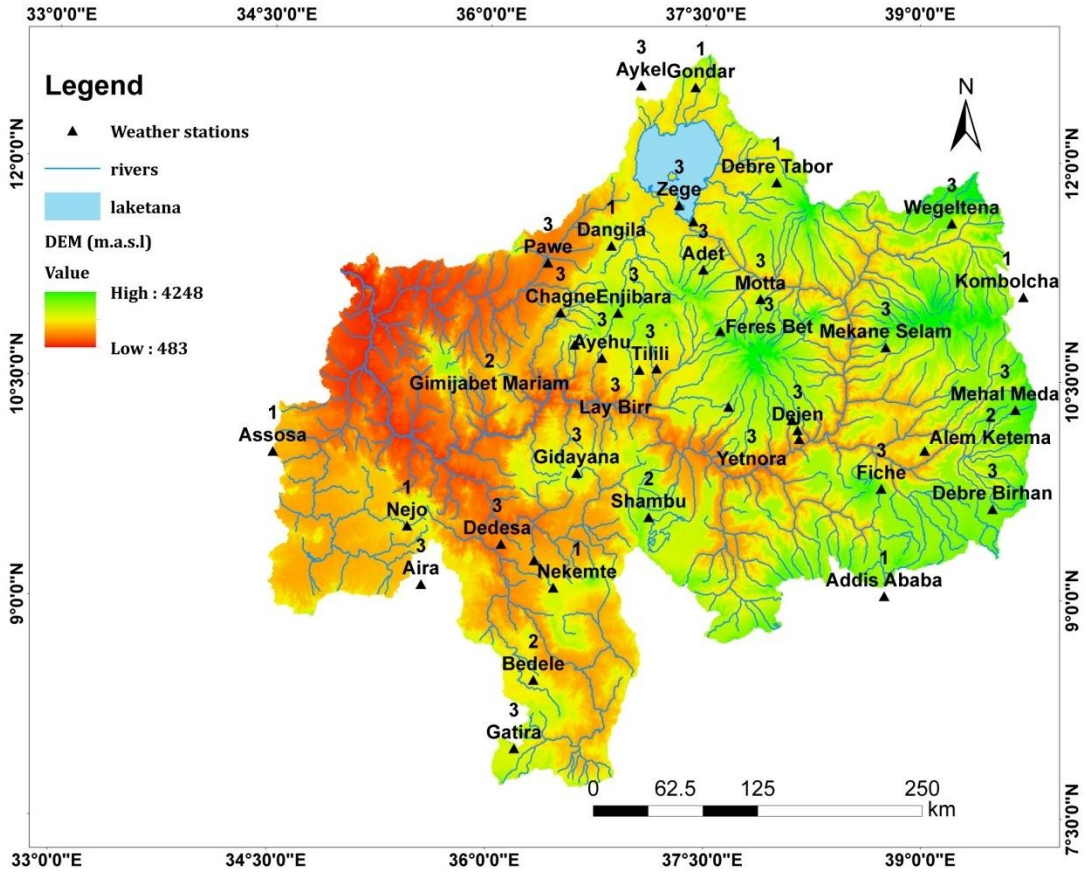

Figure 4-1: Locations of study area and meteorological and discharge stations, with the Digital Elevation Model (DEM) data as the background. where: 1: Stations used for SWAT model; 2: Stations used for trend analysis; 3: Stations used for basin wide areal rainfall analysis.

Similarly, streamflow data for sixty stations were collected from Ministry of water, irrigation and energy (MWIE) of Ethiopia as indicated in Figure 4-2 and Appendix 2.

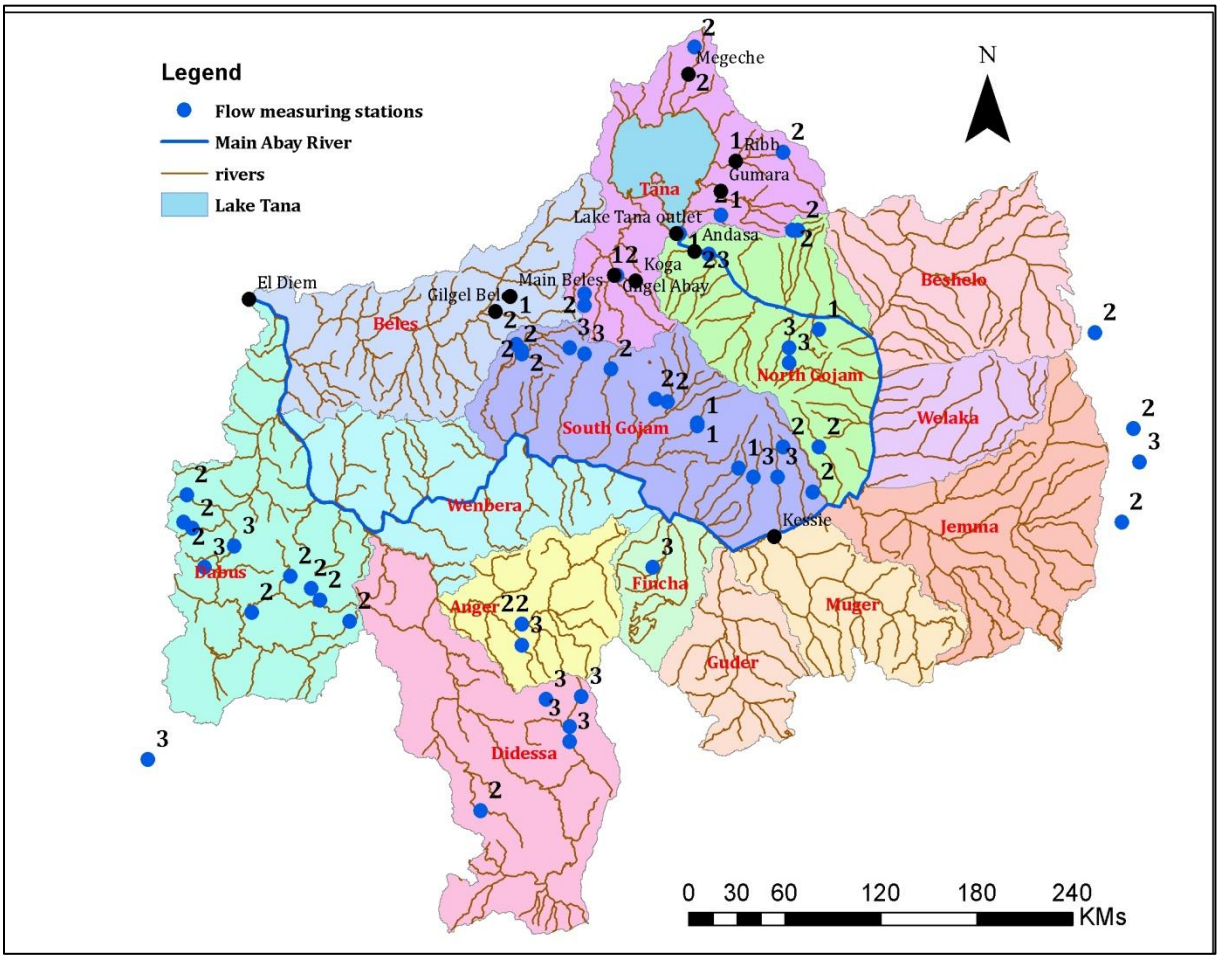

Figure 4-2: Sub-basins and flow measuring stations in the UBNRB

Where, [1] and [2] from the map denote stations considered for filling the missing records for stations which have records from (1971-2010) and (1984-2011) respectively, [3] denotes stations discarded from the analysis

4.3 Methods used for infilling

Hydro-meteorological observations are unique in space and time. If they are not observed at a given location and time, the values can only be estimated. Many applications, such as the calculation of water balances, calibration of hydrological models require full datasets. Thus, a reliable estimation of the missing observations is of great importance. The sparse gauge networks of the UBNRB exacerbate the problem. We define infilling as the process of repairing data sets where observations are missing due to many reasons. According to Campozano *et al.* (2016), the infill methods can be grouped in three major classes: (i) the deterministic, (ii) stochastic and (iii) artificial intelligence methods. In this study, we resort to both deterministic and stochastic methods or approaches for estimating missing precipitation, maximum temperature (Tmax), minimum temperature (Tmin) and streamflow datasets. Coefficient of correlation weighting (CCW), linear regression (LR), multiple linear regressions (MLR) and the inverse distance weighting method (IDW) are grouped under deterministic technique, whereas weather generator

(LARS-WG) is among many others of the stochastic methods. For precipitation data, CCW, IDW, LARS-WG methods are used for filling the missing data. Linear regression (LR) and LARS-WG were tested for infilling the missing data of Tmax and Tmin. For streamflow, missing data were fitted using eight different infilling techniques listed in Table 4-1. Let X(t)=(X1(t),...,Xi(t),...,Xm(t)) be the vector of observed values at time t. For a set of time steps Tk(1), observations are available at location k and for the rest of the time Tk(2) data for location k are missing. The purpose of infilling is to provide an estimate $\widehat{X}k(t)$ for all t ϵ Tk(2).

Table 4-1: Deterministic infilling techniques with their respective acronym for the missed streamflow data

Acronym	Details
LR-R	Linear regression of single highly correlated station
LR-ln R	As above but using log transformed streamflow
LR-D	Linear regression of single closest station
LR-ln D	As above but using log transformed streamflow
MLR-R	Multiple Linear regression of highly correlated multi/stations
MLR-ln R	As above but using log transformed streamflow
MLR- D	Multiple Linear regression of closest multi-stations
MLR-ln D	As above but using log transformed streamflow

4.3.1 Inverse distance weighting method (IDW)

The inverse distance weighting method is the most commonly used for the estimation of missing data in hydrology and geographical sciences (Di Piazza *et al.*, 2011). This method is based on the proximity of neighboring stations to the target station. The weighted distance method is given as eqn. (4-1):

$$w_i = \frac{d_{it}^{-m}}{\sum_{i=1}^{N} d_{it}} \qquad (4\text{-}1)$$

Where d_{it} is the distance between the target station and the *i*th neighboring station, and *N* is number of neighboring stations. The weight decreases as the distance from the target station increases. Greater values of *m* assign greater influence to values closer to the target station. The value of *m* usually ranges from 1.0 to 6.0, and in this study the most commonly adopted value of 2 is used. Although the success of IDW method depends on the existence of a positive spatial autocorrelation, one problem of the IDW method is the arbitrary selection of time series data from neighboring stations (Di Piazza *et al.*, 2011). The selection and number of adjacent stations for interpolations are important for the accuracy of interpolated values. As mentioned by Woldesenbet *et al.* (2017a), different authors used different criteria to select neighboring stations. Because of the relatively low number of network stations, a geographic distance of 100 km was considered for most stations when selecting neighboring stations. If no station is located within 100 km of the target station, then the search distance is increased until at least two suitable stations are reached.

4.3.2 Coefficient of correlation weighting method (CCW)

The weighting factor in this method is based on correlation coefficients instead of distance. The weighting factor is computed as eqn.(4-2):

$$W_i = \frac{r_{i,t}}{\sum_{i=1}^{N} r_{it}} \tag{4-2}$$

where *r*it is the correlation coefficient of daily time series data between the target station and *i*th neighboring station, *N* is number of neighboring stations, and *Wi* is the weighting factor.

Neighboring stations were selected for the target station with Pearson's correlation coefficient $R^2 \geq 0.25$ for daily rainfall time series. A minimum of three and a maximum of four neighboring stations were selected in this study. When the concurrent records of neighboring stations were not able to fill the missing data completely, the next neighboring station within 100 km radius and R^2 greater than 0.25 were selected and used to fill the gaps in the climate dataset.

4.3.3 Linear (LR) and multiple linear regression technique (MLR)

LR is a method used for estimating climatological data at stations with other stations, which has similar conditions. In statistics, LR is an approach for modeling the relationship between scalar dependent variable p_x and one independent parameter denoted p_i. In a method the similar station is selected by either based on the closets distance (D; lnD) or the higher Pearson correlation coefficient (R^2;lnR^2). A linear fit between the target station and the selected station is calculated using eqn. (4-3) to obtain the parameters a_0 and b.

$$\hat{X}_k(t) = a_0 + bX_{ik}(t) \tag{4-3}$$

MLR is a statistical method for estimating the relationship between a dependent variable and two or more independent, or predictor variables instead of a single variable. In essence, the additional predictors are used to explain the variation in the response not explained by a simple linear regression. It identifies the best combination of independent variables to predict the dependent variable. Eischeid *et al.* (1995) highlighted many advantages and robustness of this method in data interpolation and estimation of missing data. The missing data (Px) is estimated from eqn. (4-4).

$$\hat{X}_k(t) = a_0 + \sum_{i=1}^{n} a_i X_i(t) \tag{4-4}$$

Where Px is the dependent variable at target station x. a_0 is regression constant, a_i, is the regression coefficient for station i. p_i is predictor or independent variable for station i. n is the number of stations. The distance (D, lnD) and the Pearson correlation coefficient (R^2, lnR^2)

criteria are also used to select stations. A maximum number of four stations (n = 4) were used for the infilling of missed data at target station.

4.3.4 Weather generator (LARS-WG)

LARS-WG is a stochastic weather generator, which can be used for the simulation of weather data at a single station under both current and future climate conditions. These data are in the form of daily time series for a group of climate variables, namely precipitation, maximum temperature and minimum temperature, and solar radiation (Chen *et al.*, 2013; Semenov *et al.*, 1997). LARS-WG uses a semi-empirical distribution (SED) that is defined as the cumulative probability distribution function (CDF) to approximate probability distributions of dry and wet series, daily precipitation, minimum temperatures and maximum temperatures. The observed daily weather data at a given site is used to determine a set of parameters for probability distributions of weather variables. These parameters are used to generate a synthetic weather time series of arbitrary length by randomly selecting values from the appropriate distributions, with the same statistical characteristics as the original observed data but differing on a day-to-day basis. It can also be used to synthesize and fill in missing values daily climatic variables such as precipitation, temperature and solar radiation (Cherie, 2013). Detailed description and steps of the approach are described in Chapter 6.

4.3.5 Goodness of Fit Criteria

To establish our confidence in the outputs of such methods or techniques and justifying their continuing use, assessing model performance with quantitative tools is found to be useful, indeed most often necessary. For the performance assessment of the infilling methods 10% of the data for all stations in the time series was sampled at random and considered for cross validation with in filled values (Campozano *et al.*, 2016). This means that for a selected station 10% of observed values was treated as missing and was estimated based on the other 90% of observations. Quantitative testing or level of goodness of fit evaluation involves the calculation of suitable numerical metrics to characterize model performance. The use of metric values also minimizes potential inconsistencies arising from human judgment. The level of goodness of fit evaluation is mainly done in two different ways:

1. Visually inspecting and comparing the simulated and the observed variables. The most fundamental approach for assessing model performance in terms of behaviors is through visual inspection of the graphs between the simulated and observed data. In this approach, a modeler may formulate subjective assessments of the model behavior that are generally related to the systematic (e.g., over- or under prediction) and dynamic (e.g., timing, rising limb, falling limb, and base flow) behavior of the model.

2. Calculating objective functions. That measure the level of agreement between observed and the model output, which requires the use of a mathematical estimate of the error between the simulated and observed i.e. objective or efficiency criteria (Booij *et al.*, 2007). Usually, two different objective functions are considered, which can measure the goodness for the water balance and overall goodness agreement of shape of the hydrograph. In this study, we applied

different objective functions for measuring quantitative performance as suggested by Bennett *et al.* (2013)

Relative error and residual methods

Residual methods that calculate the difference between observed and modeled data points are the most widely used methods for model evaluation. Of the many possible numerical calculations, the most common are bias, mean absolute error (MAE), mean square error (MSE) and root mean square error (RMSE). Bias eqn.(4-8) is simply the mean of the residuals, indicating whether the model tends to under- or over-estimate the measured data, with an ideal value zero. However, positive and negative errors tend to cancel each other out. To prevent such cancellation, the MSE eqn.(4-6) criterion squares the residuals before calculating the mean, making all contributions positive and penalizing greater errors more heavily. The RMSE eqn.(4-7) takes the square root of the MSE to express the error metric in the same units as the original data. MAE eqn.(4-5) is similar to RMSE except absolute value is used instead. The MSE, RMSE and MAE can vary between 0 and ∞ but performs best when a value of 0 is generated when no difference between simulated and observed data occurs. Similar to bias measurements, a low value does not mean low errors, just balanced errors. However, at the same time the distribution of the observed and simulated data throughout the modeling period can be completely wrong. Therefore, this objective function should always be used in combination with another objective function that considers the overall shape agreement.

$$\mathrm{MAE} = \frac{\sum_{i=1}^{n} |X_i - Y_i|}{n} \tag{4-5}$$

$$\mathrm{MSE} = \frac{1}{n}\sum_{i=1}^{n} (X_i - Y_i)^2 \tag{4-6}$$

$$\mathrm{RMSE} = \sqrt{\frac{1}{n}\sum_{i=1}^{n} (X_i - Y_i)^2} \tag{4-7}$$

$$\mathrm{PBIAS} = 100 * \frac{(\mu_x - \mu_y)}{\mu_x} \tag{4-8}$$

Preserving the data pattern

To test the ability of the model in preserving the pattern of data, performance metrics must include consideration of how data points and how their errors relate to each other. To test the ability of the model to preserve the pattern of data, performance metrics must include consideration of how data points and how their errors relate to each other. A simple quantitative

and graphical measure is the cross-correlation between measured and calculated values. It measures how the similarity of the two series varies with delay along one dimension (usually time). Perhaps the best-known performance metrics in this category are the correlation coefficient and Nash-Sutcliffe coefficient.

Correlation coefficient: It is used to indicate how variation of one variable is explained by a second variable, but it is important to remember it does not indicate causal dependence. Coefficient of determination (R^2) is a commonly used to measure the efficiency of a model, but only varies between 0 and 1 eqn.(4-9). Zero indicates that the model explains none of the variability of the response data around its mean while 1 indicates that the model explains all the variability of the response data around its mean. In general, the higher the R^2, the better the model fits your data. However, R^2 cannot determine whether the coefficient estimates and predictions are biased. A perfect model would result in an R^2 equal to 1. However, normally the R^2 ends up somewhere between 0.8 and 0.95 when there are good quality input data

$$R^2 = \frac{\left[\sum_{i=1}^{n}(X_{,i} - \mu_x)(Y_{,i} - \mu_y)\right]^2}{\sum_{i=1}^{n}(X_{,i} - \mu_x)^2 \sum_{i=1}^{n}(Y_{,i} - \mu_y)^2} \qquad (4\text{-}9)$$

Nash-Sutcliffe coefficient: It measures the efficiency of the model by relating the goodness of fit of the model to the variance of the measured data. It can range from -∞ to 1 eqn.(4-10). An efficiency of 1 corresponds to a perfect match of modeled discharge to the observed data. An efficiency of 0 indicates that the model predictions are as accurate as the mean of the observed data, where as an efficiency less than 0 ($-\infty<NS<0$) occurs when the observed mean is a better predictor than the model. Besides, due to frequent use of this coefficient, it is known that when values between 0.6 and 0.8 are generated, the model performs reasonably. Values between 0.8 and 0.9 tells that the model performs well and between 0.9 and 1 indicates that the model performs extremely well (Wale, 2008).

$$NSE = 1 - \frac{\sum_{i=1}^{n}(X - Y)_i^2}{\sum_{i=1}^{n}(X_{,i} - \mu_x)^2} \qquad (4\text{-}10)$$

In the above equations, X_i and Y_i are i^{th} observation and simulated data by the model, respectively. μ_x and μ_y are the average of all data of X_i and Y_i in the study population and n is the number of all samples to be tested. Furthermore, graphical comparisons of the simulated and observed data were used.

The statistical performance indices such as correlation coefficient (R^2), Nash Sutcliffe coefficient (NSE), mean absolute error (MAE), root mean square error (RMSE) and percent bias (% bias) eqn. (4-5) to eqn.(4-10) between observed and estimated values are used to evaluate the performance of the candidate methods for filling the missing data of the target stations. Equally weighted statistical metrics are applied to compare the performances of selected methods at target stations and to establish the ranking. A score was assigned to each candidate method according to the individual metrics. For example, the candidate achieving the smallest values of RMSE and MAE, or % bias and highest values of NSE and R^2 received score 1. The final score

is obtained by summing up the score pertaining to each candidate approach at each station. The method with the smallest score is the best. While filling the missing data, uncertainty is expected due to low station density, poor correlations, and the large number of missing records.

4.4 Results and discussions of infilling missing data

Evaluation of infilling methods for precipitation and temperature data

Daily precipitation data for 24 stations, maximum and minimum temperature for 28 and 15 weather stations respectively, for the period January 1984 to December 2010 were used for this study. For the daily rainfall data, three infilling methods were applied. For daily temperature data, two infilling methods were applied. The infilling methods were evaluated on the basis of their estimation errors and preserving the pattern of the observed data. For each station, R^2, NSE, RMSE, MAE and percentage bias, between observed and estimated values of the climate variables were calculated. The ranking procedure is carried out based on the aforementioned performance indicators and candidate approaches for each target station for daily time series data. The values of performance indicators of the applied methods at Addis Ababa station (randomly chosen) for daily rainfall, Tmax and Tmin time series data are shown in Table 4-2. The result show that R^2, RMSE and MAE value between observed and in filled daily rainfall using the CCW approach exhibits better performance than other methods at Addis Ababa station. For the Tmax and Tmin at Addis Ababa station, LR has a slightly smaller value for RMSE, MAE and percentage bias, and higher R^2 and NSE than LARS-WG. The outcome of the ranking process from all target stations is summarized in Table 4-3 , showing the total scores for different candidate approaches for daily time series data of rainfall, Tmax and Tmin. Considering the daily time series for the rainfall, the total score is lowest for CCW and highest for LARS-WG. For maximum temperature and minimum temperature, LR has low score whereas LARS-WG has the highest score.

Table 4-2: Performance indices value, score and ranking for daily rainfall, Tmax and Tmin at Addis Ababa station

Variable	Infilling method	Values					Score					Total score	Rank
		R^2	RMSE	MAE	NSE	% bias	R^2	RMSE	MAE	NSE	% bias		
Rainfall	LARS-WG	0.02	7.85	3.41	-0.76	-0.18	3	3	3	3	1	13	3
	IDW	0.14	5.41	2.46	-0.05	10.35	2	1	2	2	2	9	2
	CCW	0.16	5.46	2.41	0.04	11.86	1	2	1	1	3	8	1
Tmax	LR	0.53	3.97	1.80	0.97	-2.56	1	1	1	1	2	6	1
	LARS-WG	0.20	4.38	2.29	0.96	0.12	2	2	2	2	1	9	2
Tmin	LR	0.10	2.74	2.02	0.91	0.77	2	1	1	1	2	7	1
	LARS-WG	0.22	3.01	2.23	0.90	0.18	1	2	2	2	1	8	2

Table 4-3: Total score of the candidate methods over the study period for each target station for daily time series data of rainfall, Tmax and Tmin

	Rainfall			Tmax			Tmin		
Station	LARS-WG	IDW	CCW	Station	LR	LARS-WG	Station	LR	RARS-WG
Abaysheleko	14	9	7	Abaysheleko	6	9	AddisAbaba	7	8
Addis Ababa	13	10	7	AddisAbaba	7	8	Adet	5	10
Adet	13	9	8	Adet	6	9	Ayehu	5	10
Alemketema	13	7	10	AlemKetema	6	9	Bahirdar	6	9
Angergutten	9	12	9	Angergutten	6	9	Bedele	6	9
Assosa	13	6	11	Arjo	6	9	Chagnie	5	10
BahirDar	13	10	7	Assosa	5	7	Kombolicha	5	10
Bedele	13	8	9	Ayehu	6	9	Dangila	6	9
Kombolicha	13	10	7	Ayira	6	9	Debre Birhan	6	9
Dangila	13	11	6	Bahirdar	9	6	Debre Markos	5	10
Debre Berhan	13	11	6	Bedele	5	6	Fitche	6	9
Debre Tabor	13	11	6	Chagnie	6	9	Gondar	6	9
Dedessa	13	9	8	Kombolicha	6	9	Nedjo	5	10
Dmarkos	13	10	7	Dangila	6	9	Nekemit	5	10
Fiche	13	9	8	Debre Birhan	6	9	Yege	5	10
Gimijabet	13	10	7	Debre Markos	6	9	Total score	83	142
Gidaya	13	9	8	Debre Tabor	5	10	Rank	1	2
Gondar	13	10	7	Dedesa	6	9			
Motta	13	7	10	Fitche	6	9			
Mekaneselam	13	11	6	Gondar	6	9			
Nedjo	13	8	9	Mekaneselam	6	9			
Nekemit	13	10	7	Mmeda	5	9			
Shambu	13	10	7	Motta	9	5			
Yetnora	13	11	6	Nedjo	6	9			
Total score	309	228	183	Nekemit	6	9			
Rank	3	2	1	Shambo	6	9			
				Yetnora	7	8			
				Zege	6	9			
				Total score	172	239			
				Rank	1	2			

Table 4-4 summarized the outcome of the rankings and the total scores for different performance indices and candidate approaches. Considering the R^2 performance indicator for the rainfall dataset, the total score is the lowest for CCW and the highest for LARS-WG. When RMSE is considered as a performance indicator at target stations, again CCW score is the lowest and LARS-WG is the highest for the rainfall. Similarly, considering MAE as a performance indicator for rainfall IDW shows the lowest score, LARS-WG portrays the highest score. LARS-WG scores lowest value only when the percentage bias is considered as performance index for the daily rainfall. For Tmax and Tmin, LR has comparably low scores whereas LARS-WG has the highest score, when R^2, RMSE, MAE, NSE and percentage bias are considered as a performance

indicator at target stations. In general, LARS-WG shows the highest score in all performance indices for Tmax and Tmin, when summing up the scores of the indices and, hence, less performance for filling gaps in the daily Tmax and Tmin datasets as compared to LR.

Table 4-4: Total score for each performance indices summed up from all stations for rainfall, Tmax and Tmin using different methods

Performance indices	Rainfall			Tmax		Tmin	
	LARS-WG	IDW	CCW	LR	LARS-WG	LR	LARS-WG
R^2	72	44	28	29	54	16	29
% bias	70	42	32	31	51	15	30
RMSE	70	42	32	30	52	15	30
MAE	72	41	31	31	52	15	30
NSE	25	59	60	51	30	22	23
Total score	309	228	183	172	239	83	142
Rank	3	2	1	1	2	1	2

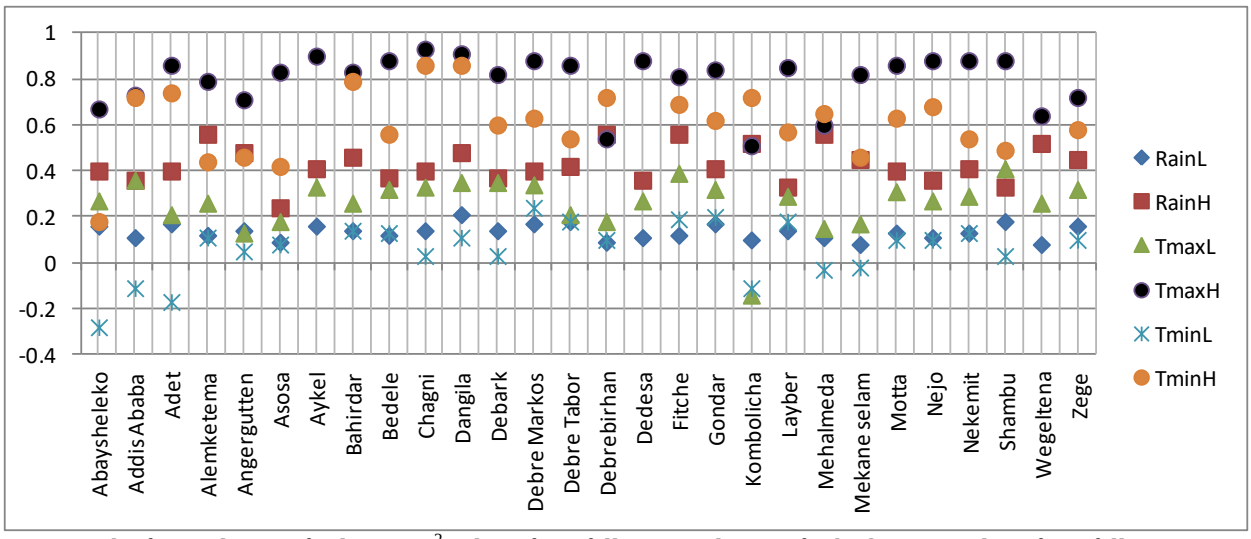

RainL on the figure denotes for lowest R^2 value of rainfall, RainH denotes for highest R2 value of rainfall, TmaxL denotes lowest R2 for Tmax, TmaxHdenotes highest R^2 for Tmax, TminL denotes lowest R2 for Tmin and TminH denotes for highest R^2 for Tmin.

Figure 4-3: Highest and lowest value of R^2 between target and neighboring stations for daily rainfall, maximum and minimum temperatures at the target stations.

Figure 4-4, Figure 4-5 and Figure 4-6 present the R^2, RMSE and MAE values calculated for daily rainfall between the observed and estimated at all rainfall stations respectively. The result from Figure 4-4 revealed that CCW method outperforms in 20 rainfall stations from 24 (i.e. 83.3

%), while IDW outperforms at 4 stations (16.7%) when considering the R^2 as performance index. When RMSE is considered as a performance index at target stations, again CCW obtained lowest RMSE values at 16 rainfall target stations from 24 (i.e. 66.7 %), IDW obtained less RMSE at 7 stations (29.2%) and LARS-WG obtained less error at 1 station (4.2%) as it is shown in (Figure 4-5). Similarly, considering MAE as performance index at target stations, the result from Figure 4-6 depict a similar pattern as RMSE, in which CCW outperforms 66.7%, IDW 29.2% and LARS-WG 4.2%. However, LARS-WG outperforms at 17 target rainfall stations (95.8%) and IDW 29.2%, when considering NSE as a performance index. In summary the analysis reveal that based on the total score and individual R^2, RMSE and MAE values, for all stations, CCW is the best performing method for infilling the daily rainfall in the UBNRB. In case one single method should be used for the daily rainfall analysis, the CCW would be most advisable, because the weighting considers Pearson's correlation, which is most appropriate for study regions with high spatial variability.

For maximum temperature, the performance comparison of the infilling methods for the performance indices of (R^2, RMSE and MAE) are shown in Figure 4-7, Figure 4-8 and Figure 4-9 respectively for all target stations. The result analysis revealed that LR method obtained higher R^2 and less error (RMSE and MAE) at more than 90 % of the stations, when observed and estimated daily Tmax are compared. This high performance of LR could be due to the existence of high correlation between the target stations and neighboring stations. Hence, LR method can be proposed the best infilling method for daily maximum and minimum temperature data at target stations in the UBNRB. According to Woldesenbet *et al.* (2017a), LARS-WG weather generator infilling method is suitable for short gaps; however, the percentage of missing records for the target stations in the study area has longer gaps. As a result, the climate variability may not be captured if gap filling is performed using weather generators.

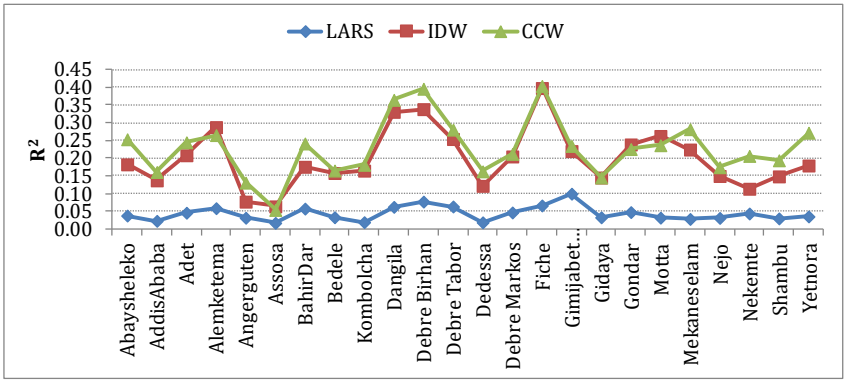

Figure 4-4: Correlation of observed and infilled daily rainfall using different filling methods

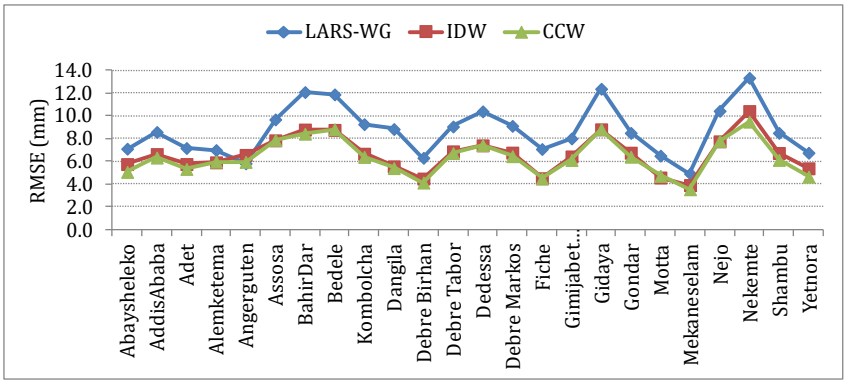

Figure 4-5: RMSE value of the observed and infilled daily rainfall using different filling methods

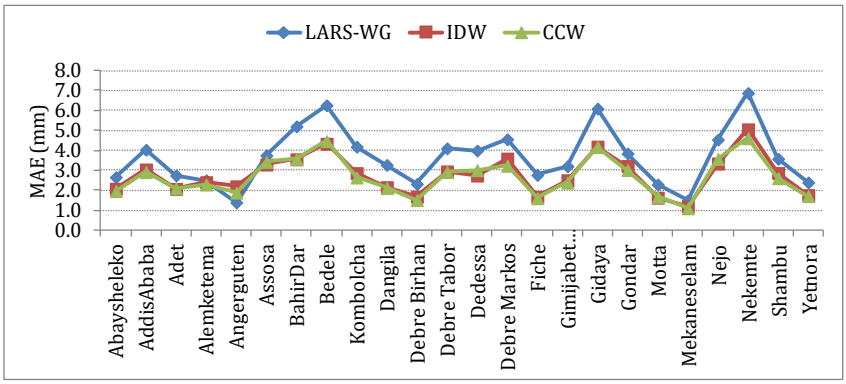

Figure 4-6: MAE value of the observed and infilled daily rainfall using different filling methods

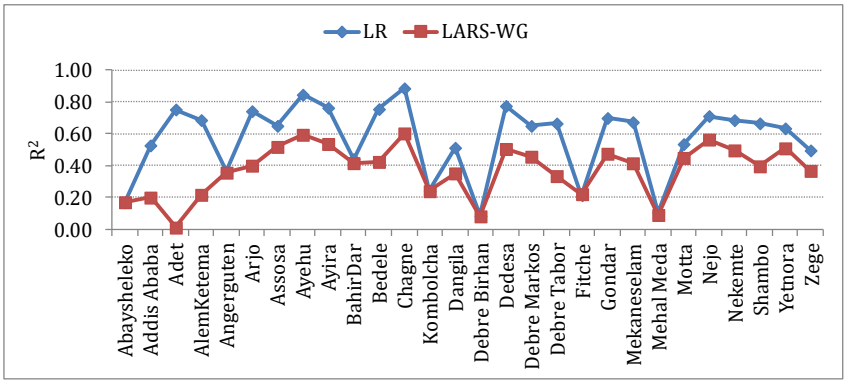

Figure 4-7: Correlation coefficient of the observed and infilled daily Tmax using different filling methods

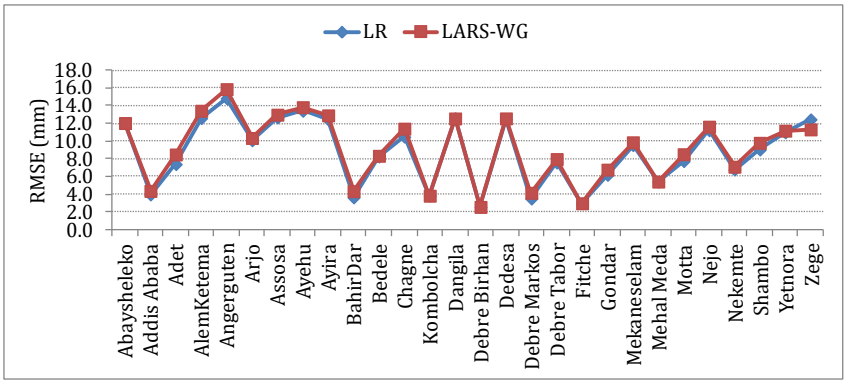

Figure 4-8: RMSE value of the observed and infilled daily Tmax using different filling methods

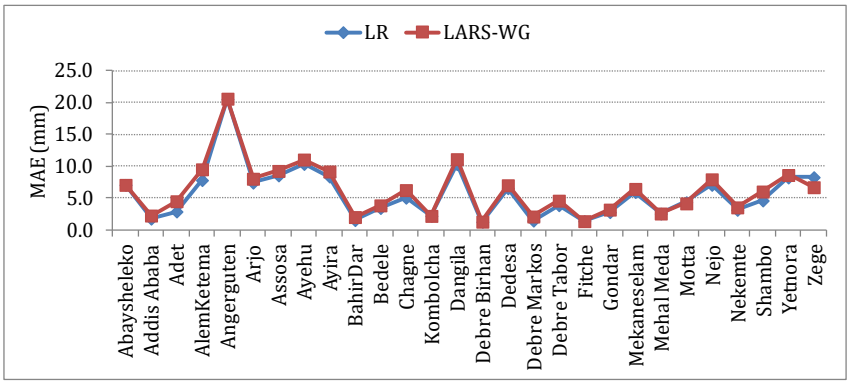

Figure 4-9: MAE value of the observed and infilled daily Tmax using different filling methods

In Ethiopia, the weather station density is less than the minimum station density (i.e. 250 km^2 per non-recording station for mountainous areas) recommended by the World Meteorological Organization (WMO); moreover, the distribution of the available stations is very uneven (WMO, 2008). In the study area, most of the stations are concentrated in the central highlands with very few stations present in the western lowlands (see Figure 4-1). While selecting neighboring stations, maximum temperature showed higher correlation between stations than minimum temperature and rainfall did (see Figure 4-3). The rainfall shows the least correlation between target stations and neighboring stations. Woldesenbet *et al.* (2017a) also reported that the CCW method performs better than other traditional gap-filling methods they considered in the same study area. As the success of IDW is based on simple distance between target and neighboring stations rather than correlation between stations (Teegavarapu and Chandramouli, 2005), its performance is lower than that of CCW for rainfall. Linear regression method is not used as infilling method for daily rainfall due to the low correlation exists between the target and neighboring stations (Figure 4-3), and also it does not satisfy the basic assumptions for linear regression (Woldesenbet *et al.*, 2017a).

Long-term, serially complete climate time series are critical in many meteorological and hydrological research applications, including for understanding climate variability and trends, planning and managing the water resources, formulating appropriate policies to increase production and productivity and reduce poverty. Hence, the present serially completed, quality-

controlled rainfall, and temperature dataset in the UBNRB could be used for the aforementioned purposes. The low correlation between the observed and the in filled daily rainfall (Figure 4-4) as compared to the correlation between the observed and in filled daily Tmax (Figure 4-7) might be due to high spatial and temporal variability of rainfall in the study area.

Evaluation of infilling methods for streamflow data

Table 4-5 presents the values of performance indices between the observed and in filled daily streamflow and score of candidate methods at El Diem station. The result analysis shows that LR-lnD method outperforms than the others at El Diem station to fill the missing streamflow data, whereas LR-D performs least. The summary of total score and ranking of the methods applied for infilling the missed streamflow data at four stations which have long time record and better quality data is shown in Table 4-6. The result revealed that LR-R^2 method has scored the highest score both at Kessi and Gilgel Abay stations while MLR-R^2 method score highest at Gumara station. However, the linear or multiple linear regression method using geometrical distance as criteria for selecting the neighbor station gives poor results. This indicates that the presence of high spatial variability of streamflow in the UBNRB.

Table 4-5: Performance evaluation of the infilling the missed flow data methods at El Diem station

Performance indices	Observed	LR-D	LR-R^2	LR-lnD	LR-lnR^2	MLR-D	MLR-R^2	MLR-lnD	MLR-lnR^2
Mean (m^3s^{-1})	1795	1808	1865	1275	1639	1518	1595	1170	1064
R^2		0.36	0.61	0.46	0.72	0.39	0.71	0.50	0.42
RMSE (m^3s^{-1})		1641	1281	1505	1088	1598	1119	1440	1559
MAE (m^3s^{-1})		1254	822	996	625	1062	690	801	967
NSE		0.35	0.60	0.39	0.71	0.37	0.69	0.41	0.29
Score									
R^2		8	3	5	1	7	2	4	6
RMSE		8	3	5	1	7	2	4	6
MAE		8	4	6	1	7	2	3	5
NSE		7	3	5	1	6	2	4	8
Total score		31	13	21	4	27	8	15	25
Rank		8	3	5	1	7	2	4	6

Table 4-6: Summary of total score and ranking for the methods for the four main streamflow stations

Station	LR-D	LR-R^2	LR-lnD	LR-lnR^2	MLR-D	MLR-R^2	MLR-lnD	MLR-lnR^2
El Diem	31	13	21	4	27	8	15	25
Kessi	8	4	16	12	27	29	27	20
Gilgel Abay	32	8	16	17	9	13	22	25
Gumara	15	18	13	25	7	5	32	27
Rank								
El Diem	8	3	5	1	7	2	4	6
Kessi	2	1	4	3	6	8	6	5
Gilgel Abay	8	1	4	5	2	3	6	7
Gumara	4	5	3	6	2	1	8	7

4.5 Hydro-climatic trend test and change point detection[1]

Trend test

Investigating the presence of trends in hydro-meteorological variables is important for existing and future water resources developments in the Nile basin. The existence of trends in the time series of rainfall, temperature, and streamflow of the UBNRB were evaluated. Daily streamflow data sets based on manual water level measurements for four gauging stations in the UBNRB for the period (1971-2011) were collected from the MWIE. Similarly, daily precipitation data for 15 stations and temperature data for 10 stations were obtained from the ENMA. The areal rainfall for the selected sub-basins (UBNRB, Kessi sub-basin, Gilgel Abay sub-basin and Gumara sub-basin) was calculated using the well-known Thiessen Polygon method from the stations located inside and around the sub-basins. Similarly, the daily, monthly and annual streamflow data from 1971 to 2010 at respective four gauging stations (El Diem, Kessi, Gilgel Abay and Gumara) were used to assess the trends of flow. The selection of study sub-basins and gauging stations was based on availability of data, catchment size (representing small, medium and large) and short missing records. The location of sub-basins, gauging stations, rainfall and temperature stations is shown in Figure 4-10. Streamflow was generated from the staff gauge readings of water level recorded twice a day at (06:00 a.m. and 06:00 p.m.). Rating curve equations were developed and regularly updated from flows measured using current meters three or four times per year at each gauging station.

[1] Based on: Mekonnen, D.F., Duan, Z., Rientjes, T., Disse, M.: Analysis of combined and isolated effects of land-use and land-cover changes and climate change on the upper Blue Nile River basin's streamflow. Hydrology and Earth System Sciences, 22(12), 6187-6207, 2018

The non-parametric Mann-Kendal (MK) test originally proposed by Mann (1945) and later reformulated by Kendall (1975) statistic is chosen to detect trends for rainfall, Tmax, Tmin and streamflow time series data, as it is widely used for water resource planning, design, and management (Yue and Wang, 2004). Its advantage over parametric tests such as t test is that the MK test is more suitable for non-normally distributed and missing data, which are frequently encountered in hydrological time series (Yue et al., 2004). MK test is nonparametric approaches and does not require any assumptions about the distribution of the variables and effective when the sample data are serially independent. The advantage of the nonparametric tests over the parametric tests, such as t-test, is that the nonparametric tests are more suitable for non normally distributed, censored, missing data, which are frequently encountered in hydrological time series (Yue *et al.*, 2004).

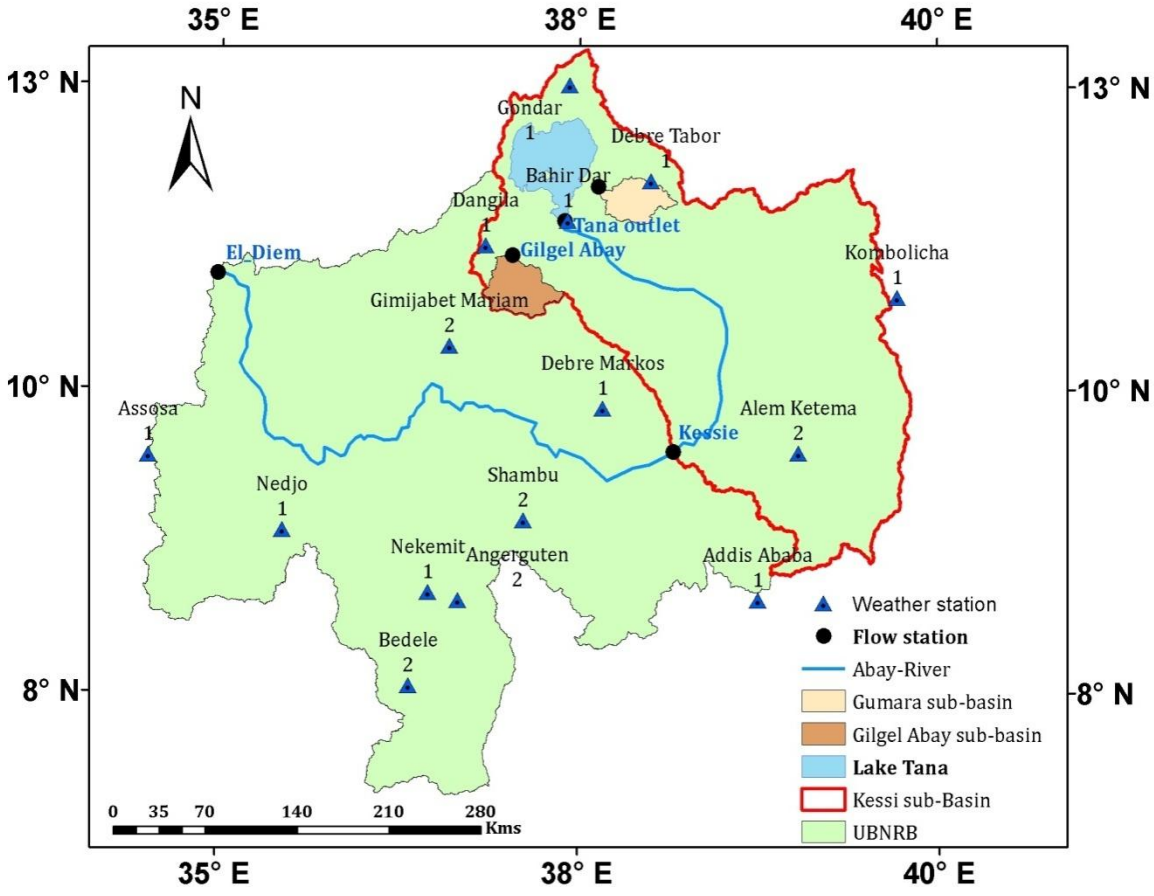

Figure 4-10: Location map of the study area, gauging stations, rainfall and temperature stations. The number (1) in the map is represnting stations, which haverecords of both rainfall and temperature variables and (2) representing the stations, which have rainfall data only.

However, the existence of positive serial correlation in time series data affects the MK test results. If serial correlation exists in time series data, the MK test rejects the null hypothesis of no trend detection more often than specified by the significance level (Von Storch, 1995). Von Storch (1995) proposed a prewhitening technique to limit the influence of serial correlation on the MK test. The effective or equivalent sample size (ESS) method developed by Hamed and Rao (1998) has also been proposed to modify the variance. However, the study by Yue et al. (2002) reported that von Storch's prewhitening is effective only when no trend exists, and the ESS approach's rejection rate after modifying the variance is much higher than the actual (Yue et al., 2004). Yue *et al.* (2002) then proposed trend free prewhitening (TFPW) technique prior to applying the MK trend test in order to minimize its limitation. This study therefore employed TFPW to remove the serial correlation and to detect a trend in time data series with significant serial correlation. Further details can be found in (Yue et al., 2002). All the trend results in this study have been evaluated at the 5% level of significance to ensure the effective exploration of the trend.

MK calculates Kendall's statistics (S), the sum of difference between data points and a measure of associations between two samples (Kendall's tau) to indicate increasing or decreasing trend using eqn.(4-11). Positive values of those parameters indicate a general tendency towards an increasing trend while negative values show a decreasing trend. Furthermore, a two-tailed probability (p-value) was computed and compared with the user defined significance level (in this study 5%) in order to identify the trend of variables. When the calculated p-value is greater than the defined significance level (5%), then it indicates acceptance of null hypothesis (no trend) and the reverse is true.

$$S = \sum_{k=1}^{n-1} \sum_{j=k+1}^{n} sgn(k_j - k_x) \qquad (4\text{-}11)$$

If S is a positive number, it indicates, observations obtained later in time tend to be larger than observations made earlier. If S is a negative number, then observations made later in time tend to be smaller than observations made earlier. Where n is the data record length and k_j and k_x are data sequential values and the function sgn(x) the sign of all n (n - 1)/2 possible differences of K_j - K_x where $j > x$ is defined as

$$sgn(x) = \begin{cases} 1, & if\ x > 0 \\ 0, & if\ x = 0 \\ -1, & if\ x < 0 \end{cases} \qquad (4\text{-}12)$$

(Mann, 1945) and (Kendall, 1975) have documented that when n > 8, the statistic S is approximately normally distributed with the mean and the variance as follows:

The mean of S is E(s) =0, and the variance δ^2

$$\delta^2 = \frac{\{n(n-1)(2n+5) - \sum_{j=1}^{p} t_j\,(t_j-1)(2t_j+5)\}}{18} \qquad (4\text{-}13)$$

Where p is the number of tied groups in the data set and t_j is the number of data points in the j^{th} tied group. The statistic S is approximately normally distributed provided that the following Z transformation is employed

$$Z = \begin{cases} \frac{s-1}{\delta}, & if\ S > 0 \\ 0, & if\ S = 0 \\ \frac{s+1}{\delta}, & if\ S < 0 \end{cases} \qquad (4\text{-}14)$$

A positive (negative) value of Z indicates that the data tend to increase (decrease) with time. If the computed value of $|Z| > Z_{1\text{-}}(\alpha/2)$, the null hypothesis ($H_0$) is rejected at α level of significance in a two-sided test. In this analysis, the null hypothesis was tested at 95% confidence level.

The statistic S is closely related to Kendall's τ as given by

$$\tau = \frac{S}{D} \qquad (4\text{-}15)$$

Where

$$D = \left[\frac{1}{2}n(n-1) - \frac{1}{2}\sum_{j=1}^{p} t_j(t_j-1)\right]^{1/2}\left[\frac{1}{2}n(n-1)\right]^{1/2} \qquad (4\text{-}16)$$

Time series homogeneity or change-point detection (Pettitt's test)

The Pettitt test is a non-parametric test that requires no assumption about the distribution of the data and is used to identify if there is a change point in the data series (Pettitt, 1979). The Pettittt test has been widely applied to detect changes in the observed climatic as well as observed hydrological time series (Salarijazi et al., 2012). This method detects one unknown change point by considering a sequence of random variables X_t=X_1, X_2, …,X_N, X_{N+1},..., X_T that may have a change point at *N*. If X_t for $t = 1, 2,..., N$ has a common distribution function $F_1(x)$ and X_t for $t = N + 1, \ldots, T$ has a common distribution function $F_2(x)$, where, $F_1(x) \neq F_2(x)$. The null hypothesis (H_0, no change, or $N = T$) is tested against the alternative hypothesis (H_a, change, or $1 < N < T$) using the non-parametric statistic: The non-parametric statistic is computed as follows:

The first step is to compute X_N statistic using eqn.(4-17)- eqn.(4-20).

$$X_N = max|U_{N,T}| \tag{4-17}$$

The next step is to define the statistical change point test (SCP) as follows:

$$U_{N,T} = \sum_{i=1}^{N} \sum_{j=N+1}^{T} sgn(x_i - x_j) \tag{4-18}$$

The change-point of the series is located at X_N, if the statistic is significant. X_{N+} for downward shift and K_{N-} for upward shift (Kahya and Kalaycı, 2004). The confidence level associated with K_{N+} or K_{N-} is determined approximately by:

$$p \cong 2 \exp\left(\frac{-6{X_T}^2}{T^3 + T^2}\right) \tag{4-19}$$

When *p* is smaller than the specific significance level, e.g. 0.05 in this study, the null hypothesis is rejected. The time, *N*, when X_N occurs is the change point time. If a significant change point exists, the time series is divided into two parts at the location of the change point, and the approximate significance probability for the change point is 1– *p*.
OR
When $U_{N,T}$ attains maximum value of *K* in a series, then a change point will occur in the series. The critical value is obtained by:

$$K_\alpha = \left[-n\, a(T^3 + T^2)/6\right]^{1/2} \tag{4-20}$$

Where *T* is number of observations and α is level of significance, which determines the critical value.

Sen's slope estimator
The trend magnitude is estimated using a non-parametric median-based slope estimator proposed by (Sen, 1968), as it is not greatly affected by gross data errors or outliers and can be computed when data are missing. The slope estimation is given by eqn. (4-21).

$$\beta = \text{Median}\left[\frac{X_j - X_k}{j-k}\right] \text{ for all } k < j, \tag{4-21}$$

Where xj and xk are the sequential data values and n is the number of the recorded data. $1 < k < j < n$, and is considered as the median of all possible combinations of pairs for the whole data set.
A positive value of β indicates an upward (increasing) trend, and a negative value indicates a downward (decreasing) trend in the time series. All MK trend tests, Pettittt change-point detections, and Sen's slope analyses were conducted using the XLSTAT add-in tool from Excel (https://www.xlstat.com).

4.6 Results and discussion of trend and change point detection analysis

4.6.1 Rainfall

The summary results of the MK trend test for the rainfall recorded at the 15 selected stations located in and around the UBNRB revealed mixed trends (increasing, decreasing, and no change) as shown in the appendices from Appendix 3 to Appendix 5. For daily time series, the computed probability values (p-values) for seven stations was greater, although for eight stations it was less, than the selected significance level (α = 5 %). This means that no statistically significant trend existed in seven stations, but a monotonic trend occurred in the remaining eight. Positive trends developed only at six stations, four of which were concentrated in the northern and central highlands (Bahir Dar, Dangila, Debre Markos, and Gimijabet). The other two stations, Assosa and Angergutten, are located in the southwestern and southern lowlands. The remained two stations, Alem Ketema and Nedjo, which are located in the east and south-west of the UBNRB, respectively, showed a decreasing trend, see Figure 4-10. On a monthly basis, the MK trend test result showed that no trend existed in 11 stations, while statistically non-significant increasing trends exist in 3 stations (Dangila, Gimijabet, and Shambu) and a decreasing trend exists in Alem Ketema station. On an annual timescale, MK trend test could not find any trend in 11 stations, but did exhibit a trend in 4 stations. The annual total rainfall of Dangila and Shambu stations showed statistically non-significant increasing trend, while Gimijabet and Alem Ketema showed statistically significant positive trends and non-significant decreasing trends, respectively.

The results from Pettitt test reveal that for the majority of the stations statistically significant upward shift have been detected for daily rainfall (Appendix 3), 11 stations showed upward shift, 3 stations downward shift and 1 station does not exhibit any change. On monthly total rainfall (Appendix 4), none of the 15 stations has shown change points, whereas, for the annual total rainfall (Appendix 5), 3 stations exhibit up ward shift, 1 station down ward shift and 11 stations did not exhibit any shift during the study period. The change points occurred for different stations are different.

The basin and sub-basin wide rainfall trend and change point detection analysis was again carried out on daily, monthly, seasonal, and annual timescales using the MK and Pettittt tests. We applied a widely used spatial interpolation technique, the Thiessen polygon method, to calculate basin and sub-basin wide rainfall series from station data. A summary results of investigated rainfall trend and change point tests for 4 sub-basins including UBNRB are provided in Table 4-7, Figure 4-11 and Figure 4-12. The MK test showed statistically significant increasing trends for annual, monthly, and long rainy-season rainfall series of UBNRB, whereas no trend for daily, short rainy and dry season rainfall series appeared. In contrast, Kessi sub-basin depicted no significant trends for daily, monthly, annual, and seasonal rainfall. For Gilgel Abay sub-basin, MK test result showed increasing trend for monthly and short rainy season rainfall, while no trend for daily, annual, long and short rainy season rainfall. Meanwhile, the MK test results indicate mixed trends for Gumara sub-basin. On daily, monthly, annual, and long rainy season rainfall, MK test could not find any trend for Gumara sub-basin. However, MK test indicate significant decreasing for dry season rainfall and significant increasing trend for short

rainy season rainfall at Gumara sub-basin. The results from the Pettit test showed daily rainfall over UBNRB, Kessi and Gilgel Abay sub-basins exhibited an upward shift, occurred around 1988, 1975 and 1983, respectively. While the daily rainfall at Gumara showed downward shift that occurred around 2001. However, the Pettittt test could not detect any jump point for monthly, annual and seasonal rainfall series in all sub-basins except for Gumara sub-basin. For Gumara sub-basin, Pettittt test indicate the presence of strong downward shift for long rainy and dry season rainfall.

Table 4-7: Mann-Kendal trend test and statistical summary of areal daily, monthly, annual and seasonal rainfall of the four sub-basins; (+) sign indicate upward shift and (-) sign indicate downward shift, numbers in bold designate p value for statistically significant trend and change points

Time period	Sub-basin	Kendall's tau	Sen's slope	MK test p-value	Pettittt test (change time)	Pettitt test (p-value)
Daily	UBNRB	0.000	5.783E-5	0.387	1998(+)	**0.001**
	Kessi	0.006	5.146E-5	0.511	1975(+)	**0.000**
	Gilgel Abay	0.009	1.123E-4	0.150	1983 (+)	**<0.0001**
	Gumara	-0.006	7.189E-5	0.983	2001 (-)	**0.014**
Monthly	UBNRB	0.014	0.009	**0.010**	1988	0.98
	Kessi	-0.002	-7.377E-4	0.603	1998	0.99
	Gilgel Abay	0.029	0.005	**< 0.0001**	1988	0.71
	Gumara	0.015	0.002	0.080	1992	0.92
Yearly	UBNRB	0.126	1.886	**0.006**	1987	0.06
	Kessi	-0.054	-0.629	0.123	2000	0.5
	Gilgel Abay	0.033	1.188	0.342	1987	0.9
	Gumara	-0.103	-2.819	0.129	1980	0.08
Long rainy-season	UBNRB	0.105	1.364	**0.010**	1987	0.21
	Kessi	0.021	0.102	0.483	1998	0.98
	Gilgel Abay	0.010	0.193	0.851	1976	0.74
	Gumara	-0.126	-2.4	0.095	1981(-)	**0.03**
Dry season	UBNRB	0.036	0.169	0.527	1996	0.32
	Kessi	-0.031	-0.23	0.468	1983	0.83
	Gilgel abay	-0.031	-0.332	0.535	2000	0.69
	Gumara	-0.208	-1.676	**< 0.0001**	1982 (-)	**0.04**
Short rainy season	UBNRB	0.010	0.068	0.822	1997	0.9
	Kessi	-0.095	-0.543	0.114	1998	0.14
	Gilgel abay	0.108	1.464	**0.017**	1990	0.28
	Gumara	0.115	0.732	**0.001**	1992	0.56

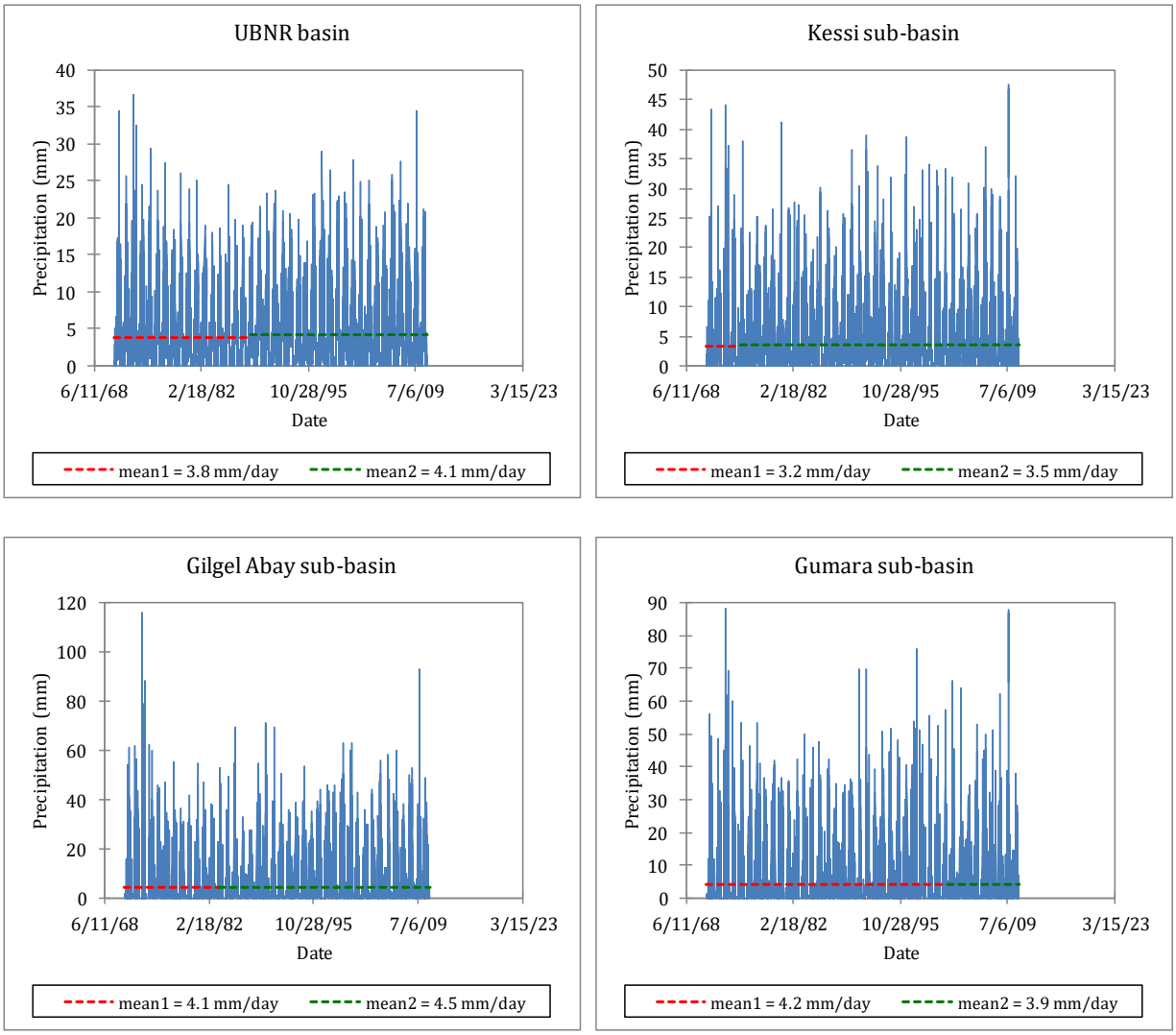

Figure 4-11: The Pettitt homogeneity test for the daily areal precipitation of the four sub-basins. The dash lines represented by mean1 and mean2 are the mean of the time series before and after the change point respectively.

The results of trend analysis in rainfall found in this work are in agreement with past research works in the area (e.g.(Gebremicael et al., 2013; Tekleab et al., 2013)). Tekleab et al. (2013) analyzed the result of MK test for the 13 rainfall stations in UBNRB and reported no significant trend existed both at monthly and seasonal scale for the majority of investigated climate stations. Gebremicael et al. (2013) reported no significant trend existed for the annual rainfall at eight out of nine climate stations during the 1973–2005 periods. Furthermore, (Conway, 2000; Gebremicael et al., 2013; Tesemma et al., 2010) conducted trend analyses of basin-wide rainfall and reported that no significant change in annual and seasonal rainfall series across the UBNRB exists, which contradicts the results of this study. This disagreement could be due to the number of stations and their spatial distribution across the basin, period of the analysis, approach used to calculate basin-wide rainfall from gauging stations, and data sources. Tesemma et al. (2010) used monthly rainfall data downloaded from Global Historical Climatology Network (GHCN)

database and 10-day rainfall data for the 10 selected stations obtained from the National Meteorological Service Agency of Ethiopia from 1963 to 2003. Conway (2000) also constructed basin-wide annual rainfall in the UBNRB for the 1900–1998 periods from the mean of 11 gauges. Furthermore, Conway (2000) employed simple linear regressions technique to detect trends in annual rainfall series without removing the serial autocorrelation effect. Gebremicael et al. (2013) used only nine stations from the 1970–2005 periods. However, in this study, we used daily-observed rainfall data from 15 stations collected from ENMA from 1971 to 2010. The stations are more or less evenly distributed over the UBNRB.

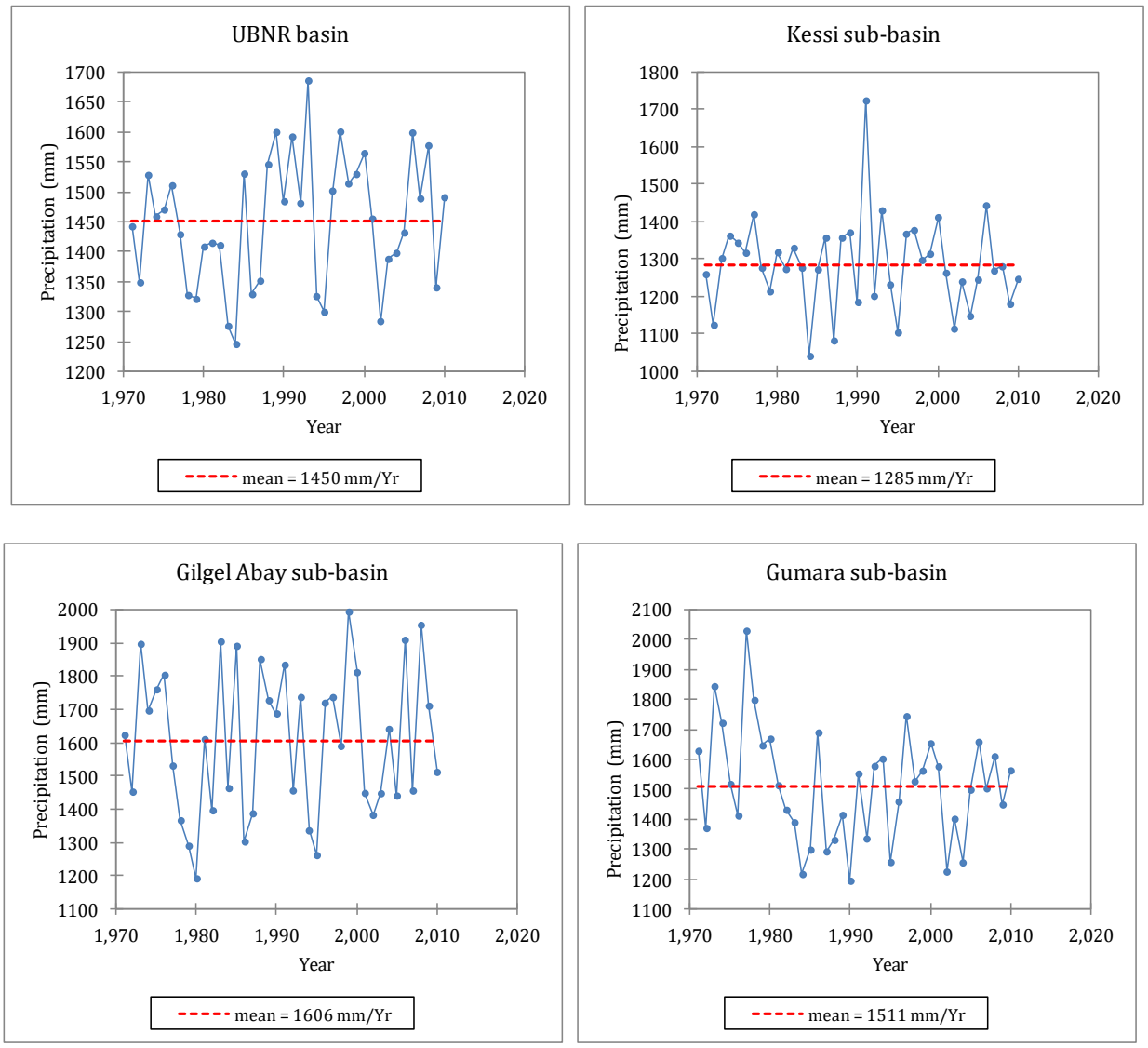

Figure 4-12: The Pettitt homogeneity test for the annual areal precipitation of the four sub-basins. The dash lines represented by mean1 and mean2 are the mean of the time series before and after the change point respectively.

4.6.2 Temperature

Ten meteorological stations were selected for analyzing the trends of Tmax and Tmin. Appendix 6, Appendix 7 and Appendix 8 summarized the MK and Pettittt test results for maximum temperature while Appendix 9, Appendix 10 and Appendix 11 presented the results for minimum temperature. The MK test result showed that maximum temperature exhibited increasing trend in all stations except Assosa station, which showed no change for daily, monthly and annual time series. For the minimum temperature, the MK test also showed increasing trend for all stations except Assosa and Debre Tabor stations. Assosa station did not exhibit any trend for daily, monthly and annual time series while Debre Tabor showed no change for daily and monthly time series.

Detection of change point for temperature time series results from Pettitt test reveal that for the majority of the stations statistically significant increasing shift have been detected Appendix 6 to Appendix 11. The Pettitt test results indicate that daily and mean annual maximum temperature exhibited upward shift at all stations except Dangila. On monthly time series maximum temperature, Assosa and Debre Markos stations did not exhibit any change, while Dangila showed downward shift. The Pettitt test showed upward shift for daily minimum temperature at all stations except Debre Tabor, which showed downward shift. For the mean monthly minimum temperature, the Pettittt test showed no change for Debre Tabor and decreasing trend for Nedjo station while increasing trend for the remaining eight stations. For the mean annual minimum temperature data, Nedjo and Assosa stations showed no change while Debre tabor station exhibited downward shift and the remained seven stations experienced upward shift respectively. It can be observed that the time for change points is quite different. It is apparent that the change point for those stations occurred around early 1980s and 1990s and mid 1980s and 1990s.

Table 4-8: Summary of MK trend test and Pettitt change point test for Tmax and Tmin for the four sub-basins; (+) sign indicate upward shift and (-) sign indicate downward shift, numbers in bold designate p value for statistically significant trend and change points.

		maximum temperature				minimum temperature			
	Stations	MK test p-value	Sen's slope	Pettitt Change time	Pettitt p-value	MK test p-value	Sen's slope	Pettitt change time	Pettitt p-value
Daily	El Diem	**< 0.0001**	3.80E-5	2001(+)	**<0.0001**	**< 0.0001**	9.399E-5	1980 (+)	**<0.0001**
	Kessi	**< 0.0001**	6.58E-5	1993 (+)	**<0.0001**	**< 0.0001**	1.020E-4	1987 (+)	**<0.0001**
	Gilgel Abay	**< 0.0001**	-1.4E-4	1988(-)	**<0.0001**	**< 0.0001**	2.022E-4	1979 (+)	**<0.0001**
	Gumara	**< 0.0001**	8.56E-5	1993(+)	**<0.0001**	0.376	-2.57E-6	1979 (+)	**<0.0001**
Monthly	El Diem	0.086	0.014	2001	0.34	**< 0.0001**	0.003	1980 (+)	**<0.0001**
	Kessi	**0.000**	0.025	1993 (+)	**0.000**	**< 0.0001**	0.003	1987 (+)	**<0.0001**
	Gilgel Abay	**< 0.0001**	-0.026	1988(-)	**<0.0001**	**< 0.0001**	0.006	1979 (+)	**<0.0001**
	Gumara	**0.000**	0.037	1993(+)	**<0.0001**	0.653	-1.94E-4	1977	0.24
Annually	El Diem	**0.005**	0.014	2001(+)	**0.009**	**< 0.0001**	0.03	1979 (+)	**0.00**
	Kessi	**< 0.0001**	0.025	1993 (+)	**<0.0001**	**< 0.0001**	0.034	1986 (+)	**<0.0001**
	Gilgel Abay	0.130	-0.026	1988 (-)	**<0.0001**	**< 0.0001**	0.057	1979 (+)	**0.001**
	Gumara	**< 0.0001**	0.037	1993 (+)	**<0.0001**	0.377	-0.003	1998	0.17

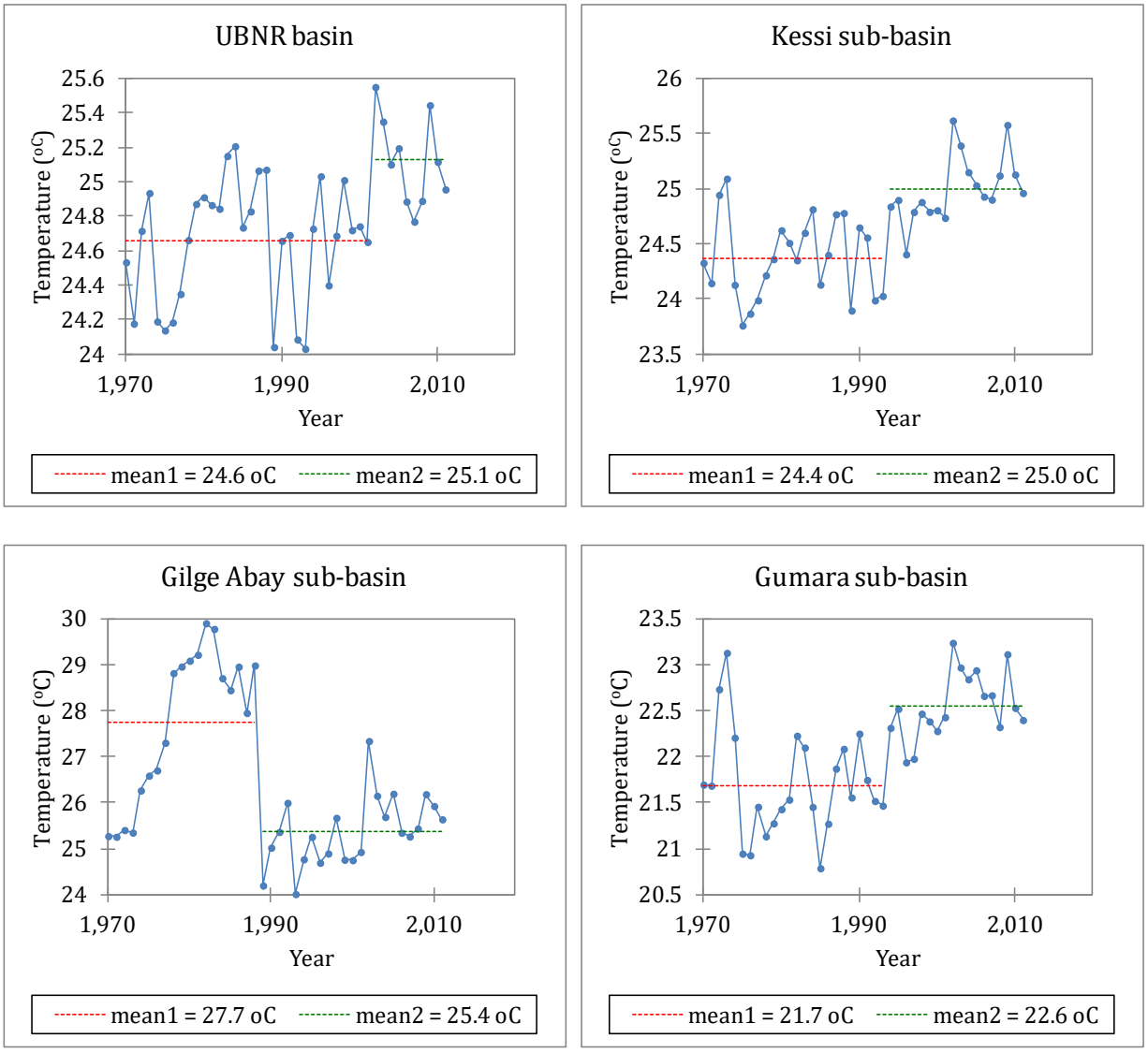

Figure 4-13: Mean annual time series plots of Tmax for the change of time. The dash lines represented by mean1 and mean2 are the mean of the time series before and after the change point respectively.

At basin and sub-basin scale, the results of MK test for the temperature showed that statistically significant increasing trends were observed in minimum and maximum temperature for the UBNRB and other three sub-basins (Table 4-8). The Pettitt test results showed that UBNRB exhibited upward shift on daily and annual average maximum temperature. Kessi and Gumara sub-basins experienced upward shift on daily, mean monthly and mean annual maximum temperature. Gilgel Abay sub-basin, major tributaries of Lake Tana exhibited downward shift on daily, mean monthly and mean annual maximum temperature. Similarly, the Pettitt test detected upward shift for the daily, mean monthly and mean annual minimum temperature over the UBNRB, Kessi and Gilgel Abay sub basins. Daily minimum temperature at Gumara sub-basin

also showed upward shift, whereas mean monthly and mean annual minimum temperature of Gumara sub-basin showed downward shift.

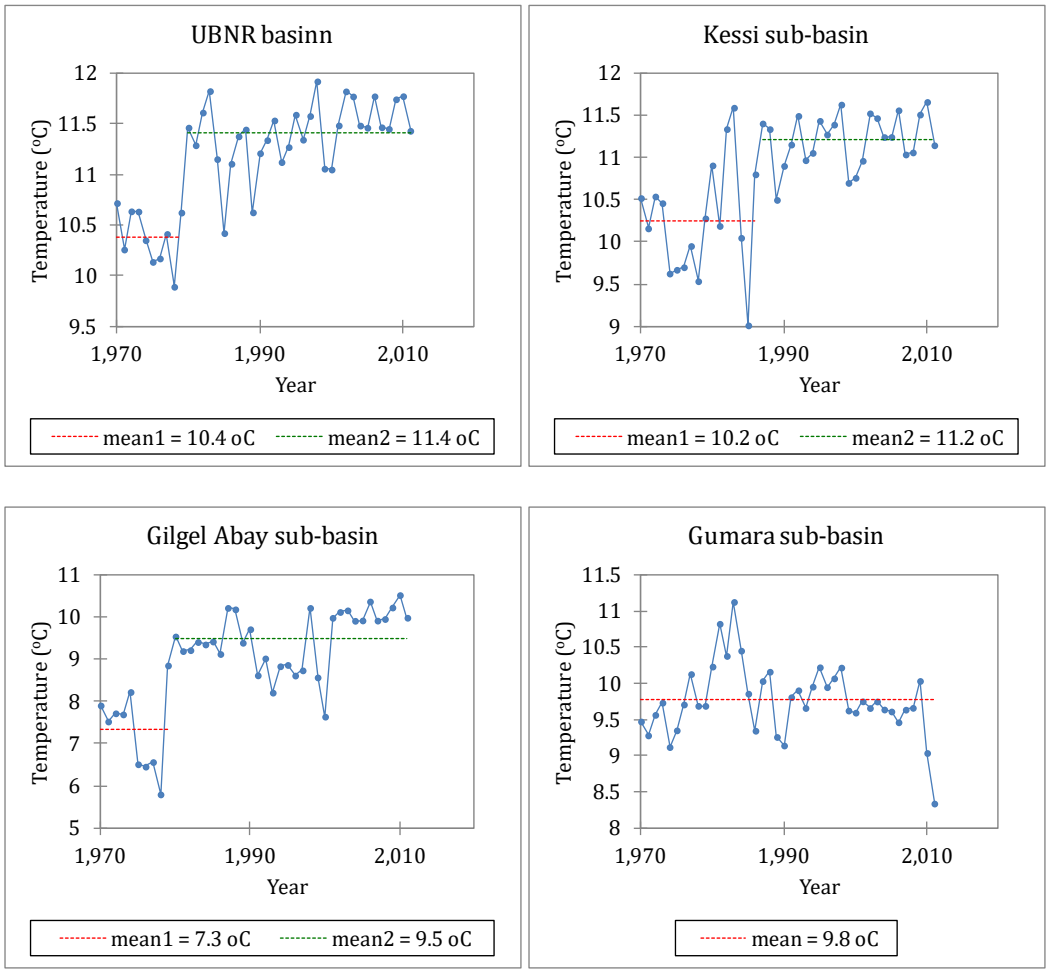

Figure 4-14: Mean annual time series plots of Tmin for the change of time. The dash lines represented by mean1 and mean2 are the mean of the time series before and after the change point respectively.

Figure 4-15 illustrates the mean annual temperature trend magnitude for the selected sub basins and UBNRB. The maximum temperature has increased about 0.14, 0.24, and 0.3 ^{o}C per decade for UBNRB, Kessi and Gumara sub-basins respectively. Similarly, the mean annual minimum temperature has increased by 0.3, 0.4, and 0.7 ^{o}C respectively for UBNRB, Kessi and Gumara sub-basins. The mean annual maximum for Gilgel Abay sub-basin and minimum temperature for Gumara sub-basin have decreased by 0.5 and 0.1 ^{o}C per decade respectively. The slope magnitudes for the change of mean annual Tmax and Tmin using standard linear regression (Figure 4-15) are similar with the corresponding magnitudes of Sen's slope (Table 4-8). The good agreement of the results from MK trend test and Pettitt change point detection indicates the robustness of the methods applied.

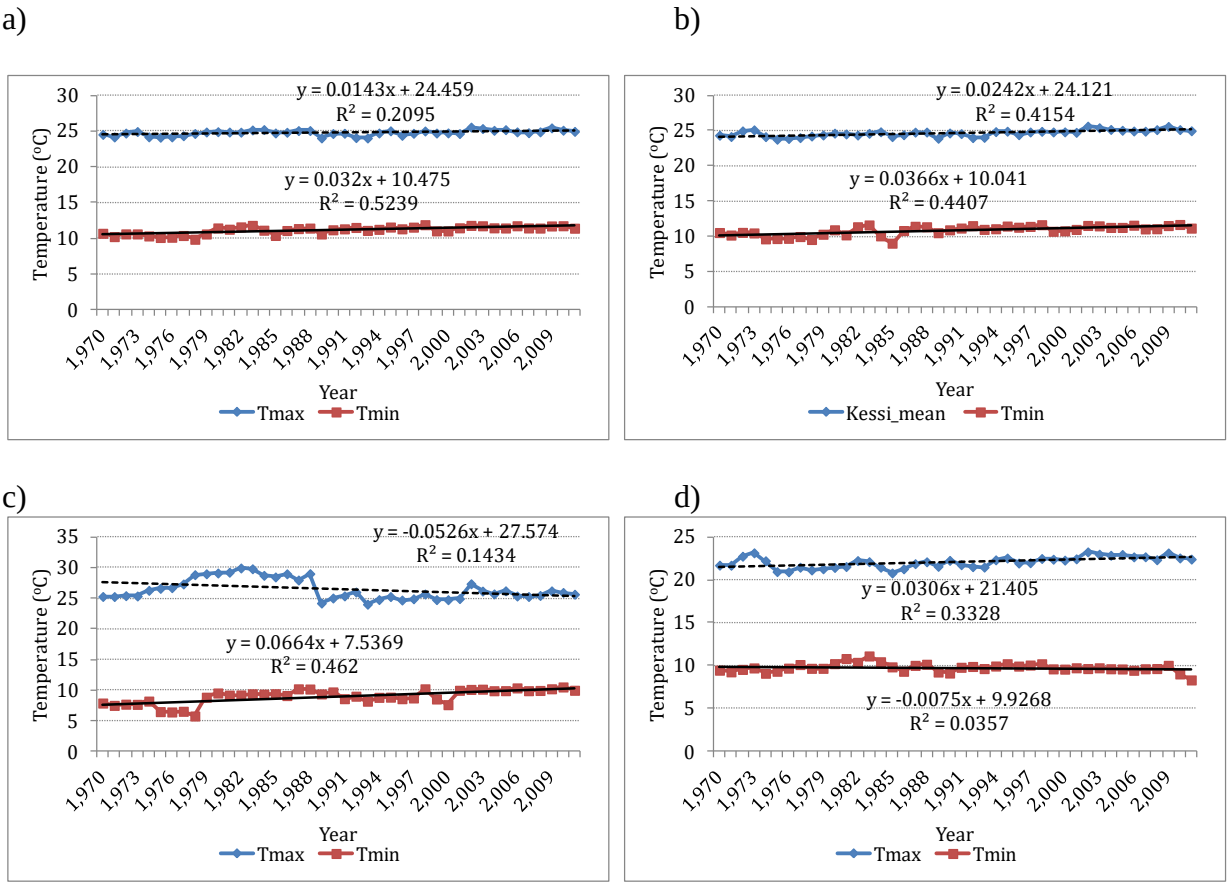

Figure 4-15: Time series plots of mean annual Tmax and Tmin for (a) UBNR basin, (b) Kessi, (c) Gilgel Abay, and (d) Gumara sub-basins.

4.6.3 Streamflow

The trend and change point detection analysis of daily, monthly, seasonal and annual streamflow at the four flow-gauging stations were computed by the MK and Pettitt tests. Table 4-9 and Table 4-10 summarized the results of MK trend test and Pettitt test for change point detection. The change point detection for the selected sub-basins are illustrated in Figure 4-16 and Figure 4-17 for daily and mean annual streamflow respectively. The MK test's result for daily, monthly, annual, and seasonal (long and short rainy season) streamflow time series showed a positive trend, the magnitude of which is statistically significant in all flow gauging stations except Gilgel Abay. For the Gilgel Abay station, MK test showed no change for monthly and seasonal (long rainy, dry and short rainy season) streamflow while decreasing trend for daily and mean annual streamflow. For the dry season, streamflow at El Diem and Kessie stations showed statistically significant increasing trend whereas no changes were observed at Gumara and Gilgel Abay stations.

The Pettitt test also detected upward shift for daily, annual, and long rainy season streamflow at El Diem, Kessi and Gumara stations. Exceptionally, Gilgel Abay exhibited downward shift for the daily time series streamflow and no change point observed for mean monthly, annual and

seasonal time series streamflow. For the monthly time series streamflow, Pettitt test detects increasing trends at Kessi and Gumara flow stations while no change at El Diem flow stations. For the dry season streamflow, the Pettitt test could not detect any change point at El Diem, Gilgel Abay and Gumara flow stations but Kessi flow station exhibited upward shift. The change points for mean annual stream flows at El Diem, Kessi and Gumara gauging stations occurred around 1995, 1990 and 1987, respectively. However, the mean annual flow at Gilgel Abay showed downward shift that occurred around 2000, though it is not statistically significant at 5% level.

The result obtained from the MK test agrees well with the findings in Gebremicael et al. (2013), who reported an increasing trend in the observed annual, short, and long rain seasons' streamflow at the El Diem and Kessi gauging stations, but our results disagree with findings for dry-season streamflow. Furthermore, the increasing trend of long rainy-season streamflow at El Diem agrees well with the result of (Tesemma et al., 2010), but it disagrees with the results of short rainy season and annual flows. (Tesemma et al., 2010) reported statistically significant increasing streamflow during the long rainy season at El Diem station while short rainy season and the annual flows are constant for the 1964–2003 periods. They also reported that dry season streamflow shows a significant decreasing trend at El Diem. This disagreement is likely attributable to the difference in analysis period, as can be seen from Figure 4-18, the last 7 years, 2004–2010, had relatively higher streamflow records. However, this study has a good agreement with their result for Kessi station. They reported significant increasing trend of long-rainy, short-rainy season and annual streamflow but no change for the dry season streamflow at Kessi station.

In general, the MK trend test and Pettitt change point detection have a good agreement in most of the cases showing the robustness of the methods and approaches applied. Furthermore, the magnitudes of Sen's slope and slope from standard linear regression are comparable in most cases. The slope magnitude difference of Sen's slope and linear regression slope (Figure 4-18) for the annual rainfall and streamflow could be due to the outliers, as Sen's slope does not affected by them. Although the magnitudes of mean annual streamflow at El Diem and annual total rainfall of UBNRB are equivalent, the magnitude of slope for streamflow (10.5 m^3s^{-1}) is much greater than it is for rainfall (1.8 $mmyr^{-1}$), see (Figure 4-18). Furthermore, the MK trend test results indicated that the annual total rainfall of UBNRB, Kessi and Gumara sub-basins did not reveal changes while the annual streamflow at El Diem, Kessi and Gumara increased significantly from 1971 to 2010. The Pettit test results for the change of point also display different times which are not consistent for both rainfall and streamflow data series. Pettitt's test shows that there was a change point for annual streamflow series around the year 1995, 1990 and 1987 at El Diem, Kessi and Gumara stations respectively while there was no change point identified for the annual precipitation series during the study period over the corresponding sub-basins.

This indicates that the relationship between the annual precipitation and streamflow presented a non-stationary state. These heterogeneous results may suggest that the degree of human interventions and natural causes, which can be attributed to the change in streamflow are different across the examined sub-basins. The responses of streamflow to the changes in rainfall could be associated with evapotranspiration and could be attributable to the combined effect of LULC change, climate change, the infiltration rate due to changing soil properties, rainfall

intensity, and rainfall extreme events. Moreover, different results for the investigated sub-basins might be related to difference in contributory factors both human interferences and physiographic characteristics like climate, vegetation, soil, geologic and topography lead to differences in responsive characteristics of the catchments. For instance, for the Gilgel Abay sub-basin, the significant decreasing trends for the annual streamflow could be related to water abstraction for irrigation and expansion of Eucalyptus plantation that extracts significant amount of ground water. Therefore, there is a need for more research linking land use change detection using remote sensing and statistical analysis of hydro-meteorological variables as it is crucial for proper utilization of the limited water resources in the region. Hence, in this dissertation quantifying the effects of LULC and climate change using hydrological modeling is carried out and discussed in (Chapter 5).

Table 4-9: Mann-Kendall trend test and statistical summary of daily, monthly and annual streamflow of the 4 sub-basins before and after TFPW; (+) sign indicate upward shift and (-) sign indicate downward shift, numbers in bold designate p value for statistically significant trend and change points

Time scale	Station	Kendall's tau	MK test p-value	Sen's slope	Pettitt test change time	Pettitt test p-value
Daily	El Diem	0.068	**< 0.0001**	0.013	1987 (+)	**<0.0001**
	Kessi	0.188	**< 0.0001**	0.013	1996 (+)	**<0.0001**
	Gilgel Abay	-0.016	**0.032**	1.269E-4	2005 (-)	**<0.0001**
	Gumara	0.101	**< 0.0001**	1.664E-4	1992 (+)	**<0.0001**
Monthly	El Diem	0.066	< 0.0001	0.377	1987	0.13
	Kessi	0.196	**< 0.0001**	0.422	1996 (+)	**<0.0001**
	Gilgel Abay	-0.009	0.192	-0.001	2005	0.41
	Gumara	0.111	**< 0.0001**	0.006	1991 (+)	**0.000**
Annual	El Diem	0.290	**< 0.0001**	9.548	1995 (+)	**0.03**
	Kessi	0.413	**< 0.0001**	9.623	1990 (+)	**<0.0001**
	Gilgel Abay	-0.105	0.348	-0.101	2000	0.34
	Gumara	0.336	**0.002**	0.374	1987 (+)	**0.003**

The results of this study in general are characterized by statistically significant increasing trends in maximum and minimum temperatures, no significant changes in mean annual or mean seasonal precipitation and both statistically significant increasing and decreasing streamflow trends in daily, monthly, annual and seasonal streamflow. From the climate variables, the minimum temperature showed more significant increase than the maximum and mean temperatures (Figure 4-15). The results from present study are in agreement with previous study in the basin done by Tekleab *et al.* (2013), who reported increasing trends of temperature and no statistically significant trends in mean annual and seasonal rainfall across the examined stations. For the hydrological variables in the Koga, Rib, Jedeb and Chemoga catchments, they reported no significant changes were seen on mean annual, seasonal and extreme flows. In contrary in the El Diem, Gumara and Neshi catchments, the annual and main rainy season mean flows exhibit significant increasing trends. However, the small rainy season mean flow show significant decreasing trend in Gilgel Abay and significant increasing trends in Gumara and Guder catchment.

Table 4-10: Mann-Kendall trend test and statistical summary of sesonal flow of the 4 sub-basins before and after TFPW; (+) sign indicate upward shift and (-) sign indicate downward shift, numbers in bold designate p value for statistically significant trend and change points

Time scale	Stations	Kendall's tau	MK test p-value	Sen's slope	Pettitt test change time	Pettitt test p-value
Long rainy season	El Diem	0.27	< **0.0001**	20.3	1995	0.06
	Kessi	0.34	< **0.0001**	18.6	1990 (+)	<**0.0001**
	Gilgel Abay	-0.20	0.07	-0.5	2001	0.29
	Gumara	0.34	**0.00**	1.0	1987 (+)	**0.01**
Dry season	El Diem	0.318	**0.004**	3.593	1985 (+)	**0.01**
	Kessi	0.623	< **0.0001**	4.639	1995 (+)	<**0.0001**
	Gilgel Abay	-0.018	0.880	-0.002	2005	0.3
	Gumara	0.485	< **0.0001**	0.048	1991 (+)	<**0.0001**
Short rainy season	El Diem	0.138	**0.000**	4.832	1995	0.06
	Kessi	0.174	**0.006**	2.202	1991 (+)	**0.019**
	Gilgel Abay	-0.008	**0.916**	-0.014	2000	0.85
	Gumara	0.072	**0.318**	0.047	1991	0.48

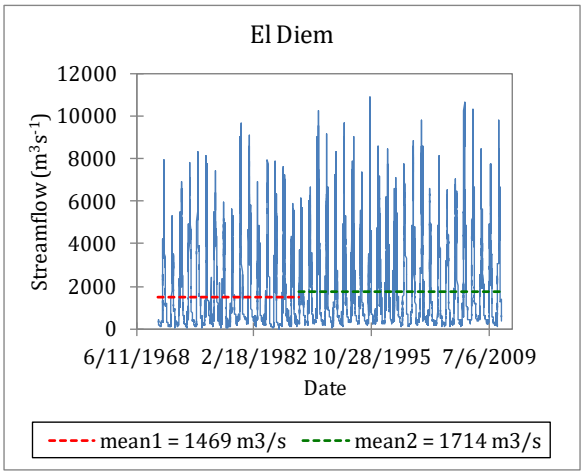

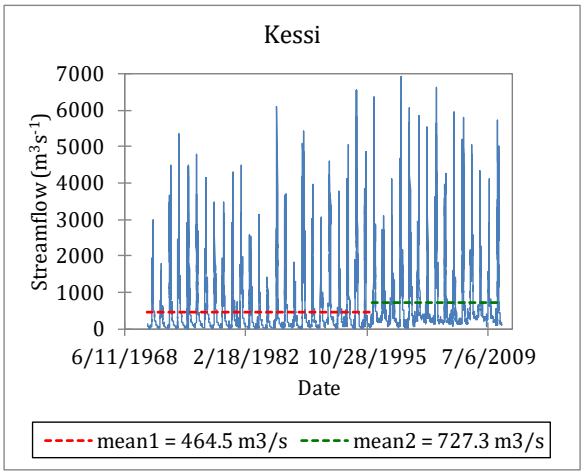

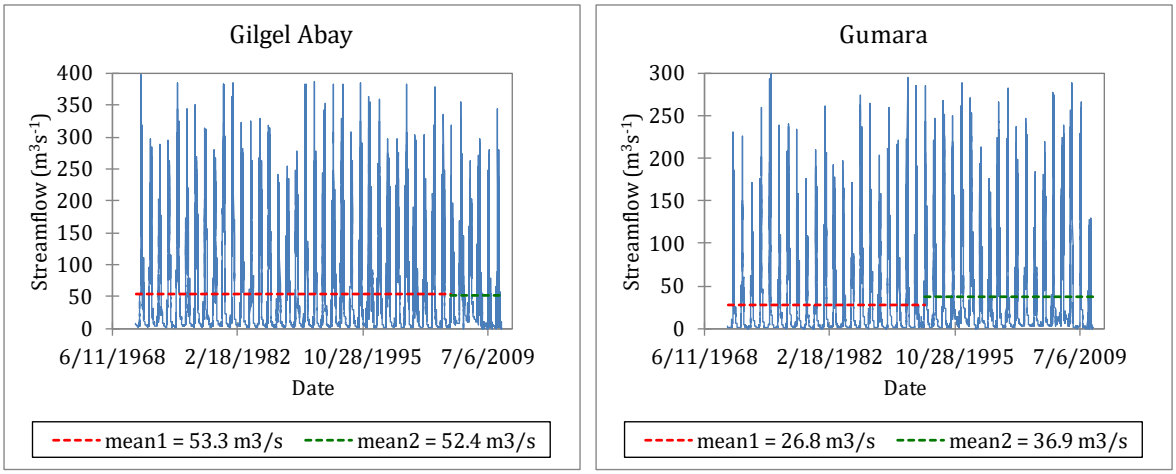

Figure 4-16: The Pettitt homogeneity test for the daily streamflows of the four sub-basins. The dash lines represented by mean1 and mean2 are the mean of the time series before and after the change point respectively.

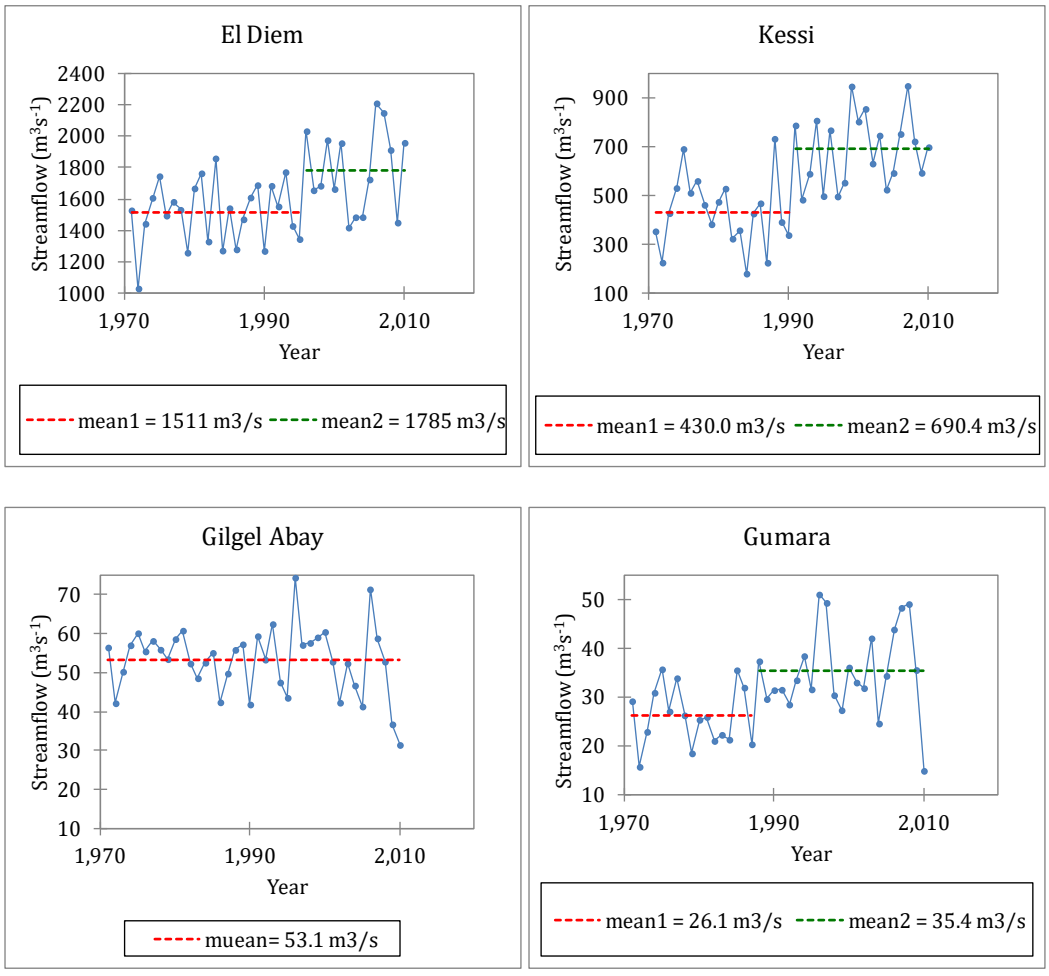

Figure 4-17: The Pettitt homogeneity test for the mean annual streamflows of the four sub-basins.

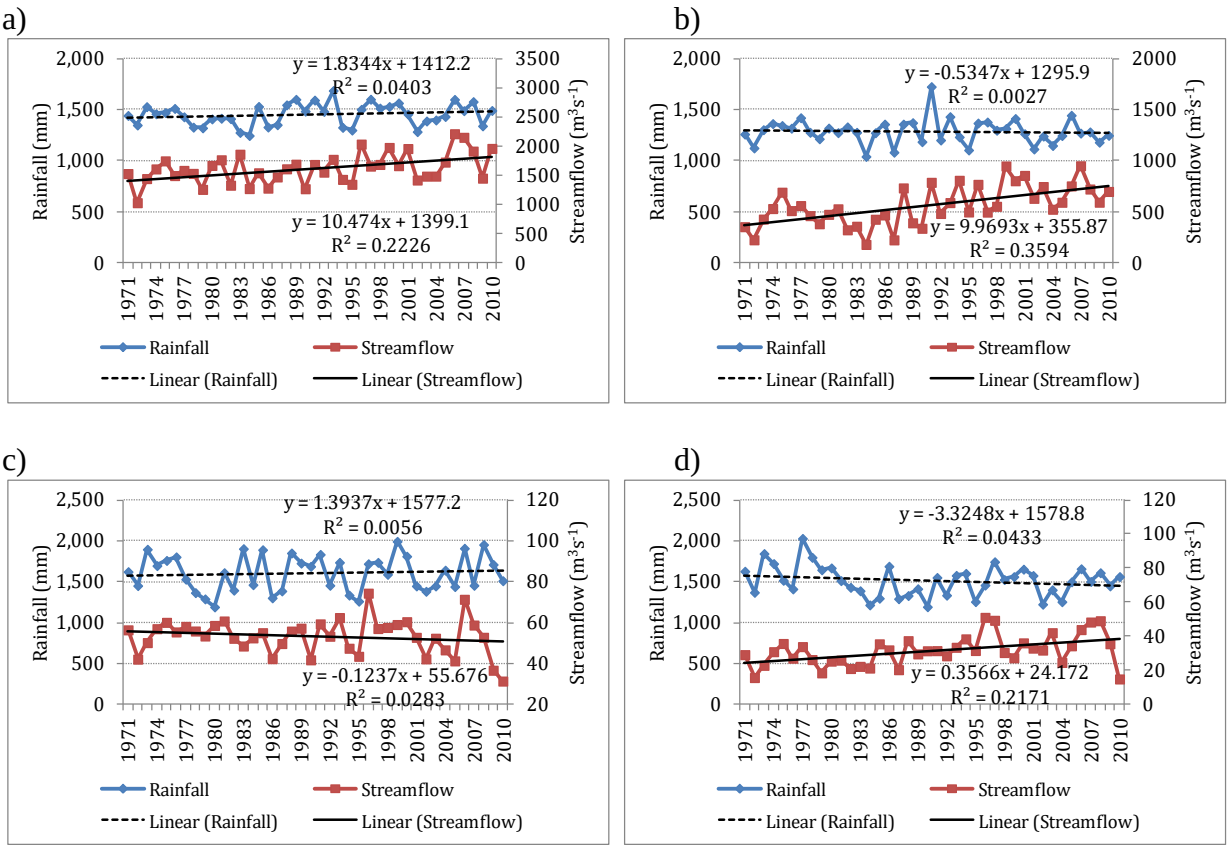

Figure 4-18: Linear trends and mean annual time series plots of rainfall and streamflow for a) El Diem b) Kessi, c) Gilgel Abay, d) Gumara sub-basins

.

Chapter 5 Hydrological responses of the streamflow of upper Blue Nile River to the changes in land use/land cover and climate[2]

5.1 SWAT hydrological model

5.1.1 Basic concepts of the SWAT Model

The Soil and Water Assessment Tool (SWAT) is an open-source-code, semi-distributed model with a large and growing number of model applications in a variety of studies ranging from catchment to continental scales (Allen *et al.*, 1998; Arnold *et al.*, 2012; Neitsch *et al.*, 2002). It enables the impact of LULC change and climate change on water resources to be evaluated in a basin with varying soil, land use, and management practices over a set period of time (Arnold *et al.*, 2012).

In SWAT, the watershed is divided into multiple sub-basins, which are further subdivided into hydrological response units (HRUs) consisting of homogeneous land use management, slope, and soil characteristics (Arnold *et al.*, 1998; Arnold *et al.*, 2012). The descritization method employed by SWAT enables the model to simulate catchment processes in detail and to understand the response of unique HRUs to hydrological processes. HRUs are the smallest units of the watershed in which relevant hydrologic components and sediment yield can be estimated. The hydrological processes involved in the water balance include: precipitation, evaporation and transpiration, Revap from shallow aquifer, surface runoff, lateral flow, return flow, water infiltration to the root zone and vadose zone, percolation to shallow aquifer, recharge to deep aquifer and flow out of the watershed **(**Figure 5-1**)** . Water balance is the driving force behind all of the processes in the SWAT calculated using eqn. (5-1),

$$SW_t = SW_o + \sum_{I=1}^{t}\left(R_{day} - Q_s - Q_l - Q_b - E_a - Revap - DA\_recharge\right) \quad (5\text{-}1)$$

Where SW_t is the final soil-water content (mm H_2O), SW_o is the initial soil-water content on day i (mm H_2O), t is the time (days), R_{day} is the amount of precipitation on day i (mm H_2O), Q_s is the amount of surface runoff on day i (mm H_2O), Q_l is the amount of return flow on day_i (mm H_2O), Q_b is the return flow from shallow aquifer on day_i (mm H2O), E_a is the amount of evapotranspiration from the canopy and soil surface on day_i (mm H_2O), Revap is the amount of water transferred from the underlying shallow aquifer reverse upward to the soil-moisture storage on day_i (mm H_2O) in response to water demand for evapotranspiration, and DA_recharge is the amount of water recharge to deep aquifer on day_i (mm H_2O).

[2] Based on: Mekonnen, D.F., Duan, Z., Rientjes, T., Disse, M.: Analysis of combined and isolated effects of land-use and land-cover changes and climate change on the upper Blue Nile River basin's streamflow. Hydrology and Earth System Sciences, 22(12), 6187-6207, 2018

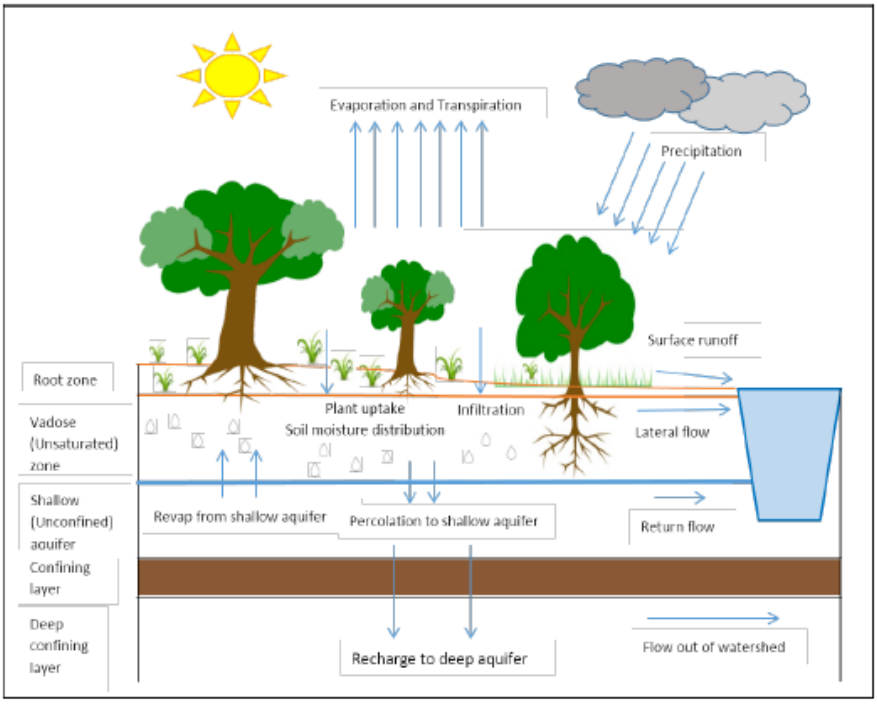

Figure 5-1: Hydrologic cycle in SWAT (Neitsch *et al.*, 2011)

SWAT has four storages: canopy storage (CS), soil moisture (SM), shallow aquifer (SA) and deep aquifer (DA). The potential pathway of water movement simulated by HRU in the SWAT is illustrated in Figure 5-1. The descended precipitation may be intercepted and held by the plant canopy or fall directly on the soil surface. The amount of water held by the plant canopy will lost in the form of canopy evaporation. Water fallen on the soil surface will infiltrate into the soil profile or flow overland as runoff. Infiltrated water may be held in the soil and later evapotranspired or it may come out to the surface water through lateral flow. The excess amount of infiltrated water further percolated to shallow aquifer. Water movement from the soil-moisture storage to the shallow aquifer is due to percolation, whereas water movement from the shallow aquifer reverse upward to the soil-moisture storage is Revap and water movement further from shallow aquifer to the deep aquifer is recharge. This study focused on the effects of LULC change and climate change on the basin's water balance components, which include the components of inflows, outflows, evapotranspiration, losses and the change in storage as shown in the general water balance (5-2).

$$P = Q_t + TAE + Losses + \Delta S \qquad (5\text{-}2)$$

where $Q_t = Q_s + Q_l + Q_b$ and $TAE = E_c + E_s + E_t + E_r$, as it is shown in Figure 5-2. P is the amount of precipitation (mm d^{-1}) as the main inflow, Qt is the total amount of streamflow (mm d^{-1}) as outflow, TAE is the total actual evapotranspiration (mm d^{-1}), E_c is evaporation from the

canopy surface (mm d^{-1}), E_t is the amount of plant transpiration (mm d^{-1}), E_s is evaporation from the soil surface (mm d^{-1}) and E_r or Revap is evaporation from the shallow aquifer (mm d^{-1}) (Abiodun *et al.*, 2018), Losses are the amount of water lost from the system as a recharge to the deep aquifer (DA_recharge) (mm d^{-1}) and ΔS is the change in soil water storage (mm d^{-1}).

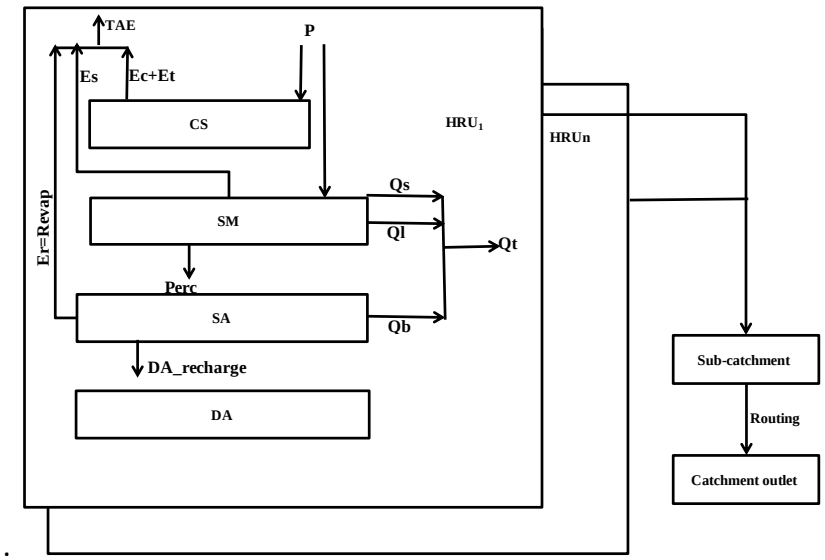

Figure 5-2: Schematic representation of the SWAT model structure modified from (Marhaento *et al.*, 2017).

Where: P is precipitation; CS is canopy storage; TAE is total actual evapotranspiration; Ec is evaporation from the canopy surface; Es is evaporation from the soil surface; Et is transpiration from plants; perc is percolation from the soil storage to shallow aquifer; SM is soil moisture storage; SA is shallow aquifer; Er=Revap is evaporation from the shallow aquifer; Qt is total streamflow; DA is deep aquifer; HRU is hydrological response unit; Qb is base flow; Ql is lateral flow; Qs is surface runoff.

Surface runoff (the SCS-CN Method)

Runoff is calculated separately for each HRU and routed to obtain the total streamflow for the watershed using either the soil conservation service (SCS) curve number (CN) method (Mockus, 1964) or Green & Ampt infiltration method (GAIM;(Green and Ampt, 1911); see Figure 5-2). However, spatial connectivity and interactions among HRUs are ignored. Instead, the cumulative output of each spatially discontinuous HRU at the sub-watershed outlet is directly routed to the channel (Pignotti *et al.*, 2017). This lack of spatial connectivity among HRUs makes implementation and impact analysis of spatially targeted management such as soil and water conservation structure difficult to incorporate into the model. Different authors have made efforts to overcome this problem for instance, a grid-based version of the SWAT model (Rathjens *et al.*, 2015) or landscape simulation on a regularized grid (Rathjens and Oppelt, 2012). Moreover, (Arnold *et al.*, 2010) and (Bosch *et al.*, 2010) further modified SWAT so that it allows landscapes to be subdivided into catenas comprising upland, hill slope, and floodplain units, and flow to be routed through these catenas. However, SWATgrid, developed to overcome this limitation, remains largely untested and computationally demanding (Rathjens *et al.*, 2015).

Hence, the standard SWAT CN method eqn.(5-3), was chosen for this study because it was applied in many Ethiopian watersheds such as (Gashaw *et al.*, 2018; Gebremicael *et al.*, 2013; Setegn *et al.*, 2008; Woldesenbet *et al.*, 2017b). Furthermore, its ability to use daily input data (Arnold *et al.*, 1998; Neitsch *et al.*, 2011; Setegn *et al.*, 2008) as compared to GAIM, which requires sub daily precipitation as a model input, and that can be difficult to obtain in data-scare regions like the UBNRB.

The Soil Conservation Service (SCS) Curve Number (CN) method developed by United States Development of Agriculture (USDA, 1972) which uses local land use, soil type, and antecedent moisture conditions can be calculated as shown in eqn.(5-3).

$$Q_{surf} = \frac{(R_{day} - I_a)^2}{(R_{day} - I_a + S)} \quad (5\text{-}3)$$

Where *Qsurf* is accumulated runoff or rainfall excess (mm H2O), *Rday* is rainfall depth for the day (mm H2O), I*a* is initial abstraction which includes surface storage, interception and infiltration prior to runoff (mm H2O), and *S* is the retention parameter (mm H2O). The *Ia* was commonly approximated as 0.2*S* (USDA, 1972). Therefore, the surface runoff will occur when *Rday>Ia*. The retention parameter S was computed as presented in the following Equation 3.

$$S = 25.4\left(\frac{1000}{CN} - 10\right) \quad (5\text{-}4)$$

Where *CN* is curve number for the day, which is a function of soils permeability, land use and antecedent soil water condition. SWAT calculates CN for antecedent moisture condition II and for 5% slope.

Evapotranspiration

The second most important hydrologic component for water balance modeling next to surface runoff is evapotranspiration. It is the primary mechanism by which water is removed from a watershed. Hence, an accurate estimation of evapotranspiration is critical in the assessment of water resources and the impact of climate and land use change on those resources. Although SWAT provides three different methods for estimating potential evapotranspiration, which are Penman–Monteith (Monteith, 1965), Priestly–Taylor (Priestley and Taylor, 1972), and Hargreaves methods (Hargreaves *et al.*, 1985), the Penman–Monteith method was used in this study since the water balance simulated with this method in SWAT better matches with the observed flow of the basin. SWAT initially calculates the potential evapotranspiration (PET) for a reference crop (alfalfa) using the Penman–Monteith equation for well-watered plants (Jensen et al., 1990)

$$ET_0 = \frac{0.408\Delta(R_n - G) + \gamma\frac{900}{T + 273}U_2(e_s - e_a)}{\Delta + \gamma(1 + 0.34U_2)} \quad (5\text{-}5)$$

Where,

ETo	reference evapotranspiration [mm day^{-1}],
Rn	net radiation at the crop surface [MJ m^{-2} day^{-1}],
G	soil heat flux density [MJ m^{-2} day^{-1}],
T	air temperature at 2 m height [°C],
u2	wind speed at 2 m height [m s^{-1}],
es	saturation vapor pressure [kPa],
ea	actual vapor pressure [kPa],
Δ	slope vapor pressure curve [kPa $°C^{-1}$],
γ	psychrometric constant [kPa $°C^{-1}$].

Total actual evapotranspiration (TAE) in SWAT is made up of four components: canopy evaporation, transpiration, soil evaporation and groundwater ET (Revap) (see **Figure 5-2**). The TAE components are calculated from the PET starting with the canopy evaporation. For a more detailed explanation and equations of AET, refer to Abiodun *et al.* (2018). For a more detailed description of the SWAT model and other water balance components, refer to Neitsch *et al.* (2011).

5.1.2 SWAT model setup

According to Setegn *et al.* (2008), the model setup involved six steps: (1) Input data preparation;(2) watershed delineation and sub-basin descritization: (3) HRU definition; (4) parameter sensitivity analysis; (5) calibration and uncertainty analysis 6) validating the model. The SWAT model setup and data preparation was done using arcSWAT2012 tool in the arcGIS environment, whereas parameter sensitivity analysis, and model calibration and validation was performed using the SWAT-CUP (Calibration and Uncertainty Procedures) interface Sequential Uncertainty Fitting (SUFI-2) algorithm (Abbaspour, 2008).

The required spatial datasets (DEM, LULC map and soil map) were prepared and projected to the same projection called Adindan UTM Zone 37N, which is the transverse mercator projection parameters for Ethiopia, using ArcGIS 10.1. The detail procedure of input data preparation is described under section 5.2. The DEM was used to delineate the watershed and to analyze the drainage patterns of the land surface terrain. The watershed and sub watershed delineation was also done using DEM data. The watershed delineation process include five major steps, DEM setup, stream definition, outlet and inlet definition, watershed outlets selection and definition and calculation of sub basin parameters. For the stream definition, the threshold based stream definition option was used to define the minimum size of the sub basin. The ArcSWAT interface allows the user to fix the number of sub basins by deciding the initial threshold area. The threshold area defines the minimum drainage area required to form the origin of a stream.

The LULC spatial data were reclassified into SWAT land cover/plant types. A user look up table was created to identify the SWAT code for the different categories of LULC on the map as per the required format. The soil map was linked with the soil database which is a soil database designed to hold data for soils not included in the U.S. For the stream definition, the threshold based stream definition option was used to define the minimum size of the sub basin. To study the differences in evapotranspiration and other hydrologic conditions for different land covers,

soils and slopes, the sub-basins further sub divided into HRUs having unique land use, soil and slope. In order to do so, the land use, soil and slope datasets were imported overlaid and linked with the SWAT2012 databases. To define the distributions of HRUs both single and multiple HRU definition options are available. For this study, multiple HRU definition option is used. Detail steps and procedures for SWAT model setup can be found in (Winchell *et al.*, 2013)

5.1.3 SWAT sensitivity analysis

Sensitivity analysis is a technique used for identifying the most important influence parameters in the model by assessing the ratio of the relative change of model output to the relative change of that parameter. Sensitivity analysis then shows the impact of input parameters on the objective function. Since parameters represent hydrological processes, sensitivity analysis can provides information on the most important processes in the study region. It also helps to decrease the number of iterations in the calibration procedure by eliminating the parameters identified as not sensitive (Abbaspour *et al.*, 2017). Sensitivity analysis was undertaken by using a SWAT CUP that uses Automated Latin Hypercube One-factor-At-a-Time (LH-OAT) global sensitivity analysis procedure.

Two general types of sensitivity analysis are usually performed. These are one-at-a-time (OAT) or local sensitivity analysis, and all-at-a-time (AAT) or global sensitivity analysis. In OAT, all parameters are held constant while changing one to identify its effect on some model output or objective function. In the AAT, however, all parameters are changing. Hence, a larger number of runs are needed for the AAT in order to see the impact of each parameter on the objective function while only few model runs are sufficient for OAT. In SWAT-CUP, OAT is used to directly compare the impact of three to five parameter values on the output signal, whereas AAT uses a multiple regression approach to quantify sensitivity of each parameter (Abbaspour *et al.*, 2017).

Global Sensitivity Analysis (AAT) was used to carry out sensitivity analysis of the parameters chosen for the calibration process. In this process, multiple regression system as shown in eqn. (5-6) regress Latin hypercube generated parameters against objective function to determine sensitivity of the parameters.

$$g = \alpha + \sum_{i=1}^{m} \beta_i b_i \qquad (5\text{-}6)$$

Where *g* is the objective function, α and β are the variables and *bi* is parameter. A t-test was then used to identify the relative significance of each parameter *bi* through the application of inverse optimization approach.

Sensitivity analyses were done prior to calibration process in order to identify important parameters for SWAT. SWAT-CUP uses t test and p-value to rank the most sensitive parameter that corresponds to direct change in stream flow response. As statistical measurements, *t*-stat and *p*-value were used. A *t*-stat is the coefficient of a parameter divided by its standard error and is a measure of the precision with which the regression coefficient is measured. Therefore, the

parameter is sensitive when the coefficient is larger than the standard error. A p-value was determined from student's *t*-distribution table with the values obtained for *t*-stat for a parameter; where a lower *p*-value suggests higher sensitivity of the parameter, and vice-versa. The overall uncertainty in the output was computed by 95 Percent Prediction Uncertainty (95 ppu) and dotty plots for each parameter. This helped in determining the new ranges and best fitted values that were applied for further iterations to maximize the objective function. The 95ppu was calculated at 2.5 and 97.5% levels of the cumulative distribution of an output variable obtained through Latin hypercube sampling. Two indices (the P-factor and R-factor) were used to quantify the goodness of calibration/uncertainty performance. P-factor is the percentage of data bracketed by the 95 PPU band (ideal value should approach closer to 1) and the R-factor, which is a measure of the thickness of the 95ppu band and calculated as the average 95ppu thickness divided by the standard deviation of the corresponding observed variable (ideal value should be close to 0). To minimize uncertainties and maximize the objective function, the number of sampling round was increased with the set of new parameter ranges.

$$\mathrm{R-factor_j} = \frac{\frac{1}{n_j}\sum_{t_{i=1}}^{n_j}\left(x_s{}^{ti,97.5\%} - x_s{}^{ti,2.5\%}\right)}{\sigma_{oj}} \qquad (5\text{-}7)$$

Where $x_s{}^{ti,97.5\%}$ and $x_s{}^{ti,2.5\%}$ are the upper and lower boundary of the 95ppu of the time step t and simulation i, n_j is the number of data points, and σ_{oj} is the standard deviation of the jth observation.

5.1.4 SWAT calibration and validation

The subsequent step after sensitivity analysis is model calibration. Both manual and automatic calibration strategies were applied to attain the minimum differences between observed and simulated streamflow in terms of surface flow, and peak and total flow following the steps recommended by Arnold *et al.* (2012), using the SUFI-2 approach within SWAT-CUP. There have been numerous local and regional hydrological modeling studies across the world carried out to assess the potential impact of climate change and LULC changes on streamflow. In these studies, hydrological models were first calibrated against baseline streamflow data, and then driven with changed climate and LULC data, with the same optimized parameter values. Then after, the modeled and baseline streamflow are compared to estimate the effects of climate change and LULC on streamflow (Kidane *et al.*, 2018; Li *et al.*, 2009; Teklay *et al.*, 2019; Woldesenbet *et al.*, 2018; Yin *et al.*, 2017). A common assumption implicit in most of these studies is that hydrological models calibrated over the historical period are valid for use in the altered regime. However, future climate and LULC changes may possibly alter the model parameters (Vaze *et al.*, 2010). There are number of factors that can affect the hydrologic responses (in particular the rainfall-runoff relationship), which include the changes in intensity of rainfall, rainfall timing, vegetation cover that affects evapotranspiration and soil infiltration rate.

Hence, to understand the dynamics of SWAT parameter values in the rainfall–runoff relationship under different climate and LULC conditions, the SWAT model is calibrated against observed monthly streamflow data for each of the four individual calibration periods representing different LULC and climate. In the model calibration, the model parameters are optimized to maximize

the objective functions. For this purpose, the period 1971–2010 was divided into four decadal periods hereafter referred as the 1970s (1971–1980), 1980s (1981–1990), 1990s (1991–2000) and 2000s (2001–2010). The SWAT model was then calibrated and validated for each decadal period by splitting 10 years of monthly record data into three data sets. The first two years were used to warm-up the model, the next five years were used for the model calibration, and the last three years were used for the model validation. For example, for the 1970s data, 1971 and 1972 used for warming-up, 1973-1977 used for calibration and 1978-1980 was used for validation. This approach also helps to analyze the combined effects of LULC and climate change on the water balance components as it can simulate the observed data better than using single parameter value for baseline and altered conditions. However, for further analysis of the isolated effects of LULC and climate changes on the streamflow and water balance components, the calibrated parameters of the baseline period (1970s) were held constant for modeling the altered conditions.

The model's performance for the streamflow was then evaluated using statistical methods (Moriasi *et al.*, 2007) such as NSE, R^2, and RVE %, which are shown by eqn.(4-5) to eqn.(4-10). Furthermore, graphical comparisons of the simulated and observed data, as well as water balance checks, were used to evaluate the model's performance. Validation is used to build confidence in the calibrated parameters. For this purpose, the calibrated parameter values are applied to an independent measured dataset without further changes. The analysis is required to do one iteration with the same number of simulations as the last calibration iteration. It is important that the data in validation period meet more or less the same physical criteria as the calibration period. For example, climate and land-use of the validation period should pertain the same kind of climate and land uses as the calibration period.

5.1.5 *SWAT simulations*

The general steps used to analyze the combined and isolated effects of LULC changes and climate change is shown Figure 5-3. Three different approaches were applied for assessing the effects of LULC change and climate change on streamflow and water balance components during the period 1971-2010. The first approach is to assess the response of streamflow for the combined effects of LULC change and climate change. We followed the approach in (Marhaento *et al.*, 2017) and divided the analysis period, 1971–2010, into four periods of similar length (four decades). These are periods when land use changes are expected to change the hydrological regime within a catchment (Marhaento *et al.*, 2017; Yin *et al.*, 2017). The first period, the 1970s, was regarded as the baseline period. The other periods, the 1980s, 1990s, and 2000s were regarded as altered periods. LULC maps of 1973, 1985, 1995, and 2010 were used to represent LULC patterns during the 1970s, 1980s, 1990s, and 2000s respectively. The baseline and altered periods were calibrated and validated separately using the respective dynamic LULC and climate data. The SWAT model simulations using the calibrated parameters for baseline and altered periods were used for analyzing the combined effects of LULC and climate changes (Table 5-1). The DEM and soil data sets remained unchanged. The differences between the simulation result of the baseline and altered periods represent the combined effects of LULC and climate changes on streamflow and water balance components.

Table 5-1: Data sets of the baseline and altered periods for the SWAT simulation used to analyze the combined and isolated effect of LULC and climate changes on streamflow and water balance components

Scenario	Description	LULC	Climate	Remark
1(Q_{base1})	LULC and meteorological data from the 1970s	1973	1970s	baseline period
2(Q_{base2})	LULC and meteorological data from the 1980s	1985	1980s	altered period1(ap1)
3(Q_{base3})	LULC and meteorological data from the 1990s	1995	1990s	altered period2 (ap2)
4(Q_{base4})	LULC and meteorological data from the 1970s	2010	2000s	alteredperiod3(ap3)
5($Q_{sim,Lc1}$)	Changing LULC while holding climate constant	1985	1970s	effect of LULC alone
6($Q_{sim,Lc2}$)	Changing LULC while holding climate constant	1995	1970s	effect of LULC alone
7($Q_{sim,Lc3}$)	Changing LULC while holding climate constant	2010	1970s	effect of LULC alone
8($Q_{sim,Cc1}$)	Changing climate while holding LULC constant	1973	1980s	effect of climate alone
9($Q_{sim,Cc2}$)	Changing climate while holding LULC constant	1973	1990s	effect of climate alone
10($Q_{sim,Cc3}$)	Changing climate while holding LULC constant	1973	2000s	effect of climate alone

The second approach included simulations to attribute effects from LULC changes alone. It aimed to investigate whether LULC change is the main driver for changes in water balance components. To identify the hydrological impacts caused solely by LULC, "A fixing-changing" method was used (Marhaento *et al.*, 2017; Teklay *et al.*, 2019; Woldesenbet *et al.*, 2017b; Yan *et al.*, 2013; Yin *et al.*, 2017). A fixing -changing method used dynamic LULC data of 1973, 1985, 1995, and 2010 but static climate data of 1970s (1971-1980) to run the models with fixed calibrated parameters of the baseline period. The DEM and soil data remained constant as suggested by (Hassaballah *et al.*, 2017b; Marhaento *et al.*, 2017; Woldesenbet *et al.*, 2017b; Yin *et al.*, 2017). This is simply running the calibrated SWAT model for the baseline period (1970s) four times changing only the LULC map for the years 1973, 1985, 1995, and 2010 and retaining the constant weather data set from the 1970s (Table 5-1). The third approach is similar to the second, but the simulations are attributed only for climate changes. The calibrated models for the base line period was run again four times, corresponding to the LULC periods using a unique LULC map of the year 1973 but altering the four different periods of weather data sets for respective periods using fixed calibrated parameter values of the baseline period.

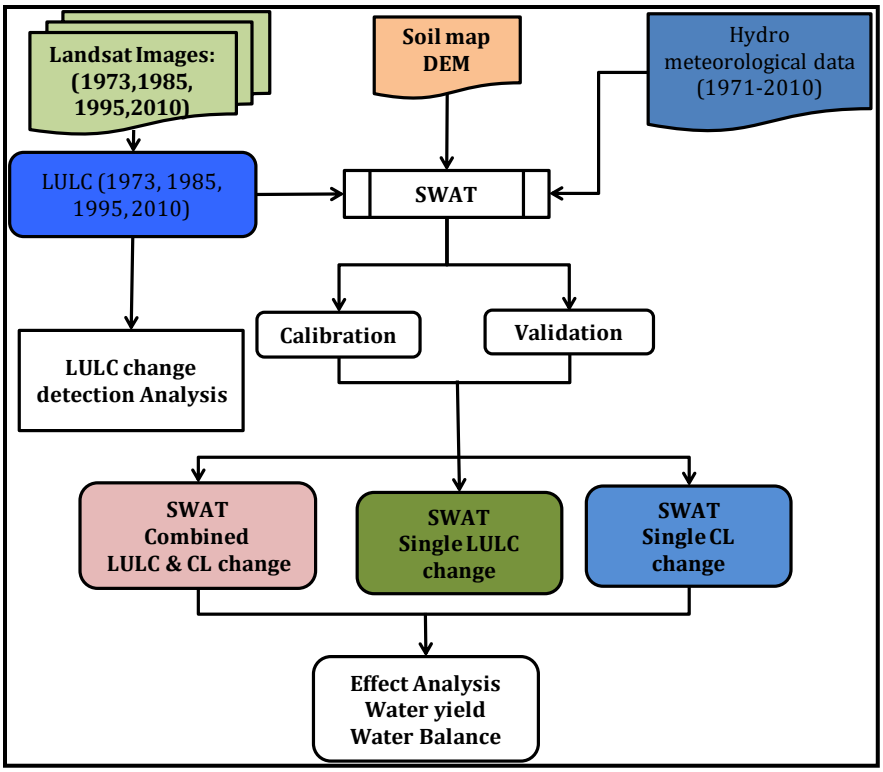

Figure 5-3: Flow chart showing the analysis of combined and single effect of LULC and climate changes on the water balnce using SWAT model

In summary, combined and isolated effects of the changes to LULC and climate on the streamflow and water balance components were evaluated by comparing the SWAT outputs of 10 scenarios. Each scenario represented 1 decade, and each simulation required an LULC map and a meteorological data set (Table 5-1). If the LULC map and the meteorological data were within the same decade (i.e., the 1970s, 1980s, 1990s, or 2000s), the simulation results represented "real streamflow" or a "baseline" affected by the combination of LULC and climate changes. Alternatively, the simulation results with varying one driving factor while holding others constant represented the effects of the variable factor alone on streamflow and water balance components (Li *et al.*, 2009; Teklay *et al.*, 2019; Yin *et al.*, 2017). For example, to assess the response of streamflow to combined LULC and climate changes in the 1970s and 1980s, the simulation of the 1970s (1971–1980) (Q_{base1}), which is used as a baseline, should be based on the current LULC (year 1973) and current climate (years 1971– 1980). The simulation of the 1980s (1980–1989) (Q_{base2}) should be based on LULC (year 1985) and future climate (years 1981–1990). The difference between the first and second simulations (Table 5-1) represents the combined effects of LULC and climate changes on streamflow. Regarding LULC changes, the fifth simulation ($Q_{sim,Lc1}$) was based on the current climate (years 1971–1980) and the LULC in the next period, (in this example, 1985). The difference between the first and fifth simulations is the effect of the LULC change on streamflow. Similarly, the difference between the first simulation and the eighth simulation ($Q_{sim,Cc1}$) based on the current LULC (year 1973) and climate of next period (in this example, 1981–1990) represents the impact of climate change alone on streamflow.

The combined effects of LULC and climate changes on streamflow ($\Delta R_{comb}\%$) and the isolated effects of LULC ($\Delta R_{iso,Lc}\%$) and climate ($\Delta R_{iso,Cc}\%$) can be assessed using eqs. (5-8) to (5-10):

$$\Delta \text{Rcomb } \% = \left(\frac{Q_{base,i+1} - Q_{base,i}}{Q_{base,i}}\right) * 100 \quad (5\text{-}8)$$

$$\Delta R_{iso,Lc,i}\% = \left(\frac{Q_{sim,Lc,i} - Q_{base,i}}{Q_{base,i}}\right) * 100 \quad (5\text{-}9)$$

$$\Delta R_{iso,Cc,i}\% = \left(\frac{Q_{sim,Cc,i} - Q_{base,i}}{Q_{base,i}}\right) * 100 \quad (5\text{-}10)$$

5.2 Input data preparation for SWAT

The final quality of a hydrological model is highly dependent on the quality of the input data. Two types of datasets were used in this study: the spatially distributed data (GIS input) needed for the ArcSWAT interface include the Digital Elevation Model (DEM), tabular and spatial soil data, tabular and spatial LULC information and stream network layers, and data on weather and river discharge which are also used for prediction of streamflow and calibration purposes.

Digital elevation model (DEM)
Topography was defined by a DEM that describes the elevation of any point in a given area at a specific spatial resolution. A Shuttle Radar Topographic Mission Digital Elevation Model (SRTM DEM) of 90 meters' resolution from the Consultative Group on International Agricultural Research-Consortium for Spatial Information (CGIAR-CSI; http://srtm.csi.cgiar.org/SELECTION/inputCoord.asp) was used to represent land surface drainage patterns. Terrain characteristics such as slope gradient, slope length of the terrain, and stream network characteristics such as channel slope, length, and width were derived from the DEM.

Soil data
The soil map (1:5000000) developed by the Food and Agriculture Organization of the United Nations (FAO-UNESCO) was downloaded from http://www.fao.org/soils-portal/soil-survey/soil-maps-and-databases/faounesco-soil-map-ofthe-world/en/. Soil information such as soil textural and physiochemical properties needed for the SWAT model were extracted from Harmonized World Soil Database v1.2, a database that combines existing regional and national soil information (http://www.fao.org/soils-portal/soil-survey/soil-maps-and-databases/harmonized-world-soil-databasev12/en/) with information provided by the FAO-UNESCO soil map (Polanco *et al.*, 2017). The soil map was linked with the soil database which is a soil database designed to hold data for soils not included in the U.S.

LULC map
The LULC maps were produced from satellite-remote-sensing Landsat images for 1973, 1985, 1995, and 2010 at a scale of 30 m x 30 m resolution. Detailed descriptions on image processing and land cover classification are available in the next section 5.3. The classified LULC spatial data were reclassified into SWAT land cover/plant types. A user look up table was created to identify the SWAT code for the different categories of LULC on the map as per the required format.

Weather data
SWAT requires daily meteorological data that can either be read from a measured data set or be generated by a weather generator model. The daily weather variables used in this study for driving the hydrological balance are daily precipitation, minimum and maximum air temperature for the period 1971– 2010. These data were obtained from ENMA for stations located within and around the watershed (Figure 4-1). For the detail description, please refer section Chapter 4.

5.3 Remote sensing land use/cover map (LULC)

Landsat image acquisition
Landsat images from the years 1973, 1985, 1995, and 2010 were accessed from the US Geological Survey (USGS) Center for Earth Resources Observation and Science (EROS) via http://glovis.usgs.gov. The Landsat images were selected based on the criteria of the acquisition period, availability, and percentage of cloud cover. Hayes and Sader (2001), recommend acquiring images from the same acquisition period to reduce image-to-image variation caused by sun angle, soil moisture, atmospheric condition, and vegetation-phenology differences. Cloud free-images were hence collected for the dry months of January to May. However, as the basin covers a large area, each of the LULC map's periods comprised 16 Landsat images. Accessing all the images during a dry season in a single year was therefore difficult. Hence, images were acquired ±1 year for each period and some images were acquired in the months of November and December. For example, 16 Landsat MSS image scenes were acquired in 1973 (10 images in January, 4 images in December and 2 images in November; ±1 years) and merged to arrive at one LULC representation for selected years. Please see supplement Table 5-2for the details on Landsat images.

Preprocessing and processing images
Several standard preprocessing methods including geometric and radiometric correction were implemented to prepare the LULC maps from Landsat images. Although many different classification methods exist, supervised and unsupervised classifications are the two most widely used methods for land cover classification from remote-sensing images. Hence, in this study, a hybrid supervised/unsupervised classification approach was adopted to classify the images from 2010 (Landsat TM). Iterative Self-Organizing Data Analysis (ISODATA) clustering was first performed to determine the image's spectral classes or land cover classes. Polygons for all of the training samples based on the identified LULC classes were then digitized using ground truth data. The samples for each land cover type were then aggregated. Finally, a supervised classification was performed using a maximum likelihood algorithm to extract four LULC classes.

Table 5-2: Summary of Landsat images and their acquisition dates

	1985	1995	2010	1973	
1. General information					
	Landsat MSS	Landsat TM	Landsat TM	Landsat TM	
Number of scene	16	16	16	18	
Pixel resolution(m)	60	30	30	30	
2. Image acquisition date					
Paths/Rows	acquisition date	acquisition date	acquisition date	Paths/Rows	acquisition date
168/052	01/18/1985	12/13/1994	11/04/2009	180/053	01/30/1973
168/053	04/22/1985	12/13/1994	11/04/2009	181/052	01/30/1973
168/054	01/18/1985	01/14/1985	12/09/2010	181/053	12/26/1972
169/051	11/12/1986	12/04/1994	01/30/2010	181/054	01/31/1973
169/052	11/09/1986	12/04/1994	01/30/2010	181/055	01/31/1973
169/053	04/15/1985	01/21/1995	01/14/2010	182/051	12/09/1972
169/054	03/14/1985	01/21/1995	01/14/2020	182/052	02/01/1973
170/051	02/17/1985	02/13/1995	12/23/2010	182/053	12/09/1972
170/052	02/17/1985	02/13/1995	01/08/2011	182/054	02/01/1973
170/053	02/01/1985	02/13/1995	01/08/2011	182/055	02/01/1973
170/054	02/01/1985	12/27/1994	01/21/2010	183/051	11/04/1972
170/055	01/19/1986	01/12/1995	11/05/2010	183/052	01/15/1973
171/052	04/13/1985	02/20/1995	01/28/2010	183/053	01/15/1973
171/053	04/13/1985	01/03/1995	01/12/2010	183/054	01/15/1973
171/054	12/28/1985	01/19/1995	01/12/2010	184/051	12/11/1972
171/055	04/16/1985	04/09/1995	11/05/2010	184/052	11/05/1972
				184/053	12/11/1972
				184/054	02/03/1973

A total of 488 Ground Control Points (GCPs) regarding land cover types and their spatial locations were collected from field observation in March and April 2017 using a Global Positioning System (GPS). Reference data were collected and taken from areas, where there had not been any significant land cover change between 2017 and 2010. These areas were identified by interviewing local elderly people, and supplemented using high resolution Google Earth Images and the first author's prior knowledge. As many as 288 GCPs were used for accuracy assessment and 200 points served as training sites to generate a signature for each land-cover type. The classifications' accuracy was assessed by computing the error matrix (also known as the confusion matrix), which compares the classification result with ground truth information as suggested by DeFries and Chan (2000). A confusion matrix lists the values for the reference data's known cover types in the columns and for the classified data in the rows (Banko, 1998). From the confusion matrix, a statistical metrics of overall accuracy, producers' accuracy and

users' accuracy are used. Another discrete multivariate technique useful in accuracy assessment is called KAPPA (Congalton, 1991). The statistical metric for KAPPA analysis is the Kappa coefficient, which is another measure of the proportion of agreement or accuracy. The Kappa coefficient is computed as

$$K = \frac{N\sum_{i=1}^{i=r} x_{ii} - \sum_{i=1}^{r}(x_{i+} * x_{+i})}{N^2 - \sum_{i=1}^{r}(x_{i+} * x_{+i})} \quad (5\text{-}11)$$

Where r is the number of rows in the matrix, x_{ii} is the number of observations in row i and column i, x_{i+} and x_{+i} are the marginal totals of row i and column i, respectively. N is the total number of observations.

Once the land cover classification of the year 2010 Landsat image had been completed and its accuracy checked, the normalized difference vegetation index (NDVI) differencing technique (Mancino *et al.*, 2014) was applied to classify the images from 1973, 1985, and 1995. This technique was chosen to increase the accuracy of classification, as it is hard to find an accurately classified digital or analog LULC map of the study area during 1973, 1985, and 1995. The information obtained from the elders is also more subjective and its reliability is questionable when there is a considerable time gap. We first calculated the NDVI from the Landsat MSS (1973) and three preprocessed Landsat TM images (1985, 1995, and 2010) following the general normalized difference between band TM4 and band TM3 images (5-12). The resulting successive NDVI images were subtracted from each other to assess the ΔNDVI image with positive (vegetation increase), negative (vegetation cleared) and no change at a 30 m x 30 m pixel resolution eqn. (5-13) to (5-15). The Landsat MSS 60 m x 60 m pixel-size data sets were resampled to a 30 m x 30 m pixel size using the "nearest neighbor" technique to have equal pixel sizes for the different images without altering the image data's original pixel values.

$$NDVI = \frac{(TM4 - TM3)}{(TM4 + TM3)} \text{ or } \frac{(MSS_3 - MSS_2)}{(MSS_3 + MSS_2)} \quad (5\text{-}12)$$

$$\Delta NDVI_{1995/2010} = NDVI_{1995} - NDVI_{2010} \quad (5\text{-}13)$$

$$\Delta NDVI_{1985/1995} = NDVI_{1985} - NDVI_{1995} \quad (5\text{-}14)$$

$$\Delta NDVI_{1973/1985} = NDVI_{1973} - NDVI_{1985} \quad (5\text{-}15)$$

The ΔNDVI image was then reclassified using a threshold value calculated as $\mu \pm n*\sigma$; where μ represents the ΔNDVI pixels value mean, and σ the standard deviation. The threshold identifies three ranges in the normal distribution: (a) the left tail ($\Delta NDVI < \mu - n*\sigma$), (b) the right tail ($\Delta NDVI > \mu + n*\sigma$), and (c) the central region of the normal distribution ($\mu - n*\sigma < \Delta NDVI < \mu + n*\sigma$). Pixels within the two tails of the distribution are characterized by significant land cover changes, whereas pixels in the central region represent no change. To be more conservative, n =

1 was selected for this study to narrow the threshold ranges for reliable classification. The standard deviation (σ) is one of the most widely applied threshold identification approaches for different natural environments based on different remotely sensed imagery (Hu *et al.*, 2004; Jensen, 1996; Lu *et al.*, 2004; Mancino *et al.*, 2014; Singh, 1989) as cited by Mancino *et al.* (2014).

ΔNDVI pixel values (2010–1995) in the central region of the normal distribution ($\mu - n*\sigma < \Delta NDVI < \mu + n*\sigma$) represent an absence of land cover change between two different periods (i.e., 1995 and 2010); therefore, pixels from 1995 corresponding to no land cover change can be classified as similar to the 2010 land cover classes. Pixels with significant NDVI change are reclassified using supervised classification, taking signatures from the already classified, no-change pixels. Likewise, 1985 and 1973 land cover images were classified based on the classified images of 1995 and 1985 respectively.

Finally, after classifying the raw Landsat images into different land cover classes, change detection, which requires the comparison of independently produced classified images (Singb, 1989), was performed by the post classification method. The post classification change-detection comparison was conducted to determine changes in LULC between two independently classified maps from images of two different dates. Although this technique has some limitations, it is the most common approach because it does not require data normalization between two dates (Singh, 1989). This is because data from two dates are separately classified, thereby minimizing the problem of normalizing for atmospheric and sensor differences between two dates.

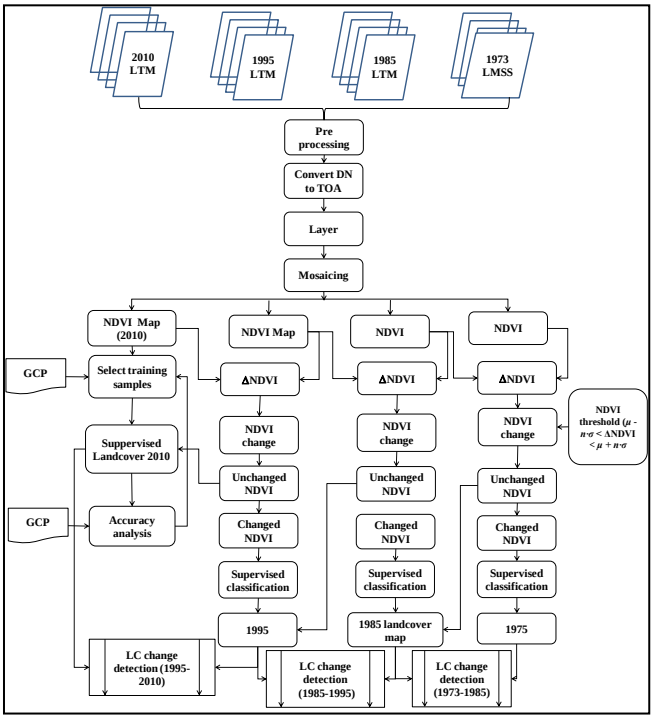

Figure 5-4: Schematic representation of Landcover classification

5.4 Results and Discussions

5.4.1 Land-cover classification, accuracy assessment and change detection

According to the confusion-matrix report, overall accuracy of 83 %, producer's accuracy values for all classes ranged from 75.4 % to 100 %, user's accuracy values ranging from 83.7 % to 91.7 % and a kappa coefficient (k) of 77% were attained for the 2010 classified image (Table 5-3). Monserud (1990) suggested a kappa value of <40 % as poor, 40–55 % fair, 55–70 % good, 70–85 % very good, and >85 % as excellent. According to these ranges, the classification in this study has very good agreement with the validation data set and meets the minimum accuracy requirements to be used for further change detection and impact analysis.

Table 5-3: Confusion (error) matrix for the 2010 land use/cover classification map

		Classified data					
	LULC class	Water	Forest	Cultivated	Bushes and shrubs	Row total	Producers' accuracy
Reference data	Water	44	0	0	0	44	100
	Forest	1	46	6	8	61	75.4
	Cultivated land	2	3	77	15	97	79.4
	Bushes and shrubs	1	3	9	73	86	84.9
	Column total	48	52	92	86	288	
	User's accuracy (%)	91.7	88.5	83.7	84.9		
	Over all accuracy (%)	83					
	Kappa (%)	77					

The classified images of the basin (Figure 5-5) have shown different LULC proportions at four distinct periods. Cultivated land dominantly covers (62.9 %) of UBNRB, followed by bushes and shrubs (18 %), forest (17.4 %), and water (1.74 %) in 1973. In 1985, cultivated land area increased to 65.6 %, followed by bushes and shrubs (18.3 %), while forest decreased to 14.4 %, and water remained unchanged at 1.7 %. In 1995, cultivated land area further increased to 67.5 %, followed by bushes and shrubs (18.5 %). Forest further decreased to 12.2 % and water remained unchanged at 1.7 %. In 2010, cultivated land decreased to 63.9 %, bushes and shrubs increased to 18.8 %, forest increased to 15.6 %, and water remained unchanged at 1.7 %. During the entire 1973–2010 period, cultivated land, along with bushes and shrubs remained the major proportions compared to the other LULC classes. The highest increase (2.7 %) and the largest decrease (−3.6 %) in cultivated land occurred during the 1973–1985 and 1995–2010 periods respectively. The largest increase in bushes and shrubs was 0.3 % from 1973 to 1985, whereas the largest increase in forest coverage (3.4 %) was recorded during the 1995–2010 period. Water coverage remained unchanged from 1973 to 2010.

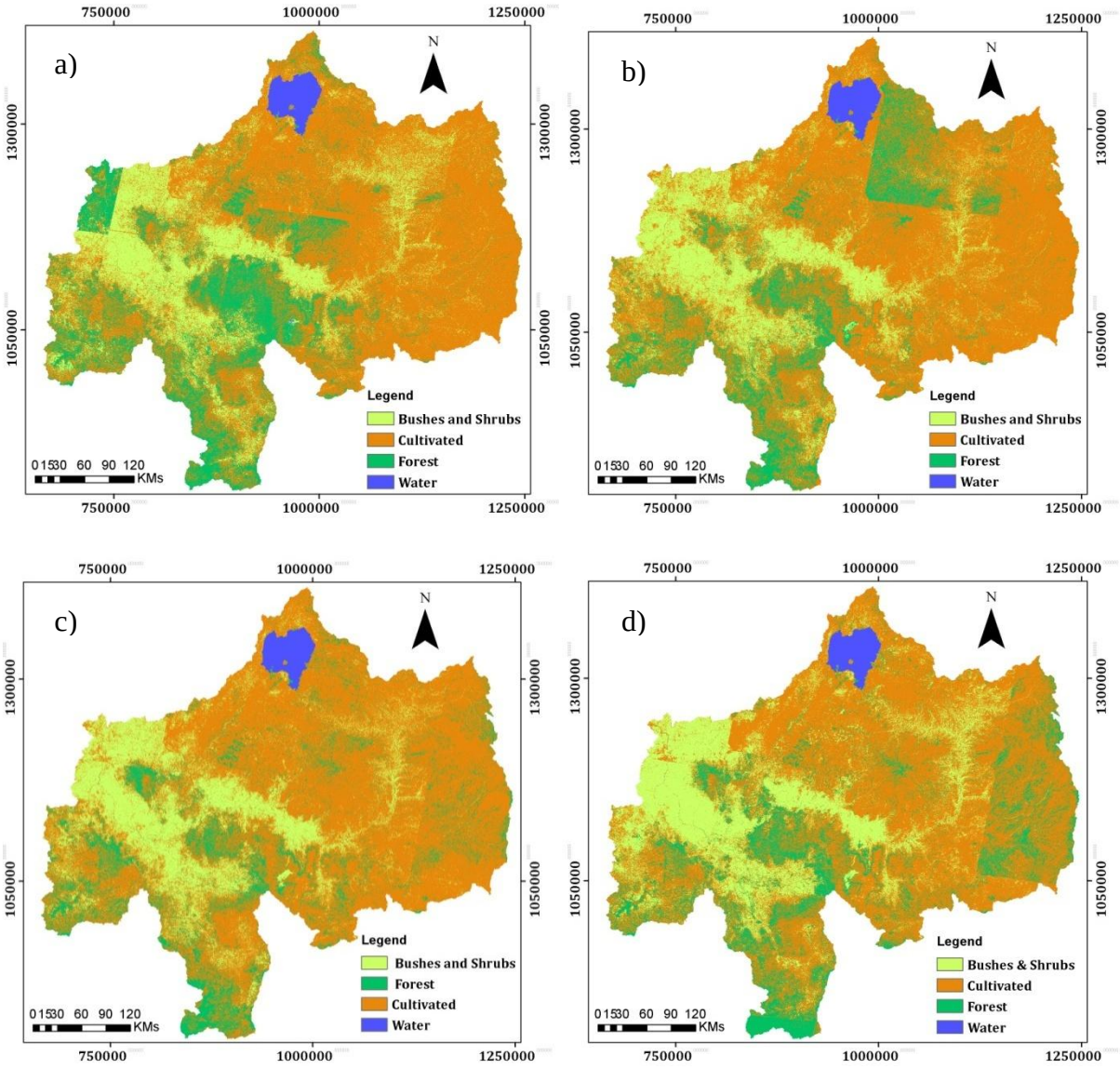

Figure 5-5: Landcover map of UBNRB derived from Landsat images for the years a) 1973, b) 1985, c) 1995, and d) 2010

Although, the image classification results show very good accuracy, uncertainties in classification could be expected. First, as elsewhere in Ethiopia, LULC may change rapidly over the land surface of the basin and image reflectance may be confusing due to the topography and variation in the image acquisition date. Landsat images were not all available for one particular year or one season (as described under section 5.3); images from different years and different seasons might harbor errors. Secondly, the workflow associated with LULC classification involves many steps and can be a source of uncertainty. The errors are observed in the classified LULC map as shown in Figure 5-5. On the western side of the map in Figure 4 (a) a rectangular section with forest appears, that completely disappears in 4(b). Rectangular forest cover appears in the northern part of the country in 4(b), which again disappears completely in 4(c). In 4(d), forest cover with linear edges (North-South) appears on the map's eastern side. That being

recognized, the land-cover mapping is reasonably accurate overall, providing a good base for land-cover estimation and for providing basic information for the hydrological impact analysis.

Table 5-4: Transition matrix of Landuse/Cover change

1973/1985 (Area Km^2)	Water	Forest	Bushes & Shrubs	Cultivated	Total	Coverage (%)
Water	3013.3	11.7	9.8	7.8	3,042.6	1.7
Forest	2.1	17,321.2	3,641.6	9,310.5	30,275.4	17.4
Bushes & Shrubs	13.1	1,385.4	25,254.6	4,651.4	31,304.4	18.0
Cultivated	2.6	6,316.6	2,947.2	100,278.0	109,544.4	62.9
Total	3,031.1	25,035.0	31,853.2	114,247.6	174,166.9	
Coverage (%)	1.7	14.4	18.3	65.6	100.0	
Change (%)	-0.4	-17.3	1.8	4.3		
1985/1995 (Area km^2)						
Water	3,027.1	1.4	0.5	2.1	3031.1	1.74
Forest	1.6	14,668.9	1,349.5	9,020.6	25,040.5	14.37
Bushes & Shrubs	0.0	875.2	27,571.3	3,409.1	31,855.6	18.28
Cultivated	7.8	5,772.9	3,382.8	105,103.0	114,266.5	65.59
Total	3,036.5	21,318.4	32,304.1	117,534.7	174,193.7	
Coverage (%)	1.7	12.2	18.5	67.5		
Change (%)	0.2	-14.9	1.4	2.9		
1995/2010 (Area km^2)						
Water	3,009.7	15.0	6.1	5.7	3036.5	1.7
Forest	0.7	16,251.6	710.7	4,355.4	21318.4	12.2
Bushes & Shrubs	1.2	1,089.5	27,766.5	3,446.9	32304.1	18.5
Cultivated	4.3	9,861.1	4,222.2	103,447.2	117534.7	67.5
Total	30,16.0	27,217.1	32,705.5	111,255.1	174,193.7	
Coverage (%)	1.7	15.6	18.8	63.9		
Change (%)	-0.7	27.7	1.2	-5.3		

Table 5-4 and Figure 5-5 depict LULC classification during the period 1973, 1985, 1995 and 2010. In 1973, the upper Blue Nile basin was dominated by cultivated land (62.9%), followed by bushes & shrubs (18%), forest (17.4%), and water (1.74%). In 1985, the cultivated land increased to (65.6%), followed by bushes & shrubs (18.3%), forest decreased to (14.4%), and water remained unchanged to (1.7%). In 1995, cultivated land further increased to (67.5%), followed by bushes & shrubs (18.5%), forest further decreased to (12.2%), and water remained (1.7%). In 2010, the cultivated land decreased to (63.9%), bushes and shrubs increased to 18.8 %, forest increased to 15.6 % and water remained unchanged to 1.7%.

Table 5-5: Summary of LULC change detection for the UBNRB

	Area (km^2)				Change			
Landcover	1973	1985	1995	2010	1973-1985	1985 -1995	1995 -2010	1973-2010
Water	3,042	3,031	3,036.5	3,016.0	-0.4	0.2	-0.7	-0.9
Forest	30,275	25,040	21,318	27,217	-17.3	-14.9	27.7	-10.1
Bushes &Shrubs	31,304	31,856	32,304	32,705	1.8	1.4	1.2	4.5
Cultivated	109,544	114,266	117,535	111,255	4.3	2.9	-5.3	1.6
Total	174,166	174,194	174,194	174,194				

Table 5-5 and Figure 5-6 show the proportion of each land cover class that made a transition from one category to another for each of the study periods. During the whole period (1973–2010), cultivated land and bushes & shrubs were the major proportions as compared to the other land use/cover classes. The highest gain (4.3%) and the highest loss (5.3%) in cultivated land occurred during the period 1973–1985 and 1995-2010 respectively. The highest gain in bushes and shrubs was (1.8%) from the period 1973 to1985, while the highest gain in forest (27.7%) was experienced during the period 1995–2010. The water coverage persists unchanged during 1973-2010. In other words, in the period 1973–1985, a decrease in the natural forest cover by 17.3% was observed while bushes & shrubs and cultivated land increases by 1.8% and 4.3% respectively from the initial states. In the period 1985-1995, a decrease of 14.9 % in forest coverage was observed while bushes &shrubs and cultivated land increased by 1.4 % and 2.9% respectively. In the period of 1995-2010, in reverse to the past periods, the forest coverage increased by 27.7% while cultivated land decreased by 5.3%, and bushes and shrubs again increased by 1.2%.

a) b) c)

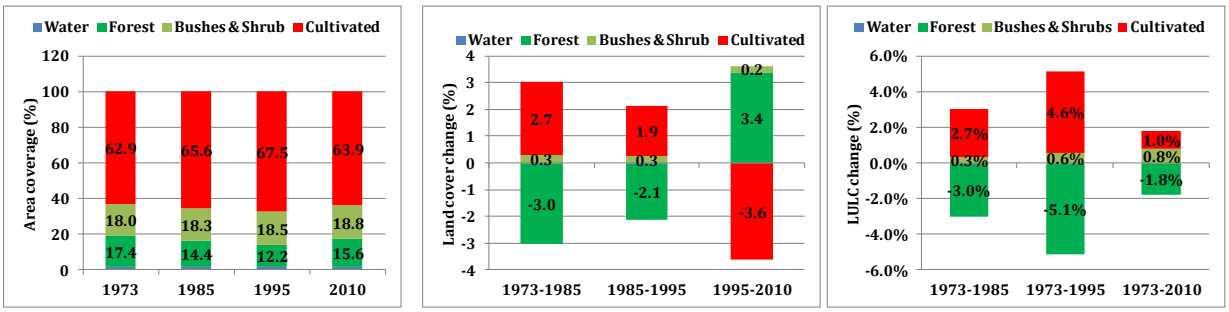

Figure 5-6: a) LULC composition, b) LULC change from consecutive periods c) LULC change in the UBNRB from the baseline period 1973

The rate of expansion of cultivated land before 1995 was higher than after 1995. Conversely, the area of the forestland decreased in 1985 and 1995 with reference to the 1973 baseline. However, after 1995, the forest's size increased again whereas cultivated land decreased. The increased forest coverage and the decrease in cultivated land over the period 1995 to 2010 showed that the

environment was recovering from the devastating drought, and forest clearing for firewood and cultivation due to population growth has been minimized. This could be due to the afforestation program, which the Ethiopian government initiated, and to the extensive soil and water conservation measures carried out by the community. Since 1995, eucalyptus tree plantation expanded significantly across the country at homestead level for fire wood, construction material, charcoal production, and income generation (Woldesenbet *et al.*, 2017b). In summary, forest coverage decreased by 1.8 %, while both bushes and shrubs as well as cultivated land increased by 0.8 % and 1 % respectively during the 2010 period from the original 1973 level (Figure 5-6 c). This result agrees well with other studies (Gebremicael *et al.*, 2013; Rientjes *et al.*, 2011a; Teferi *et al.*, 2013; Woldesenbet *et al.*, 2017b), who reported a significant conversion of natural vegetation cover into agricultural land.

5.4.2 SWAT model performance evaluation

Parameter sensitivity

The SWAT model's most sensitive parameters for simulating streamflow were identified using global sensitivity analysis of SWAT-CUP. The most sensitive input hydrologic parameters identified based on global sensitivity analysis of SWAT-CUP and used for streamflow simulations are presented in Table 5-7. Eight parameters were found to be sensitive with the relative sensitivity p values range from 0.0 to 0.50 and t values range from -6.21 to -0.67. The ranking of the parameters were different for different model runs where sensitivity test was carried out. However, the curve number (CN2) was the main sensitive parameter for all model setups. This is due to the fact that the curve number depends on several factors including soil types, soil textures, soil permeability, land use properties etc. In addition, base flow alpha factor (ALPHA_BF), soil evaporation compensation factor (ESCO), threshold water depth in the shallow aquifer required for return flow to occur (GWQMN), groundwater "revap" coefficient (GW_REVAP), and available water capacity (SOL_AWC) were found to be the most sensitive parameters for the calibration process. These sensitive parameters were considered for model calibration. Their optimized values were determined by the calibration process that Arnold *et al.* (2012) recommended.

Calibration and validation of SWAT model

The performance of the model was evaluated by comparing the simulated monthly streamflow from the model setups, which represent the four different decades, with the observed streamflow data. The model performance statistics for the calibration and validation periods are presented in Table 5-6. For calibration and uncertainty evaluation, 200 simulations have been performed in each iteration for each model run. Initial parameter estimates were taken from the default lower and upper bound values of the SWAT model database and from earlier studies in the basin e.g.(Gebremicael *et al.*, 2013). The calibration parameters were derived for four independent models that were setup for the periods 1970s, 1980s, 1990s and 2000s. Figure 5-7 shows the calibration and the validation results for monthly streamflow hydrographs for each model. These results revealed that the model represents the monthly hydrographs well as also indicated by R^2, NSE, and RVE (%) statistical performance measures (Table 5-6). For the calibration period, the values of R^2, NSE, and RVE (%) range from 0.79 to 0.91, 0.74 to 0.91, and −3.4 % to 4 %, respectively. According to the rating of Moriasi *et al.* (2007), the SWAT model's performance over the UBNRB can be categorized as very good.

Table 5-6: The SWAT model's statistical performance measure values

Period		R^2	NSE	RVE (%)	P-factor	R-factor
1970s	Calibration (1973–1977)	0.79	0.74	−3.41	0.87	1.13
	Validation (1978–1980)	0.84	0.83	7.18	0.89	1.33
1980s	Calibration (1983–1987)	0.80	0.74	−0.72	0.95	**1.87**
	Validation (1988–1990)	0.86	0.82	0.73	0.92	**1.61**
1990s	Calibration (1993–1997)	0.91	0.91	1.79	**0.67**	0.96
	Validation (1998–2000)	0.87	0.84	−3.56	**0.64**	0.88
2000s	Calibration (2003–2007)	0.86	0.86	3.99	0.98	0.92
	Validation (2008–2010)	0.94	0.92	−7.51	0.83	0.95

Table 5-7: SWAT sensitive model parameters and their (final) calibrated values for the four model runs

Parameter	Optimum value			
	1970s	1980s	1990s	2000s
R-CN2	0.88	0.91	0.92	0.9
a-Alpha-BF	0.028	0.028	0.028	0.028
V-GW_REVAPMN	0.7	0.45	0.7	0.34
V-GWQMN	750	750	750	750
V-REVAPMN	550	450	425	550
a-ESCO	−0.85	−0.85	−0.85	−0.85
R-SOL_AWC	6.5	6.5	6.5	6.5

R: value from the SWAT database is multiplied by a given value; V: replace the initial parameter by the given value; a: adding the given value to initial parameter value.

The higher R^2 for both model setups indicated a very good linear relationship between simulated and observed streamflow data. Positive and negative values of RVE (%) indicated a tendency for underestimation and over estimation of monthly streamflow respectively. However, the low magnitude of RVE values corresponded to a performance rating of "very good". The RVE result showed a very small accumulation of difference in streamflow volume between the simulated and observed data for the calibration period. The optimal parameter values of the four calibrated-model runs are shown in Table 5-7. A change was obtained for CN2 parameter values, which can be attributed to the catchment's response behavior mainly because of the difference in the LULC data between the four model setups. For instance, an increase in the absolute average (basin-wide) CN2 value in the 1980s and 1990s from 72.9 to 74.7 and 75.6 compared to the 1970s respectively, indicate a reduction in forest coverage and expansion of cultivated land. On the contrary, a decrease in CN2 value was attained during the period 1990s to 2000s from 75.6 to 73.6, attributed to the increase in forest coverage and reduction in cultivated land. These final fitted parameter values were incorporated into the SWAT2012 model for validation and further

applications. For the validation period, the values of R^2, NSE, and RVE (%) ranged from 0.84 to 0.94, 0.82 to 0.92 and −7.5 % to 7.2 % respectively.

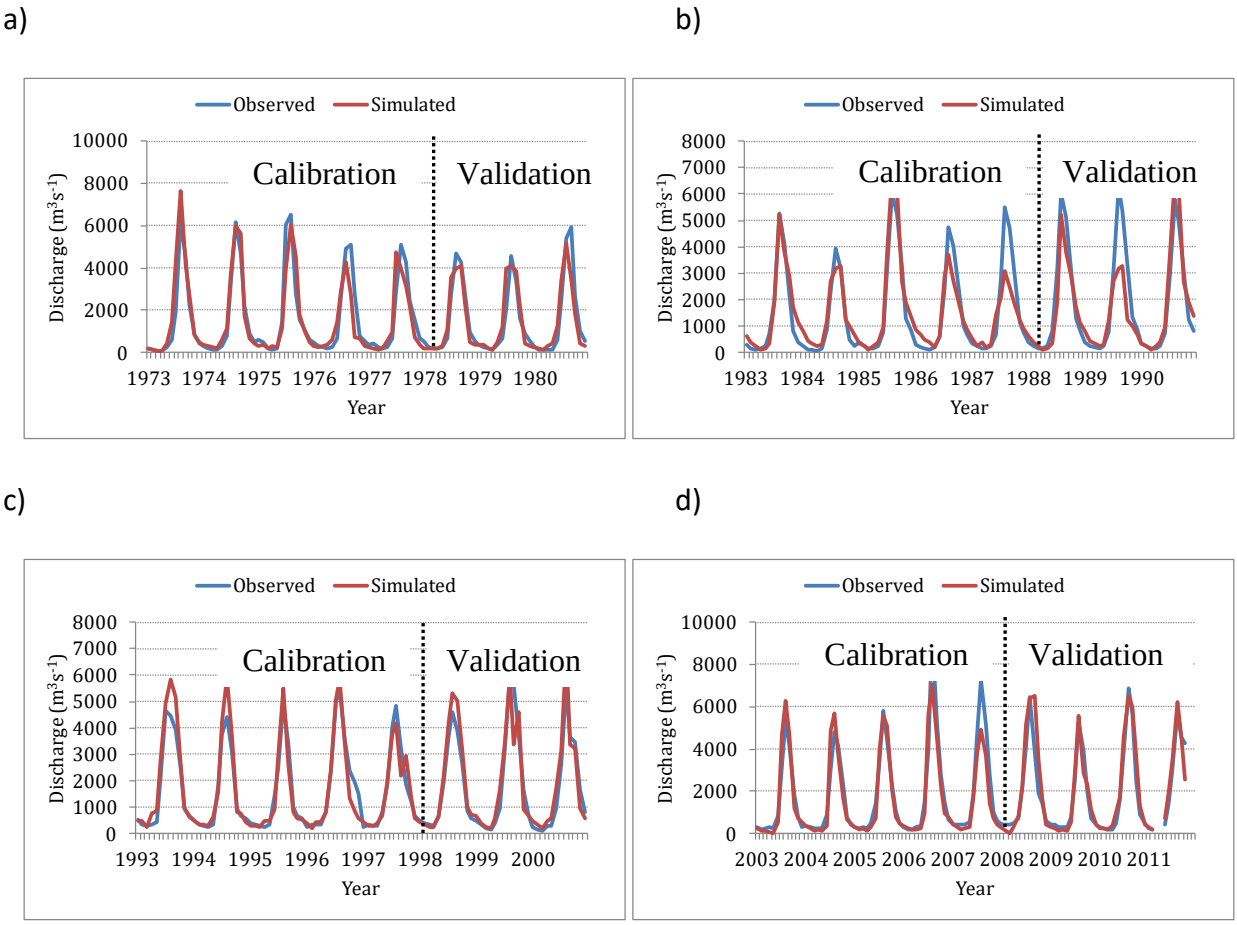

Figure 5-7: Calibration and validation of the SWAT hydrological model (left and right) respectively at monthly time scale; a) 1970s, b) 1980s, c) 1990s, and d) 2000s

Uncertainty analysis

Hydrological modeling obviously contains uncertainties in particular from (1) the uncertainty of measured or recorded spatial and temporal field data (Abbaspour, 2008), and (2) the uncertainty of the applied hydrological model itself . In this way, the present research has clear limitations. Each of the above sources of uncertainty applies, and not all of them can be quantified. Thus, the results should be treated with appropriate caution. The hydrographs of 95 PPU plots derived from four different SWAT model runs are presented in Figure 5-8. The model produced P-factor, which is the percentage of observations bracketed by the 95% prediction uncertainty (95PPU), values in the range of 0.67 to 0.98 and R-factor values in the range of 0.92 to 1.87 during calibration and from 0.64 to 0.92 and 0.88 to 1.61 during validation respectively (Table 5-7). The uncertainty factors showed acceptable model uncertainty estimates. Although performance indicators yielded fair and acceptable results, the P-factor during the period 1990s was still below the recommended model performance of 70% (Abbaspour, 2008). This problem indicates

that there is high uncertainty of simulated streamflow due to errors either in spatial or temporal inputs data. Generally, there was a good agreement between the observed and simulated flows in both model setups, but a few baseflow was underestimated.

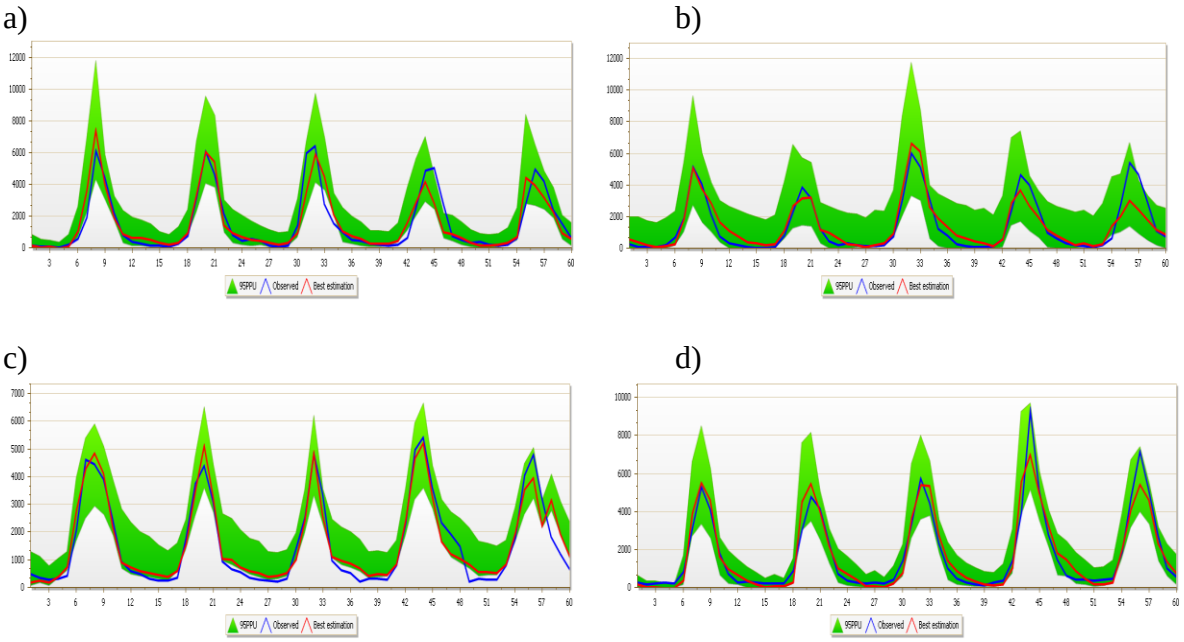

Figure 5-8: 95 PPU plots derived from running SUFI-2 within the SWAT-CUP for different model runs during calibration a) 1970s, b) 1980s, c)1990s and d) 2000s.

5.4.3 Combined effects of climate change and LULC changes

The simulation results of the four independent, decadal-time-scale calibrated and validated SWAT model runs reflect the combined effect of both LULC and climate change during the past 40 years (Table 5-9). From the simulation result, mean annual streamflow increased by 16.9 % between the 1970s and the 2000s, while the observed mean annual streamflow increased by 15.3 % for the same period. However, the rate of change is different in different decades. For example, it increased by 3.4 % and 9.9 % during the 1980s and 1990s respectively from the baseline 1970s period.

The ratio of mean annual streamflow to mean annual precipitation (Qt/P) increased from 19.4 % to 22.1 % while the actual evaporation to precipitation (Ea/P) ratio decreased from 61.1 % to 60.5 % from the 1970s to 2000s. Moreover, the ratio of surface runoff to streamflow (Qs/Qt) increased notably from 40.7 % in the 1970s to 50.1 % and 55.4 % in the 1980s and 1990s respectively, and decreased to 43.7 % in the 2000s. In contrast, the base flow to streamflow ratio (Qb/Qt) notably decreased from 17.1 % in the 1970s to 10.3 % and 3.2 % respectively during the 1980s and 1990s, but has increased to 20 % in the 2000s. The result for surface runoff agrees to findings in (Gebremicael *et al.*, 2013), but disagreement is observed for baseflow. The study reported that surface runoff (Qs) contribution to the total river discharge increased by 75 %, while the baseflow (Qb) decreased by 50 % from the 1970s to 2000s.

Furthermore, the SWAT simulation result from Table 5-9 and Figure 5-9 revealed that the Revap is a significant contributor to the total actual evapoation (TAE) in the UBNRB for the last 40 years. The mean annual contribution of Revap ranged from 21.4–25.6 %, this could be due to the large coverage of deep rooted Eucalyptus tree species that can access the saturated zone (Neitsch *et al.*, 2011). The Revap component in this study appears consistent with the results of (Abiodun *et al.*, 2018; Benyon *et al.*, 2006), who reported the annual Revap contribution to TAE ranged from 13–72 % and 20 % respectively for south-eastern Australia and Sixth Creek Catchments.

Table 5-8: Summary of the UBNRB's precipitation indices on daily time series data

Indices	1970s	1980s	1990s	2000s
Mean (mm)	4.17	4.05	4.42	4.16
95 percentile (mm)	12.57	12.52	13.66	13.31
99 percentile (mm)	17.34	17.77	19.44	19.65
1-day max (mm)	27.15	25.67	32.24	32.38
R20mm (days)	16	15	30	35
SDII (mm/day)	7.22	7.38	7.66	7.77

SDII is the ratio of total precipitation (mm) to R1mm (days).

In general, 1.8 % forest cover loss and 1 % increased cultivated land combined with 2.2 % increased rainfall from the 1970s to the 2000s led to a 16.9 % increase in simulated streamflow. The 1990s was the period during which the greatest deforestation and expansion of cultivated land was reported. Meanwhile, it was the time when the rainfall intensity and the number of rainfall events have significantly increased compared to the 1970s and 1980s, as shown in Table 5-8. Hence, the increased mean annual streamflow could be ascribed to the combined effects of LULC and climate change.

In the case of (Qs/Qt), the increasing pattern could be ascribed to increasing rainfall intensities and the expansion of cultivated land and diminution of forest coverage, which might adversely affect soil/water storage and decrease rainfall infiltration, thereby increasing water yield or streamflow. In contrast, the decreasing Qb/Qt is positively related to the increasing evapotranspiration linked to both LULC and climate factors (Table 5-9). This hypothesis can be explained with the change in CN2 parameter values obtained during calibration of the four SWAT model runs. The CN2 parameter value, which is a function of evapotranspiration derived from LULC, soil type, and slope increased in the 1980s and 1990s relative to the 1970s, and could be associated with the expansion of cultivated land and shrinkage of forestland. The increasing CN2 results reflect more surface runoff and less baseflow being generated.

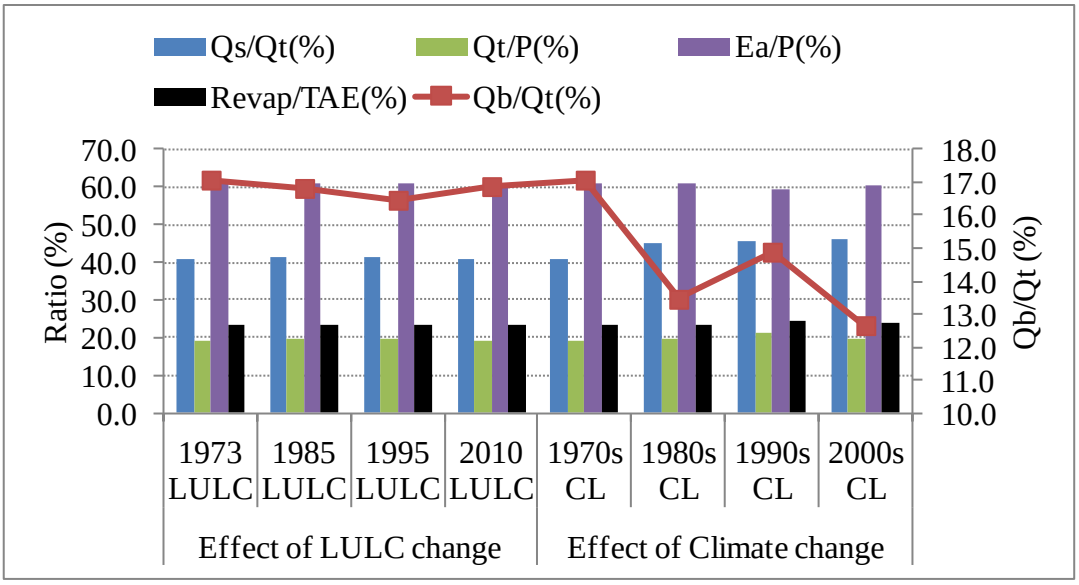

Figure 5-9: Ratio of water balance component analysis at the El Diem station using an isolated effect (LULC/climate change)

Table 5-9: Mean annual water-balance-components analysis in the UBNRB by considering LULC and climate change over respective periods. All streamflow estimates are for El Diem station.

	Unit	1970s	1980s	1990s	2000s	Change (%)		
						1970s-1980s	1970s-1990s	1970s-2000s
Precipitation (P)	mm	1428	1397	1522	1462	-2.2	6.6	2.4
Observed streamflow	(m^3s^{-1})	1549	1583	1686	1787	2.2	8.8	15.3
Surface flow (Qs)	mm	112.8	143.4	168.6	141.4	27.1	49.5	25.4
Lateral flow (Ql)	mm	116.8	113.4	125.9	117.6	-3.0	7.8	0.7
Base flow (Qb)	mm	47.3	29.6	9.8	64.7	-37.4	-79.3	36.8
Total water yield (Qt)	mm	276.9	286.3	304.3	323.7	3.4	9.9	16.9
Er=Revap	mm	269.2	257.2	310.6	241.0	-2.2	3.8	1.5
Ea (Ec+Et+Es)	mm	871.6	852.6	904.3	885.0	-4.5	15.4	-10.5
TAE	mm	1141	1110	1215	1126	-2.7	6.5	-1.3
Recharge (deep aquifer)	mm	16.7	15.0	16.7	16.3	-10.2	0.0	-2.4
Change in soil water	mm	-6.3	-14.0	-13.7	-3.5			
Qs/Qt	%	40.7	50.1	55.4	43.7			
Qb/Qt	%	17.1	10.3	3.2	20.0			
Qt/P	%	19.4	20.5	20.0	22.1			
Er (Revap)/TAE	%	23.6	23.2	25.6	21.4			
Ea/P	%	61.0	61.0	59.4	60.5			

where: water yield (Qt) =Qs+ Ql + Qb; Change in soil storage =P-Qs-Ql-Qb-Ea-Revap-Recharge

Another important factor contributing to decreasing of surface runoff and increasing base flow ratio from 1990s to the 2000s could be the establishment of soil and water conservation (SWC) measures. According to Haregeweyn *et al.* (2015), various nationwide SWC initiatives such as Food for Work (FFW), Managing Environmental Resources to Enable Transition (MERET) to more sustainable livelihoods, Productive Safety Net Programs (PSNP), Community Mobilization through free-labor days, and the National Sustainable Land Management Project (SLMP) have been undertaken since the 1980s. Haregeweyn *et al.* (2015) evaluated these initiatives' effectiveness and concluded that community labor mobilization seems to be the best approach. This can reduce mean seasonal surface runoff by 40 %, with broad spatial variability ranging from 4 % in Andit Tid (northwest Ethiopia) to 62 % in Gununo (south Ethiopia).

5.4.4 Single impacts of LULC changes

(Yan *et al.*, 2013) used "A fixing -changing" method, which was also applied to this study, to identify the hydrological impacts of LULC change alone. The calibrated and validated SWAT model and its parameter settings in the baseline period was forced by weather data from the baseline 1973–1980 period while changing only the LULC maps from 1985, 1995, and 2010, keeping the DEM and soil data constant as suggested by Hassaballah *et al.* (2017a). The result from Figure 5-9 indicated that Qs/Qt ratio changed from 40.7 % to 41.2 %, 41.9 %, and 40.9 % respectively by using the LULC maps from 1973, 1985, 1995 and 2010, whereas the Qb/Qt ratio changed from 17.1 % to 16.8 %, 16.5 %, and 16.9 % respectively. The largest Qs/Qt ratio (41.9 %) and the smallest Qb/Qt ratio (16.5 %) were recorded with the 1995 LULC map. This could be attributed to the 5.1 % reduction in forest coverage and 4.6 % increase in cultivated land with the 1995 LULC map relative to the 1973 LULC map.

On a basin scale over a decadal period, water gains mainly from precipitation. The losses are mainly due to runoff and evapotranspiration (Oki *et al.*, 2006) as the losses due to the deep percolation over the whole UBNRB is negligible (Steenhuis *et al.*, 2009). The long-term mean annual deep percolation simulated in this study is about 16.7 mm constant in four decadal periods, which is about 6 % of the total water yield. With the fixing-changing approach, the change in streamflow attributable to LULC change was essentially the change in evapotranspiration between the two periods, as the amount of precipitation was constant (1970s) and the change in water storage during the two periods was similar (Yan *et al.*, 2013). Annual Ea losses from seasonal crops are smaller than those from forests, because seasonal crops transpire during a relatively shorter time interval than perennial trees do (Yan *et al.*, 2013). As a result, the actual mean annual Ea simulated by the SWAT model was 871.6 mm at the baseline. It decreased to 871.4 mm and 871 mm in 1985 and 1995 respectively and increased to 872.1 mm in 2010. This could be due to simultaneous expansion of cultivated land and shrinkage in forest coverage in the 1985 and 1995 LULC maps relative to the 1973 base line. Furthermore, this deforestation may reduce canopy interception of the rainfall, decrease soil infiltration by increasing raindrop impacts, and reducing plant transpiration, which can significantly increase surface runoff and reducing base flow (Huang *et al.*, 2013). Here, the evapotranspiration change caused by the LULC change is minimal. As a result, the change for surface runoff and baseflow is not significant.

5.4.5 Single impacts of climate change

The impacts of climate change are analyzed by running the four models using a unique LULC map from 1973 with its model parameters while changing only the weather data sets from 1970s, 1980s, 1990s, and 2000s. The simulated water balance components shown in Figure 5-9 indicate that the Qs/Qt ratio increased from 40.7 % to 45.2 %, 45.6 %, and 46.2 % during the 1970s, 1980s, 1990s and 2000s respectively, while the Qb/Qt ratio changed from 17.1 % to 13.5 %, 14.9 %, and 12.7 % for the same simulation periods. The decreasing Qb/Qt ratio for the altered periods compared to the baseline period could be attributed to evapotranspiration changing from 872 mm to 854 mm, 906 mm, and 884 mm respectively in 1970s, 1980s, 1990s, and 2000s, which can be linked to temperature and amount of rainfall. However, to understand the effect of climate change on the water balance components, it is important to know the dominant rainfall-runoff process in the study area.

Although, no detailed research has been conducted on the Upper Blue Nile basin to investigate the runoff-generation processes, Liu *et al.* (2008) investigated the rainfall-runoff processes at three small watersheds located inside and around the Upper Blue Nile basin, namely, Mayber, AnditTid, and Anjeni. Their analysis showed that, unlike in temperate watersheds, in monsoonal climates, a given rainfall volume at the onset of the monsoon produces a different runoff volume than the same rainfall at the end of the monsoon. Liu *et al.* (2008) and Steenhuis *et al.* (2009) showed that the ratio of discharge to precipitation minus evapotranspiration, $Q/(P - ET)$, increases with cumulative precipitation from the onset of monsoon. This suggests that saturation excess processes play an important role in watershed response.

Furthermore, the infiltration rates that Engda (2009) measured in 2008 were compared with rainfall intensities in the Maybar and Andit Tid watersheds located inside and around the UBNRB. In the Andit Tid watershed, which has an area of less than 500 ha, the measured infiltration rates at 10 locations were compared with rainfall intensities considered from the 1986 –2004 period. The analysis showed that only 7.8 % of rainfall intensities were found to be higher than the lowest soil infiltration rate of 25mm h^{-1}. Derib (2005) performed a similar analysis in the Maybar watershed (with a catchment area of 113 ha). The infiltration rates measured from 16 measurements ranged from 19 mm h^{-1} to 600 mm h^{-1} with a 240 mm h^{-1} average and 180 mm h^{-1} median whereas the average daily rainfall intensity from 1996 to 2004 was 8.5 mm hr^{-1}. Hence, he suggested from these infiltration measurements that infiltration excess runoff is not a common feature in these watersheds.

From the above discussion points, it is to be noted that surface runoff could increase with increasing total rainfall amount regardless of rainfall intensity. However, the mean annual rainfall amount in this study was decreasing from the 1970s to the 1980s (1428 mm and 1397 mm respectively) while the (Qs/Qt) ratio increased from 40.7 % to 45.2 %. Similarly, the mean annual rainfall amount in the 1990s (1522 mm) was greater than the mean annual rainfall amount in the 2000s (1462 mm) while the (Qs/Qt) increased from 45.6 % to 46.2 %. In contrast, climate indexes such as 99-percentile rainfall, SDII (ratio of total precipitation amount to number of days when rainfall >1 mm (R1mm)), and number of days when rainfall >20 mm (R20mm) increase consistently from 1970 to the 2000s, as shown in Table 5-8. This indicates that the increasing of surface runoff might be due to an increasing of number of extreme rainfall events and rainfall

intensity. Although, we did not use hourly rainfall data for the SWAT model, this study suggested that infiltration excess of overland flow dominates the rainfall-runoff processes in the UBNRB, not saturation excess of overland flow. The contradiction from the previous studies might be due either to the limitation of the SWAT- CN method when applied in monsoonal climates or the overlooked of tillage activities, which significantly affect the soil infiltration rate. Extensive tillage activities are carried out across the basin at the beginning of the rainy season. Soils get disturbed as a result, which can increase the infiltration rate and ultimately decrease the amount of rainfall converted to runoff.

Although the CN method is easy to use and provides acceptable results for discharge at the watershed outlet in many cases, researchers have concerns about its use in watershed models (Steenhuis *et al.*, 1995; White *et al.*, 2011). The SWAT-CN model relies with a statistical relationship between soil moisture condition and CN value obtained from plot data in the United States with a temperate climate that was never tested in a monsoonal climate exhibiting two extreme soil moisture conditions. In monsoonal climates, long periods of rain can lead to prolonged soil saturation whereas during the dry period, the soil dries out completely, which may not happen in temperate climates (Steenhuis *et al.*, 2009). Hence, to assess the rainfall-runoff processes properly, further research that considers biophysical activities such as tillage and seasonal effects on soil moisture at representative watersheds of the basin is necessary.

Table 5-10: The mean annual hydrological response in the combined and isolated LULC and climate change effect.

		Simulated (mm)				Change (mm)			Contribution (%)		
		1970s	1980s	1990s	2000s	1970s - 1980s	1970s - 1990s	1970s - 2000s	1970s - 1980s	1970 - 1990	1970 - 2000
P	Cld	1428	1397	1522	1463						
	Cls	1428	1428	1428	1428						
LULC	LUs	1973	1973	1973	1973						
	LUd	1973	1985	1995	2010						
Qs	ClCe	112.8	125.8	147.0	132.8	13.0	34.2	20.0	87.6	90	95.7
	LuCe	112.8	114.4	115.8	113.1	1.6	3.0	0.3	10.8	7.9	1.4
	Combe	112.8	127.6	150.8	133.7	14.8	38.0	20.9			
Ql	ClCe	116.8	115.1	127.3	118.3	-1.7	10.5	1.5	82.9	98	100
	LuCe	116.8	116.4	117.0	116.8	-0.4	0.2	0.0	19.0	1.9	0.0
	Combe	116.8	114.7	127.5	118.3	-2.1	10.7	1.5			
Qb	ClCe	47.3	37.5	48.0	36.4	-9.8	0.7	-10.9	93.7	-100	94.8
	LuCe	47.3	46.7	45.9	46.7	-0.6	-1.4	-0.6	5.7	200	5.2
	Combe	47.3	36.8	46.6	35.8	-10.5	-0.7	-11.5			

Note: Cld in the table denotes climate dynamics, Cls: climate static, LUs: LULC static, LUd: LULC dynamics, ClCe: climate change effect, LuCe: LULC change effect and Combe: combined effect.

The contrast between the isolated climate change and isolated LULC changes (Table 5-10) indicated that surface runoff simulation due to combined effect increased by 14.8 mm between 1970s and 1980s periods while the isolated climate changes effect increased the surface runoff simulation by 13 mm, which accounted for about 87.6 % of the total surface runoff increment.

The isolated LULC changes increased surface runoff by 1.6 mm, which accounted for 10.8 % of the total surface runoff change (14.8 mm). Between this simulation period, combined LULC change and climate variation decreased baseflow by -10.5 mm, and the percent contributions were 93.7 % (-9.8 mm) for the climate variation and 5.7 % (-0.6 mm) for the LULC changes. The integrated effect of LULC change and climate variability increased surface runoff by 38 mm between 1970s and 1990s while the isolated effect of climate variation increased surface runoff by 34.2 mm, which accounted for 90 % of the total surface runoff change. Between these periods, the LULC changes alone increased surface runoff by 3 mm that contributed 7.9 % of the total change due to combined effects. Between this simulation period, the combined changes of LULC and climate decreased baseflow by -0.7 mm and the percent contribution were -100 % (0.7 mm) for the climate change and 200 % (-1.4 mm) for LULC change. For the period between 1970s and 2000ss, the combined effects of LULC changes and climate change increased surface runoff by 20.9 mm while the isolated effect of climate change contributed about 95.7 % (20 mm) of the total surface runoff changes (20.9 mm). During this period, the surface runoff increased by 0.3 mm due to LULC change alone, this accounted for 1.4 % of the total surface runoff change. Between this simulation period, combined changes of LULC and climate decreased baseflow by -11.5 mm, and the percent contributions were 94.8 % (-10.9 mm) for the climate change and 5.2 % (-0.6 mm) for the LULC change.

In conclusion, the above results showed that LULC change and climate variation during 1970s and 2000s increased surface runoff and decreased baseflow, but the contribution of climate change was significantly higher than that of LULC change. Teklay *et al.* (2019) showed similar findings in Gumara watershed, Lake Tana sub-basin. Likewise, Yin et al. (2017) reported a similar findings in a semi-humid and semi-arid transition zone in northwest China.

Chapter 6 Analyzing future climate changes of the upper Blue Nile River basin[3]

6.1 Statistical downscaling methods for climate change analysis

Due to the coarse spatial resolution of Global climate models (GCMs), they cannot be used at local or regional scale for impact studies; hence, there is need to bridge the gap between the large-scale variables (predictors) and local scale variables (predictands). The methods used to convert the coarse spatial resolution of GCM outputs into high-spatial resolution of point data are usually referred to as downscaling techniques (Chisanga et al., 2017). Generally, downscaling methods are classified in to dynamic and statistical downscaling (Fowler *et al.*, 2007; Wilby *et al.*, 2002). Dynamic downscaling nests higher resolution Regional Climate Models (RCMs) into coarse resolution GCMs to produce complete set of meteorological variables, which are consistent each other. The outputs from this method are still not at required scale to what the hydrological model require. These models are mostly complex and computationally expensive. In Statistical Downscaling methodologies, local climate information is derived by first determining statistical models which relate large-scale climate variables (or "predictors") to regional and local variables (or "predictands") (Wilby *et al.*, 2004a). Statistical downscaling overcomes this challenge moreover it is computationally undemanding, simple to apply and provides the possibility of uncertainty analysis (Dibike *et al.*, 2005; Semenov *et al.*, 1997; Wilby *et al.*, 2002). Extensive details on the strength and weakness of the two methods can be found (Wilby *et al.*, 2007; Wilby *et al.*, 1997). Among the different possibilities, two well recognized statistical downscaling tools, a regression based Statistical Down-Scaling Model (SDSM) (Wilby *et al.*, 2002) and a stochastic weather generator called Long Ashton Research Station Weather Generator (LARS-WG) (Semenov *et al.*, 1997; Semenov *et al.*, 2002) were chosen for this study. They have been tested in various regions e.g., (Chen *et al.*, 2013; Dibike *et al.*, 2005; Dile *et al.*, 2013; Elshamy *et al.*, 2009b; Fiseha *et al.*, 2012; Hashmi *et al.*, 2011; Hassan *et al.*, 2014; Maurer and Hidalgo, 2008; Yimer *et al.*, 2009) under different climatic conditions of the world.

[3]Based on: Mekonnen, D.F., Disse, M.: Analyzing the future climate change of Upper Blue Nile River basin using statistical downscaling techniques. Hydrology and Earth System Sciences, 22(4), 2391, 2018a. DOI:10.5194/hess-22-2391-2018

6.1.1 Description and approaches of LARS-WG Model

LARS-WG is a stochastic weather generator, which can be used for the simulation of weather data at a single station under both current and future climate conditions. These data are in the form of daily time-series for a group of climate variables, namely, precipitation, maximum and minimum temperature and solar radiation (Chen *et al.*, 2013; Semenov *et al.*, 1997).

Stochastic weather generators were originally developed for two main purposes:
1. To provide a means of simulating synthetic weather time-series with statistical characteristics corresponding to the observed statistics at a site, but which were long enough to be used in an assessment of risk in hydrological or agricultural applications.
2. To provide a means of extending the simulation of weather time-series to unobserved locations, through the interpolation of the weather generator parameters obtained from running the models at neighboring sites.

It is worth noting that a stochastic weather generator is not a predictive tool that can be used in weather forecasting, but is simply a means of generating time-series of synthetic weather statistically 'identical' to the observations. New interest in local stochastic weather simulation has arisen because of climate change studies. At present, output from GCMs is of insufficient spatial and temporal resolution and reliability to be used directly in impact models. A stochastic weather generator, however, can serve as a computationally inexpensive tool to produce multiple-year climate change scenarios at the daily time scale which incorporate changes in both mean climate and in climate variability (Semenov *et al.*, 1997).

LARS-WG uses a semi-empirical distribution (EPM) that is defined as the cumulative probability distribution function(CDF) to approximate probability distributions of dry and wet series, daily precipitation, minimum and maximum temperatures.

$$EPM = \{a_0, a_i, h_i, i = 0, \dots, 23\} \quad (6\text{-}1)$$

EPM is a histogram of the distribution of 23 different intervals (a_{i-1}, a_i) where $a_{i-1} < a_i$ (Semenov et al., 2002), which offers more accurate representation of the observed distribution compared with the 10 used in the previous version. By perturbing parameters of distributions for a site with the predicted changes of climate derived from global or regional climate models, a daily climate scenario for this site could be generated, which can be used in conjunction with a process-based impact model for assessing the impacts. In general, the process of generating synthetic weather data can be categorized in three distinct steps: model calibration, model validation and scenario generation as represented in Figure 6-1 (a), which are briefly described by (Semenov *et al.*, 2002) as follows. LARS-WG will be able to generate synthetic weather data based on as little as a single year of observed daily weather data. However, since the generated weather data will be based on probability distributions derived from this observed data, so the more data observed used the closer LARS-WG be able to match the climate for the target site. The use of at least 20-30 years of daily weather data is recommended.

Model calibration

The inputs to LARS-WG are the series of daily-observed data (precipitation, minimum and maximum temperature) of the base period (1984-2011) and site information (latitude, longitude and altitude). After the input data preparation and quality control, model calibration is done to use the function "SITE ANALYSIS" in LARS-WG. In model calibration, the observed daily weather data at a given site were used to determine a set of parameters for probability distributions of weather variables. These parameters are used to generate a synthetic weather time series of arbitrary length by randomly selecting values from the appropriate distributions, having the same statistical characteristics as the original observed data but differing on a day-to-day basis. The LARS-WG distinguishes wet days from dry days based on whether the precipitation is greater than zero. The occurrence of precipitation is modeled by alternating wet and dry series approximated by semi empirical probability distributions.

Model validation

Model validation is to analyze and compare the statistical characteristics of the observed and synthetic weather data to assess the ability of LARS-WG to simulate the precipitation, Tmax, and Tmin at the chosen sites in order to determine whether it is suitable for use in the study or not. The statistical characteristics of the observed and synthetic weather data are analyzed to determine if there are any statistically-significant differences using Chi-square goodness of fit test (KS) and the means and standard deviation using t and F test respectively by changing the parameters of LARS-WG (number of years and seed number). Each of the tests computes a test statistics and a corresponding p-value, which indicate how likely that generated and observed data are coming from the same distribution. If p-value is very low and below the significance level, set to 0.05 in this study, then the generated simulated climate is unlikely to be the same as the 'true' climate.

Generation of synthetic weather data

The parameter files derived from observed weather data during the model calibration process are used to generate synthetic weather data having the same statistical characteristics as the original observed data.

Generation of climate scenarios

To generate climate scenarios at a site for a certain future period and an emission scenario, the LARS-WG baseline parameters, which are calculated from observed weather for a baseline period (1984-2011), are adjusted by the Δ-changes for the future period and the emissions predicted by a GCM for each climatic variable for the grid covering the site. In this study, the local-scale climate scenarios based on the SRES A2, A1B and B1 scenario simulated by the selected six GCMs are generated for the periods of 2011–2030, 2046–2065, and 2080–2099 to predict the future change of precipitation and temperature in UBNRB.

Δ-changes were calculated as relative changes for precipitation and absolute changes for minimum and maximum temperatures eqn. (6-2) and (6-3), respectively. No adjustments for distributions of dry and wet series and temperature variability were made, because this would

require daily output from the GCMs which is not readily available from LARS-WG data set (Semenov and Stratonovitch, 2010).

$$\Delta T_i = \left(\bar{T}_{GCM,FUT,i} - \bar{T}_{synt,Base,i}\right) \quad (6\text{-}2)$$

$$\Delta P_i = \left(\bar{P}_{GCM,FUT,i} \Big/ \bar{P}_{synt,Base,i} \right) \quad (6\text{-}3)$$

In above equations, ΔT_i and ΔP_i are climate change scenarios of the temperature and precipitation, respectively, for long-term average for each month ($1 \leq i \leq 12$); $\overline{T}_{GCM,FUT,I}$ the long term average temperature simulated by the atmospheric observation global climate model (AOGCM) in the future periods per month for three time periods; $\overline{T}_{Synth,Base,i}$ is the long term average temperature simulated by the model in the period similar to observation period (in this study 1984-2011) for each month. The above calculations are true for precipitation as well.

For obtaining time series of future climate scenarios, climate change scenarios are added to the observations values by employing the change factor (CF) method eqns. (6-4) and (6-5) (in this study 1984-2011):

$$T = T_{obs} + \Delta T \quad (6\text{-}4)$$

$$P = P_{obs} + \Delta P \quad (6\text{-}5)$$

T and P are time series of the future climate scenarios of temperature and precipitation (2011-2100); T_{obs} and P_{obs} are observed temperature and precipitation. So, in LARS-WG downscaling unlike SDSM, large-scale atmospheric variables are not directly used in the model, rather, based on the relative mean monthly changes between current and future periods predicted by a GCM, local station climate variables are adjusted proportionately to represent climate change (Dibike *et al.*, 2005).

6.1.2 Description and approaches of SDSM

The SDSM can be described as a hybrid of the stochastic weather generator and regression based in the family of transfer function methods. A multiple linear regression model is developed between a few selected large-scale predictor variables and local-scale predictands such as temperature and precipitation to condition local scale weather parameters from large-scale circulation patterns. The stochastic component of SDSM enables the generation of multiple simulations with slightly different time series attributes, but the same overall statistical properties. (Wilby *et al.*, 2002). It requires two types of daily data, the first type corresponds to local predictands of interest (e.g. temperature, precipitation) and the second type corresponds to the data of large-scale predictors (NCEP and GCM) of a grid box closest to the station.

The SDSM model categorizes the task of downscaling into a series of discrete processes such as quality control and data transformation, screening of predictor variables, model calibration, synthesize observed data, generation of climate change scenario, and diagnostic testing and statistical analysis as shown in Figure 6-1(b). Detail procedures and steps can be found (Wilby *et al.*, 2002) for further reading. Screening potentially useful predictor-predictands relationships for model calibration is one of the most challenging but very crucial stages in the development of any statistical down scaling model. It is because of the fact that the selection of appropriate predictor variables largely determines the success of SDSM and also the character of the downscaled climate scenario (Wilby *et al.*, 2007). After routine screening procedures, the predictor variables that provide physically sensible meaning in terms of their high explained variance, correlation coefficient (r) and the magnitude of their probability (p value) were selected.

a) b)

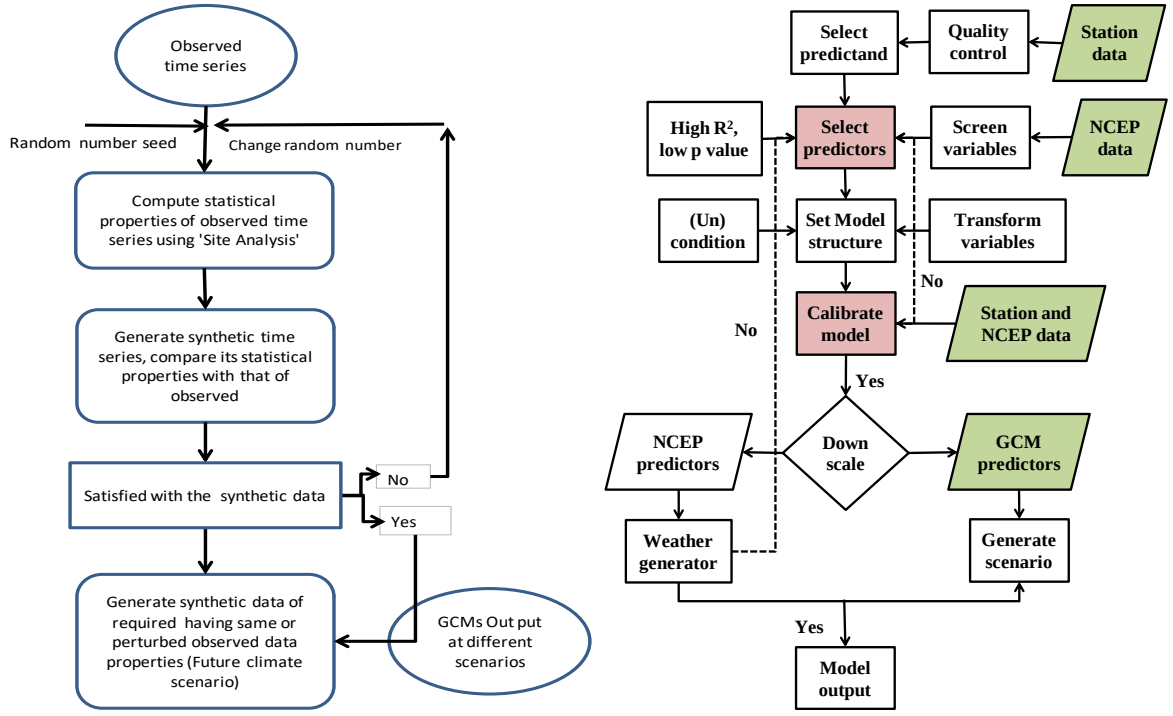

Figure 6-1: Schematic diagram of a) LARS WG analysis b) SDSM analysis source (Wilby *et al.*, 2002)

The model calibration process in SDSM was used to construct downscaled data based on multiple regression equations given daily weather data (predictands) and the selected predictor variables at each station. The model was structured as monthly model for both daily precipitation and temperature using the same set of the selected NCEP predictors for the calibration period. Hence, 12 regression equations were developed for 12 months. Bias correction and variance inflation factor was adjusted until the model replicates the observed data. Model validation was carried out by testing the model using independent data set. To compare the observed and simulated data, SDSM has provided summary statistics function that summarizes the result of

both the observed and simulated data. Time series of station data and large-scale predictor variable (NCEP reanalysis data) were divided into two groups, for the period from 1984-1995/ 1984-2000 and 1996-2001/2001-2005 for model calibration and validation of HadCM3/canESM2 GCMs respectively.

The Scenario Generator operation produces ensembles of synthetic daily weather series given observed daily atmospheric predictor variables supplied by a GCM either for current or future climate (Wilby et al., 2002). The scenario generation produced 20 ensemble members of synthetic weather data for 139 years (1961-2099) from HadCM3 A2a and B2a scenarios and for 95 years (2006-2100) from canESM2 for RCP2.6, 4.5 and 8.5 scenarios, and the mean of the ensemble members was calculated and used for further climate change analysis. The generated scenario was divided into three time windows of 30 years of data (2011-2040), (2041-2070) and (2071-2100) henceforth called 2030s, 2050s and 2080s, respectively.

6.1.3 Model performance evaluation criteria

A number of statistical tests were carried out to compare the skills of the two downscaling models categorized into two main classes. First, quantitative statistical tests, measure the average magnitude of the errors in a set of predictions without considering their direction. Performance evaluation metrics such as MAE, RMSE and bias were applied. These metrics are by far the most widely used and accepted of the many possible numerical metrics (Amirabadizadeh *et al.*, 2016; Bennett *et al.*, 2013) to evaluate the comparative performance of the models to simulate the current climate variable of precipitation on the basis of long-term monthly averages defined by using eqns.(4-5) to (4-10). In this study correlation and correlation-based measures such as coefficient of determination (R^2) and coefficient of efficiency (Nash–Sutcliffe efficiency, NSE) are not included due to the fact that these measures are oversensitive to extreme values and are insensitive to additive and proportional differences between model simulations and observations (Legates and McCabe, 1999). Evaluation was done in two steps as suggested by Goly *et al.* (2014): (i) equally weighing the metrics and (ii) varying the weights of metrics. For the case of equally weighted, the following steps were applied. (a) Compare the values of the performance metrics among the models and ranking (obtaining individual model rankings for each performance metrics) at station level. Here, score 1 will be given to the model that has smaller metrics value and score 3 to the one having larger value and 2 for the model having the value in between. (b) Summing up the score pertained to each model across all the stations. (c) Once the final scores are obtained for each evaluation metric, the models are ranked again based on the totals by summing up the metrics score value for each models.

Additionally, the varying weights technique was applied to the performance metrics as given in eqn. (6-6) to rank the models according to their skills. To avoid the discrepancy in weighing the performance measures because of differences in the order of their magnitudes, each performance measure is normalized (divided by the maximum value) and then the cumulative weighted performance measure for each downscaling model is calculated (Goly *et al.*, 2014). The weights of metrics are arranged in such a way that more emphasis is given to MAE and RMSE, followed by bias (0.5, 0.35 and 0.15 respectively).

$$Wi = R^2 \frac{{R_i}^2}{{R_{max}}^2} + MAE \frac{MAE_i}{MAE_{max}} + RMSE \frac{RMSE_i}{RMSE_{max}} + NSE \frac{NSE_i}{NSE_{max}} + Bias \frac{Bias_i}{Bias_{max}} \quad (6\text{-}6)$$

Where the index i refers to a downscaling model, Wi refers to overall performance measure, and $0 < Wi < 1$.

Secondly, qualitative tests, comparing the skill of models about capturing the distribution of the whole range observed data and in capturing the extreme precipitation events. For this purpose, statistical metrics such as IRF, ABC, 99p, 95p, 1daymax, R1, R10, R20 and SDII and graphical representations of box–whisker plots and KS cumulative distribution test were applied. KS is used to compare the probability distribution function (PDF) of the observations to the PDF of the simulated precipitation (Simard and L'Ecuyer, 2011). These plots provide a convenient visual summary of several statistical properties of the data set as they vary over time. A scoring technique is applied to compare the accuracy of the models. In this scoring technique, the bias of an evaluation metric for each station is used: score 1 will be given to the model that has smaller bias, score 3 to the one with a larger bias and 2 for the model with a value in between. Afterwards, evaluation was carried out using an equally weighted method only due to the assumption that the metrics have equal weights, as discussed above for model ranking. For the Kolmogorov–Smirnov (KS) cumulative distribution test, the observed and the simulated precipitation data from each model were compared using a *p* value at the significance level of 5% for each station. The computed p value is lower than the significance level $\alpha = 0.05$, which indicates the simulated fail to follow the same distribution as the observed. Furthermore, the *F* test and t test are applied to test the equality of monthly variances of precipitation and equality of monthly mean respectively.

IRF and ABC are recommended by (Campozano *et al.*, 2016), while 95p, 99p, 1day max, R1, R10, R20 and SDII are recommended by Expert on Climate Change Detection and Indices (ETCCDI). The inter-quartile relative fraction (IRF): to evaluate the modeled variability representation relative to the observed is defined by eqn. (6-7)

$$IRF = \frac{Q_3^m - Q_1^m}{Q_3^o - Q_1^o} \quad (6\text{-}7)$$

A value of IRF > 1 represents overestimation of the variability, IRF = 1 is a perfect representation of the variability, and IRF < 1 is an underestimation of the variability; $Q^m{}_3$ and $Q^o{}_3$ and the 75th modeled and observed percentile;$Q^m{}_1$ and $Q^o{}_1$ and the 25th modeled and observed percentile.

The absolute cumulative bias (ACB): This can be used to evaluate the bias of the 25th, 50th, and 75th percentiles eqn.(6-8);

$$ACB = abs(Q^m_1 - Q^o_1) + (Q^m_2 - Q^o_2) + (Q^m_3 + Q^o_3) \quad (6\text{-}8)$$

Where Q^m_3 and Q^o_3 are the 75th modeled and observed percentile, Q^m_2 and Q^o_2 are the 50th modeled and observed percentile Q^m_1, and Q^o_1 are the 25th modeled and observed percentile respectively. A value of ACB= 0 is a perfect representation of the modeled and observed distributions, while under- or overestimation indicates a divergence of ACB from zero to positive values. The terms 95p and 99p denote the 95th and 99th percentiles of daily precipitation amount respectively. 1 daymax is the highest 1-day precipitation amount. R1, R10 and R20 are number of precipitation days (≥1 mm), heavy precipitation days (≥10 mm) and extreme heavy precipitation days (≥20mm) respectively. SDII is the simple daily intensity index calculated as the ratio of total precipitation to the number of wet days (≥1 mm).

6.2 Datasets

6.2.1 Local data sets

The historical rainfall, maximum and minimum temperature data for the study area were obtained from ENMA, which were analyzed and checked for further quality control as described in section 4.2. Networks of 40 meteorological stations were chosen to represent the UBNRB. These were selected to cover a large range of time, space and altitude within the region. The less performed stations during calibration and validation were removed from further analysis so that the number of stations considered for SDSM and LARS-WG are different. For example, 15, 29 and 24 rainfall stations were representing for SDSM (canESM2), CMIP3 GCMs (LARS-WG) and CMIP5 GCMs (LARS-WG) respectively..

6.2.2 Large scale datasets

Global climate models (GCMs)

The GCMs used in this study were from both phases 3 and 5 of the Coupled Model Intercomparison Project phase 3 and phase 5 (CMIP3 and CMIP5) through different databases. A new version of the LARS-WG5.5 was applied for this study that incorporates predictions from 15 GCMs which were used in the intergovernmental panel on climate change fourth assessment report (IPCC's AR4) based on Special Emissions Scenarios SRES B1, A1B and A2 for three time windows as listed in Table 6-1. Furthermore, LARS-WG that incorporates three GCMs from CMIP5 climate models based on the new radiative forcing scenarios (Representative Concentration Pathway, RCP) was used for this study.

As it is difficult to process all the incorporated 15 CMIP3 GCMs and large differences in predictions of climate variables among the GCMs are expected, the performance of GCMs in simulating the current climate variables of the study area (UBNRB) should be evaluated, and the best performing GCMs were selected. The MAGICC/SCEGEN computer program tool was used for the performance evaluation of the 15 GCMs found in the LARS-WG5.5 database, as it is a standard method for selecting models based on their ability to represent current climate accurately, either for a particular region or for the globe. In this study, we used a semi

quantitative skill score that rewards relatively good models and penalizes relatively bad models as suggested by the Wigley (2008) user manual. The statistics used for model selection are pattern correlation (R^2), Root mean square error (RMSE), bias (B), and a bias-corrected RMSE (RMSE-corr). The analysis was done separately for precipitation and temperature and finally an average score value was taken for model selection. The six best-performing GCMs have been selected for this study, namely HadCM3, GFDL-CM2.1, ECHAM5-OM, CCSM3, MRI-CGCM2.3.2 and CSIRO-MK3 in the order of their performance to construct future precipitation, maximum temperature and minimum temperature in the UBNRB for the time periods of the 2030s, 2050s and 2080s under A1B, A2 and B1 scenarios; see (Table 6-1).

Table 6-1: Selected Global climate models from IPCC AR4 incorporated into the LARS-WG

Research centre	Country	GCM	Model acronym	Grid Resolution	Emission Scenarios
CMIP 3 GCMs					
Common Wealth Scientific and Industrial Research Organization	Australia	CSIRO-MK3	CSMK3	1.9x1.9^o	A1B, B1
Max-Plank Institute for Meteorology	Germany	ECHAM5-OM	MPEH5	1,9x1.9^o	A1B,A2,B1
National Institute for Environmental Studies	Japan	MRI-CGCM2.3.	MIHR	2.8x2.8^o	A1B,B1
UK Meteorological Office	UK	HadCM3	HADCM3	2.5x3.75^o	A1B,A2,B1
Geophysical Fluid Dynamics Lab	USA	GFDL-CM2.1	GFCM21	2x2.5^o	A1B,A2,B1
National Centre for Atmospheric Research	USA	CCSM3	NCCCS	1.4x1.4^o	A1B,B1
CMIP 5 GCMs used to derived the range of future climate projections (https://portal.enes.org/data/enes-model-data/cmip5/resolution)					
EC-EARTH consortium		EC-EARTH	EARTH	1.12x1.12^o	RCP4.5, 8.5
NOAA/Geophysical Fluid Dynamics Laboratory	USA	GFDL-CM3	GFDL	2x2.5^o	RCP4.5, 8.5
Met Office Hadley Centre	United Kingdom	HadGEM2-ES	HadGEM2	1.25x1.875^o	RCP2.6,4.5,8.5
Atmosphere and Ocean Research Institute	Japan	MIROC5	MIROC	1.4x1.4^o	RCP4.5,8.5
Max Planck Institute for Meteorology	Germany	MPI-ESM-MR	MPI	1.8x1.88^o	RCP4.5,8.5
Canadian Centre for Climate Modeling and Analysis (CCCma)	Canada	canESM2		2.8x2.8^o	RCP2.6, 4.5, 8.5

B: baseline; T1: 2011–2030; T2: 2046–2065; T3: 2081–2100

Moreover, atmospheric large-scale predictor variables used for representing the present condition were obtained from the National Centre for Environmental Prediction (NCEP) reanalysis data set. CanESM2, a second-generation Canadian earth system model (ESM) developed by Canadian Centre for Climate Modeling and Analysis (CCCma) of Environment Canada that represents CMIP5 and HadCM3 outputs from the Hadley Centre, United Kingdom (UK) representing CMIP3 were used in SDSM for the construction of daily local meteorological variables corresponding to their future climate scenario.

The reason for selecting these two GCMs was that they are models that made daily predictor variables freely available to be directly fed into the SDSM, covering the study area with a better resolution. Additionally, HadCM3 is the most used GCMs in previous studies such as (Dibike *et al.*, 2005; Dile *et al.*, 2013; Hassan *et al.*, 2014; Yimer *et al.*, 2009), and HadCM3 ranked first in performance evolution done by MAGICC/SCEGEN computer program tools and its downscaled results match with the ensemble mean of the six GCMs used in LARS-WG model.

Furthermore, they can represent two different scenario generations describing the amount of greenhouse gases (GHGs) in the atmosphere in the future. HadCM3 GCM used emission scenarios of A2 and B2 that were used in the CMIP3 for the IPCC's AR4 (IPCC, 2007) . Further explanation of SRES scenario and representative concentration pathways (RCPs) is presented in Table 6-2, Table 6-3 and Appendix 27.

Table 6-2: CO2 concentrations (ppm) for selected climate scenarios specified in the Special Report on Emissions Scenarios (SRES) (Semenov et al., 2010).

scenario	Key assumptions	CO2 concentration		
		2011-2030	2046-2065	2081-2100
B1 'The sustainable world'	Rapid change in economic structures, 'dematerialization' including improved equity and environmental concern. There is a global concern regarding environmental and social sustainability and more effort in introducing clean technologies. The global population reaches 7 billion by 2100.	410	492	538
B2 'The world of technological in equalities	A heterogeneous society emphasizing local solutions to economic, social and environmental sustainability rather than global solutions. Human welfare, equality and environmental protections all have high priority.	406	486	581
A1B 'The rich world'	Characterized by very rapid economic growth (3% yr–1), low population growth (0.27% yr–1) and rapid introduction of new and more efficient technology. Globally there is economic and cultural convergence and capacity building, with a substantial reduction in regional differences in per capita income.	418	541	674
A2 'The separated world'	Cultural identities separate the different regions, making the world more heterogeneous and international cooperation less likely. 'Family values', local traditions and high population growths (0.83% yr–1) are emphasized. Less focus on economic growth (1.65% yr–1) and material wealth.	414	545	754

Note: CO2 concentration for the baseline scenario, 1960–1990, is 334 ppm

Table 6-3: Types of the RCP scenarios (Moss *et al.*, 2008)

Name	Radiative forcing[1]	Concentration (ppm)[2]	Pathway
RCP8.5	>8.5Wm^{-2} in 2100	>1,370 CO2-equiv. In 2100	Rising
RCP6.5	~6Wm^{-2} at stabilization after 2100	850CO2-equiv.(at stabilization after 2100)	Stabilization without overshoot
RCP4.5	~4.5Wm^{-2} at stabilization after 2100	650 CO2-equiv.(at stabilization after 2100)	Stabilization without overshoot
RCP2.6	Peak at 3Wm^{-2} at stabilization before 2100 and then declines	peak 490 CO2-equiv. before 2100 and then declines	peak and decline

Notes:
[1] Approximate radiative forcing levels were defined as ±5% of the stated level in Wm^{-2}. Radiative forcing values include the net effect of all anthropogenic GHGs and other forcing agents.
[2] Approximate CO2 equivalent (CO2-eq) concentrations. The CO2-eq concentrations were calculated with the simple formula Conc = 278 * exp(forcing/5.325). Note that the best estimate of CO2-eq concentration in 2005 for long-lived GHGs only is about 455 ppm, while the corresponding value including the net effect of all anthropogenic forcing agents (consistent with the table) would be 375 ppm CO2-eq..

The NCEP dataset were normalized over the complete 1961-1990 period data, and interpolated to the same grid as HadCM3 (2.5^{o} latitude x 3.75^{o} longitude) and canESM2 (2.8125^{o} latitude x 2.8125^{o} longitude) from its horizontal resolution of (2.5^{o} latitude x 2.5^{o} longitude), to represent the current climate conditions. NCEP reanalysis data were normalized and interpolated using eqn. (6-9) as (Hassan *et al.*, 2014):

$$u_n = \frac{(u_t - u_a)}{\sigma_u} \qquad (6\text{-}9)$$

In which u_n is the normalized atmospheric variable at time t, u_t is the original data at time t, u_a is the multiyear average during the period, and σ_u is the standard deviation.

The canESM2 outputs for three different climate scenarios namely: RCP 2.6, RCP 4.5 and RCP 8.5 for the period 2006-2100 while the outputs of HadCM3 for A2a (medium-high) and B2a (medium-low) emission scenarios for the period 1961-2099 were obtained on a grid by grid box basis for the study area from the Environment Canada website http://ccds-dscc.ec.gc.ca/index.php?page=dst-sdi (the "a" in A2a and B2a refers the ensemble member in the HadCM3 A2 and B2 experiments). The archive of canESM2 and HadCM3 GCM output contains 26 daily predictor variables each as listed in Table 6-4.

Table 6-4: Name and description of all NCEP predictors on HadCM3 & canESM2 grid

Variables	Descriptions	variables	Descriptions
temp	Mean temperature at 2 m	s500 +	Specific humidity at 500 hpa height
mslp	Mean sea level pressure	s850+	Specific humidity at 850 hpa height
p500	500 hpa geopotential height	b_f	Geostrophic air flow velocity
p850	850 hpa geopotential height	b_z	Vorticity
rhum [a]	Near surface relative humidity	b_u	Zonal velocity component
r500[a]	Relative humidity at 500 hpa	b_v	Meridional velocity component
r850[a]	Relative humidity at 850 hpa	bzh	Divergence
shum	Near surface specific humidity	bthas	Wind direction
Prec+	Total precipitation		

(a) refers to different atmospheric levels: the surface (p_), 850 hpa height (p8), and 500 hpa height (p5), (b) refers predictors only found from HadCM3, (+) refers predictors only for canESM2

6.3 Results and discussions

6.3.1 Calibration and validation of LARS-WG

To verify the performance of LARS-WG, in addition to the graphic comparison, some statistical tests were performed. The KS test is performed to test equality of the seasonal distributions of wet and dry series (WDSeries), distributions of daily rainfall (RainD), and distributions of daily maximum (TmaxD) and minimum (TminD) temperature. The F-test is performed on testing equality of monthly variances of precipitation (RMV) while the t test is performed on verifying equality of monthly mean rainfall (RMM), monthly mean of daily maximum temperature (TmaxM), and monthly mean of daily minimum temperature (TminM). All of the tests calculate a p-value, which is used to accept or reject the hypotheses that the two sets of data (observed and generated) could have come from the same distribution at the 5% significance level. Therefore, the average number of p-values less than 5% recorded from 29 stations and percentage failed from the total of 8 seasons or 12 months has been presented in Appendix 12. It can be seen from the result LARS-WG performs very well for all parameters except RMM and RMV. On the other hand, an average of 2.9 % and 17.5% of the months of a year were recorded a p value < 5 % for the monthly mean and variance of precipitation respectively. From these numbers, it can be noted that the model is less capable in simulating the monthly variances than the other parameters.

For illustrative purpose, graphical representation of monthly mean and standard deviation of the simulated and observed precipitation, Tmax and Tmin were constructed in Figure 6-2 for randomly chosen Gondar station, as it has been difficult to present the result of all stations. Please see Appendix 24 for the other stations. It can be seen from the result that observed and simulated monthly mean precipitation, Tmax and Tmin matches very well. However, as it is known for being difficult to simulate the standard deviations in most statistical downscaling

studies, the performance of the standard deviation is less accurate as compared to the mean (Figure 6-2b).

a) b)

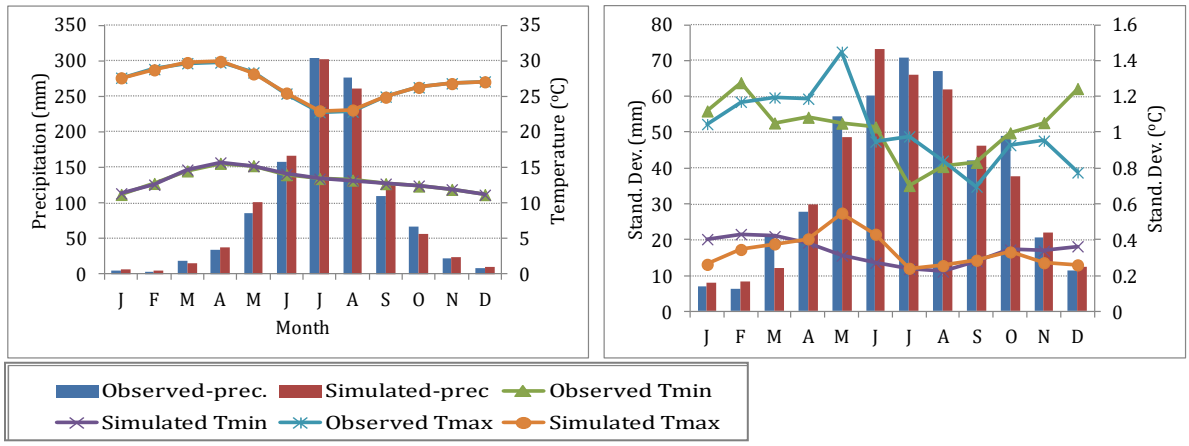

Figure 6-2: Observed and simulated a) mean monthly precipitation,Tmax and Tmin ; b) standard deviation of precipitation, Tmax and Tmin using LARS-WG

6.3.2 Screening variable, model calibration and validation of SDSM

Initially, offline correlation analysis was performed using SPSS software between predictands and NCEP reanalysis predictors to identify an optimal lag and physically sensible predictors for climate variables of precipitation, Tmax and Tmin. Analysis of the offline correlation revealed that an optimal lag or time shift does not improve the correlation of predictands and predictors for this particular study. Average partial correlation of observed precipitation with predictors as shown in Figure 6-3 indicates all stations followed the same correlation pattern (both in magnitude and direction) that illustrates all stations can have identical physically sensible predictors, with a few exceptions. Furthermore, there are predictors that have correlation coefficient values in the range of 20 to 45% for precipitation across all stations. This range is considered to be acceptable when dealing with precipitation downscaling (Wilby *et al.*, 2002) because of its complexity and high spatial and temporal variability to downscale.

The predictor variables identified for each downscaling GCM and for the corresponding local climate variables showed that different large-scale atmospheric variables control different local variables. For instance, the set of temp, mslp, s500, s850, p8_v, p500, shum comprises the most potential or meaningful predictors for temperature. While, the set of s500, s850, p8_u, p_z, pzh, p500 performs best for predicting precipitation of the study area, which is consistent with the result of offline correlation analysis. After carefully screening predictor variables, model calibration and validation was carried out. The graphical comparison between the observed and generated rainfall, Tmax and Tmin, was run to enhance the confidence of the model performance, as shown in Figure 6-4 and Figure 6-5 for Gondar station only. For the other

stations, see Appendix 25 and Appendix 26. Examination of Figure 6-4 shows that the calibrated models reproduces the monthly mean precipitation and mean standard deviation of daily Tmax and Tmin values quite well. However, the model is less accurate in reproducing variance of observed precipitation. As Wilby *et al.* (2004a) point out, downscaling models are often regarded as less able to model the variance of the observed precipitation with great accuracy.

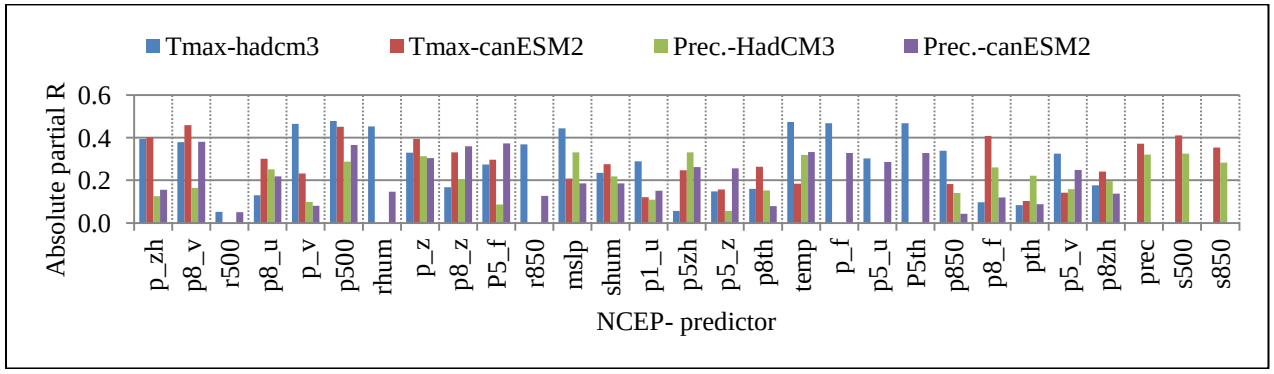

Figure 6-3: Average partial correlation coefficient values of all stations for precipitation and Tmax with NCEP- reanalysis predictors

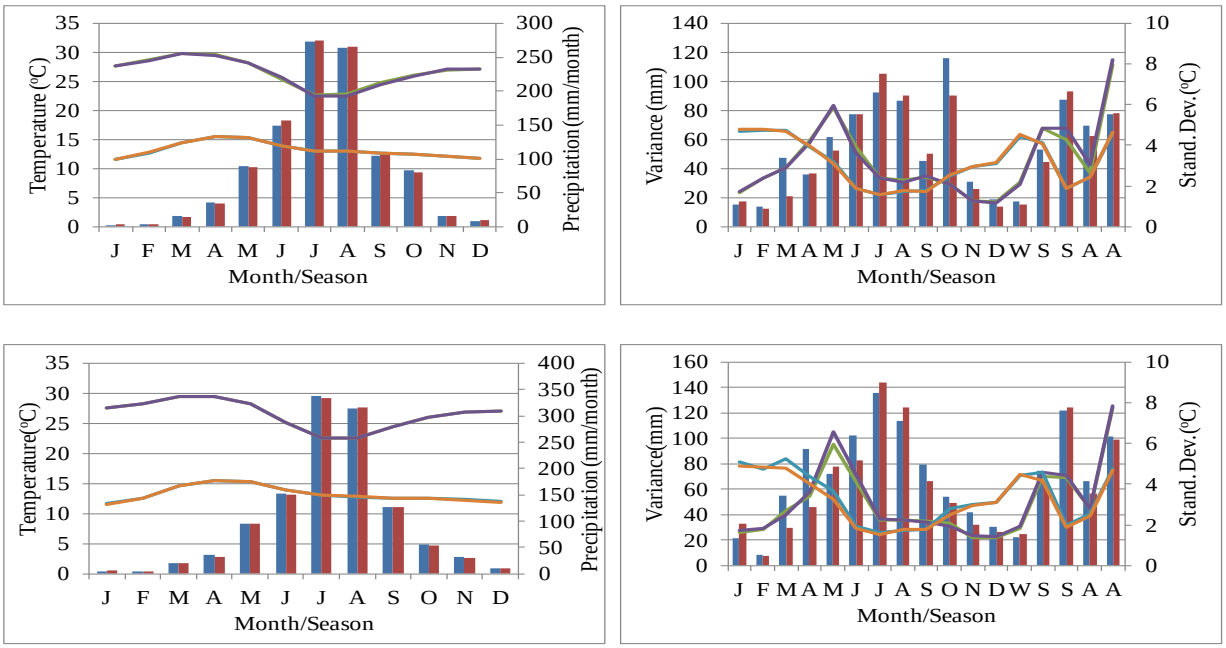

Figure 6-4: Calibration of observed and simulated of precipitation, maximum and minimum temperature for the Gondar station using SDSM from canESM2 and HadCM3 from top to bottom

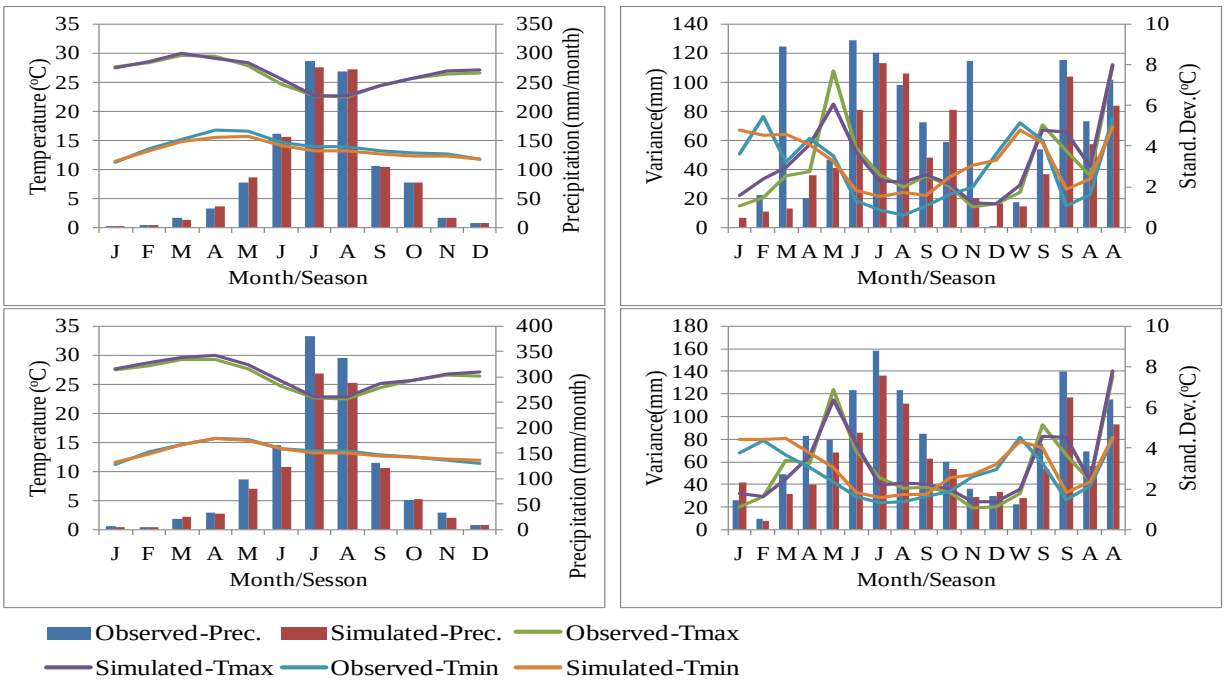

Figure 6-5: Validation of observed and simulated of precipitation, maximum and minimum temperature for Gondar station using SDSM from canESM2 and HadCM3 from left to right respectively

The statistical performance metrics of MAE and RMSE values for the monthly precipitation modeled from canESM2 range from 3.5 to 14.8 mm and 4.9 to 22.4 mm, which shows that canESM2 performs better than HadCM3, with the MAE and RMSE values ranging from 6.2 to 48.6mm and 7.6 to 73.4mm respectively. The result of statistical analysis revealed that the model is much better in simulating Tmax and Tmin than precipitation, because the high dynamical properties of precipitation make it difficult to simulate. Researchers such as (Chisanga *et al.*, 2017) and (Hassan *et al.*, 2014) indicated that downscaling of precipitation was more complex and difficult to obtain a good agreement between observed and generated values compared to downscaling of temperature. This was due to the conditional process, which depended on intermediate processes within the rainfall process such as an occurrence of humidity, cloud cover, and/or wet-days. After accomplishing a satisfactory calibration, the multiple regression models are validated using an independent set of data outside the period for which the model is calibrated. The validation result revealed that the model is successfully validated but with less accuracy compared to calibration for both GCMs as shown in Figure 6-5. In general, the result analysis of performance measure and graphical representation of observed and simulated scenarios, both for calibration and validation, revealed that the model performs very well in simulating the climate variables.

6.3.3 Future climate projections with LARS-WG

Downscaling using CMIP3 GCM3

Since the performance of LARS-WG during calibration and validation was very good, downscaling of the climate scenario can be done from six selected multimodal CMIP3 GCMs under three scenarios (A1B, B1 and A2) for three periods. After the downscaling of future climate scenarios at all stations from the selected six GCMs, the projected precipitation analysis for the areal UBNRB was calculated from the point rainfall stations using the Thiessen polygon method as it is the most appropriate method for the UBNRB (Kim *et al.*, 2008b). The result analysis (Figure 6-6 (a) and Table 6-5) revealed that GCMs disagree on the direction of precipitation change: two GCMs (CSMK3 and GFCM21) showed decreasing trends, and a majority, or four, GCMs (NCCSM, Hadcm3, MPEH5 and MIHR) showed increasing trends from the reference period in all three time periods. By the 2030s, the relative change in mean annual precipitation is projected in the range between -2.3 and 6.5% for A1B, -2.3 and 7.8% for B1, and -3.7 and 6.4% for A2 emission scenarios. In the 2050s, the relative changes in precipitation range between -8 and 22.7% for A1B, -2.7 and 22% for B1, and -7.4 and 8.7% for A2 scenarios. In the time of 2080s, the relative changes in precipitation projected may vary between -7.5 and 29.9% for A1B, -5.3 and 13.7% for B1, and -5.9 and 43.8% for A2 emission scenarios. The multimodal average result showed that in the future precipitation might generally increase over the basin in the range of 1 to 14.4 %, which is in line with the result from the HadCM3 GCM (0.8 to 16.6 %).

In a different way from precipitation, the projections of mean annual Tmax and Tmin have showed coherent increasing trends from the six GCMs under all scenarios in all three future periods (Figure 6-6 (b) and Table 6-5). The result calculated from the ensemble mean showed that mean annual Tmax may increase up to 0.5, 1.8 and 3.6^{o}C by 2030s, 2050s and 2080s respectively under the A2 scenario, which is in line with the results from both GFCM21 and HadCM3 GCMs. Likewise, the UBNRB may experience an increase in mean annual Tmin up to 0.6, 1.8 and 3.6^{o}C by the 2030s, 2050s and 2080s respectively from the multimodal average.

Table 6-5: Relative change mean annual precipitation, change in Tmax and Tmin modeled from six GCMs for three time periods of UBNRB as compared from the reference period of 1984-2011 by using LARS-WG

	1984-2011	2030s (2011-2035)			2050s (2046-2065)			2080s (2080-2099)		
GCMs/Scenario		A1B	B1	A2	A1B	B1	A2	A1B	B1	A2
Co2 concentration (ppm)		410	418	414	492	541	545	538	674	754
mean annual rainfall (mm)	1417.5									
CSMK3	Relative Change of precipitation(%)	-2.3	-2.3		-4.2	-2.7		-7.0	-5.3	
GFCM21		-1.4	-0.6	-3.7	-8.0	0.7	-7.4	-7.5	-2.2	-5.9
HADCM3		2.1	0.8	1.7	4.4	2.1	3.5	12.9	4.1	16.7
MIHR		1.9	3.7		5.5	5.5		10.2	6.0	
MPEH5		1.8	3.3	-0.5	2.5	5.8	4.2	6.0	1.4	3.3
NCCCS		6.5	7.8	6.4	22.8	22.0	8.7	29.9	13.7	43.8
Model average		1.4	2.1	1.0	3.8	5.6	2.2	7.4	3.0	14.5
Mean daily Tmax (^{o}C)	24.7									
CSMK3	Change in maximumTemperature (^{o}C)	0.4	0.4		1.3	0.9		2.2	1.5	
GFCM21		0.7	0.6	0.7	2.2	1.4	1.9	3.1	2.0	3.6
HADCM3		0.5	0.5	0.4	1.7	1.4	1.8	3.1	2.0	3.7
MIHR		0.6	0.6		2.0	1.6		3.5	2.6	
MPEH5		0.5	0.4	0.6	1.8	1.4	1.8	4.1	2.7	4.3
NCCCS		0.6	0.5	0.6	1.5	0.9	1.7	2.2	1.4	3.0
Model average		0.6	0.5	0.6	1.8	1.3	1.8	3.0	2.0	3.6
Mean daily Tmin (^{o}C)	11.4									
CSMK3	Change in minimum Temperature (^{o}C)	0.3	0.3		1.1	0.8		1.9	1.3	
GFCM21		0.7	0.6	0.7	2.2	1.4	1.9	3.1	2.0	3.6
HADCM3		0.5	0.5	0.4	1.7	1.4	1.8	3.1	2.0	3.7
MIHR		0.7	0.7		2.1	1.8		3.6	2.7	
MPEH5		0.5	0.4	0.6	1.8	1.5	1.8	4.1	2.7	4.1
NCCCS		0.6	0.5	0.6	1.5	0.9	1.7	2.2	1.4	3.0
Model average		0.6	0.5	0.6	1.7	1.3	1.8	3.0	2.0	3.6

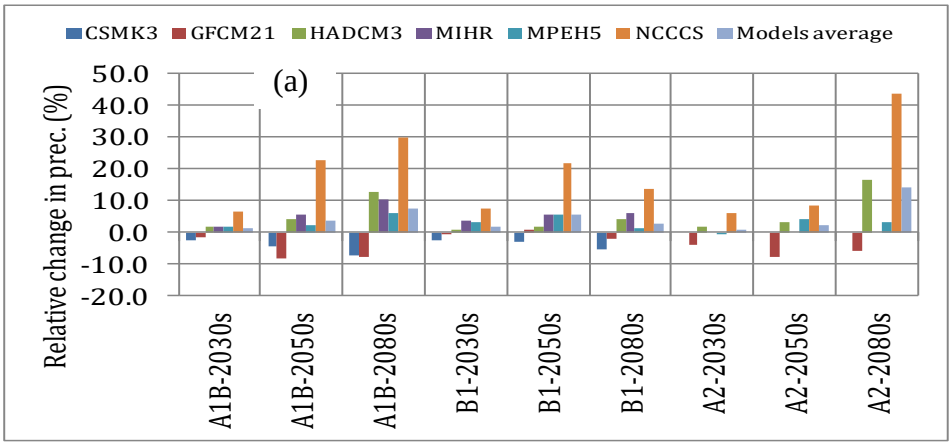
CSMK3
GFCM21
HADCM3
MIHR
MPEH5
NCCCS
Models average
(a)
Relative change in prec. (%)
50.0
40.0
30.0
20.0
10.0
0.0
-10.0
-20.0
A1B-2030s
A1B-2050s
A1B-2080s
B1-2030s
B1-2050s
B1-2080s
A2-2030s
A2-2050s
A2-2080s

(b)

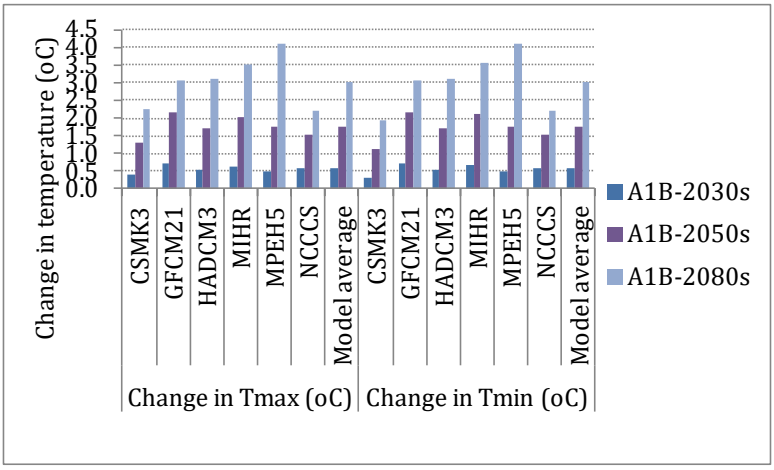
Change in temperature (oC)
CSMK3
GFCM21
HADCM3
MIHR
MPEH5
NCCCS
Model average
Change in Tmax (oC)
Change in Tmin (oC)
A1B-2030s
A1B-2050s
A1B-2080s

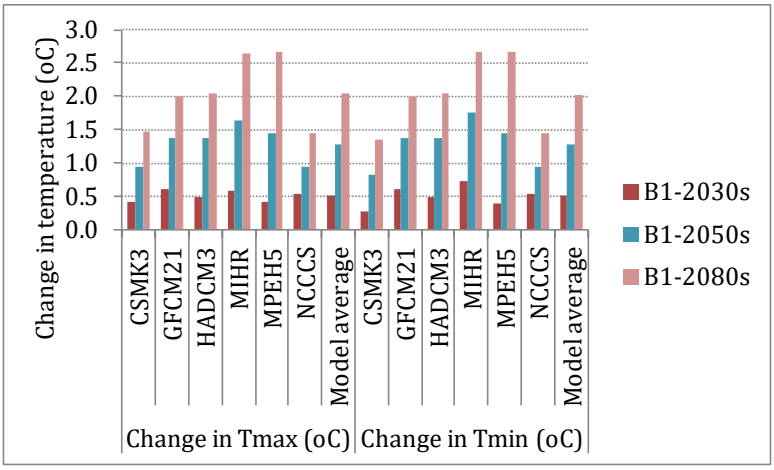
Change in temperature (oC)
3.0
2.5
2.0
1.5
1.0
0.5
0.0
CSMK3
GFCM21
HADCM3
MIHR
MPEH5
NCCCS
Model average
Change in Tmax (oC)
Change in Tmin (oC)
B1-2030s
B1-2050s
B1-2080s

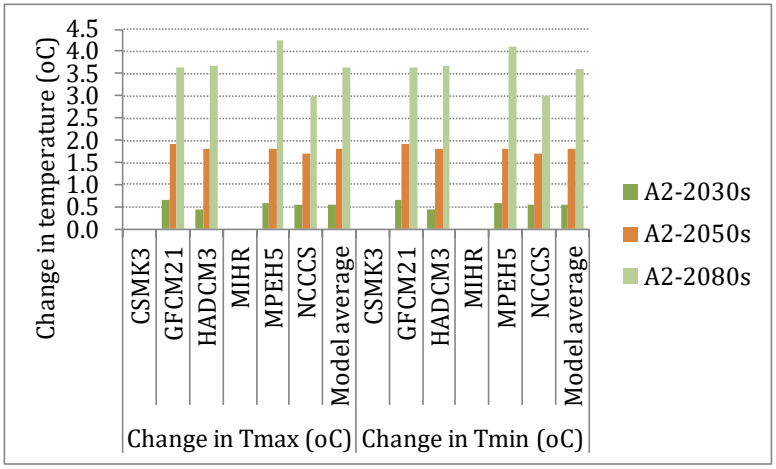

Figure 6-6: (a) Relative change mean annual precipitation and (b) change in Tmax and Tmin modeled from six GCMs for three time periods of UBNRB under three scenarios as compared from the reference period of 1984-2011 by using LARS-WG

Downscaling using CMIP5 GCMs

The downscaled precipitation from three CMIP5 GCMs using representative concentration pathways (RCP 4.5 and RCP 8.5) showed a greater tendency towards a decrease in the future in the UBNRB (Table 6-6). Two CMIP 5 GCMs showed decreasing while the other (HadGEM2) showed increasing trend. The model average result showed decreasing relative change of the long-term mean annual precipitation Figure 6-7. The magnitudes of the relative change of precipitation among the models are different. Particularly, GFDL model predicted maximum decreasing change in precipitation than the other GCM models over the basin. HadGEM2-ES GCM model projected relatively an increase average annual precipitation over the basin. MPI GCM model also projected minimum decreasing mean annual change for the basin. The long-term mean annual precipitation output may decreases in the range of -8.5% to -10.6% under RCP8.5 scenario of GFDL GCM in the period 2030s and 2080s respectively. The projected mean annual precipitation from HadGEM2 GCM showed mixed results. From HadGEM2 GCM, the mean annual precipitation may increase by maximum of 4.5% relative change under RCP4.5 by 2080s while it may decrease by a maximum of -1.7% under RCP 8.5 scenario by 2050s. Similarly, mean annual precipitation will increase by a maximum of 1.3% under RCP8.5 in the period 2030s and will decrease by a maximum of -2.1% under RCP4.5 in the period 2030s. However, the multi-model average result showed that precipitation might decrease in the future in the range of -4 % to -1.4 % under RCP4.5 and RCP8.5. For 2030`s average annual precipitation relative change projected between (-9.5 % and +0.8 %) for RCP 4.5 and between (-10.6% and +2.6%) for RCP 8.5. At 2050`s average annual precipitation change projected between (-10% and -0.7%) for RCP 4.5 and between (-10% and +0%) for RCP 8.5 emission scenario. For 2080s, average annual precipitation relative change projected between (-9.3% and +4.5%) for RCP 4.5 and between (-8.5% and +4.4%) for RCP 8.5 emission scenario.

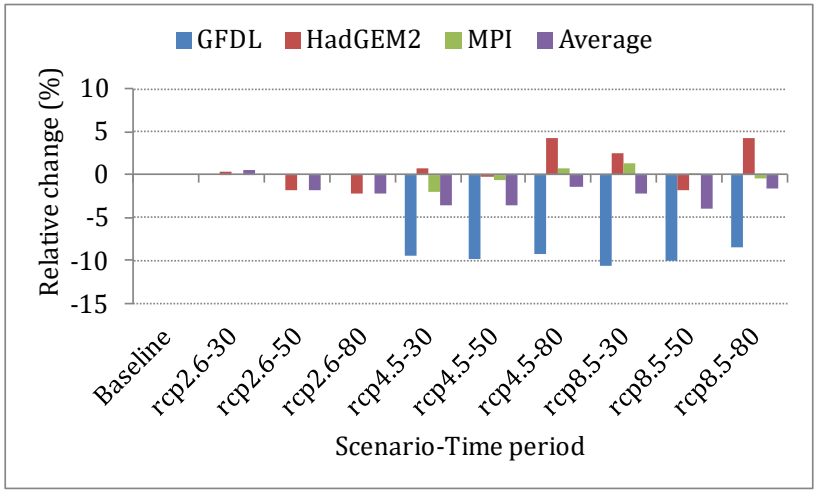

Figure 6-7: Relative change (%) of mean annual precipitation downscaled from CMIP 5 GCMs

Table 6-6: Relative change mean annual precipitation, change in Tmax and Tmin modeled from three CMIP5 GCMs for three time periods of UBNRB as compared from the reference period of 1984-2011 by using LARS-WG

	Relative change (%) for Precipitation				Change (^{o}C) for Tmin				Change (^{o}C) for Tmax			
	GFDL	HadGEM2	MPI	Average	GFDL	HadGEM2	MPI	Average	GFDL	HadGEM2	MPI	Average
Baseline	1407.7 mm				11.8 ^{o}C				25.3 ^{o}C			
RCP4.5-30	-9.5	0.8	-2.1	-3.6	1.2	1.8	0.9	1.3	1.0	1.5	1.0	1.2
RCP4.5-50	-10.0	-0.1	-0.7	-3.6	2.0	2.9	1.7	2.2	2.0	2.3	1.9	2.1
RCP4.5-80	-9.3	4.5	0.8	-1.4	2.9	4.0	2.2	3.0	2.1	3.0	2.3	2.5
RCP8.5-30	-10.6	2.6	1.3	-2.3	1.5	1.8	1.1	1.5	1.2	1.6	1.2	1.3
RCP8.5-50	-10.0	-1.7	0.0	-4.0	2.9	3.0	2.0	2.7	2.3	2.8	2.2	2.4
RCP8.5-80	-8.5	4.4	-0.5	-1.6	4.8	5.4	4.1	4.8	4.0	4.6	3.9	4.2

Average annual minimum and maximum temperature significantly increases in all future periods under RCP4.5 and RCP8.5 scenarios Table 6-6, Figure 6-8 and Figure 6-9. At 2080s of RCP4.5 and RCP8.5, the change in average maximum and minimum temperature is magnificent compared to 2030s and 2050s. At 2030s, average annual minimum temperature may increases in the range from +0.9^{o}C to +1.8^{o}C for RCP 4.5 and from +1.1^{o}C to +1.8^{o}C for RCP 8.5 emission scenario. At 2050s, mean annual minimum temperature will increase in the range of +1.7^{o}C to 2.9^{o}C under RCP4.5 and from +2^{o}C to +3^{o}C under RCP8.5. At the end of 21st century, 2080s, the mean annual minimum temperature change may increase in the range of +2.2^{o}C to +4^{o}C for RCP4.5 and between +4.1^{o}C and +5.4^{o}C under RCP8.5. Furthermore, the mean annual maximum temperature may increases in the range from +1^{o}C to +1.5^{o}C for RCP 4.5 and from

+1.2°C to +1.6°C for RCP 8.5 emission scenario by 2030s. At 2050s, mean annual maximum temperature will increase in the range of +1.9°C to 2.3°C under RCP4.5 and from +2.2°C to +2.8°C under RCP8.5. At the end of 21st century, 2080s, the mean annual maximum temperature may increase in the range of +2.3°C to +3°C for RCP4.5 and between +3.9°C and +4.6°C under RCP8.5.

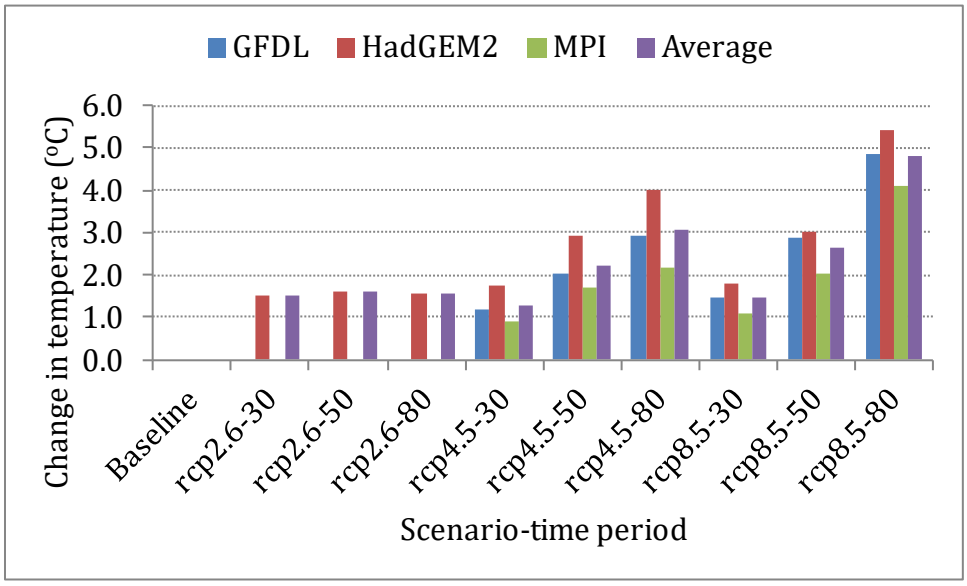

Figure 6-8: Change in mean anuual Tmin from CMIP5 GCMs

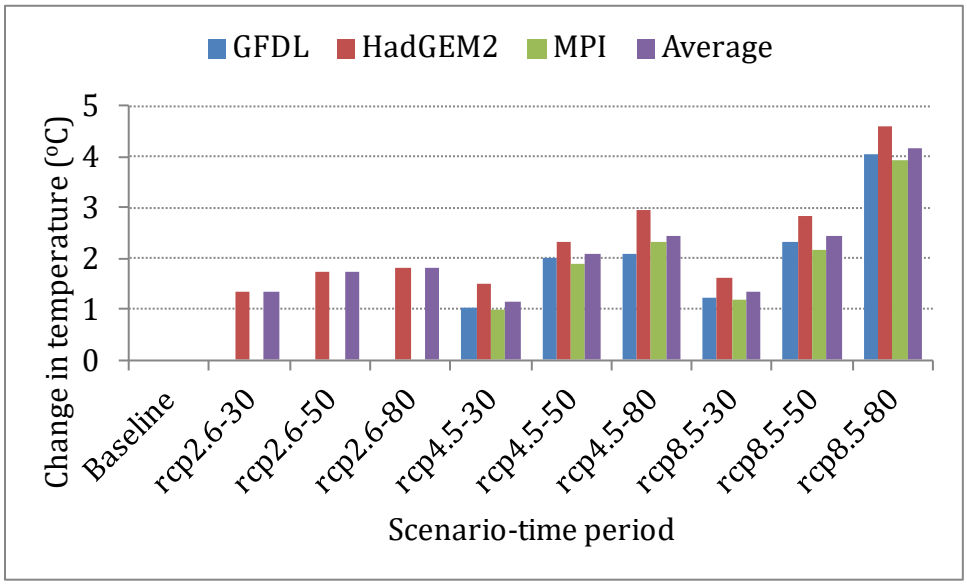

Figure 6-9: Change in mean annual Tmax from CMIP 5 GCMs

6.3.4 Future climate projections with SDSM

Here, as it is difficult to process all the selected six CMIP3 GCMs using SDSM, we choose the HadCM3 GCM as the best due to the fact that the downscaling result of HadCM3 using LARS-WG fits with the downscaling result of the ensemble mean model. In addition, canESM2 from the CMIP5 GCMs was selected to test the improvements of CMIP5 over CMIP3. Results of downscaling future climate scenario of areal UBNRB using SDSM calculated from all stations using Thiessen polygon methods are summarized in Figure 6-10. The overall analysis of the result indicates a general increase in mean annual precipitation for three time windows (2030s, 2050s and 2080s) for all five scenarios (A2a and B2a for HadCM3 and RCP2.6, RCP4.5 and RCP8.5 for canESM2) in the range of 2.1 to 43.8 %. The maximum (minimum) relative change of mean annual precipitation is projected to be 43.8% (6.2 %), 29.5% (3.5 %) and 19% (2.1 %) in the 2080s, 2050s and 2030s under the RCP8.5 scenario of canESM2 (B2a) scenario of HadCM3. In general, the RCP8.5 scenario of canESM2 GCM resulted in pronounced increases in all three-time periods, whereas scenario B2a of the HadCM3 GCM reported minimum change over the study area.

Regarding temperature, the downscaling result of Tmax and Tmin showed an increasing trend consistently in all months and seasons in three periods under all scenarios with mean annual value ranging from 0.5 to 2.6^{o}C and 0.3 to 1.6^{o}C under scenario RCP8.5 and B2a respectively. The RCP8.5 scenario reported maximum change while B2a scenario reported minimum change for both Tmax and Tmin in all three-time periods compared to other scenarios. The analysis of the downscaling result illustrates maximum temperature may become much hotter compared to minimum temperature in all scenarios and periods in the future across the UBNRB.

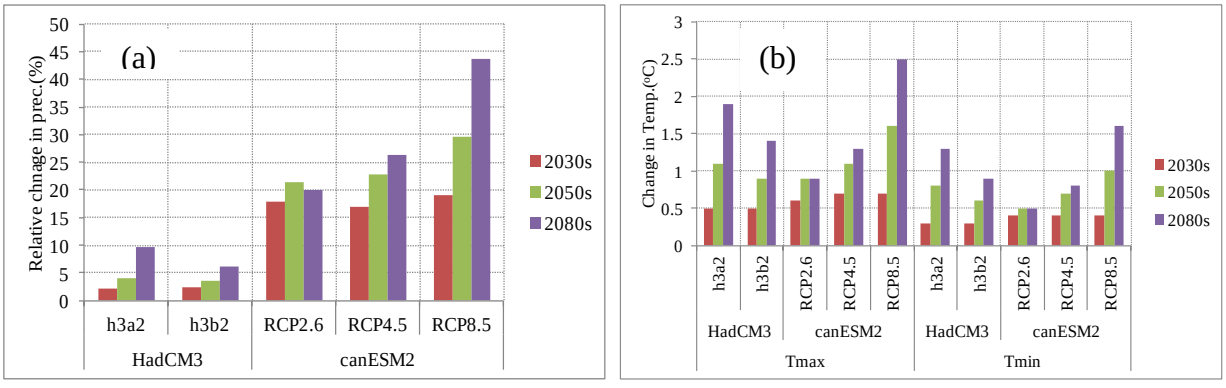

Figure 6-10: (a) Relative change of mean annual precipitation, and (b) change of mean annual Tmax and Tmin for three time periods as compared to the baseline period of UBNRB using SDSM for HadCM3 and canESM2 GCMs under different scenarios

The wide-range of downscaled future precipitation results from multi-model GCMs over UBNRB showed the uncertainties of GCMs outputs. For example, at the end of 21st century (2080s), the CMIP 5 GFDL GCM downscaled using LARS-WG for precipitation decreases by relative change of -9.3 % and canESM2 GCM downscaled using SDSM increases mean annual

precipitation by 43.8%, which can be classified as extremes of mean precipitation. Previous studies have shown different projections of annual precipitation changes for the same basin. Conway (1996) obtained -2 to 7% by the 2025s, Yates *et al.* (1998b) obtained -9 to 55% for the double carbon dioxide condition, Kim *et al.* (2008b) projected mean annual precipitation in the range of 61 and -28 % by the 2050s from six GCMs and Conway (2005) projected -40 to 100% for the 2080s. In other studies a mild increase in rainfall over the UBNRB is expected in the 2050s with a spatial mean increase over all seasons of basin 11% (Kim, 2008). Note that each study used the different target years, grid points, downscaling methods, and GCMs (Kim *et al.*, 2008b). Considering the overall results of previous studies, this study suggests a moderate range (-9.3 to 48 %) of mean annual precipitation changes for the 2080s. Since no GCM is perfect as discussed later, an ensemble value of results from the 10 GCMs of 27 different scenarios can provide a meaningful estimate. Based on this argument, the plausible mean annual precipitation might increase by 2.4%, 4.6% and 8.1% in the period 2030s, 2050s and 2080s respectively (Appendix 13).

According to Zaitchik *et al.* (2012), the results of multi-model CMIP3 GCMs and emerging results from CMIP5 have exhibited large uncertainty in regional to sub regional precipitation. This uncertainty is evident in the UBNRB, which falls in a region of particularly high uncertainty in projections of precipitation change. According to Hawkins and Sutton (2009), uncertainty in climate predictions arises from three distinct sources. The first is the internal variability of the climate system, that is, the natural fluctuations that arise in the absence of any radiative forcing of the planet that are associated with anthropogenic climate change. The second is model uncertainty (also known as response uncertainty). It is also a product of divergent representation of thresholds and feedbacks between GCMs and the computational difficulty of running large ensembles of GCMs at a spatial resolution capable of resolving local atmospheric processes. Additionally, as GCMs increase in sophistication, there is a tendency for model divergence to increase as additional coupled processes are included in increasingly complex modeling systems (Zaitchik *et al.*, 2012). The third is scenario uncertainty: uncertainty in future emissions of greenhouse gases, as it is difficult to predict what will be socio-economic and technological development over the next century that will lead to different emission pathways. There are extensive efforts underway to improve the skill of climate models, raising the possibility that the spread in future predictions will ultimately be reduced. It is unlikely, however, that the range of uncertainty in regional predictions will be narrowed to any significant extent in the near future.

Recognizing that planning for climate change is fundamentally a process of risk characterization rather than a problem for deterministic prediction, uncertain climate projections can be applied to enhance climate resilience. In this respect, applying climate model information to adaptation is not unlike many other scenario-based planning processes. Climate projections from GCMs provide scenarios that inform analysis of potential outcomes, allowing stakeholders to evaluate their risk exposures and adaptation options. Such a risk-based approach differs from conventional vulnerability assessments in that it includes a formal assessment of likelihood of impacts, clearly defined for a sector, time horizon, and time scale (i.e., events, variability, and/or trends) of interest (Zaitchik *et al.*, 2012).

6.3.5 Spatio-temporal distribution

The characteristics of spatial variation of rainfall over a basin are of great interest to agriculturalists and resource managers. Climate change across the UBNRB needs to be communicated rather than just allowing planning to be based on basin averages that ignore clear patterns across the basin. Furthermore, the amount of rains in the main rainy and dry seasons may be more important for rain-fed agriculture in order to match the growing period of the staple crops. The amount of rains in the main rainy season (Kiremet) has major impacts on rainfed agricultural crop production. The limited availability of water resources for irrigation during the dry season (bega) in the basin has been exacerbated by the characteristic of climate with a long dry season in conjunction with a population increase and human impacts on the landscape. The boundary conditions for sustainability in the UBNRB are closely linked to the climate as the productivity of agriculture is sensitive to the timing as well as the amount of rainfall (Mellander *et al.,* 2013). Hence, the spatial pattern of future prediction in seasonal distribution was exploited to improve the understanding how future climate changes might influence the Kiremet and its associated Bega on the basin. The future prediction of canESM2 GCM and GFDL GCM under RCP4.5 scenario outputs were selected for further analysis as they are representing the extremes of future climate predictions of the basin.

While the variability of mean annual precipitation is useful in long-term water resources planning and management, the variation of seasonal precipitation can affect the agricultural activities as well as the functioning of the ecosystem. Figure 6-11shows the variations of monthly precipitation of the base case and future predictions of canESM2 and GFDL GCMs. The canESM2 simulate a large increase of rainfall in the extended months of (Jun-Oct) while the GFDL simulates a large increase in the months of only (Sep-Oct) and a significant decrease in the remaining months. October is the month when most agricultural crops get matured and start harvesting, while, the months (June-August) are months when about 80 % of the annual rainfall occurred and by far the most important months for agriculture over the basin. Hence, this climate variability can be potential threat for the farmers, who have limited ability to cope with the negative impacts.

Table 6-7 and Table 6-8provide quantitative details of projected rainfall for annual and seasons of the investigated stations from canESM2 and GFDL GCMs respectively. The result show that mean annual rainfall can have extreme changes in the range of -18.3 to 70 % from canESM2 GCM while the GFDL GCM from 23 stations show in the range -18.1 to 6.2%. For Kiremet season, the relative change of the downscaled values of the selected stations show a range of -13.4 to 72 % and -19.7 to 0.3 %. For Bega (Dry season), the relative change of precipitation for the selected stations are in the range of -24 to 294 % and 3.9 to 89 % from canESM2 and GFDL GCMs respectively for the period 2080s.

The observed and predicted precipitation series were spatially interpolated from15 and 24 rainfall stations for canESM2 and GFDL GCMs respectively for communicating the amount of rain falling during the rainy and dry seasons (Figure 6-12 and Figure 6-14). This could be useful for the long-term planning of water resource management within the basin, even if the interpolation of rainfall distribution over the UBNRB does not take the topography over the region into account. An isohyetal map was produced using the Kriging interpolation package

ArcGIS with default spherical variogram. Since the Kriging method is a best linear unbiased estimator, the spatial distribution of average annual rainfall over the basin is the best reflection of spatial variation of annual rainfall for the given rain gauge network (Abtew *et al.*, 2009). Figure 6-13 and Figure 6-15 show the variations of annual and seasonal precipitation of the base case and downscaled precipitation from canESM2 and GFDL CMIP5 GCMs under RCP4.5 scenario for the period 2080s. For the baseline period, the mean annual rainfall amount varies generally from the central highland and south-west (>2000 mm) to the north and east (around 1000 mm). The highest annual average rainfall of 2082 mm is in the southern tip of the basin at Nekemit and the lowest average annual rainfall of 916 mm is in the northeast at Debre Birhan (Figure 6-14(a)). A basin-wide time series of annual rainfall constructed from 24 gauges for the period 1984 to 2011 has a mean of 1418 mm and 1465 mm for the period 1984-2005 constructed from 15 rainfall stations (Table 6-7 and Table 6-8). Abtew *et al.* (2009) reported a mean annual rainfall of 1423 mm and standard deviation of 125 mm constructed from 32 stations for a period (1960–2002). Conway (2000) reported a mean annual rainfall of 1421 mm based on 11 gauges for a period of record of 1900–1998.

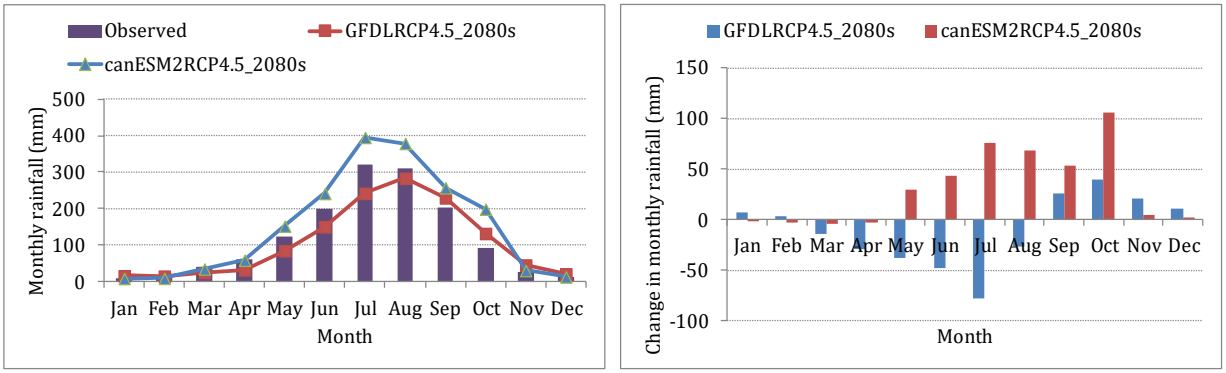

Figure 6-11: Projected areal mean monthly rainfall and relative changes from CMIP5 of canESM2 GCM and GFDL GCM under RCP 4.5 for 2080s over the UBNRB.

The noticeable result is that the canESM2 GCM simulated a significantly large increase in annual and Kiremet season rainfall Figure 6-13 (a) to (c), while GFDL GCM simulated large decrease in precipitation in annual and Kiremet season over the basin Figure 6-15 (a) to (c). The variation of annual precipitation from each GCM follows the pattern of Kiremet that controls the majority of precipitation of the study area. Both canESM2 and GFDL GCMs simulated a large increase of precipitation in bega seasons. The increase or decrease in annual and seasonal rainfall predicted for the future did not appear to be evenly distributed over the basin. A large amount of mean annual and Kiremet rainfall were expected to increase in the southeast and northeast of the basin from canESM2 GCM. However, the annual and seasonal rainfalls in the central highland and west of the basin predicted from canESM2 were expected to decrease while from GFDL a small increase was expected.

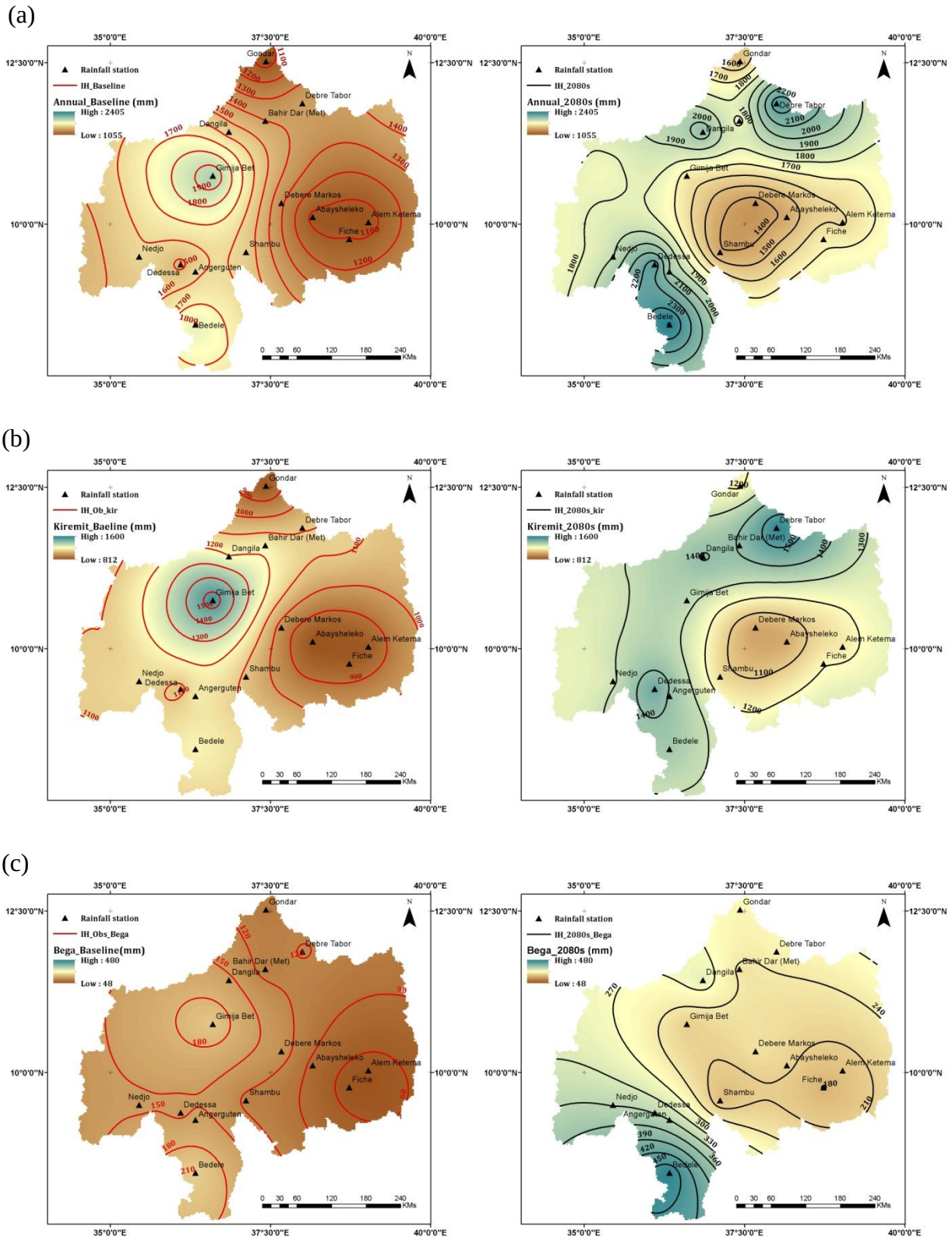

Figure 6-12: Spatial distributions of baseline (left) and simulated rainfall for the 2080s from canESM2 GCM (right): (a) annual, (b) kiremit and (c) bega seasons

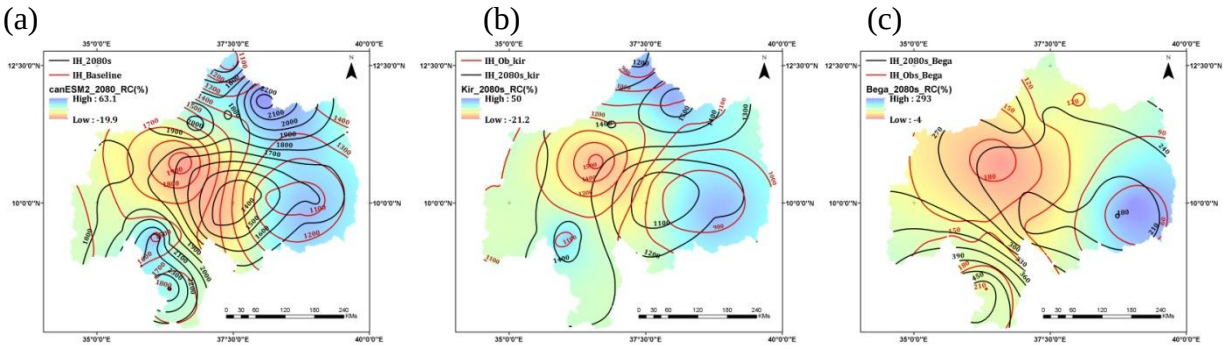

Figure 6-13: Spatial distributions of relative percent changes in annual, kiremit and bega rainfall by the 2080s from the canESM2 GCM: (a) annual, (b) kiremit and (c) bega seaon

The positive change of rainfall simulated from canESM2 GCM in the future can be a good opportunity for the farmers who are engaged in rain fed agriculture to maximize their agricultural production and to change their livelihoods. However, this information cannot be a guarantee for irrigation farming because precipitation is not the only factor contributing to affect the flow of the river, which is the main source for irrigation. Evapotranspiration, dynamics of LULC, proper water resource management and other climatic factors can influence the flow of the river directly and indirectly. In the other way, the decrease of rainfall simulated from GFDL GCM in the future might reduce the amount of streamflow, which leads to recurrent droughts and physical water scarcity of the basin. More frequent and longer periods of drought reduce the amount of runoff into rivers, streams and lakes; also, the ground water table drops. So, there is less groundwater to supply springs and shallow wells for domestic water supply. As a consequence, school dropout is expected to be high because of extra time and labor is needed to collect water from unprotected sources. Shortage of domestic and non-domestic water supply has multiple socio-economic impacts such as poor sanitation and hygiene, less industrialization and food insecurity.

(a)

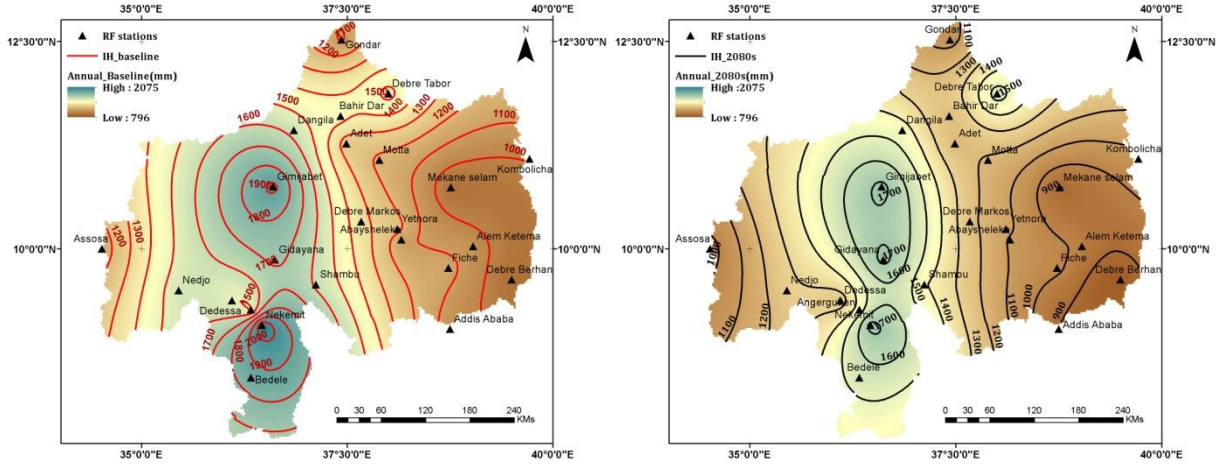

(b)

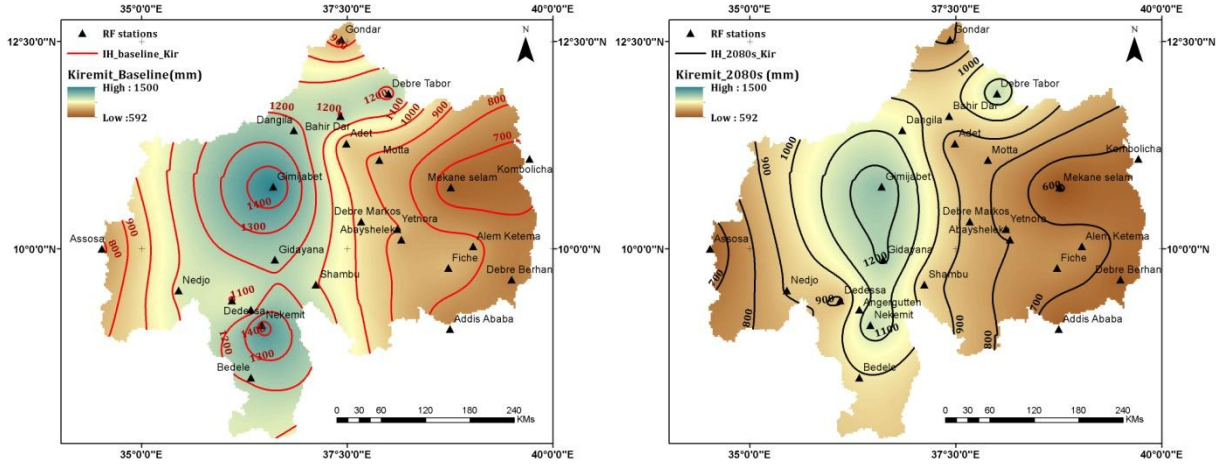

(c)

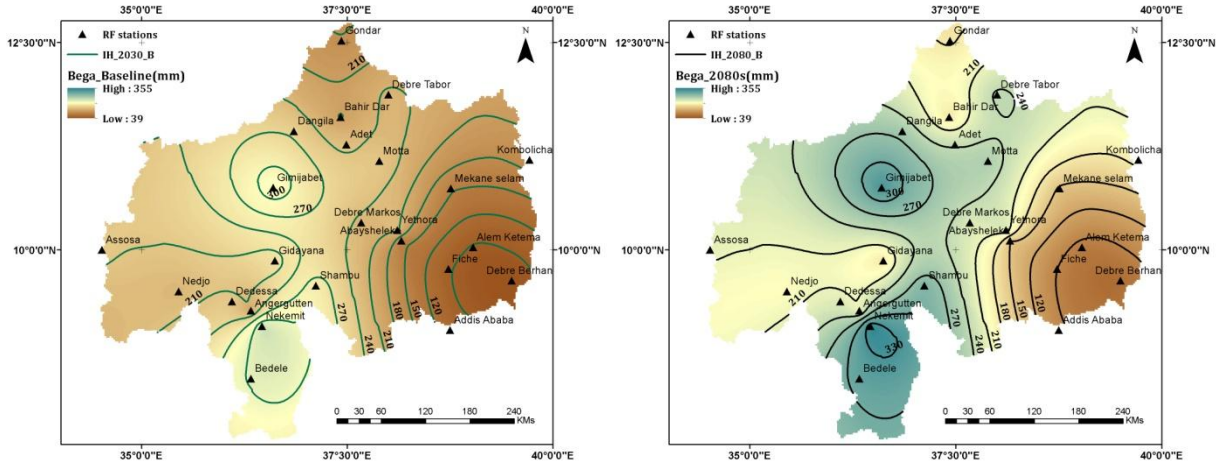

Figure 6-14: Spatial distributions of baseline and simulated rainfall for the 2080s from canESM2 GCM: (a) annual, (b) kiremit and (c) bega seasons

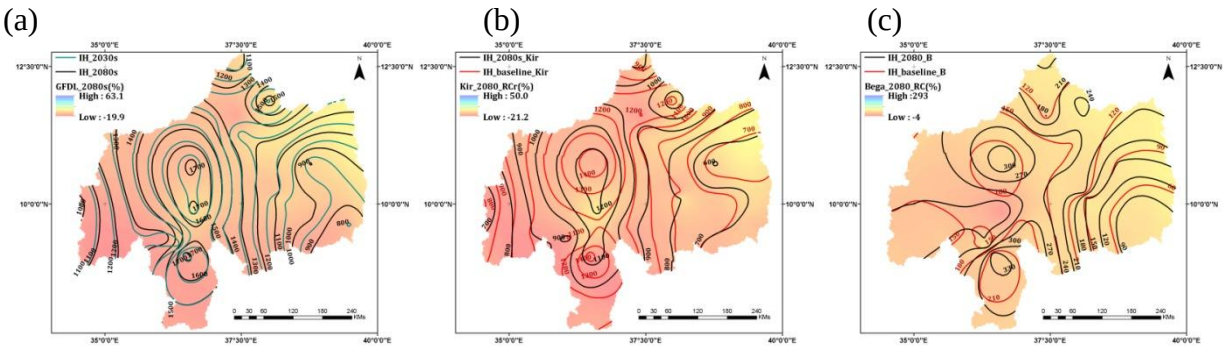

Figure 6-15: Spatial distributions of relative percent changes in annual, kiremit and bega rainfall by the 2080s from the canESM2 GCM: (a) annual, (b) kiremit and (c) bega seaon

Table 6-7: Baseline and future downscaled mean annual and seasonal rainfall data from the canESM2 GCMs under RCP4.5 scenario for the 15 selected stations in the UBNRB by the 2080s

	Annual		Kiremet (long rainy season)		Bega (dry season)		Relative change (%)		
Station	Baseline	2080	Base line	2080	Baseline	2080	Annual	Kiremet	Bega
Abaysheleko	1073	1400	816	925	82	234	30.5	13.4	186.5
Alemketema	1055	1557	826	1072	50	198	47.6	29.8	294.2
Anger	1549	2049	1126	1395	164	363	32.3	23.8	121.7
Angergutten	1580	1929	1168	1314	158	336	22.1	12.6	113.2
Bahir Dar	1401	1709	1180	1359	109	195	22.0	15.2	78.5
Bedele	1808	2474	1188	1412	211	583	36.9	18.8	176.5
Dangila	1554	2136	1203	1509	156	374	37.4	25.4	139.3
Debre Markos	1316	1336	960	896	135	270	1.5	-6.7	99.7
Debre Tabor	1391	2361	1094	1881	123	266	69.8	72.0	116.1
Dedessa	1468	2356	1078	1731	144	329	60.4	60.6	128.4
Fiche	1106	1694	836	1260	49	133	53.2	50.7	170.2
Gimija Bet	1986	1623	1557	1347	201	152	-18.3	-13.4	-24.3
Gondar	1056	1456	823	1021	103	231	37.8	24.1	123.9
Nedjo	1596	1869	1146	1191	147	318	17.1	3.9	115.6
Shambu	1557	1378	1082	1041	113	94	-11.5	-3.8	-16.6
Basin wide (UBNRB)	1465	1781	1098	1274	129	252	21.7	16.0	95.0

Table 6-8: Baseline and future downscaled mean annual and seasonal rainfall data from the GFDL GCMs under RCP4.5 scenario for the 24 selected stations in the UBNRB by the 2080s

	Annual		Kiremet (long rainy season)		Bega (dry season)		Relative change (%)		
Station	Baseline	2080	Baseline	2080	Baseline	2080	Annual	Kiremet	Bega
Abaysheleko	1101	1086	835	799	85	150	-1.3	-4.3	76.9
Addis Ababa	1052	899	736	622	61	96	-14.5	-15.6	58.5
Adet	1246	1202	910	834	144	237	-3.5	-8.3	64.6
Alemketema	1054	988	843	776	48	82	-6.2	-7.9	71.9
Anger	1492	1442	1142	1073	123	211	-3.3	-6.0	70.7
Assosa	1144	965	779	636	154	215	-15.7	-18.4	39.5
Bahir Dar	1436	1212	1205	969	116	179	-15.6	-19.6	54.8
Bedele	1851	1553	1215	989	217	311	-16.1	-18.6	42.8
Kombolicha	1006	1068	656	658	99	188	6.2	0.2	88.6
Dangila	1568	1449	1220	1074	158	261	-7.6	-11.9	65.7
Debre Birhan	916	831	720	636	39	67	-9.3	-11.8	68.8
Debre Markos	1333	1225	968	857	134	222	-8.1	-11.4	65.1
Debre Tabor	1540	1552	1232	1176	136	245	0.8	-4.6	80.3
Dedessa	1501	1244	1095	883	152	222	-17.1	-19.3	45.9
Fiche	1134	1023	878	777	53	90	-9.8	-11.4	70.7
Gidayana	1719	1731	1216	1219	173	180	0.7	0.3	3.9
Gimijabet	1927	1726	1500	1277	203	328	-10.4	-14.9	61.4
Gondar	1089	1059	847	782	100	177	-2.7	-7.7	75.9
Mekane Selam	924	896	635	590	85	146	-3.0	-7.0	71.6
Motta	1180	1188	875	824	151	255	0.7	-5.8	69.4
Nedjo	1562	1279	1123	912	137	199	-18.1	-18.7	45.1
Nekemit	2082	1733	1449	1163	232	346	-16.8	-19.7	49.5
Shambu	1582	1409	1105	935	184	289	-10.9	-15.4	57.4
Yetnora	1246	1136	910	778	144	224	-8.8	-14.5	56.0
Basin wide (UBNRB)	1418	1281	928	888	49	83	-9.6	-4.3	68.8

6.3.6 Comparative performance evaluation of LARS-WG and SDSM

Chen et al. (2013) argued that though major source of uncertainty are linked to GCMs and emission scenarios, uncertainty related to the choice of downscaling methods give less attention on climate change analysis. Therefore, in this study, comparative performance evaluation of the downscaling methods has given due emphasis and carried out in a number of statistical and graphical tests both quantitatively and qualitatively. The model skill was evaluated and ranked at each target sites for each metrics. The results are shown in Appendix 14, Appendix 15 and Appendix 16 for RMSE, MAE and bias metrics respectively. The overall rank obtained by

summing up the score of each model for each metric is presented in Table 6-9, Appendix 17 and Table 6-10 for quantitative equally weighted and varying weights respectively. Table 6-11 and Table 6-12 are showing summary results for qualitative measures. The result revealed that SDSM/canESM2 narrowly performed best in simulating the long-term average values in both equally weighted and varying weights of the quantitative metrics. However, LARS-WG performed best in qualitative measures in reproducing the distribution and extreme events of daily precipitation Table 6-11. For instance, absolute bias for the 95th percentile of daily precipitation (95p) ranges from 4.35 to 12.4mm for SDSM/canESM2, from 3.2 to 12.2mm for SDSM/HadCM3 and from 0.07 to 3.7mm for LARS-WG. For the mean of daily precipitation amount (SDII), absolute bias ranges from 1.3 to 6.3mm for SDSM/canESM2, from 2.1 to 5.6mm for SDSM/HadCM3 and from 0.01 to 3mm for LARS-WG.

Table 6-9: Summary of the total scores of each metric and methods during the baseline period (1984–2011) for equally weighted quantitative measures.

	Equally weighted overall score		
Evaluation metrics	SDSM/canESM2	SDSM/HadCM3	LARS-WG
RMSE	24	41	25
MAE	24	41	25
BIAS	31	39	20
Total	79	121	70
Rank	2	3	1

Note: The numbers in the table show the total scores summed up from 15 stations and model rankings.

Table 6-10: Summary of the total scores of each metric and methods during the baseline period (1984–2011) for varying weights quantitative measure.

	SDSM/canESM2	SDSM/HadCM3	LARS-WG
MAE	2.67	4.85	2.88
RMSE	3.86	7.22	4.47
Bias	1.29	1.83	0.70
	7.81	13.90	8.05
	1	3	2

Table 6-11: Ranking of statistical downscaling models during base line period (1984-2011) for qualitative measure (distribution and extreme events of daily precipitation).

Evaluation metrics	SDSM/canESM2	SDSM/HadCM3	LARS-WG
95p	52	41	14
99p	53	45	17
1-day max	50	48	15
SDII	47	49	19
R20	52	42	16
R10	40	36	19
R1	50	45	17
1-IRF	38	34	28
ACB	37	39	35
Total	419	379	180
Rank	3	2	1

Note: The numbers in the table show the total ranking scores obtained from 15 stations.

Furthermore, Kolmogorov-Smirnov test from Table 6-12 shows, LARS-WG captures the distribution of the observed precipitation 93.3% from all stations while SDSM captures only 20% of the 15 stations equally both from canESM2 and from HadCM3 GCMs at 5% significance level. The t-test result from all the three models revealed that 93.3% of the simulated precipitations are capturing their perspective mean values from all stations. The F test showed that 93.3% of the simulated and the observed precipitation are normally distributed around their respective variance value in LARS-WG model while only 80% from 15 stations simulate the variance correctly using SDSM. In general, the comparative performance test revealed that LARS-WG model performed best in qualitative measures while SDSM/canESM2 is best in quantitative measures in UBNRB. In addition, Figure 6-16 and Figure 6-17 confirmed graphically the ability of LARS-WG model in capturing the distribution and extreme events of the precipitation in representative stations (randomly chosen) respectively by Whisker box plot and Kolmogorov-Smirnov test. The better performance of canESM2 in quantitative measure could be attributed to the increasing performance of GCMs from time to time. CMIP5 GCMs performs better than CMIP3 GCMs due to the fact that modeling was based on the new set of radiative forcing scenario (RCPs) that replaced SRES emission scenarios, constructed for IPCC AR5 where the impacts of land use and land cover change on the environment and climate is explicitly included (Das *et al.*, 2012). Furthermore, it also includes models with improved physical parameterization schemes regarding cloud and radiation processes (Dolinar et al., 2015). The better performance of LARS-WG in capturing the distribution and extreme events of the daily precipitation may be associated with the use of 23 interval histograms for the construction of semi-empirical distribution, which offers more accurate representation of the observed distribution compared with the 10 interval used in the previous version (Semenov *et al.*, 2010).

Table 6-12: Ranking of statistical down scaling models during base line period (1984-2011) based on quality measure metrics

	Kolmogorov			t-test			F-test		
Station	model 1	model 2	model 3	model1	model2	model3	model 1	model 2	mode3
Abaysheleko	0.0	0.0	0.29	0.49	0.59	0.57	0.01	0.31	0.16
Alemketema	0.0	0.0	1.00	0.91	0.33	0.99	0.18	0.0	0.45
Anger	0.087	0.007	0.829	0.65	0.93	0.50	0.16	0.15	0.20
Angergutten	0.17	0.09	0.89	0.56	0.98	0.51	0.05	0.06	0.25
Bahirdar	0.00	0.00	0.94	0.55	0.64	0.74	0.57	0.09	0.37
Bedele	0.03	0.37	0.67	0.06	0.95	0.97	0.77	0.35	0.37
Dangila	0.05	0.07	0.37	0.76	0.01	0.03	0.07	0.0	0.0
Dedesa	0.01	0.02	0.94	0.77	0.98	0.97	0.38	0.38	0.98
Dmarkos	0.01	0.00	0.59	0.39	0.88	0.89	0.28	0.19	0.95
Debre Tabor	0.01	0.00	0.26	0.35	0.69	0.67	0.02	0.58	0.80
Fitche	0.02	0.00	0.94	0.99	0.77	0.95	0.09	0.96	0.87
Gimijabet	0.21	0.09	0.26	0.75	0.62	0.82	0.29	0.84	0.08
Gondar	0.00	0.01	0.67	0.98	0.53	0.76	0.91	0.03	0.83
Nedjo	0.00	0.01	0.97	0.57	0.68	0.98	0.80	0.30	0.97
Shambu	0.01	0.00	0.14	0.77	0.83	0.82	0.38	0.15	0.28
Total	15	15	15	15	15	15	15	15	15
No. Passed	3	3	14	14	14	14	12	12	14
% passed	20.0	20.0	93.3	93.3	93.3	93.3	80.0	80.0	93.3

model 1 in the table represents HadCM3/SDSM, model 2 represents canESM2/SDSM and model 3 represents LARS/WG

LARS-WG produces synthetic climate data of any length with the same characteristics as the input record; it simulates weather separately for single site. Therefore, the resulting weather series for different sites are independent of each other, which can lose a very strong spatial correlation that exists in real weather data during simulation. A few stochastic models have been developed to produce weather series simultaneously at multiple sites preserving the spatial correlation, mainly for daily precipitation, such as space–time models, non-homogeneous hidden Markov model and nonparametric models typically use a K-Nearest Neighbor (K-NN) procedure (King et al., 2015). However, they are complicated in both calibration and implementation and are unable to adequately reproduce the observed correlations (Khalili et al., 2007). In this study, the simple Pearson's correlation coefficient (R^2) value was checked in two stations before and after simulation of the observed data to test the capability of LARS-WG in preserving the spatial correlation of stations. The result revealed that the spatial correlation of the stations distorted /decreased/ from the original is insignificant. Further relative performance of downscaling techniques for other climatic variables such as Tmax, Tmin, dry spell length, wet spell length, inter-annual and seasonal cycle of precipitation using additional PDF-based metrics such as the Brier score and the skill score might counteract the limitations of this paper.

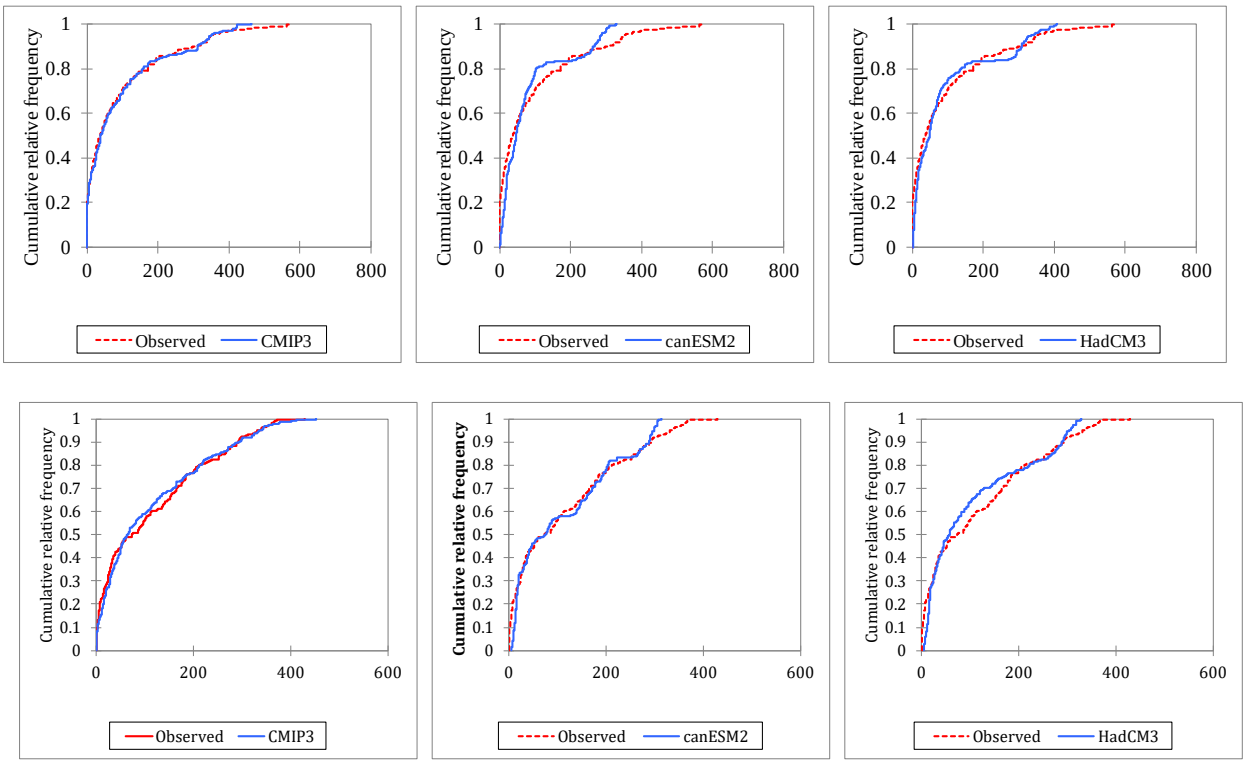

Figure 6-16: Kolmogorov-Smirnov test to compare the skill of the models for the observed precipitation distribution (Upper three Alemketema station, lower three Debre markos station)

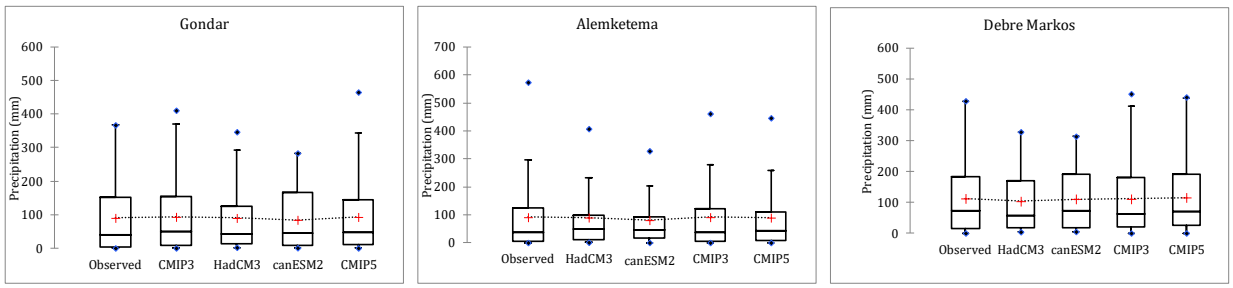

Figure 6-17: Box plot showing the model performance at three stations. Box boundaries indicate the 25th and 75th percentiles, the line within the box marks the median, whiskers below and above the box indicate the 10th and 90th percentiles, dots indicate the extremes.

For future simulation, the HadCM3 GCM A2 scenario was used in common for two (LARS-WG and SDSM) downscaling methods to test whether the downscaling methods may affect the GCM result under the same forcing scenario. The results obtained from the two downscaling models were found reasonably comparable and both approaches showed increasing trends for precipitation, Tmax and Tmin. However, the magnitude of the downscaled climate data from the two methods as presented in Figure 6-18 indicates that LARS-WG over predicts precipitation

and temperature compared to SDSM. The relative change of mean annual precipitation using LARS-WG is about 16.1% and an average increase in mean annual Tmax and Tmin is about 3.7 and 3.6^{o}C respectively in the 2080s. SDSM predicts the relative change of mean annual precipitation of only about 9.7% and an average increase in Tmax and Tmin of about 2 and 1.3^{o}C respectively in the same period. The differences in the future predictions are the result of the differences in the basic concepts behind the two downscaling techniques. The SDSM uses large-scale predictor variables from GCM outputs, which can be considered as more reliable for climate change prediction using multiple linear regressions. However, the LARS-WG uses the relative change factors (RCFs) derived from the direct GCM output of only those variables, which directly correspond to the predictands. Hence, because of the well-known fact that GCMs are not very reliable in simulating precipitation, the error induced from the GCM output for precipitation will propagate the error of downscaling that makes the performance of LARS-WG to downscale precipitation needs more caution (Dibike et al., 2005).

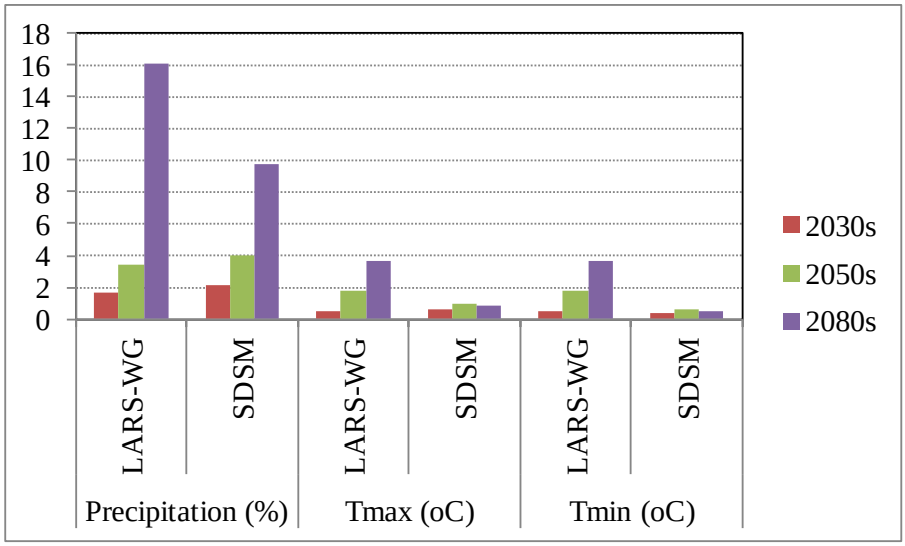

Figure 6-18: Comparison of climate change scenario downscaled using LARS-WG and SDSM from HadCM3 GCM for a2 scenario

Chapter 7 Combined impacts of climate change and water resource developments on the hydrology of the upper Blue Nile basin

7.1 Model selection and description

Application of models in hydrological studies has become an indispensible tool for understanding of the natural processes occurring at the watershed scale. Plenty of computer-based hydrological models have been developed and available to analyze the quantity and quality of stream flow, flood forecasting, reservoir system operations, water use, climate and land use change impact study, ecology and a range of water management activities (Dhami and Pandey, 2013). There is wide variability in their characteristics and potential applications, for example, spatial and temporal scale, processes modeled and the basis of relationships and algorithm used. With this increasing number of availability, wide ranging characteristics and potential applications of the models, it is becoming challenging task for the potential model users to choose a particular model best suited for the given objectives of a particular study in an individual catchment (Otieno et al., 2014). Cunderlik (2003) reviewed and evaluated a large number of existing hydrologic models (over 40) that are potentially suitable for the project aimed at assessing the potential impact of climate change on a wide range of hydrologic processes and existing water management practices. The author used a two-level selection approach to determine the most suitable model objectively. At the first level, a large number of existing hydrologic models are reviewed according to four fundamental selection criteria, and a subset of 18 models is identified.

The selected 18 models are then ranked according to several evaluation criteria reflecting different aspects of hydrologic processes that need to be modeled, required parameters to be estimated by the model, required input data and investment cost for the model. At the second level, total ranks attributed to the 18 selected models serve as an objective measure for determining the most appropriate model(s). Lumped, semi-distributed and fully distributed models were compared separately, since they reflect different approaches to hydrologic modeling. With respect to the objective of this study, a more attractive choice would be to opt for a semi-distributed model, which will be a good compromise between generally high simplification of the governing hydrologic processes used in lumped models, and extensive data requirements of distributed models. The result suggested that HEC-HMS, HFAM hydrological models were the best among the nine selected semi-distributed hydrological model category including (SWAT, HBV, TOPMODEL, HSPF, PRMS, SSARR, and SWMM) in the order of their rank.

Previously, SWAT models was tested and proved to reproduce all main hydrologic processes with high accuracy in the UBNRB (Gebremicael *et al.*, 2013; Mekonnen *et al.*, 2018b; Setegn *et al.*, 2008). However, the performance of the model on controlled reservoir operation remained questionable (Cunderlik, 2003). In SWAT, reservoir control module calculated the outflow using one of four different methods Figure 7-1: measured daily outflow, measured monthly outflow, average annual release rate for uncontrolled reservoir, and controlled outflow with target release (Winchell et al., 2013). All methods or options require predefined or measured data format to input the outflow data, which are not available for the hydropower reservoirs planned to

construct in the UBNRB. Usually these methods are used when the discharge is either observed or completely specified by an external decision processes. The method can then be used to preserve the specified release and track the storage using the inflow, outflow, and conservation of mass. SWAT reservoir simulation may suite only for irrigation dams, when the irrigation water requirement calculated externally can be used as specified released discharges. Furthermore, SWAT has limitations to simulate reservoir level that is key variable to calculate power and energy. Thus, the SWAT reservoir control module needs improvement or modification by adding the reservoir level simulation tool, and it also needs external optimization tool such as Genetic Algorithm (Holland, 1975) to obtain the optimum daily or monthly outflow for optimum power production from the unconditional inflow (Kangrang et al., 2018; Zhang et al., 2012). This modification or improvement of SWAT controlled reservoir module is beyond the scope of this study.

When measured daily outflow method is selected, the flow rate for every day of reservoir operation is required. If measured monthly outflow method is selected, the average daily flow rate for every month of operation of the reservoir is required. When the average annual release rate option is selected, the volume of water in the reservoir should be between the principal and emergency spillway volume. If the amount of water exceeding the principal spillway volume can be released at a rate <= $V_{flowout}$, than all of the water volume in excess of the principal spillway volume is released. Otherwise, the release rate, $V_{flowout}$ is used. When the water volume exceeds the emergency spillway volume, all water in excess of the emergency spillway volume is released plus the volume of water corresponding to the release rate from the principal spillway defined by $V_{flowout}$. If a target release is selected, beginning and ending month of non-flood season, number of days to reach target storage from current reservoir storage and monthly target reservoir storage is needed as input. For the details see (Arnold *et al.*, 2013).

HFAM (Hydrocomp Forecast and Analysis Modeling) is a semi-distributed model developed by Hydrocomp Inc., based on the widely used Stanford Watershed Model (SWM) and the Hydrologic Simulation Program-Fortran (HSPF). The HFAM system consists of a hydrologic simulation model and a river-reservoir model. For the hydrologic simulation, the basin is divided into hydrologically homogeneous land segments. Each segment is simulated independently using local precipitation, evapotranspiration, temperature, solar radiation and wind. HFAM simulates various hydrologic processes and currently utilized in the following applications. Optimize the design and operations of reservoirs, the effects of climate change and LULC changes on the hydrologic processes and understand the connection between groundwater and surface water to track overall water balance in a watershed. For further details, see https://hydrocomp.com/. With respect to HFAM, the concerns are its extensive data demand, not public domain (commercial) and limited technical support.

The new HEC-HMS version has substantial improvements to the model structure, including reservoir outlet structures, dam break, and user extensions. With these features, the new HEC-HMS outperforms the other semi-distributed models. Hence, HEC-HMS model found to be appropriate and selected for this study.

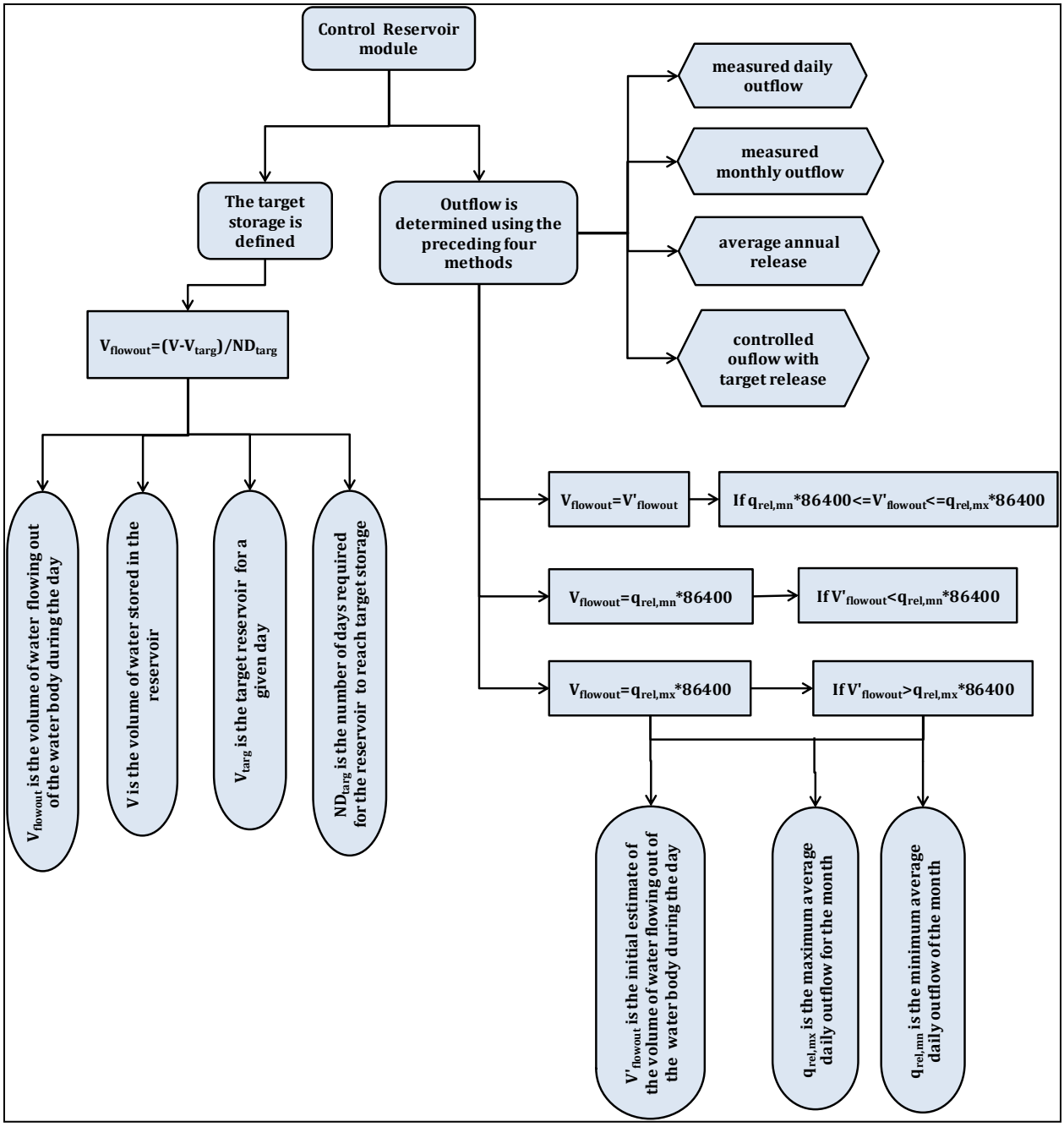

Figure 7-1: Reservoir control module of chart of the SWAT model (Zhang *et al.*, 2012)

7.1.1 HEC-HMS hydrological model

HEC-HMS is designed to simulate the complete hydrologic processes of dendritic watershed systems (Scharffenberg, 2015) to solve widespread possible hydrological problems (e.g., flood hydrology, large basin water supply, surface erosion and sediment studies and reservoir design) in a wide range of geographic regions. It has the capability to simulate both continuous and

event-based hydrological phenomena. The primary distinction is that evapotranspiration and groundwater seepage flow can be ignored for event-based modeling, but not in continuous hydrological modeling. Soil moisture has a significant influence on the hydrological response of a watershed; still, it is rarely tracked in simulation models, due to the complexity of the model structure and challenge of parameter estimation (Holberg, 2015). In HEC-HMS, the Soil Moisture Accounting Algorithm (SMA) and deficit-constant methods are the only loss methods that account for the evapotranspiration process (Scharffenberg, 2015). The HEC-HMS model is public domain software tool. The documentation and the latest version of the software can be downloaded from https://www.hec.usace.army.mil/software/hec-hms/.

The SMA loss method was applied for this study to simulate the movement of water over time through a series of storage layers as illustrated by Figure 7-3. According to Holberg (2015), SMA takes a precipitation as its input and routes it through canopy, surface, and soil storages while taking into account groundwater, baseflow, and evapotranspiration processes before outputting a streamflow hydrograph. When precipitation occurs, the canopy storage is first filled; the precipitation amount not captured by canopy storage and in excess of infiltration rate becomes inflow to the surface. Once the volume of surface interception exceeded, this excess water contributes to surface water. Furthermore, if the precipitation intensity is greater than the maximum infiltration capacity of the soil profile, the excess precipitation will become surface runoff instead of infiltrating. The infiltrated precipitation fills the tension zone first and then the upper zone. Precipitation can percolate from the upper zone, but not from the tension zone, into the groundwater layer one storage (GW1). Some water in GW1 will be routed to the first baseflow reservoir while the rest percolates down to groundwater layer two (GW2). From GW2, water can be transferred to the second baseflow reservoir; otherwise, it percolates down to a deep aquifer, which is considered lost from the system. Water in the baseflow reservoirs is transformed to streamflow based on the characteristics of the reservoirs, such as quantity and the flow coefficient.

Evapotranspiration first occurs from the canopy storage, then from the surface storage. If sufficient water is not present in the first two storage components, water is then removed from the upper zone storage to fulfill the evapotranspiration potential. If evapotranspiration is still not satisfied, water is then removed from the tension zone storage. Evapotranspiration from the tension zone storage occurs at a decreased rate based on the current soil storage depth and the maximum storage capacity of the tension zone. If potential evapotranspiration is not satisfied from the first two storage components, the algorithm removes the water from tension zone storage. Water removal from tension zone occurs at a slower pace based on maximum storage capacity of the tension zone and depth of the soil storage (Holberg, 2015; Samady, 2017).

HEC-HMS model setup (Figure 7-2) consists of a basin model, meteorological model, control specifications, time series and paired data manager (Scharffenberg, 2015). The basin model for instance, contains the hydrologic elements (sub-basin, reach, junction, reservoir, source and sink), their connectivity that represent the movement of water through the drainage system and streamflow parameters. Control specifications manager are one of the main component of the project, principally used to control time interval of simulation. The meteorological component is also the first computational element in which precipitation is distributing spatially and temporally over the river basin. The spatio-temporal precipitation distribution was accomplished

by the gauge weight method. The Thiessen polygon technique is used to determine the gauge weights of the sub-basins in order to calculate the areal rainfall depth of each sub-basins, based on an assumption that the precipitation depth at any point within the sub-basin is the same as the precipitation depth at the nearest gage (Feldman, 2000). The input data are consisting of both time series and spatial data. It requires daily precipitation, long-term average monthly potential evapotranspiration, daily streamflow and geographical information digital elevation model (DEM) of the basin as input. The paired data manager is consisting of many functions such as the physical reservoir characteristics (elevation-reservoir area function, elevation-storage function, storage-discharge function, elevation-discharge function, inflow-diversion function).

In the present study, the SMA method for a runoff volume model, the Clark unit hydrograph (CUH) for direct runoff model, Muskingum for channel routing, and exponential recession method for base flow modeling are employed.

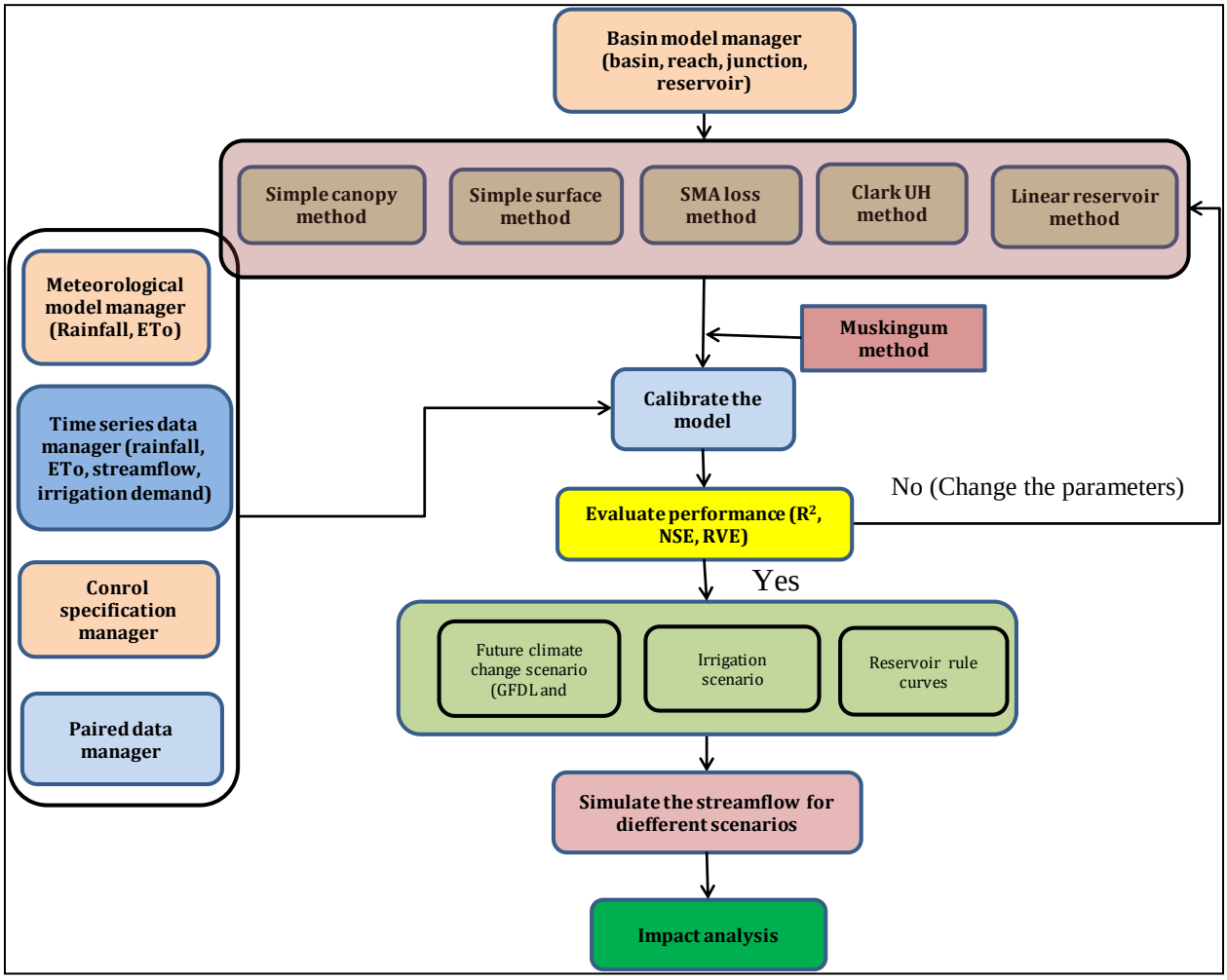

Figure 7-2: HEC-HMS model flow chart

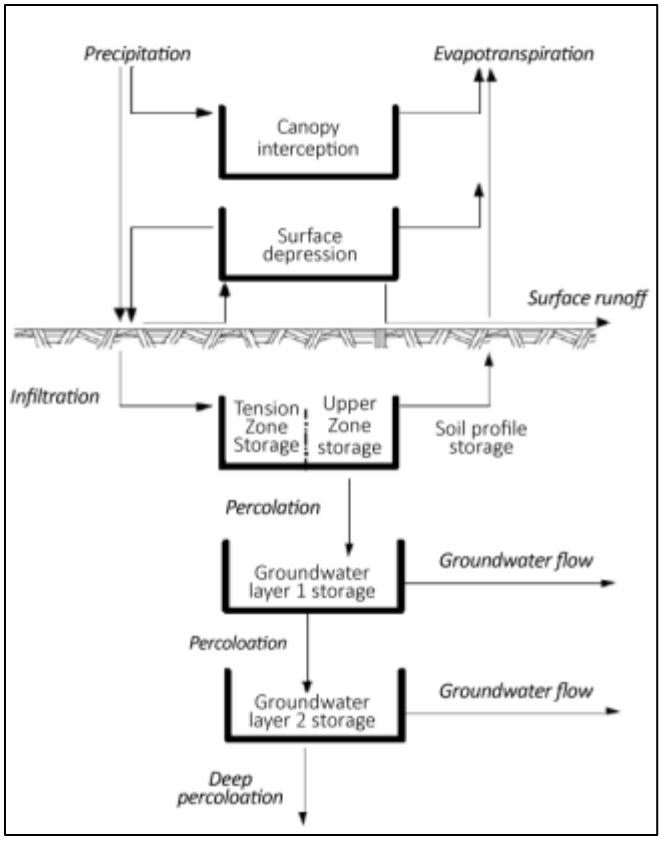

Figure 7-3: Schematic diagram of HEC-HMS soil moisture accounting model adapted from Feldman (2000)

7.1.2 Model calibration and performance assessment

Manual adjustment of model parameters using the trial-and-error method is the initial step in model calibration, which enables the modeler to make a subjective adjustment of parameters that gives an appropriate fit between observed and simulated hydrographs (Zhang *et al.*, 2013). There are many different approaches for the calibration of watershed models such as lumped, semi-distributed, 1-factor and regionalization (Wallner *et al.*, 2012). The lumped is the simplest one that can be performed in two ways either with the number of sub-basins or eliminating the sub-basins. In either of the two, the parameters value is the same for all sub-basins eqn.(7-1). In a semi-distributed HEC-HMS model, for each sub-basin the parameters $\Phi_{i,\,j}$ needs to be estimated, where the index i stand for the parameter and the index j for the sub-basin.

For the Lumped method, all particular parameter values are equal:

$$\Phi i,1 = \Phi i,2 = \Phi i,3 = \Phi i,4\,;\, i = 1,\ldots,N \qquad (7\text{-}1)$$

Where, N is the number of parameters.

According to Wallner *et al.* (2012), employing the lumped method, the spatial variability of the climate forcing is still represented due to the attribution of time series to the sub-basins, but the

spatial variability of the parameters is lost. The 1-Factor (1-F) method is the modified version of lumped method. Initial parameter values can be defined in a pre-processing step based on basin characteristics such as soil, land use and topography. As a result, spatially variable initial values for the parameters are obtained eqn. (7-2).

$$\Phi_{i,1} \neq \Phi_{i,2} \neq \Phi_{i,3} \neq \Phi_{i,4}; i = 1, \ldots, N \tag{7-2}$$

Although, the initial parameter values do not provide reliable model result, one factor is created for each parameter for the next step. These factors are calibrated and then multiplied with the particular parameter values. Hence, both (lumped and 1-factor) strategies are limiting the variability of the parameter values. Either there is no spatial variability (lumped) or the variability is given by pre-processing which depends on the modeler's subjective assessment of the catchment (1-factor).

Distributed calibration strategy (DIS) is a method, which considers all parameters for all sub-basins independently while regionalization method (REG) is assuming that the parameters of the hydrological model can be related to basin characteristics. In regionalization technique, each parameter value is calculated via transfer functions with a statistical relationship of pre-defined catchment characteristics value and the model parameters value using either linear or multiple linear regression techniques eqn.(7-3).

$$\Phi_{i,j} = \sum_{n=1}^{k} \alpha_{i,n} * S_{j,n} + \sum_{m=1}^{u} \beta_{i,m} * L_{j,m} + \gamma_i * \text{Area}_j + \cdots \tag{7-3}$$

i=1,...,N; j=1,...,N′,

where: N is number of parameters, N' is number of sub-basins, $S_{j,n}$ and $L_{j,m}$ are relative areas of soil- and land use classes, respectively and k and u are the number of different soil/land use classes defined for each sub-basin. In REG techniques, the parameters are not calibrated but the coefficients of the transfer function ($\alpha_{i,n}$, $\beta_{i,m}$, $\gamma_i \ldots$).

Therefore, semi-distributed method was employed due to the high spatial variability's of the catchment characteristics of the basin and the nature of HEC-HMS model. The entire UBNRB is sub divided into 42 different sub-basins as shown in Figure 7-4 to use the model as semi-distributed for HEC-HMS. Model parameter estimation of the sub-basins was carried out based on the observed streamflow records at eight different gauging stations namely: Gilgel Abay, Koga, Gumara, Rib, Megech, Tana, Kessi and El Diem. At Tana gauging station, we calibrated and validated for both Lake level elevation and outflow. In order to get the optimum parameter values after manually calibrating the model, an automatic optimization method was applied. The Nelder and Mead optimization method used than the univarient method. The reason behind is, the Nelder and Mead method uses downhill simplex to evaluate all parameters simultaneously and which parameters to adjust. The level of goodness of fit evaluation is mainly done using eqn.(4-5) to (4-10).

Figure 7-4: Watershed subdivision for calibrating HEC-HMS model

7.2 Input data preparation

The various types of input data needed for HEC-HMS model are:

- Geospatial data (DEM, LULC map and soil data)
- daily time series of rainfall, streamflow, and mean monthly evaporation for different sub-catchments and reservoirs
- Irrigation areas and demands for each scenario
- Characteristics of the hydropower stations (installed capacity, rated heads and discharges, etc.,)
- Reservoir characteristics (area-capacity curves, rule curves, evaporation etc.)
- Lake Tana elevation-area-capacity relationship and operation rule curves

This study uses ArcGIS; Geographic Information System (GIS) software developed by ESRI arcGIS, a Geographic Information, and manipulates spatial information. HEC-GeoHMS (https://www.hec.usace.army.mil/software/hec-geohms/) extension within the ArcGIS 10.2.1 environment is used for creating the basin model describing the physical characteristics of the watershed (slope, low accumulation, stream network, etc). It is specifically designed to process Geospatial data and create input files for HEC-HMS. It provides the connection for translating GIS spatial information into model files for HEC-HMS.

7.2.1 Hydro-meteorological data

The future climate projections generated from down scaling climate model (i.e., rainfall, temperature;(Mekonnen *et al.*, 2018a) are used as input to a hydrological model (HEC-HMS) to assess the combined impacts of climate change and water resource developments. Daily precipitation and mean monthly evapotranspiration are the main climate variables used for driving the water balance model. For the baseline scenario and for calibrating and validating the model, the weather data and flow data were obtained from the ENMA and from the Federal Ministry of Water Irrigation and Electricity of Ethiopia for the period 1971-2010 respectively. For the details of preprocessing and analysis of hydro-meteorological data please see Chapter 4 and from (Mekonnen *et al.*, 2018a; Mekonnen *et al.*, 2018b).

For the future period, six GCMs from CMIP3 and three GCMs from CMIP5 are employing in the present work. However, only two forcing data sources are selected and employed to drive HEC-HMS hydrological model. The two forcing data sources are the outputs of the downscaled canESM2 and GFDL GCMs from CMIP5 climate models under RCP4.5 scenario. The databases of the two GCMs contain precipitation and temperature data from 1984 to 2100 at monthly and daily time steps. The downscaling methods applied for the daily data are SDSM and LARS-WG, which are widely used and validated in a number of studies. The details of downscaling the future climate scenario is described under Chapter 6 of this dissertation.

These two GCMs are selected for further impact analysis for the following reasons.

- They are from CMIP5 generation climate models, which were used for the IPCC AR5. In the CMIP5 project, significant efforts were incorporated to reduce uncertainty in the model simulations, which led to a new generation of global climate models known as Earth system models (ESMs) such as canESM2 (Taylor *et al.*, 2012). These models were designed with the added capability to explicitly represent biogeochemical processes that interact with the physical climate in addition to a more detailed representation of aerosols and carbon cycles (Flato, 2011). It also includes models with improved physical parameterization schemes regarding cloud and radiation processes (Dolinar *et al.*, 2015). Therefore, CMIP5 GCMs are expected to produce more realistic results than CMIP3 as models tend to improve across generations (Das *et al.*, 2012; Mekonnen *et al.*, 2018a).
- The maximum increase of the future precipitation for the UBNRB was obtained from the downscaling canESM2 GCM while GFDL CMIP5 GCM produced the maximum decrease for the future precipitation in the UBNRB.

- Although it is hard to predict the future plausible climate scenario, RCP4.5 has chosen for this impact analysis study. Because it is the medium class radiative forcing scenario and the most likely scenario to happen in the future over the UBNRB as compared to RCP2.6 (best case scenario) and RCP8.5 the worst case scenario in terms of GHG emission. RCP 2.6 requires powerful climate politics close to the ambition of the Paris agreement $2^{o}C$ "goal" for the rise of global temperature at the end of 21^{st} century (Agreement, 2015). The RCP 8.5 scenario may also become less likely in years to come, even if the current climate most closely tracked RCP 8.5 scenario. The global coal industry should be seven times bigger than it is today to rise the world's average temperature by $4.9^{o}C$ that represents the RCP8.5 https://www.theatlantic.com/science/archive/2019/01/RCP-85-the-climate-change-disaster-scenario/579700/. These can be a real ground to exclude RCP8.5 for further impact analysis.

RCP 4.5 is a stabilization scenario in which total radiative forcing is stabilized at $4.5Wm^{-2}$ (approximately 650-ppm CO_2 equivalent) shortly after 2100 relative to the pre-industrial period, without overshooting the long-run radiative forcing target level. The RCP 4.5 scenario is developed with the following assumptions.

- Lower energy intensity
- Strong reforestation programmes
- Decreasing use of croplands and grasslands due to yield increases and dietary changes
- Stringent climate policies
- Stable methane emissions
- CO_2 emissions increase only slightly before decline commences around 2040

For the details of climate projections, please see (Mekonnen *et al.*, 2018a)

7.2.2 The evapo-transpiration data

Evapotranspiration is the combination of soil evaporation and crop transpiration. Weather parameters, crop characteristics, management and environmental aspects affect evapotranspiration. The evapotranspiration rate from a reference surface (i.e. for hypothetical grass cover of 12 cm high with no moisture constraints, surface resistance of 70 sm^{-1} and an albedo of 0.23) calculated from eqn.(5-5) is called the reference evapotranspiration and is denoted as ETo. Due to the difficulty of obtaining accurate field measurements, ETo is commonly computed from weather data. A large number of empirical or semi-empirical equations have been developed for assessing reference evapotranspiration from meteorological data. Experts consultation held in May 1990 recommended the FAO Penman-Monteith method eqn.(5-5) as the standard method for the definition and computation of the ETo (Allen et al., 1998). This method has been selected by FAO as the reference because it closely approximates grass ETo at the locations where evaluated, is physically based, and explicitly incorporates both physiological and aerodynamic parameters.

Hence, the daily evapotranspiration was calculated using FAO ETo calculator V3.2 software by means of the FAO Penman-Monteith equation at 12 stations, which have a complete climatological data sets, i.e., maximum and minimum temperature, mean relative humidity,

sunshine hours and wind speed from 1987 to 2011. The ETo Calculator is public domain software obtained from http://www.fao.org/nr/water/eto.html. After calculating ETo at station level, the areal evapotranspiration for the selected sub-basins were calculated using Thiessen polygon method based on the stations information inside and around the sub-basins. Finally, the future scenario of evapotranspiration was calculated from daily evapotranspiration at station level using SDSM from canESM2 and GFDL GCMs for the scenarios of RCP4.5. Before generating future scenarios of ETo, the statistical down scaling model (SDSM) is calibrated and validated and the potential predictors for ETo for each 12 stations were selected. Detail explanation and procedure of SDSM can be found from (Mekonnen *et al.*, 2018a). For stations, which do not have complete climatological data sets such as mean relative humidity, sunshine hours and wind speed, the baseline and future ETo was calculated using the same software based on Tmax and Tmin data. In case humidity data, wind speed data or radiation data is not available for a particular day, the software will make use of the information specified in the corresponding boxes (missing air humidity, wind speed or radiation data) to estimate the missing meteorological data.

7.2.3 Water resource development and management scenarios

In order to assess the downstream effect of the planned irrigation and hydropower projects as well as the climate change effects, thirteen development and management scenarios are established Table 7-1. The baseline scenario (s0) includes the natural flows of the UBNR before Tana Beles transfer being operational, without any man-made changes. Scenario s1 represents the current situation that consists of the currently operating irrigation schemes (Koga, Fincha sugar factory and Anger) and Tana Beles hydropower project. The remaining eleven scenarios are based on the irrigation and hydropower development combined with and without climate change. The development scenarios are classified as short term (2017-2025), medium-term (2026-2040), long term A from (2041-2070) and long term B (2071-2100). The classification of long term A and B are similar in the irrigation and hydropower developments but different for climate change scenarios.

s2, s3 and s4 scenarios are scenarios with different level of water resource development but they are not addressing the climate change effect (climate remained constant), these are used to analyze the single impacts of water infrastructure developments at different levels. S5, s6, s7 and s8 scenarios are based on the assumption that climate is changing under RCP 4.5 scenario of canESM2 GCM combined with different level of irrigation and hydropower developments, when the precipitation and streamflow might increase across the basin. S9, s10, s11 and s12 scenarios are based on the assumption that climate change of RCP 4.5 scenario of GFDL GCM combined with different level of irrigation and hydropower developments might occur in the future, when precipitation and streamflow might decrease over the basin. Detail descriptions of the scenario development can be found in Appendix 18. For each model scenario, the impacts on the hydrology, irrigation and hydropower developments are explored. Estimates of current and future irrigation and hydropower development plan were derived from data provided by government ministries and agencies or from previous studies, as well as from the basin master plan study report Appendix 20.

Table 7-1: Proposed scenario development

	Water resources development scenarios								
	Base line	Current condition	Short term	Medium term	Long term	Short term	Medium term	Long term A	Long term B
Scenario	s0	s1	s2	s3	s4	s5,s9	s6,s10	s7,s11	s8,s12
Irrigation (*1000ha)	0	23.5	214.9	382.6	424.4	214.9	382.6	424.4	424.4
MAD(Mm^3)	0	169.2	1694.9	3209.5	3583.3	1694.9	3209.5	3583.3	3583.3
AID (m^3ha^{-1})	0	7172.2	7887.5	8387.8	8524.1	7887.5	8387.8	8443.8	8443.8
Hydropower									
Tana Beles	X	√	√	√	√	√	√	√	√
Beko Abo	X	X	X	X	√	X	X	√	√
Karadobi	X	X	X	X	√	X	X	√	√
Mendiya	X	X	X	X	√	X	X	√	√
GERD	X	X	√	√	√	√	√	√	√
Climate change	X	X	X	X	X	√	√	√	√

Short term (2018-2025); medium term (2026-2040); long term A (2041-2070); long term B (2071-2100); MAD: mean annual water demand; AID: annual irrigation demand per hectare; s9, s10, s11 and s12 are based on GFDL CMIP5 GCM while s5, s6, s7 and s8 are based on canESM2 CMIP5 GCM.

Safe drinking water is one of the necessities for human beings. However, billions of people in the world have not access to it today particularly the population from the developing countries like Ethiopia. To improve this situation, the Government of Ethiopia has prepared the Second Growth and Transformation Plan (GTP-2) covering the period from 2016-2020. The GTP-2 plan has two main goals regarding to water supply and sanitation sector to accelerate the provision of safe and adequate water.

Goal 1: Provide rural water supply access with minimum service level of 25 l/c/day within a distance of 1 km from the water delivery point for 85 % of the rural population.

Goal 2: Provide urban water supply access for 75 % of the urban population with GTP-2 minimum service level standards.

The domestic and non-domestic water supply demand calculated based on the central statistics agency (CSA) population projection and revised standards of per capita demand of each sector at the end of 21st century is estimated about 7302 Mm^3. However, it is not considered in the scenarios for impact analysis due to the fact that more than 90% of the domestic water supply source is from ground water and its impact both currently and in the future is insignificant (SMEC, 2008).

7.2.3.1 Irrigation development

Irrigation led development and effective use of water resource potential is a strategic direction for the Government of Ethiopia for means of livelihood improvement. Irrigation can provide an

opportunity to improve the productivity of land and labor that increase production volumes and play a great role in confronting poverty and drought significantly. Although, irrigation potentials are not exhaustively identified, different studies reported different results. For instance, BCEOM (1998a), identified 578,000 ha net irrigable land which are economically feasible with an average water requirements calculated at 4,895Mm^3 annually. WAPCOS (1990) reported the identified 1,001,000 ha potential large and medium irrigable lands in Abay basin including the sub-basins of Rhad and Gelegu, which are not included in the current research. Hence, to maximize the advantage of irrigation development, the Ethiopian government is increasingly investing in the water sector. To this end, at the end of GTP II, the ministry of water, irrigation and electricity has been planned to carry out the construction of 280,385 hectares irrigation and drainage projects. The irrigation potential and irrigation water requirements identified and calculated by BCEOM (1998a) during the master plan study is adapted for this study see Appendix 19.

Irrigation water requirements

Diversion for the irrigation projects has designed to have two outflows, main and diverted, and one or more inflows. Six methods are available for computing the diverted flow that will be taken out of the channel. All flow that is not diverted becomes the main outflow. The specified flow diversion method designed for the known quantity of flow (irrigation demand) diverted from the channel is selected for this dissertation. In this case, a time series of specified discharges for the irrigation calculated externally based on their irrigation water requirement to be diverted from the channel can be entered in the model time series data manager.

Irrigation water requirements calculated by BCEOM (1998b) for the Abay master plan study were adopted for this dissertation. The ET_0 values were calculated based on reviewed and corrected climatic data, including altitude, average temperature, humidity, wind speed and sunshine duration for 22 stations. In order to calculate the ETo values according to the Penman-Monteith formula, the FAO CROPWAT program, version 5.7 was used. Annual effective rainfall values ranging between 50 and 70% of the annual average rainfall was considered to be on the safe side. Seven different cropping patterns had been developed with different assumptions. Here it is to be noticed that evapotranspiration for the calculation of irrigation water requirement is not considering the future climate projection due to the conservative recommended value for irrigation efficiency and assuming the irrigation efficiency in the future might improve. Gross Irrigation water requirement for the planned irrigation projects can be found on Appendix 19.

Table 7-2: Monthly average evaporation of the planned and existed reservoirs ($mmday^{-1}$)

Month	Koga	Megech	Gumara	Rib	Jemma	Gilgel Abbay	Lake Tana	Beko-Abo	Karadobi	Didesa	Mendiya	GERD
Jan	130	143	133	133	130	133	133	168	166	196	194	202
Feb	137	148	143	140	134	140	139	163	161	190	188	196
Mar	167	180	174	171	161	171	164	178	176	172	170	182
Apr	174	174	171	165	168	174	178	168	166	197	196	208
May	152	164	155	155	149	155	162	152	151	241	239	251
Jun	123	141	129	129	120	120	133	96	95	174	173	186
Jul	93	90	90	93	90	93	117	67	66	15	15	46
Aug	93	90	90	90	93	93	123	65	64	87	87	115
Sep	129	132	129	126	126	132	133	88	87	212	211	225
Oct	143	155	146	146	140	143	140	128	127	251	250	259
Nov	129	138	132	129	126	129	131	138	136	170	169	176
Dec	121	130	124	124	118	121	123	149	147	184	182	189
Total	1591	1685	1615	1600	1555	1603	1676	1560	1542	2088	2073	2236

7.2.3.2 Defining reservoirs data and model simulation

Being rich with hydraulic power potentials, dense river network, abundant rainfall and large runoff volume, the UBNRB is the most important and prospective basin for the water resource developments. According to the basin master plan studies (BCEOM, 1998a), water resource management policies and strategies, large scale reservoirs for irrigation and hydropower had been built up or under construction on the UBNRB, and planned to be constructed in the future. Because of population and socio-economic growth within the basin, assessing the demand and supply of available water turns out to be essentially urgent.

A reservoir is an element with one or more inflow and one computed outflow. Inflow comes from other elements in the basin model. If there is more than one inflow, all inflow is added together before computing the outflow. Storage reservoirs identified in the Abay basin area during the Abay master plan study (BCEOM, 1998a) are listed in Table 7-3. Their location is indicated in Figure 7-5, together with their upstream catchments. In this dissertation, one existing, three under construction and two planned reservoirs for the purpose of irrigation and three planned and one under construction reservoirs for the purpose of hydropower generation and one natural reservoir, Lake Tana, which is served to regulate the natural flow for the Tana Beles hydropower production is included in the simulation. Hence, HEC-HMS model requires physical reservoirs data as well as operational reservoirs data for simulating the required streamflow variable. The main sources for the physical data for all the reservoirs are previous

studies, feasibility studies of the projects and Hydropower Toolkits developed by Eastern Nile Technical Regional Office (ENTRO).

Reservoir routing and storage method

Several methods are available for defining the storage properties of the reservoir and for routing the reservoir. While a reservoir element conceptually represents a natural lake or a reservoir behind a dam, the actual storage calculation method is performed by a routing method contained within the reservoir. Four different routing methods are available in HEC-HMS. The first one is simply designed to represent the reservoir with a known storage-outflow relationship (Outflow curve). The second method uses a specified release and computes the storage that would result (specified release option). The third method is designed to represent individual components of the outlet works (outflow structures). The fourth method is a choice for none routing method (none). This option assumes no storage in the reservoir and all inflow is passed as outflow for each time interval of the simulation (Scharffenberg, 2015). In this dissertation, outflow structures routing method is selected because of two main reasons. First, evaporation and seepage from a reservoir can only be included using this method. Seepage loss from the reservoir is not included in this study due to data limitation. Second, there is no any developed relationship between the storage and discharge for each reservoir, which is unique. It is also possible to develop additional releases based on an operations plan for the reservoir. This is a best option to develop the different time series releases for the Lake Tana reservoir pumped irrigation based on the future development scenarios.

Elevation-Area storage method, which requires the selection of an elevation-area curve from the available curves in the paired data manager, is selected. With this choice, the model automatically transforms the elevation-area curve into an elevation-storage curve using the conic formula. After the routing is complete, the program will compute the elevation, surface area and storage for each time interval (Scharffenberg, 2015). The operational and physical data for reservoirs were taken from previous studies such as (Halcrow and GIRD, 2010; SMEC, 2008), Hydropower Toolkits and mathematical relations formulated from the long time record of Lake outflow and elevation. Elevation-Area-capacity tabulated data is entered in the paired data manager.

Reservoir evaporation

Water losses due to evaporation are an important part of water balance for a reservoir especially in dry or desert environment like GERD. The evaporation losses are different from other structures because they do not contribute to either main or auxiliary outflow. An evaporation depth is computed for each time interval and then multiplied by the corrosponding surface area. The monthly evaporation rate method is used to specify a separate evaporation rate for each month of the year, entered as a total depth for the month. Mean monthly evaporation data at the locations of reservoirs collected from previous studies is shown in Appendix 22.

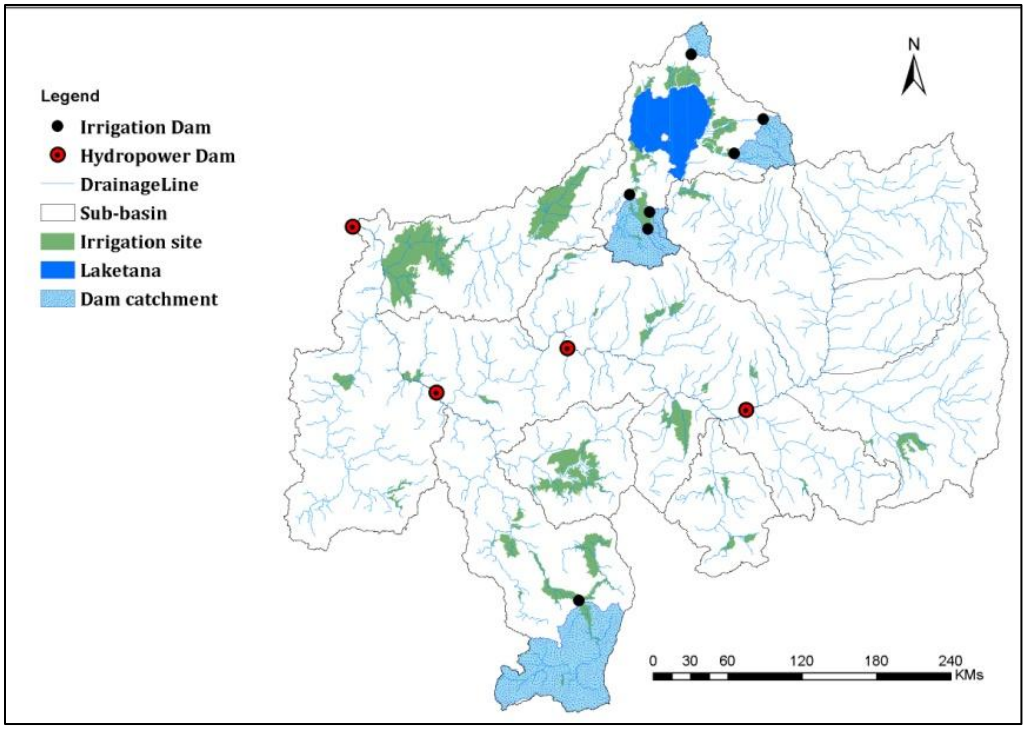

Figure 7-5: Locations of existing and proposed irrigation projects across the UBNRB

Table 7-3: Characteristics of irrigation dams identified by BCEOM (1998a)

(a) Reservoir volume characteristics

Irrigation Dam	Catchment area (km^2)	Average discharge (m^3s^{-1})	Dead storage volume (Mm^3)	Live storage volume (Mm^3)	Total storage volume (Mm^3)	Irrigation area (ha)	mean annual demand (Mm^3)
Jemma	218	5.5	10	163	173	7,786	60
Koga	165	2.75	4	73	77	7,000	54
Gilgel Abbay	1,980	70	144	419	563	16,499	160
Megech	424	5.58	20.3	161.6	181	7,311	62
Ribb	685	6.82	27	206	233	19,925	196
Gumara	410	8.15	35.9	187.1	223	13,776	117
Didessa	5537	112	537.2	1515.8	2053	88,000	477

b) Elevation characteristics

Dam Name	Bottom level (masl)	Top of dead storage (masl)	Normal water level (masl)	Spillway level (masl)
Megech	1867	1910	1947.1	1947.1
Rib	1875	1901.2	1932	1932.5
Gumara	1920	1942	1972.5	1972.5
Jemma	2055	2092.5	2130	2130
Koga	2004	2007	2015.2	2015.2
Gilgel Abay	1840	1862	1890	1890
Didessa	1312	1344	1355.2	1355.2

7.2.3.3 Hydropower development

Ethiopia needs high power to meet the growing electricity demand and help speed up the economic and social development in the country, as well as to increase the power supply reliability and earn foreign currency by exporting electricity. From the outflow at Lake Tana until the Sudanese border the Abay drops from 1800 to 500 masl over 900 km. Along this stretch its mean annual flow increases from around 110 m^3s^{-1} (outflow of Lake Tana) to 1700 m^3s^{-1} at El Diem (NORPLAN *et al.*, 2006). Due to its slope and large discharge the Abay river has enormous theoretical hydroelectric power potential estimated about 55,000 GWh as identified by (BCEOM, 1998a). However, up to the present, two small hydropower's (Tis Abay I &II), and one medium hydropower (Tana-Beles transfer HPP) schemes have been implemented in the Abay catchment Table 7-4.

Currently only Tana Beles hydropower, which can generate 460 MW is under operation in the basin. The Tana Beles hydropower scheme involves the transfer of water from Lake Tana through a 12 km long and 7.1 m diameter tunnel with 311 m elevation difference between the Lake Tana and Beles River (Salini and Pietrangeli, 2006). This enables far more electricity to generate than the power generated from Tis Abay I and II power stations. It was intended to divert approximately 2,985 Mm^3 annually through the tunnel to generate 2,310 GWh of electricity each year with a firm production estimated at 1,866 GWh (SMEC 2008). According to the data obtained from the Tana-Beles HP project office, approximately 3,139Mm^3 volume of water is diverted through the tunnel to the Tana-Beles HP each year and able to generate 2,230 GWh of electricity for the first six years operation (2011-2016).

Tis Abay I and II hydropower projects, located some 45 km downstream of Lake Tana outlet, which have total capacities of 84.4 MW are used as standby. Some part of the flow after leaving the Chara-Chara weir is diverted to these plants and the remaining part will flow to the Tis-Issat waterfall. Tis-Abay I power plant was designed for a total maximum discharge of 30 m^3s^{-1} with three turbines each 10 m^3s^{-1}, rated net head of 46 m, power factor of 0.8, and installed capacity of 11.4 MW Table 7-4. Tis-Abay II power station was designed for total maximum discharge of 150 m^3s^{-1} with 2 turbines each 75m^3s^{-1}, rated head of 53.2 m, power factor of 0.90, and with 73 MW installed capacity.

Table 7-4: Characteristics of existed operational hydropower plants in the Abbay river

Hydropower plant	No of turbines	Maximum discharge (m^3s^{-1})	Net head (m)	Installed capacity (MW)	Plant factor
Tis-Abay I	3	30	46	11.4	0.8
Tis-Abay II	2	150	53.2	73	0.9
Tana-Beles	4	160	311	460	0.48

Tana-Beles hydropower project

According to Halcrow *et al.* (2010), the Tana-Beles HPP located in the Beles river catchment is part of a multipurpose 50 year development plan for the Tana-Beles basins. It inaugurated on 14 May 2010, is now operational, and involves the diversion of water from Lake Tana through an 11km long and 7.1m diameter tunnel into the adjacent water deficient Beles catchment. Hydropower is generating by using the natural head difference of 311m between Lake Tana water level and the Beles riverbed level. Water from the tunnel feeds a vertical penstock shaft connected to a powerhouse with four turbines with a total installed capacity of 460 MW. The hydropower plant is operating with an average plant factor of 48%. The average discharge through the tunnel is 77 m^3s^{-1} with discharge peaking at 160 m^3s^{-1} at high lake levels. The aim of the Tana-Beles Scheme is to divert on average about 2,985 Mm^3 (70% of the natural outflow of Lake Tana) per annum from Lake Tana to the Beles river basin through the Tana-Beles hydropower plant generating 2,310 GWh of electricity, assuming existing development conditions in the Lake Tana basin and a minimum operation level of 1,784.0 masl. However, diversion of water to the Beles catchment will decline to 2,493 Mm^3 per annum and generate 1,907 GWh of electricity once full water resource development in the Lake Tana basin is complete and if the minimum operation level of 1,784.75 masl for Lake Tana is adopted as recommended by SMEC (2008).

According to Salini *et al.* (2006) the Beles multipurpose project has the following basic parameters:

- 1784 masl inlet minimum operating level
- 1455.5 masl tail water level in the Jehana river for 160 m^3s^{-1}
- 331.5 m gross head
- 77 m^3s^{-1} average annual flow
- 0.48 Plant factor
- 160 m^3s^{-1} design flow
- 420 MW Installed power
- 7.20 m Headrace and tailrace tunnel internal diameter
- 6.5 m Penstock shaft diameter
- 19.46 Total losses
- 31.80 Total head losses
- 299.7 Net Head

The average annual energy production can be calculated with the following expression:

$En = 9.81*\rho*Q*\eta*Hn*PF*hy*10^{-9}$ =1719 GWhyr^{-1} where:

ρ is water unit weight= 1000 kgm^{-3}, η is Plant overall efficiency= 0.87, Q is rated flow = 160 m^{3}s^{-1}, Hn is net head = 299.7m, PF is plant factor= 0.48 and hy is 8,760 hours yr^{-1}

Cascade hydropower projects

The future large scale cascaded hydropower projects to be implemented along the main stem of Abay river that has been identified by (BCEOM, 1998a) are as follows.

Karadobi hydropower project

On the middle course of the Abay, some 400 km downstream of the outflow of Lake Tana, and around 65 km downstream of the Kessi road bridge, the (USBR, 1964) identified topographically suitable Karadobi sites for a large hydropower development. The proposed Karadobi dam and power plant is located on Abay River, approximately 55km south of Debre Markos, 65km downstream of the Kessi Bridge and 1.7km downstream of the confluence of the Abay and Guder rivers. The main characteristics of Karadobi dam is shown in Appendix 23.

The analysis of 50 years data from the hydrometric station at Kessi station reported by (NORPLAN et al., 2006) concluded that the reliable average inflow of 640 m^{3}s^{-1} was recorded. Based on the average inflow of 640 m^{3}s^{-1}, Karadobi hydropower project had been identified with the installed capacity of 1,600MW that could produce 9,708GWh annual average energy, of which 9308GWh is firm energy without Tana Beles transfer (Appendix 23). Assuming upstream transfer of water to Beles catchment, the best Karadobi development option is found to be 1280MW. The annual energy production potential at Karadobi is then reduced to 8,693 GWh. A proposed of 250 m high dam on the Abay river at Karadobi will facilitate a regulated firm outflow of 526 m^{3}s^{-1} from the reservoir. The live storage of the reservoir between full supply level (FSL) at 1146 and minimum operating level (MOL) at 1100 masl is 17,300 Mm^3 corresponding to 85% of the annual average inflow.

Beko-Abo hydropower project

The proposed Beko-Abo dam and power plant will be located approximately 2 km north of the bridge on the road Nekemte-Bahir Dar crossing the Abay River, which is some 90 km (air distance) downstream of the Karadobi dam site. The distance from Addis Ababa is approximately 460 km via Debre Markos and some 530 via Nekemte (NORPLAN et al., 2013). The main features of Beko-Abo high dam is shown in Appendix 23. The 1940 MW Beko-Abo project alone can produce 12,096 GWh annual average energy, of which 11,937 GWh is firm energy in the interconnected system to Egypt. The mean annual inflow analysis carried out by NORPLAN et al. (2013) is 675m^{3}s^{-1} after deduction of the Beles abstraction of 77m^{3}s^{-1}, and this quantity is considered to be reliable (see, Appendix 23).

One alternative to avoid the over toping effect of on the Kessi Bridge is to introduce a Beko-Abo low scheme with a FSL of 910 masl, equivalent to the tailrace outlet elevation of the Karadobi project. The installed capacity is taken as 800 MW resulting in a predicted yield of 4 664 GWh. A low Beko-Abo scheme is considered to be as viable as the main Beko-Abo High (NORPLAN *et al.*, 2013).

Mandaya

Mandaya project is located at sites 220 km from Beko-Abo. While Beko-Abo and Mandaya are separate projects, the headwaters of the lower Mendiya scheme will extend all the way up to the location of Beko-Abo. Mendiya dam height 170 m, crest length 1,400m and reservoir live storage 10.3×10^6 Mm^3, Capacity 1,700MW and 8,220 $GWhyr^{-1}$ (Appendix 23).

A Mandaya low is introduced as an alternative to regulate only the average annual additional inflow downstream of a main upstream regulating reservoir. A Mandaya Low scheme with FSL 760 masl and 20 m range of regulation will have a live storage of 9.5 Bm^3. The gross storage would be 25 Bm^3 compared to 49.2 Bm^3 for the high scheme, a factor of 50 %, with significant implications for fill of the reservoir. The average annual spill (only occurring a few years under very high floods) is increased to 50 m^3s^{-1} from 23 m^3s^{-1}. The installed capacity is taken as 1,500 MW resulting in a predicted yield of between 9,400-9,625 GWh. To maintain the approximate production of 625 GWh achieved from the additional inflow from Didessa a 100 MW power plant with a 40-50 m high could be constructed in this river.

Mabil Low and High

Further variants on cascade options is the introduction of Mabil low and high schemes between Beko-Abo and Mandaya dam sites, the high or low variant being adopted dependant on which of the up-stream schemes is the main regulating reservoir. The Mabil low scheme with an FSL 800 masl and 10 m range of regulation will have a live storage of 0.3 Bm^3. After a number of years of operation due to siltation, the project will revert to a run of the river scheme, but should retain sufficient reservoir capacity to enable operation to provide a peaking regime. The installed capacity and predicted energy yield is 290 MW and 1,872 GWh respectively. The Mabil High scheme with an FSL 910 masl and 30 m range of regulation will have a live storage of 3.4 Bm^3. The installed capacity and predicted energy yield is 1,200 MW and 7 393 GWh respectively (Arnold *et al.*, 2010).

Grand Ethiopian Renaissance Dam (GERD)

The GERD is a hydroelectric power project under construction on the Abay River (UBNR) by the Government of Ethiopia, some 20 to 40 km upstream of Ethio-Sudan boarder. The dam has planned to support the economic and social development of the whole country, both in rural and urban areas. There will be exports, only if there is a total surplus of energy generated in Ethiopia to support the country's shortage of foreign currency. This is expected to happen during rainy seasons, when there is plenty of water for hydropower generation.

The electrical parameters and the storage parameters are changed from the original design parameters from 2011-2017. Originally, in 2011, the hydropower plant was designed to install 15

generating units with 350 MW each, resulting in a total installed capacity of 5,250 MW with an expected power generation of 15,128 GWh per annum. However, due to the upgrading made on the power plant, its generation capacity was uplifted to 6,000 MW from 5,250 MW, with a power generation of 15,692 GWh per annum through 16 generating units with 375 MW capacities each. In 2017, the design has again been changed to add another 450 MW, with a power generation of 16,153 GWh per annum. Upgrading 14 of the 16 generating units from 375MW to 400MW achieved that without changing the generating capacity. Not only was the electrical power parameters changed over time, but also the storage parameters. Originally, in 2011, the dam was considered 145 m height to have a volume of 66Bm^3 and a surface area of 1,680 km^2 at full supply level. In 2013, International Panel of Experts, IPoE (2013) assessed the dam and its technological parameters. At that time, the reservoir sizes were changed already. The size of the reservoir at full supply level (FSL) of 640 masl went up to 1,874 km^2. The storage volume at FSL had increased to 74 km^3. After the international panel of experts (IPoE) made its recommendations, in 2013, the dam parameters were changed to account for higher flow volumes in case of extreme floods a main dam height of 155 m with a length of 1,780 m. The outlet parameters did not change, only the crest of the main dam was raised.

The zero level of the main dam, the ground level, will be at a height of almost exactly 500 m masl, corresponding roughly to the level of the riverbed of the Blue Nile. From the ground level, the main gravity dam will be 155 m tall, 1,780m long. The crest of the dam will be at a height of 655 m above sea level. To support the main dam and reservoir, there is a curved 5.2 km long and 50 m high rock-fill saddle dam. The ground level of the saddle dam is at an elevation of about 600 m above sea level. Hydropower generation can happen between reservoir MOLs of 590 m, and 640 m, the FSL. The live storage volume, usable for power generation between both levels is then 59.2 Bm^3. The first 90 m of the height of the dam will be a dead height for the reservoir, leading to a dead storage volume of the reservoir of 14.8Bm^3 (see, Appendix 23**).**

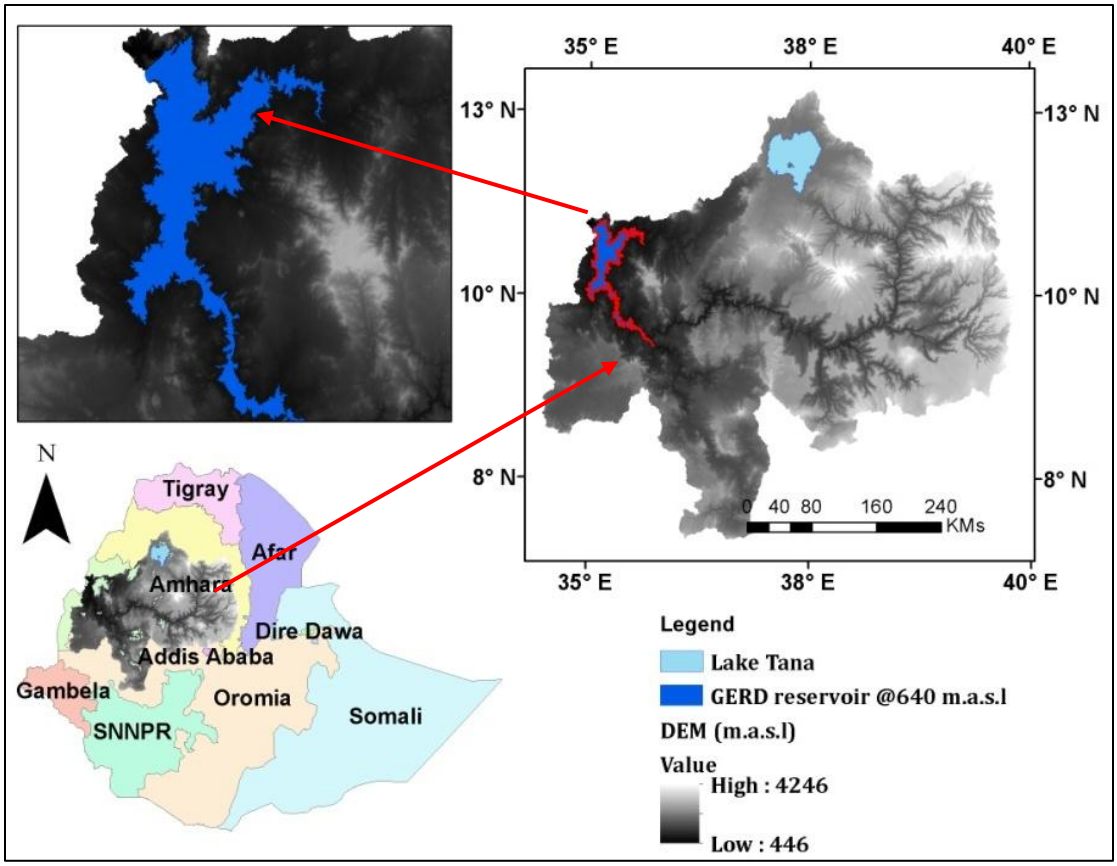

Figure 7-6: Location of GERD Reservoir

In this study, the reservoir surface area and volume were calculated via Arc GIS software based on different water level scenarios. These scenarios included storing water at different elevations behind the dam beginning from 500 m, i.e. and by increasing 10 meter in each scenario up to 640, which gives water level at 140 m. According to the elevations of the ground in the study area, the model results showed different suggestions for the area and volume of the reservoir as shown in Figure 7-6. A result showed that at level of 640 masl, i.e. 140 m behind the dam, the reservoir has 1911 km^2 and a volume of water equal to 80.5Bm^3.

7.2.4 Operational rules for planned hydropower dams

River water flow varies with time and hence water is stored in reservoirs when available in plenty and used later when it is needed. If the reservoir is properly managed and operated, it has the ability to boost the dependability of water supply in fostering livelihoods, increasing agricultural yield, and reducing the susceptibility of farmers to droughts (Neelakantan and Sasireka, 2013). The major task of reservoir operation is to decide how much water should be released in the current period and how much should be retained in storage within the reservoirs for future use, give some available and/or forecast information at the beginning of the current time period. Operating policies of reservoirs have been aimed for regulating the release of water

by keeping in mind the interests of the reservoir stakeholders and decision makers, volume of water impounded, inflows, demands of water, release capacity, and downstream constraints (Anand *et al.*, 2018).

Reservoir Operation has the potential to alter flow regimes, such as inter-annual and seasonal variations in inflow to the reservoir, which can affect the volume of water available for operating the turbines. It is a complex problem that involves numerous hydrological, technical, economical, environmental, institutional and political considerations (Mythili *et al.*, 2013). It also involves many decision variables, multiple objectives as well as considerable risk and uncertainty (Reddy and Kumar, 2006). However, effective reservoir operation is required for the sustainable water resource development in areas where there is limited water resources. Improving the reservoir operation for increased efficiency is another way of maximizing the limited supply, which does not require the physical development of reservoir.

Rule curve for reservoir system is system of curves that represent the relationship between outflow from a reservoir at any time of year and the reservoir state (current reservoir capacity and inflow to reservoir). Optimal multi-objective rule curve for reservoir system is determined such that the reservoir operation according to optimal rule curve will maximize the given objectives while satisfying all constraints. According to (Kangrang *et al.*, 2018), the purpose of the rule curves for reservoir operation was divided into two main areas. (i) Variation of hydrological conditions, such as precipitation and inflow that flows into the reservoir were affected by climate change, and (ii) water allocation for social, economic, and engineering purposes in downstream areas has changed due to the population growth and land use management. The main purpose is therefore to avoid the risk of water shortages for downstream users, minimize reservoir evaporation and maximize energy generation. During the dry season, reservoirs need to maintain water volume to reduce the risk of water levels lower than minimum storage. During the rainy season, the reservoir must release large water to reduce the storage volume, which can reduce spillage due to the increased precipitation and inflow into the reservoir (Kangrang *et al.*, 2018). Typically, reservoir operating system has been large and complex, especially in UBNRB having long dry seasons and short peak flow seasons.

Optimization models are based on clearly defined objective functions, decision variables, and constraints as limitations during optimization. Reservoir optimization models, objective functions such as efficiency (i.e. maximizing hydropower generation, irrigation area and downstream flow), and sustainability should be incorporated. The criteria are economic, social and environmental issues. The typical constraints in a reservoir optimization model, (including conservation of mass and other hydrological and hydraulic constraints, minimum and maximum storage and release, hydropower and water requirements as well as hydropower generation limitations) are presented in eqn. (7-4) to eqn.(7-8) as adapted from (Olukanni *et al.*, 2018) and with reference to (Le Ngo, 2007).

Constraints

Generally, the constraints for the optimization/simulation model can be categorized into five main types:

a) Hydrologic constraints are defined by the rainfall-runoff relationships such as sub-basins areas, rainfall losses due to canopy interceptions, depression storage and soil infiltration,

effective rainfall transform methods, watershed runoff routing methods, internal boundary conditions and initial conditions that depict the rainfall-runoff process in different components of a watershed system (Che and Mays, 2015),

$$h\left(P_{i,t}, H_{i,t,} Q_{i,t}\right) = 0 \tag{7-4}$$

Where $P_{i,\,t}$ is the matrix of precipitation data in the system; $H_{i,\,t}$ is the rainfall losses matrix of the watershed system; $Q_{i,\,t}$ is the watershed and reaches discharge matrix of the system. All the hydrologic constraints are in matrix form is because of the problem has dimension of space, i, and time, t. These constraints are solved implicitly using the HEC-HMS model each time they are required.

b) The mass balance or continuity equation between the inflows and the outflows is given as Eqn. (7-5) where:

$$S_{(t+1)} = S_{t)} + I_{(t)} - R_{(t)} - L_{(t)} - \bar{G}_{(t)} \tag{7-5}$$

S_{t+1} = final storage (initial storage of the next season) for period t + 1, (Mm^3) S_t = initial storage for period t, (Mm^3) I_t = reservoir inflow for period t, (Mm^3) R_t = turbine release for period t, (Mm^3); L_t = evaporation losses for period t, (Mm^3), $\bar{G}_t$ = excess release for period t, (Mm^3).

a) b)

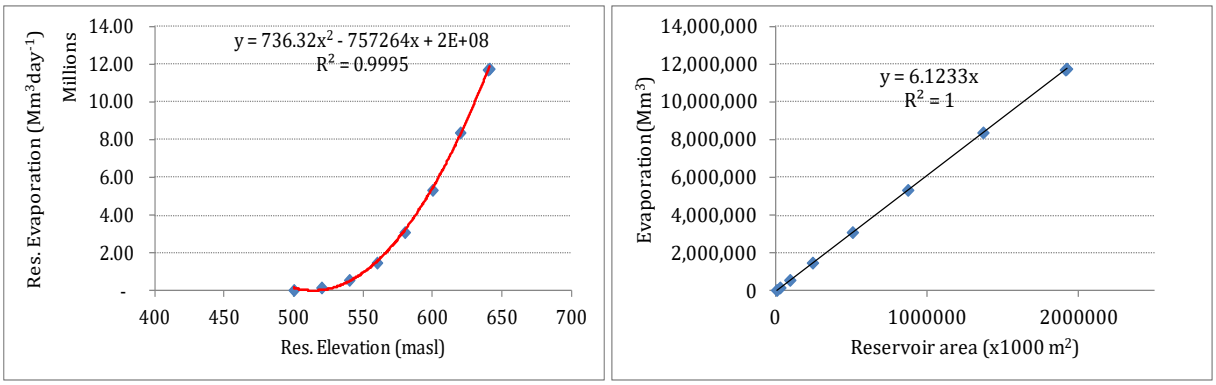

Figure 7-7: Relationship of a) water level and evaporation, b) Evaporation and reservoir are of GERD

Reservoir evaporation depth entered as monthly evaporation (Table 7-2) is multiplied by the corresponding current simulated surface area of the reservoir for each time interval. Meanwhile, a relationship of reservoir evaporation with the reservoir elevation can be established as shown in Figure 7-7 as an example for GERD.

c) Constraints on discharge defined by maximum and minimum permissible reservoir releases:

$$R_{tmin} \leq R_{(t)} \leq R_{tmax} \quad (7\text{-}6)$$

t = 1,2,…,T; where $R_{t\ min}$ = Minimum turbine release at any time t (m^3s^{-1}); $R_{t\ max}$ = Maximum turbine release at any time t (m^3s^{-1}); R_t = The turbine release at any time t (m^3s^{-1});

Eqns. (7-6) and (7-7) indicate the lower and upper bounds on reservoir storage releases and storages, respectively.

d) Constraints on storages defined by maximum and minimum permissible reservoir storages:

$$S_{tmin} \leq S_{(t)} \leq S_{tmax} \quad (7\text{-}7)$$

Where: t = 1, 2,…, T; S_{tmin} = minimum reservoir capacity at any time t (Mm^3); S_{tmax} = maximum reservoir capacity at any time t (Mm^3); S_t = the storage at any time t (Mm^3)

e) Constraints on elevations defined by maximum and minimum permissible water level at specified sites:

$$h_{tmin} \leq h_{(t)} \leq h_{tmax} \quad (7\text{-}8)$$

Where: t = 1, 2,…, T; $h_{t\ min}$ = Minimum reservoir operating water level (MOL) at any time t (masl); h_{tmax} = Maximum reservoir water level (FRL) at any time t (masl); h_t = the storage at any time t (masl). Eqn. (7-8) illustrates the minimum and maximum reservoir water level.

Finally, the available water for downstream users (Q, t), depends on the turbine release, excess release (spillage). This is expressed mathematically in eqn. (7-9) as;

$$Q_t \leq R_t + \overline{G_t} \quad (7\text{-}9)$$

Where: $\bar{Q}_t$ = incremental flow from GERD to Sudan in time t, (m^3s^{-1}) $\bar{G}_t$ = excess release at GERD (spillage) in time t, (m^3s^{-1})

Objective function

According to Olukanni *et al.* (2018), optimization problems can generally be either single objective or multi-objective. The single objective is just measuring the goal of operation of a single purpose reservoir. The main concern of single-objective optimization is to define the minimum or maximum value of an objective function, depending on the goal. However, in most cases operation objectives have trade-offs, and hence single-objective optimization cannot provide a unique optimum solution. In such situations, improvement of some objectives cannot be achieved without the sacrifice of others. The goal of the single-objective analysis should be replaced by the concept of "non-inferiority" in the multi-objective analysis.

Multi-objective optimization refers to problems with several objectives that are expected to be fulfilled simultaneously. The objectives are however often in conflict with each other and measured by different units. For a reservoir built for the purpose of hydroelectric generation like GERD, the objective function should be to maximize the annual energy production, but for trans-boundary River like Abay River, the downstream release flow should also be into account as objective function. Furthermore, in order to maximize energy production, water level in the reservoir requires being as high as possible. In contrary, the reservoir evaporation becomes high, which is not recommended as it reduces the down streamflow. There is conflict between these two objectives; therefore, it needs critical attention while establishing the operation rule curves.

Hence, the primary objective function in this study is maximizing the annual energy generation for the GERD hydropower plants as shown in eqn. (7-10):

$$Z = Max \sum_{i=1}^{T} E_{2t} \tag{7-10}$$

Where: Z is total annual energy generation (GWh); E2t is daily energy generation at GERD dam (GWh)

Energy can be calculated as shown in eqn. (7-11) as

$$E = 9.81 * R_{(2t)} * H_{(2t)} * \eta \tag{7-11}$$

Then, the objective function for maximizing energy generation becomes

$$Z = Max \sum_{i=1}^{T} (9.81 * R_{(2t)} * H_{(2t)} * \eta) \tag{7-12}$$

Furthermore, the generating head $H_{(2t)}$ in eqn. (7-12) can be expressed in terms of reservoir storage and minimum operating reservoir elevation as given in eqn. (7-13), which on substituting in eqn. (7-14) will give Equation (12).

$$H_{(2t)} = \overline{H_r} f S_{(2t)} - H_{min.2t} \tag{7-13}$$

$$Z = Max \sum_{i=1}^{T} 9.81 * \eta * \left\{ \left(R_{(2t)} \left(\left(\overline{H_r} f S_{(2t)} \right) - H_{min.2t} \right) \right) \right\} \tag{7-14}$$

Where: $\bar{H}_r$ f $S_{(2t)}$ is the average reservoir elevation expressed as a function of the average reservoir storage. It can be obtained by regression of reservoir elevation as a dependant variable and reservoir storage as the predictor. R_{2t} = turbine release at time t, (m^3s^{-1}) H_{2t} = generating head (m) H_{min2t} = minimum operating reservoir elevation (m), η = efficiency S_{2t} = reservoir storage at time t, (Mm^3). The regression analysis of reservoir elevation and reservoir storage for the GERD is shown in Figure 7-8.

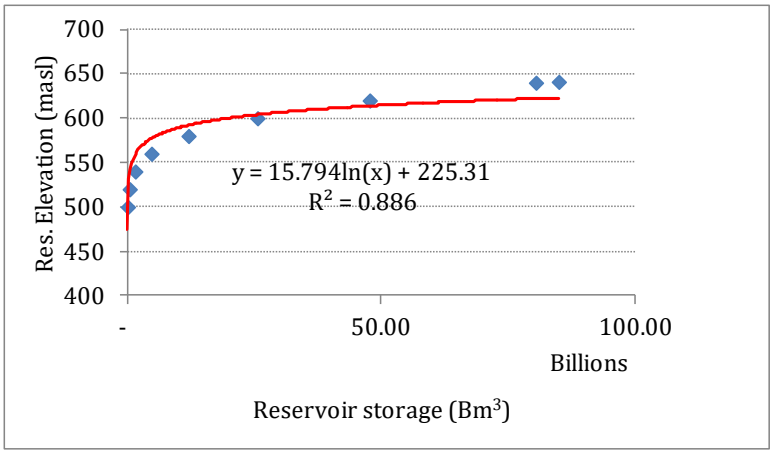

Figure 7-8: Regression relationship of water level and storage for the GERD reservoir

7.2.5 Operation rule curves for Lake Tana reservoir

Multi-purpose Lake Tana reservoir operation is a complicated process that involves a number of conflicting objectives, including the amount of water releases from reservoirs ensuring ecological and environmental flow for the downstream areas, the storage and water level in the reservoir, and ensuring reservoir releases for maximizing the energy production from Tana-Beles HPP. Hence, the operation of reservoir is critical to meet the intended objectives for the planned water resource development projects around and downstream the Lake Tana. Optimum operation of Lake Tana gives priority to maximize the energy generation of Tana-Beles HPP without affecting adversely on the environment. For the different years of the time the operations of Lake Tana was changed due to the development of new projects in and around Tana and Beles sub-basins. Before 1995, Lake Tana reservoir had no any flow regulation structures. In 1995, Chara-Chara weir with two radial gates each with a capacity of 70 m^3s^{-1} was built to regulate the flow to Tis Abay I HPP. In 2001, five additional new gates were constructed and become operational to increase the ability to regulate Lake Tana outflows and improve the flow to Tis Abay I and II HPPs. The rules attempt to maximize lake storage at the end of the wet season as a buffer for the coming dry year and this is achieved by preventing spillage over the Chara-Chara weir.

The adopted minimum operation level of the Chara-Chara weir is 1784 masl and the maximum operation level is 1987 masl. The Lake storage between 1784 and 1787 masl is about 9100 Mm^3. If all gates are opened, the total calibrated discharge at the minimum operation level is 75 m^3s^{-1} and at the maximum operation level (spillway level) 490 m^3s^{-1} (Salini *et al.*, 2006).

Regulation for power production has modified the natural lake-level regime, resulting in reduced seasonal but greater inter annual variability. The lowest level ever-recorded (1,784.4 masl) was in June 2003. This was a drought year in much of Ethiopia and hydropower production was constrained in many places. In an attempt to maintain electricity supplies, production at both Tis Abay power stations was maximized and as a result, lake levels dropped sharply. As a consequence of the low lake levels in 2003, navigation ceased for approximately four months (i.e., when lake levels dropped below 1,785 masl, the minimum level at which ships can

currently operate safely). Large areas of papyrus reed were destroyed, there was significant encroachment of agriculture on the exposed lake bed and there was a decrease in fisheries production (McCartney *et al.*, 2010). In addition, Tana-Beles hydropower scheme was commissioned on 14 May 2010, whereby releases from the tunnel generated 460 MW hydro-electricity and passed downstream along the Beles River.

Hence, in order to keep the lake level safe for navigation and prevent environmental hazards caused by low lake level, different operational rule curves were proposed at different times for the multi-purpose Tana-Beles project (Halcrow *et al.*, 2010; Salini *et al.*, 2006; SMEC, 2008) as summarized below.

According to Salini et al. (2006), a minimum level for Lake Tana of 1,784.0 masl was set to prevent difficulties with lake navigation and impacting on the environment. An average turbine discharge of 77 $m^3s^{-1}$was assumed for a wide range of lake levels (i.e. >1,784.3 but <1,787.0 masl) while the discharge to the turbines are increased to 160 m^3s^{-1} at high lake level (i.e. >1,787.0 masl). Meanwhile, the regulated outflow to the Abay River is fixed at 17 m^3s^{-1}.

SMEC (2008) recommended a minimum operational level of 1,784.75 masl to prevent serious navigation problems for shipping on Lake Tana, and an average turbine discharge of 77 m^3s^{-1}. The discharge from the turbines increases to 160 m^3s^{-1} at the high Lake level to prevent spillage over the Chara-Chara weir (>1,787 masl). The regulated outflow to the Abay River was fixed for some months to 10 m^3s^{-1} (i.e. March to June) with higher flows in other months. Comparison of the simulation results of the two operation rules were made by (SMEC, 2008). They reported that electricity production can be increased by more than 10% and spillage over the Chara-Chara weir can be reduced by almost 40% with the operation rule curves of (SMEC, 2008).

Halcrow et al. (2010) operational rule is suggesting increasing the Lake storage to store more water by the end of the wet season compared to other rules. The increasing of Lake Storage allows releasing more water during the high demands of water for upper Beles irrigation and electricity production from the months of January to April. This is achieved by releasing less water to the Tana- Beles scheme compared to the recommended (SMEC, 2008) operational rule during the wet season from July to September providing a greater buffer for the dry seasons.

In this study, the operation rule curves of the Lake Tana reservoir for model calibration and for impact analysis are different as the periods of analysis are different. Model calibration is carried out during the natural flow condition before 1995, while impact assessments are carried out post construction of Chara-Chara weir and Tana-Beles HPP. When plotting the mean daily measured discharges versus the water level of Lake Tana before and after the operation of Chara-Chara weir. The results have quite different patterns (see Figure 7-9). There existed a perfect relationship between lake level and outflow before the Chara-Chara weir with r^2=0.99 but after the Chara-Chara weir the relationship is becoming poor. Hence, based on the plotting of the measured Lake Tana's water levels and outflows for the period 1962 – 1995, the rating curve used for calibrating the hydrological model in the paired data manager is simplified to eqn.(7-15):

$$H = 0.443 \ln(Q) + 1784.8 \qquad (7\text{-}15)$$

Where: Q = discharge (m^3s^{-1}), H = Lake Tana water level (masl)

(a) (b)

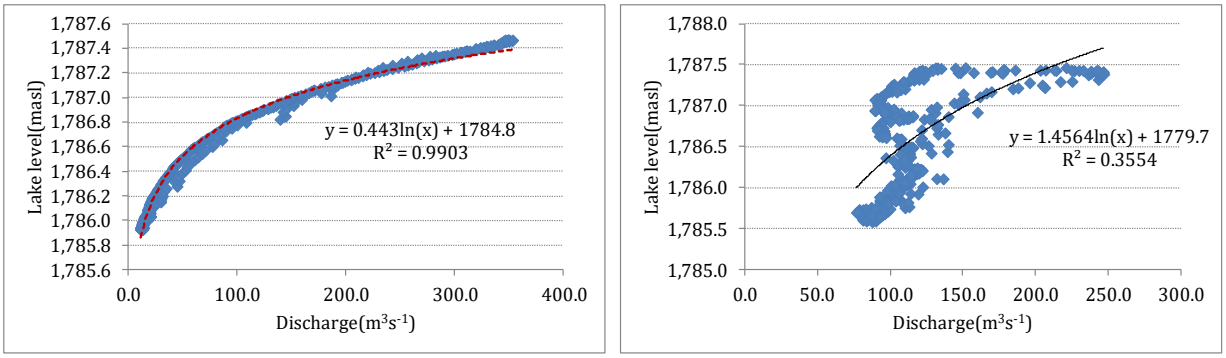

Figure 7-9: Mean daily lake level-outflow relation of Lake Tana (a) before regulation (1962-1995) and (b) after Chara-Chara weir

The rating curve of Lake Tana established for the calibration purpose above is not used any more for impact analysis because of the different operational conditions. Calibration was done in the period before the existence of Chara-Chara weir (natural flow) while the impact analysis considers the different operational scenarios of Chara-Chara weir. Hence, modifying the operation rule curve of the multi- purpose of Lake Tana reservoir is essential.

In order to do so, assumptions were made and constraints are fixed.

- The Chara-Chara weir will continue its operation in the future for regulating the outflow to the Abay River and Tana-Beles HPP.
- To preserve the Tis Issat falls as a major tourist attraction, environmental flow recommended by McCartney *et al.* (2010) has to be guaranteed through regulated outflow from the Chara-Chara weir. All other excess outflows from the lake to the Abay will then result from unregulated spills at the Chara-Chara weir during the rainy season.
- Restrictions on drawdown were applied to reduce abstractions as lake levels dropped below 1,787 masl and to ensure levels did not drop lower than the minimum operating level of 1,784.75 masl recommended by (SMEC, 2008).
- An average turbine discharge of 77 m^3s^{-1} was assumed over a wide range of lake levels and increased to 160 m^3s^{-1} at high lake level.

Optimization model

There are many optimization techniques that are applied to connect with the reservoir simulation model to search optimal rule curves of the reservoir such as dynamic programming , genetic algorithm (GA), and simulated annealing algorithm (Kangrang *et al.*, 2018). In this study, GA optimization model using analytic solver optimization and reservoir operation HEC-HMS model by adjusting the stage discharge curve of the reservoir from the paired data manager are applied.

Analytic Solver Optimization is an add-in for Microsoft Excel used for conventional optimization. It includes the PSI Interpreter, five built-in Solvers (LP/Quadratic, SOCP Barrier, GRG Nonlinear, Interval Global, and Evolutionary), solves linear models up to 8,000 variables and nonlinear models up to 1,000 variables. It can be downloaded from https://www.solver.com/. Both measured and forecasted rainfall is used to run simulations of the watershed rainfall-runoff model, HEC-HMS, and then the hydrographs are used as inputs of the optimization model to determine the reservoir water level elevation and the downstream releases of the reservoir with the objective of maximizing energy generation. The development of the optimal future rule curves use data from the future inflow flowing into the Reservoir considering the effects of climate change using different climate scenarios and land and water management scenarios. Thus, the inflows for different climate change and water and land management scenarios produced using the HEC-HMS simulation hydrological model is transferred to the optimization model as input to determine the decision variables with the set objectives. In this paper, the main objective is to maximize the energy generation and to optimize the downstream releases from GERD reservoir.

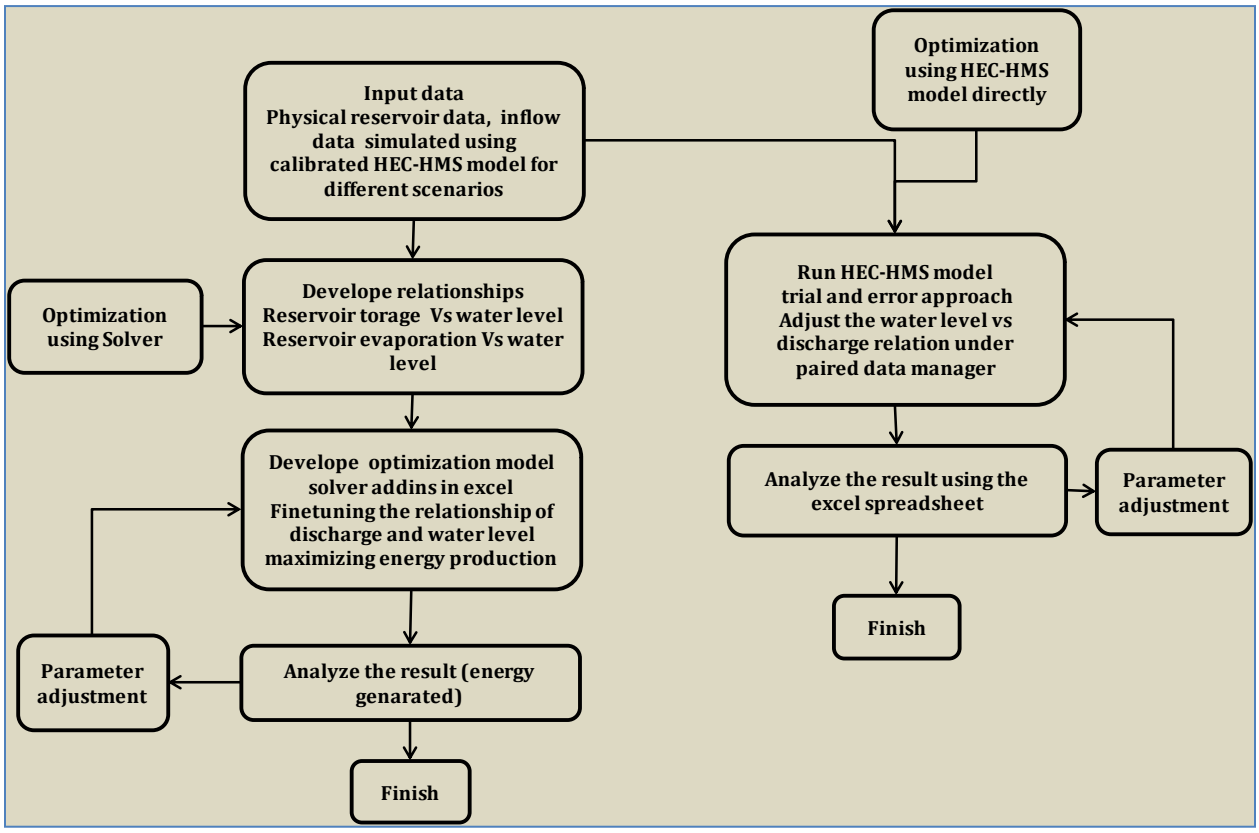

Figure 7-10: Basic steps of the optimization/simulation model

Figure 7-10shows the basic steps of the optimization/simulation model algorithm. First, the model requires rainfall data to start the rainfall-runoff simulation; once the watershed hydrographs are obtained then they are entered into an optimization model to compute the decision variables and determines whether the objective is met and pre-conditions of constraints are fulfilled, for example, are the maximum and minimum water levels under the desirable

level? Are the energy generated is maximized? If the answer is no, the model returns to the reservoir operation optimization process to determine an improved reservoir operation. When the objective is met, then the model stops.

In this dissertation, two optimization methods are applied. These are trial and error approach using the reservoir operation HEC-HMS model coupled with Excel spreadsheets and GA optimization model using analytic solver optimization in MS Excel. In trial and error approach, the constraints and the objective function described above are met by adjusting the stage discharge relationship using trial and error. Another optimization methods used in this study is genetic algorithm (GA), originally developed in the 1970's, is a model or abstraction of biological evolution based on Charles Darwin's theory of natural selection (Golberg, 1989).

The reservoir operation model must keep the storage level above the inactive storage, and below the maximum flood storage. The initial storages of the reservoirs are arbitrarily set to be at minimum operating level (MOL). Reservoir operation for irrigation supplies, the water demand is fixed and the release is based on the demand and water availability in the reservoir. If available water is sufficient to meet the demand, it satisfies the entire demand, if not, whatever the available water is utilized to meet the demand. However, this is not suitable for reservoir operation during drought periods, since it is likely to increase the maximum single period deficit. In addition, the specified release reservoir routing method in HEC-HMS model has no option to release excess water above the reservoir full supply level (FSL) when it is not needed, therefore, the excess volume of water may accumulate and exceed above the FSL.

Hence, the operation rule curves for the irrigation dams are establishing using outflows structure routing method for the following objectives.
1. Distributes the deficits in water supply across time to minimize the impact of drought and allow the spillage of excess water above the FRL to keep the dam safe.
2. Balancing the water release schedule and minimize the irrigation water deficit
3. It includes the evaporation losses of the reservoir, which is an important of the water balance for a reservoir.

Systematical representation and links of different planned and existed water resources developments, including inter basin transfer between Lake Tana sub-basin and Beles sub-basin through Tana-Beles HPP, existed and future planned reservoirs, reaches and diversion (irrigation projects) is shown below in the Figure 7-11. The model simulation starts from upstream of Lake Tana to downstream of the Blue Nile at El Diem.

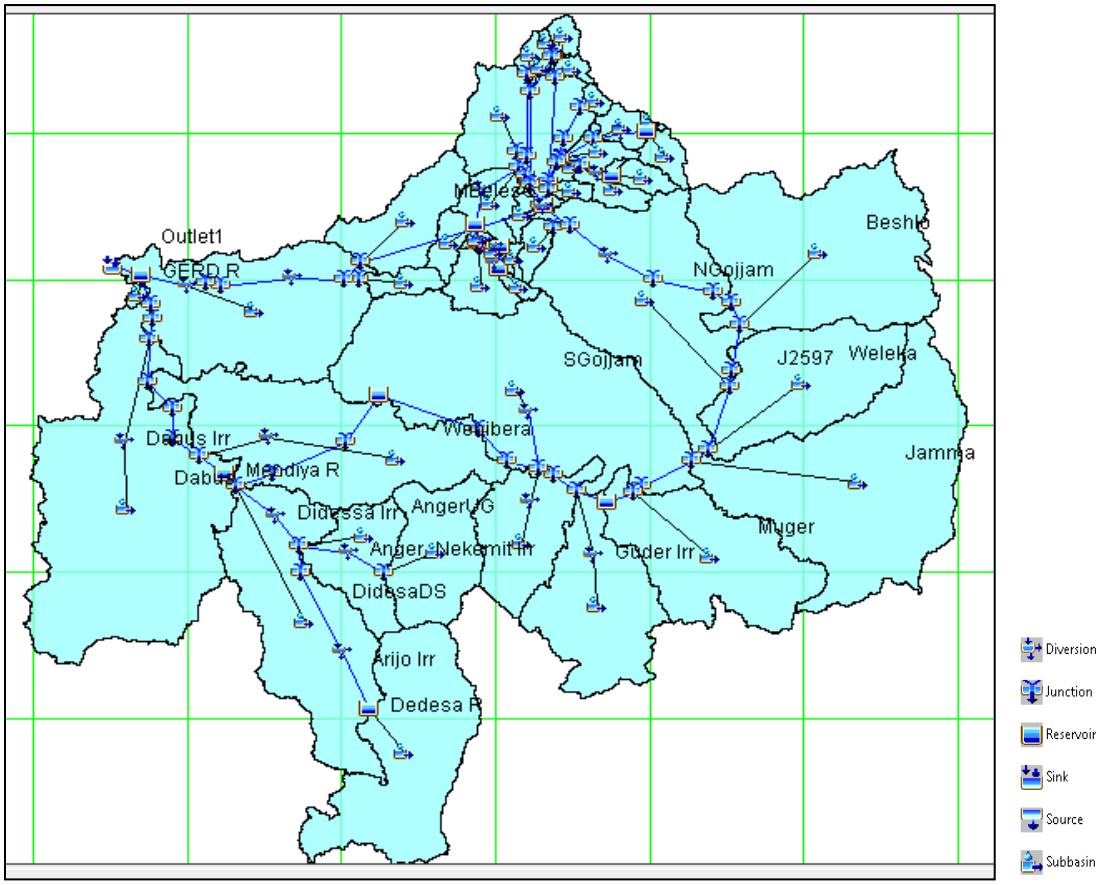

Figure 7-11: Schematic of HEC-HMS simulation model

7.3 Results and discussions

7.3.1 HEC-HMS model performance assessment

Before calibrating the model, the basin divided into multiple catchments by considering the spatial variability of land cover, soil properties, climate, and topography/altitude and with gauged and un-gauged catchments. Manual calibration using trial and error method was applied as the first step for calibrating the model. Calibration was performed at six flow-gauging stations separately as listed in Table 7-5. Model performance is assessed using three performance indicators, namely the ENS, R^2, RVE and graphical representation at the outlets of 6 flow-measuring stations, where the observed data are relatively complete.

The statistics of the observed and simulated daily streamflow during calibration and validation results in terms of criteria of fit are presented in Table 7-6. The percent volume error (RVE) calculates the volume difference between simulated and observed flows, with a positive value indicating that the model over predicts observed flows. The result indicated that HEC-HMS model underestimated the observed flow by a maximum of 6.2% and overestimated flow by a

maximum of 6.7% during the calibration period. The Nash-Sutcliff coefficient value attained during calibration is ranged from 0.77 to 0.89. Finally, according to the coefficient of determination (R^2), there is a relatively good correlation between the simulated flows and the observed flows at the gauged outlets. The R^2 value varies from 0.78 at the Ribb outlet to 0.9 at El Diem flow station. In general, according to the result depicted above using the three statistical performance indices, the model efficiency during calibration show very good result throughout calibration period.

Once the model is calibrated successfully, it is validated with separate data sets. Figure 7-13 show the graphical representation of the model performance during validation periods. The percent relative volume error (RVE) calculated during the validation period show that the model over predicts the daily time series flow with a maximum of 12.5% and under estimated the flow by 7.6% except Ribb outlet in which the model under estimated the flow by 35 % during validation period. The Nash-Sutcliff coefficient values obtained during the validation period varies from 0.53 to 0.90. Finally, the R^2 value varies from 0.70 at the Ribb outlet to 0.91 at El Diem flow station, which indicate the model performance is very good. Similar model efficiency also obtained during validation period; however, the model overestimates the simulated discharge in validation period a bit higher. Here, it is important to note that HEC-HMS model performs best for large area sub-basins (El Diem and Kessie) stations than for smaller area sub-basins like Rib, Gilgel Abay and Gumara sub-basins. The less performance of the model at Rib River could be due to the backwater effect of Lake Tana reservoir as the flow meter flooded with the backwater from the Lake Tana during the rainy season.

Table 7-5: Calibration and validation periods

	Time period		Number of years	
Flow station	Calibration	Validation	Calibration	Validation
El-Diem	1999-2005	2006-2009	7	4
Kessi	1999-2006	1992-1996	7	4
Gilgel Abay	1992-2000	2001-2005	9	5
Gumara	1990-1997	2001-2005	8	5
Rib	2000-2007	1996-1999	8	4
Tana	1985-1992	1992-1995	8	4

Table 7-6: Calibration and validation results

Performance Index	Calibration						Validation					
	El Diem	Kessi	Gilgel Abay	Gumara	Rib	Tana	El-Diem	Kessi	Gilgel Abay	Gumara	Tana	Rib
R^2	0.90	0.87	0.81	0.79	0.78	0.80	0.91	0.86	0.81	0.80	0.88	0.70
RVE	6.2	-3.2	1.5	-0.1	2.4	-6.7	11.5	-7.6	-2.5	-5.7	12.5	-34.9
NSE	0.89	0.87	0.81	0.79	0.77	0.80	0.90	0.86	0.81	0.79	0.82	0.53

The following figures show the comparison between daily simulated and observed streamflow at six discharge-measuring stations during calibration and validation periods. Figure 7-12 shows daily time series comparison between the simulated and observed flows at the gauging stations during the calibration period. The plots of observed and simulated daily streamflow indicate that the HEC-HMS well captured the observed flow relatively well at daily time step at all gauging stations. Time series comparisons between the simulated and observed flows during the validation (verification) period are shown in Figure 7-13. The hydrograph comparison also indicates that the HEC-HMS model performed well in matching the observed flows during the validation period. The visual inspection of the hydrographs of Figure 7-12 indicates generally good streamflow simulations in particular during the recession flows, while the short-term fluctuations during the high-flow season were not modeled well, in particular for the Gumara and Gilgel Abay catchments. The inability of the model to simulate the daily pattern of flood flows, could be caused by three factors. First, the given network of rainfall stations (see Figure 7-4) may not capture the areal variability of daily rainfall patterns well enough (i.e. only three stations in and around Gilgel Abay and two in Gumara were available). That interpolation errors may directly influence runoff predictions stronger in the smaller Gumra and Gilgle Abay as compared to the larger Kessi and UBNRB. Second, the daily observed discharges derived from two water level measurements (at 06:00 a.m. and 06:00 p.m.) may have smoothened a very rapid flow characteristics at the site (Uhlenbrook *et al.*, 2010). A mean rating curve may not properly capture the dynamic nature of the water level discharge relationship. Third, during floods , as the flow meter at the Gumara River is flooded with the backwater from Lake Tana may have smoothened the very dynamic natural flow.

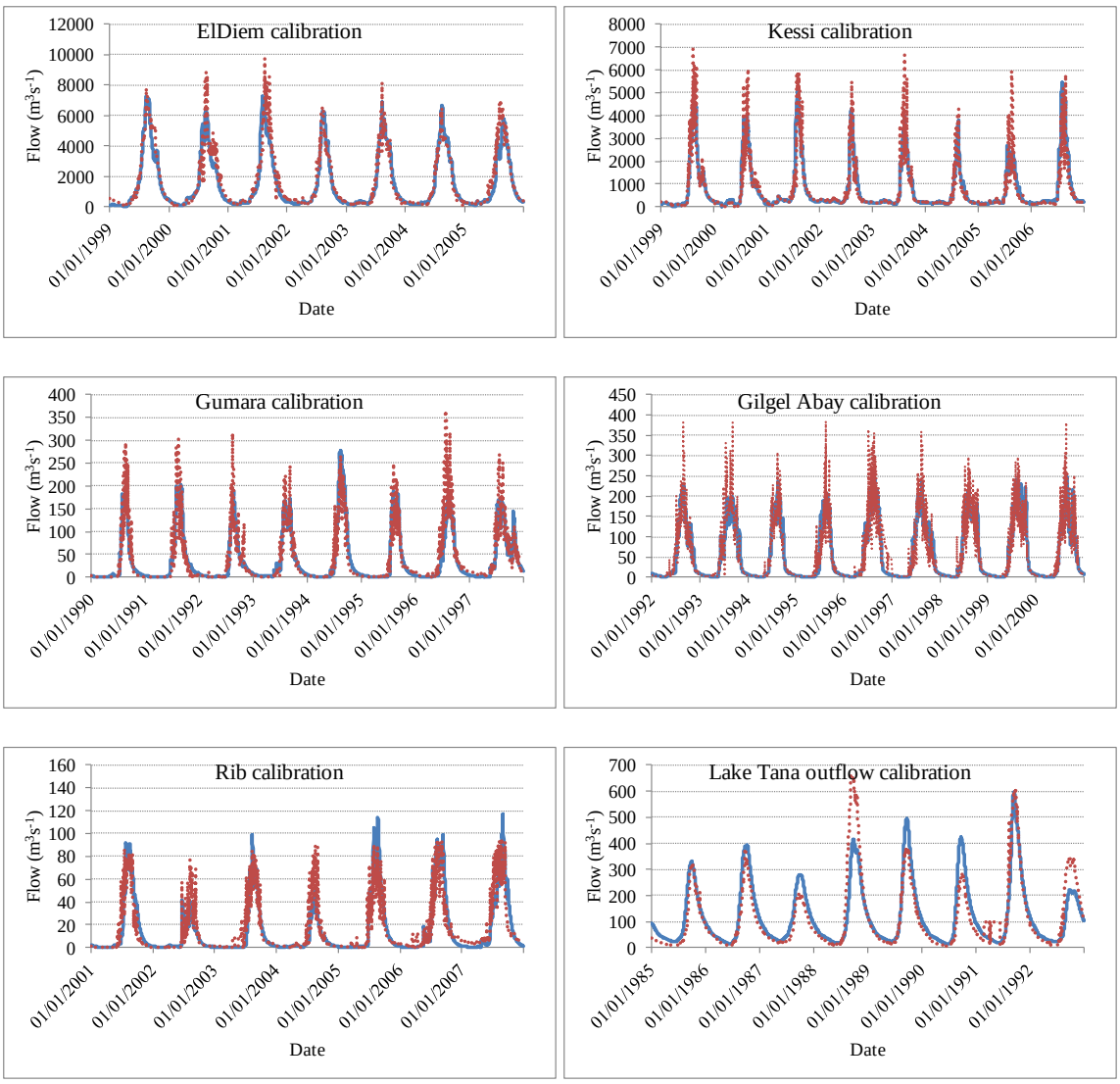

Figure 7-12: Graphical representation of model calibration

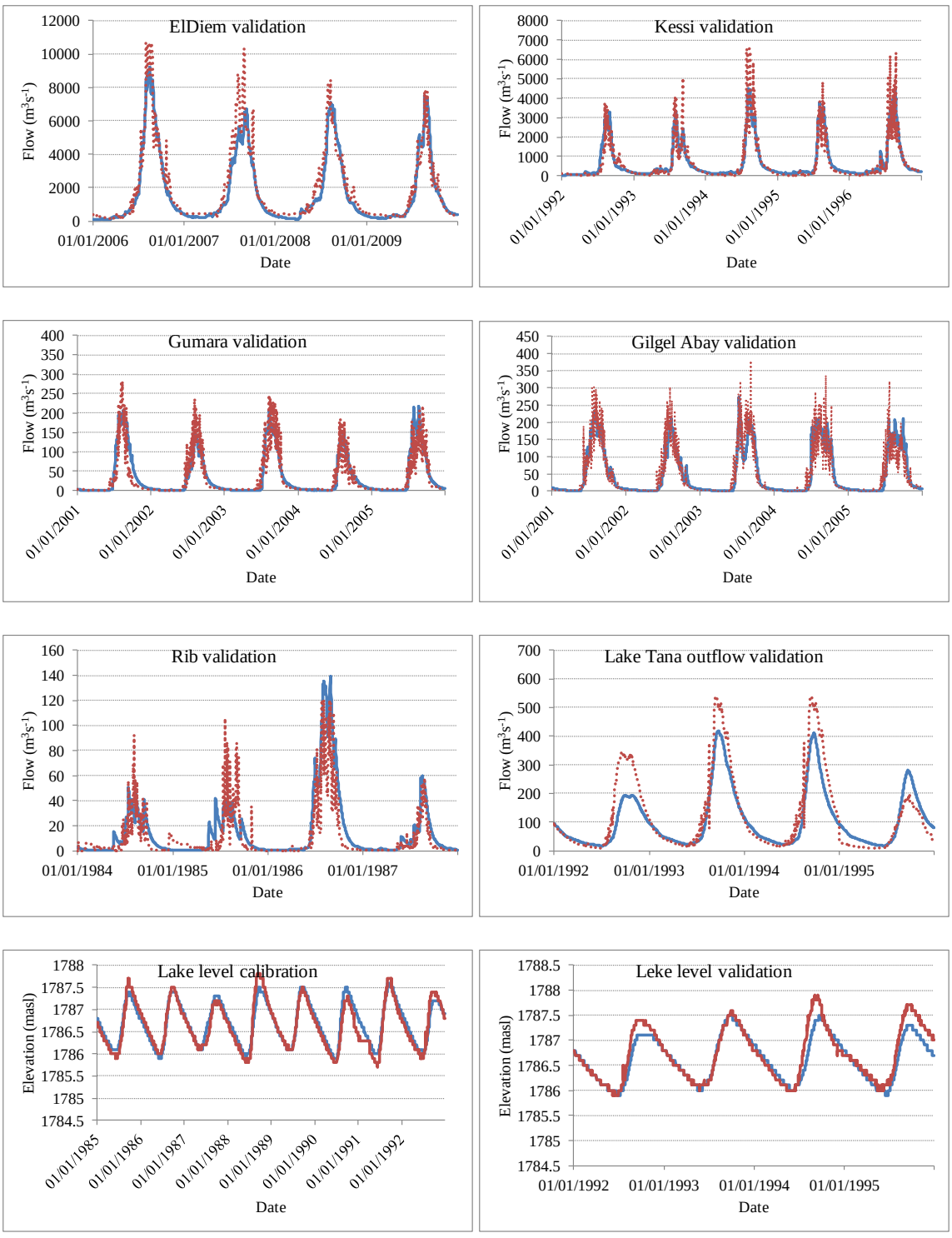

Figure 7-13: Graphical representation of model validation

In addition, performance evaluation of the model was assessed for the seasonal flows as it is necessary to make sure that the model is reliable for capturing the high and low flows so as to evaluate the effects of water resource development projects on the water availability. Dry and short rainy season flows are most important than the long rainy season flow for irrigation. Figure

7-14, and Table 7-7 show the seasonal flow comparison between the observed and simulated during the calibration period. The result revealed that the model simulation has a good agreement with the observed seasonal flows except short rainy season flows. The poor performance of the short rainy season flow could be due to the artificial extraction of water for the irrigation purpose upstream of the gauged outlets. This condition is worse in small size sub-basins than large size basin, as it has shown in Table 7-7.

The various performances evaluation measures computed for the daily streamflow including with graphical comparison of observed and simulated in the calibration and validation periods are a means to confirm the behavior of the model to represent the physical processes in UBNRB basin. Moreover as one can see, from the above graphical comparisons in both cases the simulated streamflow is in a satisfactory agreement with the observed one, and the seasonal dynamics also well reproduced, high and low flows captured very well by the model, which shows, that the capability of the model in simulating the extreme events like high flow. Overall, the calibration and validation result of HEC-HMS model revealed that the model has a good performance in the UBNRB so that it can be used for further impact assessment.

Table 7-7: Performance evaluation metrics for seasonal flows during calibration and validation

		LRS			DS			SRS		
	Stations	R^2	NSE	RVE (%)	R^2	NSE	RVE (%)	R^2	NSE	RVE (%)
Calibration	El Diem	0.77	0.88	4.37	0.85	0.90	11.29	0.35	-0.12	6.39
	Kessi	0.79	0.88	-3.90	0.85	0.89	3.15	0.66	0.77	-9.25
	Tana	0.75	0.86	-1.26	0.80	0.87	-8.87	0.10	0.29	-17.63
	Gilgel Abay	0.54	0.72	2.20	0.69	0.81	-2.94	0.39	0.61	12.70
	Gumara	0.63	0.79	1.99	0.66	0.80	-13.23	0.19	0.42	6.36
	Rib	0.61	0.78	3.66	0.67	0.66	-27.20	0.09	-0.23	47.02
Validation	El Diem	0.80	0.77	8.86	0.85	0.90	11.29	0.35	-0.12	6.39
	Kessi	0.78	0.78	-5.48	0.82	0.76	4.21	0.51	-1.05	-96.38
	Tana	0.85	0.79	21.46	0.85	0.73	13.71	0.70	-0.16	-49.69
	Gilgel Abay	0.56	0.52	3.16	0.77	0.46	-44.41	0.24	0.19	-2.54
	Gumara	0.63	0.60	-2.55	0.60	0.50	-41.93	0.25	-1.60	46.85
	Rib	0.57	0.35	-29.91	0.23	-2.83	-143.53	0.00	-3.37	12.45

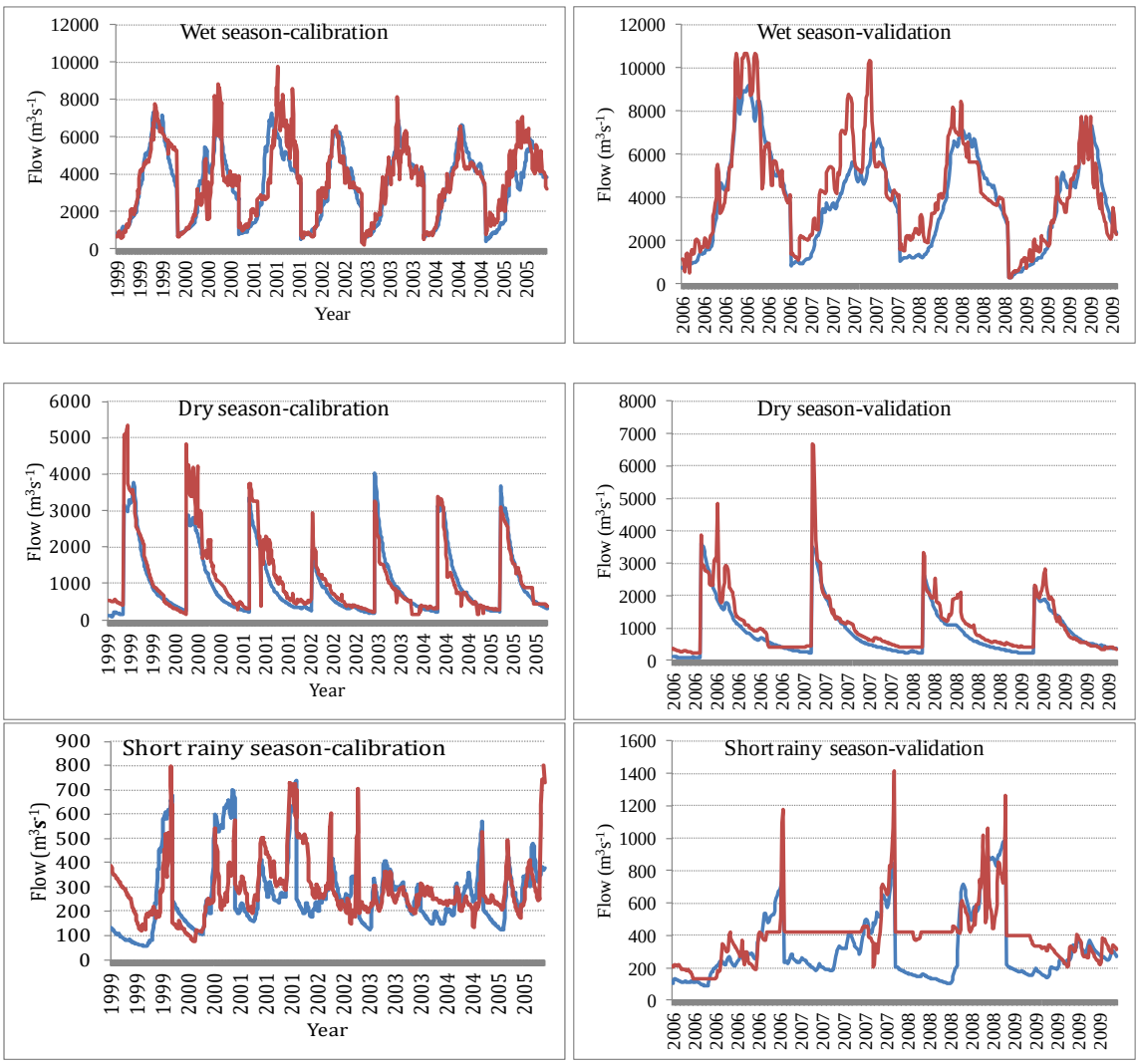

Figure 7-14: Graphical representation of model calibration for the seasonal flow

Water Balance of Lake Tana

The water balance components of the Lake Tana includes the direct rainfall over the lake surface (P), inflow from gauged rivers (Qg), surface runoff inflow from unmonitored sub-catchments (Qug), Outflow from the Lake ((Qout), Lake evaporation (El), change in water balance (closure term) (ΔS) is calculated after model calibration and validation. The general water balance equation to the Lake is shown in eqn. (7-16).

$$P + Q_g + Q_{ug} - Q_{out} - E_l = \Delta S \qquad (7\text{-}16)$$

The prediction of Lake Tana water balance is based on the simulation result from 1984 to 1995 that represents the natural flow condition. The estimated annual precipitation falling on the lake calculated using Thiessen polygon methods from the stations located around the Lake is 1234 mm and the evaporation loss from the Lake is about 1650 mm adapted from (SMEC, 2008). The model simulation of the inflow from the gauged Rivers, surface runoff from un-gauged sub-catchments and Lake outflow fluxes are indicated in Table 7-8. The analysis of the Lake Tana

water balance has shown that there is an annual surplus of 195 Mm^3 of water, which can be used for the planned pumped irrigation, domestic water supply and other unidentified abstractions. A quantitative assessment indicates that the change in storage is as large as 65$mmyr^{-1}$ of the total Lake inflow that comprised rainfall on the lake, and stream flow from gauged and un-gauged catchments. The change in storage accounts for 2.2% of the total lake inflow. In Rientjes *et al.* (2011b), the closure error was 85 mm and accounted for 2.7% of the total lake inflow or the period 1994-2000. Wale (2008) estimated the change in storage about -170 mm yr^{-1} for the period of analysis 1995-2000 and accounted for 5% of the total lake inflow.

Table 7-8: Lake Tana water balance components simulated for the period 1984–1995 (Natural flow).

Water Balance term	$mmyr^{-1}$	Mm^3yr^{-1}
Lake areal rainfall	1234.0	3730.3
Gauged inflow	1138.7	3442.2
Ungauged inflow	592.8	1792.1
Lake evaporation	1650.0	4988.0
Lake outflow	1250.8	3781.1
Change in storage	64.7	195.6

7.3.2 Future climate change impacts on monthly, seasonal, annual, low and high streamflow of the UBNRB using HEC-HMS

One of the objectives of this study was to estimate the future water availability in the basin under climate change scenarios. However, the no change assumption was made in land use patterns between the baseline and scenario periods for the future streamflow simulation. So, land use is considered stationary for the whole simulation time because its impact is less significant as compared to climate change (see Chapter 5). Therefore, the influence of the changing in land use pattern is ignored while investigating the combined impacts of climate change and water resource developments on the availability of water for power production, irrigation development and downstream streamflow of the UBNRB.

HEC-HMS model was calibrating at six discharge-measuring stations of the UBNRB with satisfactory performance results and negligible differences in volume of water. Hence, the calibrated model parameters are used for the simulation of the streamflow for the future period. It is a normal trend that, the impacts of climate change on the basin hydrology are assessed by comparing the present and projected streamflow estimates. As a result, the potential effects of climate change on the hydrology of the UBNRB can be assessed by comparing the simulated streamflow derived from downscaled climate scenarios to observed baseline (1984 - 2011) streamflow data sets.

Impacts of climate change on mean annual streamflow

In this section, we analyze the inferred changes in streamflow that would accompany the precipitation and temperature changes summarized in Chapter 6. Table 7-9 summarizes future projection of the key climatic variables and streamflow simulations using HEC-HMS

hydrological models and the relative changes as compared to baseline period. There is disagreement between the two GCMs (canESM2 and GFDL) as to the streamflow predictions under RCP4.5 scenario over the UBNRB both in magnitudes and in directions. Changes in precipitation and temperature result in disproportional changes in the hydrologic response of a river basin. Under RCP4.5 scenario from canESM2 GCM, the relative changes of the mean annual precipitation may increase by 17%, 22.8% and 26.3% by the period 2030s, 2050s and 2080s respectively. These changes associated with the increasing changes in Tmax(Tmin) by 0.7(0.4), 1.1(0.7), and 1.4(0.8) ^{o}C resulted an increasing the long-term mean annual streamflow at El Diem by 22.6%, 43% and 55% by the period 2030s, 2050s and 2080s respectively. In contrary, under RCP4.5 scenario of CMIP5 GFDL GCM, the relative changes in mean annual precipitation may decrease by -9.5%, -9.9% and -9.3% in the period 2030s, 2050s and 2080s respectively. These decreasing of precipitation associated with the increasing of Tmax(Tmin) by 1.1(1.2), 2.1(2.0), 2.2(2.9)^{o}C resulted in a decreasing of long term mean annual streamflow by -20.6%, -25% and -21% respectively in the period 2030s, 2050s and 2080s. In general, the above results indicate that precipitation is a key driving force in altering the streamflow of UBNRB.

Table 7-9: Future projections of mean annual hydro-climatic variables as compared to the baseline period of UBNRB using SDSM for canESM2 GCMs under RCP 4.5 scenario

Variable	Mean annual value				Change from the baseline (%)		
	1984-2011	2030s	2050s	2080s	2030s	2050s	2080s
CMIP5 canESM2 GCM							
Precipitation (mm)	1410.1	1650.1	1731.9	1781.2	17.0%	22.8%	26.3%
Tmax (^{o}C)	24.9	25.6	26.0	26.3	0.7	1.1	1.4
Tmin (^{o}C)	11.6	11.9	12.2	12.3	0.4	0.7	0.8
Streamflow at El Diem (m^3s^{-1})	1645.0	2016.5	2345	2542	22.6 %	43 %	55 %
CMIP5 GFDL GCM							
Precipitation (mm)	1410.1	1274.2	1267.6	1276.2	-9.5%	-9.9%	-9.3%
Tmax (^{o}C)	24.9	26.0	27.0	27.1	1.1	2.1	2.2
Tmin (^{o}C)	11.6	12.8	13.6	14.5	1.2	2.0	2.9
Streamflow El Diem (m^3s^{-1})	1645	1306	1230	1300	-21%	-25%	-21%

Impacts of climate change on mean monthly flows

The projected mean monthly streamflow for the future time periods of 2030s, 2050s and 2080s at six representative flow-measuring stations along the Abay River are shown in Figure 7-15 and Figure 7-16 for canESM2 and GFDL GCMs respectively. The results revealed that two GCMs have different pattern of mean monthly streamflow as compared to the baseline streamflow. The canESM2 GCM showed increasing streamflow in the months from May to December in most of the flow stations where as decreasing streamflow in the months of January through April. However, the percentage change is different from stations to stations.

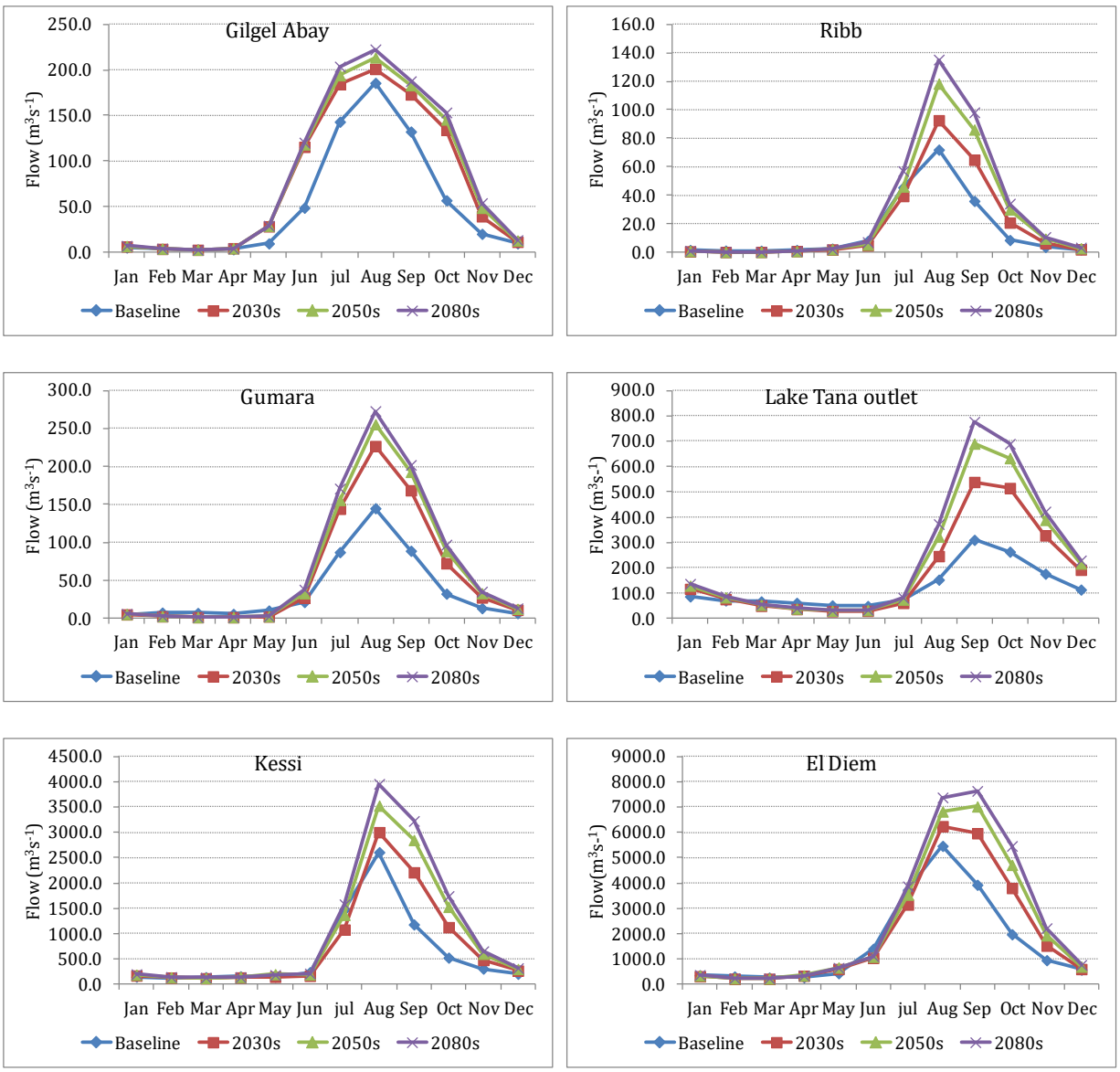

Figure 7-15: Monthly observed baseline and projected streamflow at six flow gauging stations from canESM2 GCM

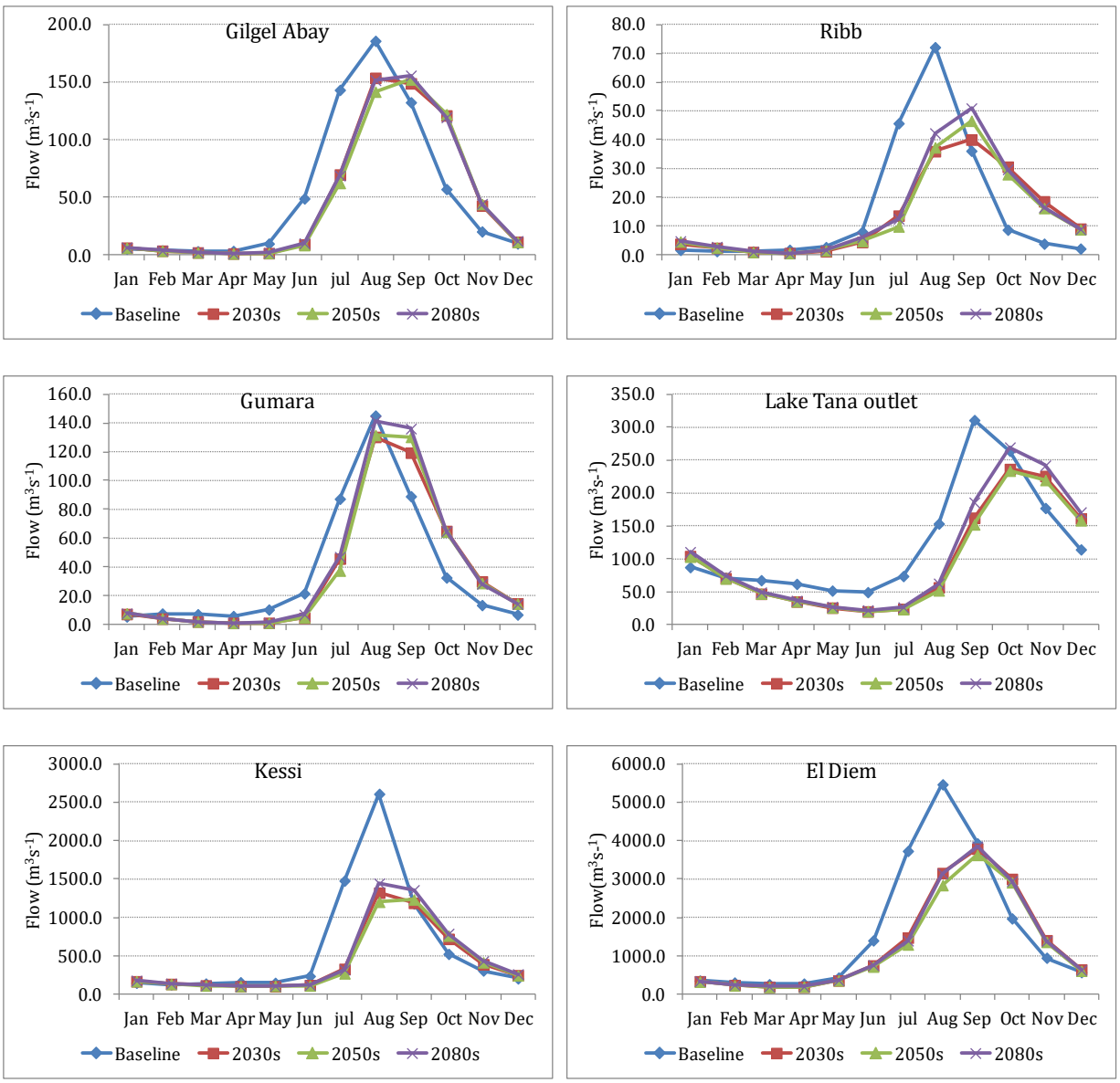

Figure 7-16: Monthly observed baseline and projected streamflow at six flow gauging stations from CMIP5 GFDL GCMs

Impacts of climate change on low and high streamflow

The mean monthly low and high flows for the baseline and future periods simulated from CMIP5 GCMs of canESM2 and GFDL for six stations is presenting in Table 7-10. The low flows of the baseline data set were occurred in the month of March for Gilgel Abay, Rib and El Diem while January for Gumara, June for the Lake Tana outlet and February for Kessi station. The future projection of low flows from canESM2 GCM showed decreasing trend at five stations except Kessi for the period 2030s as compared to the baseline low flow values. In 2030s, the low flow may decrease in the range of 9.1% to 63.1% at Gilgel Abay and Rib stations respectively. At 2050s, the low flow may decrease by 5% at Gilgel Abay and 61.5% at Rib, 32.5% at Lake Tana

outlet and 13.7% at El Diem stations while it may increase by 2.7% at Gumara and by 7.4% at Kessi stations. Similar trend my experience by the period 2080s. The low flow may decrease by 8.4%, 58.5%, 30% and 9.6% at Gilgel Abay, Rib, Lake Tana outlet and El Diem stations respectively, whereas it may increase by 9% at Gumara and 11.8% at Kessi station.

Regarding to the high flow values, all of the projected monthly streamflow from canESM2 GCM at six stations attained their high flows in the months of August. The result analysis showed that high flow in all stations might increase in the range from a minimum value of 8.2% (Gilgel Abay) to a maximum of 73.5% (Lake Tana outlet) at the 2030s period. By 2050s, the projected high flow further increase with a minimum by 15% at Gilgel Abay and by a maximum of 122% at Lake Tana outlet station. Again, the high flow might also increase in the future by a minimum of 19.8% at Gilgel Abay station and by a maximum of 150% at the Lake Tana outlet station in the period 2080s. Generally, the result indicates that, the low flow regime may decrease at four stations (Gilgel Abay, Rib, Lake Tana outlet and El Diem) in all three periods but may increase at Kessi station. In contrary, the high flow may increase throughout the month of August in the future in all stations. The decreasing of low flow value might not be a good opportunity for the farmers to produce more as it limits the use of extensive irrigation agriculture.

However, the predictions of low and high flows from CMIP5 GFDL GCM at six stations differ substantially with the predictions from canESM2 GCM. The result analysis depicted that low flow simulation from GFDL GCM might decrease with a maximum value of -59% at Lake Tana outlet to a minimum value of -14.5% at Rib by 2030s. During this period, low flow might increase at Gumara station by 30% and at Kessi by 4.7%. Similarly, by 2050s, the predictions of low flow at four stations might decrease with a maximum value of -58.4% at Lake Tana outlet to a minimum value of -16% at Rib station. The simulated low flow at Gumara and Kessi stations might increase by 38.7% and 4.1% respectively. By 2080s, the low flow simulation might further decrease in the range between -54.9% to -7.6% at Lake Tana outlet and Rib station respectively but might increase at Gumara and Kessi stations by 37.8% and 8.9% respectively.

Regarding to the high flow prediction, the result showed that high flow might decrease at all six stations in all three periods (2030s, 2050s and 2080s) in contrary to the simulation of GFDL GCM. By 2030s, the high flow might decrease with a maximum of -50% at Rib station and a minimum by -10.2% at Gumara station. In the period 2050s, the high flow might decrease by a maximum of -53.8% to a minimum of -9.3% at Kessi and Gumara stations respectively. The prediction of the high flow might decrease by a maximum of -44.6% and a minimum of -2.5% by the period 2080s at Kessi and Gumara stations respectively.

Table 7-10: Comparisons of projected low and high flows as compared to baseline from six gauging stations

	Low flows				High flows			
		Relative change (%)				Relative Change (%)		
	Baseline (m^3s^{-1})	2030s	2050s	2080s	Baseline (m^3s^{-1})	2030s	2050s	2080s
canESM2 CMIP5 GCM under RCP4.5 scenario								
Gilgel Abay	3.4	-9.3	-4.9	-8.4	185.7	8.2	15.0	19.8
Rib	1.3	-63.1	-61.5	-58.5	72.1	28.6	64.2	87.6
Gumara	5.8	-5.2	2.7	9.0	145.1	56.4	76.2	88.1
Lake Tana	49.6	-38.6	-32.5	-30.0	310.5	73.5	122.3	150.1
Kessi	131.8	0.6	7.4	11.8	2608.6	15.1	35.2	51.7
El Diem	268.7	-17.1	-13.7	-9.6	5465.0	14.2	24.9	35.0
GFDL CMIP5 GCM under RCP4.5 scenario								
Gilgel Abay	3.4	-30.5	-31.7	-27.9	185.7	-17.3	-23.7	-18.3
Rib	1.3	-14.5	-16.0	-7.6	72.1	-50.0	-48.2	-41.3
Gumara	5.8	30.0	38.7	37.8	145.1	-10.2	-9.3	-2.5
Lake Tana	49.6	-59.0	-58.4	-54.9	310.5	-47.7	-51.0	-40.2
Kessi	131.8	4.7	4.1	8.9	2608.6	-49.2	-53.8	-44.6
El Diem	268.7	-25.2	-26.1	-21.8	5465.0	-42.2	-48.0	-42.5

Table 7-11: Future projection of seasonal flows at three main gauging stations across UBNRB from canESM2 GCM under RCP4.5

Season	2030s			2050s			2080s		
	Tana	Kessi	El Diem	Tana	Kessi	El Diem	Tana	Kessi	El Diem
LRSs (m^3s^{-1})	218	1623	4111	350	1994	4703	315	2253	5010
LRSb (m^3s^{-1})	153	1538	3991	153	1538	3991	153	1538	3991
R.change (%)	42.5	5.5	3.0	129	30	18	106	47	26
DSs (m^3s^{-1})	288	515	1566	348	658	1940	369	732	2209
DSb (m^3s^{-1})	177	301	1000	178	301	1000	178	301	1000
R.change (%)	62.2	71.1	56.6	96	119	94	108	143	121
SRSs (m^3s^{-1})	47.8	135.4	352.3	44	155	368	54	154	378
SRSb (m^3s^{-1})	63.9	147.0	324.0	64	147	324	64	147	324
R.change (%)	-25.2	-7.9	8.7	-32	5	14	-16	5	17
MAs (m^3s^{-1})	185.6	760.2	2016.5	249	939	2345	247	1050	2542
MAb (m^3s^{-1})	131.5	613.3	1645.1	132	613	1645	132	613	1645
R.change (%)	41.1	24.0	22.6	89	53	43	88	71	55

Table 7-12: Future projection of seasonal flows at three main gauging stations across UBNRB from GFDL GCMs

Season	2030s			2050s			2080s		
	Tana	Kessi	El Diem	Tana	Kessi	El Diem	Tana	Kessi	El Diem
LRSs (m^3s^{-1})	66	745	2297	279	1994	4628	315	2253	5010
LRSb (m^3s^{-1})	153	1538	3991	153	1538	3991	153	1538	3991
R. change (%)	-57	-52	-42	82	30	16	106	47	26
DSs (m^3s^{-1})	181	385	1353	342	658	1927	369	732	2209
DSb (m^3s^{-1})	178	301	1000	178	301	1000	178	301	1000
R. change (%)	2	28	35	93	119	93	108	143	121
SRSs (m^3s^{-1})	44	118	255	52	155	376	54	154	378
SRSb (m^3s^{-1})	64	147	324	64	147	324	64	147	324
R. change (%)	-31	-20	-21	-19	5	16	-16	5	17
MAs (m^3s^{-1})	98	417	1307	95	410	1230	107	453	1300
MAb (m^3s^{-1})	132	613	1645	132	613	1645	132	613	1645
R. change (%)	-26	-32	-21	-28	-33	-25	-19	-26	-21

Note: LRSs: long rainy season simulated; LRSb: long rainy season baseline; DSs: dry season simulated; DSb: dry season baseline; SRSs: short rainy season simulated; SRSb: short rainy season baseline; MAs: mean annual simulated; MAb: mean annual baseline

Impacts of climate change on seasonal streamflow

To have a sense of the seasonal inter-model variability of predicted streamflow changes, changes for wet, dry and short rainy season for the three time periods (from early to late 21st century) were analyzed separately for each GCM. Table 7-11 presented the result of seasonal streamflow projection of canESM2 GCM for the future periods of 2030s, 2050s and 2080s at 3 main flow-measuring stations, as it is not suitable to present the result of all six stations. The seasonal projected streamflow analysis revealed that it might exhibit both positive and negative trends in the future. For instance, the long rainy season might increase in the range of 3% to 42.5% by 2030s; this magnitude will further increase in the range of 18% to 129% by 2050s. By 2080s, the long rainy season (high flow season), might increase by a minimum of 26% and maximum of 106%. Similarly, the dry season flow might increase in the future in all three stations in all periods. In the period 2030s, the dry season flow may increase by 62.2% at Lake Tana outlet, 71.1% at Kessi and 56.6% at El Diem. It may further increase by 96% at Lake Tana outlet, 119% at Kessi and 94% at El Diem by 2050s. At 2080s, the high flow season streamflow at Lake Tana outlet, Kessi and El Dime might increase by 108%, 143% and 121% respectively. During the short rainy season, the projected streamflow might exhibit mixed trends. The magnitude of the short rainy season (low flow season) might decrease by a maximum of -32% at the Lake Tana outlet in the period 2050s and increase to the maximum of 29% at Kessi station in the period 2080s.

Meanwhile, the simulated seasonal streamflow from GFDL GCM also showed mixed signals. During the wet season (JJAS), when the UBNRB receives more than 80% of its annual runoff, the future prediction might decrease at 2030s at all three stations by -57.2% at Lake Tana, -

51.6% at Kessi and -42.5% at El Diem stations. However, it might increase by 82% at Lake Tana, 30% at Kessi and by 16% at El Diem at the middle of 21st century by 2050s. At 2080s, the predictions of streamflow might increase by 106% at Lake Tana outlet, 47% at Kessi and by 26% at El Diem station. During dry season (ONDJ), the prediction of the streamflow might increase at all three stations for all three time periods in the range from 2.3% at Lake Tana outlet by 2030s to 121% at El Diem by 2080s. For short rainy season (FMAM), the predictions of streamflow might decrease in the range from -30.7% at Lake Tana outlet to -20% at Kessi by 2030s. By 2050s, the short rainy season streamflow might decrease by -19% at Lake Tana outlet while it might increase by 5% and 16% at Kessi and El Diem stations respectively. This again decreases by -16% at Lake Tana outlet and increase at Kessi and El Diem stations by 5% and 17% respectively at the end of 21st century.

Previous studies of the impact of climate change on Blue Nile River have produced widely different results due to the inconsistencies of global emissions scenarios and other aspects of the model simulations. Nonetheless, there is some general consistency of our results with other studies. For instance, Kim (2008) used the outputs of six GCMs to project future precipitations and temperature and analyzed the hydrological responses to the climate change effects using a simplified monthly water balance model. The study result suggested that mean annual precipitation simulated from the six GCMs might change in the range from -11% to 44% with a change of 11% from the weighted average scenario at 2050s. On the other hand, the changes in mean annual temperature range from 1.4°C to 2.6°C with a change of 2.3°C from the weighted average scenario. As a result, the relative changes in mean annual runoff are from -32% to 80% with an average change of 4%. Beyene *et al.* (2010) also used 11 CMIP3 GCMs for A2 and B1 scenarios to analyze the hydrological impacts of climate change on the entire Nile river basin and for the two large sub basins including UBNRB using the Variable Infiltration Capacity (VIC) model. The multimodal ensemble average annual precipitation relative changes for the Blue Nile sub-basin as compared to the baseline (1950–1999) annual average precipitation are 15% (19.4%), -9.2% (4.1%) and 5.1% (6.1%) for the A2 (B1) global emission scenario and periods 2010-2039, 2040-2069 and 2070-2099, respectively.

A more recent comprehensive study by Aich *et al.* (2014), which used the bias corrected model output of five ESMs (HadGEM2-ES, IPSL-5 CM5ALR, MIROC-ESM-CHEM, GFDL-ESM2M, NorESM1-M) under scenarios of RCP2.6 and RCP8.5 for analyzing the impacts of climate changes on the streamflow in four large African rivers, reported an increasing trend in precipitation. Furthermore, the projections of the SWIM model driven by the five corrected climate models agree almost completely on positive trends of streamflow at El Diem gauging station, which correspond to the precipitation. Another study done by Elshamy *et al.* (2009a), who used 17 GCMs reported that −15 % to +14 % changes in total annual precipitation but the ensemble mean of all models showed almost no change in the annual total rainfall. Moreover, all models predict the temperature to increase between 2°C and 5°C. In terms of changes to streamflow, more models (eleven) are predicting flow reductions than those showing increases (six). The ensemble mean annual streamflow at El Diem might reduce by 15% compared to the baseline. In summary, the increases in water availability will play significant benefits for small and large-scale farmers engaged in rain fed or irrigation agricultural activities to improve their livelihoods. Moreover, it assured the sustainability of water resources development projects, which are going to be implemented across the basin.

7.3.3 **Change in hydrological regime caused by the Chara-Chara Weir**

A gauging station, located immediately downstream of the outlet from Lake Tana (catchment area 15,000 km^2), has operated continuously since 1959. The natural Lake Tana reservoir regulated by the artificial man made Chara-Chara weir has an effect for changing the hydrological regime of the Lake. Daily time series flow data (1961-2014) collected from the Ministry of Water, Irrigation and Electricity were used for analyzing the impacts of Chara-Chara weir on the downstream flow to Tis Issat and Tis Abay I & II HPPs. Turbine discharge data for both Tis Abay-I and Tis Abay-II power stations were obtained from (McCartney et al., 2010) and used to estimate the monthly flows diverted to produce electricity as well as the water remaining in the river to flow over the Falls.

Analyses of outflow from Lake Tana outlet and lake level fluctuation is carried out by dividing the time horizon into four periods: January 1961 to December1995, January 1996 to December 2000, January 2001 to December 2010, and January 2011 to December 2016. These periods correspond to different levels of regulation of the Lake Tana outflow.

- Before 1996, the Lake has no any regulation
- From the period 1196-2000, two gates Chara- Chara weir became operational
- From 2001 to 2010, five additional gates at the Chara-Chara weir became operational
- Since 2011, Tana Beles hydropower starts the full operation and additional flow from Lake Tana diverts to Tana Beles hydropower.

Table 7-13 shows the mean monthly flow measured at the outlet of Lake Tana downstream of the Chara-Chara weir for the four different operational periods. The natural outflow regime from January 1961 to December 1995 has high extreme seasonal variability, ranging from a mean of 328 m^3s^{-1} in September to just 12.4 m^3s^{-1} in June. On average, only 8.3% of the natural discharge from the lake occurred in the five months from February to June. In the period 1996 to 2000, both wet and dry season flows were significantly higher than those occurred during the previous period. The higher dry season flows were a consequence of partial flow regulation by the two gates Chara-Chara Weir. The higher wet season flows were a consequence of above average rainfall during these years, particularly in 1997 and 1998. Mean annual flow in 1998 (196 m^3s^{-1}= 6182Mm^3) was the highest annual discharge measured in the whole record (Table 7-20).

The outflow from January 2001 to December 2010 characterized by the increasing of dry season flows reduced wet season flows and less seasonal variability as compared to the natural outflow condition (Figure 7-17 and Table 7-13). The increasing of dry season flow was because of the full flow regulation by the seven gates of the Chara-Chara Weir in order to satisfy the higher demands of Tis Abay II while the reduced wet season flow was a consequence of less amount of rainfall (Figure 7-18). After full flow regulation, 38% of the discharge from the lake occurred in the five months from February to June. In the period 2011 to 2014, after the Tana-Beles hydropower started operation, the mean annual discharge measured is 82m^3s^{-1}, which is the lowest released flow than the other periods. Furthermore, about 40% of the flow is occurred in the month of September while only 17% of the controlled discharge from the Lake Tana occurred in seven months from January to July. The highest flow in the months of September

indicates that the Lake reservoir reaches at the maximum level due to large river inflows in the rainy months (July-August) upstream of the Lake. Once the reservoir level reaches at its maximum, it should be discharged (spilling) in order to protect flooding around the periphery of the Lake. In general, operation of the Chara-Chara Weir has altered the flow regime of the Abay River.

Table 7-13: Mean monthly outflow of Lake Tana in four different periods under different reservoir regulation and recommended minimum environmental flow

Month	1961-1995	1996-2000	2001-2010	2011-2014	[1]EIA	[2]DRM
Jan	68.8	107.2	109.7	15.4	60	25
Feb	46.9	72.2	108.2	22.0	60	23
Mar	31.6	50.8	117.6	25.0	10	16
Apr	19.6	60.1	110.5	23.5	10	11
May	13.0	41.4	95.1	23.3	10	9
Jun	12.4	39.1	94.1	20.3	10	8
July	35.4	75.5	116.4	30.5	20	15
Aug	157.1	184.6	139.3	111.7	20	31
Sep	327.8	449.0	207.6	388.2	40	74
Oct	296.9	423.8	133.7	194.3	40	44
Nov	187.8	297.4	113.7	84.7	40	42
Dec	112.3	176.0	102.6	39.1	60	32
Mean	109.1	164.7	120.7	81.5	31.7	27.5
Volume (Mm^3)	3441	5195	3806	2569	999	867

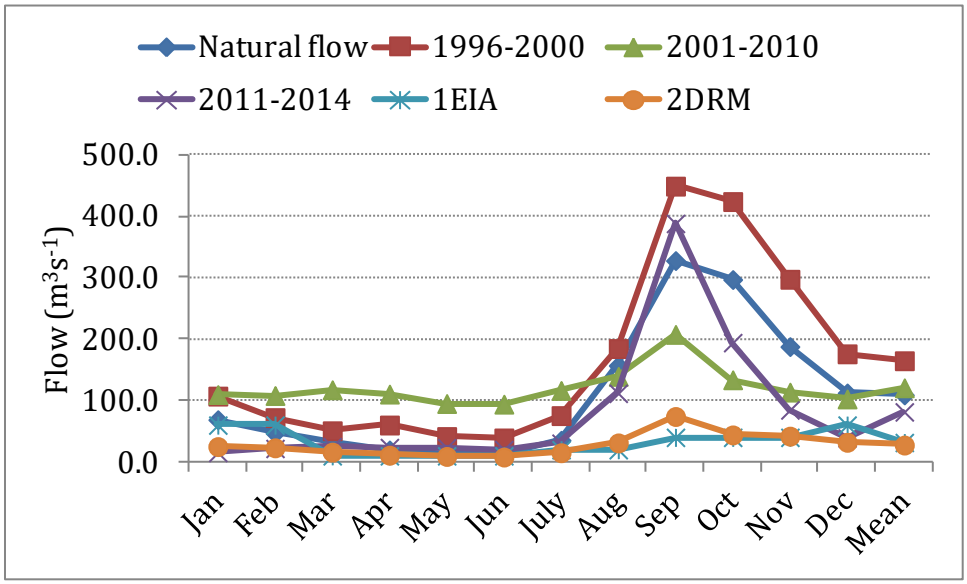

Figure 7-17: Mean monthly flow from Lake Tana for the four periods of different flow regulations and recommended minimum environmental flow

a)

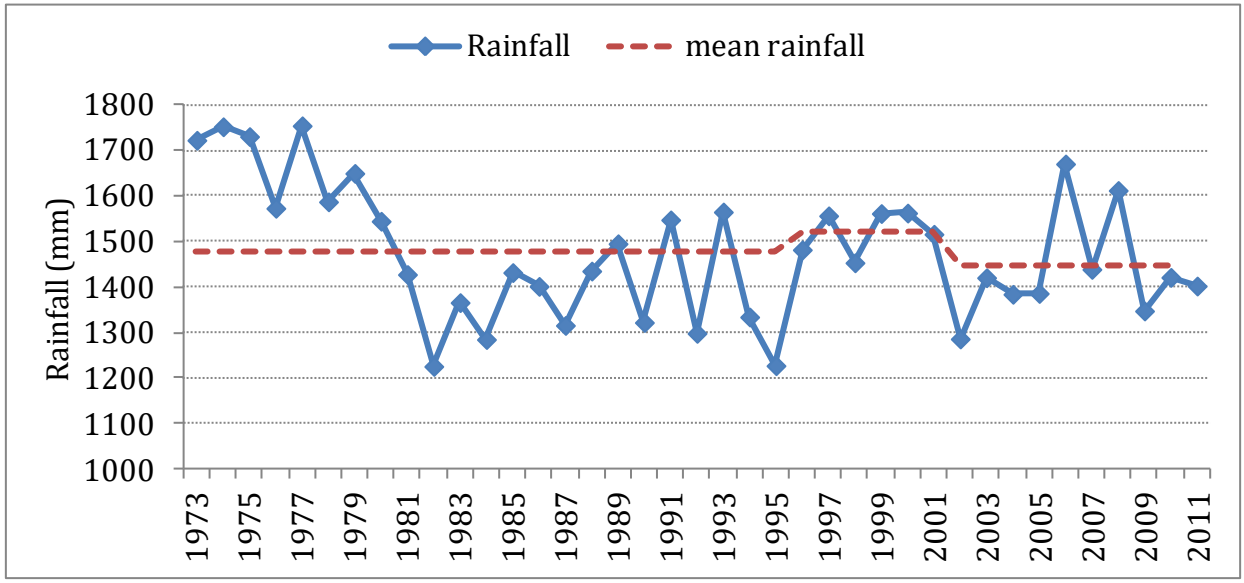

b)

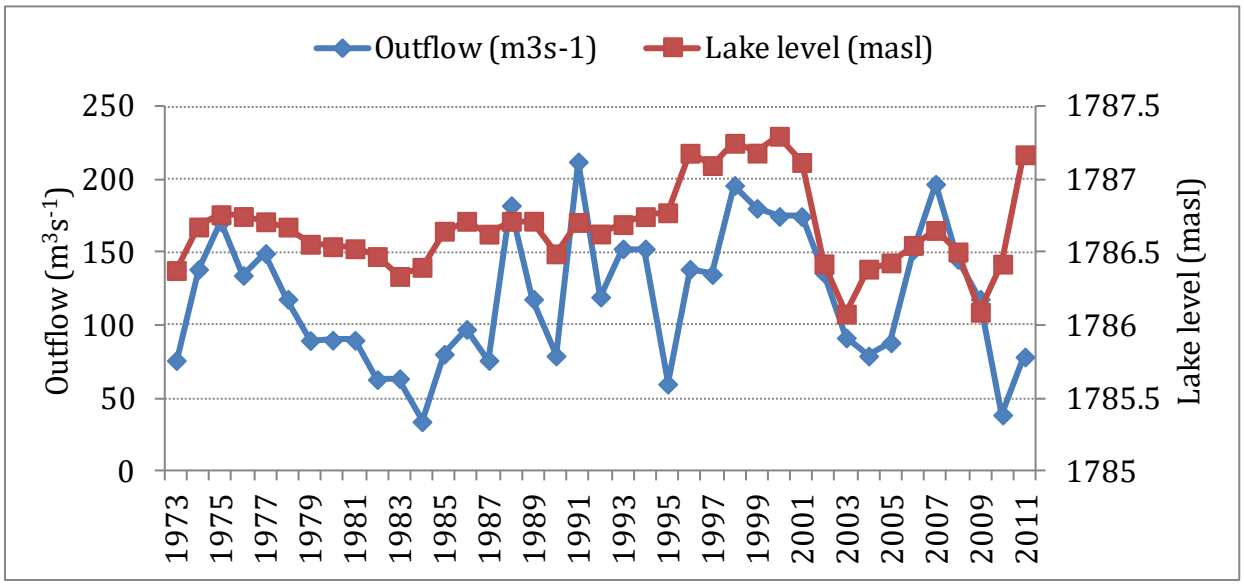

Figure 7-18: a) Annual total rainfall; b) mean annual lake level and outflow from Lake Tana

According to McCartney *et al.* (2010), when only the Tis Abay-I power station was operational (i.e., from 1964-2000) average annual turbine discharge was just 192Mm^3 (i.e., 6.1 m^{3}s^{-1}). Throughout this period just 4.5% of the average annual discharge at Tis Abay (4,227Mm^3) was diverted. Since 2001, when the Tis Abay-II power station came into operation, the average annual turbine discharge has increased to 3,090 Mm^3 (i.e., 97.9 m^{3}s^{-1}). This equates to 81.7% of the average annual discharge at the outlet of Lake Tana (3770 Mm^3) between 2001 and 2010.

According to McCartney *et al.* (2010) between 1973 and 2000 average annual discharge over the Falls is estimated to have been 128 m^3s^{-1} (i.e., 4,040 Mm^3). By comparison, between 2001 and 2010 the average annual discharge over the fall is estimated to have been just 41m^3s^{-1} (i.e., 1,305 Mm^3) including 19 m^3s^{-1} from the catchment downstream of Chara-Chara weir.

However, following the operation of the Tana Beles hydropower, Tis Abay I and II hydropower are becoming non operational, remained seated as standby. The aim of the intra-basin transfer is to generate hydropower by exploiting the 311 m difference in elevation between the lake and the Beles River generating a capacity of 460 MW. The Tana-Beles HPP generated far more electricity than the power produced by the Tis Abay power stations. Approximately 2,985 Mm3 volume of water diverted through the tunnel (rather than via the Chara-Chara Weir) each year to generate 2,310 GWh of electricity (SMEC, 2008). After passing through the Tana-Beles power station, water can be utilized for irrigation.

Consequently, the flow for the Tis Abay I and II HPPs is re-diverting and allowing to flow over Tis Issat Fall. The mean annual flow of Lake Tana outlet in the period 2011-2016 (after the Tana-Beles intra-basin transfer) has reduced from 121 m^3s^{-1} (3807Mm^3) to 82 m^3s^{-1} (2570Mm^3) as compared to the period when it was fully regulated by seven gates (2001-2010). In contrary, the mean annual flow over Tis Issat fall has increased from 41 m^3s^{-1} to 82 m^3s^{-1} as there is no need to divert (97.9 m^3s^{-1}) to the Tis Abay I and II hydropower for power production. It is to be noticed that the mean monthly flow of January, February and December after the operation of Tana-Beles HPP scheme are lower than the recommended minimum environmental flow by McCartney *et al.* (2010).

Lake Tana reservoir water level

In order to operate the Tana-Beles HPP properly and set the operation rules outlined by (Bellier *et al.*, 1997; Halcrow *et al.*, 2010; SMEC, 2008), records of Lake Tana water level are important. Lake levels fluctuate throughout the year and from day to day as shown in Figure 7-19. The regulation of Lake Tana by the Chara-Chara weir for power production at Tis Abay I and II has modified the natural lake level pattern, raised the mean lake levels and increased water storage Figure 7-19 (b). After 2001, when the Lake Tana was regulated fully by 7 gates, the draw-down of lake levels during the dry season increased most notably in June 2003 disrupting shipping, causing the desiccation of the shoreline wetlands, and reducing the lake outflow to the Abay river. The lake level is lowest at the end of the dry season, in June, and reaches a maximum in October-November after the rainy season.

Under natural conditions, outflow from Lake Tana was directly linked to rainfall with a significant seasonal variation. After the construction of the Chara-Chara weir, the outflow from Lake Tana was determined by the combined effect of the rainfall amount and demands for power stations.

a)

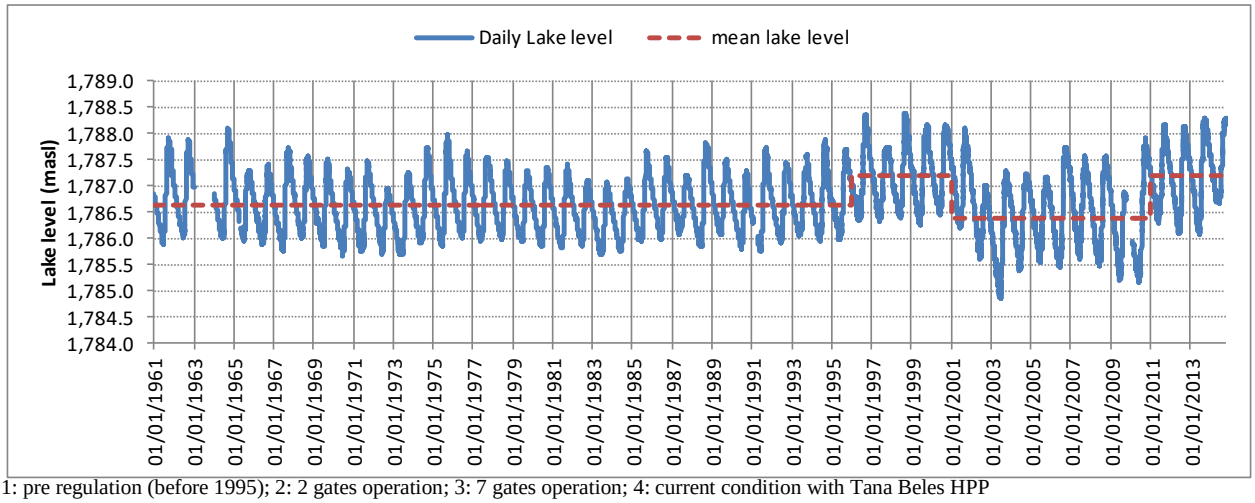

1: pre regulation (before 1995); 2: 2 gates operation; 3: 7 gates operation; 4: current condition with Tana Beles HPP

b)

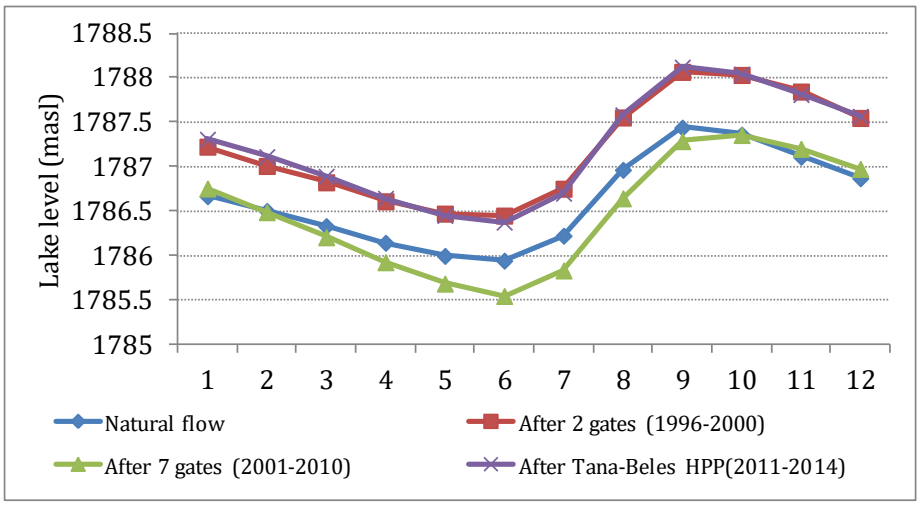

Figure 7-19: Lake Tana water level. a) daily lake level(1961-2014); b) mean monthly lake level

7.3.4 Implications of combined climate change and water resource developments to the water resource management

Because water resources management is inextricably linked with climate, the prospect of global climate change raises serious concerns as to the sustainability of water resources and regional development (Beyene et al., 2010). Efforts to provide adequate water resources in the Nile River basin will be challenged over the next century by the pressures of increasing population and resulting land use change, and with potential hydro ecological consequences. Changes in climate and climate variability (which results in droughts and flooding) will inevitably complicate water

resources management in the Nile basin. A simple reservoir HEC-HMS model was applied to identify the nature of interactions between climate change and the managed water resource systems. From both the hydrological sciences and policy-making perspectives, our knowledge about the combined impacts of water resource developments and climate change on the hydrological responses is still critically limited, particularly in data scarce areas like UBNRB. Thirteen different scenarios are developed to assess the combined impacts of climate change and water resource developments on the hydrology, hydropower and irrigation. In each scenario, the impacts on lake water levels and lake area, mean annual unmet demand for irrigation projects and mean annual downstream flow at the gauged stations and the annual energy productions are analyzed.

7.3.4.1 Impacts on the Hydrology

In order to assess the combined impacts of climate change and water resource developments, the priori task should be setting up the optimal control variables (i.e. operation rule curve) of the natural and artificial reservoirs in the UBNRB. For the purpose of this dissertation, operating rule curves both for the proposed new dams and for the Lake Tana are establishing for different scenarios following the assumptions and priorities set discussed under 7.2.4. The model was run several times using a trial and error approach to fix the operation rule curves for the Lake Tana reservoir and for the planned new reservoirs.

Table 7-14 summarized the simulated quantity of flow released from Lake Tana reservoir to the Tana Beles and Abay River, flow at Kessi and El Diem gauged stations based on different "what if" management scenarios. The mean annual flow entering the Abay River from Lake Tana was about $81.8 m^3 s^{-1}$ in the period 2011-2014 after the operation of Tana-Beles HPP started. The results under different scenarios indicate that the outflow from the Lake Tana to the Abay River may reduce by -65% at maximum and by -8% at the minimum in the scenarios s12 and s5 respectively. However, the outflow of Lake Tana to the Abay River may increase by 34% at the maximum under s8 and 11% at minimum under s6. The area of land planned for irrigation and the corresponding irrigation water requirement are the same for s4 s8, and s12 but the outflow of Lake Tana to the Abay River under s8 is higher than s4 and s12. This indicates that inflow to the Lake might increase under s8 due to the increased of precipitation as the result of climate change effect.

The mean annual flow diverted to the Tana Beles hydropower from Lake Tana reservoir during the period 2011-2016 was about $98 m^3 s^{-1}$. This flow might decrease by -36% at the maximum and by -11% at the minimum under scenarios of s11 and s2 respectively and might increase from 3.2% to 36% under scenarios of s5 and s8 respectively. Meanwhile the flow at Kessi station might decrease in the range from -24% to -48% under s2 and s9 respectively but it might increase from 1.6% to 50.6% under s5 and s8 respectively. The inflow at El Diem station might also decrease by a maximum of -35% under s11 and a minimum by -1.4% under s2. It might also increase maximum by 30% and minimum by 13% under s8 and s5 respectively.

Table 7-14: Hydrological response to the combined effect of climate change and large scale water resource development at four main stations.

	Discharge (m^3s^{-1})				Relative change from the baseline (%)			
	Abay River	Flow to Tana Beles HPP	Kessi	El Diem	Abay River	Tana Beles HPP	Kessi	El Diem
s0	81.8	97.9	613.3	1645.1				
s1	74.9	100.7	613.4	1710.2	-8.4	2.9	0.0	4.0
s2	46.4	87.1	468.8	1622.2	-43.3	-11.0	-23.6	-1.4
s3	43.1	83.8	465.5	1586.8	-47.3	-14.4	-24.1	-3.5
s4	43.5	82.0	464.3	1514.6	-46.8	-16.3	-24.3	-7.9
s5	75.3	101.0	622.8	1862.3	-7.9	3.2	1.6	13.2
s6	91.0	105.3	695.3	1979.9	11.3	7.6	13.4	20.4
s7	100.9	119.0	815.5	2111.7	23.4	21.6	33.0	28.4
s8	109.3	132.8	923.5	2147.4	33.6	35.7	50.6	30.5
s9	30.6	74.8	317.1	1178.5	-62.5	-23.5	-48.3	-28.4
s10	30.3	69.6	365.3	1234.0	-63.0	-28.9	-40.4	-25.0
s11	28.5	62.3	340.1	1064.9	-65.1	-36.4	-44.5	-35.3
s12	33.0	69.4	374.6	1124.9	-59.7	-29.1	-38.9	-31.6

*: represents the period 2001-2010, **: represents for the period 2011-2016

Impacts on the outflow of Lake Tana to the Abay River

For the operation of the Tana-Beles hydropower scheme, about 70% of the natural outflow of Lake Tana is diverted to the Tana Beles HPP scheme to generate electricity and supply water for the downstream irrigation development. The remaining 30% of lake outflow is planned to release to the Abay river as regulated flow or occasionally as unregulated flow when lake levels are particularly high spilling over the Chara-Chara weir's spillway (Halcrow *et al.*, 2010). The regulation of the Chara-Chara weir will ensure that environmental flow requirements, needed to maintain biological life in the river, are sustained. Minimum flow requirement for visual amenity of the Tis-Issat waterfall, located downstream of Lake Tana, were estimated during the feasibility study of Tis-Abay II hydropower plant prior to the construction of the five gated weir by Bellier et al. (1997) named as EIA from Table 7-15. McCartney et al. (2010) also estimated the minimum environmental flow requirement to the fall with no allowance for the aesthetic quality of the fall after the construction of the seven gates named as DRM from Table 7-15.

Table 7-15 summarizes the results of each scenario. The results indicate the decline in mean annual outflow as water resources development in the Tana sub-basin increases. As would be expected, the greatest impact of the water resources development occurs during dry climate scenario (i.e. GFDL GCM under RCP4.5 scenario) most significantly, from s9-s12 scenario simulation. During these periods, the mean annual outflow is less than the recommended environmental flow by (Bellier *et al.*, 1997).

Table 7-15: Mean monthly outflow (m^3s^{-1}) to the Abbay river from Lake Tana reservoir for different model scenarios

	Jan	Feb	Mar	Apr	May	Jun	Jul	Aug	Sep	Oct	Nov	Dec	Mean	Vol. (Mm^3)
s0	15	26	25	24	23	20	30	112	388	194	85	39	82	2580
s1	62	52	41	33	30	29	35	60	141	199	141	77	75	2362
s2	49	42	36	30	25	24	27	41	74	83	70	57	46	1463
s3	49	43	38	29	22	21	24	37	62	71	65	56	43	1361
s4	54	50	45	30	19	18	23	35	56	65	67	61	43	1372
s5	64	55	46	36	30	29	34	56	141	200	135	78	75	2376
s6	71	63	54	39	30	29	34	58	171	259	189	96	91	2871
s7	58	54	50	39	30	29	34	53	223	332	218	88	101	3183
s8	77	68	62	49	38	36	43	63	197	339	214	125	109	3446
s9	39	34	31	25	21	18	19	24	32	40	44	41	31	966
s10	40	36	33	25	18	12	15	23	32	39	47	43	30	955
s11	42	40	36	21	9	6	7	19	29	37	49	47	29	899
s12	46	44	41	26	15	10	13	23	32	41	54	51	33	1040
[1]EIA	60	60	10	10	10	10	20	20	40	40	40	60	32	999
[2]DRM	25	23	16	11	9	8	15	31	74	44	42	32	28	867

Recommended minimum flows at Tis Issat fall by 1(Bellier *et al.*, 1997); 2(McCartney *et al.*, 2010)

(a) Scenarios s0/s1

The observed flow measured at the Lake outlet to the Abay River was 3,442Mm^3 (Table 7-13) before regulation of the lake outlet by the Chara-Chara weir. Once the Tana-Beles scheme begins operating, the observed mean annual flow released to the Abay River significantly reduced to 2580Mm^3 (Table 7-15) under the current condition (s0). Although the observed mean annual outflow volume to the Abay River is higher than the recommended minimum environmental flow volume (Bellier *et al.*, 1997; McCartney *et al.*, 2010), the observed outflow in the months of January, February and December is lesser than the monthly recommended environmental flow. Meanwhile, the model simulates mean annual outflow of 2362Mm^3 to the Abay River for the current condition (s1) that is equivalent to the observed outflow. The difference between he observed and simulated outflow to the Abay River for the current condition could be due to the difference of the actual and simulated outflows to the Tana-Beles HPP (Table 7-15).

(b) Scenario s2

Under s2, 1463Mm^3 of water is going to be released from the Chara-Chara weir downstream to Abay River annually. Although the outflow is 43.3% less than the observed outflow (s0), it can satisfy the total annual environmental flow requirement of 999Mm^3 recommended by Bellier *et al.* (1997) and 867Mm^3 estimated by McCartney *et al.* (2010). However, the mean monthly flows in the months of December, January and February are less than the mean monthly flows of the recommended minimum environmental flow Table 7-15.

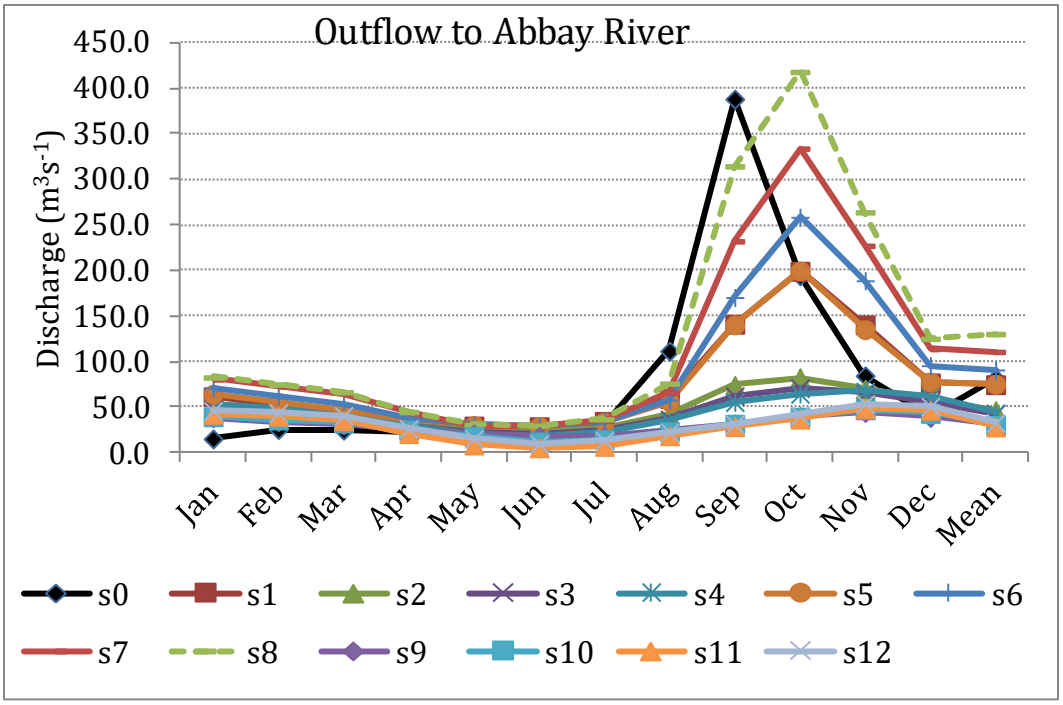

Figure 7-20: Mean monthly outflow of Lake Tana to the Abbay river under different model scenarios

(c) Scenario s3

The total mean annual Lake Tana outflow to the Abay River simulated under s3 is 1361Mm^3. Despite the flow to the Abay River decreased by 47.4% from the baseline, the criteria for environmental maintenance flows remain satisfied at the waterfall if the Tis Issat I and II hydropower's remained as standby. However, the flow in the months of January, February and December are less than the minimum environmental flows recommended by (Bellier *et al.*, 1997), while the flow in the month of only September is less as compared to the minimum EIA flow recommended by McCartney *et al.* (2010). The reduction of flow to the Abay River is due to the abstraction of 615Mm^3 of water for each year for the 68,754 ha of land to be irrigated upstream of Lake Tana Table 7-18.

(d) Scenario s4

This scenario is similar to the scenarios of s2 and s3 without climate change effect but with full irrigation development (106,754 ha) upstream of the Lake Tana. Under this scenario, it is expected to withdraw on average 953Mm^3 of water every year for the intended irrigation development upstream of Lake Tana, which is about 30% more from scenario s3. Meanwhile, the Chara-Chara weir provides a regulated mean annual outflow of 1372Mm^3 to the Abay River, which is still above the threshold for environmental maintenance flows at Tis Issat.

(e) Scenario s5, s6, s7 and s8

These scenarios are established based on the existing and future planned water resources development combined with the climate change projection under RCP4.5 scenario of canESM2 GCM. The mean annual streamflow in the future forced by RCP4.5 scenarios of canESM2 GCM is expected to increase as explained in section 7.3.2. Hence, the volume of water available for the

Tana-Beles HPP and Abay River will also increase in comparison to the respective baseline flows as it presented in the Table 7-14, Table 7-15 and Table 7-16. A mean annual flow of 2376, 2871, 3183 and 3446Mm^3 will be diverted to the Abay River under s5, s6, s7, and s8 scenarios respectively. Although the mean annual flow to the Abay River under these scenarios are higher than the other scenarios, the mean annual flows in all scenarios except s8 are less than the mean annual outflow of the Lake Tana before the regulation (3441Mm^3) Table 7-13.

(f) s9, s10, s11 and s12 (scenarios with the climate change effect of GFDL GCM under RCP4.5)

The streamflow projection under RCP4.5 scenario from GFDL GCM might decrease in the future, which might have adverse impacts on the hydrology and water resource developments by reducing the water availability. The model simulation result (Table 7-14) showed that the outflow from Lake Tana to the Abay River might reduce by -60% at the minimum and -65% at the maximum under s11 and s12 respectively from the baseline. In addition, the simulated mean annual outflows to the Abay River (Table 7-15) under s9, s10 and s11 are 966, 955, 899 and 1040 Mm^3. It shows that the mean annual outflows under s9, s10 and s11 are marginally less than the minimum environmental flow recommended by (Bellier *et al.*, 1997).

Impacts on the Lake Tana outflow to the Tana-Beles HPP

The variability of inflow to the Lake Tana reservoir due to climate change effect and different scenarios of the water resource development might have an effect on the outflow to the Tana-Beles HPP. The model simulation result under different scenarios is presented in Table 7-16.

Table 7-16: Mean monthly outflow to Tana Beles hydropower scheme under different model scenarios

Month	s0	s1	s2	s3	s4	s5	s6	s7	s8	s9	s10	s11	s12
Jan	103	97	91	91	93	98	101	128	153	86	87	88	90
Feb	104	92	88	88	92	94	97	121	145	83	85	87	89
Mar	104	88	84	85	89	90	93	113	135	79	82	81	87
Apr	104	83	78	76	75	85	86	93	111	73	71	48	72
May	103	78	72	63	53	79	79	79	90	65	43	21	34
Jun	96	77	69	58	45	77	78	78	88	45	21	12	14
Jul	98	83	75	69	65	82	83	85	100	51	31	15	26
Aug	96	96	87	84	82	94	95	112	133	71	69	52	68
Sep	89	130	102	97	94	130	138	155	159	81	81	77	80
Oct	87	148	106	101	98	148	156	160	160	87	87	84	88
Nov	92	131	101	99	100	130	144	159	160	89	91	91	93
Dec	98	104	95	95	97	104	112	146	159	87	89	90	92
Mean (m^3s^{-1})	98	101	87	84	82	101	105	119	133	75	70	62	69
Energy(GWh)	2193	2256	1952	1878	1837	2263	2359	2667	2977	1677	1559	1396	1556
Vol. (Mm^3)	3086	3175	2747	2643	2585	3184	3321	3753	4189	2360	2194	1964	2189
PF	0.61	0.63	0.54	0.52	0.51	0.63	0.66	0.74	0.83	0.47	0.43	0.39	0.43

a) Scenarios s0/s1,
S0 represents the observed outflow while s1 represents the model simulation of the baseline period to the Tana-Beles HPP that helps to evaluate the performance of established operation rule curve in representing the current condition (i.e. the condition after the operation of Tana-Beles HPP). Results from Table 7-15and Table 7-16showed that the observed mean annual

outflow both to Abay River and Tana-Beles HPP have the same magnitude with their respective simulated mean annual outflows. This indicates that the operation rule curve developed for the Lake Tana is able to represent the current operation condition of the Lake Tana reservoir.

b) Scenario s2, s3, s4 (no climate change scenarios)
These scenarios are scenarios with different level of water resource development upstream of Lake Tana but they are not addressing the climate change effect (climate remained constant). The model simulation result shows that mean annual outflows to the Tana-Beles HPP in all three scenarios ranged from $87m^3s^{-1}$ to 82 $m^3s^{-}1$, which are less than the current mean annual outflow ($98m^3s^{-1}$) but higher than the designed average flow of $77m^3s^{-1}$. This indicates that the combined effect of climate change and water resource developments upstream of Lake Tana might be insignificant when compared the simulated outflows to the designed average flow of $77m^3s^{-1}$. However, its operation needs high attention during the months of May, June and July to balance, as the outflows are less than the designed flow. Currently the project generates 2230 GWh energy annually on average, which is 62% of the plant maximum capacity. However, under s2, s3 and s4 the simulated flow to the Tana-Beles HPP can generate on average between 1952 and1837 GWh energy annually.

c) Scenario s5, s6, s7 and s8 (climate change effect under RCP4.5 scenario of canESM2 GCM)
The future climate change projection downscaled from canESM2 GCM under RCP4.5 scenario using SDSM combined with different level of water resource developments upstream of Lake Tana reservoir are used as input for the model to assess the combined impacts on the outflow to the Tana-Beles HPP. The model simulation result revealed that if the projected climate using canESM2 GCM under RCP4.5 scenario occurred in the future, Tana-Beles HPP would receive 3184, 3321, 3753 and 4189 Mm^3 volume of water every year under s5, s6, s7 and s8 respectively. These volumes of water are higher than the observed volume of water released from Lake Tana to Tana-Beles HPP. With these amount of released water, Tana-Beles HPP can generate on average from 2263 to 2507 GWh energy annually (Table 7-21). S8 is the only scenario in which all the mean monthly flows are higher than the designed mean flow ($77m^3s^{-1}$) (see Figure 7-21).

d) Scenarios s9, s10, s11 and s12 (climate change effecr from GFDL GCM under RCP4.5)
In contrary to climate change scenario of canESM2 GCM, these scenarios are the worst-case scenarios for the Tana-Beles HPP. The mean monthly outflow to the Tana-Beles HPP is lower than the mean designed flow ($77m^3s^{-1}$). The flow below the design average flow of 77 m^3s^{-1} might have multiple negative effects on generating electricity and downstream upper Beles irrigation particularly during the months of April to June when the irrigation demand is becoming high.

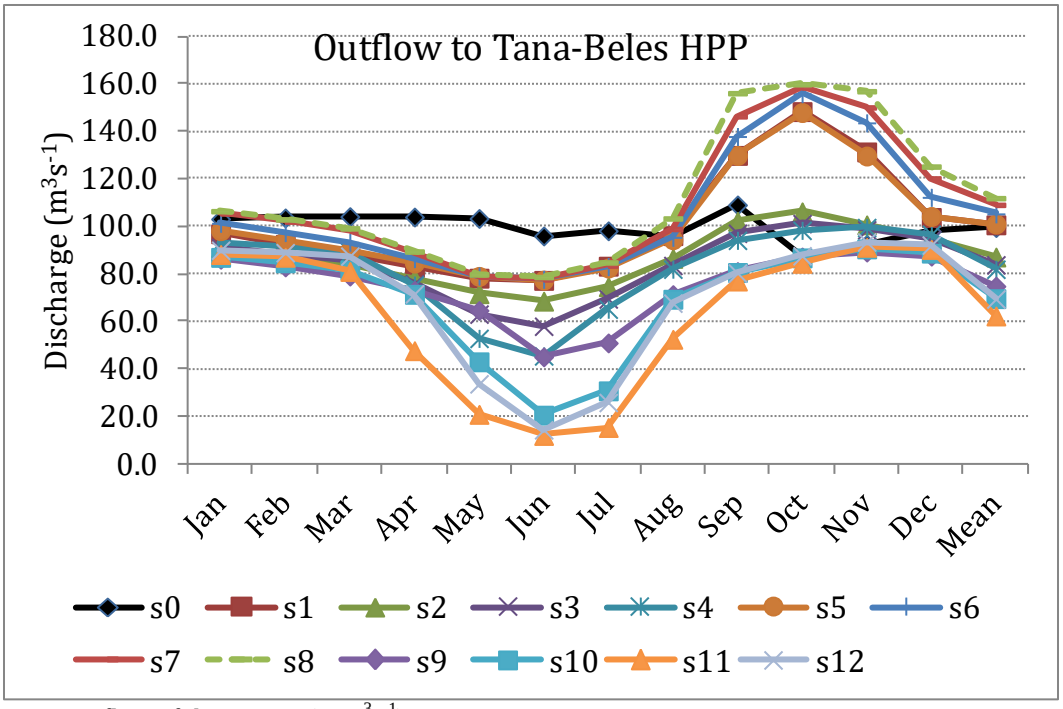

DM: design mean flow of the project ($77m^3s^{-1}$)

Figure 7-21: Mean monthly flows to the Tana Beles HP under different scenarios

In general, the model simulation results for the outflow to the Abay River in Figure 7-20 show that the minimum recommended environmental requirements are satisfied and surpassed during the wet season and dry season in all scenarios except in the months of December, January and February. The outflow below the minimum environmental requirement may have a significant negative impact on tourism, navigation and other socio-economic activities.

The seasonal pattern of flow releases to the Tana-Beles HPP is important for determining the area of irrigation that can be developed sustainably in the upper Beles irrigation project. The flow released from Lake Tana reservoir into the Beles catchment through Tana-Beles HPP has to satisfy the water requirement for the downstream irrigation development but also maintain electricity production whilst avoiding environmental damage to Lake Tana and downstream on the Abay River. Figure 7-21 and Table 7-16 present the mean monthly flow of Tana Beles HPP based on operational rules adopted for model scenarios. Salini *et al.* (2006) designed the scheme to have an average discharge of $77m^3s^{-1}$ through the tunnel with discharge peaking at $160m^3s^{-1}$at high lake levels, to operate with an average plant factor of 48%. In all scenarios except canESM2 scenarios (s5-s8), less volume of flow, below the average of 77 m^3s^{-1} is released to the Tana Beles HP during the driest season (April, May and June) and early rainy season (July).

Impacts on the flow of Kessi and El Diem stations

The mean annual streamflow of the model simulation result at Kessi showed mixed signals. It might increase for the s5, s6, s7 and s8 but might decrease under s2, s3, s4, s9, s10, s11 and s12. The flow might decrease minimum by -24% under s2 and maximum by -48% under s9 respectively. However, this flow might increase from 1.6% to 51% under scenarios of s5 and s8

respectively. At El Diem, the mean annual inflow might decease by -1.4% at minimum and by -37% at maximum under scenarios of s2 and s11 respectively while it might increase from 13.2% to 29% under scenarios of s5 and s8 respectively. The large decrease of Kessi as compared to El Diem from baseline is due to the flow that transferred to the Tana-Beles from Lake Tana upstream of Kessi, which joins the main Blue Nile upstream near to GERD. It is noticed that the existence of climate change (s5 to s8) may increase the availability of water resources for both irrigation and hydropower projects; however, if the climate remained unchanged (s2 to s4) or the climate scenario for GFDL GCM occurs, it is undoubtedly, UBNRB may experience the reduction of streamflow.

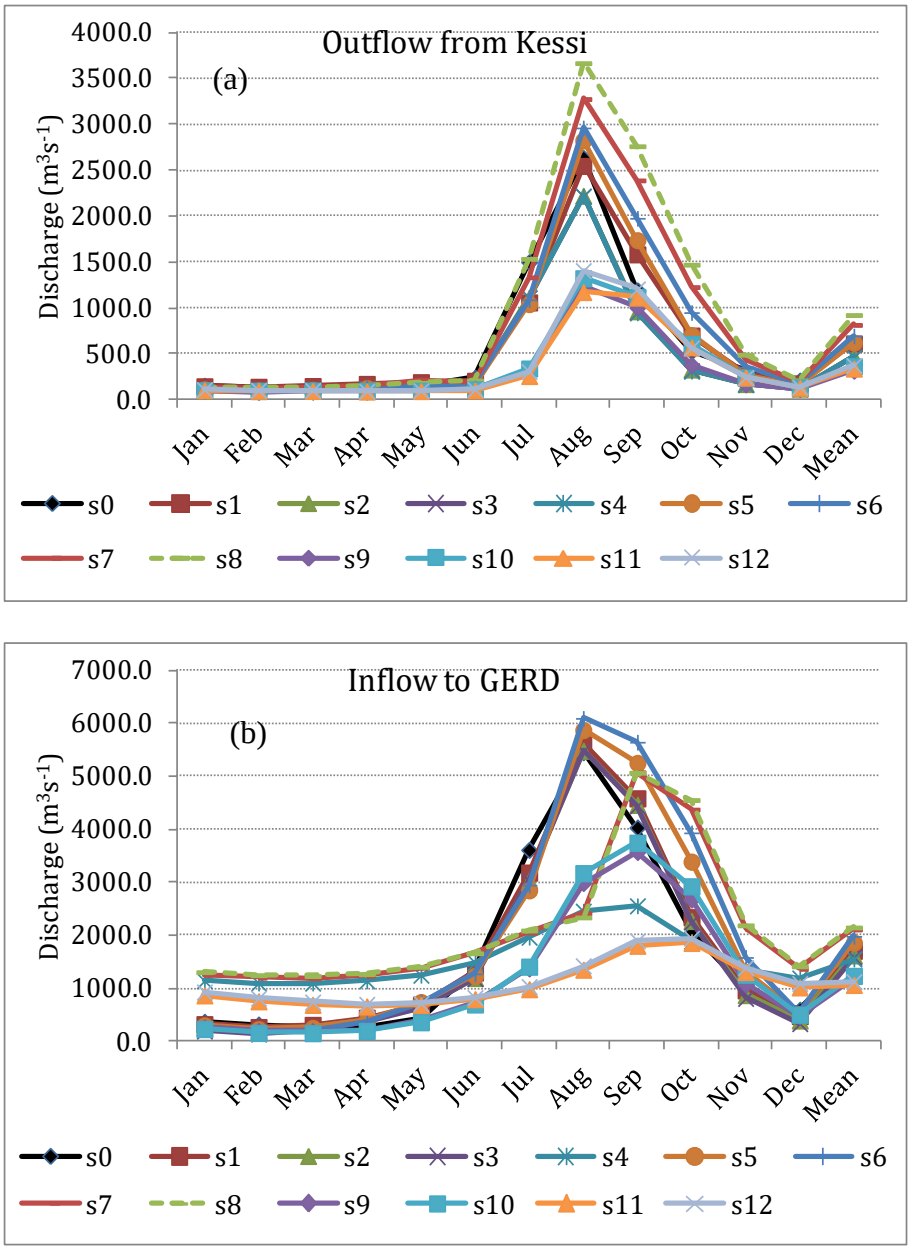

Figure 7-22: Mean monthly simulated inflow a) at Kessie and b) at El Diem station under different scenarios

Figure 7-22 shows the impact of expected water resource developments on average monthly inflows at Kessi and El Diem under different scenarios. Not surprisingly, it shows the seasonal pattern of the inflow at GERD might considerably modified under s4, s7, s8, s11 and s12, when the upstream three large-scale hydropower projects (Beko-Abo, Karadobi and Mendiya) starting operation. As a result, the flow might increase during the dry period (January–May) and a decrease of mean monthly discharges during the rainy season when discharges are used to re-fill the upstream of three large hydropower reservoirs.

The flow regime of the GERD dam is governed by the operations of the upstream hydroelectric power schemes and runoff from the catchments (the incremental flow) between the dams. The upstream reservoirs have influence on the downstream reservoirs inflow. During full operation phase of the upstream hydropower projects, in this case (s4, s7, s8, s11 and s12), the downstream GERD reservoir will gain maximum flow in the dry months and less peak discharges in wet months because of regulating effects of upstream cascades. Figure 7-22 (b) demonstrates mean monthly inflow to GERD dam for different climate change and upstream development scenarios. Releases from Karadobi, Beko-Abo and Mandaya dams constitute the major inflow into GERD dam. The values of the daily inflow coefficient of variance of GERD for scenarios without upstream hydropower projects are higher than the coefficients of variances of scenarios with upstream reservoirs (Table 7-17). For instance, the coefficients of variance are 1.14 and 0.4 for baseline and s4 scenarios respectively.

Table 7-17: Statistics of daily inflow to GERD reservoir for different scenarios

Scenario	Minimum (m^3s^{-1})	Maximum (m^3s^{-1})	Median (m^3s^{-1})	Mean (m^3s^{-1})	STDEV (m^3s^{-1})	CV
s0	20.1	10887.1	668.9	1673	1914	1.14
s1	182.2	10319.9	789.25	1719	1899	1.10
s2	116.2	10111.4	712.9	1632	1869	1.15
s3	69.4	10105.3	681.45	1596	1884	1.18
s4	956.7	7512.4	1297.1	1555	573	0.37
s5	143.5	7531	854.9	1873	1992	1.06
s6	88.5	8220.2	889.2	1991	2132	1.07
s7	1059.9	9325.4	1475.5	2113	1395	0.66
s8	1082.1	8406.6	1504.3	2150	1400	0.65
s9	147.5	5294.2	590	1184	1223	1.03
s10	98.6	5443.1	591.7	1239	1317	1.06
s11	531.7	3340.8	900.4	1066	452	0.42
s12	532.9	3178.7	958.4	1126	468	0.42

Impacts on Lake Tana water levels and lake area

Figure 7-23 presents a comparison of box plot representation of the time series of simulated lake levels for all scenarios. Table 7-19 summarizes the results of each scenario. The results indicate the decline in mean annual lake levels, and consequently lake area, as water resources development in the catchment increases. As would be expected, the greatest might occur during the climate scenarios of RCP4.5 from GFDL GCM under s9, s10, s11 and s12. During these periods, lake water levels, depending on the development scenario, up to 0.91 and 1.03m lower than natural levels under s12 and s11.

Lake Tana water level data measured at Bahir Dar station is available from 1961 to 2014. Lake level fluctuates seasonally and from year to year as shown in Table 7-19 and Figure 7-23. The analysis suggested that the Lake level increased by 0.57m in the period 1996-2000 when the outlet was regulated by two gates and only Tis Abay I hydropower was operated as compared to the natural outflow. In the period 2001-2010, when seven gates regulated the Lake and both Tis Abay I and II HPPs operated, the mean Lake water level was reduced by -0.16 m. In the period 2011-2016, when the Tana Beles hydropower has been in operation and both Tis Abay I and II functioning as standby, the mean Lake water level increased by 0.56m Table 7-23. The raising of lake level during the period 2011-2016 as compared to the lake level during 2001-2010 (before Tana-Beles) could be due to the less demand of the Tana Beles power station (i.e., 3,086Mm^3yr^{-1}) than demand of the Tis Abay I and II power stations (i.e., 3,469Mm^3yr^{-1}) (McCartney et al., 2010), which allowed the lake to store more water.

Table 7-18: Planned and ongoing irrigation and hydropower development in the Lake Tana sub-basin

	Proposed Irrigation area (ha)					Irrigation water demand (Mm^3)			
Project Name	2011-2017	2018-2025	2025-2040	2041-2070	Total	2011-2017	2018-2025	2025-2040	2041-2070
Megech Pumping		4,000	8,510	12,000	24,510	0	35	108	212
Megech gravity		7,311			7,311	0	62	62	62
North West Tana			2,000	4,720	6,720	0	0	17	58
North East Tana		3,000	2,475		5,475	0	26	48	48
Rib		8,000	6,459	5,466	19,925	0	79	143	196
Gumara			10,000	3,776	13,776	0	0	85	117
Koga	7,000				7,000	54	54	54	54
Gilgel Abay		4,000	5,999	6,500	16,499	0	39	97	160
South West Tana				5,132	5,132	0	0	0	44
Jemma			7,786		7,786	0	0	60	60
Grand Total	7,000	26,311	43,229	37,594	114,134	54	295	674	1,012

Table 7-19 summarize the results of each scenarios showing the impacts on water level and lake area based on “what if” management options of the Tana-Beles hydropower scheme and

upstream irrigation developments (Table 7-18) combined with and without climate change scenarios.

(a) Scenario s1 (current condition)
If the Tana-Beles scheme is operated with a minimum operation Lake, level of 1,784.75 masl, with the upstream Koga irrigation development, the mean annual lake level decreased by -0.2m from 1,786.6 masl to 1,786.4 masl. The mean lake area will decrease from 3,053.2 km^2 to 3,044.3 km^2, losing 8.9km^2, which is about 0.3% of its total area.

(b) Scenarios s2
For the scenario s2 described in Table 7-1, the model simulation result indicates that the mean lake level declines by -0.56m to 1,786.1masl. As a result, the mean lake area declines from 3,053.2 km^2 to 3,027.4km^2 a reduction of 25.8 km^2 of lake area (see Table 7-19).

(c) Scenario s3
If water transferring from the Lake Tana to the Tana Beles hydropower station continues and 68,754 ha of land is going to be irrigated upstream of the Lake Tana, the mean lake level falls by -0.61 m to a water level of 1,786.0 masl. As a result, the mean annual lake area therefore decreases by - 28.2km^2 to 3,024.9km^2. Lake water levels remain high, exceeding 1,785 masl for 100% of the period.

(d) Scenario s4
In this scenario, the impact analysis is carried out in the situation when full irrigation development (106,345ha), which requires 4,092Mm^3 of water annually (Table 7-18), combined with the climate that remain unchanged. The model simulation result suggested that a dramatic fall in the mean annual lake level by -0.63 m Table 7-19. Consequently, the mean annual lake area is depleted by -29.0 km^2 to 3,024.2 km^2.

(e) Scenario s5, s6, s7 and s8
In the previous scenarios, climate change has not been considered but is likely to have an adverse effect on the water resource availability of the basin. Under the conditions of these scenarios, the result suggested that the Lake level might not change or the change is insignificant Table 7-19 and Figure 7-23. The Lake level might increase at the maximum by 0.1m under s8 and as a result, the Lake surface area might increase by a maximum of 3.6km^2 to 3054.1km^2 and a minimum by 1km^2 to 3054.1km^2 Table 7-19. The Lake level rise is due to the increased mean annual inflow from the tributary rivers as the result of the climate change.

(f) Scenarios s9, s10, s11 and s12 (climate change from GFDL GCM under RCP4.5 scenario)
As would be expected, the greatest impact of the water resource development occurs when it is combined with the climate change scenarios of CMIP5 GFDL GCM under RCP4.5 scenario (Table 7-19). In these scenarios, depending on the level of development, lake water levels lower up to -0.91m and -1.03m under s12 and s11 respectively as compared to the natural flow condition of Lake Tana. The full irrigation water requirement exacerbates the drop of lake water levels in all scenarios. For the full development scenarios, the mean lake area might reduce by a maximum of -47.4 km^2 under s11 and a minimum by -42 km^2 from 3053.2km^2 to 3005.8km^2 and 3011.2 km^2 respectively.

Table 7-19: Lake Tana water level and Lake area

	Lake level (masl)					
scenario	Min.	Max.	Mean	Difference (m)	Area (km^2)	Difference (km^2)
s0	1785.7	1788.1	1786.6		3053.2	
S1	1785.5	1787.8	1786.4	-0.2	3044.3	-8.8
s2	1784.9	1787.4	1786.1	-0.56	3027.4	-25.8
s3	1784.8	1787.3	1786.0	-0.61	3024.9	-28.2
s4	1784.8	1787.3	1786.0	-0.63	3024.2	-29.0
s5	1785.3	1787.5	1786.5	-0.17	3045.4	-7.8
s6	1785.4	1787.6	1786.6	-0.08	3049.7	-3.5
s7	1785.3	1787.7	1786.7	0.02	3054.1	0.9
s8	1785.3	1787.7	1786.7	0.08	3056.8	3.6
s9	1784.8	1786.7	1785.6	-0.99	3007.7	-45.5
s10	1784.8	1786.8	1785.6	-0.99	3007.4	-45.7
s11	1784.8	1787.0	1785.6	-1.03	3005.8	-47.4
s12	1784.8	1787.0	1785.7	-0.91	3011.2	-42.0

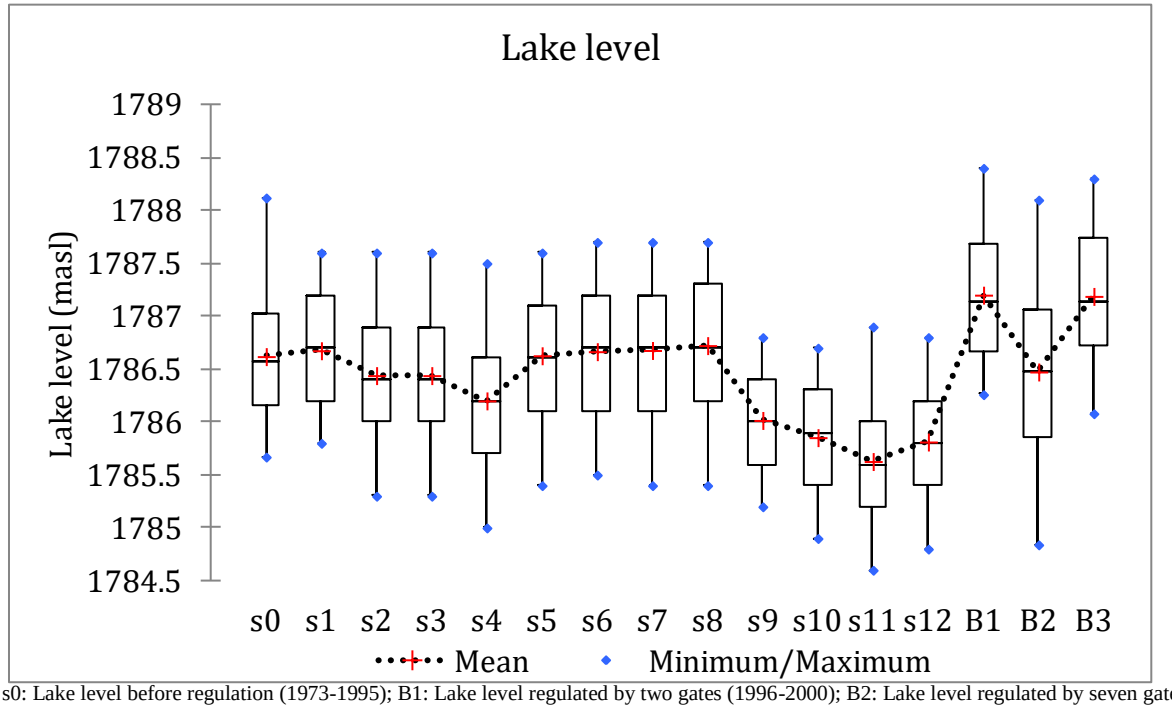

s0: Lake level before regulation (1973-1995); B1: Lake level regulated by two gates (1996-2000); B2: Lake level regulated by seven gates (2001-2010) and B3: Current condition (i.e. regulated by seven gates plus Tana Beles transfer) from 2011-2016

Figure 7-23: Box plot representation for the Lake water level under different scenarios

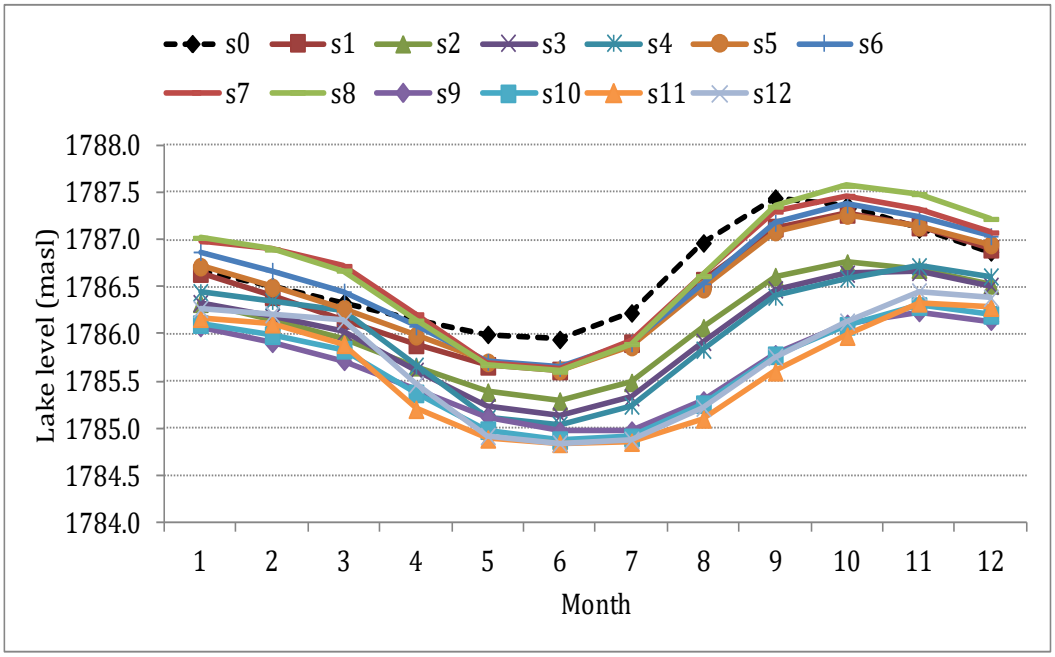

Figure 7-24: Mean monthly Lake Tana water level under different scenarios

As water resources development increases mean daily lake levels that are below 1,785 masl (Figure 7-28) exist longer periods. The result depicted that the lake level exceeds 1,785 masl just 100% of the time under s1, s5, s6, s7 and s8, when the clime change occurs with the projection scenarios of canESM2 GCMs for RCP4.5. Under the climate change scenarios of GFDL RCP4.5, the lake level exceeds 1785 masl maximum for 98.5% and minimum for 75% of the time under s10 and s11 respectively. For no climate change scenario, the lake level exceeds 1785 masl 98.5% of the time under s2 and 90% of the time under s4.

7.3.4.2 Impacts on irrigation

The mean annual water demand analysis for the total irrigation area of 23,596 ha (s1), 214,882 ha (s2,s5,s9), 382,644 ha (s3,s6,s10) and 424,370 ha (s4,s7,s8,s11,s12) in the UBNRB as presented in Table 7-20 show that 169.2, 1695, 3210 and 3583Mm^3 volume of water is required annually respectively. The full irrigation demand 3583 Mm^3 is equivalent to 7 % of the mean annual flow of Abay River under natural condition (52 Bm^3). The HEC-HMS model simulation result revealed that water deficit might exist in all scenarios with a value ranged from 31 to 692 Mm^3 annually, which is 19.3 % of the required amount. As would be expected, the maximum water deficient might occur under s4 while the minimum water deficient might occur for s1 (current condition) scenario Table 7-20. Shortfall in irrigation significantly increases as the irrigation development in the basin increases irrespective of climate change conditions of the scenarios. For instance, the shortfall for irrigation under s8, when precipitation increase in the future, is higher than the shortfall for s11, when precipitation decrease in the future at basin scale. This indicates that spatial distribution of precipitation across the basin might be influenced by the climate change as a result scarcity of water for the irrigation projects might occur even though the precipitation increases.

Table 7-20: Mean annual unmet water demand for the large irrigation developments under different scenarios

Scenario	Irrigation area (ha)	Annual average demand (m^3s^{-1})	Annual Average demand (Mm^3)	Mean Annual water demand (m^3ha^{-1})	Mean annual unmet demand (m^3s^{-1})	Mean annual unmet demand (Mm^3)	Water deficient (%)
s1	23,596	5.4	169.2	7172.2	-1.0	-31.0	-18.3
s2	214,882	53.7	1694.9	7887.5	-3.9	-123.3	-7.3
s3	382,644	101.8	3209.5	8387.8	-18.1	-571.4	-17.8
s4	424,370	113.6	3583.3	8524.1	-22.0	-692.2	-19.3
s5	214,882	53.7	1694.9	7887.5	-3.3	-102.5	-6.0
s6	382,644	101.8	3209.5	8387.8	-12.6	-396.7	-12.4
s7	424,370	113.6	3583.3	8443.8	-12.8	-404.6	-11.3
s8	424,370	113.6	3583.3	8443.8	-17.2	-543.8	-15.2
s9	214,882	53.7	1694.9	7887.5	-3.6	-112.1	-6.6
s10	382,644	101.8	3209.5	8387.8	-15.1	-476.1	-14.8
s11	424,370	113.6	3583.3	8443.8	-16.3	-514.2	-14.3
s12	424,370	113.6	3583.3	8443.8	-14.8	-466.1	-13.0

Recently, the water resources in the Upper Blue Nile River (UBNR) basin, was investigated by Stamou (2019) for four scenarios: natural, current, short- to medium-term and full development within the frame work of NIMA-NEX project. For the full development scenario, the annual irrigation requirement for the 584,110 ha of irrigated area was estimated equal to 4,568 Mm^3yr^{-1}, while the annual actual irrigation amount was calculated equal to 4,332 Mm^3yr^{-1}, while the irrigation deficit is equal to 23% of the required amount.

7.3.4.3 Impacts on hydropower production

Tana Beles hydropower project

The operation rules developed by SMEC (2008) is adapted for the model simulation of inter-basin transfer of water from Lake Tana reservoir to the adjacent Beles catchment through Tana Beles tunnel. The operation policy proposed to divert a maximum flow of 160 m^3s^{-1}at very high lake levels (> 1787 masl) but at low lake levels (< 1784.75) when water level is at or close to the minimum operating level, no water is diverted.

The model simulation result is presented in Table 7-21 for different scenarios. The result indicates that mean annual total hydropower to be generated from Tana-Beles hydropower scheme may decrease by about -11% to -36% under the s2 and s11 respectively as compared to the mean annual baseline power generated for the period (2011-2016). However, the power to be generated might increase in the range of 3.2% to 36% for the RCP 4.5 climate change scenarios combined with irrigation developments (s5-s8).

Table 7-21: Mean annual power generation from Tana Beles hydropower for different scenarios

	Q_{mean} (m^3s^{-1})	$Q_{98.5\%}$ (m^3s^{-1})	Average energy ($GWhyr^{-1}$)	Change (%)	Plant factor
s0	97.9	39.3	2193		0.62
s1	100.7	75.4	2256	2.9	0.67
s2	87.1	64.3	1952	-11.0	0.56
s3	83.8	17.0	1878	-14.3	0.56
s4	82.0	0.0	1837	-16.2	0.54
s5	101.0	72.5	2263	3.2	0.63
s6	105.3	75.0	2359	7.6	0.66
s7	119.0	75.1	2667	21.6	0.68
s8	132.8	76.8	2977	35.7	0.70
s9	74.8	20.1	1677	-23.5	0.47
s10	69.6	0.0	1559	-28.9	0.43
s11	62.3	0.0	1396	-36.4	0.39
s12	69.4	0.0	1556	-29.1	0.43

(a) Scenarios s1

The mean annual flow released to the Tana- Beles HPP during the baseline period (2011-2016) was 97.9 m^3s^{-1} (Table 7-16), which is above the average of 77 m^3s^{-1}. Although, there was a flow released 100 % of the time to the Tana-Beles HPP, only 94.3 % of the time remains above 77 m^3s^{-1} (Figure 7-21). Furthermore, it only allows high releases for 18.2% of the time (i.e. >140 m^3s^{-1}). The analysis result also indicates that an average 2256 GWh energy could produce annually with 0.67 average plant factors. The scheme was designed with a maximum flow of 160 m^3s^{-1} so as to generate 3585 GWh $year^{-1}$ with plant factor of 0.48 to generate an equivalent average energy of 1719 GWh per year (Bellier *et al.,* 1997). It is to be noticed that the mean annual energy produced in the baseline period is 30 % higher than the average design capacity.

(b) Scenario s2

If 33,311ha of land could be irrigated upstream, of the Lake Tana that required an amount of 295Mm^3 of water annually and the climate does not change in the near future, 77 m^3s^{-1} flow releases to the Tana Beles HP can only sustain for 76% of the time Figure 7-25. As a results the mean annual energy generation decreased by -11% from the baseline to 1952GWh Table 7-21. Flow might occur 100% of the time but the flow above 120 m^3s^{-1} might occur only for 3.7% of the time and 160 m^3s^{-1} flow might exist only for 0.5 % of the time.

(c) Scenario S3

Under this scenario, 615Mm^3 of water is reduced annually from the inflows of Lake Tana due to 68,754ha of upstream irrigation from the tributary rivers. In addition, an attempt was made to remain the climate unchanged from the baseline. Taking all the above factors into consideration, the outflow simulated by the model to the Tana-Beles HPP indicates that 99.5% of the time outflow might exist. Releases of 160 m^3s^{-1} can only be sustained for 0.23% of the time only in the months of September and October just after the rainy season. Flows above 77 m^3s^{-1} occur just 71.2% of the time and flows above 120 m^3s^{-1} may occur only 2.1%. As a result, the mean annual energy generated may decrease by -14.3% to 1878 $GWhyr^{-1}$with the average plant factor 0.52.

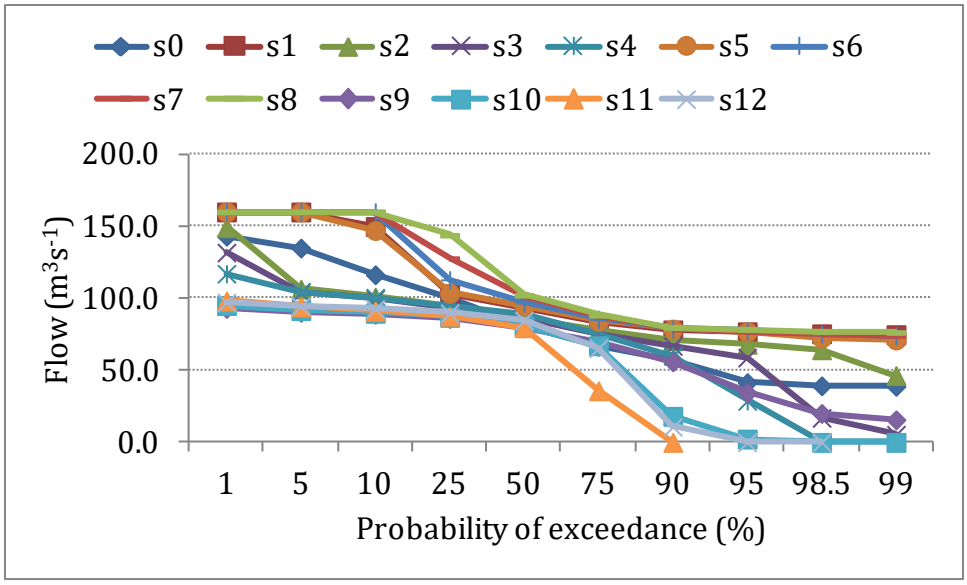

Figure 7-25: Probability of exceedence for the flow rate of Tana Beles HPP

Scenario s4

Under s4, the full irrigation development (i.e. 106,348ha of land) will be implemented and the climate is unchanged from the baseline condition. Although the flow released to the Tana-Beles HP exists 98 % of the time, the flow above the average flow of 77 m^3s^{-1} might occur for 76% of the time and flows above 120 m^3s^{-1} may occur for only 0.7% of the time. A maximum flow of 160 m^3s^{-1} may not occur in this scenario. Due to the combined effect of 953Mm^3 of withdrawal water for the irrigation in the Tana sub-basin with the unchanged climate, the mean annual energy to be generated may decrease by -16 % from the baseline to 1837 GWh. Furthermore, the average plant factor may also reduce to 0.51.

Scenario s5, s6, s7 and s8

These scenarios are based on the assumption that climate is changing under RCP 4.5 scenario (described in the previous section) combined with different level of irrigation and hydropower developments. The result of the scenarios suggested that energy production from Tana-Beles HPP might increase in the order of 3.2% to 36% as compared to the. The flow will be released 100 % of the time to the Tana Beles hydropower. The average flow of 77m^3s^{-1} will occur in the range of 94.4% to 98.3% of the time under s5 and s8 respectively. Furthermore, the high flows of 160 m^3s^{-1} may occur from 8% to 32% of the time as shown in the Figure 7-25. As the result, the mean annual energy to be generated might increase to 2977 GWh under s8 at maximum and 2359 GWh minimum under s6, consequently the average plant factor increases in the range of 0.63 to 0.83.

Scenario s9, s10, s11 and s12

As it is expected due to the combined effect of irrigation developments upstream of Lake Tana with the reduced precipitation climate change scenarios, the mean annual energy to be generated from Tana-Beles HPP may decrease at the maximum by -36% under s11 and a minimum by -24% under s9 from the baseline generated energy. The simulated minimum annual energy could be 1396 GWh yr^{-1} under s11 and the maximum would be 1677 $GWhyr^{-1}$ under s9, which all are

less than the designed capacity of 1719 $GWhyr^{-1}$. Hence, these are the worst-case scenarios that may have significant social and economic impact for the country.

Cascaded hydropower projects on the Abay River

(USBR, 1964) was the first comprehensive study harnessing the maximum hydropower potential of Abay River. The Karadobi, Mabil, Mandaya and Border dam sites were among the major cascaded hydropower potential sites identified and described. Later, (BCEOM, 1998a) adopted these options without further analysis. As the result, Ministry of Water and Energy carried out pre-feasibility study for Karadobi project in 2006 by (NORPLAN *et al.*, 2006). Subsequently, the Mandaya and Border projects pre-feasibility studies conducted in 2007. Recently, (NORPLAN *et al.*, 2013) introduced an additional option of a dam site at Beko-Abo that could be an alternative to the Karadobi project, and thereby avoid in-undation of the new bridge at Kessie, or as an element of a cascade of dams including Karadobi. Figure 7-28shows the longitudinal profile of the Abay River starting at the outflow of Lake Tana and ending at the border with Sudan that shows the full cascade development option.

Cascading options

The optimization of a cascade can depend on many factors and therefore at this stage simple comparisons are made between various options. NORPLAN *et al.* (2013) proposed four different cascading development options with two alternatives for the main upstream reservoir, Beko-Abo and Karadobi both with two downstream development options. The project options are shown as Figure 7-28 and the short summary of the cascade development options are presented below.

Option A: Beko-Abo High – Mandaya High
These two dams can utilize the full available head corresponding to the level just below the new Kessie Bridge and Mandaya dam site. The combination of the two full head developments gives the highest energy output for these two schemes combined.

Option B: Beko-Abo High – Mabil Low – Mandaya Low
The purpose of this alternative is to reduce negative impacts of the Mandaya High reservoir. The energy output is reduced mainly because of the loss of the 40m head of the Didessa inflow. To maintain the loss of this production estimated to 625 GWh a dam would need to be constructed in the Didessa River. The Mabil low dam is introduced to utilize the available head due to the reduced height of the Mandaya reservoir.

Option C: Karadobi – Beko-Abo Low – Mandaya High
Utilization of energy potential upstream the Kessie Bridge in a feasible way is found to be by development of the Karadobi dam. The Karadobi study implied that the optimum dam could be higher than the one presented in the prefeasibility study thus increasing the power and energy output. The dam site has the narrowest valley profile indicating the cheapest dam development. The Beko-Abo Low is introduced to utilize the head downstream of Karadobi followed by the Mandaya High reservoir. This cascade option is viable with small environmental impacts from the Beko-Abo Low. With Karadobi as the upstream main reservoir, this option gives the highest energy output and therefore chosen for this study for further analysis.

Option D: Karadobi - Mabil High – Mandaya Low

The purpose of this alternative is again to reduce negative impacts of the Mandaya High reservoir. The head downstream Karadobi and the Mandaya Low is utilized with a higher dam at the site described in Option B. The energy output for this option is only some 200 GWh less than Option C.

Impacts on hydropower production

Like many large-scale projects, the GERD is subject to a number of concerns and criticism with regard to jeopardizing downstream water security and livelihoods (Taye *et al.*, 2016), which created tension particularly between Egypt and Ethiopia (Liersch *et al.*, 2017). An assessment of the likely impacts of GERD, which is not in operation mode yet, comes along with a number of uncertainties is therefore crucial. Hence, optimizing the hydroelectric generation and the amount of water released to satisfy the water demand targets of the downstream countries should be taken into account for establishing the operation rule curve. The data for the target demands of the downstream countries are not available. Hence, the average historical annual flow of the Blue Nile being available for power generation expected to be 1,547 m^3s^{-1} (IPoE, 2013) during the design period was assumed as the average water demands of the downstream countries.

Cascading development option C described above is selected for further impact assessment in this study. Before proceeding to model simulation, establishing the operation rule curves for the proposed hydropower projects is a priori task. Two optimization models are applied as described under section 7.2.4 to attain the maximum energy and optimum downstream flow released to satisfy the demands of the downstream countries. The reservoir operation HEC-HMS model coupled with Excel spreadsheet and GA are applied for establishing the optimum operation rule curves. For the purpose of comparison, the monthly power production using two optimization methods are presented in Figure 7-26. Furthermore, the total annual energy generation, power production, reservoir evaporation and down stream flows of the two optimization methods are depicted in the Figure 7-27 below. The results envisaged that the two-optimization methods have a good agreement in all scenarios with minor differences. A trial and error optimization methods using HEC-HMS model by adjusting the stage discharge curves of the reservoirs simulates less amount of total annual energy for s9-s12 but higher for the other scenarios as compared to the simulation results of GA optimization method. However, the downstream outflow from GERD using a trial and error approach is higher than GA methods for all scenarios but less than the historical average flow with the exception of s7 and s8. Minimizing reservoir evaporation can also be another parameter for comparison. Reservoir evaporation at GERD for different scenarios using two candidate optimization methods is shown Figure 7-27. The result indicates that reservoir evaporations from the two-optimization methods have also a good match. Therefore, henceforth, the model outputs of HEC-HMS trial and error optimization methods is used for further impact analysis taking into account the high downstream flow simulation as an advantage to minimize the impacts of the downstream countries.

Table 7-22: Hydropower production and Energy generation simulation using HEC-HMS trial and error optimization method for GERD

	Power (MW)							
col. 1	col. 2	col.3	col. 4	col. 5	col. 6	col. 7	col. 8	col. 9
	Min	Max	Mean	St.dev.	EP99	EP95	EP90	Energy (GWh)
s1	367	5577	1559	770	501.4	1134.2	1311.9	14536
s2	321	4907	1512	548	1092.8	1092.8	1260.2	13699
s3	305	4750	1479	468	1088.1	1088.1	1212.7	13274
s4	927	1613	1434	78	1062.0	1062.0	1231.5	12116
s5	362	4729	1696	802	379.1	643.4	1118.9	14570
s6	363	4936	1861	1071	395.6	1203.7	1265.1	16274
s7	945	6271	1949	875	963.9	1149.1	1680.7	18623
s8	943	5754	1984	995	964.6	1131.9	1659.4	18982
s9	331	1319	1102	180	337.6	540.4	636.0	8266
s10	340	1392	1152	185	367.9	638.4	721.3	8913
s11	558	1126	1004	114	565.3	596.6	629.7	7081
s12	520	1130	1059	112	557.9	663.8	696.9	7572

a) b)

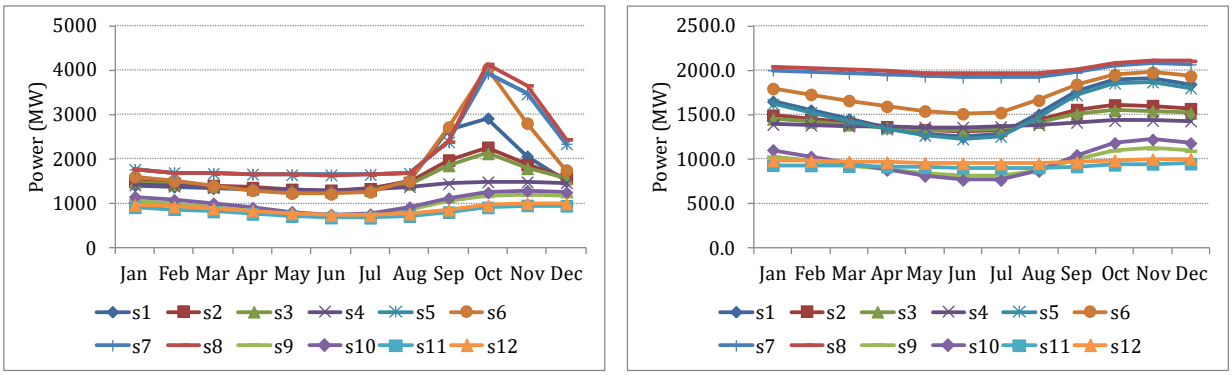

Figure 7-26: Average hydropower production of GERD under different climatic and water development scenarios: a) using HEC-HMS coupled with Excel spreadsheet rule curves, b) using GA rule curves.

The impact analysis result of the GERD hydropower projects under twelve different scenarios on the power and energy generation is presented in Table 7-22. The second, third and fourth columns in Table 7-22 shows the minimum, maximum and average hydropower production for different scenarios. The fifth column indicates the variations of the hydropower production using standard deviation. The sixth, seventh and eighth columns characterize the level of firm energy yields assuming exceedance probabilities (EP) of 90%, 95% and 99% of the daily HPP time series. The last column shows the total energy generation in $GWhyr^{-1}$. The installed capacity of GERD is 6450 MW with the aim to produce annual total energy of $16,153GWhyr^{-1}$

(Wikipedia, 2019). To meet this electricity target, an equivalent power of 1844MW would have to be produced. The loss due to seepage is not accounted for in this study, because related data are not available and are officially not envisaged.

In the case of no climate change effect, the total annual energy from GERD alone is around 12,116 to 13,699 GWh. In the case of canESM2 GCM under RCP4.5 climate change scenarios, the mean annual energy is increased to around 14,570 to 18,982 GWh, this again decreased to 7,081 $GWhyr^{-1}$ in GFDL GCM under RCP4.5 climate change scenarios. The total annual energy simulated from GERD under the climate scenarios of GFDL GCM is 50% less than the total annual designed energy, whereas, the energy generated under canESM2 GCM could be 17 % higher than the total annual energy during the design period. Hence, the highest energy could be generated under wet climate condition of canESM2 GCM under RCP4.5 scenario and the least energy could be generated under the dry climate condition of GFDL GCM under RCP4.5 scenario.

From an economic or engineering perspective, continuity (variability) and reliability (firm yields) of electricity supply are usually more important than average annual hydropower production (Liersch *et al.*, 2017). Considering these indicators, the upstream hydropower developments and climate change have large impacts on the performance of HPP. As the average annual energy is different among scenarios, the variations of daily power production are also different. S5 and s6 scenarios show much higher variations throughout the year with standard deviations > 57% of the mean daily power, while s4, s11 and s12 show small variations around 10 % of the mean daily power. The small variation under s4, s11 and s12 are because of the operation of the upstream hydropower dams. The highest EP values are achieved in the wet climatic conditions s7 scenarios with an EP90 of 1681MW, meaning that a daily minimal production of 1681MW is guaranteed for 90% of the days. The s8 scenario is in the same order, whereas the EP90 in the dry climate condition scenarios (i.e. projected using GFDL GCM) are only in the range of 630 to 721 MW. This indicates that the impacts of hydro-climatic conditions on the reliability of power generation are significant. For the wet climatic canESM2 GCM condition, the reliability of the power generation is high while for the dry climate condition (GFDL GCM) the reliability for power generation is low.

The maximal simulated daily hydropower value of GERD in the no climate change scenarios (s1-s4) is 5577 MW, which is less than the maximal capacity. This indicates that based on current climate condition, the target of 16,153 GWh annual total energy is never reached on average in the simulations, although it can be topped in extraordinary wet climatic conditions such as canESM2 GCM RCP4.5 climate scenario. The total annual energy generations under the current climate condition are 14,536, 13,699, 13,279 and 12,116 $GWhyr^{-1}$ for s1, s2, s3 and s4 respectively. Under the wet climate condition (canESM2 GCM of RCP 4.5 scenarios), the total annual simulated energy generations are increased to 14,570, 16,274, 18,623 and 18,982 $GWhyr^{-1}$ for s5, s6, s7 and s8 respectively. Under dry climate conditions (GFDL GCM of RCP4.5 scenario), the total annual simulated energy generations are decreasing to 8,266, 8913, 7081 and 7572 $GWhyr^{-1}$ for s9, s10, s11 and s12 scenarios respectively. The result envisaged that under the current climate scenarios, the highest simulated average annual energy value is 90% of the target. Under the wet climate scenarios, the maximum simulated total annual energy value is

117% of the target and for dry climate scenarios, the highest simulated total annual energy is only 55% of the target.

s1, s2, s3 and s4 are scenarios, used to analyze the single impacts of water resource developments with the assumption of no climate change effect. The result from s2 indicates that the evaporation loses from GERD alone and water demand for 214,882 ha of irrigation land (i.e. abstraction of 1695 Mm^3) could reduce the power generation of GERD by -15.2 % from the design capacity (16,153 $GWhyr^{-1}$). If the irrigation area increase to 382,644 ha and mean annual irrigation demand also increased to 3,210Mm^3 under s3, the power generation will decrease by -17.8 % from the target. Under s4, full irrigation development, when 42,0370 ha of land is irrigated with the mean annual water abstraction of 3,583Mm^3 associated with the full upstream hydropower developments, the power generation capacity of GERD might reduce by -25 % from the annual average designed capacity.

The maximum simulated daily hydropower production of GERD could be 6270 MW under s7, which is almost equivalent to the design capacity of 6,450MW. The simulation result also revealed that the target capacity of GERD generating 16,153$GWhyr^{-1}$ electricity could never be reached in all scenarios except s6, s7 and s8. The target energy can be obtained only when the canESM2 GCM RCP4.5 climate change scenario occurs. Liersch *et al.* (2017) carried out detail impact assessment of different operation management scenarios of GERD under current and future climate change on the hydropower and downstream flows. They applied five operation rules under the current and future climate change scenarios. To investigate the potential impact of climate change on the management of the GERD, an ensemble of four downscaled and bias-corrected global Earth System Models (ESMs) and six Regional Climate Models (RCMs) were used as input for SWIM hydrological model. Liersch *et al.* (2017) reported the simulated mean annual energy of around 13,000 GWh for low seepage rate scenarios and between 11,000 and 11,500 GWh for assuming medium seepage rates and around 9,000 GWh for the assumption of high seepage rate under current climate scenario (1961-1999). Hence, they concluded that even under optimistic conditions, the target is not reached under reference climate conditions, where 13,000 $GWhyr^{-1}$ are generated on average. In the RCP 8.5 climate scenario at the end of the 21st Century, the ensemble mean projects the mean annual energy potentials increasing by 650 $GWhyr^{-1}$, but the ensemble median a decrease by 340 $GWhyr^{-1}$. The simulated energy of this study under climate condition (s1-s4) has a good agreement with the low seepage rate scenario of the previous study as expected because seepage is not considered in this study. This indicates the robustness of the simulation result of this study.

Another recent study done by Mulat *et al.* (2018), evaluated the impacts of future water developments in the Eastern Nile region on energy generation by considering the current water use situation and proposed reservoirs in the UBNR basin in Ethiopia using different scenarios. The study was carried out by using a monthly time step and historical ensemble time series data as representative of possible near future scenarios. They indicated that at full development level, GERD could generate a maximum energy of 16,256 $GWhyr^{-1}$ when there is no cascade upstream of GERD. When there are more reservoirs in operation above GERD, there could be slight energy reduction of GERD to 15,376$GWhyr^{-1}$.

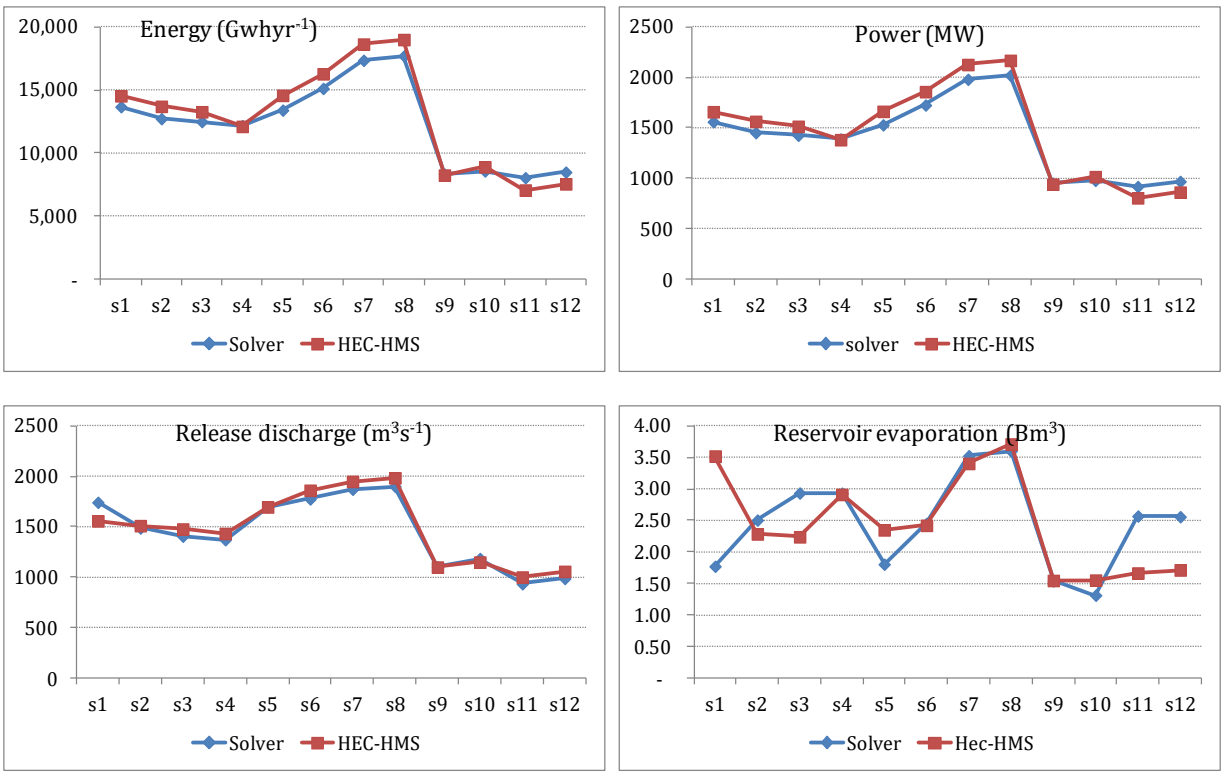

Figure 7-27: Comparisons of the two optimization methods.

This study also evaluates the impact of the four cascade dams for twelve different climate change, water, and land management scenarios, with the objective of maximizing power generation and releasing the downstream flow to acceptable quantity. The impact analysis result of the four cascaded hydropower projects under different scenarios on the energy generation is presented in Table 7-23. It is to be noted that for the midterm and short-term development scenario, only GERD hydropower project is supposed to be operational.

The simulation result of energy production for the different scenarios is provided in Tables 7-29. At full hydropower development level, maximum total energy of 50,047 $GWhyr^{-1}$ and minimum total energy of 24,213 $GWhyr^{-1}$ could be generated from four cascade projects under s8 and s11 respectively. Meanwhile GERD alone can produce total annual energy in the range from 7,081 $GWhyr^{-1}$ to 18,982 $GWhyr^{-1}$, and the minimum could be under s11 and the maximum could be under s8. The total amount of energy simulated from the four cascaded hydropower projects has a good agreement with the result of Abay basin master plan study, which estimated 55,000 GWh annual total energy by (BCEOM, 1998a). The preliminary study carried out by NORPLAN *et al.* (2013) during the pre-feasibility study of Beko-Abo hydropower project indicated that 50 year average of 31,255 GWh energy can be generated for option A, 30,283 GWh for option B, 33,062GWh for option C and 32,864 GWh for option D. The result of option C has a good agreement with the result of this report under s4 (without climate change condition) that revealed to generate 35,293 $GWhyr^{-1}$, see Table 7-23. A difference could be due to the size difference of the Border dam considered in the analysis of previous study and GERD in this report. During the pre-feasibility study, Border dam now called GERD was designed to the installed capacity of

1200 MW but now it is re-designed to 6450 MW. Mulat *et al.* (2018) also reported the maximum mean annual energy production of about 38,200 $GWhyr^{-1}$ under scenario's that combines four reservoirs (GERD, Karadobi, Beko-Abo low and Mandaya) in UBNR basin. Stamou (2019) calculated the mean annual energy equal to 46,620 $GWHyr^{-1}$ for the full development scenario that included 23 HPPs.

The economic damage due to the reduction of total energy production because of climate change as compared from the base line would be enormous. The Ethiopian electric utility (EEU), which is a public enterprise established for the purpose of selling and purchasing bulk electric power, amended a new tariff effected on 1st January 2019 (http://www.eeu.gov.et/index.php/current-tariff). If we take the average rate of 0.7807 birr/KWh, the annual economic damage due to the worst climate change scenario in the UBNRB (s11) will be around 13.7 billion Birr as compared to the base line scenario (s0). From this damage around 7.1 billion Birr is from GERD alone. In contrary, 6.4 billion birr per year benefit can be gained due to positive climate change effect of canESM2 RCP4.5 scenario as compared to the designed energy production capacity of the cascaded hydropower projects along the main stem of Abay River. GERD alone has a benefit of 2.2 billion Birr per year. SMEC (2008) reported a loss of about 200 million birr annually due to 12 % decrease in power production from only Tana-Beles HPP because of an additional irrigation development of 107,000 ha in the Tana Basin. This implies that climate change effect on water resource development over the UBNRB is enormous.

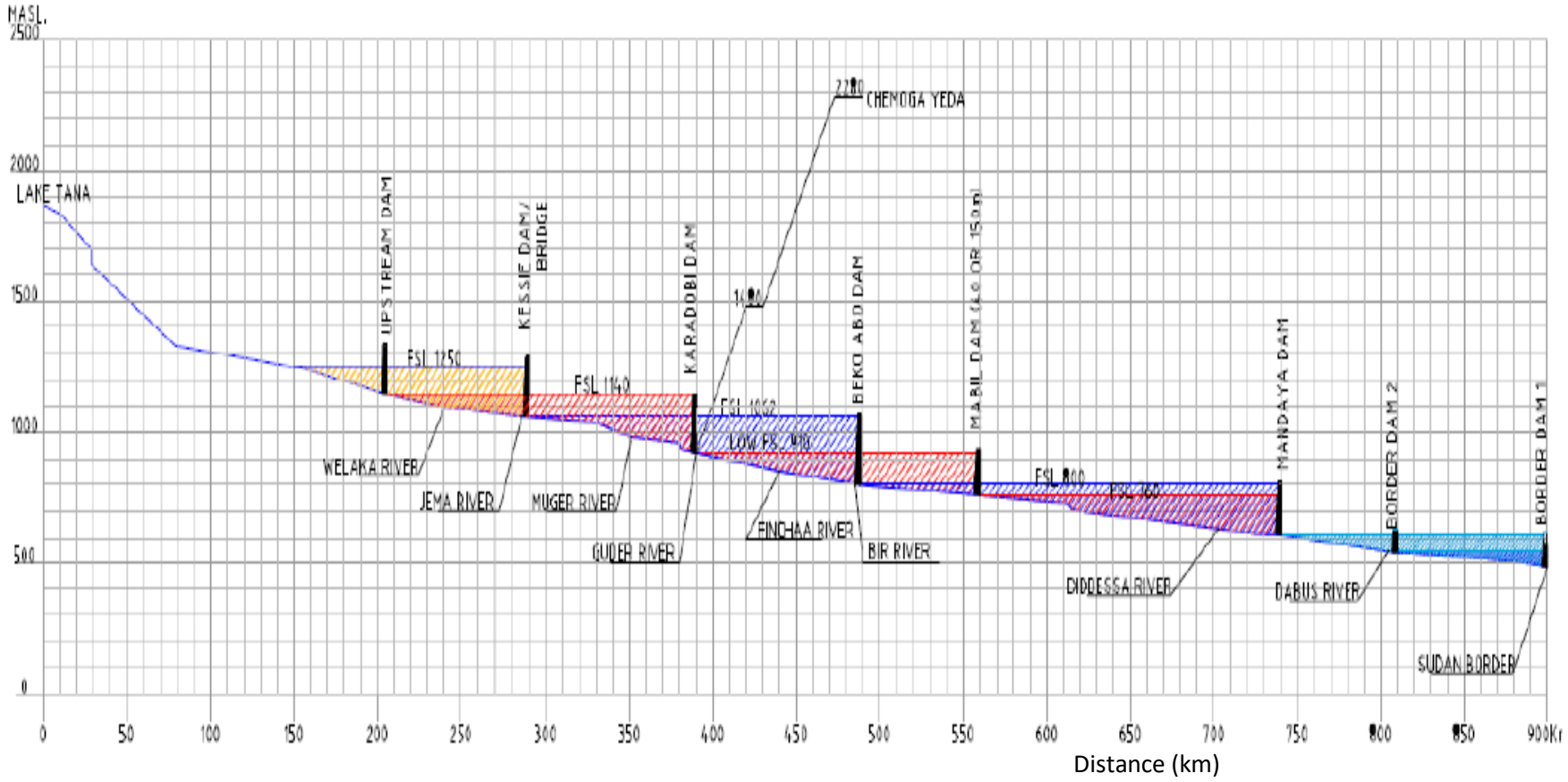

Figure 7-28: Longitudinal profile of Abbay River (UBNR) and proposed hydropower projects (NORPLAN *et al.*, 2013)

Table 7-23: Energy production from the cascaded hydropower projects at the Abbay River for different scenarios

	Design	s1	s2	s3	s4	s5	s6	s7	s8	s9	s10	s11	s12
		Turbine discharge (m^3s^{-1})											
Karadobi	800				495			708	714			334	370
Beko-Abo	900				877			847	843			629	678
Mandaya	1200				782			1163	1158			714	762
GERD	5400	1559	1512	1479	1434	1696	1861	1949	1984	1102	1152	1004	1059
		mean annual energy (GWh)											
Karadobi	8634				6829			11882	12066			5425	6133
Beko-Abo	4662				4352			4819	4698			3131	3603
Mandaya	12419				11996			14397	14301			8576	9215
GERD	16153	14536	13699	13274	12116	14570	16274	18623	18982	8266	8913	7081	7572
Total	41868	**14536**	**13699**	**13274**	**35293**	**14570**	**16274**	**49720**	**50047**	**8266**	**8913**	**24213**	**26523**
Change (%)		-10.0	-15.2	-17.8	-25.0	-9.8	0.7	15.3	17.5	-48.8	-44.8	-56.2	-53.1
		Hydropower production (MW)											
Karadobi	1600				780			1356	1377			619	700
Beko-Abo	800				497			550	536			357	411
Mandaya	2000				1369			1643	1633			979	1052
GERD	6450	1659	1564	1515	1383	1663	1858	2126	2167	944	1017	808	864
Total		**1659**	**1564**	**1515**	**4029**	**1663**	**1858**	**5676**	**5713**	**944**	**1017**	**2764**	**3028**

Impacts of GERD reservoir operation on downstream flow

Discharges released from a reservoir are depend on various factors, such as targets for hydropower, inflows into the reservoir (depending on hydro-climatic conditions and upstream land and water management), losses by seepage, and evapotranspiration from the reservoir area. In the case of GERD, many of these variables are uncertain. Dam operation strategies can have major impacts on seasonal discharge patterns, particularly in the Blue Nile River, characterized by one peak discharge season and a prolonged low flow period. Figure 7-30 shows the monthly pattern of outflow of GERD before and after the operation. Surprisingly, the model simulation result of all scenarios indicates an increase of discharges during the dry period (January–May). For instance, a comparison is made between the model simulation result of s0 and s1 to analyze the impacts of GERD without any climate and anthropogenic effect on the downstream flow. The result indicates that the discharge during the dry period increases of up to 450% (from around 270–1300 m^3s^{-1}) and a decrease of average monthly discharges during the rainy season from maximal 5454m^3s^{-1} down to 1358 m^3s^{-1} in August, when discharges are used to re-fill the reservoir.

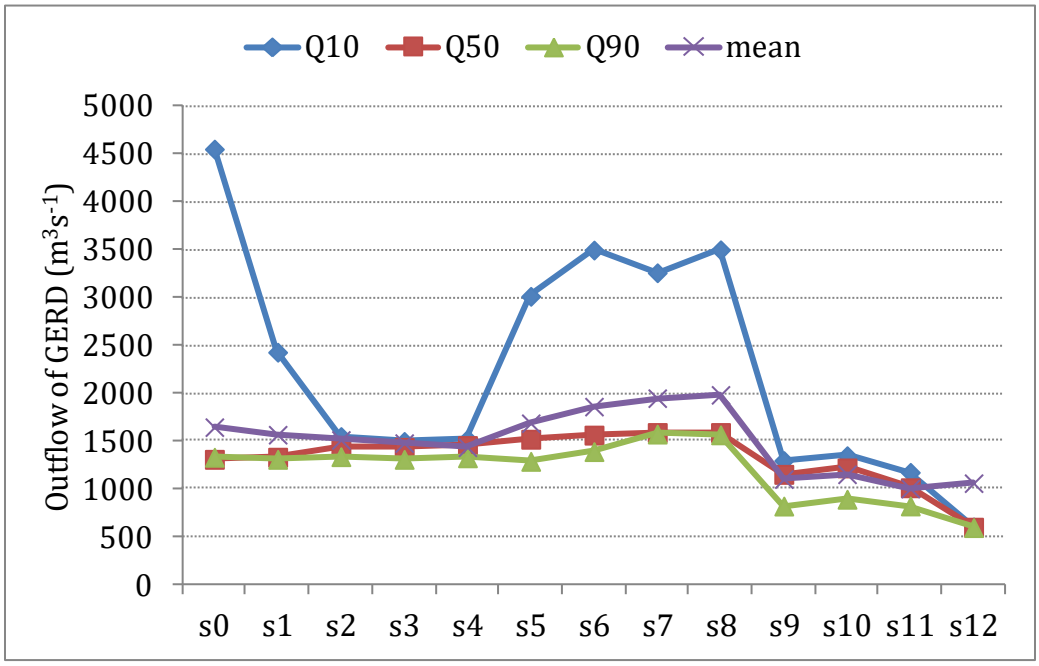

Figure 7-29: Low, median and high streamflows of GERD under different sceanrios

Furthermore, GERD can reduce the inter-annual variability of downstream discharges (Figure 7-30). Given the large capacity of the GERD, this is not surprising. The most obvious simulation result that significantly decreases the interannual variability are under s4, s7, s8, s11 and s12, where the inflows to GERD are also regulated by the upstream reservoirs. Besides the reduced inter-annual variability, daily dynamics are also significantly influenced (Figure 7-29). Not surprisingly, with the GERD online, low flows are augmented to the extent that about 1337 m^3s^{-1} are secured at least 90% of the time, compared to only 225m^3s^{-1} under natural condition Figure 7-29. The low flow (Q_{90}) further increased to a maximum about 1573 m^3s^{-1} under s7 and a minimum about 596 m^3s^{-1} under s12 due to the climate change effects. In contrast, the high flow

(Q_{10}) decrease from 4550 m^3s^{-1} under natural condition (s0) to 603 m^3s^{-1} under s12 and 3498 m^3s^{-1} under s8, at an exceedance probability of 10%, see Figure 7-29 and Figure 7-30. The flow above the average flow of 1547 m^3s^{-1} under natural condition (s0) might occur for a maximum of 98.5% of the time under s8 scenario, while under s3; this flow is available only for 24.8 % of the time. However, 1547 m^3s^{-1} may not occur under s9, s10, s11 and s12. Hence, the operational strategy of the GERD may change the annual hydrologic cycle, particularly for downstream countries.

Table 7-24: Outflow statistics from GERD for different scenarios

Scenario	Min	Max	Median	Mean	Stdev	CV
s0	20	10887	669	1673	1914	1.14
s1	496	4839	1331	1559	639	0.41
s2	440	4291	1441	1512	410	0.27
s3	419	4160	1434	1479	363	0.25
s4	1177	1550	1454	1434	84	0.06
s5	529	3644	1533	1686	605	0.36
s6	501	4589	1563	1861	857	0.46
s7	1189	5996	1589	1949	788	0.40
s8	1188	4985	1589	1984	826	0.42
s9	456	1370	1153	1102	197	0.18
s10	468	1407	1219	1152	195	0.17
s11	744	1302	1012	1004	133	0.13
s12	701	1304	1073	1059	125	0.12

The impact of the GERD on the quantity of discharges released downstream is also influenced by losses via reservoir evaporation (ETRes). Table 7-25 shows average annual ETRes, inflows and outflows. Mean annual inflow volumes are in the range between 34Bm^3 and 68Bm^3 while the mean annual outflow volumes are between 32BM^3 and 63Bm^3, mean reservoir evaporation volume between 1.5Bm^3 and 5.2Bm^3. The evaporative losses from the reservoir surface area are on average 6.1$mmday^{-1}$ in the reference period (1984-2011), which amounts to approximately 2235 $mmyr^{-1}$. The reservoir simulations at GERD for the twelve scenarios indicate that annual reservoir evaporation losses relative to the annual inflow volumes into the GERD estimated to 3.4–6.5 % (Table 7-25). During the design period, evaporation of water from the reservoir was estimated to be at 3% of the annual inflow volume of 48.8 km^3, which corresponds to an average volume lost through evaporation of around 1.5 Bm^3 annually (Wikipedia, 2019).

The simulated reservoir evaporation of this study has an agreement with the previous study done by Liersch *et al.* (2017), which reported evaporative losses values under regular operation in the range between 7% and 8% of average annual inflows (3.8 Bm^3) under reference climate conditions that corresponds to 5.6 $mmday^{-1}$ or 2044 $mmyr^{-1}$. They also reported that the volume evaporating from the reservoir area to increase by 0.1 Bm^3yr^{-1} under ensemble mean of RCP 8.5

scenarios of five CMIP5 Earth system models (ESMs) and 10 regional climate models (RCMs) from CORDEX in 2070–2099.

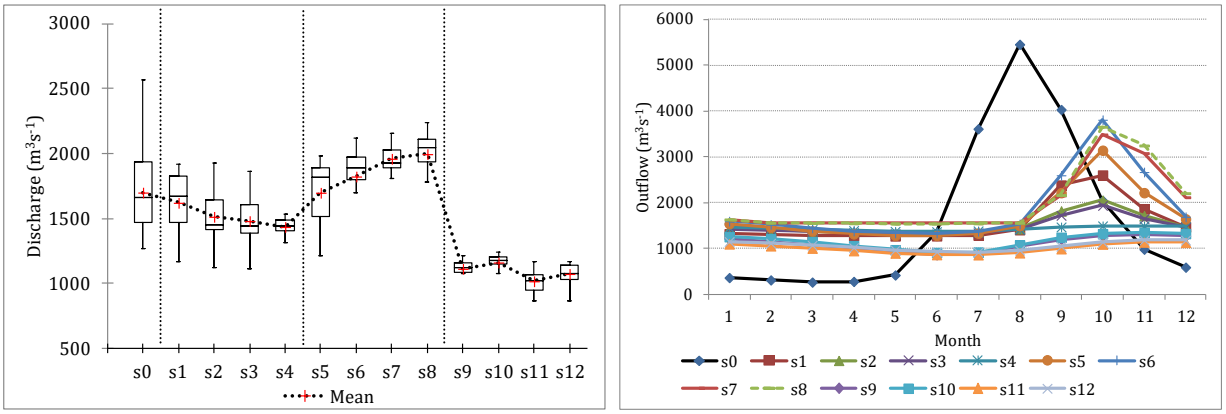

Figure 7-30: Outflow of GERD: a) inter-annual variability, b) mean monthly outflow

Table 7-25: Mean annual inflow, outflow and evaporation of GERD

	Inflow (m^3s^{-1})	Inflow (Bm^3)	Outflow (m^3s^{-1})	Outflow (Bm^3)	ET GERD (Bm3)	Ratio (%) EtRes/inflow
s0	1645	51.9	1645	51.9	0.0	
s1	1709	53.9	1566	49.4	3.5	6.5
s2	1622	51.2	1511	47.7	2.3	4.5
s3	1587	50.0	1478	46.6	2.3	4.5
s4	1552	48.9	1434	45.2	2.9	5.9
s5	1862	58.7	1695	53.5	2.4	4.1
s6	1980	62.4	1860	58.7	2.1	3.4
s7	2110	66.6	1948	61.4	3.7	5.6
s8	2147	67.7	1983	62.5	3.7	5.5
s9	1179	37.2	1102	34.8	1.6	4.4
s10	1234	38.9	1152	36.3	1.7	4.3
s11	1065	33.6	1004	31.7	1.9	5.7
s12	1125	35.5	1060	33.4	2.0	5.6

Considering the large capacity of the reservoir, which could store approximately 1.5 years of long-term average discharges of the Upper Blue Nile River, and the fact that its main purpose is the generation of hydropower, the GERD will significantly alter the discharge regime downstream. Almost independent of how the dam will be operated, drastic impacts on the annual cycle of discharges can be expected, shifting from a strong seasonal to a completely balanced regime with almost constant discharges each month (Liersch *et al.*, 2017). The daily outflow coefficient of variance for GERD under natural condition (s0) is higher as compared to other

scenarios, when GERD and other upstream hydropower project start operation. The value of the coefficient of variance at El Diem under natural condition is 1.14 but for other scenarios, it is less than 0.5, see Table 7-24. This is especially important for Sudan due to the limited water storage capacity within the country, which is not the case for Egypt with the large storage capacity of the Aswan High Dam (AHD). These results are similar to those found by (Arjoon *et al.,* 2014; McCartney *et al.,* 2010), who showed a significant reduction in wet season flow and increases in dry season flow due to regulation from GERD. The GERD will also retain significant amounts of silt within the reservoir, likely extending the effective life of downstream hydropower facilities.

Comparison of Lake Tana drawn-down with previous study

The current research output is consistent with the result of the previous studies. For instance, McCartney *et al.* (2010) developed a water balance model of Lake Tana to evaluate current and future water resources development in the Lake Tana Basin. McCartney *et al.* (2010) reported the mean annual Lake water level will be lowered by 0.44 m if the full development scenario in the Lake Tana catchment is implemented without allowing the environmental flow to the Abay River. Furthermore, the average surface area of the lake will decrease by 30 km^2. In some years, this will be reduced by as much as 81km^2 during the dry season. According to McCartney *et al.* (2010) variable environmental flow requirements exacerbate the drop in lake water levels. For the full development scenario, lake level exceeds 1785 masl just 60% of the time and the mean lake area is reduced by 57km^2. Furthermore, the amount of power produced from Tana-Beles HPP is reduced between 1% and 3% depending on the scenario, declines from 2247.0 GWh to 2207.1 GWh and 2197.1 GWh if all the planned and all the possible irrigation schemes are developed respectively.

Halcrow *et al.* (2010) did detail water balance modeling and impact assessment on different development scenarios in the Tana and Beles sub-basins. They reported a reduction of mean lake level by 0.45m and mean lake area by 36 km^2. The Lake level remains above 1785 masl 85 % of the time when the Tana-Beles scheme is operated using the SMEC operation rule (min. 1784.75 masl) under full development scenario. Furthermore, the analysis showed that a 3% reduction of mean annual outflow from Lake Tana to Tana-Beles HPP, about 2,305 Mm^3 annual flows could be diverted. Meanwhile, the mean annual lake outflow to the Abay river simulated about 975Mm3. Despite a small decline in annual flows, the criteria for environmental maintenance flows remain satisfied at the waterfall. In regard to hydropower, (Halcrow et al., 2010) also reported a reduction of electricity production by 3% to about 1,805 $GWhyr^{-1}$.

SMEC (2008) also assessed some of the scenario impacts in the Tana-Beles sub-basin by applying the river basin simulation model MIKE BASIN, using the operation rule curves developed by them. The result revealed that the variation between maximum and minimum levels is almost 3m as compared with 2.3 m under natural conditions. The annual flow volumes entering the Abay from Lake Tana are about 29% of the natural flow volumes in the current condition. In the full irrigation development scenario, this percentage decreases to about 19% of the natural flow volumes. With regard to the hydropower, the total hydropower production under full development scenario decreases by about 11% as compared to the current condition due to an additional irrigation development of 107,000 ha in the Tana sub-basin.

Chapter 8 Conclusions and recommendations

Upper Blue Nile River Basin is one of the prospective basins for Ethiopia to develop huge amount of hydropower and irrigation projects, because of its ample water resources potential and its geographical landscape providing a good opportunity for hydropower production. Moreover, the untouched land in the lowland part of the basin and land suitability for irrigation around Lake Tana makes it favorable for irrigation development. Hence, the government of Ethiopia has planned large-scale irrigation and hydropower projects across the basin as a strategy for alleviating poverty. However, land degradation, deforestation, increasing water demand due to population and economic growth, and urbanization are becoming the major challenges and threatening issues for future water resource developments by altering the dynamics of the hydrology and water availability of the basin. The implication of climate change effect on the availability of water resources should also be a great concern for the sustainability of these large scale projects otherwise the consequences becomes catastrophic. Under such circumstances quantifying the amount of the water resources potential due to the competing demands for power generation, irrigation, water supply and other useful developmental projects is becoming crucial for sustainability of the developmental projects.

This dissertation assessed long-term trends of main driving forces of streamflow such as rainfall and temperature, which have an enormous advantage for planning and management of limited water resources. A physically based SWAT hydrological model was applied for characterization and quantification of catchment processes primarily how changes in LULC and climate have affected streamflow and water balance components. This can be essential for setting alternative strategies for future developments particularly to the shared water resource in the case of Abay River. Statistical downscaling techniques (LARS-WG and SDSM) have been used to assess the possible future climate change of UBNRB employing a multi-model approach. Furthermore, research on the interdependencies of the water users upstream-downstream in conjunction with the future climate change scenarios, on water availability is indispensable for sustainable water resources development and for providing concrete and concise information for water managers, policy and decision makers. Hence, HEC-HMS semi-distributed model was used to quantify the impacts of combined future climate change and water resource developments on the hydrology of the basin, Lake Tana water level, irrigation and hydropower sectors.

The long-term trends and change points of hydro-climatic variables such as rainfall, maximum temperature, minimum temperature and streamflow in the UBNRB were investigated using Mann-Kendall (MK) trend test and Pettitt change point detection (Chapter 4). The results of trends of meteorological variable in the basin depict a number of significant trends, both increasing and decreasing. With regard to rainfall time series, the study could not find any consistent change or patterns of trends among the investigated 15 rainfall stations. Thus, the results of the trends across the investigated rainfall stations are heterogeneous. For the daily time series, no statistically significant trend existed in seven stations, but a statistically significant trend existed in six rainfall stations and decreasing trend in the remaining two. On monthly and annual time scale, the MK trend test result showed that no trend existed in 11 stations, while statistically non-significant increasing trends exist in three stations and a decreasing trend exists

in one station. The MK test showed increasing trends for annual, monthly, and long rainy-season basin wide areal rainfall series, whereas no trend for daily, short rainy and dry season rainfall series appeared. For streamflow, the MK test's result for daily, monthly, annual, and seasonal (dry, long and short rainy seasons) streamflow time series at El Diem station showed a positive trend, the magnitude of which is statistically significant. The Pettitt test also detected increasing trends for daily, annual, long-rainy and short rainy-season streamflow at El Diem. For the monthly and dry season's streamflow, Pettitt test detects no change at El Diem flow station. However, the minimum and maximum temperature in ten stations in the basin reveals statistically significant increasing trends. The mismatch between the rainfall and the streamflow trend magnitude could be associated with evapotranspiration, which is attributable to the combined effect of LULC change and climate change, the infiltration rate due to changing soil properties, rainfall intensity and rainfall extreme events.

This dissertation also investigated the driving forces to the observed changes in hydrological variables (e.g. the combined and isolated effects of climate change and LULC changes) on the streamflow of UBNRB using SWAT hydrological model (Chapter 5). LULC change detection during the period 1973-2010 was assessed by comparing the classified Landsat images. The results indicated that the expansion of cultivated land and diminish in forest coverage were the dominant processes. The rate of deforestation was high during the 1973–1995 periods. This was probably due to the severe drought that occurred in the mid-1980s and a large population increase resulting from the expansion of agricultural land. On the other hand, forest coverage increased by 3.4% during the period 1995 to 2010. This indicates that the environment was recovering from the devastating drought in the 1980s, regenerating of forests as the result of afforestation program initiated by the Ethiopian government, and due to soil and water conservation activities accomplished by the communities.

SWAT was developed in the United States with a temperate climate, which has different characteristics with monsoonal climate. In monsoonal climates, long periods of rain can lead to prolonged soil saturation whereas during the dry period, the soil dries out completely, which may not happened in temperate climates. Nevertheless, the results from calibration and validation revealed that the SWAT model represents the monthly hydrographs very well, and therefore, SWAT can be applied in the study area if additional site-specific data containing soil and land use information is properly integrated into the model with high confidence. For the calibration period, the values of coefficient of determination (R^2), Nash-Sutcliffe coefficient (NSE), and Relative volume error (RVE%) range from 0.79 to 0.91, 0.74 to 0.91, and −3.4 % to 4 %, respectively.

The SWAT hydrological model result showed that the combined effects of the LULC and climate changes increased the mean annual streamflow by 16.9 % from the 1970s to the 2000s. The increased mean annual streamflow could be ascribed to the combined effects of LULC and climate change. The LULC change alters the catchment responses. As a result, SWAT model parameter values could be changed. For instance, the expansion of cultivation land and the shrinkage of forest coverage from 1973 to 1995 changed the basin average curve number (CN2) parameter values from 72.9 in 1973 to 74.7 and 75.6 in 1985 and 1995 respectively. Increasing

of CN2 value might increase surface runoff and decrease base flow. Similarly, the increase in rainfall intensity and extreme precipitation events led to a substantial increase in ratio of surface runoff to total streamflow (Qs/Qt), a substantial decrease in baseflow to total streamflow ratio (Qb/Qt), and ultimately to an increases in the streamflow during the 1971–2010 simulation period.

The "fixing-changing" approach (changing LULC data of 1973, 1985, 1995, and 2010 but fixing constant climate data of 1970s) result revealed that the isolated effect of LULC change could potentially alter the streamflow generation processes. The result shows that surface runoff is increasing while baseflow is decreasing due to expansion of cultivated land and reduction of forest coverage that reduce evapotranspiration during the periods 1985 and 1995 as compared to the baseline period 1973 LULC map. In general, a 5.1 % reduction in forest coverage and a 4.6 % increase in cultivated land led to a 9.9 % increase in mean annual streamflow from 1973 to 1995. The contribution of the effects of isolated climate change and isolated LULC changes indicated that surface runoff simulation due to combined effect increased by 20.9 mm between 1970s and 2000s periods while the isolated climate changes effect increased the surface runoff simulation by 20 mm, which accounted for about 95.7 % of the total surface runoff increment. The isolated LULC changes increased surface runoff by 0.3 mm, which accounted for 1.4 % of the total surface runoff change (20.9 mm). Between this simulation period, combined changes of LULC and climate decreased baseflow by -10.9 mm, and the percent contributions were 94.8 % (-10.9 mm) for the climate change and 5.2 % (-0.6 mm) for the LULC change. The SWAT simulation indicated that the impacts of climate change are more substantial than the impacts of LULC change. Surface water is no longer used for agriculture and plant consumption in areas such as the UBNRB, where water-storage facilities are scarce. On the other hand, base flow provides the most reliable source for the irrigation needed to increase agricultural production. Hence, the increasing amount of surface water and diminished base flow caused by both LULC and climate changes negatively affect socio-economic developments in the basin. The analysis provides a better understanding and substantial information about how climate and LULC change affects streamflow and water balance components separately and jointly, which is useful for basin-wide water resources management.

The future climate change of the UBNRB was analyzed using two widely used statistical downscaling techniques (Chapter 6). General circulation models (GCMs) are the prime tools used in the projection of climate into the future. However, their coarse resolution hinders their direct use in catchment scale studies. Downscaling techniques are therefore used to bridge the coarse resolution GCM outputs with the catchment scale climatic variables. Reliability of downscaling results is an important issue in climate change impact studies due to the presence of model errors and uncertainties associated with the GCMs and downscaling techniques. Hence, in order to overcome the uncertainties originating from different GCMs, a multi-model approach was employed. In total, 27 systematically selected future climate scenarios were produced for each period, which might be representative to understand fully and to project plausibly the future climate change in the study area and to retain information about the full variability of GCMs.

- 6 CMIP3 GCM3x3 SRES (A1B, B1 and A2) scenarios= 16 scenarios using LARS-WG (3 GCMs had no A2 scenarios)
- 3 CMIP5 GCMs x 2 RCP scenarios (RCP4.5, RCP8.5) = 6 scenarios using LARS-WG

- 1 CMIP5 GCM (canESM2) x 3 RCP scenarios (RCP2.6, RCP4.5, RCP8.5) = 3 scenarios using SDSM
- 1 CMIP3 GCM (HadCM3) x 2SRES (A2a, B2a) scenarios = 2 scenarios using SDSM

Moreover, two widely used statistical downscaling methods were applied, namely the regression downscaling technique (SDSM) and the stochastic weather generation method (LARS WG) for this particular study.

Three weather parameters: precipitation, minimum and maximum temperature were simulated using LARS-WG for 26 observed stations. The statistical result analysis of performance measure between observed and generated climatic variables revealed that both LARS-WG and SDSM models perform very well in simulating the climate variables and therefore they can be used with high confidence for further climate change studies.

Further comparative performance evaluation between the three models (HadCM3/SDSM, canESM2/SDSM and LARS-WG) were tested for the base line period of 1984-2011 in representing the current situation quantitatively and qualitatively particularly for precipitation, as it is the most difficult climate variables to model. The result suggested that SDSM using canESM2 GCM captures the long term monthly average very well at most of the stations and it ranked first from others. However, LARS-WG performed best in qualitative measures in capturing the distribution and extreme events of the daily precipitation than SDSM. The reason for the superiority of one method to another one, can be attributed to each model's methods of modeling. For instance, in SDSM a regression equation is established between the large-scale predictor variables and the predictors with local scale. This equation is created by bias correction and variance inflation in a way that the model can produce a close output to the observed data. While in LARS-WG model no large-scale weather variables is used in the modeling process. But this model analyzes the observed data of precipitation and temperature, and calculates the statistical characteristics based on the observed data, and in the next step, it changes its statistical characteristics based on the change factor in large-scale weather variables. The poor performance of SDSM would indicate the difficulty in finding climate variables from the NCEP data that could explain well the variability of daily precipitation. Therefore, LARS-WG would be more preferred in areas of the UBNRB with its high climatic variability to simulate the distribution and extreme events of the precipitation correctly, which is crucial for a realistic assessment of flood events and agricultural production.

Future climate projections downscaled by the two statistical down scaling techniques (LARS-WG and SDSM) are used to assess impacts on the hydrology of the upper Blue Nile River Basin. The major interest is to evaluate if the downscaled climate projections provide consistent results among the GCMs and downscaling methods. In LARS-WG model, the downscaling result reported from the six GCMs showed large inter model differences, two GCMs reported precipitation might decrease while four GCMs reported precipitation might increase in the future. The multimodal average result showed that the future precipitation may generally increases over the basin in the range of 1 % to 14.4 %. The downscaled precipitation from three CMIP5 GCMs using representative concentration pathways (RCP 4.5 and RCP 8.5) showed a greater tendency towards a decrease in the future in the UBNRB. The multi-model average result showed that precipitation might decrease in the future in the range of -4 % to -1.4 % under

RCP4.5 and RCP8.5. The downscaling result using SDSM indicates a general increase in mean annual precipitation for three time windows of the 21st century period for all five scenarios (A2a and B2a for HadCM3 and RCP2.6, RCP4.5 and RCP8.5 for canESM2) in the range of 2.1 to 43.8 %. Since no GCM is perfect as discussed below, and high uncertainities in simulating precipitation in the UBNRB, an ensemble value of results from the 10 GCMs with 27 different scenarios can provide a meaningful estimate. Based on this argument, the plausible mean annual precipitation might increase by 2.4, 4.6 and 8.1% for the period 2030s, 2050s and 2080s respectively.

Regarding temperature, the downscaling result of Tmax and Tmin showed an increasing trend consistently in all months and seasons for the 21th century period in all 27 different scenarios. The large inter model differences for simulating precipitation or uncertainties in climate predictions arises from three distinct sources (the natural variability of the climate system e.g. changes in solar activity, scenario and model uncertainties). Usually sequences of steps are undertaken to produce a climate change projection at global and regional scales. The first step to produce a climate change modeling is generation of scenarios of green house gas (GHG) and aerosol emissions based on hypotheses of future socio-economic and technological development. It is indeed essentially impossible to predict what will be socio-economic and technological development over the next century that will lead to different emission pathways. This source of uncertainty thus falls under the category of "intrinsic" and essentially will never be eliminated (Giorgi, 2010). GCMs are affected by uncertainties due to poor knowledge of the biogeochemical cycles and approximate representation of relevant processes associated with their differences of resolution and assumptions of physical atmospheric processes to represent local scale climate variables, which are typical characteristics for Africa. Climate model projections have generally a low convergence in the area of UBNRB (Gebre and Ludwig, 2015). This also illustrates that more GCMs should be considered in the study of climate change to reduce the uncertainty of GCMs.

In addition, climate projections are produced via statistical down scaling tools, which are also affected by substantial uncertainties related to our imperfect knowledge and description of relevant processes in the climate system. A further comparison between two downscaling methods was made for future simulation to understand uncertainties related to modeling tools. The HadCM3 GCM A2 scenario was used in common for two (LARS-WG and SDSM) downscaling methods to test whether the downscaling methods may affect the GCM result under the same forcing scenario. The results obtained from the two downscaling models were found reasonably comparable and both approaches showed increasing trends for precipitation, Tmax and Tmin. However, the magnitude of the downscaled climate data from the two methods indicates that LARS-WG over predicts precipitation and temperature compared to SDSM. The differences in the future predictions are the result of the differences in the basic concepts behind the two downscaling techniques. The SDSM uses large-scale predictor variables from GCM outputs, which can be considered as more reliable for climate change prediction using multiple linear regressions. However, the LARS WG uses the relative change factors (RCFs) derived from the direct GCM output of only those variables, which directly correspond to the predictands. Hence, because of the well-known fact that GCMs are not very reliable in simulating precipitation, the error induced from the GCM output for precipitation will propagate the error of downscaling. Therefore, the performance of LARS-WG to downscale precipitation needs more caution (Dibike *et al.*, 2005).

In general, this dissertation has shown that climate change will likely occur that may affect the water resources and hydrology of the UBNRB. Moreover, it provides substantial information that the choice of downscaling methods has a contribution in the uncertainty of future climate prediction. With respect to the future climate in the UBNRB, there is high confidence that temperatures will rise. However, there is much less certainty about future precipitation because of the low convergence in climate model rainfall projections in the UBNRB (Conway, 2005). Based on the performance evaluation results obtained, both SDSM and LARS-WG models can be adopted with reasonable confidence as downscaling tools to undertake climate change impact assessment studies for the future. However, LARS-WG is more suitable for extreme rainfall impact assessment study such as floods and droughts.

Finally, the combined effects of climate change and water resource developments on the availability of water, Lake Tana reservoir level fluctuation, irrigation and hydropower production was analyzed using HEC-HMS model (Chapter 7). Before applying the model for impact assessment, the model is calibrated and validated. The statistical performance indices of NSE, R^2 and RVE are used for performance evaluation. The results obtained during the calibration and validation periods are satisfactory and acceptable. Once the HEC-HMS hydrological model is calibrated and validated the future streamflow projection is simulated under the RCP 4.5 forcing scenario of canESM2 and GFDL GCMs. The model simulation results indicate that the changes in climate will affect the basin hydrology. Under a midrange climate scenario of (RCP4.5) from canESM2 climate model, streamflow at El Diem station may increase by 22.6 %, 43 % and 55 % in the period 2030s, 2050s and 2080s respectively over the UBNRB. However, the streamflow may decrease by -21 %, -25 % and -21 % using climate variables downscaled from GFDL CMIP5 GCM under RCP4.5 scenario as input.

Furthermore, this dissertation also analyzed the possible impacts arising from the combined future water managements and the climate changes of the UBNRB basin and its sub-basins. In order to analyze the impact assessment, optimization rule curves for the reservoirs and for the Lake Tana are established. The reservoir operation HEC-HMS model coupled with Excel spreadsheet and genetic algorithm (GA) are tested for establishing the optimum rule curves. The simulation results of two methods with regard to energy, outflow from GERD and GERD reservoir evaporation are similar. The impact assessment results indicate that the impacts of climate change over the UBNRB is significant on the Lake Tana level fluctuation, hydrology and water infrastructure developments (irrigation and hydropower) than the impacts arising from physical developments of water resources.

Overall, the results from the combined impact assessments in this study and others (Halcrow *et al.*, 2010; McCartney *et al.*, 2010; SMEC, 2008) showed that the magnitude of the rise and drop of Lake level is depend on the operation of Tana-Beles HPP, future climate change scenario and level of future irrigation area developed in the Lake Tana sub-basin. If the climate change projection of canESM2 GCM under RCP4.5 scenario occurred and combined with full development, (s8) then it would have positive impacts on the Lake Tana level that might increase maximum by 0.1m and the reservoir surface area might increase by 4.2 km^2 when compared with the area during the natural flow condition. Meanwhile, under these scenarios, the mean annual energy simulated from Tana-Beles HPP might increase to 2977 GWh from 2193 GWh energy during the baseline period. In contrary, when climate change projection of GFDL GCM under

RCP4.5 scenario is combined with the full planned water developments in the Tana sub-basin (s11), the environmental and social impacts arising from the drawing down of water levels and reduction of lake area and flow to the Abay River will exacerbate. Under such circumstances, lake water levels lower up to by 1.03 m as compared to the natural flow condition of Lake Tana. Consequently, the mean lake area might reduce by a maximum of 47.4 km^2 from 3053.2 km^2 to 3005.8 km^2. The mean annual energy to be generated from Tana-Beles HPP may decrease at the maximum by -36 % to 1396 $GWHyr^{-1}$ under s11 from the baseline generated energy (2193 $GWhyr^{-1}$).

The decline in water levels is likely to have significant impacts on the ecology of the lake, particularly in the littoral zone, and result in the desiccation of the wetlands surrounding the lakeshore. The reduction of Lake Area can allow the community who are living around the Lake to extend their farming activities towards the receded fringe of the Lake. The expansion of recession wetland cultivation has caused the loss of riparian vegetation, increase run off and soil erosion (McCartney *et al.*, 2010). Application of fertilizer, insecticide and pesticide chemicals for the irrigation and recession wetland cultivation has a direct effect on the Lake water quality. As the water level declines and the lake retreats, the natural ecosystem will be seriously disrupted.

Increased desiccation of reed beds is likely to result in the loss of fish breeding habitats affecting the livelihood of many people who depend on fishing from Lake Tana. The potential fish production of the lake is estimated to be 10,000 tons yearly (Janko, 2015). However, its current fish production is less than 1,000 tons a year due to the spread of the aquatic weed water hyacinth around fish spawning grounds. To make matters worse, inflowing rivers carry heavy loads of soil and suspended sediment into the lake, which affects the water quality and creates favorable conditions for the spread of the weed. A trade-off also exists between the lake ecosystem and the ecosystem of the Abay River and the Tis Issat Falls. It is also important that Lake outflows attempt to preserve flows over the Tis Issat Falls for aesthetic reasons, as these falls are an important tourist attraction in Ethiopia for domestic and international visitors. The simulated mean annual outflows to the Abay River under s9, s10 and s11 are 966, 955 and 899 Mm^3, which are marginally less than the minimum environmental flow recommended by Bellier et al. (1997). A further decline in flows over the Tis Issat Falls would likely impact on tourist numbers resulting in a loss of income for many local people who rely on tourist for their livelihoods. Since the livelihoods and well-being of many people are directly dependent on Tis Issat Falls, careful consideration is needed regarding the partitioning of lake outflows between the Abay river and those transferred to the Tana-Beles HPP.

At full irrigation development stage, 114,134 ha of land that corresponds to 24% of the total planned irrigation area in the UBNRB is planned to be implemented in the Lake Tana sub-basin, which requires 1012 Mm^3 volume of water annually that accounts 25 % of the natural outflow of Lake Tana. From the total irrigation demand 362 Mm^3 of water is planned to be pumped from Lake Tana. Furthermore, an average of $77m^3s^{-1}$ equivalent to 2428 Mm^3 or 61 % of the natural flow should be diverted to Tana-Beles HPP. Meanwhile, a minimum environmental requirement flow of 867 Mm^3 recommended by McCartney *et al.* (2010) should be available annually to the main Abay River. This indicates a minimum of 3,657 Mm^3 of water should be available from Lake Tana sub-basin to meet the demands of full water resource developments and environmental sustainability. However, the total annual simulated outflow to the Abay River and

to the Tana-Beles HPP from Lake Tana under the full development and dry climate change scenario (s11) is about 2,863 Mm^3, which can satisfy 78.3 % of the minimum demand. This revealed that Tana sub-basin is more prone to water scarcity because of the large size future planned water resource developments and climate change effects.

This dissertation also provide quantitative analysis of water resources management by considering the current and future climate change combined with the proposed cascades reservoirs for power generation. The scenarios were evaluated on energy production and on the magnitude of released discharges for the downstream countries. The installed capacity of GERD is 6450 MW with the aim to produce a total energy of 16,153 $GWhyr^{-1}$ (Wikipedia, 2019). The model simulation results indicate that the target energy is not reached under reference and dry climatic conditions of GFDL GCM RCP8.5 climate change scenarios. The target might be achieved only if the wet climatic condition (canESM2 GCM under RCP8.5 scenario) occurs. In the canESM2 GCM RCP 8.5 climate scenario at the end of the 21st century, the total energy generation might increase by 2,829 $GWhyr^{-1}$ to 18,982 $GWhyr^{-1}$, but under dry climatic condition (i.e. GFDL GCM RCP8.5); it might decrease by 9,072 $GWhyr^{-1}$ to 7,081 $GWhyr^{-1}$. The cascaded hydropower projects along the main stem of Abay River can generate a maximum total annual energy of 50,047 $GWhyr^{-1}$ and a minimum of 24,213 $GWhyr^{-1}$ under s8 and s11 respectively.

In order to understand the significance of the single impacts of climate change and water resources development, scenarios with similar magnitudes of developments but different climate change scenarios were compared. For instance, the impacts of full development and no climate change scenario (s4), full development and wet climate change (canESM2) scenario (s8) and full development and dry climate condition (GFDL) scenario (s11) were compared. The simulation result indicated that mean annual outflow from GERD increased to 1984 m^3s^{-1} under s8 and decrease to 1004 m^3s^{-1} and 1434 m^3s^{-1} under s11 and s4 respectively from the natural condition streamflow of 1645 m^3s^{-1}. Moreover, under s4 (i.e. the impact arises due to full development alone), the simulated total energy generated from GERD decreases by -25 %. However, if the climate is changing and precipitation increases by 26 % (s8), total annual energy might increase by 17.5 % and If precipitation decreases by 9.9 % (s11), total annual energy decreases by -56.2 % as compared to baseline scenario. This indicates that climate change effect is more significant than the anthropogenic effects for altering the performance of water infrastructure developments and hydrology of the basin. It is to be noted that projected climate change adds another dimension of uncertainties on future water availability and its variability of the UBNRB, as some models project higher others lower rainfall and streamflow. Hence, water storages could be a better adaptation option allowing for balancing responses to changing hydrology.

The evaporative losses from the GERD reservoir surface area estimated on average 6.1 $mmday^{-1}$ in the reference period (1984-2011), which amounts to approximately 2235 $mmyr^{-1}$. This volume also be an additional limiting water balance component for altering the quantity of downstream flow. The model simulates mean annual reservoir evaporation volume between 1.5 Bm^3 and 5.2 Bm^3, which corresponds to 3.4-6.5% of the mean annual inflow volumes into the GERD. The amount of water flowing to the downstream countries Sudan and Egypt will be more regulated and more constant due to the upstream cascades.

Overall, there are many, often-competing water demands and water user sectors in the UBNRB. As agriculture is a major livelihood strategy in the Nile Basin, sustaining hundreds of millions of people, and energy is vital to the future growth of the Nile Basin riparian states, water scarcity in terms of both physical water scarcity and economic water scarcity remains the major limiting factor for agricultural and energy development in the basin. Hence, effective planning, management and regulation of water resource developments are essential to prevent conflict between competing water users and sectors. Careful management of the energy and irrigation sectors are needed to gain the benefit of a future increase in food production but without a significant cost in terms of assured electricity production (McCartney et al., 2010).

Recommendations

Based on the statistical performance evaluation results obtained from the calibrations and validations, it can be said that SWAT is able to simulate the hydrological process correctly and successfully when the simulated streamflow compared with the observed streamflow data. However, the SWAT model does not adjust CN2 for slopes greater than 5%. This could be significant in areas where the majority of the area has a slope greater than 5%, such as in the UBNRB. We therefore suggest adjusting CN2 values for slope >5 % outside of the SWAT model might improve the results. Furthermore, the SWAT water balance modeling results suggested that the effects of climate change is significant than the effects of LULC change for altering the hydrology and water balance components of the UBNRB. However, this is not enough to understand the spatial and temporal variability of the dominant hydrological processes and runoff generation mechanism in the basin. On the one hand, the heterogeneities in climate, topography, soil, vegetation and geology could influence the responses of the basin. Hence, to gain further insights about the runoff generation mechanisms, more in-depth studies on runoff generation processes involving rainfall intensity, infiltration rate, and event-based analysis of hydrographs and critical evaluation of rainfall-runoff processes are recommended.

The large inter model differences of the GCMs for simulating precipitation showed the uncertainties of GCMs associated with their differences of resolution and assumptions of physical atmospheric processes to represent local scale climate variables which are typical characteristics for Africa and because of low convergence in climate model projections in the area of UBNRB (Gebre *et al.*, 2015). This also illustrates that incorporating more GCMs is highly recommended in the climate change study to reduce the uncertainty of GCMs particularly for precipitation.

In future, there is significant potential for further water resource development with increased water demand of water in the Tana sub-basin. However, great care is needed to ensure that such development is sustainable and does not adversely affect those communities that depend on the natural resources of the lake (fishing, navigation, tourism, agriculture) and the rivers that feed into it. Further comprehensive research is needed to improve quantitative understanding of the impacts of climate change and future water resource developments on socio-economic and environmental sustainability.

Before embarking into implementation of the cascaded hydropower projects, it is highly recommended to extend the model to demonstrate more specific downstream impacts, such as:

- The effect of the filling rate policy on the electricity generation of the downstream hydropower projects,
- The effects of upstream developments on the downstream water demands (Egypt and Sudan).
- Optimal operational strategies for cascaded water resource development projects both from Ethiopia, Sudan and Egypt,
- Detail cost-benefit analysis from the perspectives of Ethiopia and downstream riparian countries Sudan and Egypt.

Cooperation among the three riparian countries at all stages (planning, designing, construction, filling and operational management) is critical for project sustainability and future regional developments that increases benefits and reduces downstream risks.

Further research to establish the optimum operation rules that include all planned and existed water infrastructure developments in the entire Eastern Nile basin, including irrigation, hydropower generation, and domestic/industrial demand would certainly provide added value. As well, levels of cooperation or integrating stakeholders during the planning and decision processes, other than that explored in this dissertation, could be assessed. Therefore, designing appropriate decision support system (DSS) tool that can provides a framework for sharing knowledge, understanding river system behavior, evaluating alternative development and management strategies, and supporting informed decision making would be highly recommended.

Chapter 9 References

Abbaspour, C.K.: SWAT Calibrating and Uncertainty Programs. A User Manual. Eawag Zurich, Switzerland, 2008.

Abbaspour, K.C., Vaghefi, S.A., Srinivasan, R.: A guideline for successful calibration and uncertainty analysis for soil and water assessment: A review of papers from the 2016 International SWAT Conference. Multidisciplinary Digital Publishing Institute, 2017.

Abdulkarim H, S., Milly, M., Mohsen, A.: Nile Basin Water Resources Atlas. 2016.

Abiodun, O.O., Guan, H., Post, V.E., Batelaan, O.: Comparison of MODIS and SWAT evapotranspiration over a complex terrain at different spatial scales. Hydrology and Earth System Sciences, 22(5), 2775-2794, 2018. DOI:10.5194/hess-22-2775-2018

Abtew, W., Melesse, A.M., Dessalegne, T.: El Niño southern oscillation link to the Blue Nile River basin hydrology. Hydrological Processes: An International Journal, 23(26), 3653-3660, 2009.

Adeloye, A.J.: An opportunity loss model for estimating the value of streamflow data for reservoir planning. Water resources management, 10(1), 45-79, 1996.

Adem, G., Batelaan, O.: Modeling groundwater-surface water interaction by coupling MODFLOW with WetSpa. Geophysical Research, 8, 03181, 2006.

Agreement, P.: United nations. United Nations Treaty Collect, 1-27, 2015.

Aich, V., Liersch, S., Vetter, T., Huang, S., Tecklenburg, J., Hoffmann, P., Koch, H., Fournet, S., Krysanova, V., Müller, E.: Comparing impacts of climate change on streamflow in four large African river basins. Hydrology and Earth System Sciences, 18(4), 1305-1321, 2014.

Alemseged, T.H., Tom, R.: Evaluation of regional climate model simulations of rainfall over the Upper Blue Nile basin. Atmospheric research, 161, 57-64, 2015. DOI:10.1016/j.atmosres.2015.03.013

Allen, R.G., Pereira, L.S., Raes, D., Smith, M.: Crop evapotranspiration-Guidelines for computing crop water requirements-FAO Irrigation and drainage paper 56. FAO, Rome, 300(9), D05109, 1998.

Amirabadizadeh, M., Ghazali, A.H., Huang, Y.F., Wayayok, A.: Downscaling daily precipitation and temperatures over the Langat River Basin in Malaysia: A comparison of two statistical downscaling approaches. International Journal of Water Resources and Environmental Engineering, 8(10), 120-136, 2016.

Anand, J., Gosain, A.K., Khosa, R.: Optimisation of Multipurpose Reservoir Operation by Coupling Soil and Water Assessment Tool (SWAT) and Genetic Algorithm for Optimal Operating Policy (Case Study: Ganga River Basin). Sustainability, 10(5), 1660, 2018.

Arjoon, D., Mohamed, Y., Goor, Q., Tilmant, A.: Hydro-economic risk assessment in the eastern Nile River basin. Water Resources and Economics, 8, 16-31, 2014.

Arnold, J., Kiniry, J., Srinivasan, R., Williams, J., Haney, E., Neitsch, S.: SWAT 2012 input/output documentation, Texas Water Resources Institute, 2013.

Arnold, J.G., Srinivasan, R., Muttiah, R.S., Williams, J.R.: Large area hydrologic modeling and assessment part I: Model development1. Wiley Online Library, 1998. DOI:10.1111/j.1752-1688.1998.tb05961.x

Arnold, J.G., Allen, P., Volk, M., Williams, J., Bosch, D.: Assessment of different representations of spatial variability on SWAT model performance. Transactions of the ASABE, 53(5), 1433-1443, 2010.
Arnold, J.G., Moriasi, D.N., Gassman, P.W., Abbaspour, K.C., White, M.J., Srinivasan, R., Santhi, C., Harmel, R., Van Griensven, A., Van Liew, M.W.: SWAT: Model use, calibration, and validation. Transactions of the ASABE, 55(4), 1491-1508, 2012.
Authority, A.b.: Atlas of Abbay Basin. 2015.
Awulachew, S.B., McCartney, M., Steenhuis, T.S., Ahmed, A.A.: A review of hydrology, sediment and water resource use in the Blue Nile Basin, 131. IWMI, 2008.
Ayenew, T., Gebreegziabher, Y.: Application of a spreadsheet hydrological model for computing the long-term water balance of Lake Awassa, Ethiopia. Hydrological sciences journal, 51(3), 418-431, 2006.
Banko, G.: A review of assessing the accuracy of classifications of remotely sensed data and of methods including remote sensing data in forest inventory IASA Interim Report. IIASA, Laxenburg, Austria, IR-98-08, 1998.
BCEOM: Abbay river basin integrated development master plan project. Ministry of Water Resources, Addis Ababa, Ethiopia, Phase 3, Volume I, Main report, 1998a.
BCEOM: Abbay river basin integrated development master plan Ministry of Water Resources, Addis Ababa, Ethiopia, section II, volume V-water resources development(part 1-irrigation and drainage), 1998b.
Bellier, C., Humphreys, H., Kennedy, R., Donkin: Environmental Impact Assessment for the medium scale hydropower plant study project Tis Abay II. Federal Republic of Ethiopia, Ministry of Water Resources, 1997.
Bennett, N.D., Croke, B.F., Guariso, G., Guillaume, J.H., Hamilton, S.H., Jakeman, A.J., Marsili-Libelli, S., Newham, L.T., Norton, J.P., Perrin, C.: Characterising performance of environmental models. Environmental Modelling & Software, 40, 1-20, 2013.
Benyon, R.G., Theiveyanathan, S., Doody, T.M.: Impacts of tree plantations on groundwater in south-eastern Australia. Australian Journal of Botany, 54(2), 181-192, 2006. DOI:10.1071/BT05046
Bewket, W., Sterk, G.: Dynamics in land cover and its effect on stream flow in the Chemoga watershed, Blue Nile basin, Ethiopia. Hydrological Processes, 19(2), 445-458, 2005. DOI:10.1002/hyp.5542
Beyene, T., Lettenmaier, D.P., Kabat, P.: Hydrologic impacts of climate change on the Nile River Basin: implications of the 2007 IPCC scenarios. Climatic change, 100(3-4), 433-461, 2010.
Booij, M.J., Deckers, D.L., Rientjes, T.H., Krol, M.S.: Regionalization for uncertainty reduction in flows in ungauged basins. 2007.
Bormann, H., Breuer, L., Gräff, T., Huisman, J., Croke, B.: Assessing the impact of land use change on hydrology by ensemble modelling (LUCHEM) IV: Model sensitivity to data aggregation and spatial (re-) distribution. Advances in water resources, 32(2), 171-192, 2009.
Bosch, D., Arnold, J., Volk, M., Allen, P.: Simulation of a low-gradient coastal plain watershed using the SWAT landscape model. Transactions of the ASABE, 53(5), 1445-1456, 2010.
Brooks, K.N., Ffolliott, P.F., Gregersen, H.M., DeBano, L.F.: Hydrology and the management of watersheds. Iowa State University Press, 2003.

Campozano, L., Sánchez, E., Avilés, Á., Samaniego, E.: Evaluation of infilling methods for time series of daily precipitation and temperature: The case of the Ecuadorian Andes. Maskana, 5(1), 99-115, 2014.
Campozano, L., Tenelanda, D., Sanchez, E., Samaniego, E., Feyen, J.: Comparison of statistical downscaling methods for monthly total precipitation: case study for the paute river basin in Southern Ecuador. Advances in Meteorology, 2016, 13, 2016. DOI:10.1155/2016/6526341
Casajus, N., Périé, C., Logan, T., Lambert, M.-C., de Blois, S., Berteaux, D.: An Objective Approach to Select Climate Scenarios when Projecting Species Distribution under Climate Change. PloS one, 11(3), e0152495, 2016. DOI:10.1371/journal.pone.0152495
Chakilu, G., Moges, M.: Assessing the Land Use/Cover Dynamics and its Impact on the Low Flow of Gumara Watershed, Upper Blue Nile Basin, Ethiopia. Hydrol Current Res, 7(268), 2, 2017.
Che, D., Mays, L.W.: Development of an optimization/simulation model for real-time flood-control operation of river-reservoirs systems. Water resources management, 29(11), 3987-4005, 2015.
Chen, H., Guo, J., Zhang, Z., Xu, C.-Y.: Prediction of temperature and precipitation in Sudan and South Sudan by using LARS-WG in future. Theoretical and Applied Climatology, 113(3-4), 363-375, 2013.
Chen, H., Swain, A.: The Grand Ethiopian Renaissance Dam: Evaluating its sustainability standard and geopolitical significance. Energy Development Frontier, 3(1), 11, 2014.
Cherie, N.Z.: Downscaling and modeling the effects of climate change on hydrology and water resources in the upper Blue Nile river basin, Ethiopia, Kassel, Univ., Diss., 2013, 2013.
Cheung, W.H., Senay, G.B., Singh, A.: Trends and spatial distribution of annual and seasonal rainfall in Ethiopia. International Journal of Climatology, 28(13), 1723-1734, 2008. DOI:10.1002/joc.1623
Chisanga, C.B., Phiri, E., Chinene, V.R.: Statistical Downscaling of Precipitation and Temperature Using Long Ashton Research Station Weather Generator in Zambia: A Case of Mount Makulu Agriculture Research Station. American Journal of Climate Change, 6(03), 487, 2017.
Chow, V.T., Maidment, D.R., Larry, W.: Mays. Applied Hydrology. International edition, MacGraw-Hill, Inc, 149, 1988.
Collick, A.S., Easton, Z.M., Ashagrie, T., Biruk, B., Tilahun, S., Adgo, E., Awulachew, S.B., Zeleke, G., Steenhuis, T.S.: A simple semi-distributed water balance model for the Ethiopian highlands. Hydrological processes, 23(26), 3718-3727, 2009.
Congalton, R.G.: A review of assessing the accuracy of classifications of remotely sensed data. Remote sensing of environment, 37(1), 35-46, 1991.
Conway, D.: The impacts of climate variability and future climate change in the Nile Basin on water resources in Egypt. International Journal of Water Resources Development, 12(3), 277-296, 1996.
Conway, D.: The climate and hydrology of the Upper Blue Nile River. The Geographical Journal, 166(1), 49-62, 2000.
Conway, D.: From headwater tributaries to international river: observing and adapting to climate variability and change in the Nile basin. Global Environmental Change, 15(2), 99-114, 2005.

Cunderlik, J.: Hydrologic model selection for the CFCAS project: assessment of water resources risk and vulnerability to changing climatic conditions. Department of Civil and Environmental Engineering, The University of Western Ontario, 2003.
Das, L., Annan, J., Hargreaves, J., Emori, S.: Improvements over three generations of climate model simulations for eastern India. Climate Research, 51(3), 201-216, 2012.
DeFries, R., Chan, J.C.-W.: Multiple criteria for evaluating machine learning algorithms for land cover classification from satellite data. Remote Sensing of Environment, 74(3), 503-515, 2000.
DeFries, R., Eshleman, K.N.: Land-use change and hydrologic processes: a major focus for the future. Hydrological processes, 18(11), 2183-2186, 2004.
Derib, S.D.: Rainfall-runoff processes at a hill-slope watershed: case of simple models evaluation at Kori-Sheleko Catchments of Wollo, Ethiopia, M. Sc. Thesis, 2005.
Deser, C., Phillips, A., Bourdette, V., Teng, H.: Uncertainty in climate change projections: the role of internal variability. Climate dynamics, 38(3-4), 527-546, 2012.
Desta, G.: Estimation of Runoff Coefficient at different growth stages of crops in the highlands of Amhara Region, MSc Thesis, Alemaya University, Ethiopia, 2003.
Dhami, B.S., Pandey, A.: Comparative review of recently developed hydrologic models. Journal of Indian Water Resources Society, 33(3), 34-42, 2013.
Di Piazza, A., Conti, F.L., Noto, L.V., Viola, F., La Loggia, G.: Comparative analysis of different techniques for spatial interpolation of rainfall data to create a serially complete monthly time series of precipitation for Sicily, Italy. International Journal of Applied Earth Observation and Geoinformation, 13(3), 396-408, 2011.
Dibike, Y.B., Coulibaly, P.: Hydrologic impact of climate change in the Saguenay watershed: comparison of downscaling methods and hydrologic models. Journal of hydrology, 307(1), 145-163, 2005.
Dile, Y.T., Berndtsson, R., Setegn, S.G.: Hydrological Response to Climate Change for Gilgel Abay River, in the Lake Tana Basin-Upper Blue Nile Basin of Ethiopia. PloS one, 8(10), e79296, 2013. DOI:10.1371/journal.pone.0079296
Dingman, S.L.: Physical hydrology. Prentice Hall, 2002.
Dolinar, E.K., Dong, X., Xi, B., Jiang, J.H., Su, H.: Evaluation of CMIP5 simulated clouds and TOA radiation budgets using NASA satellite observations. Climate Dynamics, 44(7-8), 2229-2247, 2015.
Dwarakish, G., Ganasri, B.: Impact of land use change on hydrological systems: A review of current modeling approaches. Cogent Geoscience, 1(1), 1115691, 2015.
Ebrahim, G.Y., Jonoski, A., van Griensven, A., Di Baldassarre, G.: Downscaling technique uncertainty in assessing hydrological impact of climate change in the Upper Beles River Basin, Ethiopia. Hydrology Research, 44(2), 377-398, 2013.
Eischeid, J.K., Bruce Baker, C., Karl, T.R., Diaz, H.F.: The quality control of long-term climatological data using objective data analysis. Journal of Applied Meteorology, 34(12), 2787-2795, 1995.
Elshamy, M., Seierstad, I.A., Sorteberg, A.: Impacts of climate change on Blue Nile flows using bias-corrected GCM scenarios. 2009a.
Elshamy, M.E., Seierstad, I.A., Sorteberg, A.: Impacts of climate change on Blue Nile flows using bias-corrected GCM scenarios. Hydrology and Earth System Sciences, 13(5), 551-565, 2009b.

Engda, T.A.: Modeling rainfall, runoff and soil loss relationships in the northeastern highlands of Ethiopia, andit tid watershed, Citeseer, 2009.
Feldman, A.D.: Hydrologic Modeling System HEC-HMS Technical Reference Manual. U:S: Army Corps of Engineers, Hydrologic Engineering Center, HEC, 609 Second St., Davis, CA 95616-4687, 2000.
Fiseha, B., Melesse, A., Romano, E., Volpi, E., Fiori, A.: Statistical downscaling of precipitation and temperature for the Upper Tiber Basin in Central Italy. International Journal of Water Sciences, 1, 2012. DOI:10.5772/52890
Flato, G.M.: Earth system models: an overview. Wiley Interdisciplinary Reviews: Climate Change, 2(6), 783-800, 2011.
Fowler, H., Blenkinsop, S., Tebaldi, C.: Linking climate change modelling to impacts studies: recent advances in downscaling techniques for hydrological modelling. International journal of climatology, 27(12), 1547-1578, 2007.
Gashaw, T., Tulu, T., Argaw, M., Worqlul, A.W.: Modeling the hydrological impacts of land use/land cover changes in the Andassa watershed, Blue Nile Basin, Ethiopia. Science of the Total Environment, 619, 1394-1408, 2018.
Gebre, S.L., Ludwig, F.: Hydrological Response to Climate Change of the Upper Blue Nile River Basin: Based on IPCC Fifth Assessment Report (AR5). Journal of Climatology & Weather Forecasting, 2015, 2014.
Gebre, S.L., Ludwig, F.: Hydrological Response to Climate Change of the Upper Blue Nile River Basin: Based on IPCC Fifth Assessment Report (AR5). Journal of Climatology & Weather Forecasting, 3(121), 2015. DOI:10.4172/2332-2594.1000121
Gebrehiwot, S.G., Taye, A., Bishop, K.: Forest cover and stream flow in a headwater of the Blue Nile: complementing observational data analysis with community perception. Ambio, 39(4), 284-294, 2010.
Gebrekristos, S.T.: Understanding Catchment Processes and Hydrological Modelling in the Abay/Upper Blue Nile Basin, Ethiopia. 2015.
Gebremicael, T., Mohamed, Y., Betrie, G., van der Zaag, P., Teferi, E.: Trend analysis of runoff and sediment fluxes in the Upper Blue Nile basin: A combined analysis of statistical tests, physically-based models and landuse maps. Journal of Hydrology, 482, 57-68, 2013. DOI:10.1016/j.jhydrol.2012.12.023
Giorgi, F.: Uncertainties in climate change projections, from the global to the regional scale, EPJ Web of conferences. EDP Sciences, pp. 115-129, 2010.
Girma, M.M.: Potential impact of climate and land use changes on the water resources of the Upper Blue Nile Basin. 2013.
Golberg, D.E.: Genetic algorithms in search, optimization, and machine learning. Addion wesley, 1989(102), 36, 1989.
Goly, A., Teegavarapu, R.S., Mondal, A.: Development and evaluation of statistical downscaling models for monthly precipitation. Earth Interactions, 18(18), 1-28, 2014.
Goodarzi, E., Dastorani, M., Talebi, A.: Evaluation of the change-factor and LARS-WG methods of downscaling for simulation of climatic variables in the future (Case study: Herat Azam Watershed, Yazd-Iran). Ecopersia, 3(1), 833-846, 2015.
Gosain, A., Mani, A., Dwivedi, C.: Hydrological Modelling-Literature Review. Disponible en internet en: http://web. iitd. ac. in/~ akgosain/CLIMAWATER.[Citado en 2010]. Reporte(1), 2009.

Green, W.H., Ampt, G.: Studies on Soil Phyics. The Journal of Agricultural Science, 4(01), 1-24, 1911.
Halcrow, GIRD: Water Balance Modelling of Lake Tana and Operational Rules and Irrigation Development in The Upper Beles Catchment. Federal Democratic Republic of Ethiopia Ministry of Water Resources, Addis Ababa, Ethiopia, 2010.
Hamed, K.H., Rao, A.R.: A modified Mann-Kendall trend test for autocorrelated data. Journal of Hydrology, 204(1-4), 182-196, 1998.
Hansen, A., De Fries, R., Turner, W.: Land Use Change and Biodiversity: A Synthesis of Rates and Consequences during the Period of Satellite Imagery. Pgs 277-299 Land Change Science: Observing, Monitoring, and Understanding Trajectories of Change on the Earth's Surface. New York: Springer Verlag, 2004.
Haregeweyn, N., Yohannes, F.: Testing and evaluation of the agricultural non-point source pollution model (AGNPS) on Augucho catchment, western Hararghe, Ethiopia. Agriculture, ecosystems & environment, 99(1-3), 201-212, 2003.
Haregeweyn, N., Tsunekawa, A., Nyssen, J., Poesen, J., Tsubo, M., Tsegaye Meshesha, D., Schütt, B., Adgo, E., Tegegne, F.: Soil erosion and conservation in Ethiopia: a review. Progress in Physical Geography, 39(6), 750-774, 2015. DOI:10.1177/0309133315598725
Hargreaves, G.L., Hargreaves, G.H., Riley, J.P.: Agricultural benefits for Senegal River basin. Journal of irrigation and Drainage Engineering, 111(2), 113-124, 1985.
Hashmi, M.Z., Shamseldin, A.Y., Melville, B.W.: Comparison of SDSM and LARS-WG for simulation and downscaling of extreme precipitation events in a watershed. Stochastic Environmental Research and Risk Assessment, 25(4), 475-484, 2011.
Hassaballah, K., Mohamed, Y., Uhlenbrook, S., Biro, K.: Analysis of streamflow response to land use and land cover changes using satellite data and hydrological modelling: case study of Dinder and Rahad tributaries of the Blue Nile (Ethiopia–Sudan). Hydrology and Earth System Sciences, 21(10), 5217, 2017a. DOI:10.5194/hess-21-5217-2017
Hassaballah, K., Mohamed, Y., Uhlenbrook, S., Biro, K.: Analysis of streamflow response to land use land cover changes using satellite data and hydrological modelling: case study of Dinder and Rahad tributaries of the Blue Nile (Ethiopia/Sudan). 2017b.
Hassan, Z., Shamsudin, S., Harun, S.: Application of SDSM and LARS-WG for simulating and downscaling of rainfall and temperature. Theoretical and applied climatology, 116(1-2), 243-257, 2014.
Hawkins, E., Sutton, R.: The potential to narrow uncertainty in regional climate predictions. Bulletin of the American Meteorological Society, 90(8), 1095-1108, 2009.
Hayes, D.J., Sader, S.A.: Comparison of change-detection techniques for monitoring tropical forest clearing and vegetation regrowth in a time series. Photogrammetric engineering and remote sensing, 67(9), 1067-1075, 2001.
Holberg, J.: Downward model development of the soil moisture accounting loss method in HEC-HMS: Revelations concerning the soil profile. 2015.
Holland, J.H.: Adaptation in natural and artificial systems: an introductory analysis with applications to biology, control, and artificial intelligence. University of Michigan press Ann Arbor, 1975.
Hu, Y., De Jong, S., Sluiter, R.: A modeling-based threshold approach to derive change/no change information over vegetation area, Proceedings of the "12 International Conference on Geoinformatics-Geospatial Information Research: Bridging the Pacific and Atlantic". University of Gävle (Sweden), pp. 647-654, 2004.

Huang, J., Wu, P., Zhao, X.: Effects of rainfall intensity, underlying surface and slope gradient on soil infiltration under simulated rainfall experiments. Catena, 104, 93-102, 2013. DOI:10.1016/j.catena.2012.10.013

Hurni, H., Tato, K., Zeleke, G.: The implications of changes in population, land use, and land management for surface runoff in the upper Nile basin area of Ethiopia. Mountain Research and Development, 25(2), 147-154, 2005.

IPCC: Climate Change 2007: Synthesis Report. Contribution of Working Groups I, II and III to the Fourth Assessment Report of the Intergovernmental Panel on Climate Change [Core Writing Team, Pachauri, R.K and Reisinger, A.(eds.)]. IPCC, Geneva, Switzerland, 104 pp, 2007.

IPCC: Climate Change 2014–Impacts, Adaptation and Vulnerability: Regional Aspects. Cambridge University Press, 2014a.

IPCC: Climate Change 2014: Synthesis Report. Contribution of Working Groups I, II and III to the Fifth Assessment Report of the Intergovernmental Panel on Climate Change [Core Writing Team, R.K. Pachauri and L.A. Meyer (eds.)]. IPCC, Geneva, Switzerland, 151 pp, 2014b.

IPoE: Grand Ethiopian Renaissance Dam Project. Final Report, 2013.

Jajarmizadeh, M., Harun, S., Salarpour, M.: A review on theoretical consideration and types of models in hydrology. Journal of Environmental Science and Technology, 5(5), 249-261, 2012.

Janko, A.M.: Fish production, consumption and management in Ethiopia, NJF Congress: Nordic view to sustainable rural development, 25, Riga (Latvia), 16-18 Jun 2015. NJF Latvia, 2015.

Jensen, J.R.: Introductory digital image processing: a remote sensing perspective. Prentice-Hall Inc., 1996.

Kahya, E., Kalaycı, S.: Trend analysis of streamflow in Turkey. Journal of Hydrology, 289(1-4), 128-144, 2004.

Kangrang, A., Prasanchum, H., Hormwichian, R.: Development of Future Rule Curves for Multipurpose Reservoir Operation Using Conditional Genetic and Tabu Search Algorithms. Advances in Civil Engineering, 2018, 2018.

Kebede, S., Travi, Y., Alemayehu, T., Marc, V.: Water balance of Lake Tana and its sensitivity to fluctuations in rainfall, Blue Nile basin, Ethiopia. Journal of hydrology, 316(1), 233-247, 2006.

Kendall, M.: Rank correlation methods. 1975.

Khalili, M., Leconte, R., Brissette, F.: Stochastic multisite generation of daily precipitation data using spatial autocorrelation. Journal of hydrometeorology, 8(3), 396-412, 2007.

Khan, M.S., Coulibaly, P., Dibike, Y.: Uncertainty analysis of statistical downscaling methods. Journal of Hydrology, 319(1), 357-382, 2006.

Kidane, M., Tolessa, T., Bezie, A., Kessete, N., Endrias, M.: Evaluating the impacts of climate and land use/land cover (LU/LC) dynamics on the Hydrological Responses of the Upper Blue Nile in the Central Highlands of Ethiopia. Spatial Information Research, 1-17, 2018.

Kim, U., Kaluarachchi, J.J.: Application of parameter estimation and regionalization methodologies to ungauged basins of the Upper Blue Nile River Basin, Ethiopia. Journal of Hydrology, 362(1-2), 39-56, 2008a.

Kim, U., Kaluarachchi, J.J., Smakhtin, V.U.: Generation of Monthly Precipitation Under Climate Change for the Upper Blue Nile River Basin, Ethiopia 1. JAWRA Journal of the American Water Resources Association, 44(5), 1231-1247, 2008b.
Kim, U.K., J. J.; Smakhtin, V. U.: Climate change impacts on hydrology and water resources of the Upper Blue Nile River Basin, Ethiopia. Colombo, Sri Lanka: International Water Management Institute, 27p (IWMI Research Report 126), 2008.
King, L.M., McLeod, A.I., Simonovic, S.P.: Improved weather generator algorithm for multisite simulation of precipitation and temperature. JAWRA Journal of the American Water Resources Association, 51(5), 1305-1320, 2015.
Le Ngo, L.: Optimising reservoir operation: A case study of the Hoa Binh reservoir, Vietnam. DTU Environment, 2007.
Legesse, D., Vallet-Coulomb, C., Gasse, F.: Hydrological response of a catchment to climate and land use changes in Tropical Africa: case study South Central Ethiopia. Journal of Hydrology, 275(1-2), 67-85, 2003.
Lewarne, M.: Setting Up ArcSWAT hydrological model for the verlorenvlei Catchment, Stellenbosch: University of Stellenbosch, 2009.
Li, Z., Liu, W.-z., Zhang, X.-c., Zheng, F.-l.: Impacts of land use change and climate variability on hydrology in an agricultural catchment on the Loess Plateau of China. Journal of hydrology, 377(1-2), 35-42, 2009.
Liersch, S., Koch, H., Hattermann, F.F.: Management scenarios of the Grand Ethiopian Renaissance Dam and their impacts under recent and future climates. Water, 9(10), 728, 2017.
Liu, B.M., Collick, A.S., Zeleke, G., Adgo, E., Easton, Z.M., Steenhuis, T.S.: Rainfall-discharge relationships for a monsoonal climate in the Ethiopian highlands. Hydrological Processes, 22(7), 1059-1067, 2008. DOI:10.1002/hyp.7022
Lørup, J.K., Refsgaard, J.C., Mazvimavi, D.: Assessing the effect of land use change on catchment runoff by combined use of statistical tests and hydrological modelling: case studies from Zimbabwe. Journal of Hydrology, 205(3-4), 147-163, 1998.
Lu, D., Mausel, P., Batistella, M., Moran, E.: Comparison of land-cover classification methods in the Brazilian Amazon Basin. Photogrammetric engineering & remote sensing, 70(6), 723-731, 2004.
Mancino, G., Nolè, A., Ripullone, F., Ferrara, A.: Landsat TM imagery and NDVI differencing to detect vegetation change: assessing natural forest expansion in Basilicata, southern Italy. iForest-Biogeosciences and Forestry, 7(2), 75, 2014. DOI:10.3832/ifor0909-007
Mann, H.B.: Nonparametric Tests Against Trend. Econometrica, 13(3), 245-259, 1945.
Marhaento, H., Booij, M.J., Rientjes, T., Hoekstra, A.Y.: Attribution of changes in the water balance of a tropical catchment to land use change using the SWAT model. Hydrological Processes, 31(11), 2029-2040, 2017. DOI:10.1002/hyp.11167
MARKERT, K., Griffin, R., Limaye, A., McNider, R., Anderson, E.: Investigation Into the Effects of Climate Variability and Land Cover Change on the Hydrologic System of the Lower Mekong Basin, AGU Fall Meeting Abstracts, 2016.
Maurer, E.P., Hidalgo, H.G.: Utility of daily vs. monthly large-scale climate data: an intercomparison of two statistical downscaling methods. Hydrology and Earth System Sciences, 12(2), 551-563, 2008.
McCartney, M., Alemayehu, T., Shiferaw, A., Awulachew, S.: Evaluation of current and future water resources development in the Lake Tana Basin, Ethiopia, 134. IWMI, 2010.

McCartney, M., Alemayehu, T., Easton, Z.M., Awulachew, S.B.: Simulating current and future water resources development in the Blue Nile River Basin. The Nile River Basin: water, agriculture, governance and livelihoods. Routledge-Earthscan, Abingdon, 269-291, 2012.
McColl, C., Aggett, G.: Land-use forecasting and hydrologic model integration for improved land-use decision support. Journal of environmental management, 84(4), 494-512, 2007.
Meher, J.K., Das, L., Akhter, J., Benestad, R.E., Mezghani, A.: Performance of CMIP3 and CMIP5 GCMs to simulate observed rainfall characteristics over the Western Himalayan region. Journal of Climate, 30(19), 7777-7799, 2017.
Mekonnen, D.: Satellite remote sensing for soil moisture estimation: Gumara catchment, Ethiopia. International Institute for Geo-information Science and Earth Observation, Enschede, 2009.
Mekonnen, D.F., Disse, M.: Analyzing the future climate change of Upper Blue Nile River basin using statistical downscaling techniques. Hydrology and Earth System Sciences, 22(4), 2391, 2018a. DOI:10.5194/hess-22-2391-2018
Mekonnen, D.F., Duan, Z., Rientjes, T., Disse, M.: Analysis of combined and isolated effects of land-use and land-cover changes and climate change on the upper Blue Nile River basin's streamflow. Hydrology and Earth System Sciences, 22(12), 6187-6207, 2018b.
Melesse, A., Abtew, W., Dessalegne, T., Wang, X.: Low and high flow analyses and wavelet application for characterization of the Blue Nile River system. Hydrological processes, 24(3), 241, 2009. DOI:10.1002/hyp.7312
Mellander, P.-E., Gebrehiwot, S.G., Gärdenäs, A.I., Bewket, W., Bishop, K.: Summer rains and dry seasons in the Upper Blue Nile Basin: the predictability of half a century of past and future spatiotemporal patterns. PloS one, 8(7), e68461, 2013.
Meze-Hausken, E.: Contrasting climate variability and meteorological drought with perceived drought and climate change in northern Ethiopia. Climate research, 27(1), 19-31, 2004.
Mockus, V.: National engineering handbook,Section 4:Hydrology, 630, 1964.
Mohamed, Y., Bastiaanssen, W., Savenije, H.: Spatial variability of evaporation and moisture storage in the swamps of the upper Nile studied by remote sensing techniques. Journal of hydrology, 289(1-4), 145-164, 2004.
Mohammed, A.K.: The Effect of Climate Change on Water Resources Potential of Omo Gibe Basin, Ethiopia, Universitätsbibliothek der Universität der Bundeswehr München, 2013.
Monserud, R.A.: Methods for comparing global vegetation maps. IIASA Working Paper. IIASA, Laxenburg, Austria, WP-90-040, 1990.
Monteith, J.L.: Evaporation and environment, Symp. Soc. Exp. Biol, pp. 4, 1965.
Moriasi, D.N., Arnold, J.G., Van Liew, M.W., Bingner, R.L., Harmel, R.D., Veith, T.L.: Model evaluation guidelines for systematic quantification of accuracy in watershed simulations. Trans. Asabe, 50(3), 885-900, 2007.
Moss, R., Babiker, W., Brinkman, S., Calvo, E., Carter, T., Edmonds, J., Elgizouli, I., Emori, S., Erda, L., Hibbard, K.: Towards new scenarios for the analysis of emissions: Climate change, impacts and response strategies. Intergovernmental Panel on Climate Change Secretariat (IPCC), 2008.
Mulat, A.G., Moges, S.A., Moges, M.A.: Evaluation of multi-storage hydropower development in the upper Blue Nile River (Ethiopia): regional perspective. Journal of Hydrology: Regional Studies, 16, 1-14, 2018.

Mythili, B., Devi, U.G., Raviteja, A., Kumar, P.S.: Study of optimizing techniques of reservoir operation. International Journal of Engineering Research and General Science, 1(1), 2091-2730, 2013.
Nakicenovic, N., Alcamo, J., Grubler, A., Riahi, K., Roehrl, R., Rogner, H.-H., Victor, N.: Special report on emissions scenarios (SRES), a special report of Working Group III of the intergovernmental panel on climate change. Cambridge University Press, 2000.
Nandakumar, N., Mein, R.G.: Uncertainty in rainfall—runoff model simulations and the implications for predicting the hydrologic effects of land-use change. Journal of Hydrology, 192(1-4), 211-232, 1997.
Neelakantan, T., Sasireka, K.: Hydropower reservoir operation using standard operating and standard hedging policies. Int J Eng Techn, 5(2), 1191-6, 2013.
Neitsch, S., Arnold, J., Kiniry, J.e.a., Srinivasan, R., Williams, J.: Soil and water assessment tool user's manual version 2000. GSWRL report, 202(02-06), 2002.
Neitsch, S.L., Arnold, J.G., Kiniry, J.R., Williams, J.R.: Soil and water assessment tool theoretical documentation version 2009, Texas Water Resources Institute, 2011.
Nkomozepi, T.D., Chung, S.-O.: Uncertainty of Simulated Paddy Rice Yield using LARS-WG Derived Climate Data in the Geumho River Basin, Korea. Journal of the Korean Society of Agricultural Engineers, 55(4), 55-63, 2013.
NMA: Annual climate buletien for the year 2013. National Meteorological Agency, Meteorological Data and Climatology Directorate, Addis Ababa, Ethiopia, http://www.ethiomet.gov.et/bulletins/bulletin_viewer/bulletins/348/2013_Annual_Bulletin/en, 2013.
NORPLAN, Norconsult, international, L., Engineering, S., WWDSE: Karadobi Multipurpose Project Pre-Feasibility Study Final Report. Volume 1 - Main Report, 2006.
NORPLAN, Norconsult, Wilson, S., eDF, consult, S., engineers, T.c.: Beko-Abo multipurpose project pre-feasibilty study. Main report. Ministry of Water and Energy, Addis Ababa, Ethiopia., Final report, 2013.
Oki, T., Kanae, S.: Global hydrological cycles and world water resources. science, 313(5790), 1068-1072, 2006. DOI:10.1126/science.1128845
Olukanni, D., Adejumo, T., Salami, A., Adedeji, A.: Optimization-based reliability of a multipurpose reservoir by Genetic Algorithms: Jebba Hydropower Dam, Nigeria. Cogent Engineering, 5(1), 1438740, 2018.
Onyutha, C., Willems, P.: Spatial and temporal variability of rainfall in the Nile Basin. Hydrology and Earth System Sciences, 19(5), 2227-2246, 2015.
Oogathoo, S.: Runoff Simulation in the CANAGAGIGUE CREEK Watershed using the MIKE SHE Model, McGill University Montreal, 2006.
Otieno, H., Han, D., Woods, R.: Comparative performance assessment of hydrological models. 2014.
Pervez, M.S., Henebry, G.M.: Projections of the Ganges–Brahmaputra precipitation—Downscaled from GCM predictors. Journal of Hydrology, 517, 120-134, 2014.
Pettitt, A.: A non-parametric approach to the change-point problem. Applied statistics, 126-135, 1979.
Pignotti, G., Rathjens, H., Cibin, R., Chaubey, I., Crawford, M.: Comparative Analysis of HRU and Grid-Based SWAT Models. Water, 9(4), 272, 2017. DOI:10.3390/w9040272
Polanco, E.I., Fleifle, A., Ludwig, R., Disse, M.: Improving SWAT model performance in the upper Blue Nile Basin using meteorological data integration and subcatchment

discretization. Hydrology and Earth System Sciences, 21(9), 4907, 2017. DOI:10.5194/hess-21-4907-2017
Polanco, E.I.A.: Simulating Hydrogeomorphological Processes to Assess Land Degradation in the Upper Blue Nile Basin in Ethiopia Using SWAT, Technische Universität München, 2017.
Priestley, C., Taylor, R.: On the assessment of surface heat flux and evaporation using large-scale parameters. Monthly weather review, 100(2), 81-92, 1972.
Qian, B., Hayhoe, H., Gameda, S.: Evaluation of the stochastic weather generators LARS-WG and AAFC-WG for climate change impact studies. Climate Research, 29(1), 3-21, 2004.
Rathjens, H., Oppelt, N.: SWATgrid: An interface for setting up SWAT in a grid-based discretization scheme. Computers & geosciences, 45, 161-167, 2012. DOI:10.1016/j.cageo.2011.11.004
Rathjens, H., Oppelt, N., Bosch, D., Arnold, J.G., Volk, M.: Development of a grid-based version of the SWAT landscape model. Hydrological processes, 29(6), 900-914, 2015. DOI:10.1002/hyp.10197
Reddy, M.J., Kumar, D.N.: Optimal reservoir operation using multi-objective evolutionary algorithm. Water Resources Management, 20(6), 861-878, 2006.
Rientjes, T., Haile, A., Kebede, E., Mannaerts, C., Habib, E., Steenhuis, T.: Changes in land cover, rainfall and stream flow in Upper Gilgel Abbay catchment, Blue Nile basin-Ethiopia. Hydrology and Earth System Sciences, 15(6), 1979, 2011a. DOI:10.5194/hess-15-1979-2011
Rientjes, T., Perera, B., Haile, A., Reggiani, P., Muthuwatta, L.: Regionalisation for lake level simulation–the case of Lake Tana in the Upper Blue Nile, Ethiopia. Hydrology and Earth System Sciences, 15(4), 1167-1183, 2011b.
Salarijazi, M., Akhond-Ali, A.-M., Adib, A., Daneshkhah, A.: Trend and change-point detection for the annual stream-flow series of the Karun River at the Ahvaz hydrometric station. African Journal of Agricultural Research, 7(32), 4540-4552, 2012.
Salarpour, M., Rahman, N.A., Yusop, Z.: Simulation of flood extent mapping by InfoWorks RS-case study for tropical catchment. J. Software Eng, 5, 127-135, 2011.
Salini, C., Pietrangeli, S.: Beles mpp. Level 1 Design January 2006, 2006.
Samady, K.: Continuous hydrologic modeling for analyzingthe effects of drought on the lower Colorado River in Texas. Open Access Master's Thesis, Michigan Technological University, 2017.
Sarkar, A., Kumar, R.: Artificial neural networks for event based rainfall-runoff modeling. Journal of Water Resource and Protection, 4(10), 891, 2012.
Scharffenberg, W.: Hydrologic Modeling System HEC-HMS User's Manual. U:S: Army Corps of Engineers, Institute for Water Resources, Hydrologic Engineering Center, 609 Second Street, Davis, CA 95616-4687, 2015.
Seleshi, Y., Zanke, U.: Recent changes in rainfall and rainy days in Ethiopia. International journal of climatology, 24(8), 973-983, 2004. DOI:10.1002/joc.1052
Semenov, M.A., Barrow, E.M.: Use of a stochastic weather generator in the development of climate change scenarios. Climatic change, 35(4), 397-414, 1997.
Semenov, M.A., Barrow, E.M., Lars-Wg, A.: A stochastic weather generator for use in climate impact studies. User Manual: Hertfordshire, UK, 2002.

Semenov, M.A., Stratonovitch, P.: Use of multi-model ensembles from global climate models for assessment of climate change impacts. Climate research (Open Access for articles 4 years old and older), 41(1), 1-14, 2010. DOI:doi: 10.3354/cr00836
Setegn, S.G., Srinivasan, R., Dargahi, B.: Hydrological modelling in the Lake Tana Basin, Ethiopia using SWAT model. The Open Hydrology Journal, 2(1), 2008.
Shirke, Y., Kawitkar, R., Balan, S.: Artificial neural network based runoff prediction model for a reservoir. International Journal of Engineering Research and Technology, 1(3), 1-4, 2012.
Simane, B., Beyene, H., Deressa, W., Kumie, A., Berhane, K., Samet, J.: Review of Climate Change and Health in Ethiopia: Status and Gap Analysis. Ethiopian Journal of Health Development, 30(1), 28-41, 2016.
Simard, R., L'Ecuyer, P.: Computing the two-sided Kolmogorov-Smirnov distribution. Journal of Statistical Software, 39(11), 1-18, 2011.
Singb, A.: Digital change detection techniques using remotely sensed data. International Journal of Remote Sensing, 10(6), 989L1003, 1989.
Singh, A.: Review article digital change detection techniques using remotely-sensed data. International journal of remote sensing, 10(6), 989-1003, 1989. DOI:10.1080/01431168908903939
Singh, V.P., Frevert, D.K.: Watershed models. CRC Press, 2005.
SMEC, X.: Hydrological study of the Tana-Beles sub basins. Surface water investigation, MOWR, Addis Ababa, Ethiopia, 2008.
Stamou, A.-T.: Water Resources Optimization using the Nexus Approach, Technische Universität München, 2019.
Steenhuis, T.S., Winchell, M., Rossing, J., Zollweg, J.A., Walter, M.F.: SCS runoff equation revisited for variable-source runoff areas. Journal of Irrigation and Drainage Engineering, 121(3), 234-238, 1995.
Steenhuis, T.S., Collick, A.S., Easton, Z.M., Leggesse, E.S., Bayabil, H.K., White, E.D., Awulachew, S.B., Adgo, E., Ahmed, A.A.: Predicting discharge and sediment for the Abay (Blue Nile) with a simple model. Hydrological processes, 23(26), 3728-3737, 2009. DOI:10.1002/hyp.7513
Suliman, A.H.A., Jajarmizadeh, M., Harun, S., Darus, I.Z.M.: Comparison of semi-distributed, GIS-based hydrological models for the prediction of streamflow in a large catchment. Water resources management, 29(9), 3095-3110, 2015.
Sutcliffe, J., Parks, Y.: The hydrology of the Nile, IAHS Special publication No. 5. Int. Assoc. Hydrol. Sci., Wallingford, UK, 1999.
Tang, L., Yang, D., Hu, H., Gao, B.: Detecting the effect of land-use change on streamflow, sediment and nutrient losses by distributed hydrological simulation. Journal of hydrology, 409(1-2), 172-182, 2011.
Taye, M.T., Ntegeka, V., Ogiramoi, N., Willems, P.: Assessment of climate change impact on hydrological extremes in two source regions of the Nile River Basin. Hydrology and Earth System Sciences, 15(1), 209-222, 2011.
Taye, M.T., Willems, P., Block, P.: Implications of climate change on hydrological extremes in the Blue Nile basin: A review. Journal of Hydrology: Regional Studies, 4, 280-293, 2015.
Taye, M.T., Tadesse, T., Senay, G.B., Block, P.: The Grand Ethiopian Renaissance Dam: Source of Cooperation or Contention? Journal of Water Resources Planning and Management, 142(11), 02516001, 2016.

Taylor, K.E., Stouffer, R.J., Meehl, G.A.: An overview of CMIP5 and the experiment design. Bulletin of the American Meteorological Society, 93(4), 485-498, 2012.
Teegavarapu, R.S., Chandramouli, V.: Improved weighting methods, deterministic and stochastic data-driven models for estimation of missing precipitation records. Journal of Hydrology, 312(1-4), 191-206, 2005.
Teferi, E., Bewket, W., Uhlenbrook, S., Wenninger, J.: Understanding recent land use and land cover dynamics in the source region of the Upper Blue Nile, Ethiopia: Spatially explicit statistical modeling of systematic transitions. Agriculture, ecosystems & environment, 165, 98-117, 2013. DOI:10.1016/j.agee.2012.11.007
Teklay, A., Dile, Y.T., Setegn, S.G., Demissie, S.S., Asfaw, D.H.: Evaluation of static and dynamic land use data for watershed hydrologic process simulation: A case study in Gummara watershed, Ethiopia. Catena, 172, 65-75, 2019.
Tekleab, S., Mohamed, Y., Uhlenbrook, S.: Hydro-climatic trends in the Abay/upper Blue Nile basin, Ethiopia. Physics and Chemistry of the Earth, Parts A/B/C, 61, 32-42, 2013.
Tekleab, S., Mohamed, Y., Uhlenbrook, S., Wenninger, J.: Hydrologic responses to land cover change: the case of Jedeb mesoscale catchment, Abay/Upper Blue Nile basin, Ethiopia. Hydrological Processes, 28(20), 5149-5161, 2014. DOI:10.1002/hyp.9998
Tesemma, Z.K., Mohamed, Y.A., Steenhuis, T.S.: Trends in rainfall and runoff in the Blue Nile Basin: 1964–2003. Hydrological processes, 24(25), 3747-3758, 2010. DOI:10.1002/hyp.7893
Turner, B.L., Lambin, E.F., Reenberg, A.: The emergence of land change science for global environmental change and sustainability. Proceedings of the National Academy of Sciences, 104(52), 20666-20671, 2007.
Uhlenbrook, S.: Biofuel and water cycle dynamics: what are the related challenges for hydrological processes research? Hydrological Processes: An International Journal, 21(26), 3647-3650, 2007.
Uhlenbrook, S., Mohamed, Y., Gragne, A.: Analyzing catchment behavior through catchment modeling in the Gilgel Abay, upper Blue Nile River basin, Ethiopia. Hydrology and Earth System Sciences, 14(10), 2153-2165, 2010. DOI:10.5194/hess-14-2153-2010
USBR: Land and water resources of the Blue Nile basin, Ethiopia. Main report. United States Bureau of Reclamation, Washington, DC., 1964.
USDA: National engineering handbook, Section 4, hydrology. US Government Printing Office Washington DC, 1972.
Van Griensven, A., Ndomba, P., Yalew, S., Kilonzo, F.: Critical review of SWAT applications in the upper Nile basin countries. Hydrology and Earth System Sciences, 16(9), 3371, 2012.
Vaze, J., Post, D., Chiew, F., Perraud, J.-M., Viney, N., Teng, J.: Climate non-stationarity–validity of calibrated rainfall–runoff models for use in climate change studies. Journal of Hydrology, 394(3-4), 447-457, 2010.
Von Storch, H.: Misuses of Statistical Analysis in Climate Research, Analysis of Climate Variability. Springer, pp. 11-26, 1995.
Wale, A.: Hydrological Balance of Lake Tana Upper Blue Nile Basin, Ethiopia. ITC thesis, 2008, 159-180, 2008.
Wallner, M., Haberlandt, U., Dietrich, J.: Evaluation of different calibration strategies for large scale continuous hydrological modelling. Advances in Geosciences 31 (2012), 31, 67-74, 2012.

Wang, Z.-M., Batelaan, O., De Smedt, F.: A distributed model for water and energy transfer between soil, plants and atmosphere (WetSpa). Physics and Chemistry of the Earth, 21(3), 189-193, 1996.
WAPCOS: Preliminary water resources development master plan for Ethiopia. Prepared for EVDSA. Addis Ababa, Final report., 1990.
White, E.D., Easton, Z.M., Fuka, D.R., Collick, A.S., Adgo, E., McCartney, M., Awulachew, S.B., Selassie, Y.G., Steenhuis, T.S.: Development and application of a physically based landscape water balance in the SWAT model. Hydrological Processes, 25(6), 915-925, 2011.
Wigley, T.M.: MAGICC/SCENGEN 5.3: User manual (version 2). NCAR, Boulder, CO, 80, 2008.
Wikipedia: Grand Ethiopian Renaissance Dam. Wikipedia, The Free Encyclopedia, 2019.
Wilby, R., Charles, S., Zorita, E., Timbal, B., Whetton, P., Mearns, L.: Guidelines for use of climate scenarios developed from statistical downscaling methods. available from the DDC of IPCC TGCIA 27, 2004a.
Wilby, R., Charles, S., Zorita, E., Timbal, B., Whetton, P., Mearns, L.: Guidelines for use of climate scenarios developed from statistical downscaling methods. 2004b.
Wilby, R., Dawson, C., Barrow, E.: SDSM user manual-a decision support tool for the assessment of regional climate change impacts, London, UK, 2007.
Wilby, R.L., Wigley, T.: Downscaling general circulation model output: a review of methods and limitations. Progress in Physical Geography, 21(4), 530-548, 1997.
Wilby, R.L., Hay, L.E., Leavesley, G.H.: A comparison of downscaled and raw GCM output: implications for climate change scenarios in the San Juan River basin, Colorado. Journal of Hydrology, 225(1-2), 67-91, 1999.
Wilby, R.L., Dawson, C.W., Barrow, E.M.: SDSM—a decision support tool for the assessment of regional climate change impacts. Environmental Modelling & Software, 17(2), 145-157, 2002.
Winchell, M., Srinivasan, R., Di Luzio, M., Arnold, J.: ArcSWAT interface for SWAT 2012–User's guide. Blackland Research and Extention Center Texas Agrilife Research & Grassland, Soil and Water Laboratory USDA Agricultural Research Service, Available at: Temple, Texas, USA, 2013.
WMO: Guide to Hydrological Practices. Volume I: Hydrology–From Measurement to Hydrological Information. World Meteorological Organization Geneva, 2008.
Woldesenbet, T.A., Elagib, N.A., Ribbe, L., Heinrich, J.: Gap filling and homogenization of climatological datasets in the headwater region of the Upper Blue Nile Basin, Ethiopia. International Journal of Climatology, 37(4), 2122-2140, 2017a. DOI:10.1002/joc.4839
Woldesenbet, T.A., Elagib, N.A., Ribbe, L., Heinrich, J.: Hydrological responses to land use/cover changes in the source region of the Upper Blue Nile Basin, Ethiopia. Science of the Total Environment, 575, 724-741, 2017b. DOI:10.1016/j.scitotenv.2016.09.124
Woldesenbet, T.A., Elagib, N.A., Ribbe, L., Heinrich, J.: Catchment response to climate and land use changes in the Upper Blue Nile sub-basins, Ethiopia. Science of the Total Environment, 644, 193-206, 2018.
Worqlul, A.W., Maathuis, B., Adem, A.A., Demissie, S.S., Langan, S., Steenhuis, T.S.: Comparison of rainfall estimations by TRMM 3B42, MPEG and CFSR with ground-observed data for the Lake Tana basin in Ethiopia. Hydrology and Earth System Sciences, 18(12), 4871-4881, 2014.

WRB, I.W.G.: World Reference Base for Soil Resources 2014, update 2015 International soil classification system for naming soils and creating legends for soil maps. World Soil Resources Reports No. 106, 192, 2015.
Xu, C.-Y., Singh, V.P.: A review on monthly water balance models for water resources investigations. Water Resources Management, 12(1), 20-50, 1998.
Xu, C.-y.: From GCMs to river flow: a review of downscaling methods and hydrologic modelling approaches. Progress in Physical Geography, 23(2), 229-249, 1999.
Yan, B., Fang, N., Zhang, P., Shi, Z.: Impacts of land use change on watershed streamflow and sediment yield: an assessment using hydrologic modelling and partial least squares regression. Journal of Hydrology, 484, 26-37, 2013. DOI:10.1016/j.jhydrol.2013.01.008
Yates, D.N., Strzepek, K.M.: An assessment of integrated climate change impacts on the agricultural economy of Egypt. Climatic Change, 38(3), 261-287, 1998a.
Yates, D.N., Strzepek, K.M.: Modeling the Nile Basin under climatic change. Journal of Hydrologic Engineering, 3(2), 98-108, 1998b.
Yimer, G., Jonoski, A., Van Griensven, A.: Hydrological response of a catchment to climate change in the upper Beles river basin, upper blue Nile, Ethiopia. Nile Basin Water Engineering Scientific Magazine, 2, 49-59, 2009.
Yin, J., He, F., Xiong, Y.J., Qiu, G.Y.: Effects of land use/land cover and climate changes on surface runoff in a semi-humid and semi-arid transition zone in northwest China. Hydrology and Earth System Sciences, 21(1), 183-196, 2017. DOI:10.5194/hess-21-183-2017
Yue, S., Pilon, P., Phinney, B., Cavadias, G.: The influence of autocorrelation on the ability to detect trend in hydrological series. Hydrological Processes, 16(9), 1807-1829, 2002. DOI:10.1002/hyp.1095
Yue, S., Wang, C.: The Mann-Kendall test modified by effective sample size to detect trend in serially correlated hydrological series. Water Resources Management, 18(3), 201-218, 2004.
Zaitchik, B.F., Simane, B., Habib, S., Anderson, M.C., Ozdogan, M., Foltz, J.D.: Building climate resilience in the Blue Nile/Abay Highlands: A role for earth system sciences. International journal of environmental research and public health, 9(2), 435-461, 2012.
Zeleke, G.: Landscape dynamics and soil erosion process modelling in the north-western Ethiopian highlands, 2000.
Zhang, H., Wang, Y., Wang, Y., Li, D., Wang, X.: The effect of watershed scale on HEC-HMS calibrated parameters: a case study in the Clear Creek watershed in Iowa, US. Hydrology and Earth System Sciences, 17(7), 2735-2745, 2013.
Zhang, N., He, H.M., Zhang, S.F., Jiang, X.H., Xia, Z.Q., Huang, F.: Influence of reservoir operation in the upper reaches of the Yangtze River (China) on the inflow and outflow regime of the TGR-based on the improved SWAT model. Water resources management, 26(3), 691-705, 2012.

Appendices

Appendix 1: List of weather stations and percentage gaps

			Location		Rainfall		Temperature	
No.	Station Name	Elevation (masl)	Easting	Northing	Period of records	Percentage of missing (%)	Period of records	Percentage of missing (%)
1	Gondar[a]	1967	37.43	12.52	1952-2011	7.5	1952-2012	10.1
2	Debre Markos[a]	2515	37.67	10.33	1954-2012	1.9	1953-2012	3.0
3	Debre Tabor[a]	2612	38	11.87	1954-2011	27.8	1951-2011	28.6
4	Dangila[a]	2116	36.85	11.43	1954-2011	34.2	1954-2011	31.3
5	Enjibara[d]	2670	36.9	10.97	1954-2011	38.7		
6	Debark[d]	1900	37.9	13.16	1955-2011	57.7	1973-2011	44.9
7	Dejen[d]	2420	38.15	10.17	1957-2011	60.8		
8	Gimijabet[c,b]	2320	36.6	10.75	1958-2011	32.4		
9	Feres bet[d]	2870	37.61	10.85	1959-2007	54.7		
10	Bahir Dar [a,b,c]	1770	37.42	11.6	1961-2012	1.6	1961-2012	1.5
11	Shambu[c,b]	2460	37.12	9.57	1961-2014	33.5	1974-2014	33.1
12	Ayikel[d]	2150	37.05	12.53	1968-2011	37.4	1969-2011	31.9
13	Angerguten[c,b]	1350	36.33	9.27	1972-2011	39.5	1972-2011	33.0
14	Zege[b]	1800	37.32	11.71	1974-2011	38.9	1974-2011	20.5
15	Tillili[d]	2570	37.05	10.58	1974-2011	31.9		
16	Nedjo[a,b,c]	1800	35.45	9.5	1974-2014	20.3	1974-2014	24.9
17	Abaysheleko[b,c]	1790	38.16	10.11	1983-2011	10.6	1983-2011	33.0
18	Alem Ketema[c,b]	2280	39.03	10.03	1973-2013	7.6	1973-2013	32.5
19	Mehal Meda [d]	3084	39.66	10.31	1984-2014	9.7	1984-2014	12.2
20	Gidayana[b]	1850	36.62	9.87	1970-2011	7.5	1989-2011	33.6
21	Dedessa[b]	1310	36.1	9.38	1984-2014	12.7	1984-2014	35.0
22	Fiche[b]	2784	38.73	9.77	1984-2015	1.4	1984-2014	4.3
23	Anger[d]	1350	36.33	9.27	1984-2014	14.6	1984-2011	37.6
24	Gatira[d]	2358	36.2	7.98	1984-2014	14.9	1990-2014	47.3
25	Wegel Tena[d]	2952	39.22	11.59	1984-2014	21.6	1984-2014	35.3
26	Chagni[d]	1614	36.5	10.97	1973-2011	14.6	1984-2014	26.9
27	Debre Berhan[b]	2750	39.5	9.63	1984-2014	1.9	1984-2014	1.2
28	Bedele[c,b]	2011	36.33	8.45	1970-2011	10.2	1970-2013	17.2
29	Adet[b]	2179	37.49	11.27	1986-2014	4.5	1986-2014	10.3
30	Pawe[d]	1119	36.41	11.31	1986-2014	3.1	1986-2014	21.6
31	Ayira[d]	1555	35.55	9.1	1987-2014	11.4	1987-2014	41.5
32	Mekane selam[b]	2605	38.76	10.74	1988-2014	29.1	1988-2014	29.5
33	Yetnora [b]	2420	38.11	10.24	1988-2014	8.7	1988-2014	38.4
34	Lay Birr[d]	1707	37.17	10.59	1989-2015	7.4	1989-2012	21.7

35	Ayehu[d]	1771	36.79	10.66	1989-2014	12.9	1987-2014	48.1
36	Motta[b]	2417	37.89	11.07	1990-2014	5.6	1988-2014	6.9
37	Addis Ababa[a,b,c]	2354	38.75	9.03	1970-2011	0.6	1970-2011	1.8
38	Kombolcha[a,b,c]	1857	39.72	11.08	1970-2011	0.4	1970-2011	1.2
39	Nekemit[a,b,c]	2080	36.46	9.08	1970-2011	2.4	1970-2011	8.3
40	Assosa[a,b,c]	1600	34.52	10.00	1970-2011	20.0	1970-2011	24.8

[c]: stations selected for statistical trend analysis, [a]: stations selected for SWAT hydrological model, and [b]: stations selected for HEC-HMS model, [d]: stations discarded for further analysis

Appendix 2: List of hydrology stations and percentage gaps in the UBNRB

No.	Station Name	Lat.	Long.	Drainage area (km^2)	Period of records	% of missed records	Sub-basin
1	Abay Nr.Kessie[1]	11.07	38.18	65784	1961-2004	6.80	N/Gojam
2	Aleltu Nr. Nedjo[2]	9.50	35.00	168	1980-2006	10.19	Dabus
3	Amen Nr. Dangila[2]	11.27	36.87	89	1988-2005	15.89	Tana
4	Anger Nr. Nekemte[2]	9.43	36.52	4674	1982-2004	17.52	Anger
5	Angreb Nr.Gonder[2]	12.63	37.48	41	1983-2005	4.71	Tana
6	Ardy Nr. Metekel[2]	10.95	36.52	219	1977-2004	5.53	S/Gojam
7	Ataye Nr Ataye[3]	10.33	39.98	166.4	1981-2004	10.31	
8	Azuari Nr. Motta[3]	10.97	38.02	209	1980-2004	13.13	N/Gojam
9	BorekenaNr. kombolicha[2]	11.05	39.73	281	1976-2001	42.57	
01	Chemoga Nr. Debre Markos[1]	10.30	37.73	364	1973-2007	4.89	S/Gojam
11	Chena Nr. Estie[2]	11.62	38.03	33	1985-2008	14.63	N/Gojam
12	Dabana Nr. Bedelle[2]	8.40	36.28	47	1984-2004	8.49	Dedessa
13	Didesa Nr. Arjo[3]	8.68	34.42	9981	1963-2007	24.05	Dedessa
14	Dilla Nr. Nedjo[2]	9.45	35.55	69	1981-2005	23.31	Dabus
15	Dondor Nr. Metekel[2]	10.93	36.52	184	1980-2004	6.76	S/Gojam
16	Dura Nr. Metekel[1]	10.98	36.48	539	1962-2005	10.97	S/Gojam
17	Gambella Nr. Asosa[2]	10.00	34.62	5.5	1979-2006	28.87	Dabus
18	Gelda Nr. Ambesame[2]	11.70	37.63	32	1984-2006	12.94	Tana
19	Gilgel Abay Nr.Merawi [1]	11.37	37.03	1664	1970-2011	9.8	Tana
20	Gilgel Beles Nr. Mandura[2]	11.17	36.37	675	1980-2008	2.72	Beles
21	Gudla Nr.Denbecha[1]	10.55	37.50	242	1962-2003	8.27	S/Gojam
22	Gumara Nr. Bahir Dar[1]	11.83	37.63	1394	1970-2009	11	Tana
23	Hafa Nr. Assosa[2]	9.97	34.67	194	1980-2003	10.68	Dabus
24	Hoha Nr.Asosa[1]	10.15	34.63	161	1966-2005	10.97	Dabus
25	Hujur Nr.Nedjo[2]	9.63	35.33	94	1980-2003	18.12	Dabus

26	Jara Nr Jara[2]	10.52	39.95	235.4	1981-2003	3.54	
27	Koga nr. Merawi[2]	12.37	37.05	244	1980-2008	10.20	Tana
28	Komis Nr.Gori[2]	9.57	35.38	112	1984-2000	4.62	Dabus
29	Lah Nr.Finote-Selam[2]	10.68	37.27	288	1984-2003	4.61	S/Gojam
30	Lake Tana Bahir Dar[1]	11.60	37.38	15154	1961-2014	3.45	Tana
31	Leza Nr.Jiga[2]	10.67	37.33	175	1981-2003	24.65	S/Gojam
32	Main Beles Nr.Metekel[1]	11.25	36.45	3431	1962-2005	22.05	Beles
33	Megech Azezo[2]	12.48	37.45	462	1980-2008	2.03	Tana
34	Muga Nr Dejen[2]	10.17	38.15	375	1981-2003	7.72	
35	Quasheni Nr. Addis Kidame[2]	11.20	36.87	42	1984-2006	13.51	Tana
36	Ribb River Nr. Addis Zemen[1]	12.00	37.72	1664	1961-2014	8.23	Tana
37	Ribb Nr. Debratabor[2]	12.05	37.98	844	1980-2008	7.70	Tana
38	Robi @ Robit[2]	10.00	39.88	263	1983-2004	14.55	
39	Sechi Nr.Mendi[2]	9.70	35.22	562	1979-2003	19.08	Dabus
40	Suha Nr. Bichena[2]	10.42	38.18	359	1985-2004	7.11	N/Gojam
41	TemechaNr.Denbecha[1]	10.53	37.50	406	1962-2004	8.21	S/Gojam
42	Teme Nr. Motta[2]	10.42	37.98	156	1984-2003	2.67	S/Gojam
43	Upper FettamNr. Tilili[2]	10.85	37.02	282	1980-2004	24.88	S/Gojam
44	Wenka Nr. Estie[2]	11.62	38.07	110	1987-2003	13.92	N/Gojam
45	Andasa Nr. Bahir Dar[2]	11.50	37.48	573	1990-2004	3.30	N/Gojam
46	Tigder Nr. Gumde-Woin[3]	10.88	38.02	**NA**	1995-2004	6.02	N/Gojam
47	Neshi Nr. Shambo[3]	9.75	37.25	322	1985-2008	0.99	Fincha
48	Bongeno Nr.Lummame[3]	10.25	37.95	166	1987-2003	18.23	S/Gojam
49	Missini Nr.Kossober[3]	10.93	36.87	16	1988-2004	4.80	S/Gojam
50	Anger Nr. Nekemte[2]	9.43	36.52	4674	1994-2004	11.69	Anger
51	Sifa Nr. Nekemte[3]	8.87	36.78	951	1962-1967	0.59	Dedessa
52	Wama Nr. Nekemte[3]	8.78	36.78	844	1980-1985	38.78	Dedessa
53	Tatto Nr. Gutie Nekemte[3]	9.02	36.65	42.5	1996-2009	0.04	Dedessa
54	Endris Nr. Sire[3]	9.03	36.85	49	1988-2006	0.23	Dedessa
55	Dabus Nr. Asosa[3]	9.87	34.90	10139	1963-1979	32.55	Dabus
56	Mutsa Nr. Bambasi[3]	9.75	34.73	16	1989-1999	41.52	Dabus
57	Ayo_Nr.Kosober[3]	10.97	36.78	398	1995-2004	6.00	S/Gojam
58	Yeda Nr. Amber[3]	10.25	37.82	125	1988-2005	4.44	S/Gojam
59	Uke Nr. Nekmete[3]	9.32	36.52	204	1985-2005	2.61	Anger
60	Mendel Nr. Tis Abay[3]	11.48	37.57	72	1987-2003	4.80	N/Gojam

[1] and [2] in the table denote stations considered for filling the missing records for stations which have records from (1971-2010) and (1984-2011) respectively, [3] denotes stations discarded from the analysis and Nr. represents near.

Appendix 3: Mann-Kendal trend test and statistical summary of daily rainfall at 15 selected stations of UBNRB (1971-2010) ; (+) sign indicate upward shift and (-) sign indicate downward shift, numbers in bold designate p value for statistically significant trend and change points

Station	Kendall's tau	MK test p-value	Sen's slope	Pettitt test change time	Pettitt test p-value
Addis Ababa	-0.002	0.798	7.651E-5	1983	0.14
Alemketema	-0.018	**0.004**	6.455E-5	1978 (-)	**<0.0001**
Angergutten	0.048	**< 0.0001**	1.059E-4	1989 (+)	**<0.0001**
Assosa	0.024	**< 0.0001**	1.221E-4	1989 (+)	**<0.0001**
Bahirdar	0.016	**0.008**	1.004E-4	1988 (+)	**<0.0001**
Bedele	-0.001	0.916	1.223E-4	1983 (-)	**0.036**
Kombolicha	0.006	0.328	9.884E-5	1986 (+)	**0.003**
Dangila	0.014	**0.019**	1.195E-4	1983 (+)	**<0.0001**
Debre tabor	-0.002	0.764	8.482E-5	1986 (-)	**0.002**
Debre Markos	0.019	**0.001**	1.284E-4	1989 (+)	**<0.0001**
Gimija-bet	0.019	**0.001**	0	1980 (+)	**<0.0001**
Gondar	-0.001	0.898	7.889E-5	1977 (-)	**0.023**
Nedjo	-0.023	**0.000**	7.394E-5	1977 (-)	**<0.0001**
Nekemit	0.010	0.080	1.643E-4	1992 (+)	**<0.0001**
Shambu	-0.003	0.591	1.414E-4	1993 (+)	**0.012**

Appendix 4: Mann-Kendal trend test and statistical summary of monthly rainfall at 15 selected stations of UBNRB (1971-2010) ; (+) sign indicate upward shift and (-) sign indicate downward shift, numbers in bold designate p value for statistically significant trend and change points

Stations	Kendall's tau	p-value	Sen's slope	Pettitt test change time	Pettitt test p-value
Addis Ababa	-0.003	0.925	-0.003	1998	0.99
Alemketema	-0.029	0.340	-0.002	1993	0.66
Angergutten	0.003	0.914	0	1989	0.89
Assosa	0.012	0.709	0	1997	0.37
Bahirdar	0.009	0.770	0	1988	0.94
Bedele	-0.002	0.956	-6.281E-4	1983	0.98
Kombolicha	-0.009	0.772	0	1998	0.77
Dangila	0.031	0.317	0.003	1988	0.67
Debre Tabor	0.018	0.561	8.608E-4	1992	0.98
Debre Markos	0.020	0.518	0.009	1991	0.89
Gimija-bet	0.047	0.127	0.031	1984	0.38
Gondar	-0.009	0.765	0	1980	0.88
Nedjo	-0.017	0.584	-3.420E-4	1981	0.65
Nekemit	0.004	0.897	3.547E-4	1992	0.96
Shambu	0.028	0.362	0.016	1984	0.64

Appendix 5: Mann-Kendal trend test and statistical summary of annual rainfall at 15 selected stations of UBNRB (1971-2010) ; (+) sign indicate upward shift and (-) sign indicate downward shift, numbers in bold designate p value for statistically significant trend and change points

Stations	Kendall's tau	p-value	Sen's slope	Pettitt test change time	Pettitt test p-value
Addis Ababa	-0.077	0.494	-1.58	1986	0.75
Alemketema	-0.223	**0.043**	-4.09	1991 (-)	**0.0**15
Angergutten	0.056	0.619	2.25	1987	0.297
Assosa	0.018	0.880	0.47	1988	0.51
Bahirdar	-0.013	0.917	-0.69	1976	0.15
Bedele	-0.041	0.720	-1.27	1983	0.45
Kombolicha	0.008	0.954	0.13	2000	0.22
Dangila	0.054	0.635	1.58	1982	0.94
Debre tabor	-0.074	0.509	-2.30	1982	0.13
Debre Markos	0.269	**0.014**	5.02	1995 (+)	**0.012**
Gimija-bet	0.369	**0.001**	16.21	1986 (+)	**0.000**
Gondar	0.064	0.571	1.41	1977	0.27
Nedjo	-0.049	0.669	-2.26	1973	0.57
Nekemit	0.031	0.790	0.71	1991	0.26
Shambu	0.259	**0.019**	6.58	1983 (+)	**0.001**

Appendix 6: Mann-Kendal trend test and statistical summary of daily Tmax at 10 selected stations of UBNRB (1971-2010) ; (+) sign indicate upward shift and (-) sign indicate downward shift, numbers in bold designate p value for statistically significant trend and change points

Stations	p-value	Sen's slope	Pettitt test change time	Pettitt test p-value
Addis Ababa	< **0.0001**	8.135E-5	1987 (+)	**<0.0001**
Assosa	0.708	1.256E-5	1979 (+)	**<0.0001**
Bahirdar	< **0.0001**	4.390E-5	1994 (+)	**<0.0001**
Kombolicha	< **0.0001**	1.225E-4	1997 (-)	**<0.0001**
Dangila	**0.004**	-1.601E-4	1988 (-)	**<0.0001**
Debre Markos	**0.000**	4.068E-5	1993 (+)	**<0.0001**
Debre Tabor	< **0.0001**	8.781E-5	1993 (+)	**<0.0001**
Gondar	< **0.0001**	6.470E-5	1993 (+)	**<0.0001**
Nedjo	< **0.0001**	7.059E-5	1997 (+)	**<0.0001**
Nekemit	< **0.0001**	7.416E-5	1993 (+)	**<0.0001**

Appendix 7: Mann-Kendal trend test and statistical summary of monthly Tmax at 10 selected stations of UBNRB (1971-2010) ; (+) sign indicate upward shift and (-) sign indicate downward shift, numbers in bold designate p value for statistically significant trend and change points

Stations	p-value	Sen's slope	Pettitt test change time	Pettitt test p-value
Addis Ababa	< **0.0001**	0.002	1987 (+)	<**0.0001**
Assosa	0.846	1.849E-4	1979	0.274
Bahirdar	**0.029**	0.001	1994 (+)	**0.026**
Combolicha	< **0.0001**	0.004	1994 (+)	<**0.0001**
Dangila	< **0.0001**	-0.005	1988 (-)	<**0.0001**
Debre Markos	0.118	0.001	1993	0.09
Debre Tabor	**0.000**	0.003	1993 (+)	<**0.0001**
Gondar	**0.014**	0.002	1993 (+)	**0.008**
Nedjo	**0.017**	0.002	1997 (+)	**0.036**
Nekemit	**0.005**	0.002	1993 (+)	**0.016**

Appendix 8: Mann-Kendal trend test and statistical summary of annual Tmax at 10 selected stations of UBNRB (1971-2010) ; (+) sign indicate upward shift and (-) sign indicate downward shift, numbers in bold designate p value for statistically significant trend and change points

Stations	p-value	Sen's slope	Pettitt test change time	Pettitt test p-value
Addis Ababa	< **0.0001**	0.031	1990 (+)	<**0.001**
Assosa	0.730	0.002	1979 (+)	**0.029**
Bahirdar	**0.005**	0.021	1994 (+)	**0.003**
Combolicha	< **0.0001**	0.047	1996 (+)	<**0.0001**
Dangila	0.124	-0.03	1988 (+)	<**0.0001**
Debre Markos	**0.008**	0.015	1993 (+)	**0.001**
Debre Tabor	< **0.0001**	0.038	1993 (+)	<**0.0001**
Gondar	**0.000**	0.027	1993 (+)	<**0.0001**
Nedjo	< **0.0001**	0.027	1997 (+)	<**0.0001**
Nekemit	< **0.0001**	0.031	1994 (+)	<**0.0001**

Appendix 9: Mann-Kendal trend test and statistical summary of daily Tmin at 10 selected stations of UBNRB (1971-2010) ; (+) sign indicate upward shift and (-) sign indicate downward shift, numbers in bold designate p value for statistically significant trend and change points

Stations	MK test p-value	Sen's slope	Pettitt test change time	Pettitt test p-value
Addis Ababa	< **0.0001**	1.485E-4	1995 (+)	<0.0001
Assosa	< **0.0001**	6.119E-5	1980 (+)	**<0.0001**
Bahirdar	< **0.0001**	1.965E-4	1980 (+)	**<0.0001**
Kombolicha	< **0.0001**	1.110E-4	1986 (+)	**<0.0001**
Dangila	< **0.0001**	2.035E-4	1979 (+)	**<0.0001**
Debre Markos	< **0.0001**	1.209E-4	1991 (+)	<0.0001
Debre tabor	< **0.0001**	-1.638E-5	1988 (-)	**<0.0001**
Gondar	< **0.0001**	8.143E-5	1991 (+)	**<0.0001**
Nedjo	< **0.0001**	-3.588E-5	1977 (-)	**<0.0001**
Nekemit	< **0.0001**	9.424E-5	1990 (+)	**<0.0001**

Appendix 10: Mann-Kendal trend test and statistical summary of monthly Tmin at 10 selected stations of UBNRB (1971-2010) ; (+) sign indicate upward shift and (-) sign indicate downward shift, numbers in bold designate p value for statistically significant trend and change points

Stations	MK test p-value	Sen's slope	Pettitt test change time	Pettitt test p-value
Addis Ababa	< **0.0001**	0.004	1995 (+)	**<0.0001**
Assosa	**0.010**	0.001	1980 (+)	**<0.0001**
Bahirdar	< **0.0001**	0.005	1980 (+)	**<0.0001**
Kombolicha	**0.000**	0.003	1986 (+)	**<0.0001**
Dangila	< **0.0001**	0.006	1979 (+)	**<0.0001**
Debre Markos	< **0.0001**	0.003	1991 (+)	**<0.0001**
Debre tabor	0.078	-7.217E-4	1988	0.079
Gondar	**0.000**	0.002	1991 (+)	**<0.0001**
Nedjo	**0.002**	-0.002	1987 (-)	**0.000**
Nekemit	< **0.0001**	0.003	1990 (+)	**<0.0001**

Appendix 11: Mann-Kendal trend test and statistical summary of annual Tmin at 10 selected stations of UBNRB (1971-2010) ; (+) sign indicate upward shift and (-) sign indicate downward shift, numbers in bold designate p value for statistically significant trend and change points

Stations	MK test p-value	Sen's slope	Pettitt test change time	Pettitt test p-value
Addis Ababa	< **0.0001**	0.049	1990 (+)	**<0.0001**
Assosa	0.546	0.006	1980	0.058
Bahirdar	**0.000**	0.063	1986 (+)	**0.000**
Kombolicha	0.072	0.023	1981 (+)	**0.006**
Dangila	< **0.0001**	0.057	2000 (+)	**0.001**
Debre Markos	< **0.0001**	0.04	1990 (+)	**<0.0001**
Debre tabor	0.053	-0.01	1998 (-)	**0.037**
Gondar	**0.000**	0.026	1990 (+)	**<0.0001**
Nedjo	0.079	-0.025	2002	0.086
Nekemit	< **0.0001**	0.031	1989 (+)	**<0.0001**

Appendix 12: Calibration results of the average statistical tests comparing the observed data from 26 stations with synthetic data generated through LARS-WG 6.

		KS				t-test			F-test
No.	Station	WD series	Rain D	Tmin D	Tmax D	RM M	Tmin M	Tmax M	RM V
1	Abaysheleko	0	0	0	0	0	0	0	1
2	Addis Ababa	0	0	0	0	0	0	1	2
3	Adet	0	0	0	0	0	0	0	2
4	Alemketema	0	0	0	0	0	0	0	2
5	Angergutten	0	0	0	0	1	0	0	6
6	Arijo	0	0	0	0	0	0	0	4
7	Assosa	0	0	0	0	0	0	0	1
8	Ayehu	0	0	0	0	0	0	1	2
9	Ayira	0	0	0	0	0	1	1	2
10	Bahirdar	0	0	0	0	0	0	1	3
11	Bedele	0	0	0	0	0	0	1	0
12	Komibolicha	0	0	0	0	0	0	0	1
13	Dangila	0	0	0	0	0	0	0	1
14	Debre Birhan	0	0	0	0	2	0	0	3
15	Dedesa	0	0	0	0	0	0	0	1
16	Debre Markos	0	0	0	0	1	0	1	2
17	Debre Tabor	0	0	0	0	0	0	0	2
18	Fitche	0	0	0	0	0	0	0	0
19	Gatira	0	0	0	0	1	0	1	2
20	Gidayana	0	0	0	0	1	0	1	1
21	Gimijabet	0	0	0	0	0			7
22	Gondar	0	0	0	0	2	0	1	1
23	Motta	0	0	0	0	0	0	0	1
24	Nedjo	0	0	0	0	0	0	0	2
25	Nekemit	0	0	0	0	0	0	0	2
26	Shambu	0	0	0	0	1	0	1	2
27	Yetnora	0	0	0	0	1	0	0	4
28	Zege	0	0	0	0	0	0	0	2
29	Mekane Selam	0	0	0	0	0	0	0	2
	Average	0	0	0	0	0.34	0.036	0.36	2.1
	Number	8	12	12	12	12	12	12	12
	% failed	0.0	0.0	0.0	0.0	2.9	0.3	3.0	17.5

Note: The numbers in the table show the average numbers of tests gave P value less than 5 % significance level.

Appendix 13: Mean annual and relative percent changes of precipitation statistics by the 2030s, 2050s and 2080s relative to the mean of the base case.

GCM	scenario	2030s	2050s	2080s	2030s	2050s	2080s
CSMK3-A1B	A1B	1385	1358	1319	-2.3	-4.2	-7.0
CSMK3-B1	B1	1385	1379	1342	-2.3	-2.7	-5.3
GFCM21-A1B	A1B	1397	1305	1311	-1.4	-8.0	-7.5
GFCM21-B1	B1	1409	1428	1387	-0.6	0.7	-2.2
GFCM21-A2	A2	1365	1312	1334	-3.7	-7.4	-5.9
HADCM3-A1B	A1B	1448	1480	1600	2.1	4.4	12.9
HADCM3-B1	B1	1429	1447	1475	0.8	2.1	4.1
HadCM3-A2	A2	1441	1467	1654	1.7	3.5	16.7
MIHR-A1B	A1B	1445	1495	1563	1.9	5.5	10.2
MIHR-B1	B1	1470	1496	1502	3.7	5.5	6.0
MPEH5-A1B	A1B	1443	1453	1503	1.8	2.5	6.0
MPEH5-B1	B1	1465	1499	1437	3.3	5.8	1.4
MPEH5-A2	A2	1410	1477	1464	-0.5	4.2	3.3
NCCCSM-A1B	A1B	1510	1740	1842	6.5	22.8	29.9
NCCCSM-B1	B1	1528	1730	1612	7.8	22.0	13.7
NCCCSM-A2	A2	1508	1541	2038	6.4	8.7	43.7
GFDL-RCP4.5	RCP4.5	1274	1268	1276	-9.5	-10.0	-9.4
GFDL-RCP8.5	RCP8.5	1259	1267	1288	-10.6	-10.0	-8.5
HadGEM2-RCP4.5	RCP4.5	1420	1406	1471	0.8	-0.1	4.5
HadGEM2-RCP8.5	RCP8.5	1444	1383	1470	2.6	-1.7	4.4
MPI-RCP4.5	RCP4.5	1378	1398	1419	-2.1	-0.7	0.8
MPI-RCP8.5	RCP8.5	1426	1408	1401	1.3	0.0	-0.5
canESM2-RCP2.6	RCP2.6	1663	1711	1694	17.9	21.4	20.2
canESM2-RCP4.5	RCP4.5	1650	1732	1781	17.0	22.8	26.3
canESM2-RCP8.5	RCP8.5	1678	1826	2028	19.0	29.5	43.8
HadCM3-A2a	A2a	1553	1583	1670	2.1	4.0	9.7
HadCM3-B2a	B2a	1559	1575	1617	2.4	3.5	6.2
Model average					2.4	4.6	8.1

Appendix 14: Performance measure and ranking of models during the baseline period (1984-2011) for the evaluation metric RMSE (equally weighted)

	Value (mm)			Score		
Stations	canESM2/SDSM	HadCM3/SDSM	LARS-WG	canESM2/SDSM	HadCM3/SDSM	LARS-WG
Abaysheleko	7.42	15.68	18.86	1	2	3
Alemketema	19.43	7.6	10.48	3	1	2
Anger	11.05	13.13	10.01	2	3	1
Angergutten	8.18	16.11	9.81	1	3	2
Bahirdar	8.49	21.67	11.51	1	3	2
Bedele	6.42	46.07	14.67	1	3	2
Dangila	13.18	53.84	8.97	2	3	1
Dedesa	8.24	18.02	13.84	1	3	2
Debre Markos	5.04	19.11	12.53	1	3	2
Debre Tabor	22.39	39.37	10.71	2	3	1
Fitche	17.75	11.23	10.77	3	2	1
Gimijabet	14.49	32.4	11.41	2	3	1
Gondar	4.96	18.19	3.58	2	3	1
Nedjo	8.35	15.35	11.66	1	3	2
Shambu	8.6	15.68	10.74	1	3	2
				24	41	25

Appendix 15: Performance measure and ranking of models during the baseline period (1984-2011) for the evaluation metric MAE (equally weighted)

	Value (mm)			Score		
Stations	canESM2/SDSM	HadCM3/SDSM	LARS-WG	canESM2/SDSM	HadCM3/SDSM	LARS-WG
Abaysheleko	5.35	12.41	12.54	1	2	3
Alemketema	12.84	6.17	6.79	3	1	2
Anger	7.9	8.73	7.7	2	3	1
Angergutten	6.33	12.3	8.22	1	3	2
Bahirdar	6.05	12.87	7.78	1	3	2
Bedele	4.44	36.25	10.81	1	3	2
Dangila	9.32	37.52	7.13	2	3	1
Dedesa	5.67	11.9	9.89	1	3	2
Debre Markos	3.66	13.43	9.98	1	3	2
Debre Tabor	14.82	25.03	8.83	2	3	1
Fitche	8.39	8.17	7.48	3	2	1
Gimijabet	11.01	21.87	7.63	2	3	1

Gondar	3.52	13.29	2.66	2	3	1
Nedjo	5.09	11.73	8.98	1	3	2
Shambu	6.01	12.41	7.99	1	3	2
				24	41	25

Appendix 16: Performance measure and ranking of models during the baseline period (1984-2011) for the evaluation metric Bias (equally weighted)

	Value (mm)			Score		
Stations	canESM2/ SDSM	HadCM3/ SDSM	LARS-WG	canESM2/ SDSM	HadCM3/ SDSM	LARS-WG
Abaysheleko	2.59	12.17	5.06	1	3	2
Alemketema	8.42	0.9	-0.53	3	2	1
Anger	-7.08	5.8	1.46	3	2	1
Angergutten	-2.51	7.59	-0.33	2	3	1
Bahirdar	1.11	8.33	-5.67	1	3	2
Bedele	-1.48	23.89	-0.77	2	3	1
Dangila	-8.86	2.89	1.67	3	2	1
Dedesa	-3.02	3.42	-2.02	2	3	1
Debre Markos	1.02	8.9	0.58	2	3	1
Debre Tabor	-14.26	-14.6	-4.84	2	3	1
Fitche	-3.9	0.04	2.60	3	1	2
Gimijabet	-5.72	5.4	0.81	3	2	1
Gondar	0.51	2.16	-0.71	1	3	2
Nedjo	-4.19	-7.23	2.94	2	3	1
Shambu	-0.69	12.17	-3.79	1	3	2
				31	39	20

Appendix 17 : Weighted performance measures for different models based on weights defined under section 6.1.3 during the baseline period (1984-2011) for all stations.

	RMSE			MAE			Bias			Overall weight performance			Score		
Stations	canESM2/SDSM	HadCM3/SDSM	LARS-WG	canESM2/SDSM	HadCM3/SDSM	LARS-WG	canESM2/SDSM	HadCM3/SDSM	LARS-WG	canESM2/SDSM	HadCM3/SDSM	LARS-WG	canESM2/SDSM	HadCM3/SDSM	LARS-WG
Abaysheleko	0.14	0.29	0.35	0.21	0.49	0.50	0.03	0.15	0.06	0.38	0.94	0.91	1	3	2
Alemketema	0.35	0.14	0.19	0.50	0.24	0.26	0.15	0.02	0.01	1.00	0.39	0.46	3	1	2
Anger	0.29	0.35	0.27	0.45	0.50	0.44	0.15	0.12	0.03	0.90	0.97	0.74	2	3	1
Angergutten	0.18	0.35	0.21	0.26	0.50	0.33	0.05	0.15	0.01	0.48	1.00	0.55	1	3	2
Bahirdar	0.14	0.35	0.19	0.24	0.50	0.30	0.02	0.15	0.10	0.39	1.00	0.59	1	3	2
Bedele	0.05	0.35	0.11	0.06	0.50	0.15	0.01	0.15	0.00	0.12	1.00	0.27	1	3	2
Dangila	0.09	0.35	0.06	0.12	0.50	0.10	0.15	0.05	0.06	0.36	0.90	0.21	2	3	1
Dedesa	0.16	0.35	0.27	0.24	0.50	0.42	0.13	0.15	0.09	0.53	1.00	0.77	1	3	2
Debre Markos	0.09	0.35	0.23	0.14	0.50	0.37	0.02	0.15	0.01	0.25	1.00	0.61	1	3	2
Debre Tabor	0.20	0.35	0.10	0.30	0.50	0.18	0.15	0.15	0.05	0.64	1.00	0.32	2	3	1
Fitche	0.35	0.22	0.21	0.50	0.49	0.45	0.15	0.00	0.10	1.00	0.71	0.76	3	1	2
Gimijabet	0.16	0.35	0.12	0.25	0.50	0.17	0.15	0.14	0.02	0.56	0.99	0.32	2	3	1
Gondar	0.10	0.35	0.07	0.13	0.50	0.10	0.04	0.15	0.05	0.26	1.00	0.22	2	3	1
Nedjo	0.19	0.35	0.27	0.22	0.50	0.38	0.09	0.15	0.06	0.49	1.00	0.71	1	3	2
Shambu	0.19	0.35	0.24	0.24	0.50	0.32	0.01	0.15	0.05	0.44	1.00	0.61	1	3	2
Total score													24	41	25
Rank													1	3	2

Appendix 18: Scenario developments and their definitions

Name	scenario	Water resource developments description	Climate change scenario	HPP installed capacity (MW)	Irrigation area (ha)
s0	Natural condition	No development of water resources. The "natural" system without any water infrastructure	Baseline condition (no climate change)	0	0
s1	Current condition	Current development of water resources (2018) that includes Koga, Fincha and Anger irrigation projects and Tana-Beles HPP	Baseline condition (no climate change)	460	23596
s2	Short-term development	Short-term planned water resources development; that includes all projects that are existing, under construction and anticipated to start operation in the future before 2025	Baseline condition (no climate change)	6910	214882
s3	Medium term developments	Medium-term planned development of water resources that includes all projects under s2 plus anticipated projects to start operation before 2040	Baseline condition (no climate change)	6910	382644
s4	Long term A developments	Long-term planned development of water resources that includes all projects that are likely to occur in the future before 2070	Baseline condition (no climate change)	49762	420370
s5	Short term development	Short-term planned development of water resources; that includes all projects that are existing, under construction and anticipated to start operation in the future before 2025	Based on RCP4.5 scenario of canESM2 GCM (2017-2025)	6910	23596
s6	Medium term developments	Medium-term planned development of water resources that includes all projects under s2 plus anticipated projects to start operation before 2040	Based on RCP4.5 scenario of canESM2 GCM (2026-2040)	6910	214882
s7	Long term A developments	Long-term planned development of water resources that includes all projects that are likely to occur in the future before 2070	Based on RCP4.5 scenario of canESM2 GCM (2041-2070)	49762	382644

s8	Long term B developments	Long-term planned development of water resources that includes all projects that are likely to occur in the future before 2100	Based on RCP4.5 scenario of canESM2 GCM (2071-2100)	49762	420370
s9	Short term development	Short-term planned development of water resources; that includes all projects that are existing, under construction and anticipated to start operation in the future before 2025	Based on RCP4.5 scenario of GFDL GCM (2017-2025)	6910	23596
s10	Medium term developments	Medium-term planned development of water resources that includes all projects under s2 plus anticipated projects to start operation before 2040	Based on RCP4.5 scenario of GFDL GCM (2026-2040)	6910	214882
s11	Long term A developments	Long-term planned development of water resources that includes all projects that are likely to occur in the future before 2070	Based on RCP4.5 scenario of GFDL GCM (2041-2070)	49762	382644
s12	Long term B developments	Long-term planned development of water resources that includes all projects that are likely to occur in the future before 2100	Based on RCP4.5 scenario of GFDL GCM (2071-2100)	49762	420370

Appendix 19: Monthly irrigation water requirment

Project Name	sub-basin	total area (ha)	Monthly irrigation requirement (mm month^{-1})											
			Jan	Feb	Mar	Apr	May	Jun	Jul	Aug	Sep	Oct	Nov	Dec
Megech Pumping	Lake Tana	24,510.00	132.1	161.4	196.1	93.5	0.0	0.0	0.0	0.0	0.0	24.0	122.8	136.6
Megech gravity	Lake Tana	7,311.00	130.7	159.4	194.2	91.4	0.0	0.0	0.0	0.0	0.0	21.7	121.7	135.9
North West Tana	Lake Tana	6,720.00	131.8	161.1	195.8	93.3	0.0	0.0	0.0	0.0	0.0	23.9	122.7	136.5
North East Tana	Lake Tana	5,475.00	150.6	191.8	201.4	92.5	0.0	0.0	0.0	0.0	0.0	0.0	113.6	125.7
Ribb 1800	Lake Tana	19,925.00	289.6	138.2	155.3	197.1	60.0	0.0	0.0	0.0	0.0	53.4	77.9	17.3
Gumara	Lake Tana	13,776.00	143.0	170.6	189.8	97.1	0.0	0.0	0.0	0.0	0.0	0.0	124.6	129.5
Koga	Lake Tana	7,000.00	131.0	177.1	162.7	64.7	0.0	0.0	0.0	0.0	0.0	0.0	116.4	126.8
Middle Birr	South Gojam	8,500.00	134.1	172.6	143.7	77.4	0.0	0.0	0.0	0.0	0.0	0.0	77.3	135.1
Lower Birr	South Gojam	3,659.00	146.6	187.0	166.6	95.8	0.0	0.0	0.0	0.0	18.4	2.1	95.5	142.3
Gilgel	Lake Tana	16,499.00	285.1	145.9	136.4	177.3	0.0	0.0	121.1	0.0	0.0	18.1	73.3	14.9
South West Tana	Lake Tana	5,132.00	139.4	184.2	201.5	113.4	0.0	0.0	0.0	0.0	0.0	0.0	90.8	139.2
Tis Abay Pumping	North Gojam	4,132.00	139.4	184.2	201.5	113.4	0.0	0.0	0.0	0.0	0.0	0.0	90.8	139.2
TIS 3-5	North Gojam	7,167.00	139.4	184.2	201.5	113.4	0.0	0.0	0.0	0.0	0.0	0.0	90.8	139.2
Fettam	South Gojam	600.00	111.7	148.4	103.1	15.2	0.0	0.0	0.0	0.0	0.0	0.0	60.0	102.9
Azena	South Gojam	426.00	151.5	181.4	173.9	91.7	0.0	0.0	0.0	0.0	0.0	0.0	105.1	135.1
Jema	Jemma	7,786.00	129.5	175.2	160.4	62.0	0.0	0.0	0.0	0.0	0.0	0.0	115.0	125.8
Weberi	Jemma	10,608.00	129.5	175.2	160.4	62.0	0.0	0.0	0.0	0.0	0.0	0.0	115.0	125.8
Weserbi	Jemma	1,000.00	138.1	157.0	93.2	13.2	0.0	0.0	0.0	0.0	0.0	0.0	84.7	111.9
Lumame	Jemma	4,012.00	111.7	148.4	103.1	15.2	0.0	0.0	0.0	0.0	0.0	0.0	60.0	102.9

Upper Beles	Beles	53,720.00	156.5	163.6	141.1	135.6	43.1	0.0	0.0	0.0	0.0	0.0	151.6	194.5
Lower Beles	Beles	10,000.00	174.5	217.6	203.8	107.9	6.1	0.0	0.0	0.0	0.0	0.0	143.1	148.4
Anonu	Guder	804.00	141.2	166.3	125.0	23.0	0.0	0.0	0.0	0.0	12.0	0.0	63.4	134.4
Upper Guder	Guder	4,896.00	122.8	122.8	65.4	0.0	0.0	0.0	0.0	0.0	0.0	1.4	96.4	141.1
Kale	Guder	1,537.00	142.0	167.5	126.8	24.5	0.0	0.0	0.0	0.0	14.9	0.0	64.2	135.0
Anonu	Guder	803.00	141.2	166.3	125.0	23.0	0.0	0.0	0.0	0.0	12.0	0.0	63.4	134.4
Neshe	Finchaa	7,217.00	137.4	136.6	100.1	76.8	10.4	0.0	0.0	0.0	27.2	105.1	168.9	170.4
Angar	Angar	14,450.00	142.5	168.9	97.1	20.6	0.0	0.0	0.0	0.0	0.0	0.0	87.7	120.1
Nekemte	Angar	11,220.00	142.5	168.9	97.1	20.6	0.0	0.0	0.0	0.0	0.0	0.0	87.7	120.1
Dembi Gusu	Angar	893.00	142.5	168.9	97.1	20.6	0.0	0.0	0.0	0.0	0.0	0.0	87.7	120.1
Didessa Pumping	Didessa	2,402.00	138.1	157.0	93.2	13.2	0.0	0.0	0.0	0.0	0.0	0.0	84.7	111.9
Didiga	Didessa	4,633.00	138.1	157.0	93.2	13.2	0.0	0.0	0.0	0.0	0.0	0.0	84.7	111.9
Dimtu	Didessa	534.00	139.1	158.6	95.9	15.5	0.0	0.0	0.0	0.0	0.0	0.0	85.5	113.2
Negeso	Didessa	21,315.00	120.2	137.9	75.9	0.0	0.0	0.0	0.0	0.0	0.0	0.0	70.8	125.2
Felemtu Dila	Dabus	1,092.00	120.3	124.5	105.2	70.6	39.1	0.0	0.0	0.0	1.6	42.2	62.3	84.5
Upper Dila	Dabus	2,669.00	145.9	183.7	155.5	25.4	0.0	0.0	0.0	0.0	0.0	0.0	65.7	142.1
Arjo-Didessa	Didessa	14,280.00	138.1	157.0	93.2	13.2	0.0	0.0	0.0	0.0	0.0	0.0	84.7	111.9
Dabana	Didessa	1,500.00	139.4	159.0	96.6	16.0	0.0	0.0	0.0	0.0	0.0	0.0	85.7	113.5
Upper Dabana	Didessa	1,105.00	138.1	157.0	93.2	13.2	0.0	0.0	0.0	0.0	0.0	0.0	84.7	111.9
Didessa	Didessa	2,401.00	138.1	157.0	93.2	13.2	0.0	0.0	0.0	0.0	0.0	0.0	84.7	111.9
Hida	Didessa	1,190.00	138.1	157.0	93.2	13.2	0.0	0.0	0.0	0.0	0.0	0.0	84.7	111.9
Nedi	Didessa	3,936.00	138.1	157.0	93.2	13.2	0.0	0.0	0.0	0.0	0.0	0.0	84.7	111.9
Finicha sugar factory	Finchaa	8,145.00	113.1	112.0	80.6	61.0	4.3	0.0	0.0	0.0	17.7	85.0	138.8	140.8
Urgesa	Didessa	2,933.00	113.1	112.0	80.6	61.0	4.3	0.0	0.0	0.0	17.7	85.0	138.8	140.8
Dabus	Dabus	9,100.00	120.3	124.5	105.2	70.6	39.1	0.0	0.0	0.0	1.6	42.2	62.3	84.5
Lugo	Didessa	285.00	113.1	112.0	80.6	61.0	4.3	0.0	0.0	0.0	17.7	85.0	138.8	140.8
Bar	Wombera	253.00	179.2	228.5	229.9	107.6	14.7	0.0	0.0	31.9	17.3	0.0	165.9	146.3
Lower Dura	Wombera	1,819.00	179.2	228.5	229.9	107.6	14.7	0.0	0.0	31.9	17.3	0.0	165.9	146.3
Lower Beles	Beles	85,000.00	174.5	217.6	203.8	107.9	6.1	0.0	0.0	0.0	0.0	0.0	143.1	148.4

Appendix 20: Proposed Irrigation development during Master plan period (ha)

		Area	Proposed Irrigation development during Master plan period (ha)					Irrigation water demand (MM3MM3)			
Project Name	sub-basin	(ha)	P1	P2	P3	P4	Total	P1	P2	P3	P4
Megech Pumping	Tana	24,510		4,000	8,510	12,000	24,510	-	35	108	212
Megech gravity	Tana	7,311		7,311			7,311	-	62	62	62
North West Tana	Tana	6,720			2,000	4,720	6,720	-	-	17	58
Lower Dindir	Dindir	25,000					-	-	-	-	-
North East Tana	Tana	5,475		3,000	2,475		5,475	-	26	48	48
Ribb 1800	Tana	19,925		8,000	6,459	5,466	19,925	-	79	143	196
Gumara	Tana	13,776			10,000	3,776	13,776	-	-	85	117
Koga	Tana	7,000	7,000				7,000	54	54	54	54
Middle Birr (Acres)	South Gojam	8,500		3,500	5,000		8,500	-	26	63	63
Lower Birr	South Gojam	3,659		3,659			3,659	-	31	31	31
Gilgel	Tana	16,499		4,000	5,999	6,500	16,499	-	39	97	160
South West Tana	Tana	5,132				5,132	5,132	-	-	-	44
Tis Abbay Pumping	North Gojam	4,132				4,132	4,132	-	-	-	36
TIS 3-5	North Gojam	7,167		7,167			7,167	-	62	62	62
Fettam	South Gojam	600		600			600	-	3	3	3
Azena	South Gojam	426			426		426	-	-	4	4
Jema	Jemma				7,786						

		7,786					7,786	-	-	60	60
Weberi	Jemma	10,608			10,608		10,608	-	-	81	81
Weserbi	Jemma	1,000			1,000		1,000	-	-	6	6
Lumame	Jemma	4,012			4,012		4,012	-	-	22	22
Upper Beles	Beles	53,720		53,720			53,720	-	528	528	528
Lower Beles	Beles	10,000			10,000		10,000	-	-	100	100
Gelegu	Gelegu	9,860					-	-	-	-	-
Rahad	Rahad	45,135					-	-	-	-	-
		297,953	**7,000**	**94,957**	**74,275**	**41,726**	**217,958**	**54**	**946**	**1,574**	**1,948**
Anonu	Guder	804		804			804	-	5	5	5
Upper Guder	Guder	4,896		4,896			4,896	-	27	27	27
Kale	Guder	1,537			1,537		1,537	-	-	10	10
Anonu	Guder	803		803			803	-	5	5	5
Neshe	Finchaa	7,217		5,000	2,217		7,217	-	47	67	67
Angar	Angar	14,450	8,450	6,000			14,450	54	92	92	92
Nekemte	Angar	11,220		3,000	8,220		11,220	-	19	71	71
Dembi Gusu	Angar	893		893			893	-	6	6	6
Negeso	Didessa	21,315		21,315			21,315	-	113	113	113
Felemtu Dila	Dabus	1,092			1,092		1,092	-	-	7	7
Upper Dila	Dabus	2,669			2,669		2,669	-	-	19	19

Arjo-Didessa	Didessa	80,000		80,000			80,000	-	477	477	477
Finicha sugar factory	Finchaa	8,145	8,145				8,145	61	61	61	61
		155,041	**16,595**	**122,711**	**15,735**		**155,041**	**115**	**852**	**961**	**961**
Dabus	Dabus	9,100		9,100			9,100	-	59	59	59
Bar	Wombera	253		253			253	-	3	3	3
Lower Dura	Wombera	1,819			1,819		1,819	-	-	20	20
Lower Dindir	Dindir	24,555					-	-	-	-	-
Lower Beles	Beles	85,000		12,000	73,000		85,000	-	120	849	849
		120,727		**21,353**	**74,819**		**96,172**	**-**	**182**	**931**	**931**
		573,721	23,595	239,021	164,829	41,726	469,171	169	2,040	3,622	4,144
			23,595	262,616	427,445	469,171					

Where p1 represents (2017-2025), p2 represents (2026-2040), p3 represents (2041-2070) and p4 represents (2071-2100)

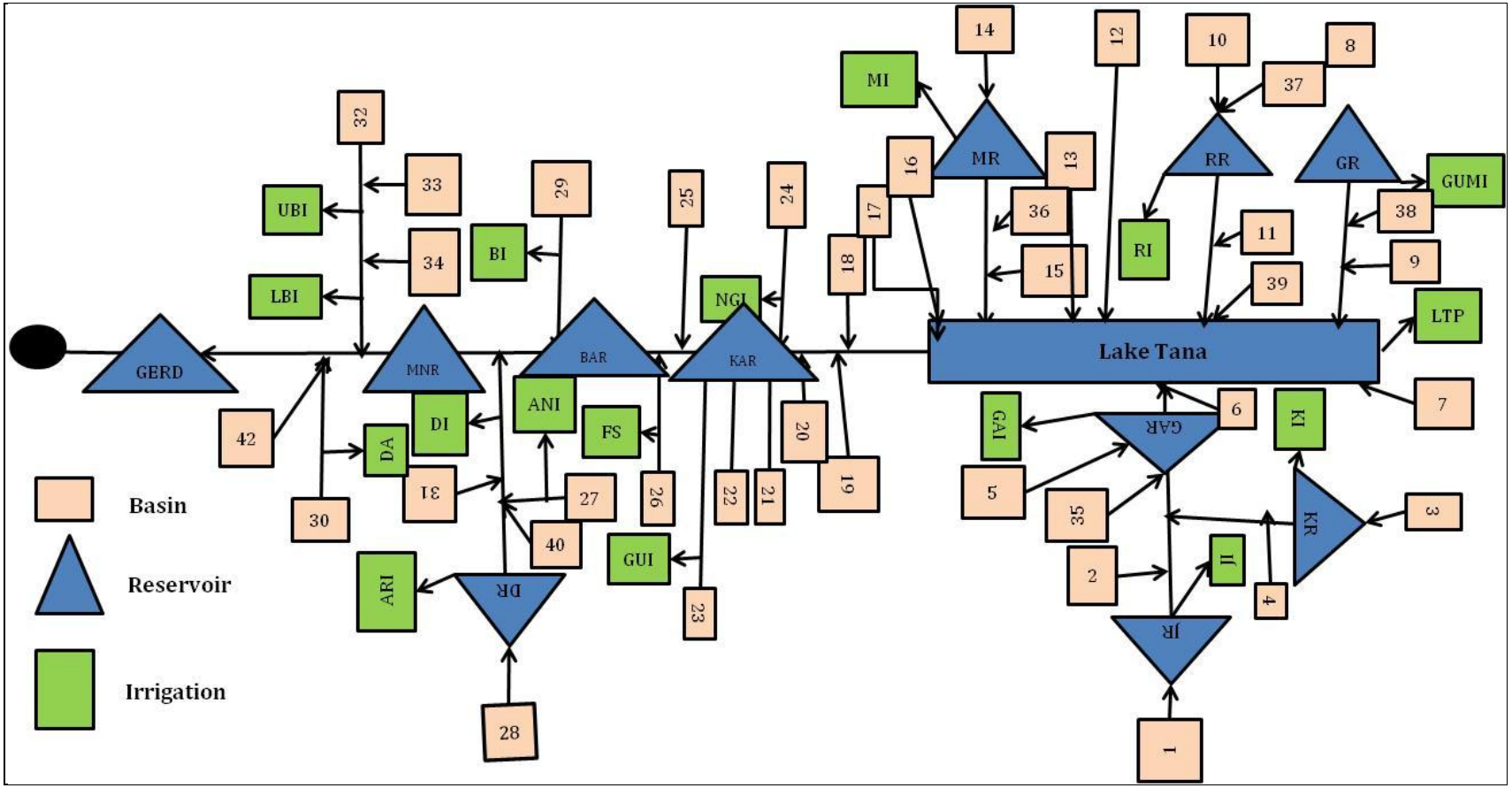

Appendix 21: Schematic of existing and planned water resource developments in the UBNRB as simulated in the HEC-HMS model,showing model basin, reservoirs and control points (diversions).

Basin code	Basin description	Basin code	Basin description	Reservoir code	Reservoir description	Irrigation code	Irrigation description
1	Jema basin	22	Muger basin	JR	Jemma reservoir	JI	Jemma Irrigation
2	Upper Gilgel abay basin	23	Guder basin	KR	Koga reservoir	KI	Koga Irrigation
3	Upper Koga basin	24	North Gojjam basin	GAR	Gilgel abay reservoir	GAI	Gilgel Abay irrigation
4	Lower Koga basin	25	South Gojjam basin	GR	Gumara reservoir	GUMI	Gumara irrigation
5	Kilti basin	26	Fincha basin	RR	Rib reservoir	RI	Rib Irrigation
6	Lower Gilgel abay basin	27	Anger basin	MR	Megech reservoir	MI	Megech Irrigation
7	Gelda basin	28	Didesa basin	LT	Lake Tana	LTPI	Lake Tana pump irrigation
8	Upper Gumara basin	29	Wenibera basin	DR	Didesa reservoir	NGI	North Gojjam irrigation
9	Lower Gumara basin	30	Dabus basin	KAR	Karadobi reservoir	BI	Birr irrigation
10	Rib U/S reservoir1	31	Lower Didesa basin	BAR	Bekoabo reservoir	GUI	Guder irrigation
11	Rib D/S gage station	32	Main beles basin	MNR	Mendiya reservoir	FSFI	Finch sugar factory irrigation
12	Garno basin	33	Gilgel beles basin	GERD	Grand renaissance dam	ARI	Arijo Irrigation
13	Gumero basin	34	Lower beles basin			ANI	Anger Nekemit irrigation
14	Megech U/S reservoir	35	Gilgel Abay D/S gage station			DI	Didessa (Negesso) irrigation
15	Megech D/S gage station	36	Megech D/S reservoir			DABI	Dabus irrigation
16	Gabi Kura basin	37	Rib U/S reservoir2			UBI	Upper Beles irrigation
17	Lake Tana periphery basin	38	Gumara d/s reservoir			LBI	Lower Beles irrigation
18	Andasa basin	39	Rib D/S reservoir				
19	Beshilo basin	40	Anger D/s gage station				
20	Weleka basin	41	Upper Tis isat basin				
21	Jemma basin	42	Lower Dabus				

Appendix 22: Mean monthly reservoirs evaporation

Month	Koga	Megech	Gumara	Rib	Jemma	Gilgel Abay	Lake Tana	Beko-Abo	Karadobi	Didessa	Mendiya	GERD
Jan	130	143	133	133	130	133	133	168	166	196	194	202
Feb	137	148	143	140	134	140	139	163	161	190	188	196
Mar	167	180	174	171	161	171	164	178	176	172	170	182
Apr	174	174	171	165	168	174	178	168	166	197	196	208
May	152	164	155	155	149	155	162	152	151	241	239	251
Jun	123	141	129	129	120	120	133	96	95	174	173	186
Jul	93	90	90	93	90	93	117	67	66	15	15	46
Aug	93	90	90	90	93	93	123	65	64	87	87	115
Sep	129	132	129	126	126	132	133	88	87	212	211	225
Oct	143	155	146	146	140	143	140	128	127	251	250	259
Nov	129	138	132	129	126	129	131	138	136	170	169	176
Dec	121	130	124	124	118	121	123	149	147	184	182	189
Total	1591	1685	1615	1600	1555	1603	1676	1560	1542	2088	2073	2236

Appendix 23: Key data for the cascade hydropower projects (IPoE, 2013; NORPLAN *et al.*, 2006; NORPLAN *et al.*, 2013)

Data	Parameters	Karadobi	Beko-Abo	Mendaya	GERD
Power and Energy	Total rated output (MW)	1600	1 940	2000	6450
	Mean annual energy generation (GWh)	8634	12096	12119	16,153
	Plant factor	0.67	0.71	0.69	0.29
	Design discharge (m3s-1)	800	900	1200	5400
	Maximum gross head (m)	236	272		133
Hydrologic Data	Abay river catchment area upstream of dam (km2)	66 910	93 490	128729	172,250
	Mean river flow at dam site (m3s-1)	649	675	1091	1547
Reservoir	Full Supply Level (masl)	1146	1 062	800	640
	Minimum Operation Level (masl)	1100	1 010	760	590
	Total volume at FSL (Bm3)	40.2	31.7	49.2	74.01
	Active reservoir volume (Bm3)	17.0	17.4	24.6	59.22
	Surface at FSL (km^2)	445	403	736	1874
	Extension of reservoir towards upstream (Km)	150	150	300	246
Dam	Dam crest elevation (masl)	1150.0	1063.7	803	645
	Maximum height of dam above foundation (m)	260	282	200	145
	Crest length of dam (m)	684	1 080	1400	1780
	Dam volume (Mm3)	6.5	12.8	13	10.1
Spillway	Spillway capacity(m3s-1)	21 450	13 260	30000	38,500

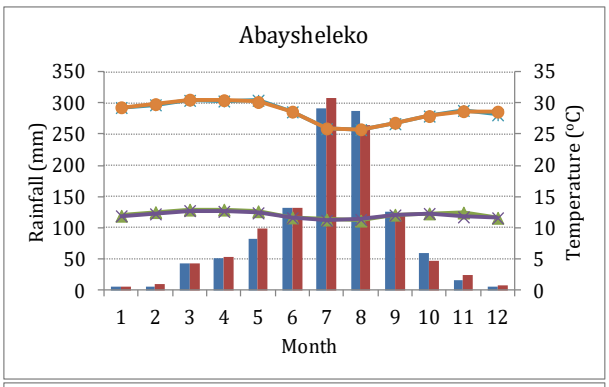
Abaysheleko
Rainfall (mm)
Temperature (°C)
Month

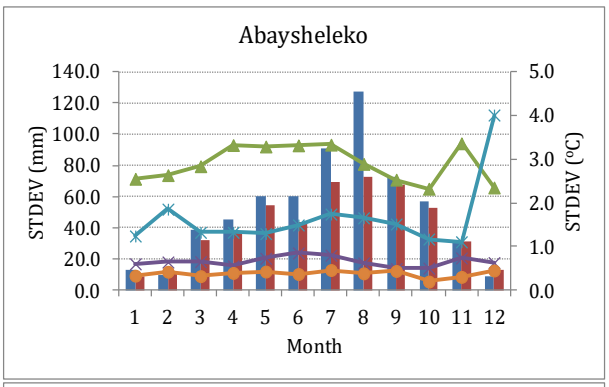
Abaysheleko
STDEV (mm)
STDEV (°C)
Month

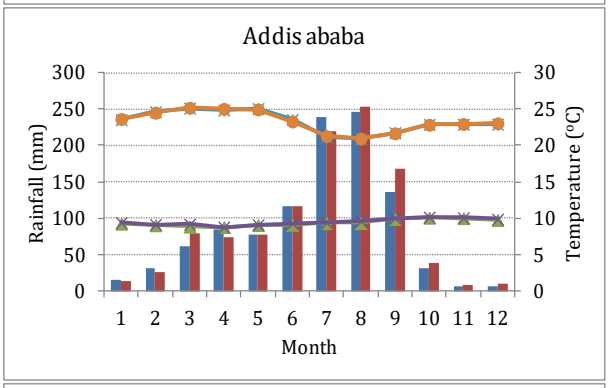
Addis ababa
Rainfall (mm)
Temperature (°C)
Month

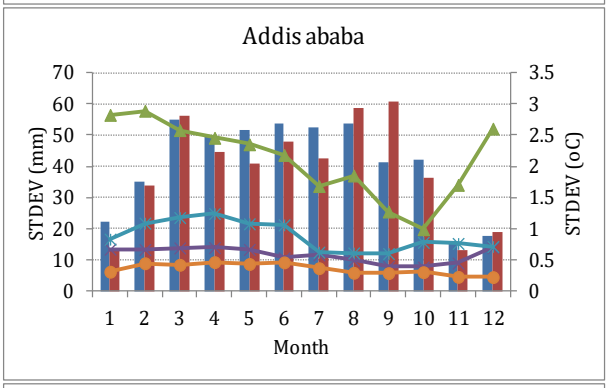
Addis ababa
STDEV (mm)
STDEV (oC)
Month

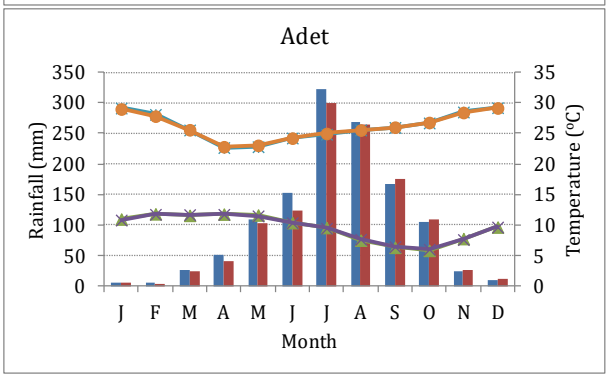
Adet
Rainfall (mm)
Temperature (°C)
Month

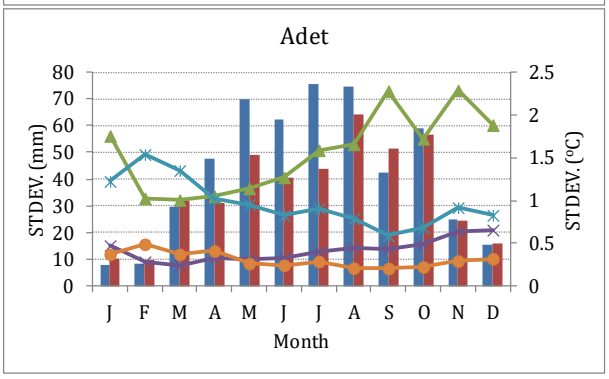
Adet
STDEV. (mm)
STDEV. (°C)
Month

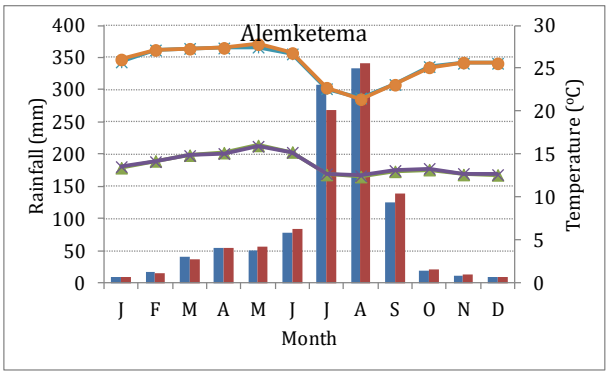
Alemketema
Rainfall (mm)
Temperature (°C)
Month

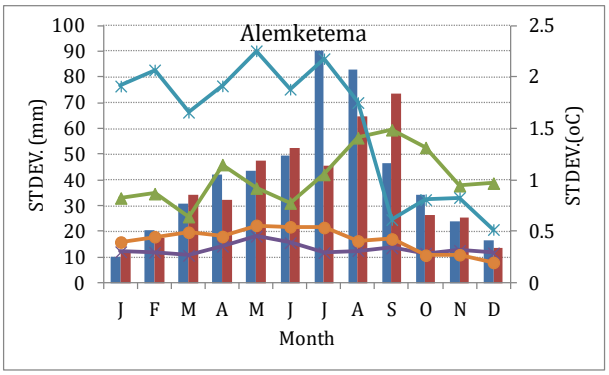
Alemketema
STDEV. (mm)
STDEV.(oC)
Month

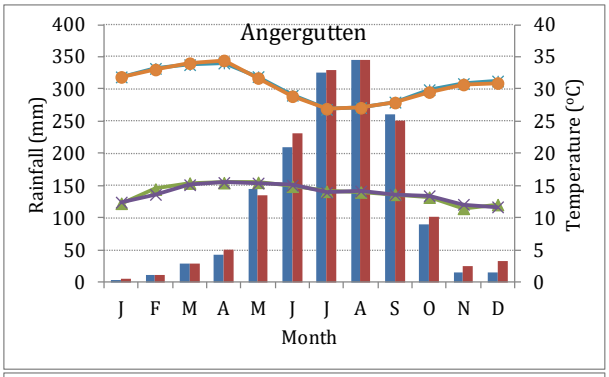
Angergutten
Rainfall (mm)
Temperature (°C)
Month
J F M A M J J A S O N D

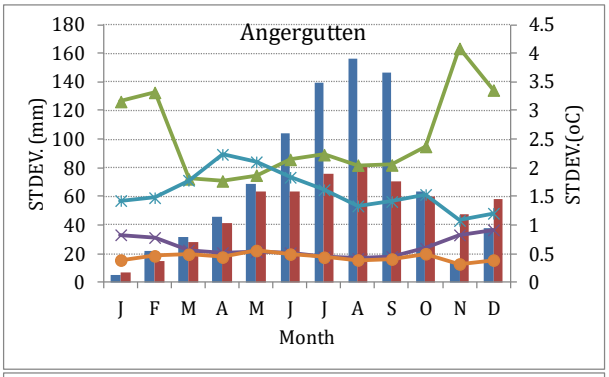
Angergutten
STDEV. (mm)
STDEV.(oC)
Month
J F M A M J J A S O N D

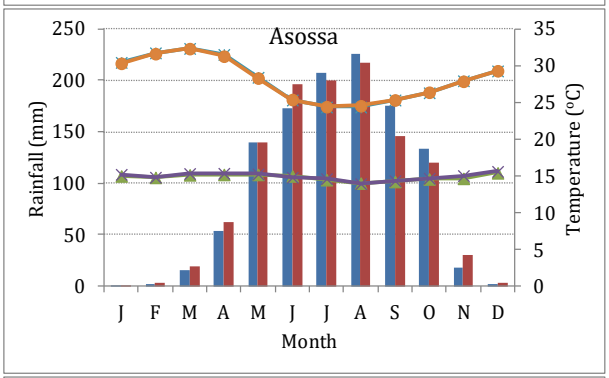
Asossa
Rainfall (mm)
Temperature (°C)
Month
J F M A M J J A S O N D

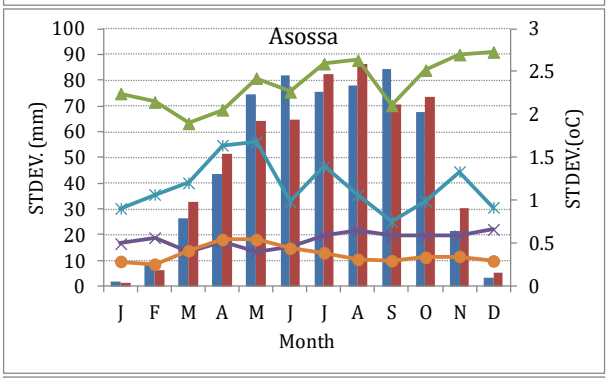
Asossa
STDEV. (mm)
STDEV.(oC)
Month
J F M A M J J A S O N D

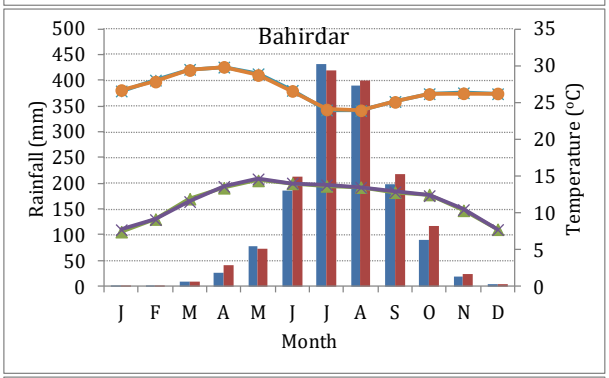
Bahirdar
Rainfall (mm)
Temperature (°C)
Month
J F M A M J J A S O N D

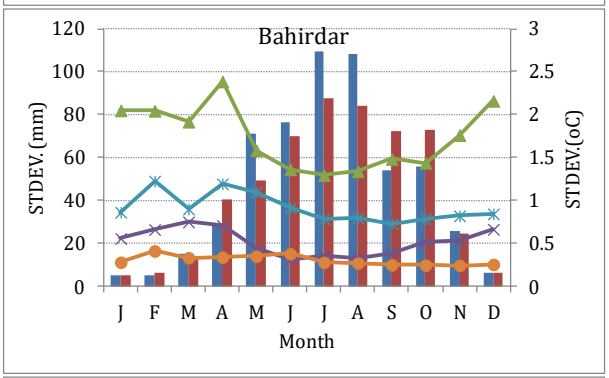
Bahirdar
STDEV. (mm)
STDEV.(oC)
Month
J F M A M J J A S O N D

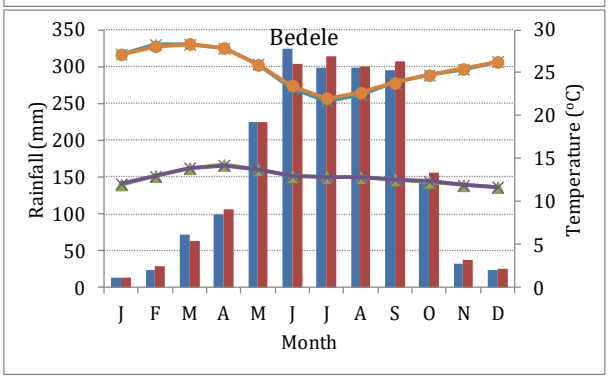
Bedele
Rainfall (mm)
Temperature (°C)
Month
J F M A M J J A S O N D

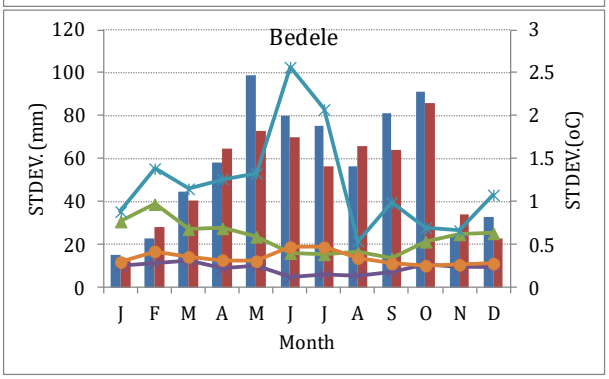
Bedele
STDEV. (mm)
STDEV.(oC)
Month
J F M A M J J A S O N D

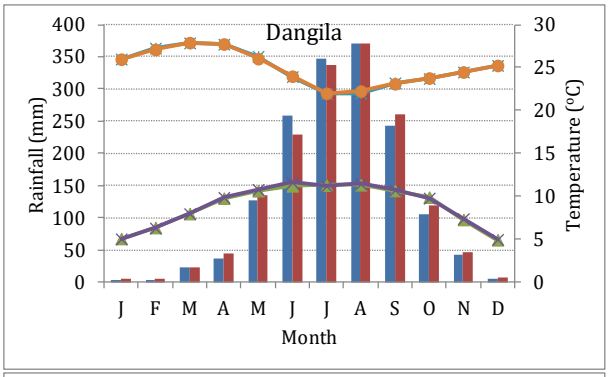
Dangila
Rainfall (mm)
Temperature (°C)
Month
J F M A M J J A S O N D

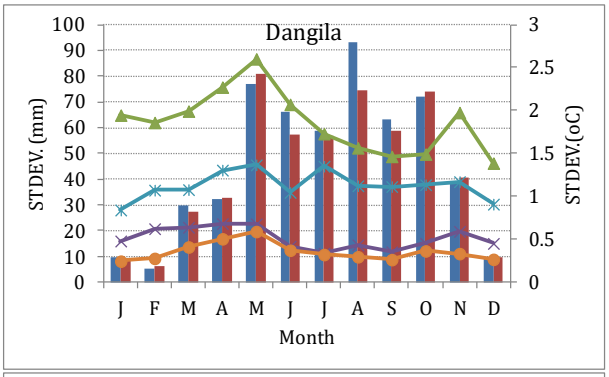
Dangila
STDEV. (mm)
STDEV.(oC)
Month
J F M A M J J A S O N D

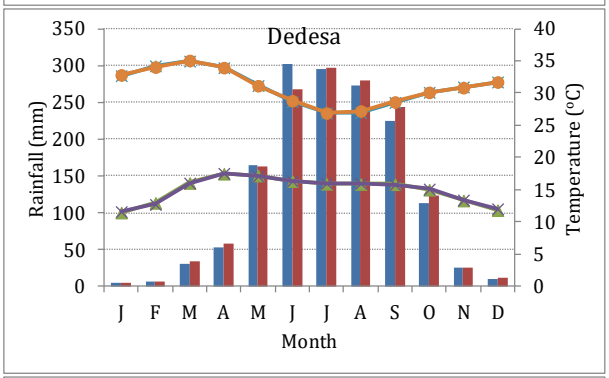
Dedesa
Rainfall (mm)
Temperature (°C)
Month
J F M A M J J A S O N D

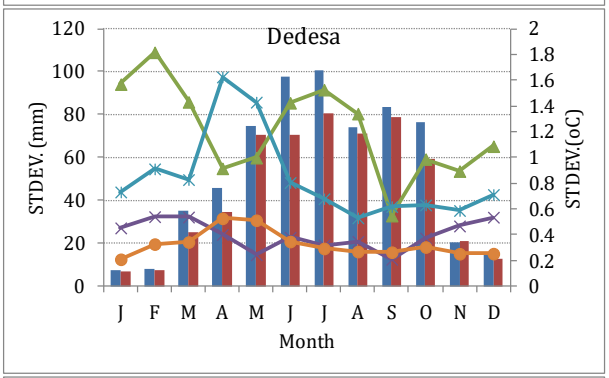
Dedesa
STDEV. (mm)
STDEV.(oC)
Month
J F M A M J J A S O N D

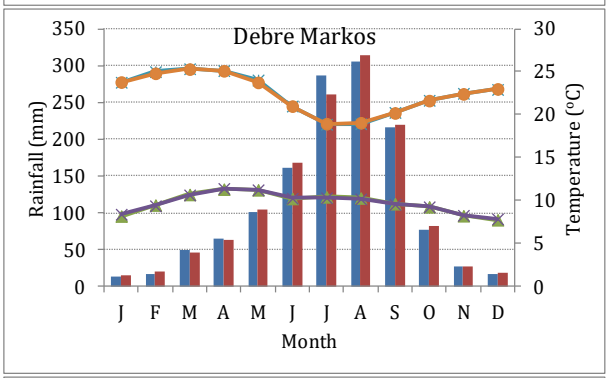
Debre Markos
Rainfall (mm)
Temperature (°C)
Month
J F M A M J J A S O N D

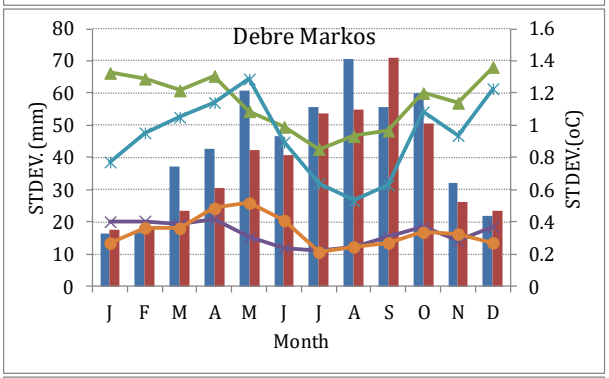
Debre Markos
STDEV. (mm)
STDEV.(oC)
Month
J F M A M J J A S O N D

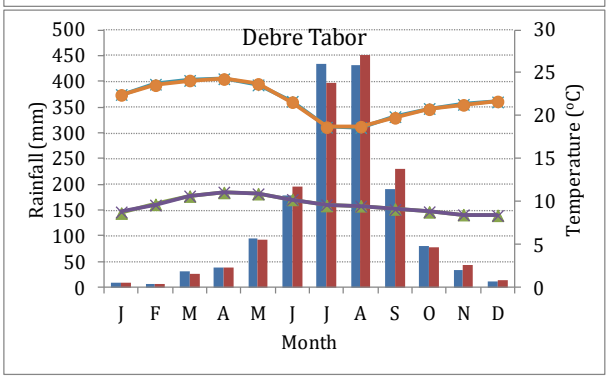
Debre Tabor
Rainfall (mm)
Temperature (°C)
Month
J F M A M J J A S O N D

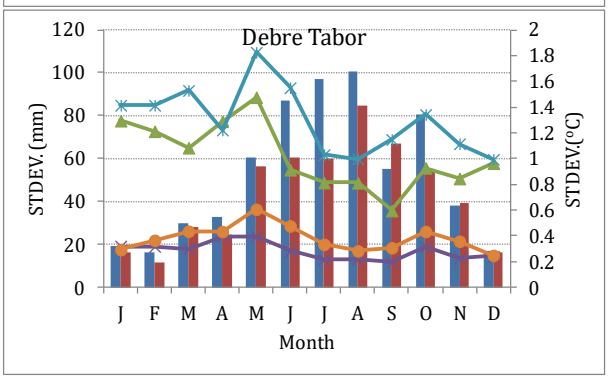
Debre Tabor
STDEV. (mm)
STDEV.(°C)
Month
J F M A M J J A S O N D

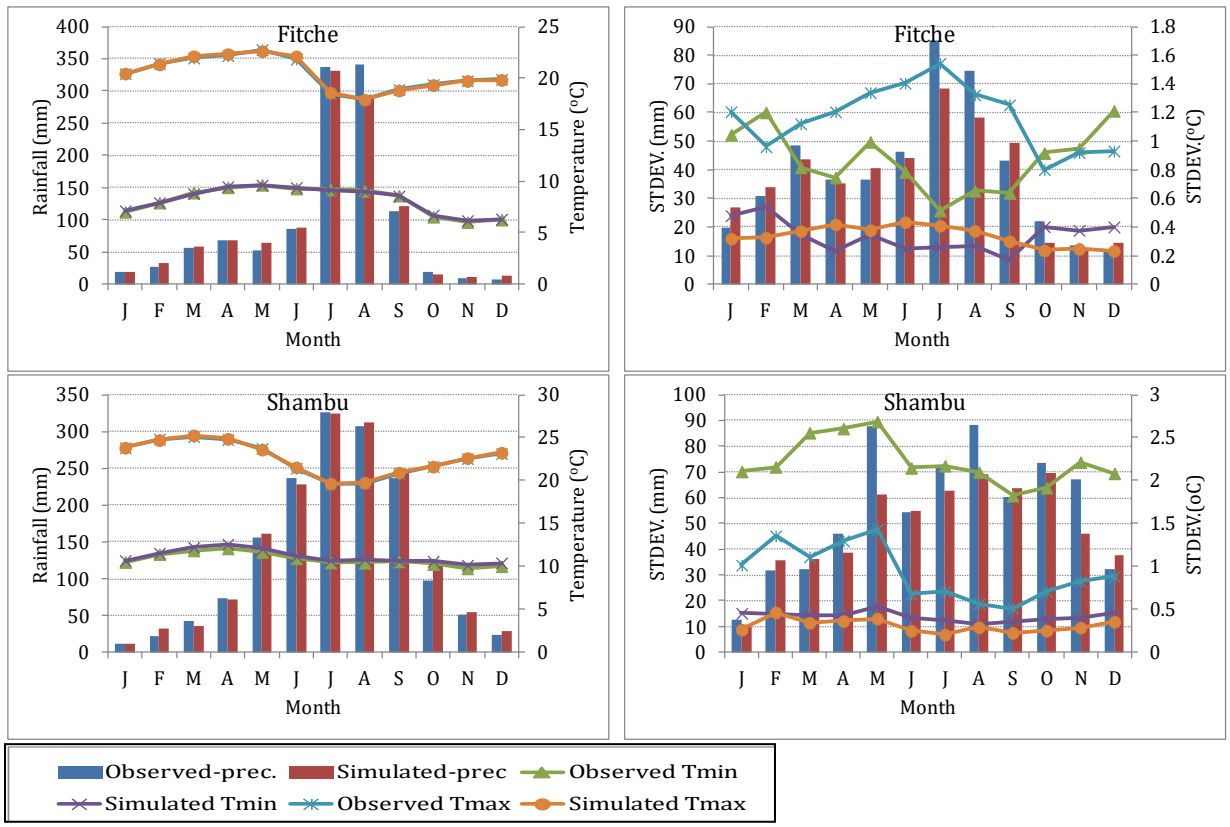

Appendix 24: Observed and simulated (left) mean monthly precipitation,Tmax and Tmin; (right) standard deviation of precipitation, Tmax and Tmin using LARS-WG

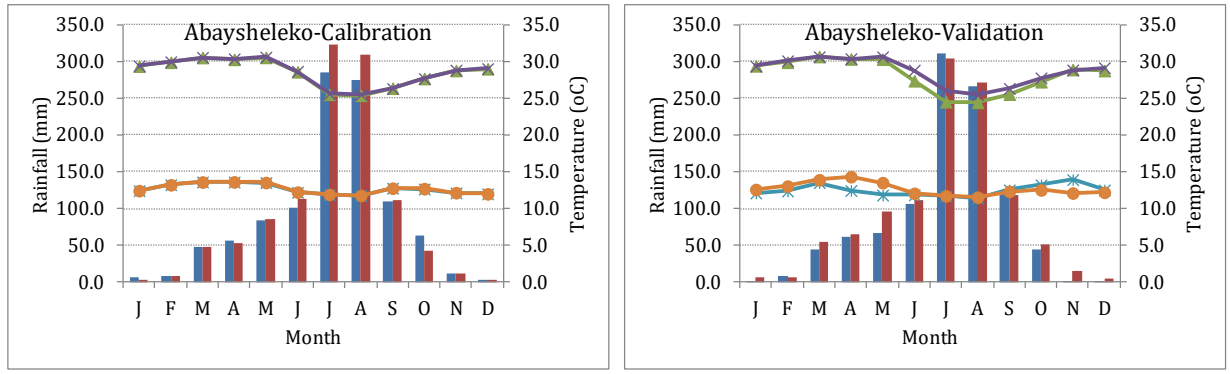

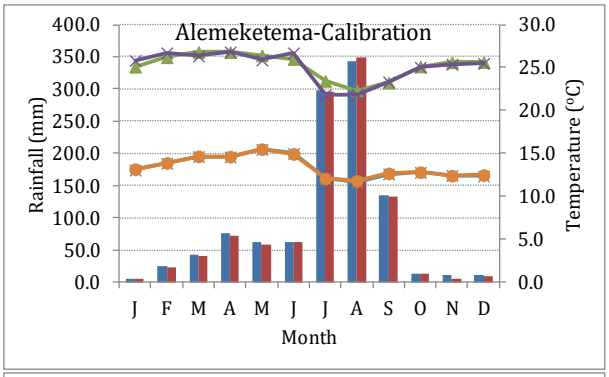
Alemeketema-Calibration
Rainfall (mm)
Temperature (°C)
Month
J F M A M J J A S O N D

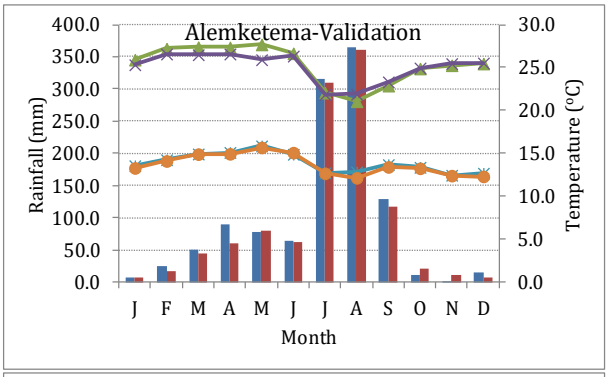
Alemketema-Validation
Rainfall (mm)
Temperature (°C)
Month
J F M A M J J A S O N D

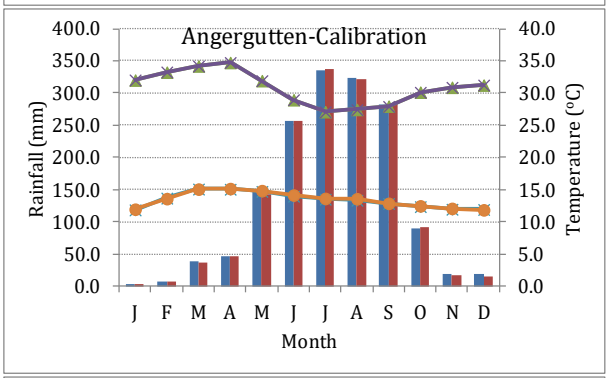
Angergutten-Calibration
Rainfall (mm)
Temperature (°C)
Month
J F M A M J J A S O N D

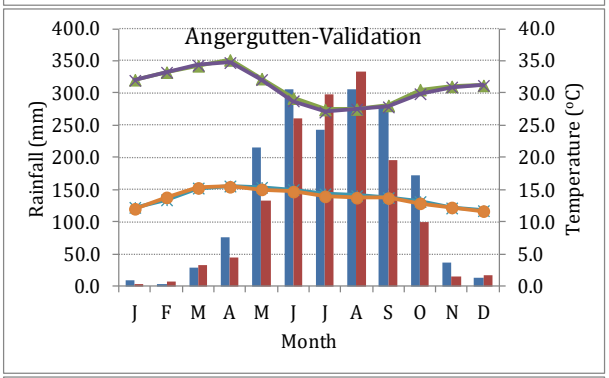
Angergutten-Validation
Rainfall (mm)
Temperature (°C)
Month
J F M A M J J A S O N D

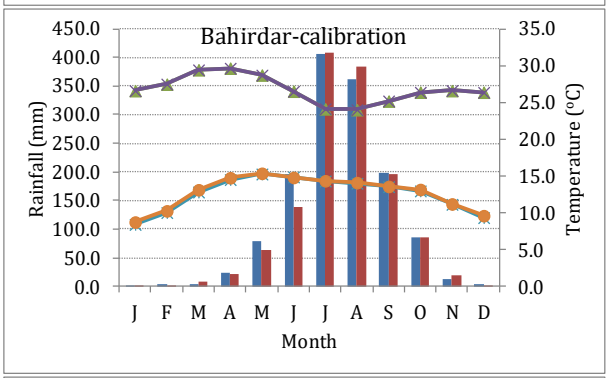
Bahirdar-calibration
Rainfall (mm)
Temperature (°C)
Month
J F M A M J J A S O N D

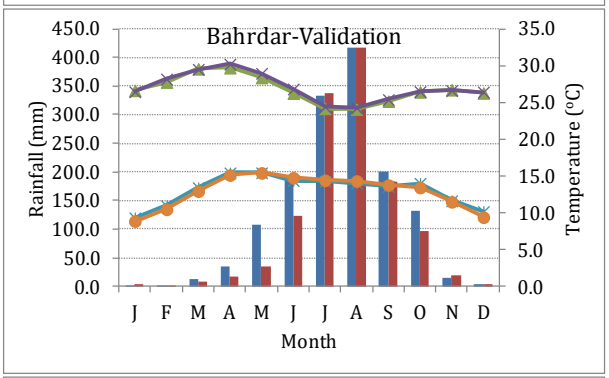
Bahrdar-Validation
Rainfall (mm)
Temperature (°C)
Month
J F M A M J J A S O N D

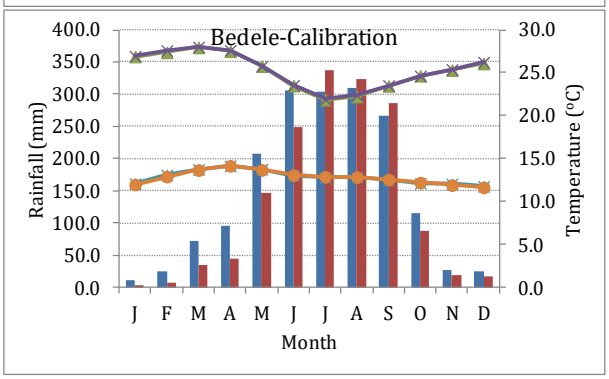
Bedele-Calibration
Rainfall (mm)
Temperature (°C)
Month
J F M A M J J A S O N D

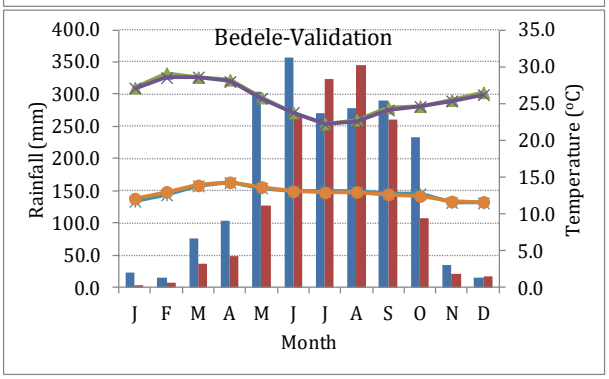
Bedele-Validation
Rainfall (mm)
Temperature (°C)
Month
J F M A M J J A S O N D

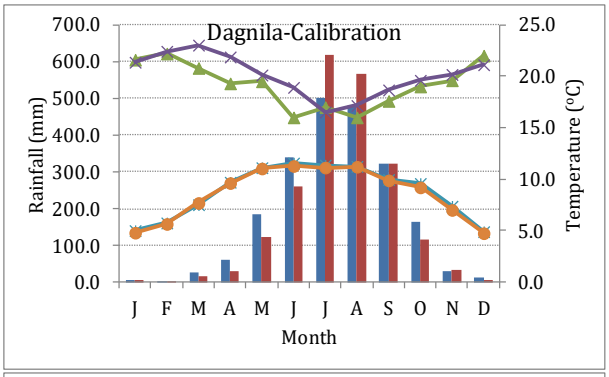
Dagnila-Calibration
Rainfall (mm)
Temperature (°C)
Month
J F M A M J J A S O N D

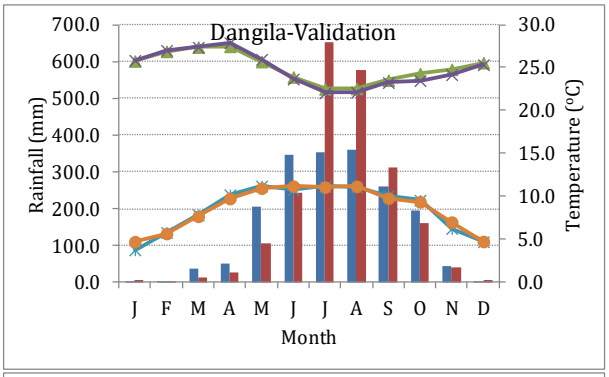
Dangila-Validation
Rainfall (mm)
Temperature (°C)
Month
J F M A M J J A S O N D

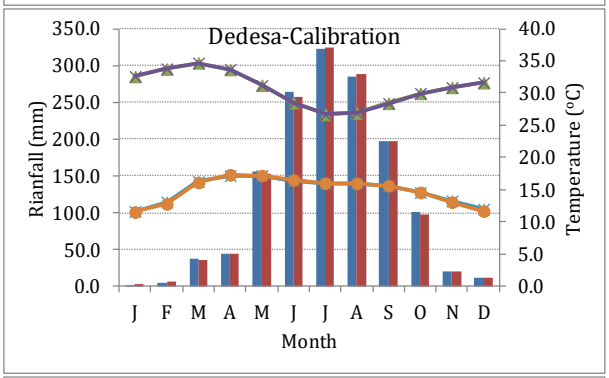
Dedesa-Calibration
Rianfall (mm)
Temperature (°C)
Month
J F M A M J J A S O N D

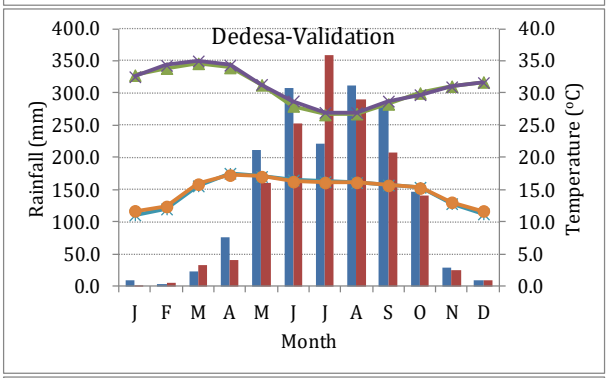
Dedesa-Validation
Rainfall (mm)
Temperature (°C)
Month
J F M A M J J A S O N D

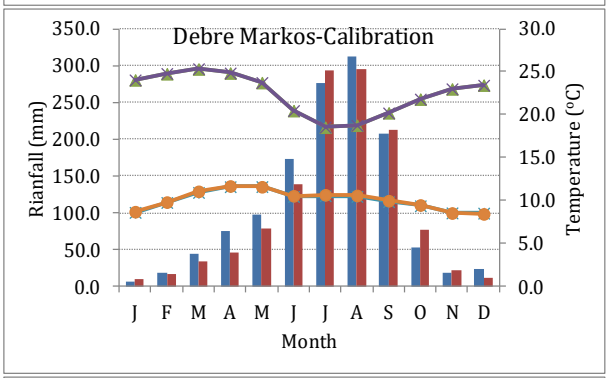
Debre Markos-Calibration
Rianfall (mm)
Temperature (°C)
Month
J F M A M J J A S O N D

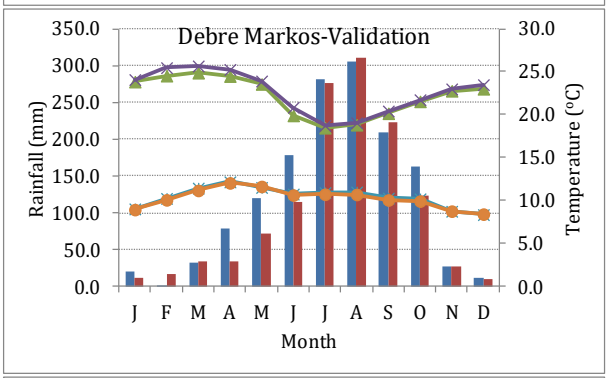
Debre Markos-Validation
Rainfall (mm)
Temperature (°C)
Month
J F M A M J J A S O N D

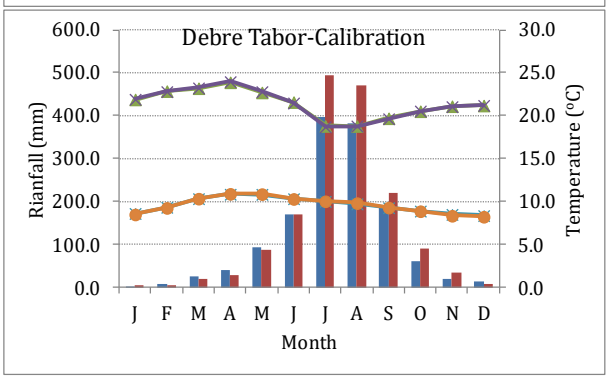
Debre Tabor-Calibration
Rianfall (mm)
Temperature (°C)
Month
J F M A M J J A S O N D

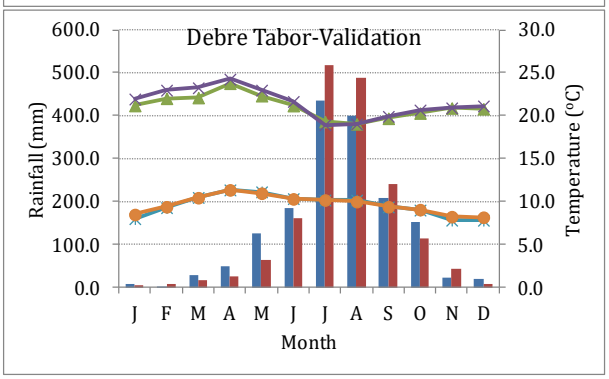
Debre Tabor-Validation
Rainfall (mm)
Temperature (°C)
Month
J F M A M J J A S O N D

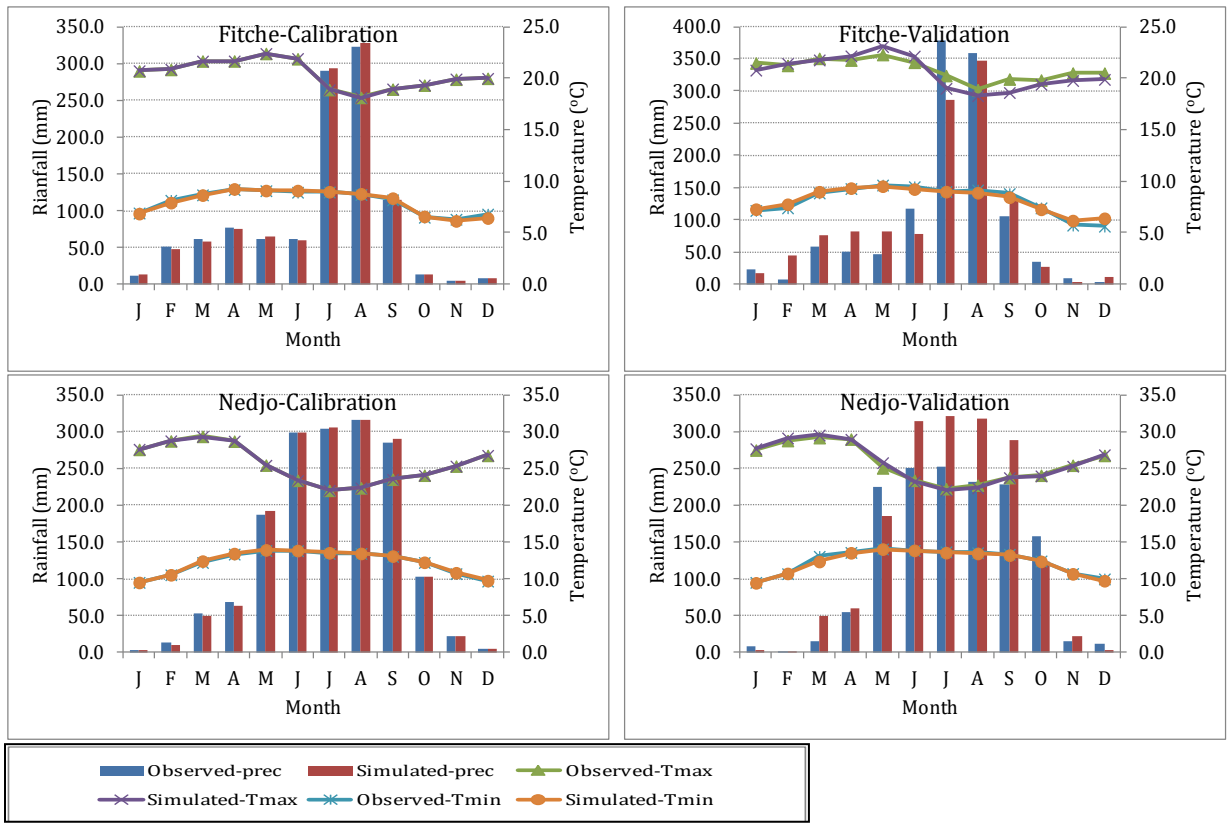

Appendix 25: Calibration and validation of observed and simulated of precipitation, maximum and minimum temperature for all stations using SDSM from NCEP of HadCM3 GCM from left to right respectively

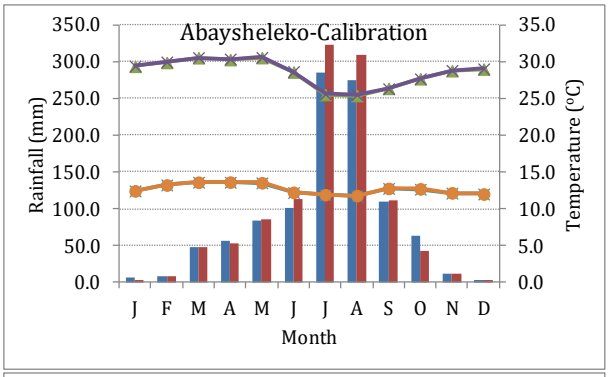
Abaysheleko-Calibration
Rainfall (mm)
Temperature (°C)
Month
J F M A M J J A S O N D

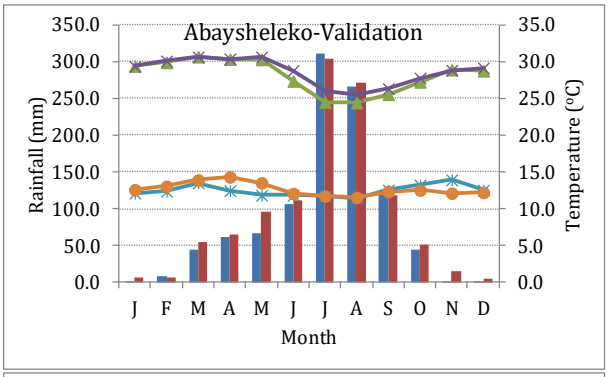
Abaysheleko-Validation
Rainfall (mm)
Temperature (°C)
Month
J F M A M J J A S O N D

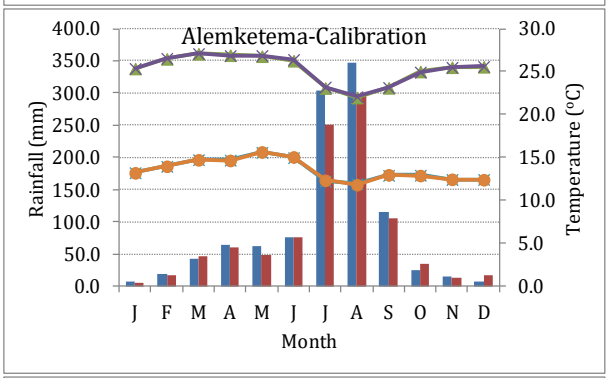
Alemketema-Calibration
Rainfall (mm)
Temperature (°C)
Month
J F M A M J J A S O N D

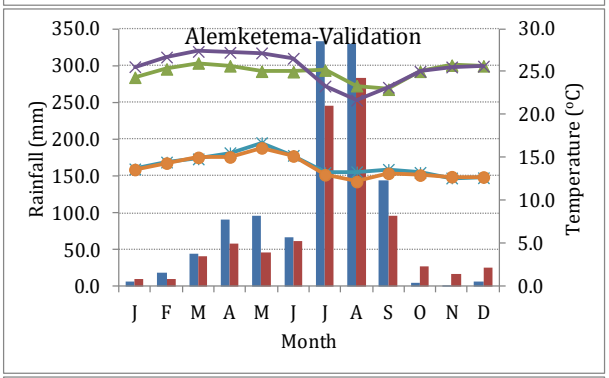
Alemketema-Validation
Rainfall (mm)
Temperature (°C)
Month
J F M A M J J A S O N D

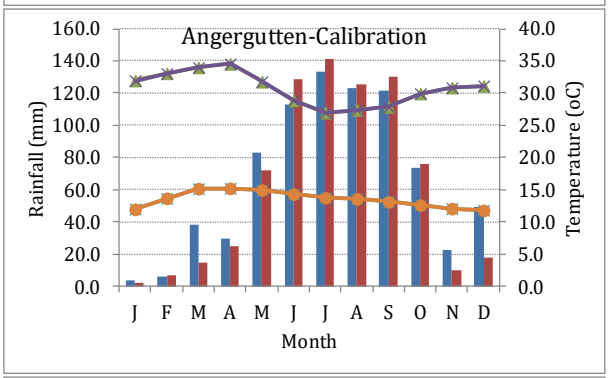
Angergutten-Calibration
Rainfall (mm)
Temperature (oC)
Month
J F M A M J J A S O N D

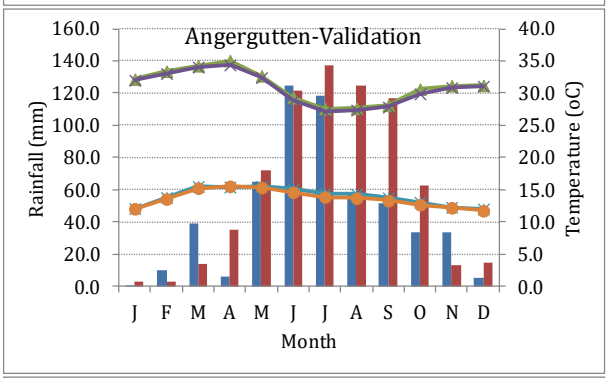
Angergutten-Validation
Rainfall (mm)
Temperature (oC)
Month
J F M A M J J A S O N D

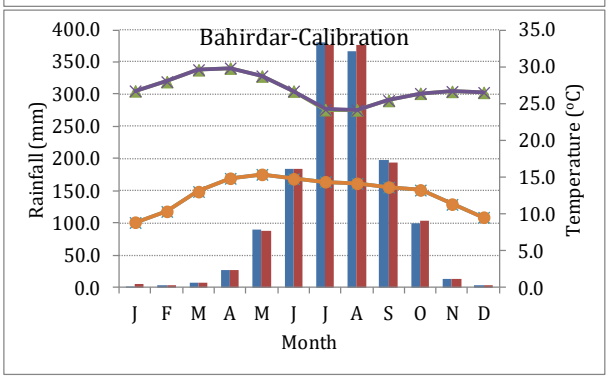
Bahirdar-Calibration
Rainfall (mm)
Temperature (°C)
Month
J F M A M J J A S O N D

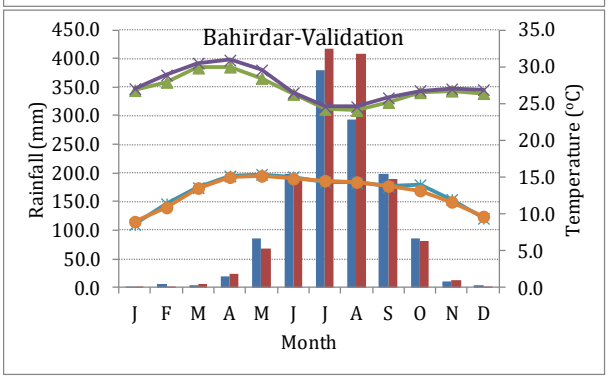
Bahirdar-Validation
Rainfall (mm)
Temperature (°C)
Month
J F M A M J J A S O N D

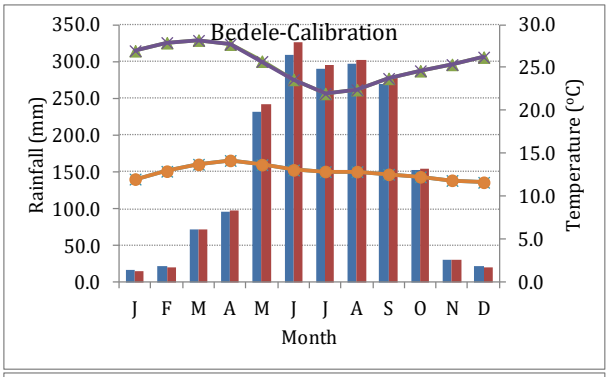
Bedele-Calibration
Rainfall (mm)
Temperature (°C)
Month
J F M A M J J A S O N D

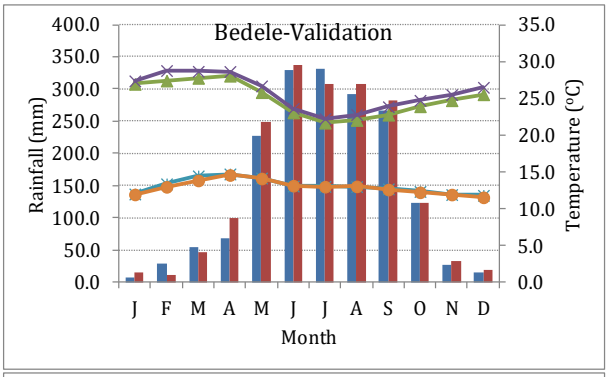
Bedele-Validation
Rainfall (mm)
Temperature (°C)
Month
J F M A M J J A S O N D

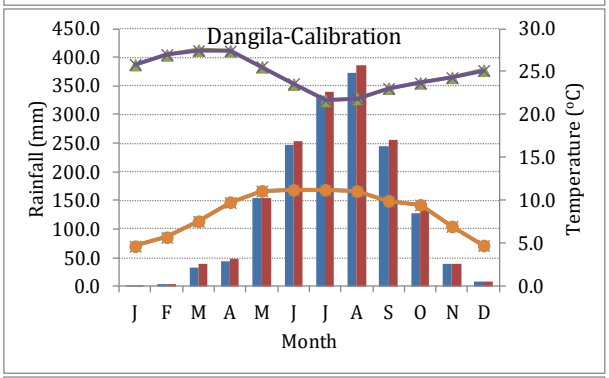
Dangila-Calibration
Rainfall (mm)
Temperature (°C)
Month
J F M A M J J A S O N D

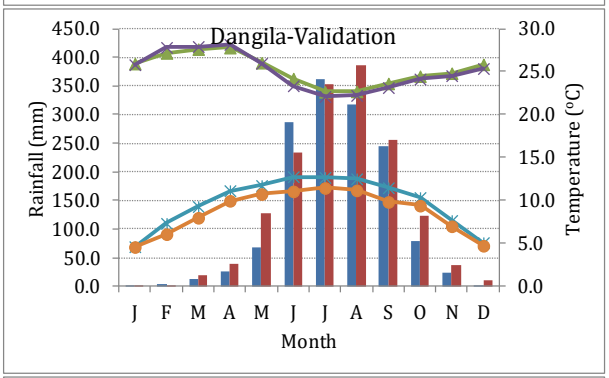
Dangila-Validation
Rainfall (mm)
Temperature (°C)
Month
J F M A M J J A S O N D

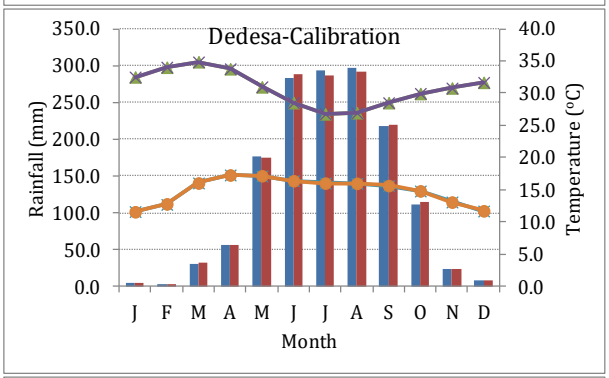
Dedesa-Calibration
Rainfall (mm)
Temperature (°C)
Month
J F M A M J J A S O N D

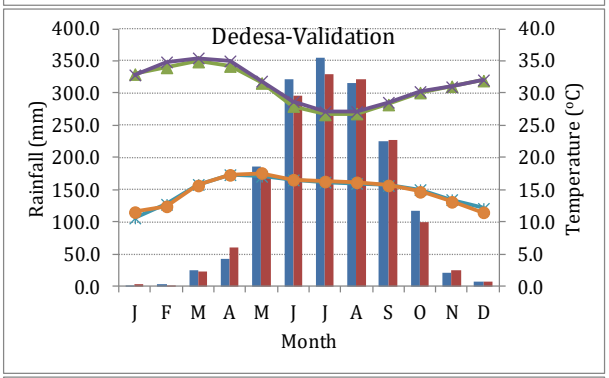
Dedesa-Validation
Rainfall (mm)
Temperature (°C)
Month
J F M A M J J A S O N D

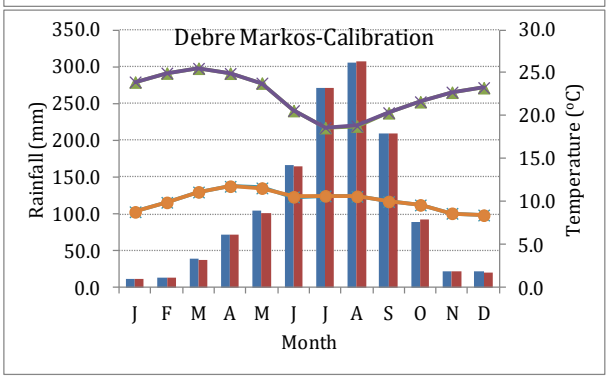
Debre Markos-Calibration
Rainfall (mm)
Temperature (°C)
Month
J F M A M J J A S O N D

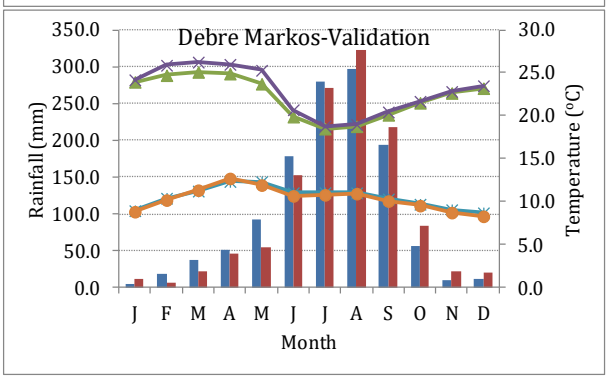
Debre Markos-Validation
Rainfall (mm)
Temperature (°C)
Month
J F M A M J J A S O N D

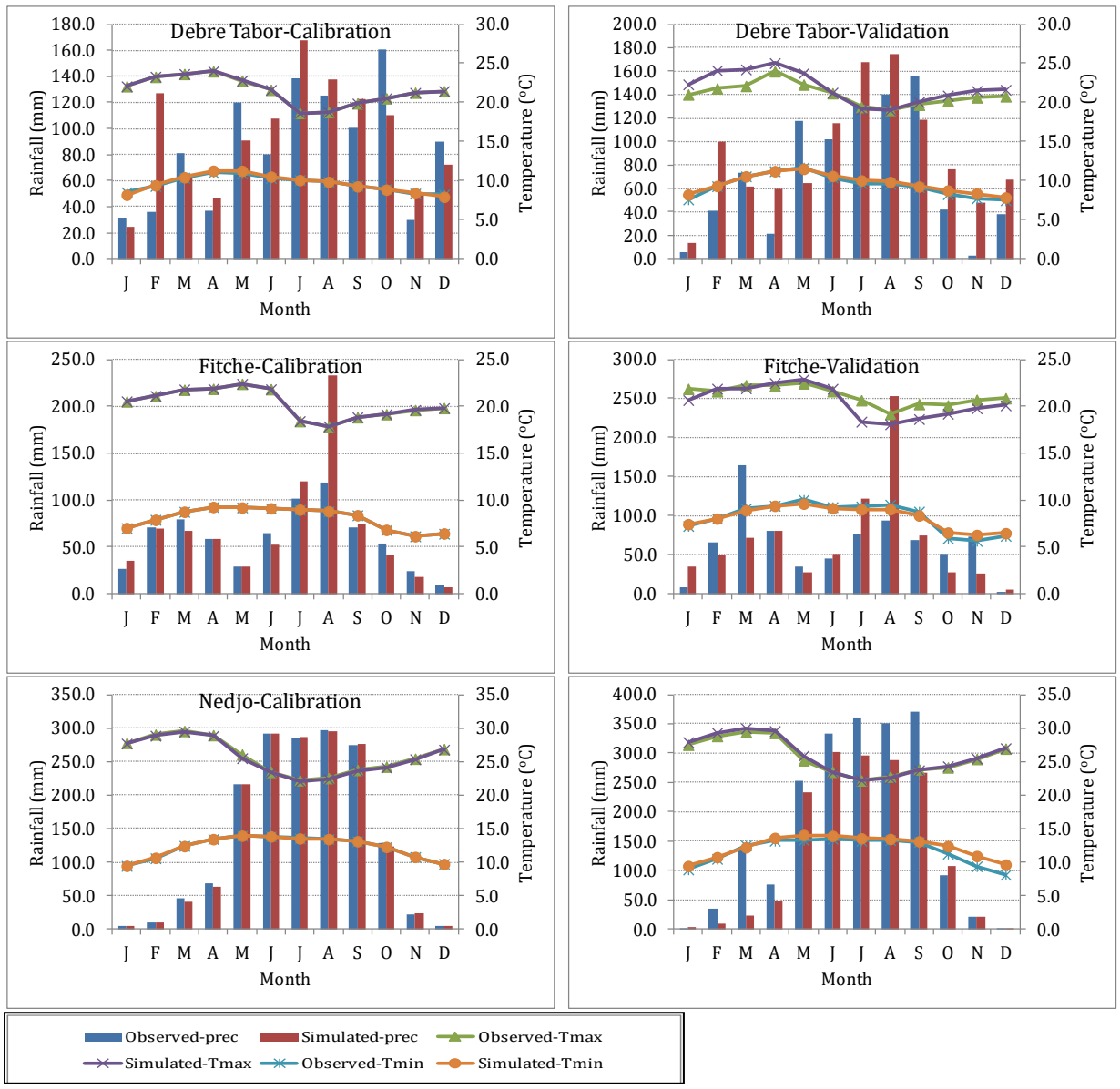

Appendix 26: Calibration and validation of observed and simulated of precipitation, maximum and minimum temperature for all stations using SDSM from NCEP-canESM2 GCM from left to right respectively

Appendix 27: Emissions Scenarios and Representative Concentration Pathways (RCPs)

Future greenhouse gas (GHG) emissions are the product of very complex dynamic systems, determined by driving forces such as demographic development, socio-economic development, and technological change. Their future evolution is highly uncertain. Scenarios are alternative images of how the future might unfold and are an appropriate tool with which to analyze how driving forces may influence future emission outcomes and to assess the associated uncertainties(Nakicenovic *et al.*, 2000). Hence, climate models require data on the time-evolving emissions or concentrations of radiatively active constituents, and some have additional requirements for information about the time-evolving paths for land use and land cover. Climate projections are typically presented for a range of plausible pathways, scenarios, or targets that capture the relationships between human choices, emissions, concentrations, and temperature change. A set of scenarios was developed to represent the range of driving forces and emissions in the scenario literature to reflect current understanding and knowledge about underlying uncertainties. New sets of scenarios for climate change research are needed periodically to take into account scientific advances in understanding of the climate system as well as to incorporate updated data on recent historical emissions, climate change mitigation, and impacts, adaptation, and vulnerability. These sets of standard scenarios have become more comprehensive with each new generation, as the original Scientific Assessment (SA90) scenarios were replaced by the IS92 emission scenarios of the 1990s, which were in turn succeeded by the Special Report on Emissions Scenarios in 2000 (SRES) and by the Representative Concentration Pathways in 2010 (RCPs). These scenarios have been widely used in the analysis of possible climate change, its impacts, and options to mitigate climate change (Nakicenovic et al., 2000).

A90 emission scenarios were used in the first Intergovernmental Panel on Climate Change Assessment Report (IPCC FAR) in 1990. IS92-based projections were used in the IPCC Second and Third Assessment Reports (SAR and TAR). Projections based on SRES scenarios were used in the IPCC TAR and Fourth Assessment Reports (AR4). The most recent set of time-dependent scenarios, RCPs, builds on these two decades of scenario development were used in the most recent IPCC Fifth Assessment Report (AR5).

The SRES scenarios are grouped into four scenario families (A1, A2, B1 and B2) that explore alternative development pathways, covering a wide range of demographic, social, economic, technological and environmental driving forces and resulting green house gas (GHG) emissions (Nakicenovic et al., 2000). In simple terms, the four storylines combine two sets of divergent tendencies: one set varying between strong economic values and strong environmental values, the other set between increasing globalization and increasing regionalization. The A-families are characterized by a domination of economic drivers, whereas the B families assume environmental concerns to be the driving force. The number associated with the scenario families gives a further differentiation. While the A1 and B1 scenario families are rather globally orientated, the A2 and B2 scenario families pursue a rather regional policy (Table 6-2).

The storylines are summarized as follows (Nakicenovic et al., 2000):

- A1 storyline and scenario family: a future world of very rapid economic growth, global population that peaks in mid-century and declines thereafter, and rapid introduction of new and more efficient technologies. The A1 scenario family develops into three groups

that describe alternative directions of technological change in the energy system. The three A1 groups are distinguished by their technological emphasis: fossil intensive (A1FI), non-fossil energy sources (A1T), or a balance across all sources (A1B).

- A2 storyline and scenario family: a very heterogeneous world with continuously increasing global population and regionally oriented economic growth that is more fragmented and slower than in other storylines.
- B1 storyline and scenario family: a convergent world with the same global population as in the A1 storyline but with rapid changes in economic structures toward a service and information economy, with reductions in material intensity, and the introduction of clean and resource-efficient technologies.
- B2 storyline and scenario family: a world in which the emphasis is on local solutions to economic, social, and environmental sustainability, with continuously increasing population (lower than A2) and intermediate economic development.

The IPCC Fifth Assessment Report (AR5) findings were based on a new set of scenarios that replace the Special Report on Emissions Scenarios (SRES) standards employed in two previous reports (TAR and RA4). The new scenarios are called Representative Concentration Pathways (RCPs). According to Moss *et al.* (2008), the word 'representative' signifies that each RCP provides only one of many possible scenarios that would lead to the specific radiative forcing characteristics. The term 'pathway' emphasizes that not only the long-term concentration levels are of interest, but also the trajectory taken over time to reach that outcome. In summary, the new parallel process starts with the selection of four RCPs (RCP2.6, RCP4.5, RCP6, and RCP8.5), and each was named according to the radiative forcing it projected by the year 2100 (Table 6-3). Therefore, canESM2 and GFDL CMIP5 GCMs represent the latest plausible radiative forcing scenarios, a wide range that includes RCP2.6, RCP4.5, RCP6 and RCP8.5.

RCP2.6 is a very low forcing level, where radiative forcing peaks at approximately $3Wm^{-2}$ relative to pre-industrial values, peaks approximately 490 ppmCO2 equivalent before 2100, and then declines to $2.6Wm^{-2}$ relative to pre-industrial values. This scenario is close to the ambition of the Paris agreement, which aims to strengthen the global response to the threat of climate change by keeping a global temperature rise this century well below 2 ^{o}C above pre-industrial levels and to pursue efforts to limit the temperature increase even further to 1.5 ^{o}C with powerful climate politics.

RCP4.5 is one of the two medium stabilization scenarios (RCP6 and RCP 4.5), in which strategies for reducing green house gas emissions cause radiative forcing to stabilize at $4.5Wm^{-2}$ relative to pre-industrial values (approximately 650 ppm CO2 equivalent) before 2100.
RCP 6 is another medium stabilization scenario in which radiative forcing is stabilized at $6Wm^{-2}$ relative to pre-industrial values (approximately 850 ppmCO2 equivalent).

RCP8.5 is a very high baseline emission scenario for which radiative forcing reaches $>8.5Wm^{-2}$ relative to pre-industrial values (1370 ppm CO2 equivalent) by 2100 and continues to rise for some time (IPCC, 2014b). This scenario is closest to the currently measured trends in green house gas concentration.